

For Reference

NOT TO BE TAKEN FROM THIS ROOM

Ex LIBRIS
UNIVERSITATIS
ALBERTAENSIS



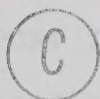
Digitized by the Internet Archive
in 2022 with funding from
University of Alberta Library

<https://archive.org/details/Floriano1984>

THE UNIVERSITY OF ALBERTA

ELECTRON AND ION TRANSPORT IN SYMMETRICAL
AND UNSYMMETRICAL METHANES

by



Michele Antonio Floriano

A THESIS

SUBMITTED TO THE FACULTY OF GRADUATE STUDIES AND RESEARCH
IN PARTIAL FULFILMENT OF THE REQUIREMENTS FOR THE DEGREE
OF DOCTOR OF PHILOSOPHY

DEPARTMENT OF CHEMISTRY

EDMONTON, ALBERTA

FALL, 1984

To my parents and to my wife

ABSTRACT

The mobilities μ of electrons and μ_+ of ions generated by ionization of CH_4 and deuterated analogues were measured as functions of electric field E along the vapor-liquid coexistence curve and in the gas along isochores. The density range from $n \approx 1 \times 10^{25} \text{ molec/m}^3$ (dilute gas) to $n \approx 17 \times 10^{27} \text{ molec/m}^3$ (liquid near triple point) was investigated.

In the gas, μ was independent of electric field strength up to a threshold $(E/n)_{\text{thr}}$. Electron heating either by fields above $(E/n)_{\text{thr}}$ or by T caused μ to increase because of the energy dependence of the scattering cross section σ_m . Values of σ_m did not change with isotopic substitution. The ratio of the drift velocity at the threshold field, v_d^{thr} , to the speed of sound, c_0 , is ~ 1 when electrons lose energy predominantly by elastic scattering. The ratio is >1 when inelastic scattering occurs. In low density methane gas at constant n $(v_d^{\text{thr}})/c_0 \approx 1$ at low T but increased to ~ 14 at 636K. This was attributed to the opening of vibrational channels at high temperatures. In the saturated gas the normalized mobility $n\mu$ at low fields was $\sim 2 \times 10^{25} \text{ molec/Vsm}$ for $n \leq 3 \times 10^{25} \text{ molec/m}^3$. $n\mu$ decreased to $\sim 1 \times 10^{25} \text{ molec/Vsm}$ at $n \approx 4 \times 10^{27} \text{ molec/m}^3$ and increased on approaching the

critical density, $n_c = 6.1 \times 10^{27}$ molec/m³. The decrease was due to electron quasilocalization in density fluctuations. The temperature coefficient of mobility E_μ along isochores increased superlinearly with density at $5 \lesssim n(10^{26} \text{ molec/m}^3) \lesssim 61$, independent of isotopic substitution. At n_c , E_μ was ~ 140 kJ/mol. Heating the gas at constant n lowered the extent of fluctuations and thereby electron quasilocalization. The increase in $n\mu$ at $n \gtrsim 4 \times 10^{27}$ molec/m³ was due to conduction band formation. In the liquid at $n \approx 10.7 \times 10^{27}$ molec/m³ a maximum $n\mu_{\text{max}} \approx 1 \times 10^{27}$ molec/Vsm was reached. Values of $n\mu_{\text{max}}$ were ~ 50 times larger than $n\mu$ in the dilute gas. The values of $n\mu_{\text{max}}$ were in the order $\text{CH}_4:\text{CD}_4:\text{CHD}_3:\text{CH}_3\text{D}:\text{CH}_2\text{D}_2 = 1.00:0.73:0.72:0.66:0.59$. Altering the spherelike symmetry of CH_4 led to enhanced scattering in the liquid. The field dependence of mobility $d\mu/dE$ was positive at $n < 8.5 \times 10^{27}$ molec/m³ but it was negative at higher n . The change of sign also caused a cusp in the value of $(v_d^{\text{thr}})/c_0$ at 8.5×10^{27} molec/m³. In the normal liquid at $n/n_c > 2$, $(v_d^{\text{thr}})/c_0$ was ~ 4 , which indicated appreciable inelastic scattering.

The ion mobility was independent of E/n between 0.1 and 15 Td. In the gas at $n \lesssim 12 \times 10^{25}$ molec/m³, μ_+ increased with T due to: (1) declustering of the ion and (2) energy dependence of the scattering cross section.

Values of $n\mu_+$ were independent of n in the saturated vapors between 1×10^{25} and 6.1×10^{27} molec/m³ (n_c). The temperature coefficients of μ_+ in the gas at constant n were similar to E_μ for electrons. At $n > n_c$, $n\mu_+$ increased, reaching a maximum at $\sim 11 \times 10^{27}$ molec/m³. This was approximately the same density where the electron $n\mu_{\max}$ occurred. In the liquid at $n/n_c \gtrsim 2$ the product $\eta\mu_+$ was independent of viscosity η . At lower densities, $\eta\mu_+$ attained a maximum at $\eta \approx 6 \times 10^{-5}$ kg/sm and then decreased as the critical region was approached. The decrease was attributed to electrostriction increasing the local viscosity around the ion. No isotope effect was observed in the ion mobilities.

ACKNOWLEDGEMENTS

I am sure I will benefit, in years to come, from my association with Professor G.R. Freeman. The assistance and guidance I received during the course of this work were greatly appreciated.

I would like to thank the past and present members of the Radiation Chemistry Group for creating a stimulating and pleasant atmosphere in which to work, the many persons associated with me during the course of this study, including the staff of the Department of Chemistry and of the supporting departments and Mrs. Jacki Jorgensen for typing the final draft of this thesis.

I am indebted to Dr. Norman Gee for the many useful discussions and for the help I received at the beginning of this project.

Thanks are due to Mr. Ron Gardner and Mr. Larry Coulson of the Radiation Research Center for technical help and for developing a special lubricant for a particularly squeaky wheel.

I would also like to thank the Department of Chemistry and the Faculty of Graduate Studies Scholarship Committee of the University of Alberta for a Research Assistantship and a Dissertation Fellowship I received in the latter part of my program.

TABLE OF CONTENTS

Chapter I	INTRODUCTION.....	1
A.	General	1
B.	Historical Aspects.....	4
1.	Early Works.....	4
2.	Electron Mobilities.....	5
a.	Gas Phase Experiments.....	5
b.	Electron Mobilities in Hydrocarbon Vapors...	8
i)	Methane.....	8
ii)	Methane-d ₄	10
iii)	Ethane and Propane.....	11
iv)	Other <u>n</u> -Alkanes.....	12
v)	Branched Alkanes.....	13
c.	Liquid Phase Experiments.....	14
3.	Ion Mobilities.....	17
a.	Gas Phase.....	17
b.	Liquid Phase.....	18
C.	Theory and Models.....	19
1.	Gas Phase.....	19
a.	Electron Mobilities.....	19
b.	Ion Mobilities.....	20
2.	Liquid Phase.....	22
a.	Quasifree Electrons.....	23
b.	Localized Electrons.....	26
c.	Ions.....	27

D. Present Study.....	28
E. Condensed Phase Isotope Effects.....	29
1. Theory	29
2. Applications. The Isotopic Methanes.....	39
Chapter II EXPERIMENTAL.....	44
A. Materials	44
B. Apparatus and Procedure.....	45
1. The Vacuum System.....	45
2. Sample Purification.....	48
3. Conductance Cells.....	49
4. Filling the Cell.....	53
5. Temperature Control.....	56
6. van de Graaff Accelerator.....	62
7. Mobility Measurements.....	62
C. The Analysis of the Measured Signal.....	67
1. Effect of Finite Width of the Xray Pulse.....	72
2. Effect of Random Diffusion.....	73
3. Effect of Space Charge.....	74
D. Physical Properties.....	81
Chapter III RESULTS.....	84
A. Electron Mobilities.....	85
1. CH ₄	85
2. CH ₃ D	113
3. CH ₂ D ₂	140
4. CHD ₃	163

5. CD_4	191
B. Cation Mobilities	215
1. CH_4	217
2. CH_3D	228
3. CH_2D_2	239
4. CHD_3	251
5. CD_4	272
Chapter IV DISCUSSION	292
A. Electrons	292
1. Low Density Gas ($n/n_c \lesssim 0.05$)	294
a. Electric Field Effect	294
i) CH_4	294
ii) Deuterated Methanes	300
b. Temperature Effect	301
i) CH_4	301
ii) Deuterated Methanes	305
2. Dense Gas ($0.05 \lesssim n/n_c \leq 1$)	309
a. Electric Field Effect	309
i) CH_4	309
ii) Deuterated Methanes	311
b. Temperature and Density Effects	311
i) CH_4	311
ii) Deuterated Methanes	317

3. Liquid ($1 < n/n_c \lesssim 2.8$).....	332
a. Electric Field Effect.....	332
i) CH_4 and Deuterated Analogues.....	332
b. Density Effect.....	341
c. Isotope Effect.....	351
B. Ions	359
1. Low Density Gas.....	359
2. Effect of Density.....	380
a. Dense Gas.....	380
b. Liquid Phase.....	391
REFERENCES	399
APPENDIX Average Deviations.....	418

LIST OF TABLES

TABLE	Description	PAGE
I-1	Parameters for Equation I-42.....	40
I-2	Relative A's in Equation I-42 for Methanes of Same Mass and Different Moments of Inertia.	41
II-1	Physical Properties.....	82
III-1 to III-5	Summaries of Electron Results	
	1. CH ₄	109
	2. CH ₃ D.....	136
	3. CH ₂ D ₂	160
	4. CHD ₃	187
	5. CD ₄	211
III-6 to III-10	Summaries of Ion Results	
	6. CH ₄	226
	7. CH ₃ D.....	237
	8. CH ₂ D ₂	247
	9. CHD ₃	268
	10. CD ₄	288
IV-1	Temperature Coefficients of Thermal Electron Mobilities in Methane Gases at Different Densities.....	328
IV-2	Calculation of Electron Mobility Maxima in Liquids from Equation IV-21.....	348
IV-3	Temperature Coefficients of Thermal Electron and Ion Mobilities.....	392

LIST OF FIGURES

FIGURE	Description	PAGE
Chapter II EXPERIMENTAL		
1	Main Vacuum Manifold.....	46
2	Auxiliary Manifold Used for Filling Cells.....	47
3	Low Pressure Gas Cell.....	50
4	High Pressure Liquid Cell.....	51
5	High Pressure Gas Cell.....	52
6	Circuit to Measure Cell Capacitance.....	54
7	Cooling Apparatus.....	57
8	Block Diagram of Temperature Regulation Apparatus.....	59
9	Block Diagram of Temperature Controller.....	60
10	High Temperatures Apparatus.....	61
11	System for Measuring Current Transient Signals..	63
12	Amplifier #8.....	65
13	Block Diagram of Data Collection System.....	66
14	The Measured Signal.....	68
15	Examples of Space Charge Limited Signals.....	80

Chapter III RESULTS

A. Electrons

1. CH₄

1-1 to 1-14 Mobilities in Gas Phase Plotted Against E/n at
Different Temperatures (K) and Densities
(molec/m³).

FIGURE	Description	PAGE
1	$n = 2.95 \times 10^{25}$ at 116.5K to 636K.....	86
2	$n = 5.3 \times 10^{25}$ at 110.0K to 293.5K.....	87
3	$n = 5.8 \times 10^{25}$ at 124.0K to 488.5K.....	88
4	$n = 7.5 \times 10^{25}$ at 152.0K to 293.0K.....	89
5	Coexistence Vapor at 100.5K, $n = 2.65 \times 10^{25}$ to 108.7K, $n = 5.4 \times 10^{25}$	91
6	Coexistence Vapor at 123.5K, $n = 1.54 \times 10^{26}$ to 146.2K, $n = 5.2 \times 10^{26}$	92
7	$n = 5.5 \times 10^{26}$ at 152.0K to 292.3K.....	93
8	Coexistence Vapor at 149.0K, $n = 5.7 \times 10^{26}$ to 169.1K, $n = 14.2 \times 10^{26}$	94
9	Coexistence Vapor at 169.5K, $n = 14.4 \times 10^{26}$ to 184.0K, $n = 28.5 \times 10^{26}$	95
10	$n = 2.90 \times 10^{27}$ at 188.7K to 195.2K.....	97
11	Coexistence Vapor at 185.8K, $n = 32 \times 10^{26}$ to 188.7K, $n = 4.0 \times 10^{27}$	98
12	Coexistence Vapor at 189.1K, $n = 4.17 \times 10^{27}$ to 190.2K, $n = 4.92 \times 10^{27}$	99
13	Supercritical Gas at $n_c = 6.1 \times 10^{27}$ at 190.7K to 194.6K.....	100
1-14 to 1-17	Mobilities in Equilibrium Liquid Phase Plotted Against E/n at Different Densities (10^{27} molec/m ³)	
14	7.5 to 9.1.....	101
15	9.7 to 10.8.....	103

FIGURE	Description	PAGE
16	11.3 to 13.7.....	104
17	14.0 to 17.0.....	105
1-18	Threshold Fields Against Temperature at Different Gas Densities.....	106
1-19	Threshold Fields Against Density of Saturated Gas and Liquid Phases.....	107
2. <u>CH₃D</u>		
2-1 to 2-3	Mobilities in Gas Phase Plotted Against E/n at Different Temperatures (K) and Densities (molec/m ³)	
1	n = 2.35 x 10 ²⁵ at 146.3K to 637K.....	114
2	n = 3.30 x 10 ²⁵ at 112.5K to 407K.....	115
3	n = 4.9 x 10 ²⁵ at 109.3K to 423K.....	116
2-4	Threshold Fields Against Temperature at Different Gas Densities.....	117
2-5 to 2-14	Mobilities in Gas Phase Plotted Against E/n at Different Temperatures (K) and Densities (molec/m ³)	
5	Coexistence Vapor at 99.0K, n = 2.30 x 10 ²⁵ to 109.3K, n = 4.9x10 ²⁵	118
6	Coexistence Vapor at 115.7K, n = 8.9 x 10 ²⁵ to 130.5K, n = 22.6 x 10 ²⁵	119
7	Coexistence Vapor at 136.5K, n = 3.11 x 10 ²⁶ to 149.8K, n = 6.0 x 10 ²⁶	120

FIGURE	Description	PAGE
8	$n = 6.0 \times 10^{26}$ at 154.8K to 294.0K.....	121
9	$n = 6.7 \times 10^{26}$ at 153.9K to 293.0K.....	123
10	Coexistence Vapor at 154.8, $n = 7.5 \times 10^{26}$ to 163.0K, $n = 10.7 \times 10^{26}$	124
11	$n = 1.50 \times 10^{27}$ at 171.0K to 210.0K.....	125
12	Coexistence Vapor at 181.0K, $n = 2.36 \times 10^{27}$ to 191.0K, $n = 5.5 \times 10^{27}$	126
13	$n = 2.70 \times 10^{27}$ molec/m ³ at 186.9K to 195.2K....	127
14	Supercritical Gas at $n_c = 6.1 \times 10^{27}$ at 191.3K to 193.3K.....	128
2-15 to 2-18	Mobilities in Equilibrium Liquid Phase Plotted Against E/n at Different Densities (10^{27} molec/m ³)	
15	7.5 to 8.6.....	130
16	9.1 to 10.3.....	131
17	10.6 to 12.3.....	132
18	13.5 to 17.0.....	134
2-19	Threshold Fields Against Density of Saturated Gas and Liquid Phases.....	135

3. CH₂D₂

3-1 to 3-5	Mobilities in Gas Phase Plotted Against E/n at Different Temperatures (K) and Densities (molec/m ³)
------------	---

1	Coexistence Vapor at 94.0K, $n = 1.40 \times 10^{25}$
---	---

FIGURE	Description	PAGE
	to 102.8K, $n = 3.3 \times 10^{25}$	141
2	$n = 3.7 \times 10^{25}$ at 133.0K to 450K.....	142
3	$n = 6.1 \times 10^{25}$ at 113.0K to 408.5K.....	143
4	Coexistence Vapor at 120.8K, $n = 1.37 \times 10^{26}$ to 147.8K, $n = 5.9 \times 10^{26}$	144
5	$n = 7.3 \times 10^{26}$ at 155.7K to 292.0K.....	146
3-6	Threshold Fields Against Temperature at Different Gas Densities.....	147
3-7 to 3-11	Mobilities in Gas Phase Plotted Against E/n at Different Temperatures (K) and Densities (molec/m ³)	
7	Coexistence Vapor at 154.0K, $n = 7.7 \times 10^{26}$ to 180.1K, $n = 24.8 \times 10^{26}$	148
8	$n = 2.60 \times 10^{27}$ at 184.2K to 195.5K.....	149
9	Coexistence Vapor at 181.4K, $n = 2.65 \times 10^{27}$ to 186.0K, $n = 3.55 \times 10^{27}$	150
10	Coexistence Vapor at 186.6K, $n = 3.70 \times 10^{27}$ to 189.2K, $n = 6.1 \times 10^{27}$	151
11	Supercritical Gas at $n_c = 6.1 \times 10^{27}$ at 189.6K to 193.9K.....	153
3-12 to 3-15	Mobilities in Equilibrium Liquid Phase Plotted Against E/n at Different Densities (10^{27} molec/m ³)	
12	7.5 to 9.1.....	154
13	9.4 to 10.4.....	155

FIGURE	Description	PAGE
14	10.5 to 14.2.....	156
15	15.2 to 17.0.....	157
3-16	Threshold Fields Against Density of Saturated Gas and Liquid Phases.....	159
4. <u>CHD₃</u>		
4-1 to 4-6	Mobilities in Gas Phase Plotted Against E/n at Different Temperatures (K) and Densities (molec/m ³)	
1	n = 2.30 x 10 ²⁵ at 102.0K to 622K.....	164
2	n = 4.3 x 10 ²⁵ at 106.6K to 434K.....	165
3	Coexistence Vapor at 111.1K, n = 7.0 x 10 ²⁵ and 115.8, n = 9.9 x 10 ²⁵	166
4	n = 12.2 x 10 ²⁵ at 121.5K to 293.7K.....	167
5	Coexistence Vapor at 125.5K, n = 1.35 x 10 ²⁶ to 147.5K, n = 5.8 x 10 ²⁶	169
6	n = 6.8 x 10 ²⁶ at 155.0K to 369.5K.....	170
4-7	Threshold Fields Against Temperature at Different Gas Densities.....	171
4-8 to 4-14	Mobilities in Gas Phase Plotted Against E/n at Different Temperatures (K) and Densities (molec/m ³)	
8	Coexistence Vapor at 152.0K, n = 7.1 x 10 ²⁶ to 156.0K, n = 8.7 x 10 ²⁶	172
9	n = 9.3 x 10 ²⁶ at 161.0K to 293.8K.....	173

FIGURE	Description	PAGE
10	Coexistence Vapor at 159.5K, $n = 1.00 \times 10^{27}$ to 176.2K, $n = 2.07 \times 10^{27}$	174
11	Coexistence Vapor at 176.8K, $n = 2.12 \times 10^{27}$ to 182.3K, $n = 2.83 \times 10^{27}$	175
12	$n = 2.91 \times 10^{27}$ at 182.3K to 192.0K.....	177
13	Coexistence Vapor at 183.6, $n = 3.03 \times 10^{27}$ to 188.5K, $n = 4.7 \times 10^{27}$	178
14	Supercritical Gas at $n_c = 6.1 \times 10^{27}$ at 189.0K to 193.0K.....	179
4-15 to 4-18	Mobilities in Equilibrium Liquid Phase Plotted Against E/n at Different Densities (10^{27} molec/ m^3)	
15	8.3 to 94.....	180
16	9.7 to 10.3.....	182
17	10.6 to 13.0.....	183
18	14.0 to 16.9.....	184
4-19	Threshold Fields Against Density of Saturated Gas and Liquid Phases.....	185
5. <u>CD₄</u>		
5-1 to 5-6	Mobilities in Gas Phase Plotted Against E/n at Different Temperatures (K) and Densities (molec/ m^3)	
1	Coexistence Vapor at 98.3K, $n = 2.2 \times 10^{25}$ to 107.8K, $n = 4.8 \times 10^{25}$	192

FIGURE	Description	PAGE
2	$n = 3.20 \times 10^{25}$ at 106.0K to 598K.....	193
3	$n = 5.0 \times 10^{25}$ at 111.8K to 521K.....	194
4	Coexistence Vapor at 119.3K, $n = 1.23 \times 10^{26}$ to 142.0K, $n = 4.46 \times 10^{26}$	195
5	$n = 3.70 \times 10^{26}$ at 138.4K to 433.0K.....	197
6	$n = 5.5 \times 10^{26}$ at 146.5K to 397.0K.....	198
5-7	Threshold Fields Against Temperature at Different Gas Densities.....	199
5-8 to 5-11	Mobilities in Gas Phase Plotted Against E/n at Different Temperatures (K) and Densities (molec/m ³)	
8	Coexistence Vapor at 164.8K, $n = 1.24 \times 10^{27}$ to 182.5K, $n = 2.83 \times 10^{27}$	200
9	$n = 2.90 \times 10^{27}$ at 182.7K to 195.5K.....	201
10	Coexistence Vapor at 186.1K, $n = 3.60 \times 10^{27}$ and 188.7K, $n = 4.7 \times 10^{27}$	203
11	Supercritical Gas at $n_c = 6.1 \times 10^{27}$ at 189.3K to 193.2K.....	204
5-12 to 5-15	Mobilities in Equilibrium Liquid Phase Plotted Against E/n at Different Densities (10^{27} molec/m ³)	
12	7.6 to 9.4.....	205
13	9.7 to 10.5.....	206
14	10.9 to 14.7.....	207
15	15.1 to 17.1.....	208

FIGURE	Description	PAGE
5-16	Threshold Fields Against Density of Saturated Gas and Liquid Phases.....	210
B. <u>IONS</u>		
1. <u>CH₄</u>		
1-20 to 1-25	Mobilities in Gas Phase Plotted Against E/n at Different Temperatures (K) and Densities (molec/m ³)	
20	n = 2.95 x 10 ²⁵ at 116.5K to 494K.....	218
21	Coexistence Vapor at 123.5, n = 1.54 x 10 ²⁶ to 146.2, n = 5.2 x 10 ²⁶	219
22	n = 5.5 x 10 ²⁶ at 152.0K to 292.3K.....	220
23	Coexistence Vapor at 154.0K, n = 7.4 x 10 ²⁶ to 184.0K, n = 28.5 x 10 ²⁶	221
24	n = 2.90 x 10 ²⁷ at 188.7K to 195.2K.....	222
25	Supercritical Gas at n _c = 6.1 x 10 ²⁷ at 191.2K and 192.2K.....	223
1-26	Mobilities in Equilibrium Liquid Phase Plotted Against E/n at 8.6 x 10 ²⁷ to 17.0 x 10 ²⁷	224
2. <u>CH₃D</u>		
2-20 to 2-26	Mobilities in Gas Phase Against E/n at Different Temperatures (K) and Densities (molec/m ³)	
20	Coexistence Vapor at 91.9K, n = 1.24 x 10 ²⁵ to	

FIGURE	Description	PAGE
	99.0K, $n = 2.30 \times 10^{25}$	229
21	$n = 2.35 \times 10^{25}$ at 108.2K to 535K.....	230
22	Coexistence Vapor at 115.7, $n = 0.89 \times 10^{26}$ to 149.5K, $n = 5.8 \times 10^{26}$	231
23	$n = 6.7 \times 10^{26}$ at 153.9K to 293.0K.....	232
24	Coexistence Vapor at 155.0K, $n = 7.6 \times 10^{26}$ to 184.2K, $n = 27.0 \times 10^{26}$	233
25	$n = 1.50 \times 10^{27}$ at 171.0K to 210.0K.....	234
26	$n = 2.70 \times 10^{27}$ at 160.0K to 195.2K.....	235
3. <u>CH₂D₂</u>		
3-17 to 3-22 Mobilities in Gas Phase Plotted Against E/n at Different Temperatures (K) and Densities (molec/m ³)		
17	$n = 3.70 \times 10^{25}$ at 133.0K to 450K.....	240
18	$n = 6.1 \times 10^{25}$ at 113.0K to 408.5K.....	241
19	Coexistence Vapor at 120.8K, $n = 1.37 \times 10^{26}$ to 181.4K, $n = 26.5 \times 10^{26}$	242
20	$n = 7.3 \times 10^{26}$ at 155.7K to 292.0K.....	243
21	$n = 26.0 \times 10^{26}$ at 184.2K to 195.5K.....	244
22	Supercritical Gas at $n_c = 6.1 \times 10^{27}$ at 190.5K to 193.9K.....	245
3-23 to 3-24 Mobilities in Equilibrium Liquid Phase Plotted Against E/n at Different Densities (10^{27} molec/m ³)		

FIGURE	Description	PAGE
23	8.8 to 12.2.....	247
24	13.1 to 17.0.....	248

4. CHD₃

4-20 to 4-31 Mobilities in Gas Phase Plotted Against E/n
at Different Temperatures (K) and Densities
(molec/m³)

20	Coexistence Vapor at 91.5K, $n = 1.11 \times 10^{25}$ to 97.7K, $n = 2.20 \times 10^{25}$	252
21	$n = 2.30 \times 10^{25}$ at 102.0K to 568.7K.....	253
22	$n = 4.3 \times 10^{25}$ at 106.6K to 434K.....	254
23	Coexistence Vapor at 102.0K, $n = 3.0 \times 10^{25}$ to 115.8, $n = 10.5 \times 10^{25}$	255
24	$n = 1.22 \times 10^{26}$ at 136.0K to 293.7K.....	256
25	Coexistence Vapor at 125.5K, $n = 1.85 \times 10^{26}$ to 147.5K, $n = 5.8 \times 10^{26}$	257
26	$n = 6.8 \times 10^{26}$ at 155.0K to 369.5K.....	259
27	Coexistence Vapor at 152.0K, $n = 7.1 \times 10^{26}$ to 156.0K, $n = 8.7 \times 10^{26}$	260
28	$n = 9.3 \times 10^{26}$ at 161.0K to 293.8K.....	261
29	$n = 29.1 \times 10^{26}$ at 184.0K to 193.8K.....	262
30	Coexistence Vapor at 158.5K, $n = 9.7 \times 10^{26}$ to 183.6, $n = 30.3 \times 10^{26}$	263
31	Supercritical Gas at $n_c = 6.1 \times 10^{27}$ at 189.5K to 193.0K.....	264

FIGURE	Description	PAGE
4-32 to 4-33	Mobilities in Equilibrium Liquid Phase Plotted Against E/n at Different Densities (10^{27} molec/ m^3)	
32	9.4 to 11.7.....	265
33	12.3 to 16.9.....	266
5. <u>CD</u> ₄		
5-17 to 5-28	Mobilities in Gas Phase Plotted Against E/n at Different Temperatures (K) and Densities (molec/ m^3)	
17	$n = 2.50 \times 10^{24}$ at 95.0K to 535.5K.....	273
18	Coexistence Vapor at 94.0K, $n = 1.5 \times 10^{25}$ to 107.8K, $n = 4.8 \times 10^{25}$	274
19	$n = 3.20 \times 10^{25}$ at 106.0K to 598K.....	275
20	$n = 5.0 \times 10^{25}$ at 111.6K to 184.7K.....	276
21	$n = 5.0 \times 10^{25}$ at 225.0K to 521K.....	277
22	Coexistence Vapor at 119.3K, $n = 1.23 \times 10^{26}$ to 135.1K, $n = 3.22 \times 10^{26}$	278
23	$n = 3.70 \times 10^{26}$ at 138.4K to 433K.....	279
24	Coexistence Vapor at 141.0K, $n = 4.21 \times 10^{26}$ to 151.0K, $n = 6.8 \times 10^{26}$	280
25	$n = 5.5 \times 10^{26}$ at 146.5K to 397K.....	282
26	Coexistence Vapor at 164.8K, $n = 1.24 \times 10^{27}$ to 182.5K, $n = 2.83 \times 10^{27}$	283
27	$n = 2.90 \times 10^{27}$ at 182.7K to 195.5K.....	284

FIGURE	Description	PAGE
28	Supercritical Gas at $n_c = 6.1 \times 10^{27}$ at 189.3K to 193.0K.....	285
5-29 to 5-30	Mobilities in Equilibrium Liquid Phase Plotted Against E/n at Different Densities (10^{27} molec/ m^3)	
29	8.4 to 11.6.....	286
30	12.7 to 17.1.....	287
Chapter IV - DISCUSSION		
1	Density Normalized Electron Mobilities in CH_4 Coexistence Vapor and Liquid Against n	293
2	Drift Velocities Against E/n in CH_4 Gas at $n = 5.3 \times 10^{25}$ molec/ m^3 and $T = 293.5K$	296
3	Plot of $(v_d^{thr})/c_0$ vs. T in CH_4 Gas at n from 2.95 to 5.8 (10^{25} molec/ m^3).....	297
4	Maxwellian Energy Distributions for Thermal Electrons in CH_4 gas at 110K and 640K.....	298
5	Density Normalized Low Field Electron Mobilities Against T in CH_4 Gas at n from 2.95 to 7.5 (10^{25} molec/ m^3).....	302
6	Momentum Transfer Cross Section for Electrons in Low Density CH_4 Gas as a Function of Energy.....	304
7	Average Cross Section Against T of Low Density CH_4 Gas.....	306

FIGURE	Description	PAGE
8	Density Normalized Low Field Electron Mobilities Against T in the Gases CH ₃ D at n from 2.35 to 4.9 (10 ²⁵ molec/m ³) and CH ₂ D ₂ at n = 3.7 and 6.1 (10 ²⁵ molec/m ³).....	307
9	Density Normalized Low Field Electron Mobilities Against T in the Gases CHD ₃ at n from 2.30 to 12.2 (10 ²⁵ molec/m ³) and CD ₄ at n = 3.20 and 5.0 (10 ²⁵ molec/m ³).....	308
10	Plot of (v _d ^{thr})/c _O in Saturated CH ₄ Vapor as Function of n.....	310
11	Thermal Electron Mobilities Against T ⁻¹ in CH ₄ Gas at Different Densities.....	313
12	Thermal Electron Mobilities Against T ⁻¹ in CH ₄ Gas at Different Densities.....	314
13 to 16	Density Normalized Low Field Electron Mobilities in Coexistence Vapor and Liquid against n.	
13	CH ₃ D.....	318
14	CH ₂ D ₂	319
15	CHD ₃	320
16	CD ₄	321
17 to 20	Thermal Electron Mobilities Against T ⁻¹ in Gas Phase	
17	CH ₃ D.....	322
18	CH ₂ D ₂	323
19	CHD ₃	324

FIGURE	Description	PAGE
20	CD ₄	325
21	Temperature Coefficients of Electron Mobility Against n in Methane Gases.....	326
22	Density Dependence of ΔH° in Methane Gases.....	330
23	Density Dependence of ΔS° in Methane Gases.....	331
24	Density Dependence of $(E/n)_{thr}$ in Liquid and Supercritical Methanes and Argon.....	333
25	Plot of $(v_d^{thr})_{hd}/(v_d^{thr})_d]S(K)$ in Liquid and Supercritical CH ₄ and CD ₄	336
26	Plot of $(v_d^{thr})/c_0$ in Liquid and Supercritical Methanes.....	338
27	Thermal Electron Mobilities Against n in Saturated Vapor and Supercritical CH ₄	342
28	Density Normalized Low Field Electron Mobilities Against n and n/n_c in the Liquids CH ₄ , Ar, Kr, Xe and C(CH ₃) ₄	344
29	Density Normalized Low Field Electron Mobilities Against n in the Liquid Methanes.....	352
30	Thermal Electron Mobilities Against T/T_c in the Liquid Methanes.....	353
31	Thermal Electron Mobilities Against T/T_c in the Liquid and Supercritical Methanes in the Vicinity of T_c	354
32	Thermal Electron Mobility Maxima Against the Number of D Atoms in Liquid Methanes.....	356

FIGURE	Description	PAGE
33	Ratios of the Electron Mobility in Liquid CH_4 to that of the Deuterated Analogues.....	358
34	Density Normalized Cation Mobilities Against T in CH_4 Gas at $n = 2.95 \times 10^{25}$ molec/ m^3	361
35	Density Normalized Cation Mobilities Against T in CD_4 Gas at n from 0.25 to 5.0 (10^{25} molec/ m^3).....	362
36	Ion-Molecule Momentum Transfer Cross Section of Low Density CH_4 Gas Against Energy.....	364
37	Density Normalized Cation Mobilities Against E/n for CH_5^+ and C_3H_7^+ in CH_4 Gas at P = 0.7 - 1.3 torr and T = $300 \pm 5\text{K}$	366
38	Density Normalized Cation Mobilities Against the Effective Temperature for CH_5^+ and C_3H_7^+ in CH_4 Gas at P = 0.7 - 1.3 torr and T = $300 \pm 5\text{K}$	369
39	Plot of Methane Clusters Equilibrium Constants Against T^{-1}	371
40	Distribution of Clusters $\text{CH}_5^+(\text{CH}_4)_m$ as Functions of T at $n_{\text{CH}_4} = 2.95 \times 10^{25}$ molec/ m^3	372
41	Temperature Dependence of the Average Cluster Size and of the Density Normalized Cation Mobility in CH_4 Gas at $n = 2.95 \times 10^{25}$ molec/ m^3 ..	373
42	Temperature Dependence of the Average Scattering Cross Section for Cations in CH_4 Gas at $n = 2.95 \times 10^{25}$ molec/ m^3	375

FIGURE	Description	PAGE
43 to 45	Density Normalized Cation Mobilities Against T in Low Density Methane Gases	
43	CH ₃ D at n = 2.35 x 10 ²⁵ molec/m ³	377
44	CH ₂ D ₂ at n = 3.70 and 6.1 (10 ²⁵ molec/m ³).....	378
45	CHD ₃ at n = 2.30 and 4.3 (10 ²⁵ molec/m ³).....	379
46	Electron and Ion Mobilities in Vapor, Liquid and Supercritical CH ₄ against T.....	382
47	Density Normalized Cation Mobilities Against n in Coexistence Vapor and Liquid Methanes.....	383
48 to 52	Cation Mobilities Against T ⁻¹ in Methane Gases	
48	CH ₄	385
49	CH ₃ D.....	386
50	CH ₂ D ₂	387
51	CHD ₃	388
52	CD ₄	389
53	Cation Mobilities in Supercritical Methane Gases at n _c as Functions of T _c /T.....	390
54	Plots of the Cation Mobilities and Liquid Viscosities in CH ₄ Against T.....	394
55	Cation Mobilities Against T in Liquid and Supercritical Methanes.....	395
56	Plot of the Viscosity Normalized Cation Mobilities Against the Viscosity in Liquid Methanes.....	397

Considerate la vostra semenza:
fatti non foste a viver come bruti
ma per seguir virtute e conoscenza'.

Dante Alighieri, La Divina Commedia
Inferno XXVI, 118-120

CHAPTER I

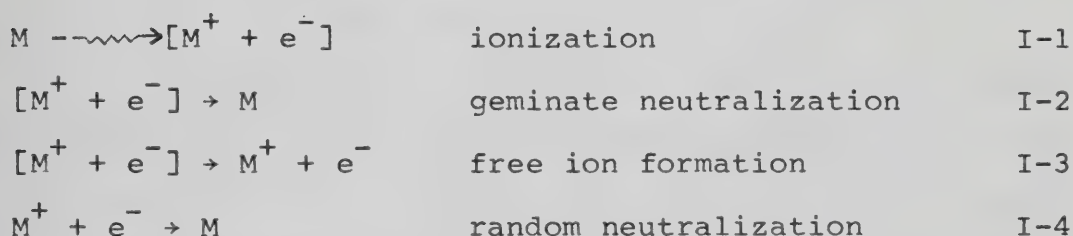
INTRODUCTION

A. General

High energy radiation causes ionization of the medium in which it is absorbed. The result of this process is an ion and an energetic electron. The electron generated in this process initially has excess kinetic energy which it loses through interactions with the molecules of the medium. When its energy is high enough (≥ 10 eV) the electron will cause further ionization events. At energies below ~ 10 eV the electron will continue to lose energy in electronic excitation of the molecules until its kinetic energy drops below the electronic excitation threshold (~ 4 eV). Below this value further losses can occur by intramolecular vibrational (~ 0.1 eV), rotational (~ 0.01 eV) and intermolecular vibrational (~ 0.01 eV) excitations.

While the electron is losing its energy it travels a distance y from its parent ion. The magnitude of the distance y is usually small enough that, when the electron reaches thermal energy, it is still subject to an appreciable coulombic attraction to its parent ion. This

potential tends to draw the ion and electron back together to undergo geminate neutralization.^{1,2,3} However not all the ion pairs undergo geminate neutralization. Some of the ions and electrons diffuse away from each other's coulombic field. They then diffuse at random in the fluid as free ions. Eventually they will recombine with other free ions (random recombination). These processes can be described by



where M is a molecule and e^- is an electron. The square brackets indicate the existence of an electrostatic potential that is appreciable compared to thermal energy.

For an ion and electron to escape their mutual coulombic attraction they must overcome the attraction energy $\xi^2/\epsilon y$, where ξ is the charge on the electron and ϵ is the dielectric constant of the medium between the ions. The probability, P, that a pair of ions escapes geminate recombination is given by the Onsager expression.⁴

$$P = \exp(-r/y) \quad \text{I-5}$$

where r is the distance from an ion at which the coulombic potential energy is equal to thermal energy, kT

$$\xi^2/\epsilon r = kT \quad \text{I-6}$$

or

$$r = \xi^2/\epsilon kT \quad \text{I-7}$$

For a nonpolar liquid ($\epsilon \approx 2$) this distance is of the order of 3×10^{-8} m at room temperature.

In the presence of an electric field E , the ions and electrons will be accelerated by the electric force eE and gain energy.⁵ In a fluid the particles will undergo collisions and lose energy. A constant average velocity in the direction of the field, the drift velocity, v_d , is attained. The particles are collected at the electrodes. This method has been used to measure the yield of free ions. These measurements have led, under more or less strict assumptions, to calculations of thermalization distances.⁶⁻⁹

At not too high fields v_d is directly proportional to E . The proportionality constant between the drift velocity and the electric field strength is called the mobility μ .

B. Historical Aspects.

1. Early Works.

It has been known since the turn of the century that normally insulating liquids become conducting when exposed to high energy radiation.¹⁰⁻¹³ This phenomenon has attracted considerable experimental and theoretical attention over the years. However the majority of early works was concerned with the degree of ionization in the presence of relatively high electric fields. The first reported observation of radiation induced conductivity is due to Thomson.¹⁰ He found that not only gases but also liquids and solids under exposure to Xrays showed an increase in conductivity. Townsend^{11,12} showed that the radiation induced current in air was proportional to the applied field strength at low fields, it reached a saturation value at intermediate fields and increased sharply at high fields. He suggested that only at the saturation value was the field high enough to collect all the ions generated by the radiation and, at even higher fields, electrical breakdown was occurring.

The first Xray induced conductance experiments on dielectric liquids were carried out by Pierre Curie in 1902.¹³ He performed an extensive investigation of the effects of electric field strengths, molecular structure, temperature and phase in the radiation induced

conductivities in liquids. He is also responsible for the first determination of the induced conductivity in a cryogenic fluid since he performed measurements in liquid air.

In the 1940's Xray induced conductance was observed by Gerritsen¹ in liquid nitrogen and liquid helium. With field strengths up to 2 MV/m ionization currents up to 40 picoamps were obtained. The current was directly proportional to the voltage in liquid nitrogen at 77K but in liquid helium between 1 and 4K the curves showed a tendency towards saturation.

2. Electron Mobilities

a. Gas Phase Experiments.

Much of the work done until the 1950's dealt with gas phase experiments, mainly because of purification problems in the liquid phase.

If a beam of electrons is passed through a gas sample, the beam will be attenuated by collisions of the electrons with the molecules. If the sample is sufficiently thin, that is an electron once scattered from the beam is unlikely to undergo a second collision that scatters it back into the beam, the intensity of the beam is given by

$$I = I_0 \exp (-n\sigma x)$$

where I_0 is the intensity in vacuum, x the distance that the beam travels through the sample and σ is the scattering cross section of a molecule.

Ramsauer¹⁴ developed a method to directly measure the electron-molecule total scattering cross section by measuring the extent of attenuation of the electron beam by the gas. He found that the cross sections depended on the electron energy. Extension of this work to energies lower than 1 eV showed that the cross-sections in the heavy rare gases passed through a minimum and then increased again.¹⁵ The same effect was found in methane.¹⁶ The method was used to measure electron mobilities in other molecular systems.^{17,18} It was found that in the n-alkane series, increasing the carbon chain length increased the cross-section.

Soon it was realized that this technique was limited in its applications because it could not be used to determine cross sections at high densities. In addition, most of these studies could not be extended to near thermal energies.¹⁹ The implementation of swarm experiments overcame these problems. In this technique one measures the flight time of a pulse of charged particles travelling a known distance.^{20,21} From the flight time the drift velocity could be determined.

Using this method Townsend measured the drift velocity and the ratio of the mean kinetic energy of the electron to

that of the gas molecules in a variety of simple compounds.²²⁻²⁶ He found that the mean free path of the electron in Ar was ten times larger than that in nitrogen or oxygen at the same pressure in the low field region. At higher field the mean free path in Argon decreased by an order of magnitude. Such effect was not found in hydrogen²⁵ or helium.³⁰ The large mean free path in argon corresponded to the small scattering cross section of the Ramsauer-type experiments. The relative transparency of the heavy rare gases to electrons of a certain energy near 1 eV was confirmed only six years later by direct measurements of the scattering cross sections. It is called the Ramsauer-Townsend effect.

Another method, originally developed to measure ion mobilities, is the shutter technique described in references 20 and 21. It involves the use of electrical shutters both to form the groups of charged particles as well as to determine the drift time. Absolute values of electron mobilities were determined in hydrogen²⁷ as well as oxygen, air, nitrous oxide and ammonia.²⁸ Mobilities were also determined in nitrogen at 80 kPa, hydrogen at 85 kPa and carbon monoxide at 96 kPa.²⁹⁻³¹

Wahlin³¹ found that, over the voltage range $0.45 < E < 4.8$ kV/m, the mean free path was independent of E . This was one of the first determinations in the thermal electron region in a gas, that is, when all the energy

gained from the field by the electrons is being lost at a collision.

b. Electron Mobilities in Hydrocarbon Vapors.

From about 1940 the number of swarm experiments in the gas phase has increased enormously.^{19,32-36} Of particular interest to this work are the measurements performed on hydrocarbon systems, especially small alkanes. Available information about the systems pertinent to this work will be reviewed in this section.

i) Methane

Methane can be considered as an extension of the monoatomic rare gases to spherelike polyatomic molecules. It is also the simplest alkane beginning the sequence of alkane molecules, which increase in complexity with size: C_nH_{2n+2} , $n = 1, 2, \dots$.

English and Hanna³⁷ measured electron drift velocities in the rare gases, in methane and carbon dioxide and in mixtures of the rare gases with the molecular gases.

Davis and Crowe³⁸ investigated methane as part of the alkane series. Many more recent works³⁹⁻⁴⁵ attempted to extract the electron molecule momentum transfer cross section from measurements of the drift velocity and of the

ratio of the diffusion coefficient to the mobility (D/μ). In spite of the scatter between and within data sets and of the high fields used, the general features were the same. The measured drift velocity curves possessed a maximum at $E/n \sim 3 \times 10^{-21} \text{ m}^2\text{V/molec}$ and decreased to a minimum at $4 \times 10^{-20} \text{ m}^2\text{V/molec}$. The cross sections calculated by Duncan and Walker⁴⁵ in the range $0.02 < \epsilon < 4 \text{ eV}$ showed a minimum at 0.25 eV with a value of $1 \times 10^{-20} \text{ m}^2$.

All the previous studies were performed in the dilute gas regime ($P < 500 \text{ torr}$). Measurements have been made in compressed methane as well. Lehning⁴⁶ performed drift velocity measurements at $6 \times 10^{-23} < E/n < 2 \times 10^{-21} \text{ m}^2\text{V/molec}$. He plotted the ratio of the drift velocity at the pressure of the measurement to the drift velocity at 500 torr and he showed that this ratio increased with E/n up to 3×10^{-22} , decreased between 3×10^{-22} and 3×10^{-21} and was roughly constant at higher fields. The amount of increase depended on the pressure. The greater the pressure, the larger the increase. Above 3×10^{-21} the ratio was independent of pressure. The mobility was measured in methane as a function of density at temperatures between 196K and 295K .⁴⁷ In all cases the electron mobility varied as n^{-1} at low densities, reached a minimum at about $3.6 \times 10^{27} \text{ molec/m}^3$ and then increased, passing through a maximum at about $10 \times 10^{27} \text{ molec/m}^3$. The mobility was higher for a higher temperature.

Gee and Freeman⁴⁸ conducted an extensive study on methane in both vapor and liquid phases along the coexistence curve. In the vapor they found that the density normalized mobility, $n\mu$, was independent of density at $\sim 2 \times 10^{25}$ molec/Vs m up to $\sim 7 \times 10^{26}$ molec/m³. They found that $n\mu$ decreased to reach a minimum at about 3×10^{27} molec/m³ and then increased sharply on approaching the critical region and in the liquid. At densities higher than 7×10^{26} molec/m³ ($n/n_c > 0.1$) they found that the mobility increased at constant density with increasing temperature and they calculated activation energies from plots of $\lg \mu$ vs $1/T$. The observed decrease in $n\mu$ with increasing density was attributed to quasilocalization of the electrons in clusters of molecules which were regarded as density fluctuations. An increase in temperature decreased the extent of quasilocalization and therefore raised the mobility.

ii) Methane-d₄.

Measurements of the drift velocity have been performed in gas phase CD₄.^{39,42} At field strengths up to $E/P = 0.5$ V/cm torr ($\sim 1.5 \times 10^{-21}$ m²V/molec) the CH₄ and CD₄ curves were the same. At higher fields the CD₄ curve was lower than that of CH₄. This was explained in terms of inelastic losses of the electron to vibrational channels. At low

fields the scattering process was elastic. The small differences in sizes between CH_4 and CD_4 did not produce a detectable difference in drift velocities. At high fields inelastic losses were invoked to explain the difference because the vibrational quanta in CD_4 are smaller than in CH_4 .

Cottrell and Walker⁴³ also estimated the fractional energy loss per collision (λ) and the momentum transfer cross section (Q_D). They found that λ was much smaller in CD_4 than in CH_4 but Q_D was found to be the same in the two compounds.

iii) Ethane and Propane.

Drift velocities in low density ethane and propane gases have been measured by Cottrell and co-workers^{39,49} and Christophorou and co-workers.^{50,51} Huber^{52,53} determined drift velocities in ethane and in propane from low pressures (0.06 MPa) to high pressure (4.5 MPa for ethane and 1 MPa for propane).

The drift velocity curve as a function of E/n for both compounds had the same shape. At 298K the propane curve fell below that of ethane, for all values of E/n up to $1.2 \times 10^{-20} \text{ m}^2\text{V/molec.}$ Gee and Freeman⁵² measured the electron mobility in gaseous and liquid ethane along the coexistence curve. A plot of the density normalized

mobility, $n\mu$, against the density n in the gas displayed a minimum at $n \approx 3 \times 10^{27}$ molec/m³ that, as in CH₄, was attributed to quasilocalization. The value of $n\mu$ increased to a maximum in the liquid and then it decreased sharply at $n/n_c > 1.5$.

iv) Other n -Alkanes.

Christophorou and his collaborators made extensive measurements over the past twenty five years of drift velocities in the dilute gases. The work prior to 1970 is collected in reference 53.

György and Freeman⁵⁴ studied n -pentane along the entire coexistence curve as well as along isochores. A plot of the mobility vs n along the coexistence curve showed that the mobility varied as n^{-1} for $n \leq 1 \times 10^{26}$ molec/m³. A plot of $n\mu$ vs n revealed this as a constant $n\mu$ up to 1×10^{26} molec/m³. At higher densities $n\mu$ decreased, reaching a minimum at about 1.7×10^{27} molec/m³.

Huang and Freeman⁵⁵ made similar measurements in n -hexane. Measurements were made along the coexistence curve and along isochores. A plot of $n\mu$ vs n showed that $n\mu$ was independent of n for $n \leq 4 \times 10^{25}$ molec/m³. At higher n the $n\mu$ curve decreased to a minimum at $n = 1.3 \times 10^{27}$ molec/m³ and then increased as the critical region was approached.

v) Branched Alkanes.

Christophorou and co-workers have measured the drift velocity in isobutane at room temperature⁵⁶ and in neopentane, both at room temperature⁵⁶ and as a function of temperature at 100 torr and as a function of pressure at 373K.⁵¹

Freeman and co-workers have measured electron mobilities in neopentane along the coexistence curve and at fixed densities as functions of temperature from the dilute gas up to the supercritical fluid.^{54,55}

Huang made measurements of electron mobilities in neopentane in a cell constructed so that the liquid level rose up to the center of the electrodes as the critical region was approached.⁵⁷ As a result, two distinct signals were observed, one corresponding to each phase. The critical point was reached when the two signals merged into a single signal. Huang found that the mobility at the critical point was higher than those at $0.5 \leq n < n_c$, which the experimental scatter in György's work could not confirm. The smooth transition of the mobility curve through the critical region showed that the large density fluctuations that characterize the critical fluid have correlation lengths that are too great to hinder electron motion. The prediction⁵⁸ that such scattering would occur was earlier shown to be untrue for electron mobilities in critical xenon.⁵⁹

More recently many of the data on hydrocarbons have been reanalyzed.⁶⁰ This work stressed the importance of the effect of the shape of the molecules on the electron mobility in hydrocarbons. It was known that the shape is the dominant molecular property in liquid hydrocarbons (see next section) but it appeared to be important in the low density gas as well. As will be discussed later on, the electron mobility in a liquid composed of spherelike molecules is orders of magnitude greater than that in liquids composed of rodlike molecules. The opposite is true in the dilute gas. It was pointed out that the density normalized mobility in low density neopentane gas is a factor of 3 lower than that in n-pentane. A low energy resonance involving a spherical shape was suggested. To further elucidate this effect, the electron mobility was measured in mixtures of neopentane and n-pentane.⁶¹ It was found that in a 50:50 mixture the stronger scatterer dominates in each phase. Neopentane dominates in the low density gas and n-pentane dominates in the liquid.

c. Liquid Phase Experiments

Electron mobilities have been measured in liquified rare gases since 1951.⁶² However, because of purification problems (electrons are readily scavenged by oxygen, for

example, even at concentrations of parts per million), the first observation of a signal that could definitely be attributed to electrons was not accomplished in liquid hydrocarbons until 1968.⁶³ An initial sharp peak was found on the current vs time trace obtained when neohexane or neopentane were exposed to a pulse of Xrays. Addition of oxygen or SF_6 eliminated the "overshoot" (as the initial spike was called) and decreased the free ion yield. Although not confirmed until the next year,⁶⁴ this overshoot was the first recorded observation of a true thermal electron signal in a liquid hydrocarbon. This finding led to a series of other studies and measurements were made in a wide number of systems.⁶⁵⁻⁷¹ These studies were limited in the temperature range over which measurements could be made because the cells used could only withstand gas pressures up to about 0.4 MPa. Despite this limitation a great amount of data were collected, especially after 1972.⁷²⁻⁸⁹ Higher pressures had been used in work with liquified rare gases^{90,91} and later, with hydrocarbons.⁹²⁻⁹⁶

Freeman and co-workers developed a glass cell which allowed measurements over a continuous density range from the normal liquid to the critical fluid and into the dilute gas.^{48,52,54,55,57,97-100} The electron mobilities first reported in molecular liquids immediately indicated the great diversity of values which was to be found in later

work. For liquid hydrocarbons at room temperature for example, mobility values have been found to range from $70 \times 10^{-4} \text{ m}^2/\text{Vs}$ for neopentane to as low as 1.3×10^{-6} for trans decalin.¹⁰¹ Large differences have been found even between geometrical isomers. For example, the values of $1.5 \times 10^{-4} \text{ m}^2/\text{Vs}$ and $3 \times 10^{-6} \text{ m}^2/\text{Vs}$ found in cis- and trans-butene-2 respectively.⁹⁹ Rather than being related to any particular bulk property of the liquids studied, the electron mobility has been found to reflect more or less the shape of the constituent molecules.^{61,63,72,98,103} As measurements were extended into the critical region, it was found that all the mobility curves increased as the temperature was raised above the boiling point of the compound. Mobility maxima were found in methane,^{48,93,94} ethane,^{52,95}, cis-butene,⁹⁹ cyclopentane, neopentane and neohexane,⁹⁸ cyclohexane⁵⁵ and 2,3-dimethylbutane, 3,3-dimethylpentane, 2,2,4-trimethylpentane and 2,2,4,4-tetramethylpentane.¹⁰⁰ The size of the maximum decreased drastically as the molecular shape was changed from the spherelike methane to rodlike ethane. It was also found that the existence and the density where the maximum occurs in methane were independent of temperature.⁴⁷ Cipollini⁴⁷ made measurements in dense methane gas and found that the existence and density of the maximum were also independent of phase since the density of the maximum agreed with that found in the liquid.^{48,93,94}

3) Ion Mobilities

a. Gas Phase

The first extensive work on ion mobilities in gas phase is due to Tyndall.²¹ He reviewed the work done to date (1938) and concluded that the ions were in two states. They could be moving through the gas unattached to other molecules, or they could be in clusters of varying sizes. The measured mobility depended upon the ratio of unattached to attached ions. He applied Langevin's mobility equation (see section C) to calculate the cluster sizes. In the subsequent years all work in ion transport involved studies of inorganic systems. Ion work up to 1973 is summarized in reference 104.

Wada and Freeman¹⁰⁵ observed droplet nucleation in isobutene by observing that under certain conditions the ion mobility plunged by one or two orders of magnitude. The decrease in mobility was attributed to droplet formation around the positive ion. They found that the critical temperature for droplet formation was lower than the normal liquid/vapor critical temperature.

Huang and Freeman¹⁰⁶ measured cation mobilities in gaseous, critical and liquid cyclopentane, cyclohexane and n-hexane. Gee and Freeman¹⁰⁷ measured cation mobilities in

C₁-C₄ hydrocarbon gases at densities up to the critical. They found that the temperature coefficient of cation mobility, $d\mu/dT$, at constant gas density μ , was positive and increased with increasing density n . This was attributed to the clustering of molecules about the ion. In a subsequent work¹⁰⁸ the same authors compared the transition from low to high density behavior for ions and neutral molecules in Ar, Xe, N₂ and CH₄.

b. Liquid Phase

One of the first extensive investigations of ion mobilities in liquid hydrocarbons was performed by Adamczewski.^{109,110} He measured ion mobilities in the series n-pentane to n-decane to investigate the effect of the carbon chain length. Other molecular properties such as boiling point, density and viscosity are correlated to the carbon number. Adamczewski found that the product of the viscosity, η , and the mobility in the alkane series varied as $\eta^{-3/2}$. By Stokes' law this product should have been constant if the ions were of the same size. Huang and Freeman¹¹¹ found that $\eta\mu$ was constant in benzene but not in toluene. They also found¹⁰⁶ that the viscosity normalized cation mobilities in liquid cyclopentane, cyclohexane and n-hexane were not constant. They suggested that ion migration in liquids made up of non spherelike molecules is

more closely linked to solvent molecular rotation than to shear viscosity. Gee and Freeman¹¹² measured cation mobilities in liquid C₁-C₄ hydrocarbons. They found a maximum in a plot of $\eta\mu$ against η^{-1} and concluded that Stokes' law is only a rough approximation when the molecular radius is assumed to be independent of density.

C. Theory and Models

1. Gas Phase.

a. Electron Mobilities

J.L. Pack and A.V. Phelps used simple models to extract electron-molecule scattering cross-sections from transport data.¹¹³ One method used obtained cross-sections by the variation of the low field mobility as a function of temperature. A more recent method used the variation of mobility and the variation of the ratio of the diffusion coefficient to the mobility, D/μ , as a function of electric field strength. Both led to solutions of Maxwell equation of transport, given in reference 114. The mobility of electrons in the low density gas was expressed as:

$$\mu = \frac{4\pi e}{3mn} \int_0^{\infty} \frac{v^2}{\sigma_v} \frac{df_0}{dv} dv \quad \text{I-9}$$

where e and m are the charge and mass of the electron, respectively, n is the number of molecules/ m^3 , σ_v is the scattering cross section of the molecules for electrons of velocity v ,¹¹⁵ and f_0 is the spherically symmetric term in the series expansion of the electron velocity distribution function. At low fields the distribution is Maxwellian:

$$f_0 = \left(\frac{m}{2\pi kT}\right)^{3/2} \exp\left(-\frac{mv^2}{2kT}\right) \quad \text{I-10}$$

where k is Boltzmann's constant.

The temperature variation of the mobility could be used to obtain σ_v vs v curves. This method and an equivalent formulation by Viehland and Mason for ions^{116,117} have been widely used.^{40,48,51,52,54,55,57,97,106,118}

b. Ion Mobilities

Langevin¹¹⁹ assumed the molecules to be elastic, polarizable spheres in the field of the ions. The mutual attraction force, f , is:

$$f = \frac{2\bar{m}e}{3r} \quad \text{I-11}$$

where \bar{m} is an average effective moment induced on the molecule by the ion, e is the electronic charge and r the distance between the ion and the molecule. The effective moment is given by

$$\bar{m} = \frac{\gamma e}{r^2} \quad \text{I-12}$$

where γ is the total effective molecular polarizability and is given by:

$$\gamma = \frac{\epsilon - 1}{4\pi n} \quad \text{I-13}$$

where n is the density of molecules and ϵ is the dielectric constant. The force of attraction is therefore

$$f = \frac{(\epsilon - 1)e^2}{2\pi n r^5} \quad \text{I-14}$$

Assuming that the random velocities of the ions followed a Maxwellian distribution, Langevin obtained

$$\mu = A \left[\frac{1 + m/M}{n(\epsilon - 1)} \right]^{1/2} \quad \text{I-15}$$

where μ is the mobility, m the mass of the molecule, M the mass of the ion and A a function of a quantity λ which is a measure of the relative importance of the size of the particles and the polarization forces in determining the path of the ion and is given by

$$\lambda = \frac{\sigma^2}{e} \left(\frac{8\pi P}{\epsilon - 1} \right)^{1/2} \quad \text{I-16}$$

where σ is the sum of the radii of the molecule and ion, and P is the pressure. The final result is

$$\mu = \frac{(\lambda A)e}{\sigma^2} \left(\frac{1+m/M}{8\pi P n} \right)^{1/2} \quad \text{I-17}$$

This formula was used by Tyndall in his study of ion sizes.²¹

As mentioned earlier, Viehland and Mason^{116,117} developed a model similar to that proposed for electrons to calculate ion mobilities. Their equation is

$$\mu = \frac{3e}{8M_r} \frac{\sqrt{\pi}}{n} \left(\frac{2kT}{M_r} \right)^{5/2} / \int_0^{\infty} v^5 \sigma_v \exp(-M_r v^2 / 2kT) dv \quad \text{I-18}$$

where M_r is the reduced mass of the ion-molecule pair. This equation has been used to calculate ion mobilities in a variety of systems.¹⁰⁶⁻¹⁰⁸

2. Liquid Phase

In general the properties of electrons in the pseudo-spherical molecular liquids resemble very closely those of electrons in the liquid and solid rare gases and in the crystalline semiconductors silicon and germanium.¹²⁰⁻¹²⁴ In these materials electrons are considered to be in a completely extended, quasi-free state. On the other hand, in liquids composed of rodlike molecules electrons are

thought to be localized in regions of lower potential energy in the medium due to preferential orientation of the molecules. In general, in a liquid exhibiting a mobility $\geq 10^{-2} \text{ m}^2/\text{Vs}$ electrons are thought to be quasi free. In this section the two states will be distinguished according to this criterion.

a. Quasifree Electrons

Cohen and Lekner^{125,126} developed a model to calculate drift velocities in liquid argon. At low fields electrons were assumed to have a Maxwellian distribution of velocities and that they could be treated as "scattered plane waves whose total scattering amplitude at a point in the system is the coherent sum of amplitudes scattered singly from individual scattering centers".¹²⁸ The necessary condition for the validity of the single scatterer approximation and the sufficient condition for the validity of the Boltzmann equation was that the mean free path λ between scattering events be large compared with the De Broglie wavelength of the electron. The solution of the Boltzmann equation led, for low fields, to the expression

$$\mu = \left(\frac{2e}{3}\right) \left(\frac{2}{\pi m k T}\right)^{1/2} \lambda \quad \text{I-19}$$

Cohen and Lekner regarded the atoms or molecules of the liquids as scattering centers. This resulted in the following equation for λ in monoatomic liquids:

$$\lambda = [4\pi a^2 n S(0)]^{-1} \quad \text{I-20}$$

Here a is the scattering length and $S(0)$ the long wavelength (low momentum) limit of the structure factor of the liquid;

$$S(0) = nkT\chi_T \quad \text{I-21}$$

with χ_T being the isothermal compressibility. The mobility was then given by:

$$\mu = \frac{2}{3} \left(\frac{2}{\pi m k T} \right) \frac{e}{4\pi a^2 n S(0)} \quad \text{I-22}$$

This equation is equivalent to the expression Bardeen and Shockley developed to calculate electron mobilities in non polar crystals.¹²⁹⁻¹³¹ Calculated values agreed well with the data of reference 127.

Schnyders and co-workers⁹⁰ had extended the measurements in liquid argon and krypton to densities considerably lower than the normal liquid. They found that the mobility decreased with decreasing density, went through a minimum and then increased. Lekner observed that

the value of the scattering length was negative in gaseous argon, as found by Ramsauer and Kollath¹⁵ and positive in the liquid as calculated by him.¹²⁵ He proposed that the scattering length goes through zero at an intermediate density and at that density the mobility goes through a maximum.¹³² This maximum was found in liquid argon near the critical region.⁹¹ Equation I-22 would predict an infinite mobility for $a = 0$ but density fluctuations keep it a finite value.¹³² The Cohen-Lekner model has been used for a long time to calculate the mobility of quasi-free electrons in hydrocarbons.¹³³⁻¹³⁵

Recently the energy level of the electron, V_O , was determined by photoemission experiments in neopentane.¹³⁶ It was found that at approximately the density of maximum mobility the energy of the electron in the liquid with respect to vacuum passed through a minimum. It was suggested that, in that density region, the mobility was being controlled by fluctuations in the ground state energy level of the electron resulting from fluctuations in the density of the medium. The impedance to electron motion due to such fluctuations would then pass through a minimum for $dV_O/dn = 0$. The same conclusions have been drawn from measurements of dV_O/dn in xenon, krypton, methane and propane.¹³⁷ Equations explicitly containing the energy level fluctuation parameter have been derived.^{138,139}

b. Localized Electrons

In most liquid hydrocarbons electron mobilities were found to be orders of magnitude larger than those of the ions. However they were orders of magnitude smaller than those found in the liquified rare gases, except in methane. Although this is not of direct interest to the present work, brief mention will be made of those models developed to describe the behavior of electrons in these liquids.

After a series of experiments conducted by Minday, Schmidt and Davis,⁶⁹⁻⁷¹ it became apparent that the electron had to exist in two states, one corresponding to the quasi free electron and one to a slower mobility state. The identity of the slow mobility state was not clear until they measured the temperature dependence of the electron mobility in a mixture of neopentane and n-hexane. They found that the temperature coefficient depended on the mole fraction of n-hexane and concluded that the electron was trapped by a multimolecular process rather than being localized as on a single molecule as a negative ion. Later this was further shown to be true by the detection of an optical absorption signal from electrons solvated in liquid hydrocarbons.¹⁴⁰⁻¹⁴⁵

Several models have been developed. Schiller developed a two state model in which the localized state of

the electron was a bubble.^{138,146,147} Freeman developed a model from observations of electron mobility and optical absorption energies in ethers^{79,148} and he applied it to liquid hydrocarbons.^{54,55,81,98-100} Freeman made no assumptions on the nature of the localized state and derived an equation relating the mobility to the temperature by an activation energy.

c. Ions

The liquid phase ion mobility is correlated to the viscosity η .^{73,78,59,98,109-112} According to Stokes' law the product $\eta\mu_+$ is a constant if the effective radius of a sphere moving through a fluid is a constant.¹⁴⁹ In general this is valid in the normal liquid but it fails as the density decreases.¹⁰⁹⁻¹¹²

The first attempt to connect the ideal gas and ideal liquid limits of ion transport involved a modification of Stokes' law to:¹⁵⁰

$$\eta\mu_+ = \left(\frac{e}{6\pi r}\right)[1 + b\lambda(r)] \quad \text{I-23}$$

where the 6π refers to stick conditions, b is a constant, and λ is the mean free path between collisions. In normal liquids, $\lambda \ll r$, so Stokes' law is recovered. As the density decreases λ will increase and eventually will

become similar in magnitude to r . At a given density $\eta\mu$ should increase. In fact this is not true. It was shown¹⁰⁸ that in some simple liquids $\eta\mu_+$ at first decreases with decreasing η and density and only gives the expected increase in the gas at $\eta/\eta_c < 0.7$.

D. Present Study

The purpose of this work was to further investigate the effect of molecular structure on the electron and ion mobilities in nonpolar fluids. The electron mobilities in liquid methane, a spherelike molecule, and ethane, a rodlike compound, each at their normal boiling points, are different by three orders of magnitude. This enormous difference is mainly attributable to the different molecular shapes. There was an enormous gap to be explored between methane and ethane. This was done by only slightly perturbing the symmetry of the methane molecule by progressive deuterium substitution.

The electron and ion mobilities were measured in the fluids CH_4 , CH_3D , CH_2D_2 , CHD_3 and CD_4 . Measurements were performed at a fixed density and temperature as functions of the applied field strength over a wide density range, from the low density gas, through the critical region, to the dense liquid. Measurements were also performed at a fixed density as functions of temperature.

E. Condensed Phase Isotope Effects

1. Theory

The most thoroughly studied of all condensed phase isotope effects is the Vapor Pressure Isotope Effect (VPIE). The first quantitative treatment of this effect was given independently by Stern¹⁵¹ and Lindemann.^{152,153} They considered the equilibrium between a Debye solid and an ideal gas composed of monoatomic molecules and introduced the following assumptions: a) harmonic oscillations in the solid lattice; b) isotope independent potential energy; c) existence of a vibrational zero point energy. Under these assumptions they obtained the following expression:

$$\ln \frac{P'}{P} = \left(\frac{3}{40}\right) \left(\frac{\theta}{T}\right)^2 \delta + \dots \quad \text{I-24}$$

where P' and P are the vapor pressures of a light and heavy isotope respectively, θ is the Debye temperature, $h\nu/k$, of the heavy isotope and $\delta = [(M/M')-1]$.

According to equation I-24 the difference in vapor pressure of isotopes is a purely quantum mechanical phenomenon. The vapor pressure ratio approaches the classical limit at high temperature, as T^{-2} .

Roth and Bigeleisen^{154,155} confirmed the T^{-2} law through their investigation of the vapor pressures of the neon isotopes and showed that the systematic investigation of the VPIE in simple substances could give new information about the lattice energy, the anharmonic vibrations in crystals, the melting process and the mean square force between molecules in the liquid state which is related to the intermolecular potential and the radial distribution function. Investigations of the vapor pressures of argon¹⁵⁶ and krypton¹⁵⁷ isotopes have proved this point.^{158,159}

A more general form of equation I-24 was obtained by Herzfeld and Teller.¹⁶⁰ They developed the partition function of the liquid in terms of the classical partition function by the use of the Wigner quantum correction to the Boltzmann distribution:¹⁶¹

$$Z = Z_{cl} \left\{ 1 - \frac{\hbar^2}{24(kT)^2} \left\langle \sum_i \frac{1}{m_i} \frac{\partial^2 V}{\partial x_i^2} \right\rangle_{Av} \right\} \quad \text{I-25}$$

where Z is the partition function, Z_{cl} is the classical partition function and the expression in parentheses represents the mean value of the interaction potential in the condensed phase. The average is taken over the classical probability distribution in configuration space. This formula, applied to the harmonic oscillator, yields:¹⁶⁰

$$Z = Z_{cl} \left\{ 1 - \frac{1}{24} \left(\frac{\bar{r}_w}{kT} \right)^2 \right\} \quad \text{I-26}$$

The correction always diminishes the partition function and its absolute value increases with the mean square value of the forces and diminishing mass of the particle. Thus the correction will be greater for the liquid phase than for the gas phase because of the stronger forces and the difference between gas and liquid is greater for the lighter isotopes. Equation I-25 therefore predicts that the lighter isotope will always have the higher vapor pressure. This qualitative prediction has failed in several systems which show a cross over phenomenon and among them is the system of the deuterated methanes. At low temperature, in this system, the vapor pressure of a lighter isotope is higher than that of a heavier one; at higher temperatures the vapor pressure curves cross giving a higher vapor pressure to the heavier compound (Table I-1 and ref. 162).

The problem was reinvestigated by Bigeleisen¹⁶³ who gave a demonstration of the important connection between the VPIE and studies of molecular structure in terms of reduced partition function ratios.¹⁶⁴ This method will be described in some detail because it represents the basis for most of the modern VPIE studies.

Consider the equilibrium between the condensed and vapor phases. In the gas the freely rotating and translating molecule may be considered as a set of $3n-6$, $n \geq 3$, coupled oscillators (n is the number of atoms, if the molecules are linear there are $3n-5$, $n \geq 2$, oscillators, if they are monoatomic there are no oscillators and rotation is not defined). Upon condensation intermolecular forces in the condensed phase will perturb the energy levels of the oscillators. A given energy level may be either raised or lowered with respect to its gas phase value depending on the specific nature of the intermolecular potential; in methane, because of the dispersion interaction, stretching motions are shifted to a lower frequency.^{165,166,167} In addition, the six (five for linear, three for monoatomic molecules) external motions of the molecule become hindered as the molecules condense. These modes are necessarily shifted to higher frequencies than the gas phase values. For both internal and external modes the reduced masses are such that the light molecule undergoes the larger shift. Since the intramolecular motions can shift either to higher or lower frequencies the net isotopic effect can be either positive or negative leading therefore to positive (normal) or negative (inverse) VPIE.

These ideas have been quantified by Bigeleisen^{162,163} who derived an expression for the VPIE. Following his treatment,¹⁶² the Gibbs free energy in the condensed phase, G_c , is given by:

$$G_C = -kT \ln Q + PV \quad \text{I-27}$$

where Q is the partition function for a system of N molecules. An average partition function \bar{Q} can be defined as:

$$\bar{Q} = Q^{1/N} \quad \text{I-28}$$

and therefore G_C can be written as

$$G_C = -RT \ln \bar{Q} + PV \quad \text{I-29}$$

The equation of state for the gas can be expressed in terms of a virial expansion:

$$PV = RT(1 + B_O P + C_O P^2 + \dots \quad \text{I-30}$$

and therefore the Gibbs free energy for the vapor, G_V , has the form

$$\frac{G_V}{RT} = \ln P + \frac{3}{2} \ln M + \frac{5}{2} \ln T - \ln Q_{\text{int}} + (B_O P + \frac{1}{2} C_O P^2) + K_{ST} \quad \text{I-31}$$

where M is the molecular weight, Q_{int} represents the product of rotational and vibrational partition functions

and K_{ST} is the Sackur-Tetrode constant. At equilibrium $G_c = G_v$ and therefore

$$\ln P = \ln \frac{Q_{int} M^{3/2}}{\bar{Q}} + \frac{PV}{RT} + \frac{5}{2} \ln T - (K_{ST} + B_O P + \frac{1}{2} C_O P^2) \quad \text{I-32}$$

For a pair of isotopic molecules the vapor pressure (P and P') ratio at the temperature T is

$$\begin{aligned} \ln \frac{P'}{P} = \ln \frac{Q'_{int} M'^{3/2} \bar{Q}}{Q_{int} M^{3/2} \bar{Q}'} + (RT)^{-1} (P'V' - PV) \\ - (B_O P + \frac{1}{2} C_O P^2)' + (B_O P + \frac{1}{2} C_O P^2) \end{aligned} \quad \text{I-33}$$

The prime refers to the lighter isotope and V and V' are the condensed phase molar volumes. At this point the author introduces the reduced partition function ratio defined as:¹⁶³

$$\frac{s}{s'} f = \frac{s}{s'} \frac{Q}{Q'} \prod_{i=1}^n \left(\frac{m'_i}{m_i} \right)^{3/2} = \left(\frac{Q}{Q'} \right)_{qm} / \left(\frac{Q}{Q'} \right)_{cl} \quad \text{I-34}$$

(the product runs over the n atoms in the molecule, m_i is the mass of the i th atom, qm and cl denote the quantum mechanical and classical partition functions). Comparing the two isotopic systems at the same molal volume equation I-33 becomes

$$\ln \frac{P'}{P} = \left(\ln \frac{s}{s'} f_c - \ln \frac{s}{s'} f_g \right) + (RT)^{-1} (P'V' - PV) + \\ - (B_O P + \frac{1}{2} C_O P^2)' + (B_O P + \frac{1}{2} C_O P^2) + (RT)^{-1} \int_V^{V'} P' dV \quad \text{I-34}$$

For most calculations equation I-34 can be simplified if $\ln P'/P$ is small, i.e., $\ln P'/P \approx (P' - P)/P$. In this case $B_O' \approx B_O$, $V' = V$ and, neglecting $(RT)^{-1} \int_V^{V'} P' dV$ and terms of order $C_O P^2$, equation I-34 becomes

$$\ln \frac{f_c}{f_g} = \ln \frac{P'}{P} \left[1 + P \left(B_O - \frac{V}{RT} \right) \right] \quad \text{I-35}$$

By using a treatment developed by Stern, Van Hook and Wolfsberg^{168,169} the VPIE could be calculated. Input data such as force fields obtained from spectroscopic data are needed and the calculation is performed in the harmonic approximation. In the gas phase the partition functions for translation and rotation are evaluated in the classical approximation and no vibrational rotational interaction is assumed.

$$\frac{s}{s'} f_g = \frac{Q_{\text{vibr qm}}}{Q'_{\text{vibr qm}}} / \frac{Q_{\text{vibr cl}}}{Q'_{\text{vibr cl}}} = \\ = \frac{\pi^{3n-6}}{\prod_{i=1}^n} \frac{u_i}{u'_i} \frac{\exp(-u_i^2/2)/(1-\exp(-u_i^2))}{\exp(-u_i'^2/2)/(1-\exp(-u_i'^2))} \quad \text{I-36}$$

where $Q_{\text{vibr qm}}$ is the quantum mechanical vibrational partition function

$$Q_{\text{vibr qm}} = \frac{1}{\pi} \prod_{i=1}^{3n-6} \frac{\exp(-u_i/2)}{1 - \exp(-u_i)} \quad \text{I-37}$$

$Q_{\text{vibr cl}}$ is the classical vibrational partition function

$$Q_{\text{vibr cl}} = \frac{1}{\pi} \prod_{i=1}^{3n-6} \frac{1}{u_i} \quad \text{I-38}$$

and $u_i = hc\nu_i/kT$; ν_i is the i th normal mode harmonic frequency.

In order to evaluate f_c the authors chose a simplified cell model which assumed an average condensed phase molecule with $3n$ degrees of freedom. The $3n-6$ vibrational modes were treated in a fashion similar to that used in the gas phase and the remaining six external degrees of freedom corresponding to gas phase translations and rotations were assumed to be harmonic. Then equations I-39 and I-40 apply

$$\frac{s}{s'} f_c = \prod_{i=1}^{3n-6} \left[\frac{u_i}{u'_i} \frac{\exp(-u_i/2)(1 - \exp(-u_i))}{\exp(-u'_i/2)(1 - \exp(-u'_i))} \right] \quad \text{I-39}$$

$$\frac{f_c}{f_g} = \frac{3n-6}{\pi} \frac{\text{internal frequencies}}{\text{frequencies}} \left[\frac{(u_i/u'_i)_c \exp((u'_i - u_i)_c/2)}{(u_i/u'_i)_g \exp((u'_i - u_i)_g/2)} \right] \times$$

$$\times \left[\frac{(1 - \exp(-u'_i)_c) / (1 - \exp(-u_i)_c)}{(1 - \exp(-u'_i)_g) / (1 - \exp(-u_i)_g)} \right] \times$$

$$\times \frac{6}{\pi} \frac{u_i}{\text{ext } u'_i} \times \left[\exp\left(\frac{u'_i - u_i}{2}\right) \right] \left[\frac{1 - \exp(-u'_i)}{1 - \exp(-u_i)} \right] \quad \text{I-40}$$

therefore, in order to calculate VPIE, one needs a complete set of all frequencies in both gas and liquid phase. When there is not enough input information to define the complete problem, it is advantageous to have available an approximate relation. The most common approximation applied to VPIE makes use of the fact that very often the $3n$ molecular frequencies happen to fall neatly into two groups; the first group contains the high frequencies $u_i = h\nu_i/kT \gg 1$, the second contains the low frequencies. The first group may be treated in the low temperature (zero point energy) approximation because the excitation factors of these frequencies all approach one, the second is treated in the high temperature approximation. Another assumption is often made that the low-frequency group contains the external gas phase

frequencies (assigned zero value) together with corresponding condensed phase values, while the high frequency group contains only internal modes.

With these assumptions equation I-40 becomes

$$\ln \frac{f_c}{f_g} = \frac{1}{24} \left(\frac{\hbar c}{kT} \right)^2 \left[\sum^{\text{ext}} (v_i'^2 - v_i^2) \right] +$$

$$- \frac{1}{2} \frac{\hbar c}{kT} \left[\left(\sum^{\text{int}} v_{ig}' - \sum^{\text{int}} v_{ic}' \right) - \left(\sum^{\text{int}} v_{ig} - \sum^{\text{int}} v_{ic} \right) \right]$$

I-41

thus

$$\ln \frac{P'}{P} \approx \ln \frac{f_c}{f_g} = \frac{A}{T^2} - \frac{B}{T}$$

I-42

with

$$A = \frac{1}{24} \left(\frac{\hbar c}{k} \right)^2 \left[\sum^{\text{ext}} (v_i'^2 - v_i^2) \right]$$

I-43

$$B = \frac{1}{2} \frac{\hbar c}{k} \left[\left(\sum^{\text{int}} v_{ig}' - \sum^{\text{int}} v_{ic}' \right) - \left(\sum^{\text{int}} v_{ig} - \sum^{\text{int}} v_{ic} \right) \right]$$

I-44

The A term is always positive and predicts a normal VPIE. The B term is the contribution due to the change in zero-point energies of the large internal frequencies on condensation. An increase in force constants of the internal degrees of freedom on condensation will lead in the direction of a normal isotope effect, while a decrease will tend to an inverse isotope effect. The A and B terms

display different temperature dependencies. At low enough temperatures the A/T^2 term must predominate and the isotope effect will be normal and fall off proportional to T^{-2} . At intermediate temperatures the B term, which may be positive, negative or zero can dominate and accounts for a cross over to an inverse isotope effect.

2. Applications. The Isotopic Methanes.

Bigeleisen, Craag and Jeevanandam¹⁷⁰ used a single isotope independent force field to rationalize their own and other¹⁶² vapor pressure data. In this calculation the point of primary interest was the rotational contribution. They fitted experimental vapor pressure data to equation I-42 and their results are summarized in Table I-1. The contributions of the internal modes is found primarily in the B term. The lattice contribution (A term) is from both translational and rotational motions. Data from a single isotopic pair, such as $\text{CH}_4/\text{CH}_3\text{D}$, only fixes the total lattice contribution, which in turn could be consistent with a large number of ratios of rotational to translational contributions. The effects may be sorted out by considering the behavior of molecules of the same total mass but different moments of inertia. In Table I-2 are summarized results for isotopic molecules having the same mass; according to the authors a comparison between the experimental A's and the same factors calculated assuming

Table I-1*
Coefficients for equation I-42

Species ^a	A ^b	B ^b	T _{CO} , K ^c
¹³ CH ₄	94±6	0.95±0.06	
¹⁴ CH ₄	231±10	1.4±0.1	
CH ₃ D	292±4	2.99±0.03	97.6
CH ₃ T	503±7	4.83±0.07	103.9
CH ₂ D ₂	536±5	5.85±0.05	91.5
CHD ₃	749±6	8.69±0.06	79.3
CD ₄	895±7	11.10±0.06	73.6

* From reference 170.

a. All isotopic species referred to ¹²CH₄.

b. Liquid phase.

c. Cross over temperatures; temperature at which the sign of the isotope effect changes.

Table I-2*

Relative A values for the isotopic methanes of
equal total mass.

Species	Calculated for free rotor ^a	Experimental
$\text{CH}_3\text{D}/^{13}\text{CH}_4$	0.83	3.12
$\text{CH}_2\text{D}_2/^{14}\text{CH}_4$	0.90	2.32
$\text{CH}_3\text{T}/^{14}\text{CH}_4$	0.74	2.17

* From reference 170.

a. Refer to Table II-1 for moments of inertia.

free rotation from the moments of inertia (see Table II-1), unequivocally shows that rotation must contribute in the liquid and therefore must be hindered. This point has not found definite experimental proof yet because the experiments have been rather contradictory^{166,171,172,186} or inconclusive.¹⁷³⁻¹⁷⁶ It has been claimed that the Raman spectrum¹⁶⁶ proves free rotation whereas the infrared spectra^{171,176} demonstrate hindered rotation. Other works dealing with scattering of long wavelength neutrons¹⁷³⁻¹⁷⁶ have not solved the problem but the most recent ones tend to indicate a hindrance in rotation in both liquid and solid (plastic) phases. A theoretical calculation of the spectral line shapes in the liquid phase¹⁸⁷ shows that rotation is hindered and this result has been confirmed by a more recent Molecular Dynamics calculation.¹⁸⁸

It is probably instructive, at this point, to compare the methane system with another which has been proven to be highly hindered in rotation in the liquid phase. The isotopic ethylenes belong to the same general class as methane: non polar, non associated liquids. The VPIE measurements in ethylene have been analyzed in detail.^{189,190} The experimental data were found to follow the approximate form of eq. I-42 and vapor pressure differences between cis-, trans- and gem-C₂H₂D₂ in particular were shown to be principally due to hindered rotation in the liquid (these molecules have the same mass but the moments of inertia are different). In addition,

superimposed on this effect, there is a zero point energy effect due to coupling of the hindered rotation with certain internal vibrations. In a more refined analysis¹⁹⁰ anharmonic effects were also taken into consideration. The data were corrected for molar volume, nonclassical rotation and gas imperfection and values of the reduced partition functions which were directly comparable with the theory were derived. The set of derived equations are in good agreement with the experimental data and such agreement extends to details of rather subtle rotational effects showing consistency with spectroscopic studies within the experimental precision of the latter.

Another example is given by the NNO isotopic isomers. The results are old ones by Bigeleisen and Ribnikar.¹⁹¹ The vapor pressure difference between the isomers $^{15}\text{N}^{14}\text{N}^{16}\text{O}$ ($M = 45$) and $^{14}\text{N}^{15}\text{N}^{16}\text{O}$ ($M = 45$) is as large as that between $^{14}\text{N}^{15}\text{N}^{16}\text{O}$ ($M = 45$) and $^{14}\text{N}^{14}\text{N}^{16}\text{O}$ ($M = 44$). In the first pair the mass ratio is unity, but there is an isotope effect on the moments of inertia; in the second there is an isotope effect on mass but the moments of inertia are equal within 7 parts in 10^5 . It was concluded that a sizable barrier to rotation exists in this condensed phase. This prediction was confirmed by infrared measurements 11 years later.

From this information it can be concluded that there probably is a rotational barrier in liquid methane.

CHAPTER II

EXPERIMENTAL

A. Materials

Methane (99.99%) was supplied by Matheson of Canada Limited. Methane- d_1 (99%) was obtained from Stohler Isotope Chemicals, Inc. Methane d_1 , d_2 , d_3 and d_4 , all with a minimum chemical purity of 99%, were supplied by Merck, Sharp and Dohme of Canada Limited. All of these gases were further purified with either Molecular Sieves or successive treatments with silica gel and sodium potassium alloy and, in both cases, a final treatment with potassium mirrors. The procedure is more extensively described below.

Davison 3A Molecular Sieves M564 were supplied by Fisher Scientific Company; potassium metal was obtained from American Chemicals Limited and from Matheson, Coleman and Bell; sodium metal from Fisher Scientific Company. Silica gel S157 28-200 mesh was supplied by Fisher Scientific Company, passed through a 80 mesh sieve and caught on a 120 mesh sieve to obtain a ~ 100 mesh fraction.

B. Apparatus and Procedure

1. The Vacuum System

A typical layout of the main manifold is shown in Figure II-1. A vacuum of $\leq 10^{-4}$ Pa was achieved using a Welch duo-seal vacuum pump in series with a mercury diffusion pump and cold traps at liquid nitrogen temperature. The pressure was measured with a Controller series 260 coupled with an ionization gauge supplied by Granville-Phillips.

All the stopcocks on the upstream side of the mercury pump were grease free metal-teflon valves supplied by Hoke Inc. (model 4251N6Y) or by Nupro Company (model 5S-513WTSW).

Two auxiliary manifolds were attached to the main vacuum line. Traps containing the Molecular Sieves, the sodium potassium alloy and silica gel, 2l bulbs whose internal surface had been covered with potassium mirror and traps used in degassing the samples were attached to the auxiliary lines. The measuring pipette, two mercury manometers and the conductivity cells were also attached to the auxiliary lines.

A typical configuration showing the portion of line used to fill the cells is shown in Figure II-2.

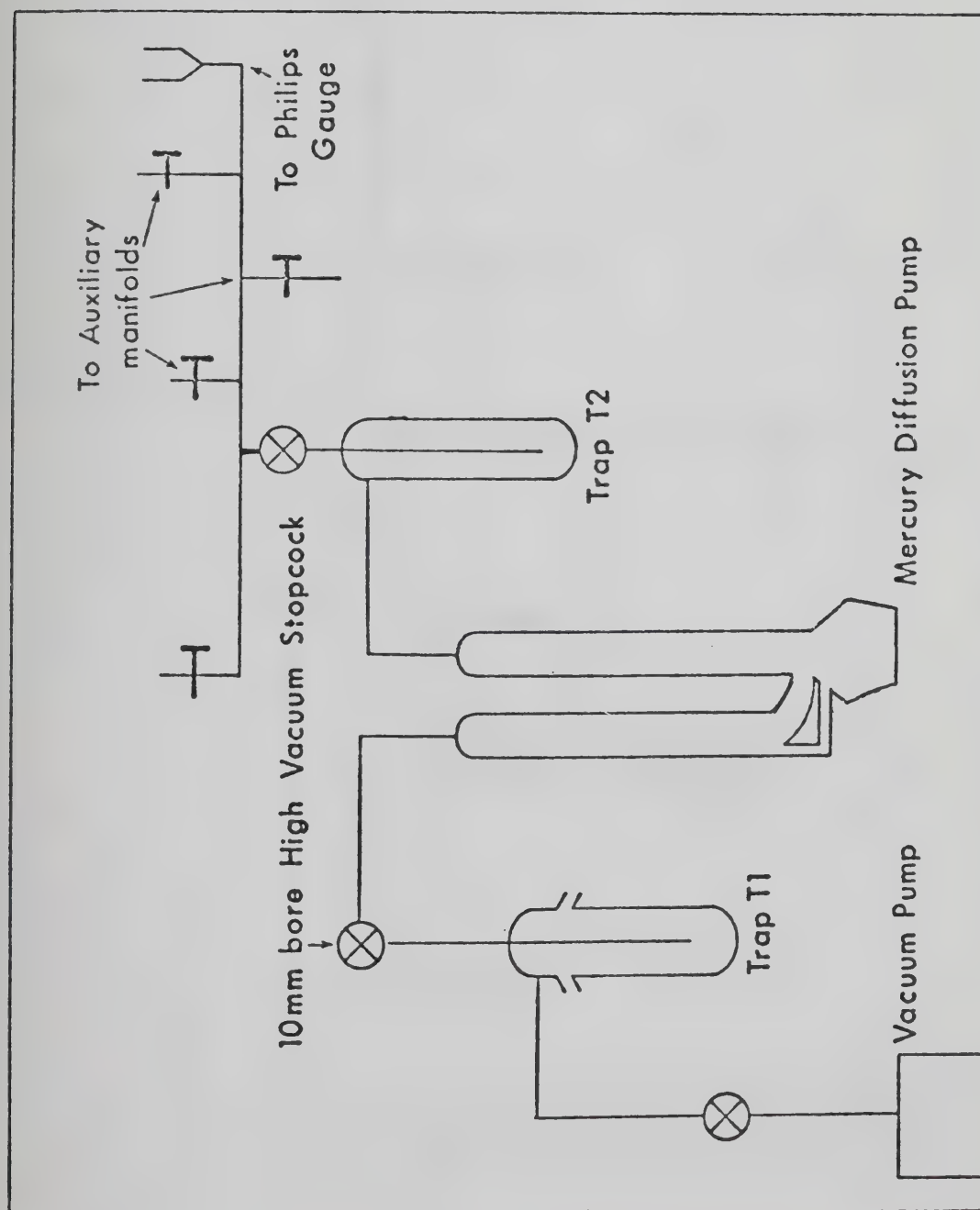


Figure II-1 Main Vacuum Manifold

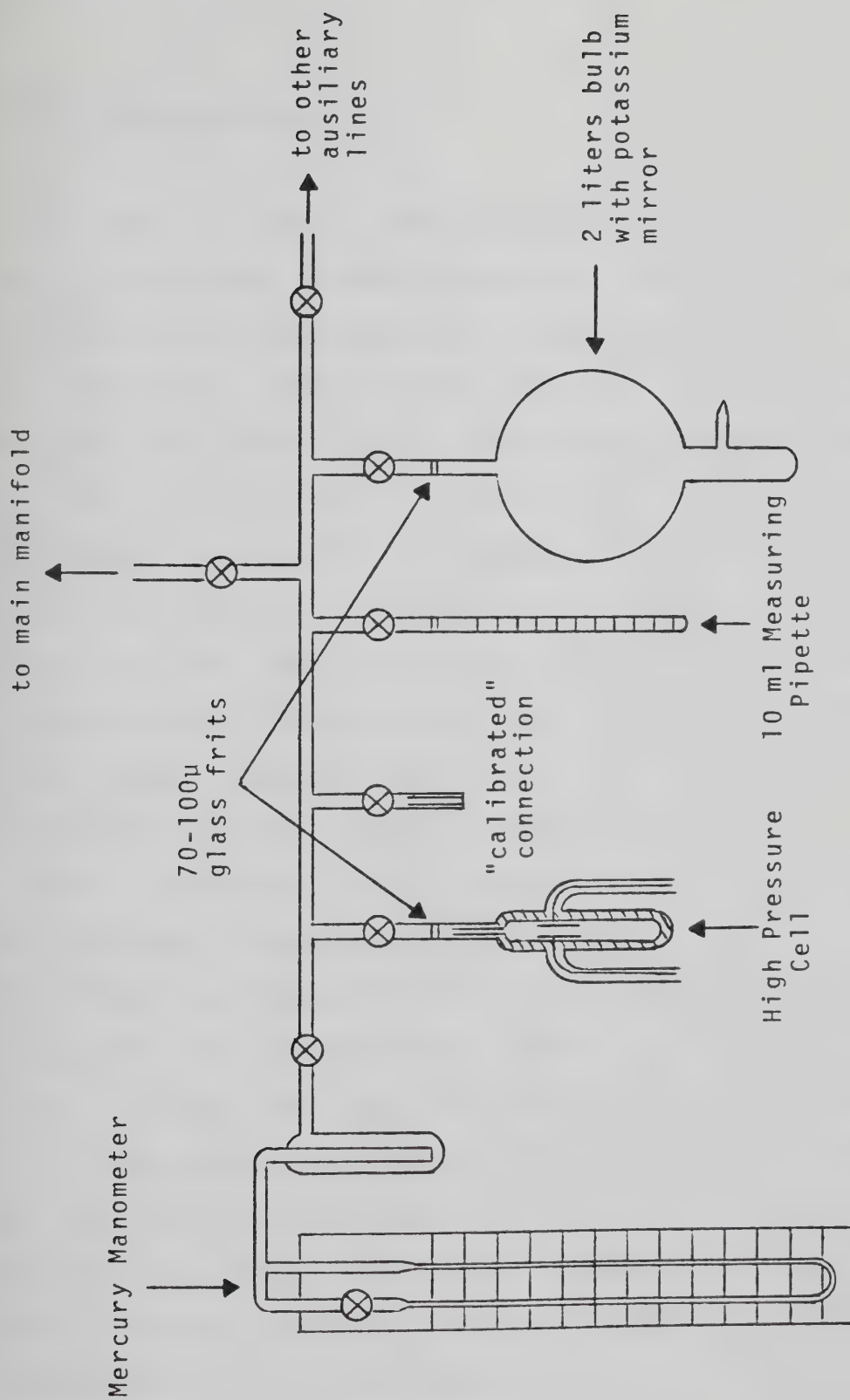


Figure II-2 Portion of the line used to fill the cell. The "calibrated" connection consisted of a valve whose internal volume was known and a 3 mm ID capillary.

2. Sample Purification

The gas cylinders were connected directly to the vacuum line through flexible stainless steel tubing welded to a Kovar seal. Two procedures were followed: 1. CH_4 , CH_3D and CH_2D_2 ; after the line had been thoroughly evacuated, the gases were flowed through Molecular Sieves which had been activated at 530K under vacuum, flushed twice before use and held at isopentane slush temperature ($\sim 110\text{K}$); the gases were introduced keeping a constant pressure of ~ 100 torr measured with a mercury manometer (consisting of a 3 mm capillary tube imbedded in a pool of mercury whose surface was exposed to atmosphere) and collected in a trap at liquid nitrogen temperature.

About 10 cm^3 of liquid sample were collected every time, degassed twice by pumping on the liquid for about half a minute and transferred to a 2 l bulb whose internal surface had been covered with freshly generated potassium mirror. 2. CHD_3 and CD_4 ; the vapor was passed through a $30 \times 1.5\text{ cm}$ silica gel column that had been activated at 500K under vacuum and flushed twice with the gas in question; the column was held at dry ice temperature ($\sim 200\text{K}$). The gas was then bubbled through liquid sodium-potassium alloy at room temperature. The samples were collected in a trap at liquid nitrogen temperature, degassed as above and transferred to 2l bulbs containing freshly generated potassium mirrors.

It was found that for CH_4 , CH_3D and CH_2D_2 no further treatment was required and the samples were used after they had been kept on the mirrors for at least ten days.

The CHD_3 and CD_4 required a longer period (one month) and more fresh mirrors (at least four). The criterion used to determine the purity of the deuterated samples was a comparison of the electron lifetime at low fields with that in CH_4 .

3. Conductance Cells

Two types of cells were used, one for low pressure (<4 atm) gas measurements and one for high pressure and liquid measurements.

The low pressure cell is shown in Figure II-3 and the high pressure cell for liquid measurements in Figure II-4. Cells for high pressure gas phase measurements were similar to that in Figure II-4 except that the side arms pointed up instead of down (Figure II-5). A third type of high pressure cell was used where the electrodes were placed at the center therefore allowing measurements in both liquid and gas phases at the same time. This cell was used for measurements in the vicinity of the critical point in order to monitor the disappearance of the liquid phase.

The separation between the electrodes was measured directly with precision calipers to ± 0.001 cm. The cell

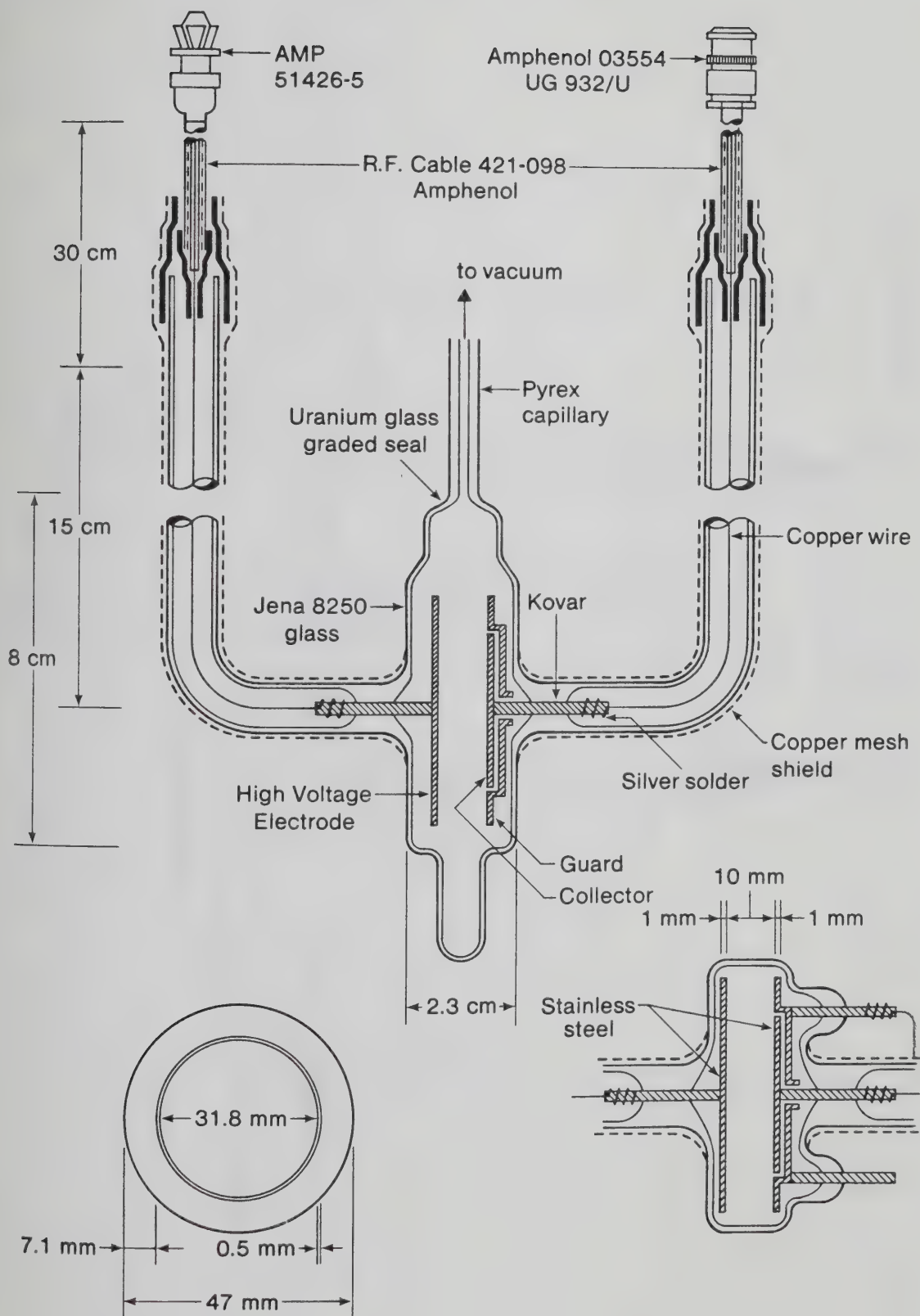


Figure II-3 Low Pressure Gas Cell

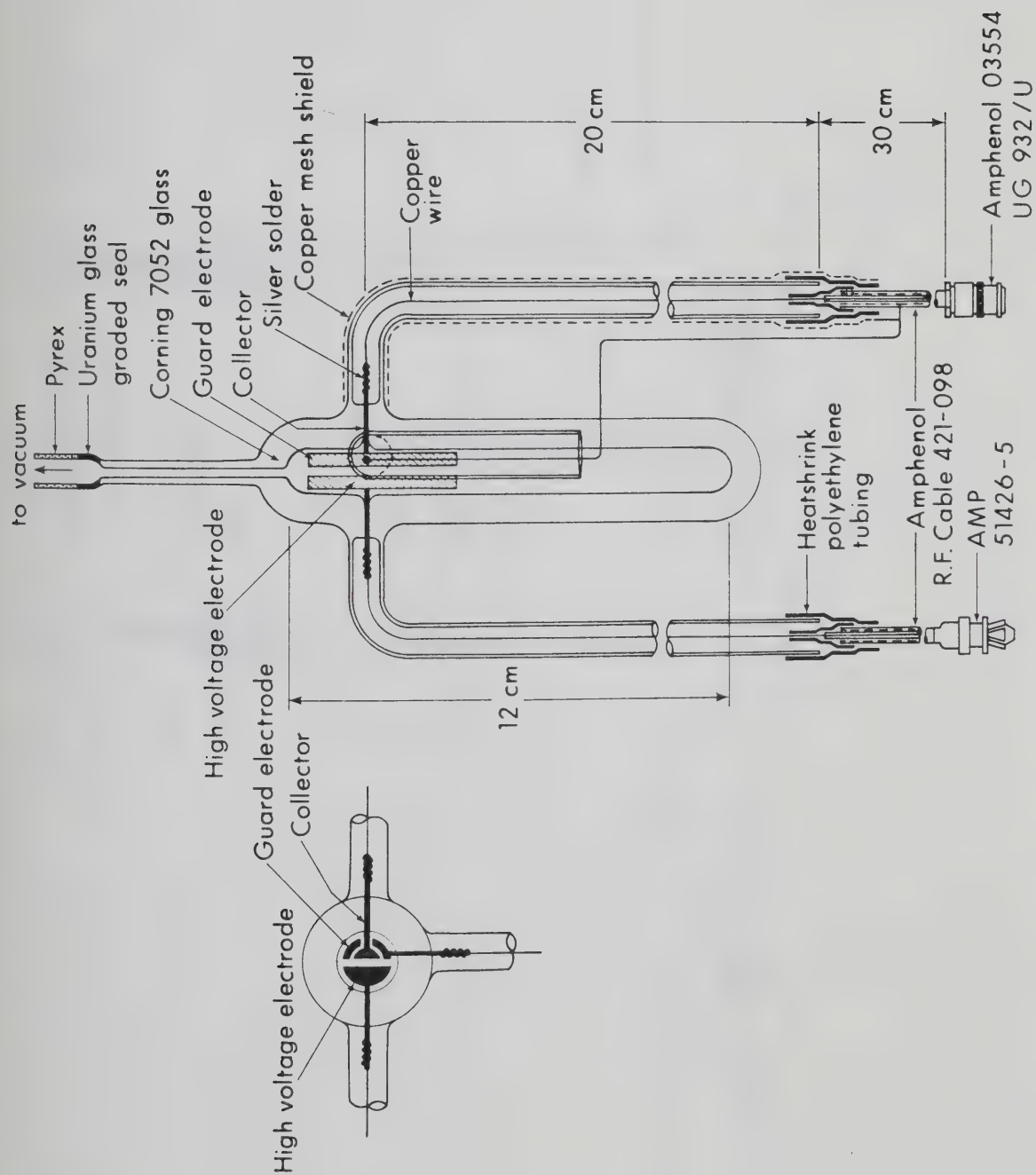


Figure II-4. High Pressure Liquid Cell.

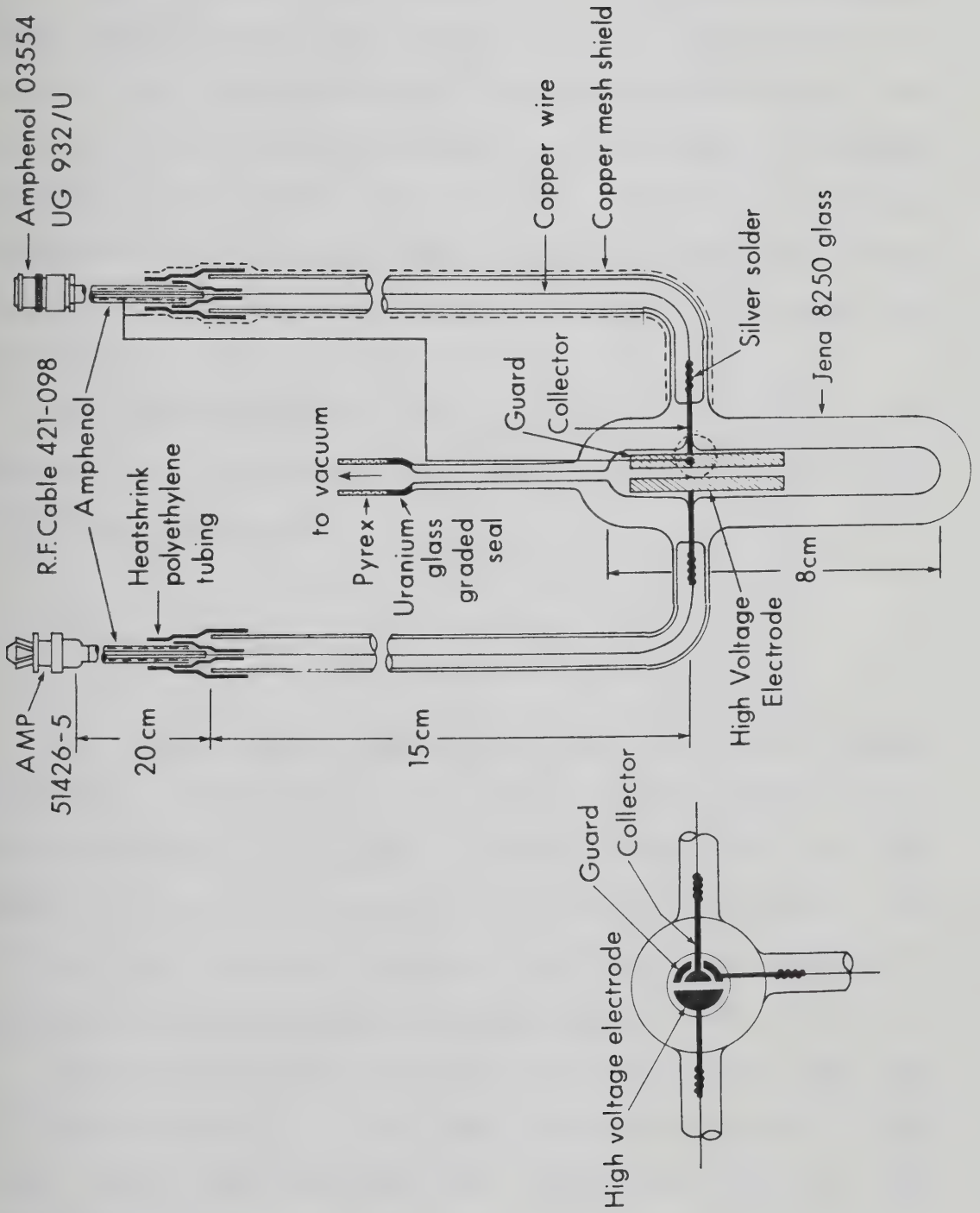


Figure II-5 High Pressure Gas Cell

constant was determined by a capacitance measurement. The cell was connected to an Electro Scientific Industries Capacitance Bridge model 173 as shown in the schematic of Figure II-6; an equilibrium condition was obtained. The cell was replaced by a General Radio Company Precision Capacitor type 1422 and the same null in the bridge obtained. This procedure was followed, rather than reading directly from the instrument, in order to increase the resolution.

The ratio between the cell constant and the separation between the electrodes gave the effective area of the collecting electrode.

4. Filling the Cell

The cells were heated to 50K above the highest temperature that was to be used in the experiment or to 500K whichever was higher. During heating the cell was pumped on until a pressure of 10^{-5} Pa was achieved. The cell was left in this state for at least two consecutive nights and cooled slowly before filling.

The outer surface of the cell was coated with Aqua Dag (G.C. Electronics T.V. tube coat) which was grounded to the copper braid that shielded the leads connected to both electrodes.

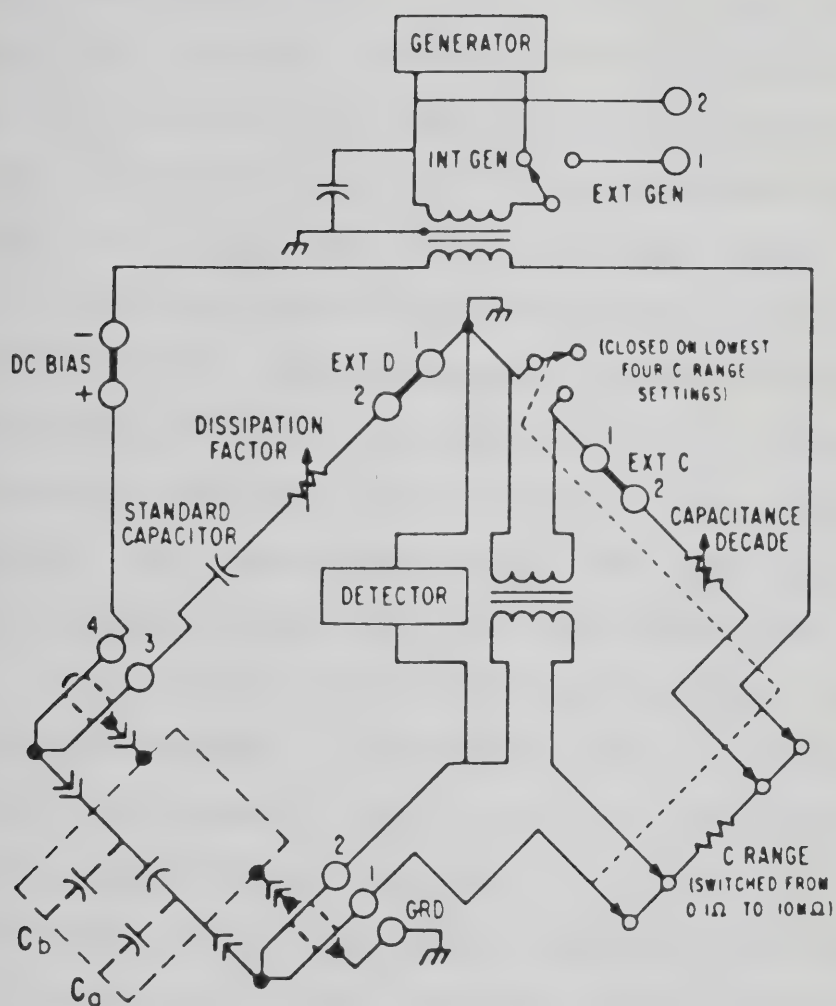


Figure II-6. Apparatus for measuring the cell capacitance.

For densities $< 1 \times 10^{26}$ molec/m³ the following procedure was then used. The whole line was flushed with a portion (~10 torr) of purified gas from one of the storage bulbs and evacuated; the cell was surrounded with an isopentane slush at 110K and the desired amount of gas giving the pressure needed was introduced. The pressure was measured with a mercury manometer connected to the same portion of line as shown in Figure II-2. After closing the valve connecting the cell to the rack, the isopentane slush was removed, the lower tip of the cell cooled at liquid nitrogen temperature and the cell was sealed off with a torch.* The density was calculated from the measured values of the pressure, temperature and the volume of the cell plus the volume of the valve and connecting tubing which had been previously measured.

For higher densities, after flushing, the necessary amount of sample was taken from one of the reservoirs and transferred to a 10 ml measuring pipette cooled at liquid nitrogen temperature. The amount to give the needed density was then transferred to the cell which was then sealed off with a torch.

*For some of the lower densities the cell was filled at room temperature.

5. Temperature Control

A box made of polystyrene foam was used to achieve low temperatures. A stream of cold nitrogen from a 50ℓ Dewar of liquid nitrogen was introduced through a port at the bottom of the box. The stream passed through channels up the walls of the box and entered the cell compartment through narrow slits opening near the top. The gas exited through a tube which extended from 1 cm above the floor of the chamber up through the lid. The rate of flow of nitrogen was controlled by varying the current passing through a 1 kW resistor immersed in the liquid nitrogen. This resistor was connected to an LFE Corp. model 226-A21 temperature controller.

A second set up was used in the latter part of the work in order to reduce temperature differences inside the chamber. It is illustrated in Figure II-7. It consisted of a large silvered Dewar and a polystyrene lid. The cell was fitted to the lid and lowered into the Dewar so that it hung freely with a space of about 10 cm beneath it. In the bottom 2 cm of the space the temperature changed appreciably with position because of gas turbulence. A stream of nitrogen gas entered the lid, was deflected by a circular buffer in order not to directly hit the cell, and exited through the sides. The rate of flow of nitrogen was fixed and regulated by a Variac connected to a heater

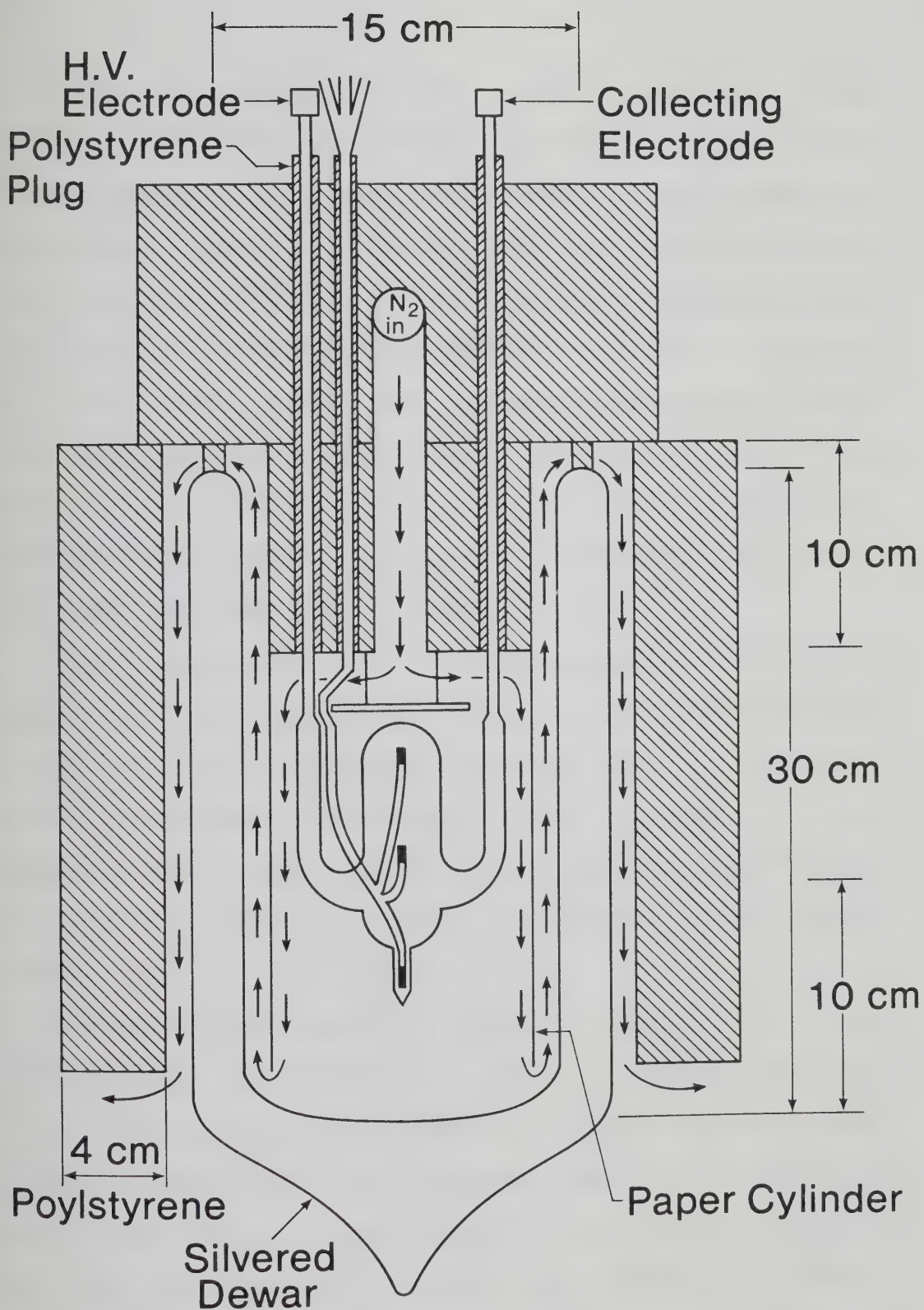


Figure II-7 Cooling Apparatus

placed at the bottom of a 50 l Dewar containing liquid nitrogen. The nitrogen gas was heated by a Hotwatt heater before entering the cell compartment. The heater was connected to a Taylor Micro Scan 1300 Indicating Controller which had been modified as shown in the diagram of Figure II-8 to improve stability and resolution, and to a Sorensen D.C. Power Supply (model DCR 150/1813). In Figure II-9 is shown a block diagram of the actual controller. This configuration allowed for a reasonably stable temperature and a maximum difference between the temperature at the top of the cell and that at the bottom of 0.5 K.

Three calibrated type T thermocouples were used to measure the cell temperature, one placed at the bottom of the cell, one in the electrode area and one at the top. A platinum resistance thermometer acted as monitor for the temperature controller. The cooling system was surrounded by a polystyrene box and placed in a well grounded aluminum Faraday cage.

The set up for heating is shown in Figure II-10. The cell was either positioned on asbestos supports glued to the wall of a clear walled Dewar or fitted to an asbestos lid and lowered in a large silvered Dewar. The heat gun (Master Appliance Co. model AH0751) was fitted to a glass tube. The heating coil of the gun was connected to either of the temperature controllers already described. The heat gun fan was powered from a normal 60 cycle outlet.

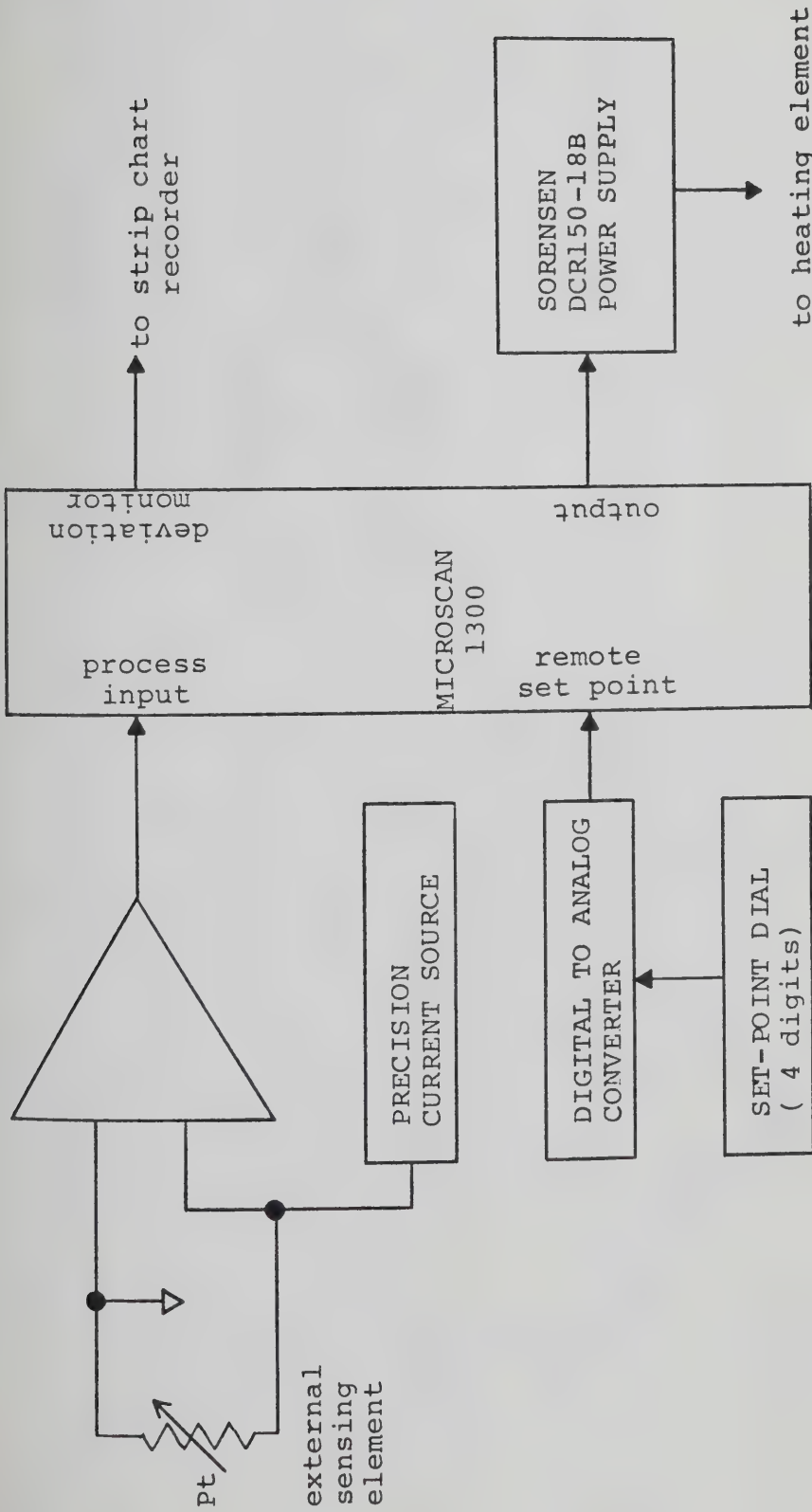


Figure II-8 Block diagram of the temperature regulation apparatus

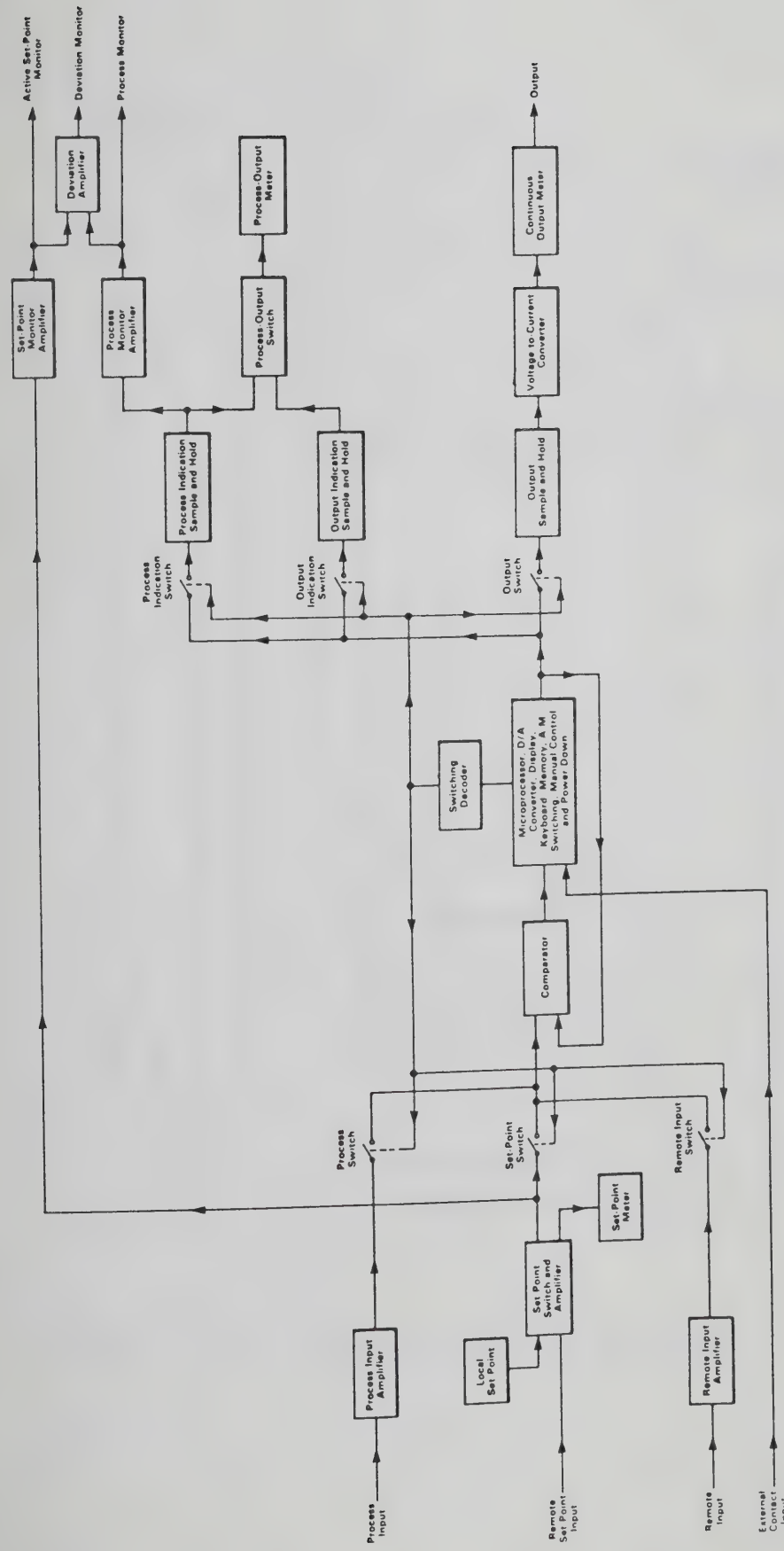


Figure II-9 Block diagram of temperature controller

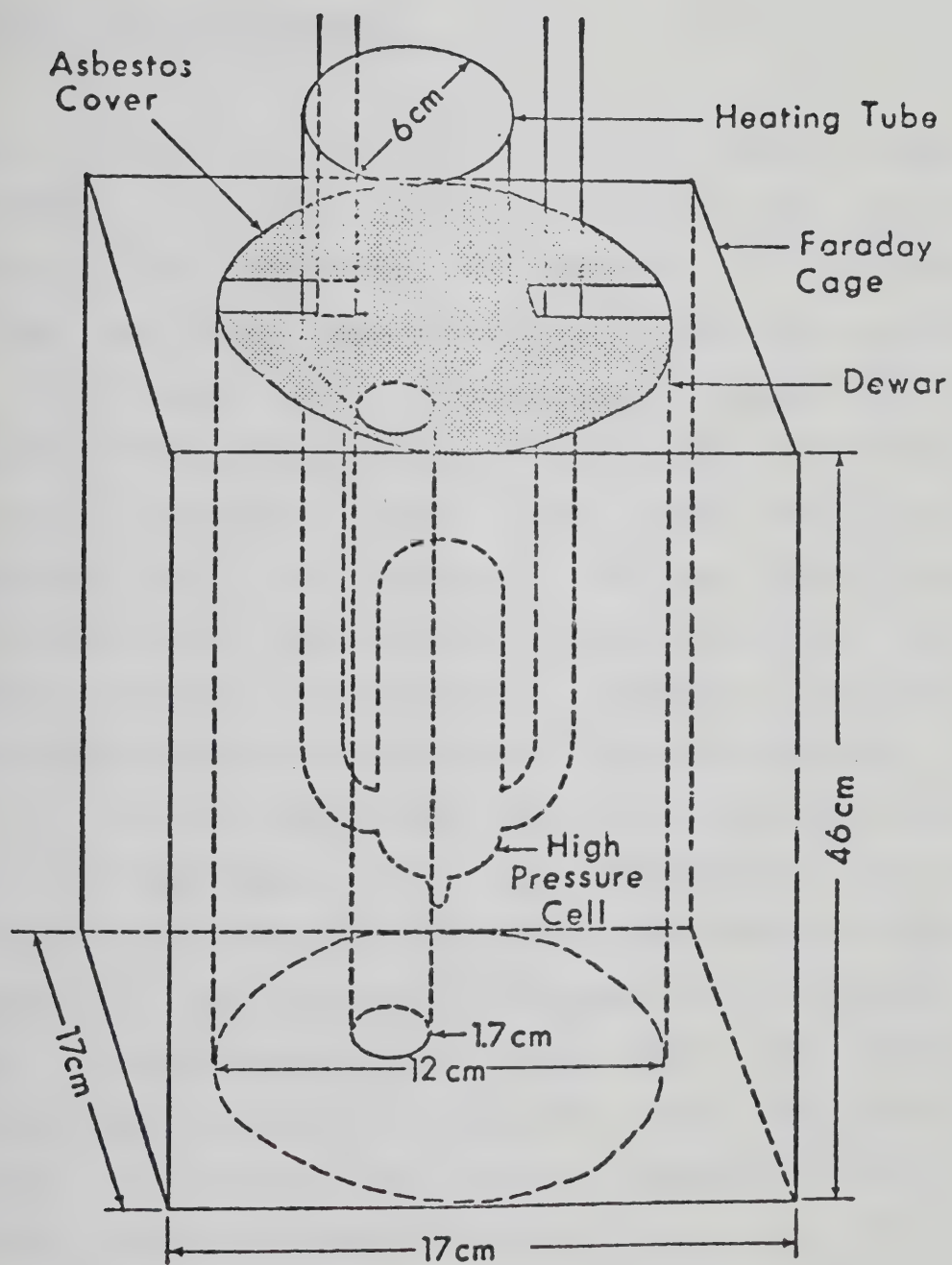


Figure II-10. High Temperature Apparatus

6. Van de Graaff Accelerator

A 2.0 MeV Van de Graaff accelerator (High Voltage Engineering Co.) was used to produce high energy electrons. The accelerator was operated at 1.7 MeV for this work and pulse lengths of 10, 30 and 100 ns were used. The vacuum inside the accelerator tube was of the order of 10^{-5} Pa. The beam was focussed with the aid of a piece of phosphorescent paper placed at the end of the accelerator tube. Each pulse of electrons hitting the paper produced a visible glow which could be seen on closed circuit television. Steering and focussing of the beam were achieved by controlling current to electromagnets.

A 3.2 mm thick gold target was used to produce Xrays to irradiate the sample. The target was placed at the end of the beam pipe and was insulated from the ground so that the beam of 1.7 MeV electrons could cause the build up of a charge for measurement of the pulse dose. The charge generated was measured by an ORTEC model 439 current digitizer. A TSI model 1535 counter was used to display the signal as nanocoulombs of charge.

7. Mobility Measurements

The system used to measure current transient signals is shown in Figure II-11. For ion mobility measurements

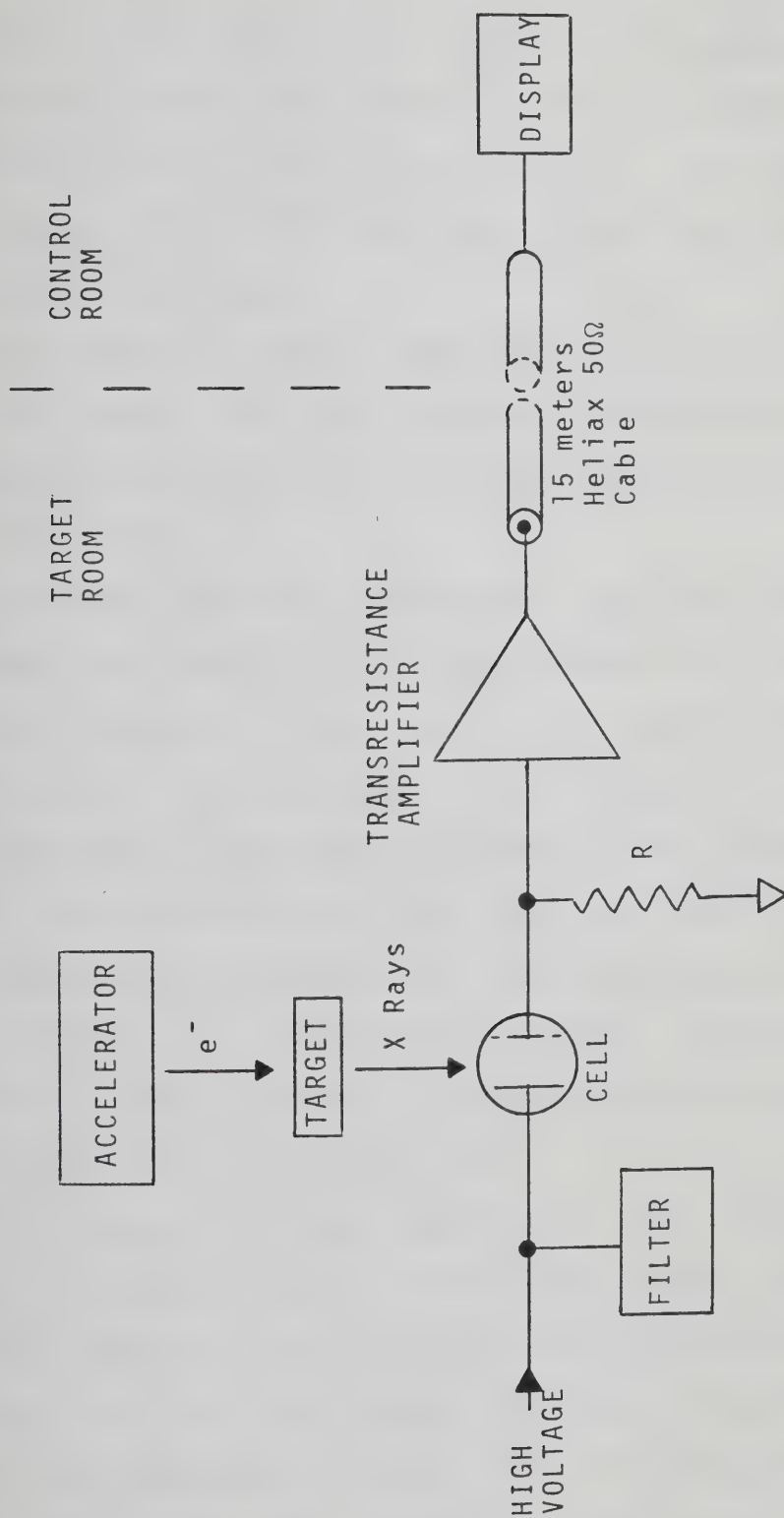


Figure II-11 System for measuring current transient signals

amplifier P.A.R. mod 113 was used. The response time and gain of the circuit were varied by the gain setting on the amplifier and the value of the resistor R. For most of the work a gain of 5×10^8 was used. The 0 to 97% response time was about 15 μ s.

For electron signals amplifier #8 shown in Figure II-12 was used. The gain was 5×10^4 and the 0 to 97% response time was about 60 ns. The amplifier was designed by Mr. Ron Gardner.

Collection of data was computer assisted as shown in the diagram of Figure II-13. The software was developed by Mr. Larry Coulson. The signals, as plots of voltage against time, were displayed on a scope and printed on graph paper by an incremental plotter. All the information related to the particular run such as applied voltage, dose, temperature, sensitivity, time scale and others were also printed. A preliminary mobility calculation was performed by the computer. Signal averaging was used to increase the signal to noise ratio.

The electron and ion mobilities were obtained by a time of flight measurement. Electrons and ions were formed uniformly between two electrodes of separation λ . A measurement of the time needed for the charges to drift across the separation led to the determination of the average velocity in the direction of the field, the drift velocity v_d

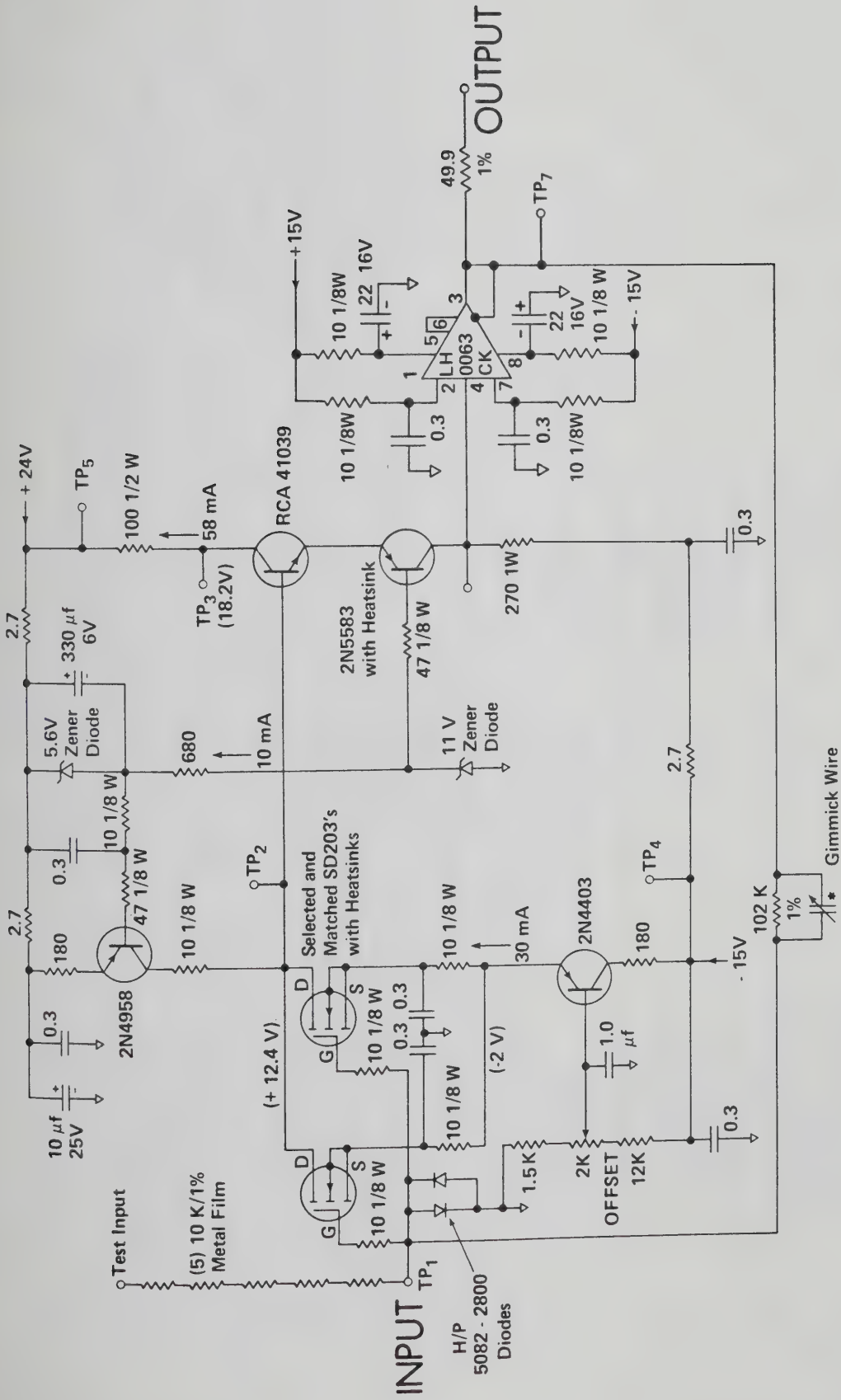


Figure II-12 Transresistance Amplifier #8, used with a 50 ohms termination.
Gain= 5×10^4

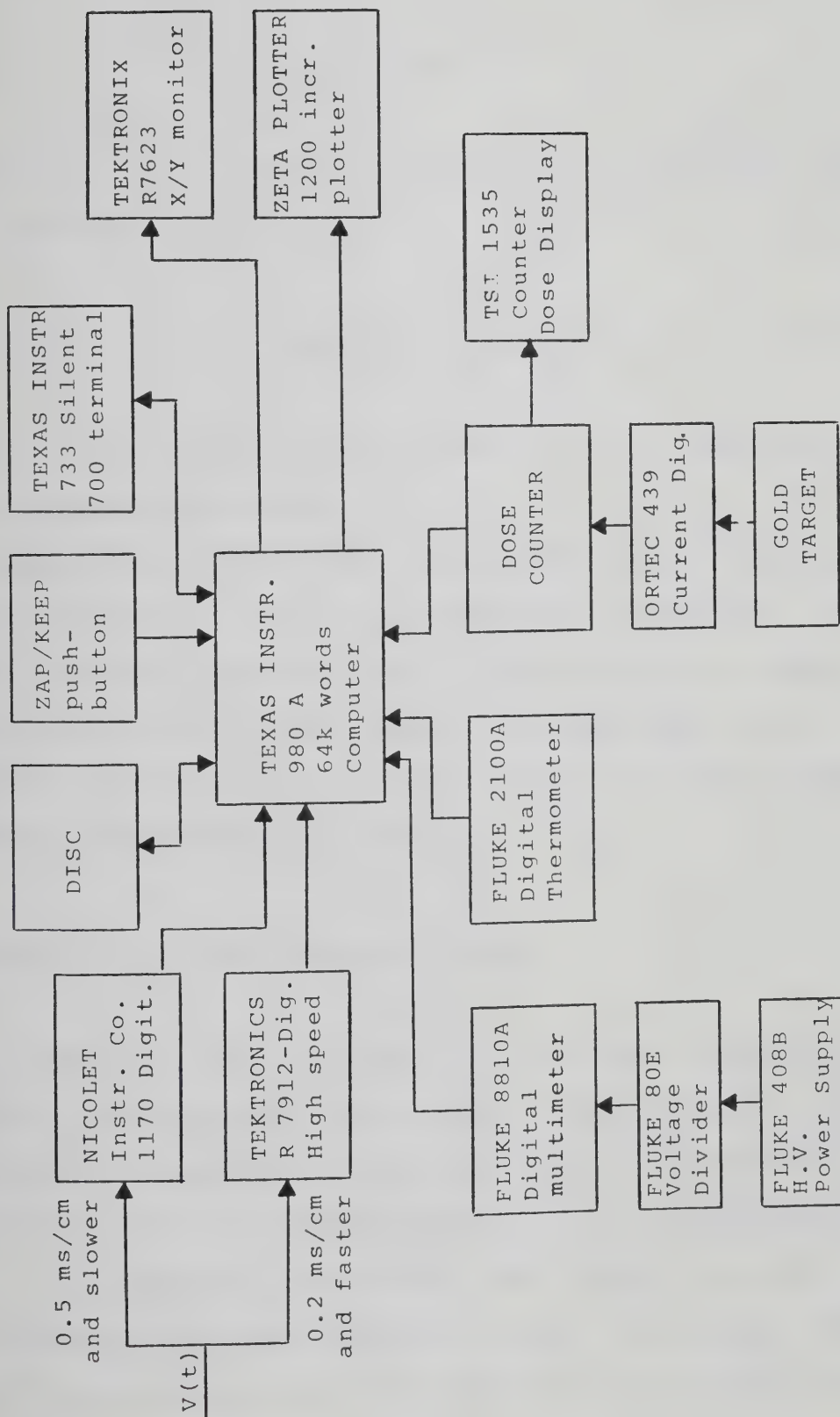


Figure II-13 Block diagram of data collection system

$$v_d = \ell / t_d \quad \text{II-1}$$

The mobility, μ , is defined as the drift velocity per unit field strength

$$\mu = \frac{v_d}{E} = \frac{\ell^2}{t_d V} \quad \text{II-2}$$

where E is the electric field strength and V is the voltage applied across the plates.

Measurements were made with positive and negative applied voltages. The two different polarities gave results agreeing to within 5%. The averages of results obtained with positive and negative voltages were used.

More details on the analysis of the measured signal are given in the following section.

C. The Analysis of the Measured Signal

In Figure II-14 A is shown an idealized schematic of the measuring apparatus. It consists of two plates of area A , placed at a distance ℓ , under the voltage V generated by the battery. If one electron (charge = $-e$) is generated at time $t = 0$ somewhere between the two plates, it will be accelerated by the field and gain energy. This energy will be lost by collisions with the molecules of the surrounding

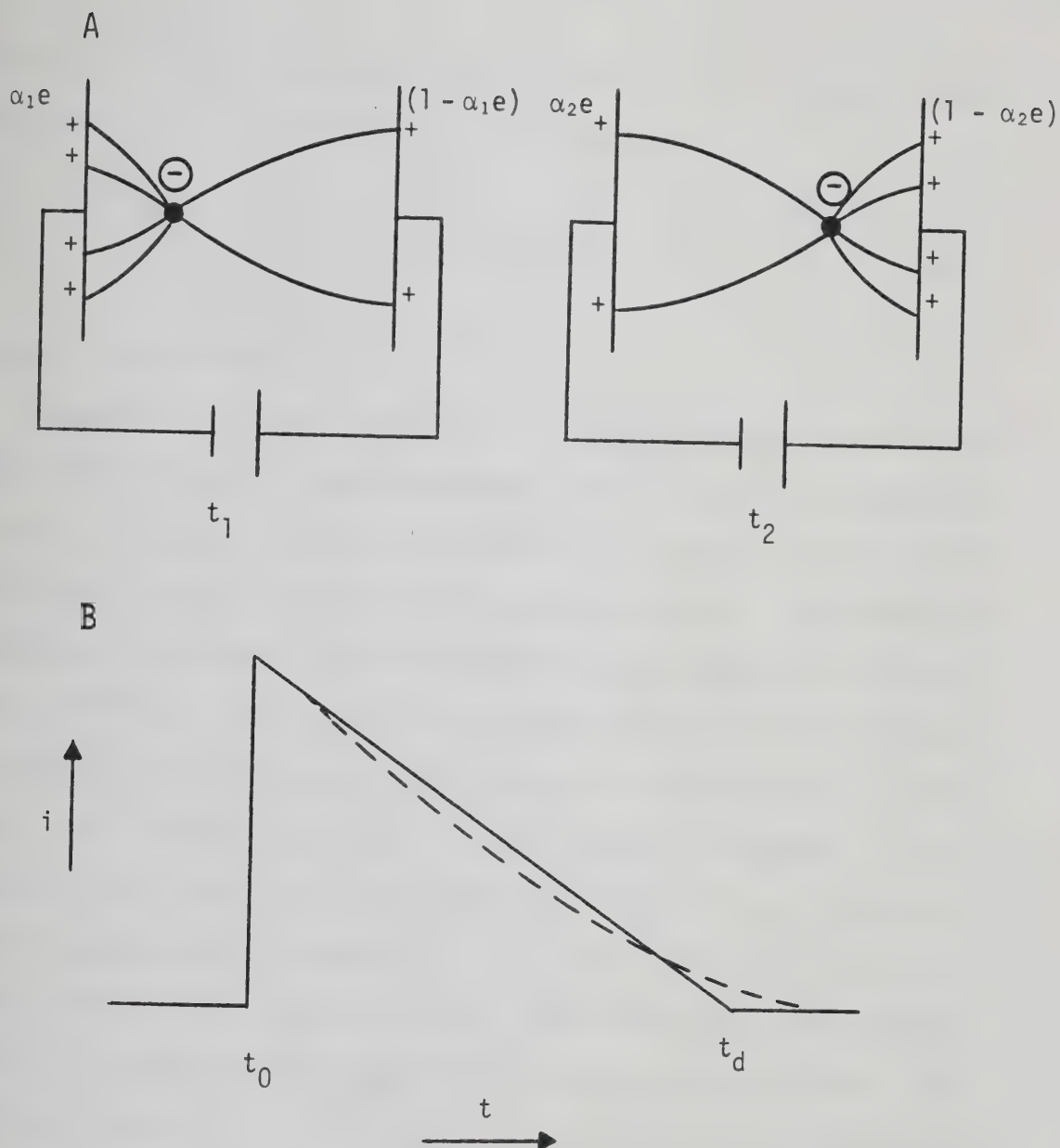


Figure II-14 A: Drift of a charge (-) between two plates at different times t_1 and t_2 .

B: Idealized current transient signal. The dashed line represents space charge distortion.

medium. The electron will achieve an average drift velocity, v_d , in the direction of the field.

$$v_d = \mu \frac{V}{l} = \mu E \quad \text{II-3}$$

where μ is the mobility.

Suppose that at time $t = t_1$, the electron is in the position shown in the diagram on the left of Figure II-14A. It will induce a charge $= \alpha_1 e$ on the negative electrode and $(1 - \alpha_1 e)$ on the positive plate. The induced charge is inversely proportional to the distance from the charge.²³⁹ At time t_2 the electron will have moved closer to the positive terminal as shown in the diagram on the right of Figure II-14A. The induced charges on the negative and positive terminals will now be $\alpha_2 e$ and $(1 - \alpha_2 e)$ respectively, where $\alpha_2 < \alpha_1$. Thus, when the electron moves through the space between the electrodes the induced positive charge on the negative electrode moves through the external circuit to the positive electrode or, during the whole drift if the electron travels the whole distance l , a charge $-e$ moves in the external circuit in the opposite direction. A current flows in the circuit in the same direction as that of the electron moving in the drift space.

The electron is moving with a drift velocity

$$v_d = \frac{dx_d}{dt} \quad \text{II-4}$$

along a line of force due to the electric field $E = V/\lambda$.

An amount of work dW will be performed.²³⁹

$$dW = eEdx_d \quad \text{II-5}$$

This energy has been supplied by the current i from the battery and is given by

$$dW = Vidt \quad \text{II-6}$$

Therefore

$$eEdx_d = Vidt \quad \text{II-7}$$

or

$$i = \frac{eE}{V} \frac{dx_d}{dt} = \frac{e}{\lambda} v_d = \frac{e\mu E}{\lambda} \quad \text{II-8}$$

The induced current is proportional to the number of moving charges. If n_d charges/ m^3 are drifting at time t the resulting current/ m^2 will be

$$i = n_d\mu E \quad \text{II-9}$$

Electrons are being collected at the positive electrode. Their concentration will decrease according to zeroth order kinetics. If n_0 is the number of charges of either sign/m³ generated by the Xray pulse, the concentration n being neutralized at the electrode per unit area will be given by

$$-\frac{dn}{dt} = \frac{n_0 e}{t_d} = n_0 e \mu E \quad \text{II-10}$$

$$n(t) = n_0 e \mu E t \quad \text{II-11}$$

The concentration, $n_d(t)$, of charges contributing to the current will be

$$n_d(t) = n_0 - n(t) = n_0 e (1 - \mu E t) \quad \text{II-12}$$

The current will then be

$$i(t) = n_0 e \mu E (1 - \mu E t) \quad \text{II-13}$$

The current decays linearly with time. The solid line in Figure II-14 B shows an idealized current decay. At time $t = 0$, for an infinitely short Xray pulse, the current is directly proportional to the concentration of charges generated, to their mobility and to the applied electric

field strength. The area underneath the signal is equal to $n_0 e$ and is velocity independent. A fast signal will be higher and proportionately shorter than a slow one, n_0 being the same in the two cases.

At time $t = t_d$ the current is zero. This is the measured quantity. In this section several limitations producing changes from ideality in the observed current decay traces will be discussed.

The three major sources of distortion in the traces are: (1) finite width of the Xray pulse, (2) random diffusion of the swarm, (3) space charge. Their effects will be discussed in this order.

1. Effect of Finite Width of the Xray Pulse

The effect of a non zero duration of the Xray pulse has been discussed in Reference 192. Briefly, when the pulse width is not negligible with respect to the drift time, a tail appears at the end of the linear part of the decay. This makes it difficult to determine the real end of the signal. The problem was minimized by always using pulses which were much shorter than the drift times. Typically the electron drift times were in the order of μs . The pulses used were 10 or 30 ns long. The ion drift times were in the order of ms. The pulses used were 100 ns long. In those cases (fast electron signals, high fields)

where the width of the pulse was considered to be an appreciable fraction of the drift time, Equation 2 of Reference 192 was used.

2. Effect of Random Diffusion

At low fields and large values of t_d , the current decay was no longer linear. This is due to random diffusion of the electrons during the drift to the collecting electrode. Random diffusion spreads the tail of the current decay signal. In general this problem was not important because the threshold fields were sufficiently high (see Results section) to ensure that diffusion effects were negligible. In those cases where it was necessary to reduce the applied voltage the effect of diffusion was taken into consideration.

The mobility from Equation II-3 is given by

$$\mu = \frac{v_d \ell}{V} = \frac{\ell^2}{V t_d} \quad \text{II-14}$$

If diffusion is important ℓ can be replaced by $(\ell + \Delta x)$ where Δx is the mean distance of diffusion opposite to the field direction during the time t_d . This quantity is given by¹⁹²

$$\Delta x = (2Dt_d)^{1/2} \quad \text{II-15}$$

where D is the diffusion coefficient of the electrons which is assumed to be given by the Einstein relation

$$D = (kT/e)\mu \quad \text{II-16}$$

Using this correction Equation II-14 becomes

$$\mu = \lambda^2 [1 + (2kT/eV)^{1/2}] / Vt_d \quad \text{II-17}$$

where k is Boltzmann's constant, T the absolute temperature and e the electron charge. For a signal measured at 510 V/m and 636 K the correction is 15%.

3. Effect of Space Charge

Because the electron mobility in methane is much larger than the ion mobility ($\mu/\mu_+ \approx 10^4$) the electrons are cleared out of the volume between the electrodes leaving the ions essentially unmoved. Under certain conditions (high dose, low fields ...) this can severely alter the field and lead to distortion of the current vs time decay.

An example of how the trace could look is shown with a dashed line in Figure II-14B.

If a field E_0 is applied between two parallel infinite plates the charge density on each electrode is given by¹⁹³

$$\sigma_{+} = E_0 \epsilon_0 \quad \text{II-17}$$

where ϵ_0 is the permittivity of free vacuum

$$(\epsilon_0 = 8.9 \times 10^{-12} \text{ C}^2 \text{ N}^{-2} \text{ m}^{-2}).$$

It can be assumed that the whole charge is on the negative electrode.

$$\sigma_{-} = 2E_0 \epsilon_0 \quad \text{II-18}$$

and

$$\sigma_{+} = 0 \quad \text{II-19}$$

Assume that N electron-ion pairs/ m^2 are generated between the electrodes, that the thickness of the zone cleared of electrons is x and that the number of ions left in this zone is Nx/ℓ , where ℓ is the electrode separation. A layer dx of this zone will contain dn_{+} ions where

$$dn_{+} = \frac{Ndx}{\ell} \quad \text{II-20}$$

A layer dx of ions at distance x from the negative electrode will induce σ_{-}^{ind} charges on it and σ_{+}^{ind} on the positive plate

$$\sigma_{-}^{ind} = \frac{(\ell-x)Ndx}{\ell^2} \quad \text{II-21}$$

and

$$\sigma_{+}^{ind} = \frac{x Ndx}{\ell^2} \quad \text{II-22}$$

As the electrons are cleared out of the space, the net field, E_{sc} , generated by the positive ions and the resultant charges induced on the electrodes is¹⁹⁴

$$-E_{sc} = \frac{1}{2\epsilon_0} \left[\int_0^x \frac{Ndx}{\ell} - \int_0^x \frac{N(\ell-x)dx}{\ell^2} + \int_0^x \frac{Nxdx}{\ell^2} \right] = \quad \text{II-23a}$$

$$= \frac{N}{\epsilon_0 \ell^2} \left[\int_0^x xdx \right] = \quad \text{II-23b}$$

$$= \frac{N}{2\epsilon_0} \left(\frac{x}{\ell} \right)^2 \quad \text{II-23c}$$

The net field E_x is

$$E_x = E_0 - E_{sc} = E_0 - \frac{N}{2\epsilon_0} \left(\frac{x}{\ell} \right)^2 \quad \text{II-24}$$

or

$$E_x (\text{V/m}) = E_o - 9 \times 10^{-9} N \left(\frac{x}{\ell}\right)^2 \quad \text{II-25}$$

where N is in units of ion-electron pairs/ m^2 .

The drift velocity is given by equation II-4. The time dt_x for the electrons to drift in the space dx is

$$dt_x = \frac{dx}{\mu [E_o - 9 \times 10^{-9} \left(\frac{x}{\ell}\right)^2]} \quad \text{II-26}$$

The time t_x to drift in the space x is

$$t_x = \frac{1}{\mu} \int_0^x \frac{dx}{E_o - 9 \times 10^{-9} \frac{N}{\ell^2} x^2} \quad \text{II-27}$$

Integration of this formula gives

$$t_x = \frac{\ell}{9 \times 10^{-9} N \mu x^2 \left(\frac{E_o}{9 \times 10^{-9} N} \right)^{1/2}} \ln \frac{\left(\frac{E_o \ell^2}{9 \times 10^{-9} N} \right)^{1/2} + x}{\left(\frac{E_o \ell^2}{9 \times 10^{-9} N} \right)^{1/2} - x} \quad \text{II-28}$$

This formula can be written as

$$t_x = \frac{\ell}{2\mu (9 \times 10^{-9} N E_o)^{1/2}} \ln \frac{\ell \left(\frac{E_o}{9 \times 10^{-9} N} \right)^{1/2} + x}{\ell \left(\frac{E_o}{9 \times 10^{-9} N} \right)^{1/2} - x} \quad \text{II-29}$$

where N is in ions/ m^2 and E_o in V/m . The drift time t_o in

the absence of space charge effects is

$$t_o = \frac{\ell}{\mu E_o} \quad \text{II-30}$$

The ratio of these two times is

$$\frac{t_x}{t_o} = \frac{1}{2} \left(\frac{E_o}{9 \times 10^{-9} N} \right)^{1/2} \ln \frac{\ell \left(\frac{E_o}{9 \times 10^{-9} N} \right)^{1/2} + x}{\ell \left(\frac{E_o}{9 \times 10^{-9} N} \right)^{1/2} - x} \quad \text{II-31}$$

The current i_x generated by the exposed ions and the resultant charges induced on the electrodes is

$$i_x = \mu e N \left(1 - \frac{x}{\ell} \right) E_x = \quad \text{II-32a}$$

$$= \mu e N \left(1 - \frac{x}{\ell} \right) \left[E_o - 9 \times 10^{-9} N \left(\frac{x}{\ell} \right)^2 \right] \quad \text{II-32b}$$

The current i_o in the absence of space charge effects is

$$i_o = \mu e N E_o \quad \text{II-33}$$

The ratio of these two currents is

$$\frac{i_x}{i_o} = \left(1 - \frac{x}{\ell} \right) \left[1 - \frac{9 \times 10^{-9} N}{E_o} \left(\frac{x}{\ell} \right)^2 \right] \quad \text{II-34}$$

This formula shows that the effect will increase with N and $1/E_0$ and that, at given N and E_0 , the effect will be greater at long times giving rise to a long tail at the end of the signal. This is shown with the dashed line in Figure III-14B.

A plot of i_x/i_0 vs. t_x/t_0 in the absence of space charge effects is a straight line with slope of -1 . By plotting these quantities at a given N and different values of E_0 one can get information about the minimum field strength to use for space charge effects to be negligible. Alternatively, plots of i_x/i_0 vs. t_x/t_0 at a given E_0 and different values of N give the maximum concentration of ions producing a negligible field distortion.

In Figure III-15, is shown an example at $N_{\text{ions}}/n_{\text{molec}} \approx 1 \times 10^{-14}$, the maximum concentration used in gas phase measurements in this work. The four curves correspond to values of E/n of 1.7×10^{-3} Td, 3.3×10^{-3} Td, 1×10^{-2} Td and 3.3×10^{-2} Td ($\text{Td} = 10^{-21} \text{ m}^2\text{V/molec}$) respectively. In the low density gas the threshold field is about 2×10^{-2} Td near the coexistence curve and increases with temperature at constant density and with density (see Results section).

In liquid phase measurements lower ion concentrations were used and the ratio $N_{\text{ion}}/n_{\text{molec}}$ was of the order of 1×10^{-16} .

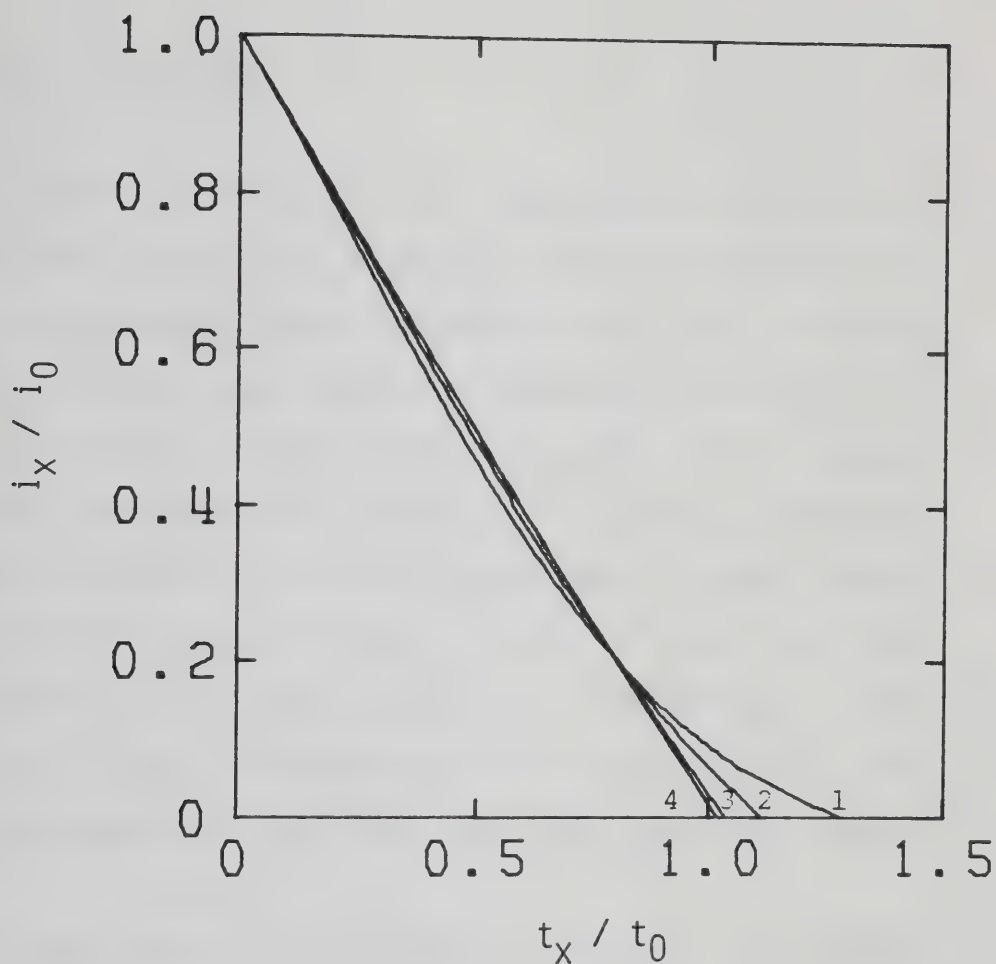


Figure II-15 Examples of space charge limited signals. $n_{\text{ions}} / n_{\text{molec}} = 10^{-14}$ ions/molec.
 1: $E/n = 1.7$ mTd ; 2: $E/n = 3.3$ mTd ; 3: $E/n = 10$ mTd
 4: $E/n = 33$ mTd .

D. Physical Properties

The physical properties of the gases, liquids and molecules were taken from References 162,179-185,195-199. Relevant values are listed in Table II-1. The critical temperature, pressure and density were known for CH_4 ^{195,196} and CD_4 ,¹⁹⁷ but not for the other compounds. The critical temperatures were measured in the present work by observing the sudden appearance of the liquid phase signal, while cooling from the supercritical fluid in the cell that allowed simultaneous measurements in both phases. The calibration of the thermocouples was verified by the critical temperatures obtained for CH_4 and CD_4 (Table II-1).

The liquid density n (molec/m³) of CD_4 is 0.8% greater than that of CH_4 at the same T/T_c .^{195,197} The densities of the other compounds were interpolated between those of CH_4 and CD_4 at the same T/T_c , but the differences were negligible for the purposes of this work. The gas densities of CH_4 were obtained from Reference 195 and were assumed to be the same in all the other compounds at the same T/T_c .

Table II-1. Physical Properties

PROPERTY	UNITS	CH ₄	CH ₃ D	CH ₂ D ₂	CHD ₃	CD ₄	REF	NOTE
Triple point T _t	K	90.7	90.4	90.2	90.0	89.8	162	
Density n _{ts} ^a	10 ²⁷ m ⁻³	18.30				18.57	198	
Density n _{tl} ^b	10 ²⁷ m ⁻³	17.08	17.11	17.15	17.19	17.22	195, 197	
Normal boiling T _b	K	111.8				112.0	179	
Density n _b	10 ²⁷ m ⁻³	15.90				16.03	195, 197	
Critical T _c	K	190.6				189.2	195, 197	
		190.6	191.1 ^c	189.2	189.0	189.2	this work	
Density n _c	10 ²⁷ m ⁻³	6.09				6.14	196, 197	
Pressure P _c	MPa	4.60				4.66	196, 197	
Polarizability α	10 ⁻³⁰ m ³	2.63				2.60	180, 181, 198	gas at STP
		2.60				2.54	182	liquid, 100K
		2.61				2.57	198	solid 90.4 & 89.2K
Dipole moment D ^d	5.4x10 ⁻⁶						183	gas
			5.6x10 ⁻³				184	gas

Table II-1 (continued)

C-H distance	10^{-10}m	1.106		180	gas
C-D distance	10^{-10}m	1.093		199	gas
			1.102	180	gas
			1.089	199	gas
Molar Volume	10^{-6}m^3	36.5	36.1	182	liquid, 100K
Hypersonic velocity	m/s	1540	1380	182	liquid at mp
		1340	1200	182	liquid at bp
Moment A	10^{-47}kg m^2	5.34	5.34	185	
of B		5.34	7.22	185	
Inertia C		5.34	7.22	185	
			6.52		
			8.54		
			8.00		
			9.19		

a. Solid.

b. Liquid.

c. Seems ~1.0K too high.

d. $D = 3.34 \times 10^{-30} \text{ Cm}$.

CHAPTER III

RESULTS

The electron and ion mobilities were measured in methane and its deuterium substituted analogues as functions of the applied electric field strength. Measurements were made as a function of density along the saturated vapor curve in the region from the normal gases to the liquids near the triple point, and at fixed gas densities as a function of temperature.

The electron mobilities are given first, followed by the ion mobilities. In each case the order of presentation is CH_4 first followed by CH_3D , CH_2D_2 , CHD_3 and CD_4 .

The results are presented in order of increasing density beginning with the gas, followed by the critical region, then the liquid phase.

All the data are given as plots of the mobility $\mu(\text{m}^2/\text{Vs})$ against the density normalized field strength E/n ($T_d = 10^{-21} \text{ m}^2 \text{ V/molec}$). For each compound a table summarizing the low field values of the mobility is also given.

All of the curves of Chapters III and IV were drawn empirically unless otherwise specified.

A discussion of errors is given in the Appendix.

A. Electron Mobilities

1. CH₄

In Figure III-1-1 are shown the mobilities as functions of E/n in the gas at $n = 2.95 \times 10^{25}$ molec/m³ at different temperatures. At all temperatures the mobility is field independent at low fields and then it increases when the field is greater than a threshold value. The threshold field increases with temperature. It is ~ 0.02 Td at $T = 116.5\text{K}$ and ~ 0.14 Td at $T = 636\text{K}$.

The low field mobility increases with temperature, from $0.8 \text{ m}^2/\text{Vs}$ at 116.5K to $1.48 \text{ m}^2/\text{Vs}$ at 636K . The mobility curves tend to merge at $E/n \approx 0.5$ Td.

Figures III-1-2 and III-1-3 show the effect of an increase in density by a factor of about 2. Again, both the threshold field and the low field mobility increase with temperature. The rate of change of the threshold field with temperature has not been altered by the change in density. Also the value of the field where the mobility curves merge is unchanged.

The effect of a further increase in density to $n = 7.5 \times 10^{25}$ molec/m³ is illustrated in Figure III-1-4. The absence of measurements between 0.013 Td and 0.027 Td makes it difficult to estimate the threshold fields. However the slope of the curves above 0.013 Td decreases

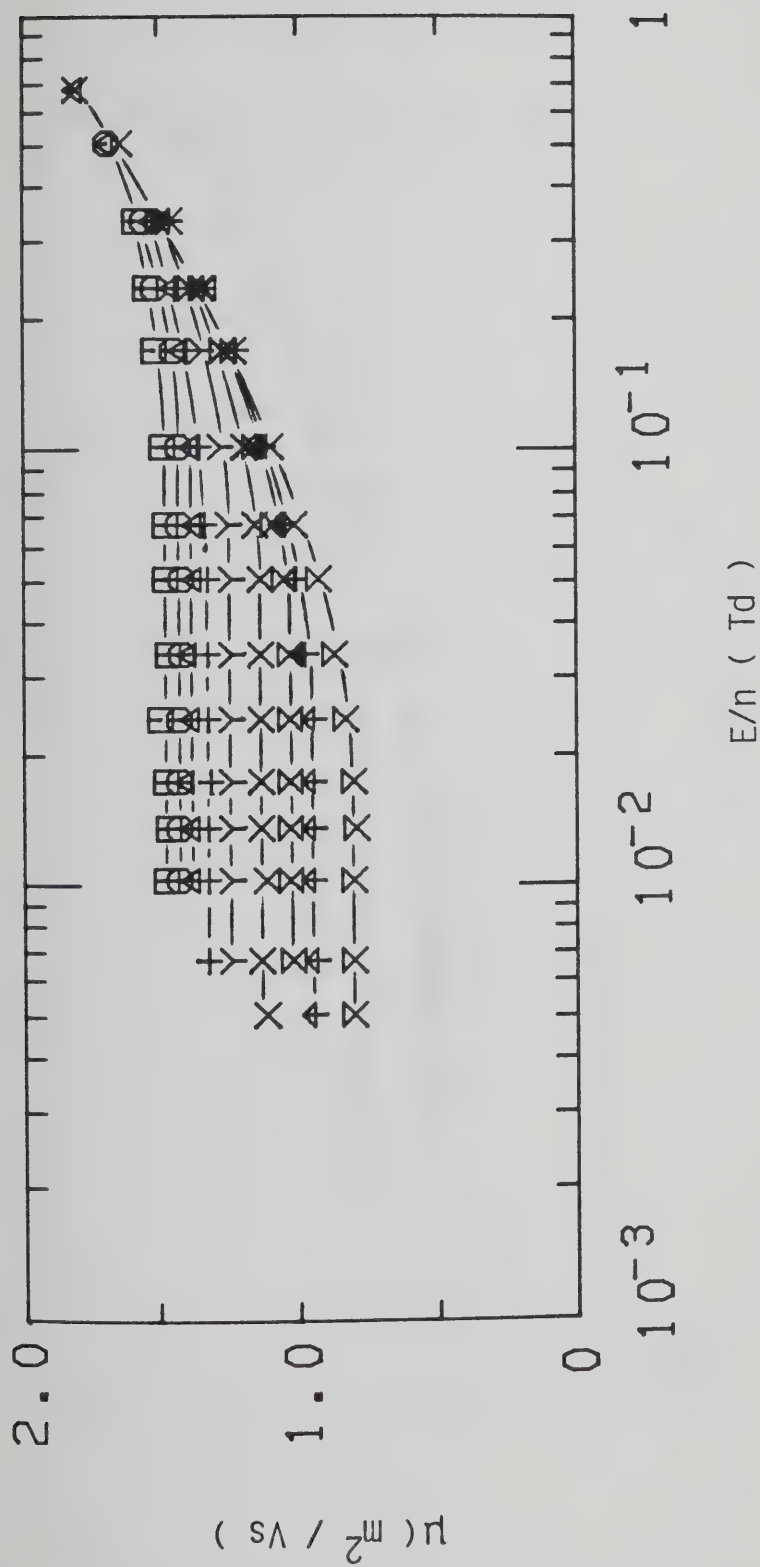


Figure III-1-1. Electron mobilities in CH_4 gas at $n = 2.95 \times 10^{25} \text{ molec/m}^3$ and different temperatures (K). \otimes , 116.5; \uparrow , 163.7; \otimes , 226.0; x, 292.5; y, 372.6; +, 441.2; Δ , 494; \circ , 555; \square , 636.

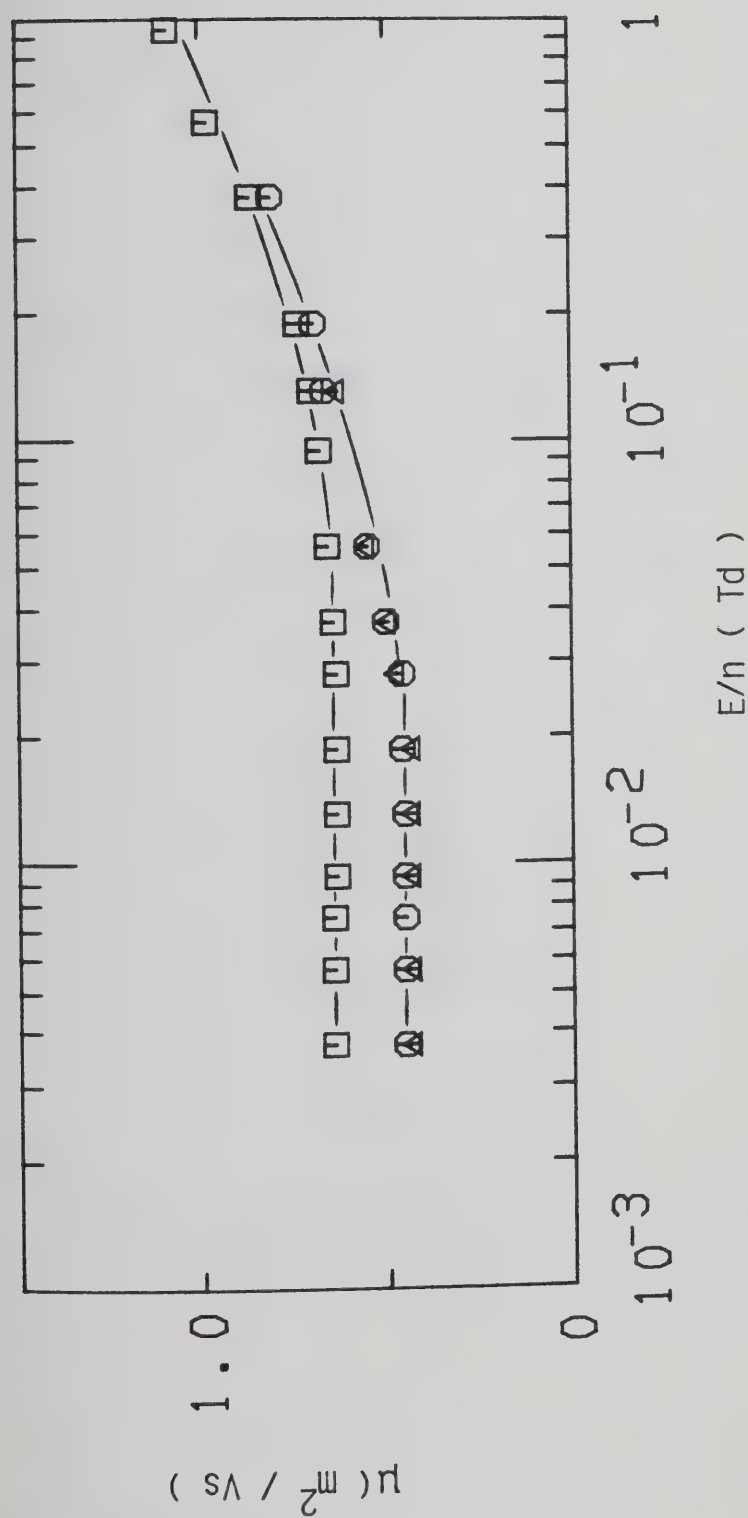


Figure III-1-2. Electron mobilities in CH_4 gas at $n = 5.3 \times 10^{25} \text{ molec}/\text{m}^3$ and different temperatures (K). Δ , 110.0; \circ , 113.6; \square , 293.5.

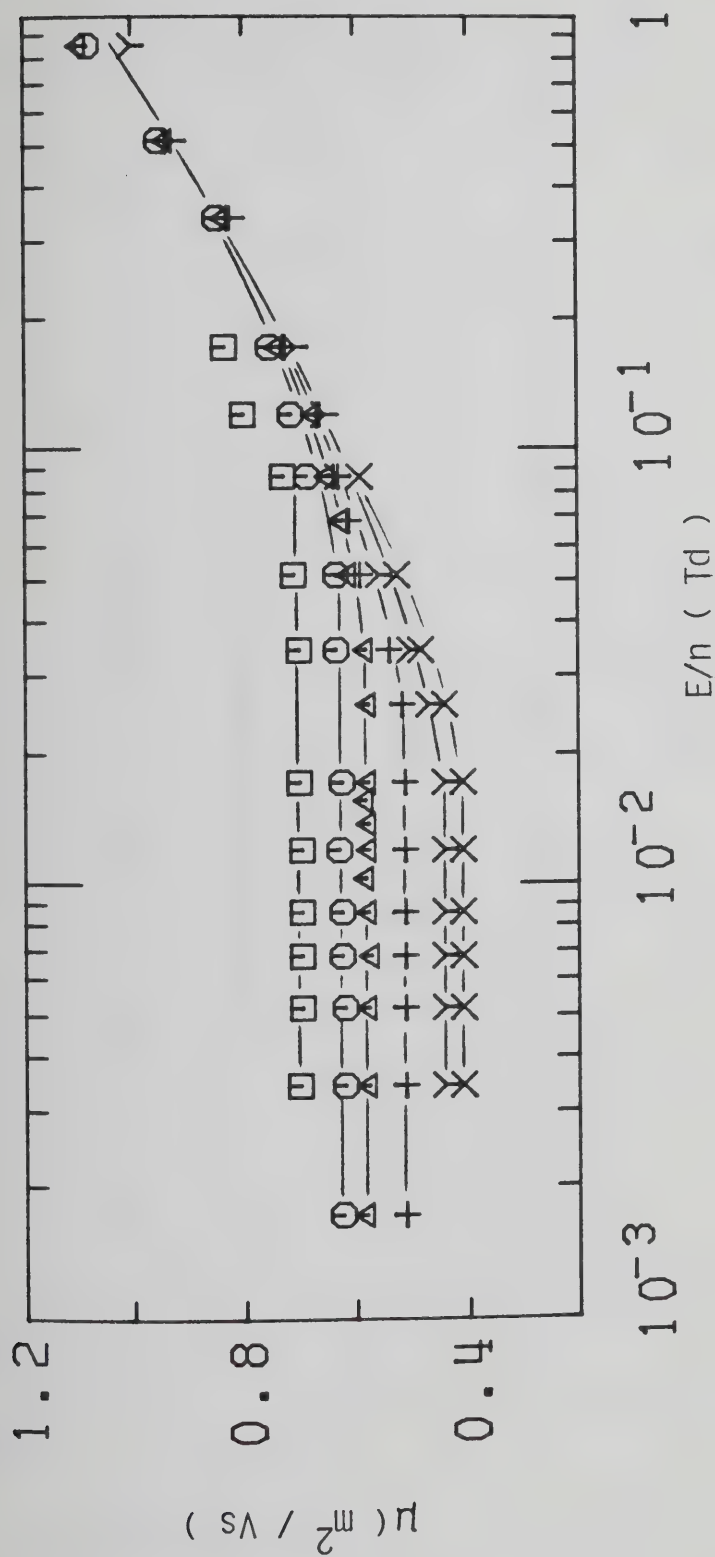


Figure III-1-3. Electron mobilities in CH_4 gas at $n = 5.8 \times 10^{25} \text{ molec/m}^3$ and different temperatures (K). X, 124.0; Y, 151.8; +, 225.0; Δ , 294.0; \circ , 370.5; \square , 488.5.

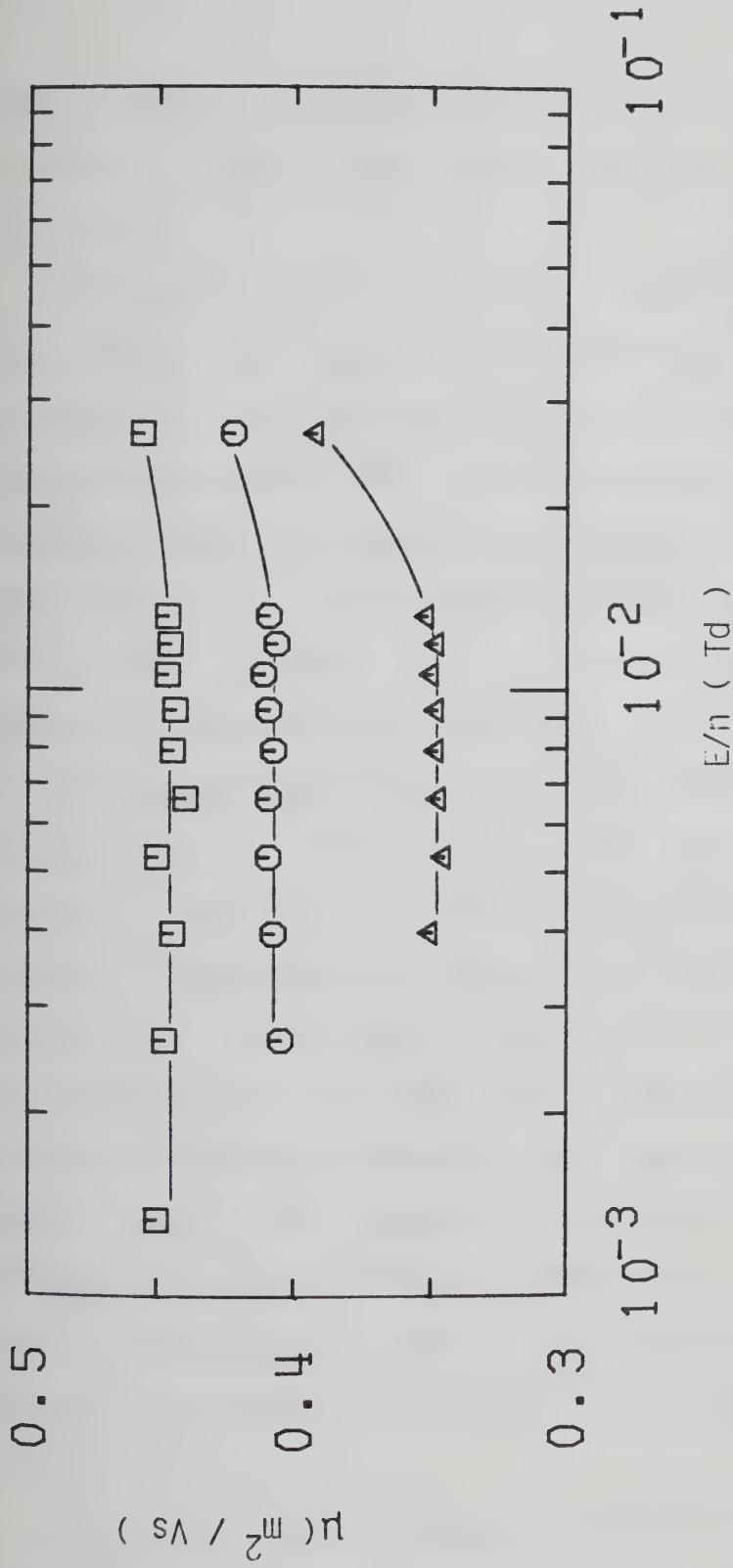


Figure III-1-4. Electron mobilities in CH_4 gas at $n = 7.5 \times 10^{25} \text{ molec/m}^3$ and different temperatures (K). Δ , 152.0; \circ , 228.8; \square , 293.0.

with temperature indicating that the threshold field increases. The low field mobility increases with temperature.

In Figures III-1-5 and -6 are reported measurements in the coexistence gas. The density increases with temperature. In this density region the low field mobility decreases by roughly the inverse ratio of the density. A change in density by more than an order of magnitude causes little effect on the threshold field which increases by approximately a factor of 2. However the corresponding change in temperature is only 46K.

In Figure III-1-7 is shown the effect of raising the temperature from 152.0K to 292.3K at $n = 5.5 \times 10^{26}$ molec/m³. The rate of change of the threshold field with density is approximately the same as that observed at lower densities. The threshold field approximately doubles as the temperature is increased by a factor of about 2. The low field mobility increases with temperature by a factor greater than that observed at lower densities. It increased by about 40% on doubling the temperature from 226K to 555K at $n = 2.95 \times 10^{25}$ molec/m³ while at this density the mobility at 292.3K is 75% larger than that at 152K.

The effect of a further increase in density by a factor of 5 is shown in Figures III-1-8 and III-1-9. The low field mobility drops by a factor of 6.5. The threshold

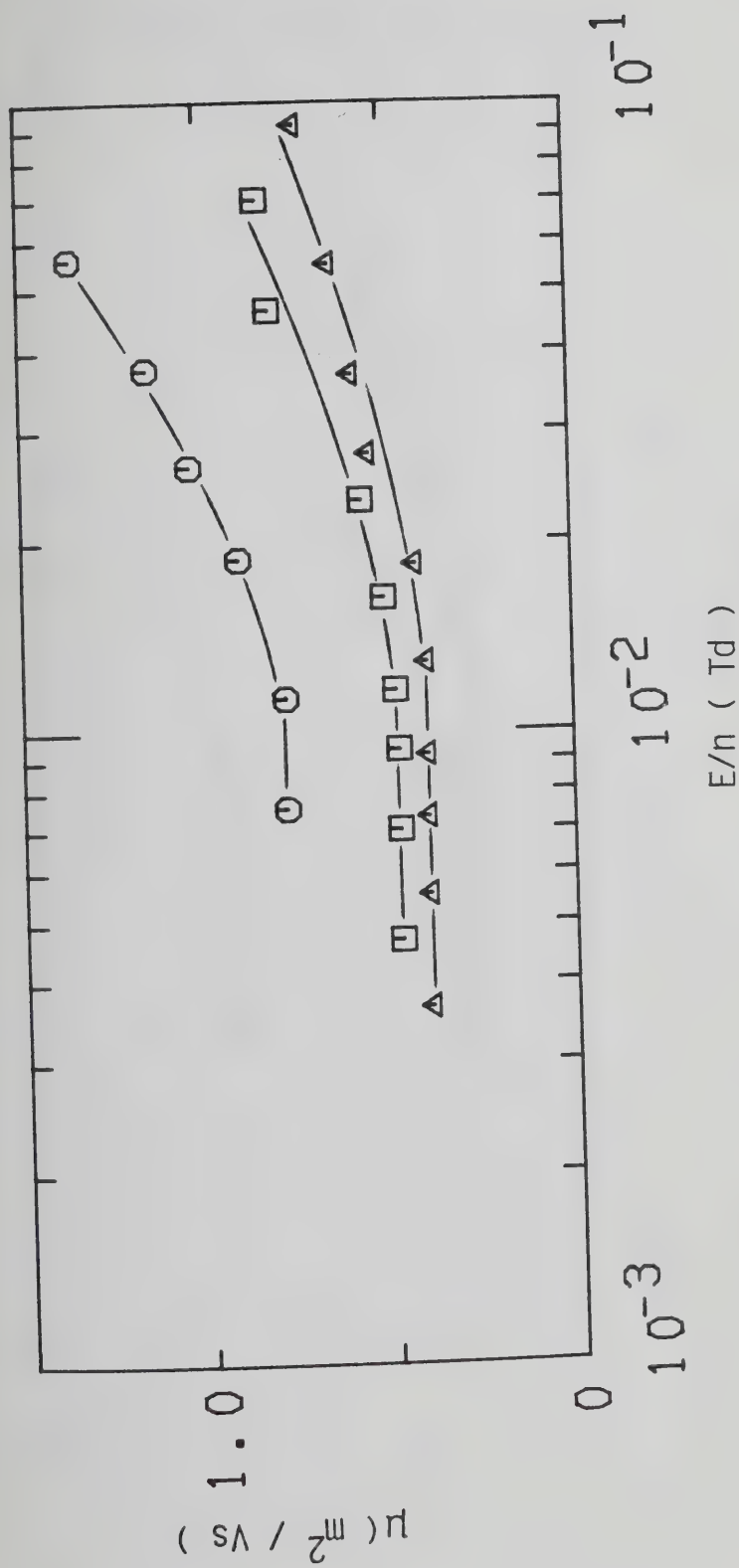


Figure III-1-5. Electron mobilities in saturated CH_4 vapor at different densities ($10^{25} \text{ molec/m}^3$) and temperatures (K). \bigcirc , 2.65, 100.5; \square , 4.3, 105.8; \triangle , 5.4, 108.7.

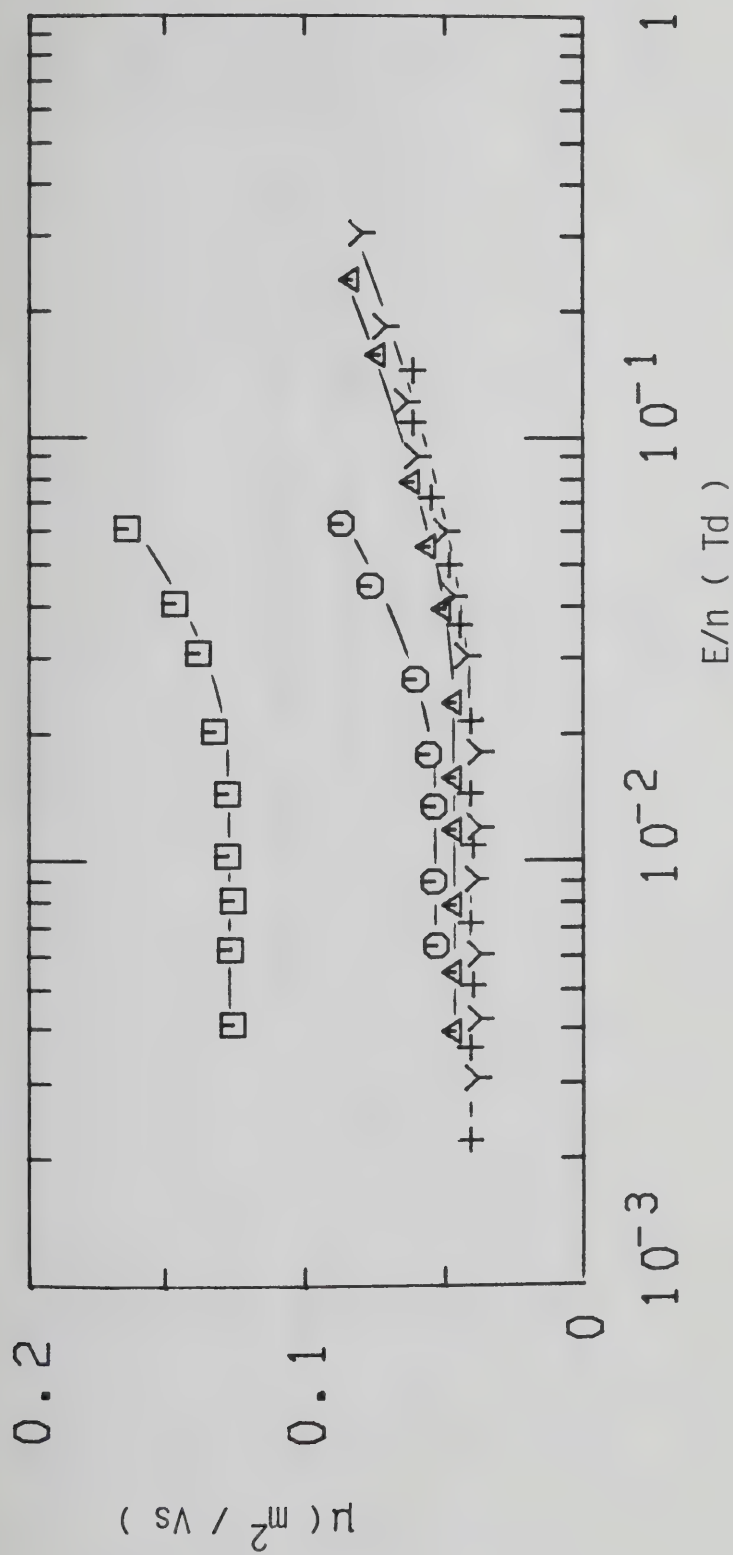


Figure III-1-6. Electron mobilities in saturated CH_4 vapor at different densities ($10^{26} \text{ molec/m}^3$) and temperatures (K). \square , 1.54, 123.5; \circ , 3.60, 139.0; Δ , 3.90, 140.5; +, 4.36, 142.5; γ , 5.2, 146.2.

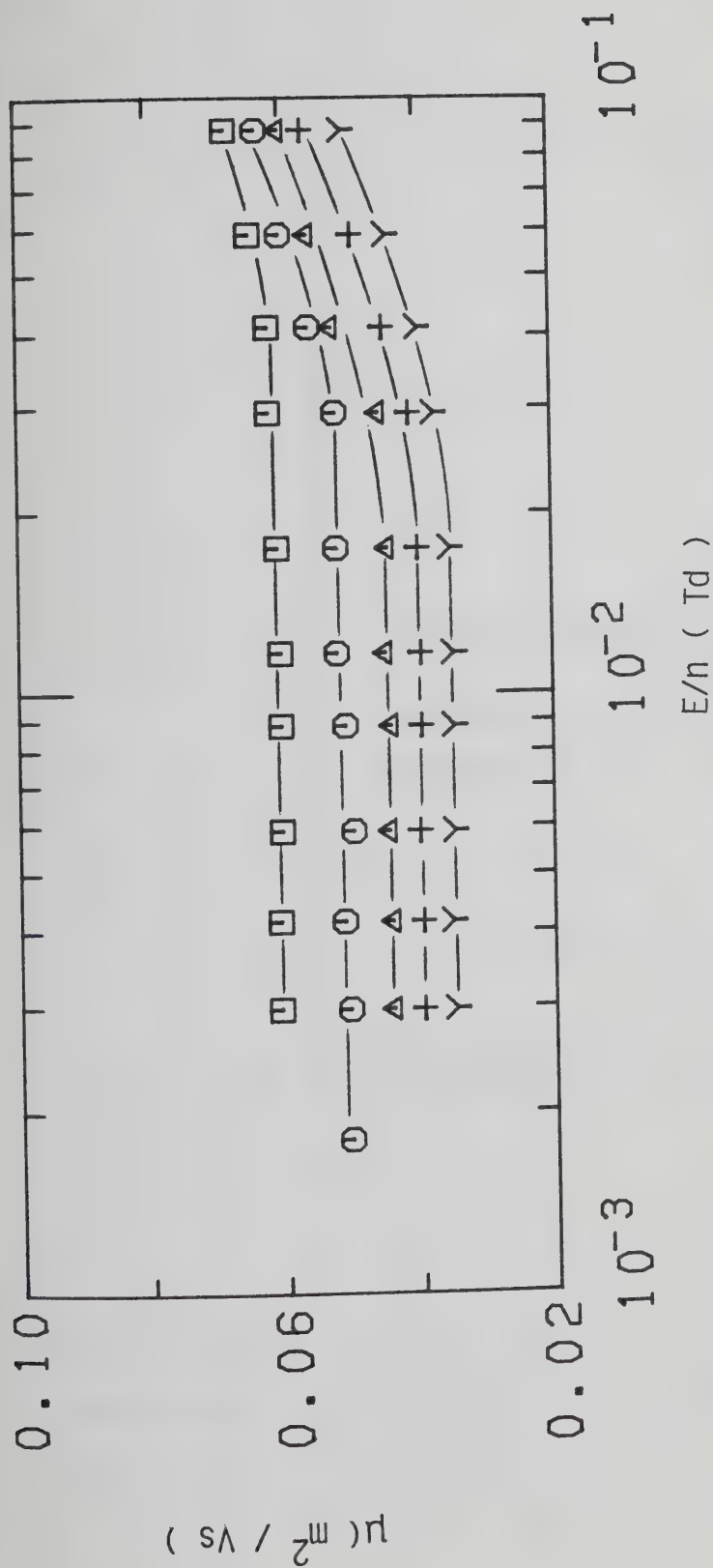


Figure III-1-7. Electron mobilities in CH_4 gas at $n = 5.5 \times 10^{26} \text{ molec/m}^3$ and different temperatures (K). Y, 152.0; +, 172.5; Δ , 201.5; O, 228.0; \square , 292.3

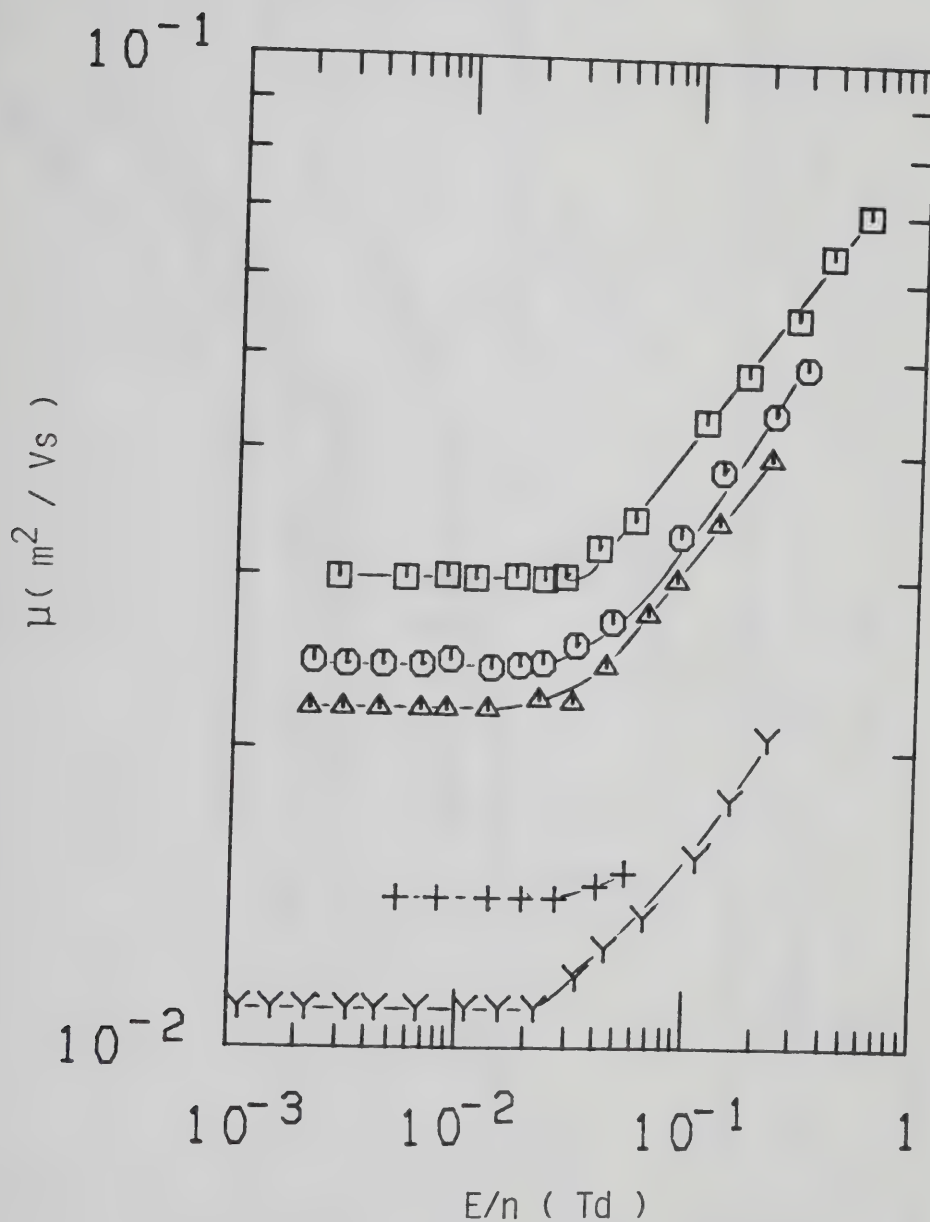


Figure III-1-8. Electron mobilities in saturated CH_4 vapor at different densities (10^{26} molec/ m^3) and temperatures (K). \square , 5.7, 149.0; \circ , 7.0, 152.8; Δ , 7.4, 154.0; +, 11.7, 164.6; Y, 14.2, 169.1.

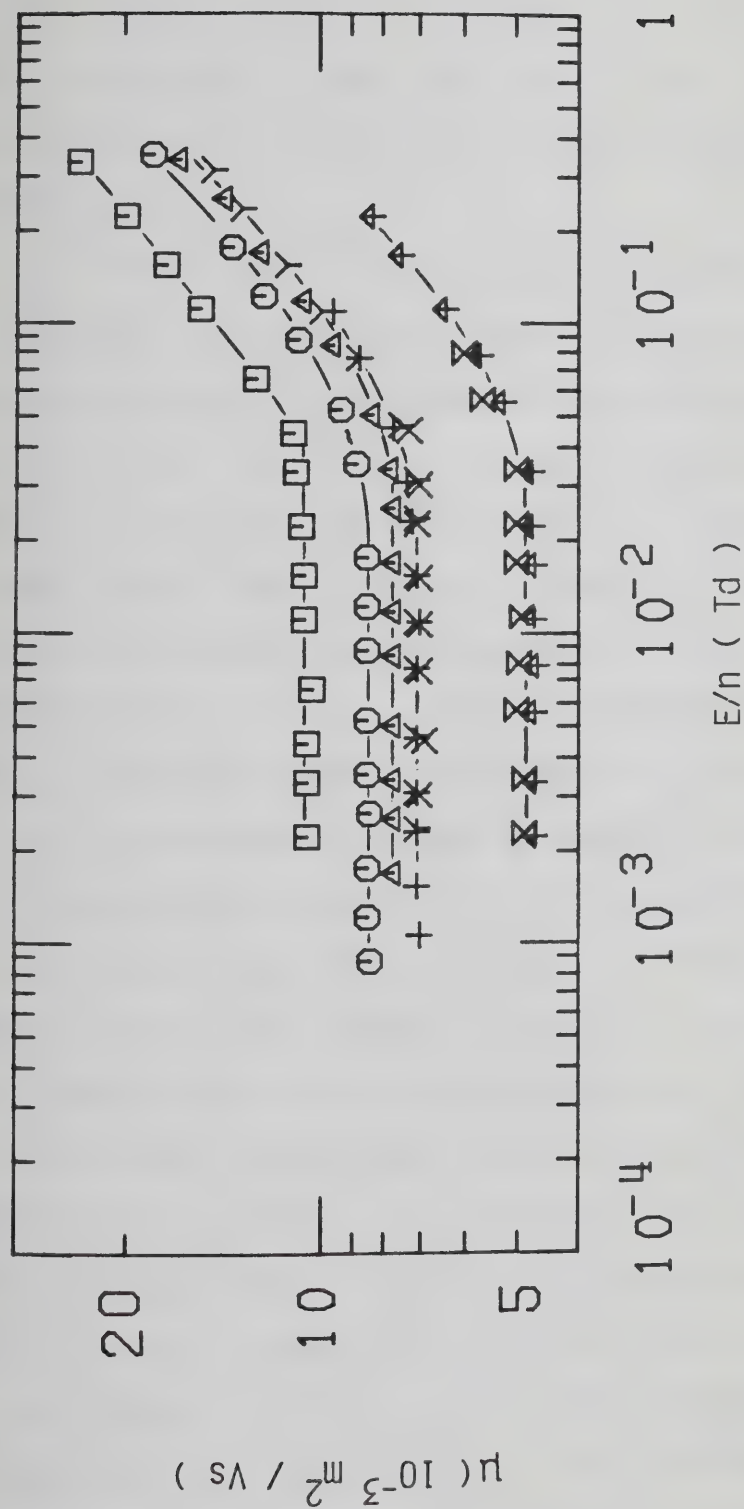


Figure III-1-9. Electron mobilities in saturated CH_4 vapor at different densities ($10^{27} \text{ molec/m}^3$) and temperatures (K). \square , 1.44, 169.5; \circ , 1.77, 174.8; Δ , 1.89, 175.7; $+$, 2.05, 177.4; γ , 2.06, 177.6; \times , 2.10, 178.1; \boxtimes , 2.80, 183.7; \uparrow , 2.85, 184.0.

field increases by 40% on going from $n = 5.7 \times 10^{26}$ molec/m³ and $T = 149.0\text{K}$ to $n = 28.5 \times 10^{26}$ molec/m³ and $T = 184\text{K}$.

In Figure III-1-10 are shown results obtained at $n = 29 \times 10^{26}$ molec/m³ at different temperatures. Not much change is observed in threshold field, which stays constant at $E/n \approx 0.04$ Td between 188.7K and 195.2K. At this density an increase of less than 4% in temperature causes the low field mobility to increase by about 25%. An increase in density to values close to the critical point has virtually no effect on the threshold field (Figures III-1-11 and III-1-12). The change in temperature is only 4K. The corresponding change in density is about 50%. The low field mobility decreases with increasing density.

In Figure III-1-13 is shown the effect of field and temperature on the electron mobility in the supercritical gas. The low field mobility increases by about a factor of 2 on increasing the temperature from 190.7K to 194.6K, a change of about 2%; $T_c = 190.6\text{K}$. In this temperature region the threshold field stays approximately constant with increasing temperature at $E/n \approx 0.03$ Td.

In Figure III-1-14 are shown measurements in the liquid phase at densities near the critical point. At densities up to $n \approx 8.9 \times 10^{27}$ molec/m³ the threshold field and low field mobility increase with density. At higher densities the low field mobility increases but the

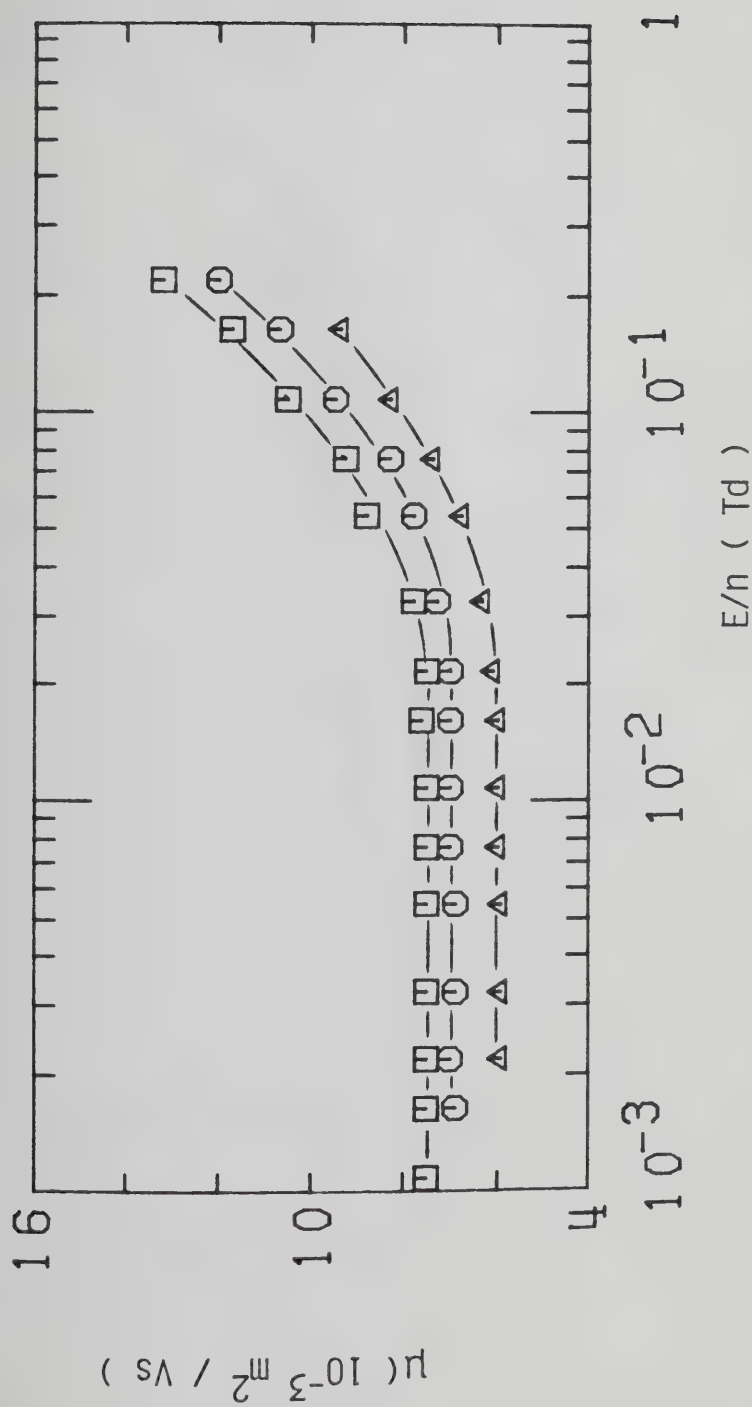


Figure III-1-10. Electron mobilities in CH_4 gas at $n = 29.0 \times 10^{26} \text{ molec/m}^3$ and different temperatures (K). Δ , 188.7; \circ , 192.0; \square , 195.2.

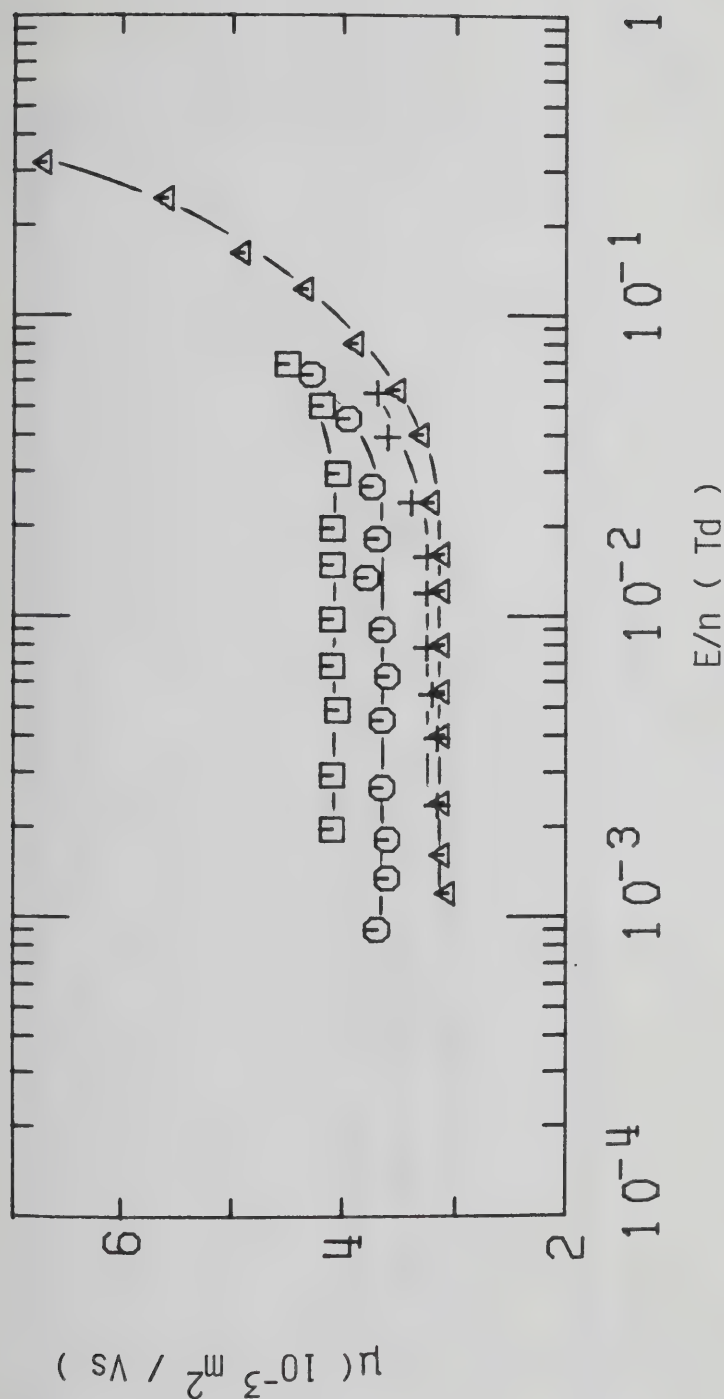


Figure III-1-11. Electron mobilities in saturated CH_4 vapor at different densities (10^{27} molec/m³) and temperatures (K). □, 3.20, 185.8; ○, 3.50, 187.1; Δ, 3.93, 188.5; +, 4.0, 188.7,

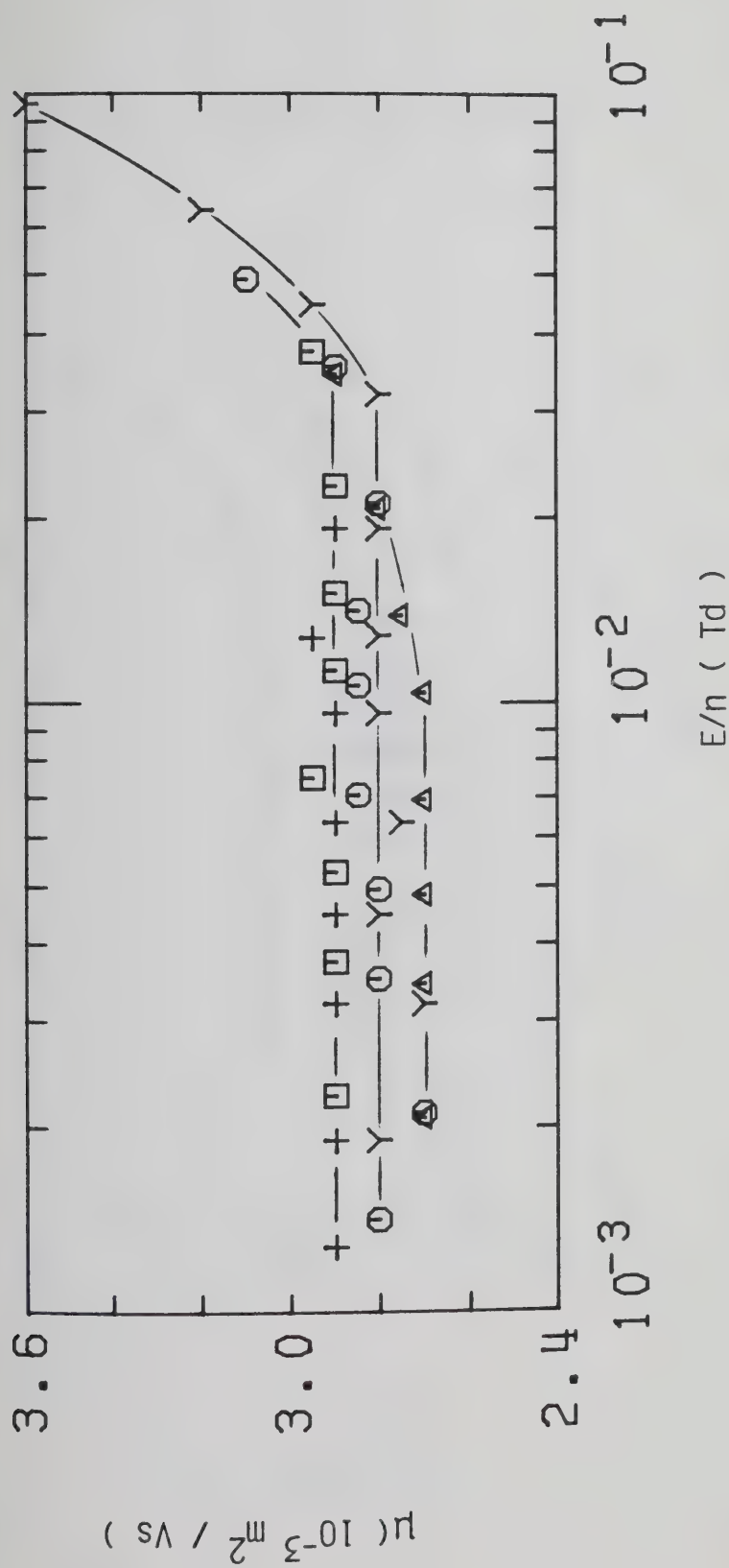


Figure III-1-12. Electron mobilities in saturated CH_4 vapor at different densities ($10^{27} \text{ molec/m}^3$) and temperatures (K). \square , 4.17, 189.1; \circ , 4.45, 189.7; \triangle , 4.55, 189.9; +, 4.92, 190.2; Y, 4.92, 190.2

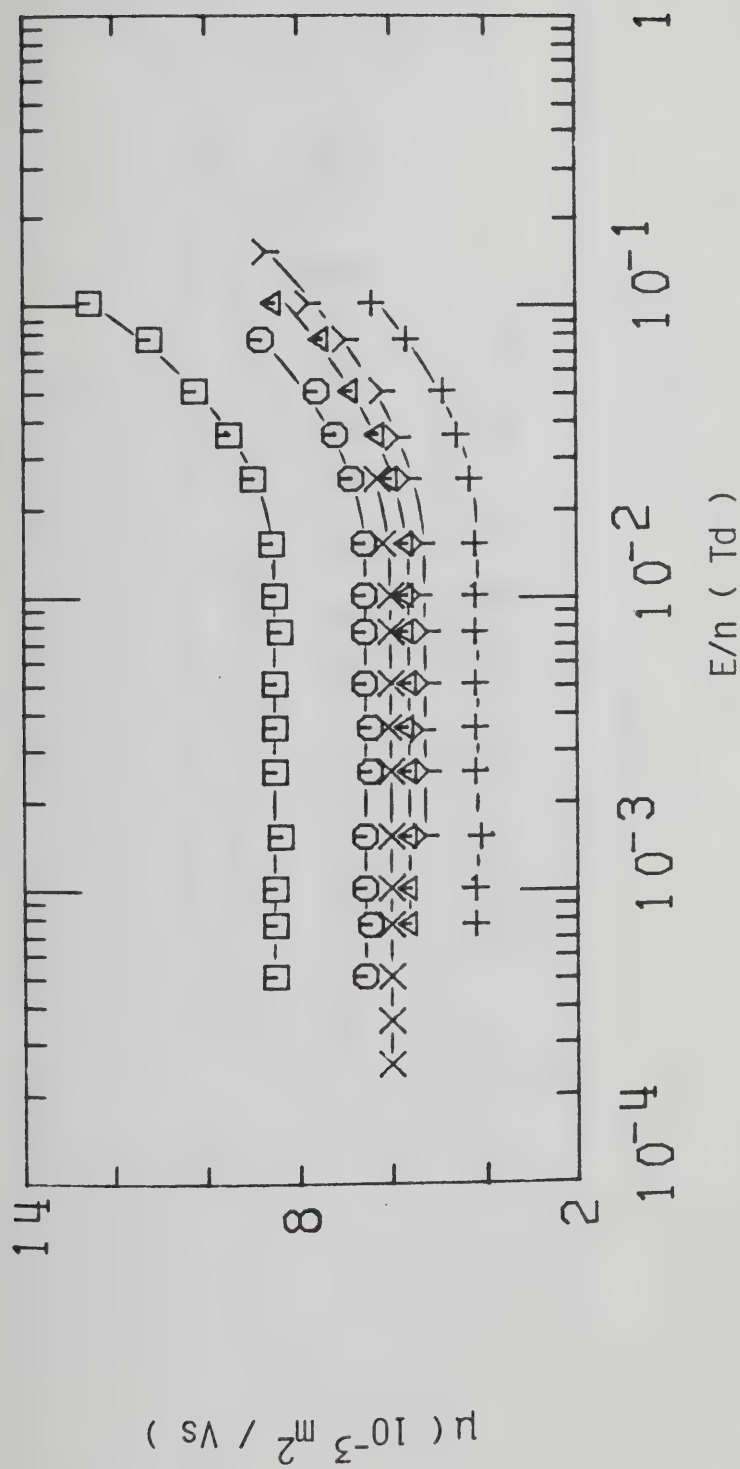


Figure III-1-13. Electron mobilities in supercritical CH_4 gas at $n_c = 6.1 \times 10^{27}$ molec/ m^3 and different temperatures (K). +, 190.7; Y, 191.2; Δ , 191.4; X, 192.4; O, 192.9; \square , 194.6. $T_c = 190.6$.

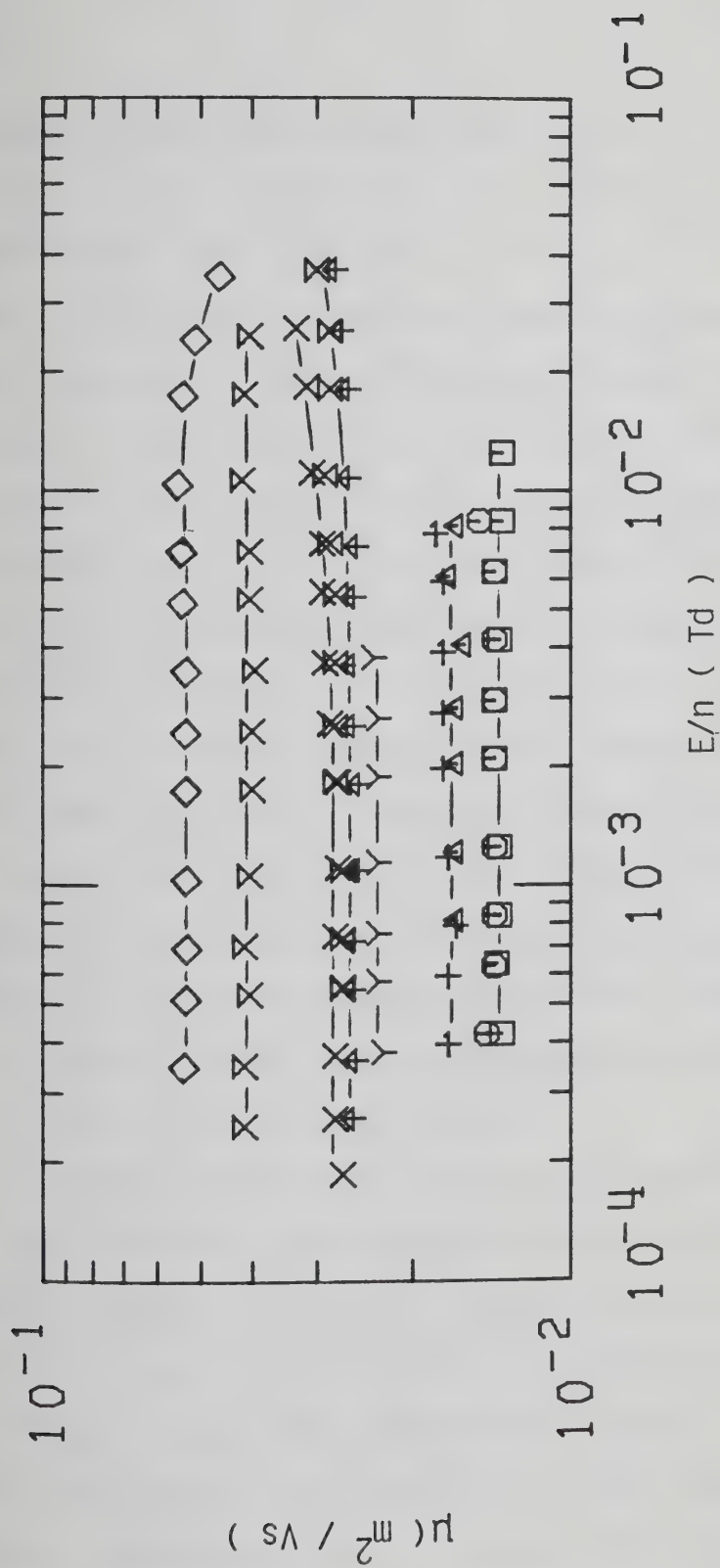


Figure III-1-14. Electron mobilities in liquid CH_4 at different densities ($10^{27} \text{ molec/m}^3$) and temperatures (K). \square , 7.5, 190.3; \circ , 7.5, 190.2; \triangle , 7.8, 189.9; +, 8.0, 189.7; y, 8.3, 189.1; x, 8.5, 188.7; \boxtimes , 8.6, 188.5; \uparrow , 8.6, 188.2; \diamond , 9.1, 186.5.

threshold field decreases. At $n = 9.1 \times 10^{27}$ molec/m³ the effect of the field on the electron mobility is the opposite of that observed in the gas. In this density region the mobility decreases with increasing field above the threshold. The transition between the two effects occurs in the liquid at $n \approx 8.9 \times 10^{27}$ molec/m³. By increasing the density of the liquid the low field mobility increases and the threshold field decreases (Figure III-1-15). A further increase in density (Figure III-1-16) produces a decrease in low field mobility while the threshold field remains approximately constant at $E/n \approx 6$ mTd. This value is smaller than any value observed in the gas. On approaching the triple point (Figure III-1-17) the low field mobility decreases with density up to $n \approx 15 \times 10^{27}$ molec/m³ and then it increases with increasing density. The threshold field does not appreciably change in spite of the change in temperature of 50K.

In Figure III-1-18 is shown the effect of temperature on the threshold field along several isochores. In this density range the field at which electron heating becomes noticeable is a linear function of temperature. The effect of density along the coexistence curve on the threshold field is reported in Figure III-1-19. The points at low density correspond to a temperature of approximately 100K. The points in the gas at high density correspond to a temperature of about 180K. In this region the electron

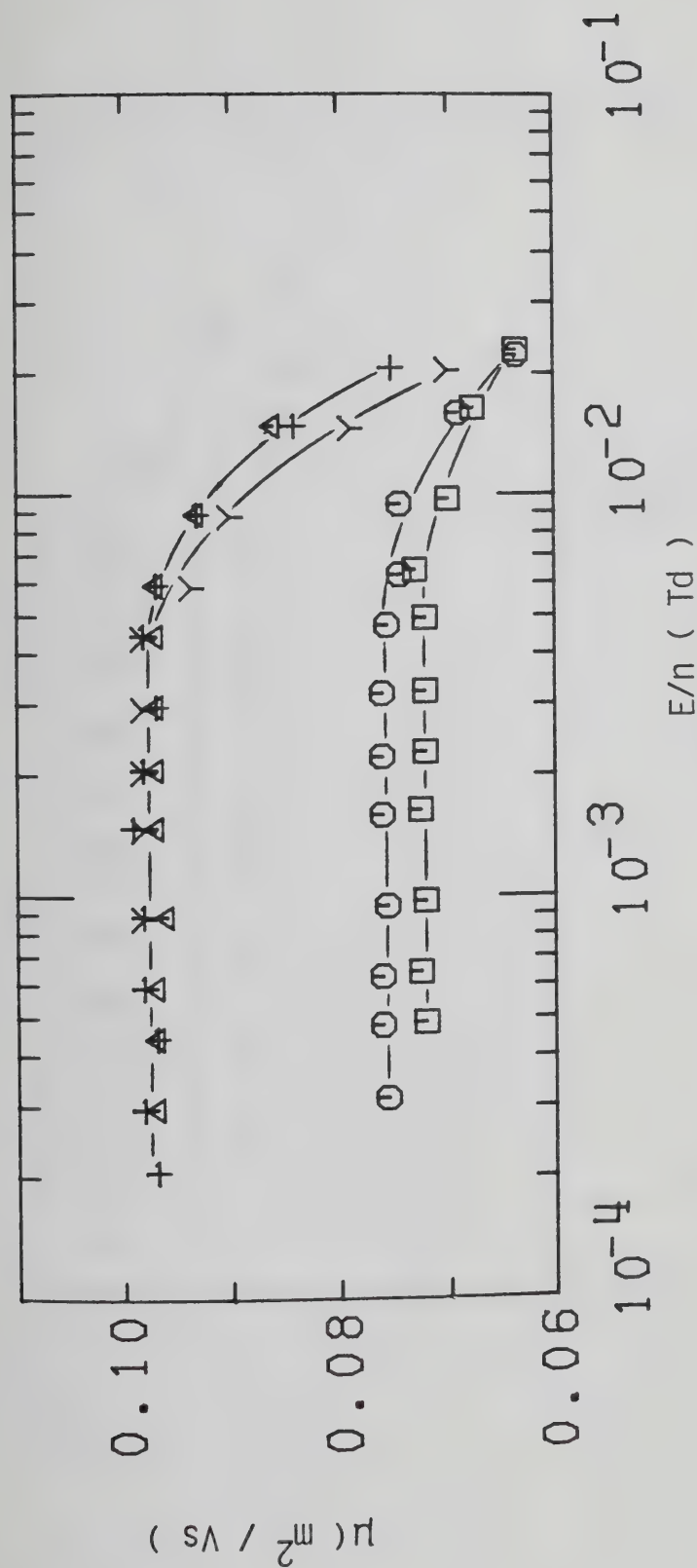


Figure III-1-15. Electron mobilities in liquid CH_4 at different densities (10^{27} molec/ m^3) and temperatures (K). \square , 9.7, 183.7; \circ , 9.9, 183.0; Δ , 10.7, 178.1; $+$, 10.7, 177.6; γ , 10.8, 177.4.

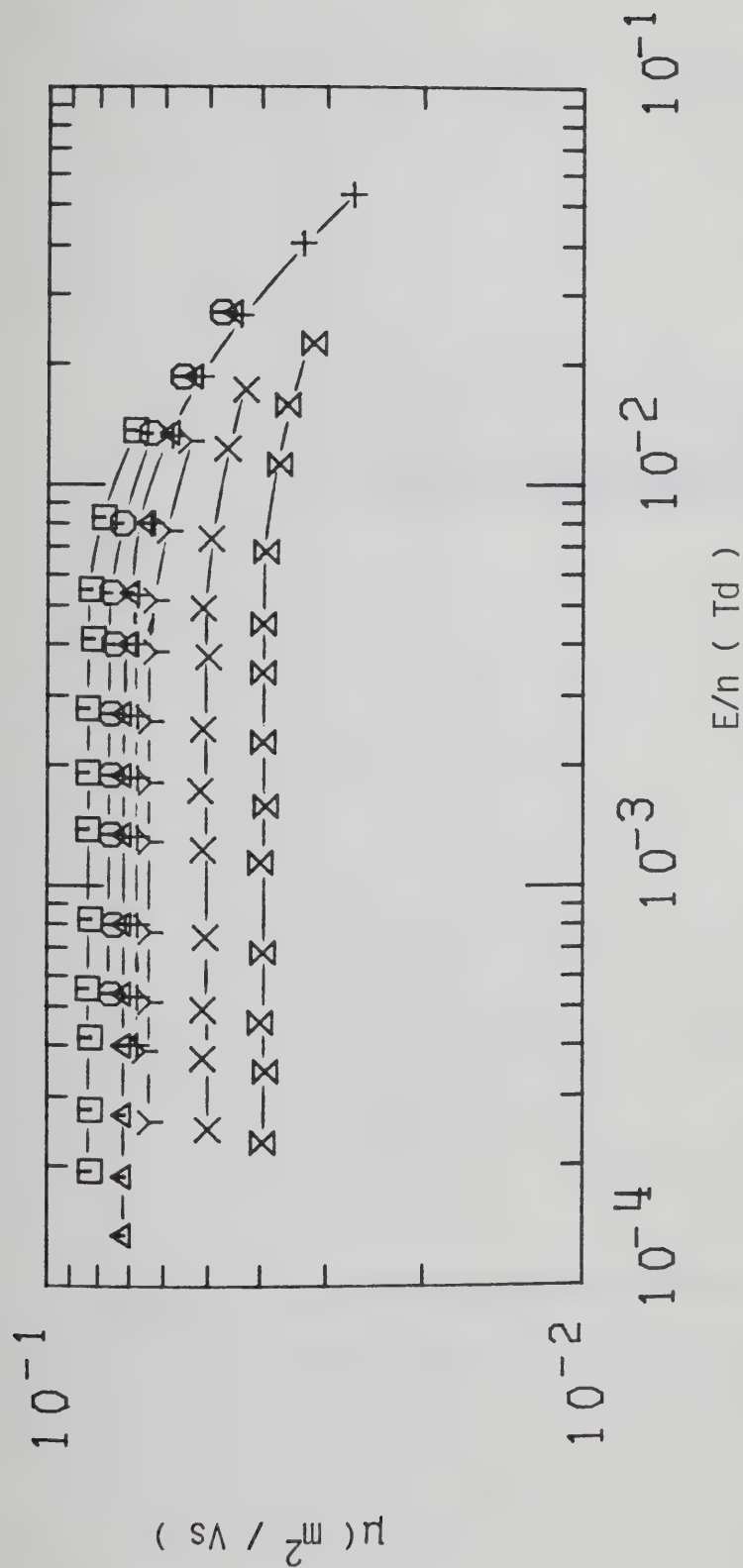


Figure III-1-16. Electron mobilities in liquid CH_4 at different densities

(10^{27} molec/ m^3) and temperatures (K). \square , 11.3, 173.0; \circ , 11.7, 169.5;

Δ , 11.7, 169.1; $+$, 12.0, 166.6; γ , 12.2, 164.6; \times , 12.6, 160; \boxtimes , 13.6, 146.5.

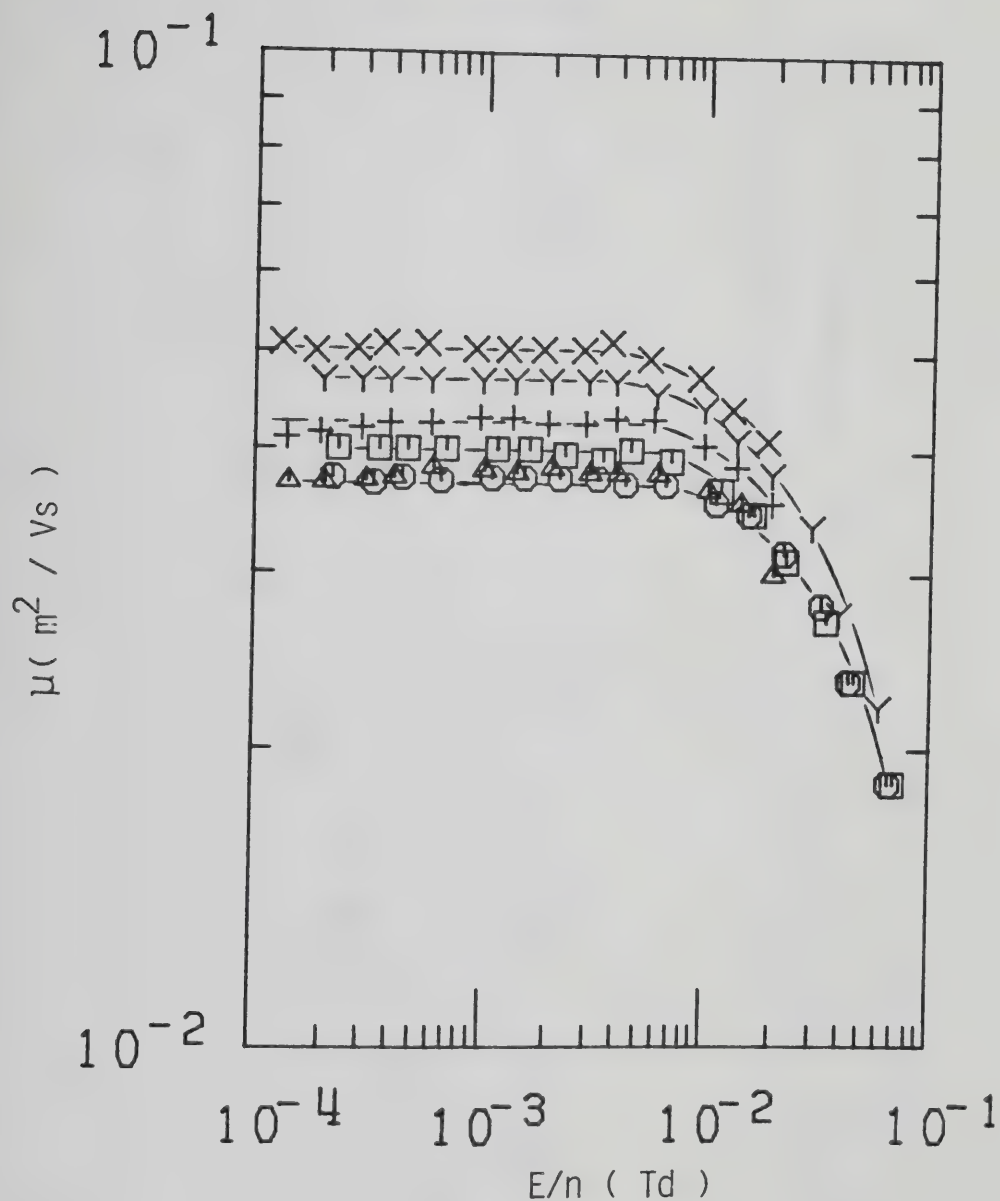


Figure III-1-17. Electron mobilities in liquid CH_4 at different densities (10^{27} molec/ m^3) and temperatures (K). \square , 14.0, 143.0; \bigcirc , 14.7, 130.3; \triangle , 15.5, 118.5; +, 16.2, 104.5; Y, 16.4, 101.5; X, 17.0, 92.0.

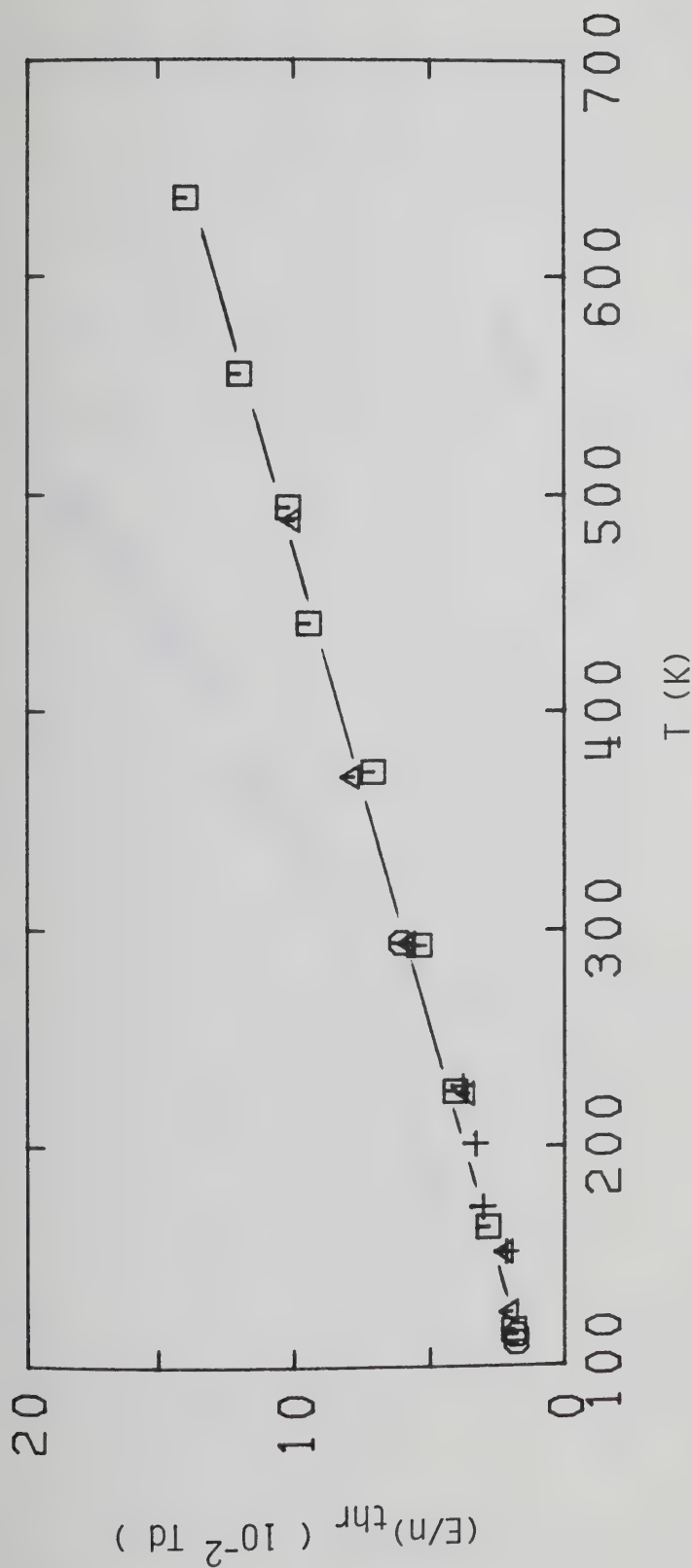


Figure III-1-18. Electric field threshold, $(E/n)_{thr}$, for electron heating in CH_4 gas at different densities ($10^{25} \text{ molec/m}^3$) as a function of temperature.

\square , 2.95; \circ , 5.3; Δ , 5.8; $+$, 55.

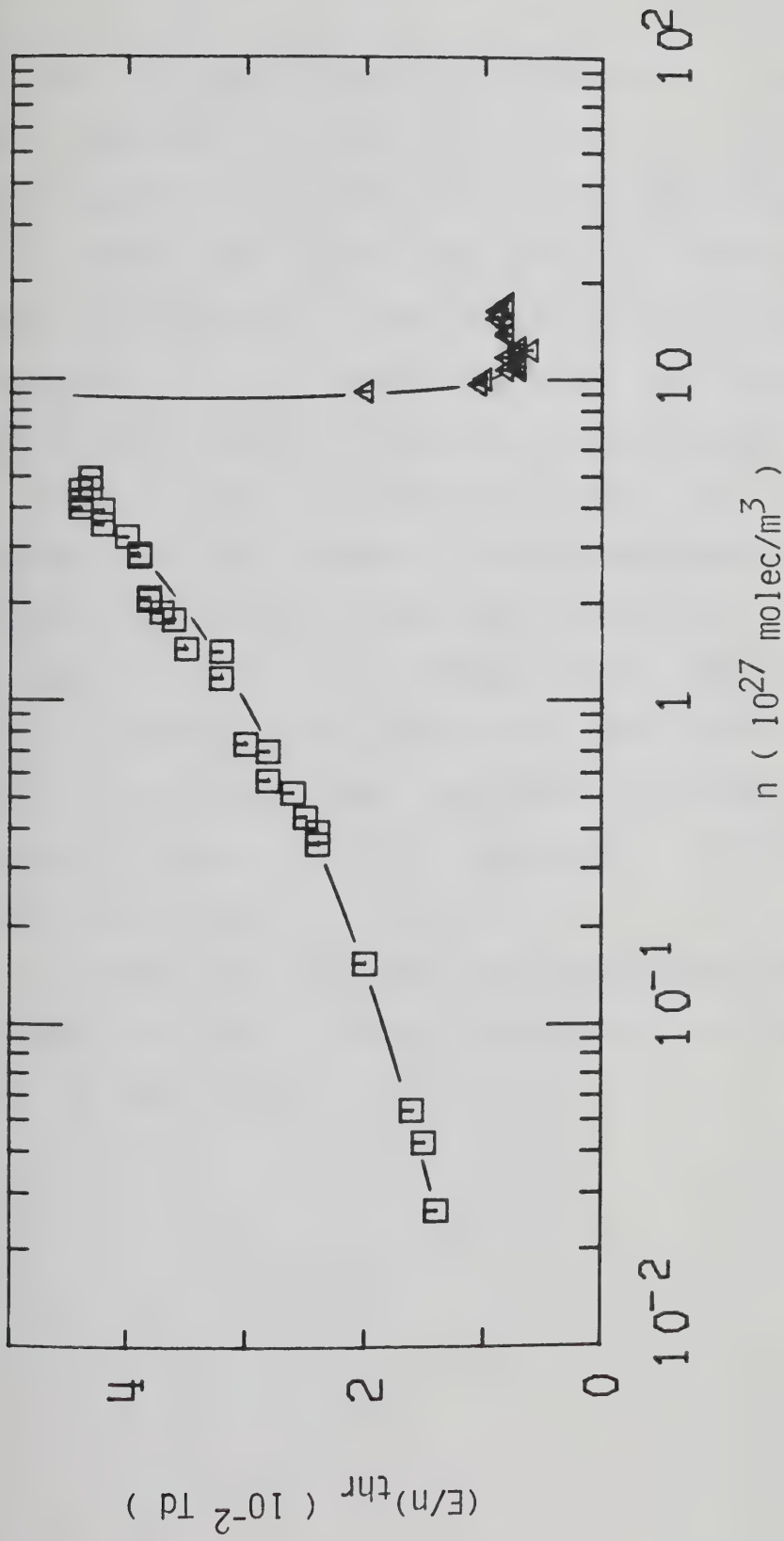


Figure III-1-19. Electric field threshold, $(E/n)_{thr}$, for electron heating in coexistence vapor and liquid CH_4 as a function of density.
 \square , $d_\mu / d(E/n) > 0$; Δ , $d_\mu / d(E/n) < 0$

mobility increases above the threshold. The threshold field increases by a factor of about 3. At a density of approximately 8.9×10^{27} molec/m³ the field effect changes sign. Above this value the electron mobility decreases above the threshold. The threshold field decreases with density up to $n \approx 10 \times 10^{27}$ molec/m³ to a value of about 0.08 Td and at higher densities it remains constant.

The results in Figures III-1-1 to III-1-5 were obtained with low pressure type conductance cells. The electrode separations were 1.002 ± 0.002 cm. All the other gas phase results were obtained with high pressure type cells. The electrode separations were 0.318 ± 0.007 cm. Liquid phase data were obtained in liquid type high pressure cells. The electrode separations were 0.316 ± 0.004 cm.

A listing of the low field mobilities and threshold voltages at the different temperatures and densities is given in Table III-1.

TABLE III-1
Summary of Electron Results for CH₄^a

T (K)	n (10 ²⁶ m ⁻³)	μ (m ² /Vs)	nμ [10 ²⁵ (Vsm) ⁻¹]	(E/n) _{thr} (mTd)	dμ/d(E/n)
116.5	0.295	0.80	2.36	20	+
163.7	0.295	0.95	2.80	28	+
226.0	0.295	1.03	3.04	41	+
292.5	0.295	1.13	3.33	54	+
372.6	0.295	1.24	3.66	71	+
441.2	0.295	1.33	3.92	92	+
494.0	0.295	1.38	4.08	100	+
555	0.295	1.43	4.20	120	+
636	0.295	1.48	4.35	140	+
110.0	0.53	0.43	2.28	18	+
113.6	0.53	0.46	2.41	18	+
293.5	0.53	0.64	3.40	60	+
124.0	0.58	0.41	2.37	20	+
151.8	0.58	0.44	2.55	22	+
225.0	0.58	0.51	2.98	36	+
294.0	0.58	0.58	3.36	58	+
370.5	0.58	0.62	3.62	80	+
488.5	0.58	0.70	4.05	100	+
152.0	0.75	0.35	2.62		+
228.8	0.75	0.41	3.07		+
293.0	0.75	0.45	3.35		+
100.5	0.265	0.78	2.07	14	+
105.8	0.43	0.475	2.03	15	+
108.7	0.54	0.40	2.17	16	+
123.5	1.54	0.127	1.96	20	+
139.0	3.60	0.054	1.93	24	+
140.5	3.90	0.046	1.79	24	+

(continued....)

Table III-1 continued

142.5	4.36	0.0405	1.96	25	+
146.2	5.2	0.0370	1.92	26	+
152.0	5.5	0.0348	1.91	22	+
172.5	5.5	0.0397	2.18	30	+
201.5	5.5	0.0445	2.45	33	+
228.0	5.5	0.051	2.81	38	+
292.3	5.5	0.061	3.36	56	+
149.0	5.7	0.0300	1.71	28	+
152.8	7.0	0.0245	1.72	28	+
154.0	7.4	0.0220	1.62	30	+
164.6	11.7	0.0142	1.66	32	+
169.1	14.2	0.0110	1.56	32	+
169.5	14.4	0.0106	1.53	35	+
174.8	17.7	0.0085	1.50	36	+
175.7	18.9	0.0077	1.46	37	+
177.4	20.5	0.0071	1.46	38	+
177.6	20.6	0.0071	1.46	38	+
178.1	21.0	0.0070	1.47	38	+
183.7	28.0	0.00490	1.37	39	+
184.0	28.5	0.00465	1.33	39	+
188.7	29.0	0.0060	1.73	40	+
192.0	29.0	0.0070	2.03	40	+
195.2	29.0	0.0075	2.18	37	+
185.8	32.0	0.0041	1.31	40	+
187.1	35.0	0.00370	1.22	42	+
188.5	39.3	0.00310	1.22	42	+
188.7	40.0	0.0032	1.28		+
189.1	41.7	0.00290	1.21	44	+
189.7	44.5	0.00282	1.25	44	+

(continued....)

Table III-1 continued

189.9	45.5	0.00281	1.25	44	+
190.2	49.2	0.00290	1.43	43	+
190.2	49.2	0.00285	1.40	43	+
190.7	61 ^b	0.0042	2.56	28	+
191.1	61 ^b	0.0051	3.11	27	+
191.2	61 ^b	0.0053	3.23	29	+
191.4	61 ^b	0.0057	3.45	29	+
192.4	61 ^b	0.0066	4.00	29	+
192.9	61 ^b	0.0061	3.69	30	+
193.0	61 ^b	0.0064	3.90	30	+
194.6	61 ^b	0.0085	5.19	28	+
190.3	75	0.0137	10.3		
190.2	75	0.0140	10.5		
189.9	78	0.0165	12.8		
189.7	80	0.0175	14.0		
189.1	83	0.0230	19.1		
188.7	85	0.0275	23.4		
188.5	86	0.0275	23.7	40	+
188.2	86	0.0256	22.0	40	+
187.1	89	0.0405	36.0		~0
186.5	91	0.0535	48.7	20	-
183.7	97	0.072	70	10	-
183.0	99	0.076	75	10	-
178.1	107	0.097	104	8	-
177.6	107	0.098	105	7	-
177.4	108	0.098	106	7	-
173.0	113	0.083	93	7	-
169.5	117	0.075	88	8	-
169.1	117	0.071	83	7	-

(continued....)

Table III-1 continued

166.6	120	0.067	80	7	-
164.6	122	0.064	78	6	-
160.0	126	0.051	64	7	-
146.5	137	0.0395	54	8	-
143.0	140	0.0398	56	8	-
130.3	147	0.0373	55	8	-
118.5	155	0.0378	59	9	-
104.5	162	0.0425	69	9	-
101.5	164	0.047	77	8	-
92.0	170	0.051	86	8	-

- a. The results appear in this table in the same order as the figures. They are give in order of increasing density.
- b. $n_c = 6.1 \times 10^{27}$ molec/m³ , $T_c = 190.6K$
 Some of these points have been omitted from Figure III-1-13 to avoid overcrowding.

2. CH₃D

In Figure III-2-1 is shown the variation of the electron mobility with electric field strength and temperature in the low density gas at $n = 2.35 \times 10^{25}$ molec/m³. As in the case of CH₄, the mobility is field independent at low fields and increases above a threshold value. This value is a linear function of temperature. The mobility curves tend to merge at $E/n \approx 0.8$ Td. The value of the low field mobility increases with temperature.

Increasing the density to $n = 3.3 \times 10^{25}$ molec/m³ (Figure III-2-2) and $n = 4.9 \times 10^{25}$ molec/m³ (Figure III-2-3) does not change these effects. In Figure III-2-4 is reported the effect of temperature on the threshold field in this density region. At $T \approx 100$ K the threshold value of E/n is about 0.01 Td ($\text{Td} = 10^{-21} \text{ m}^2\text{V/molec}$). It is about 0.15 Td at $T \approx 600$ K. Increasing the density of the coexistent vapor by a factor of 26 (Figures III-2-5, 6, 7) causes the low field value of the mobility to drop by a factor of 34. The corresponding change in temperature of 50K causes the value of the threshold field to increase by a factor of 2. In Figure III-2-8 the effect of raising the temperature from 154.8K to 294.0K at a fixed gas density $n = 6.0 \times 10^{26}$ molec/m³ is illustrated. The low field mobility increases by 70%. At the lowest density $n = 2.35 \times 10^{25}$ molec/m³ the same change in temperature

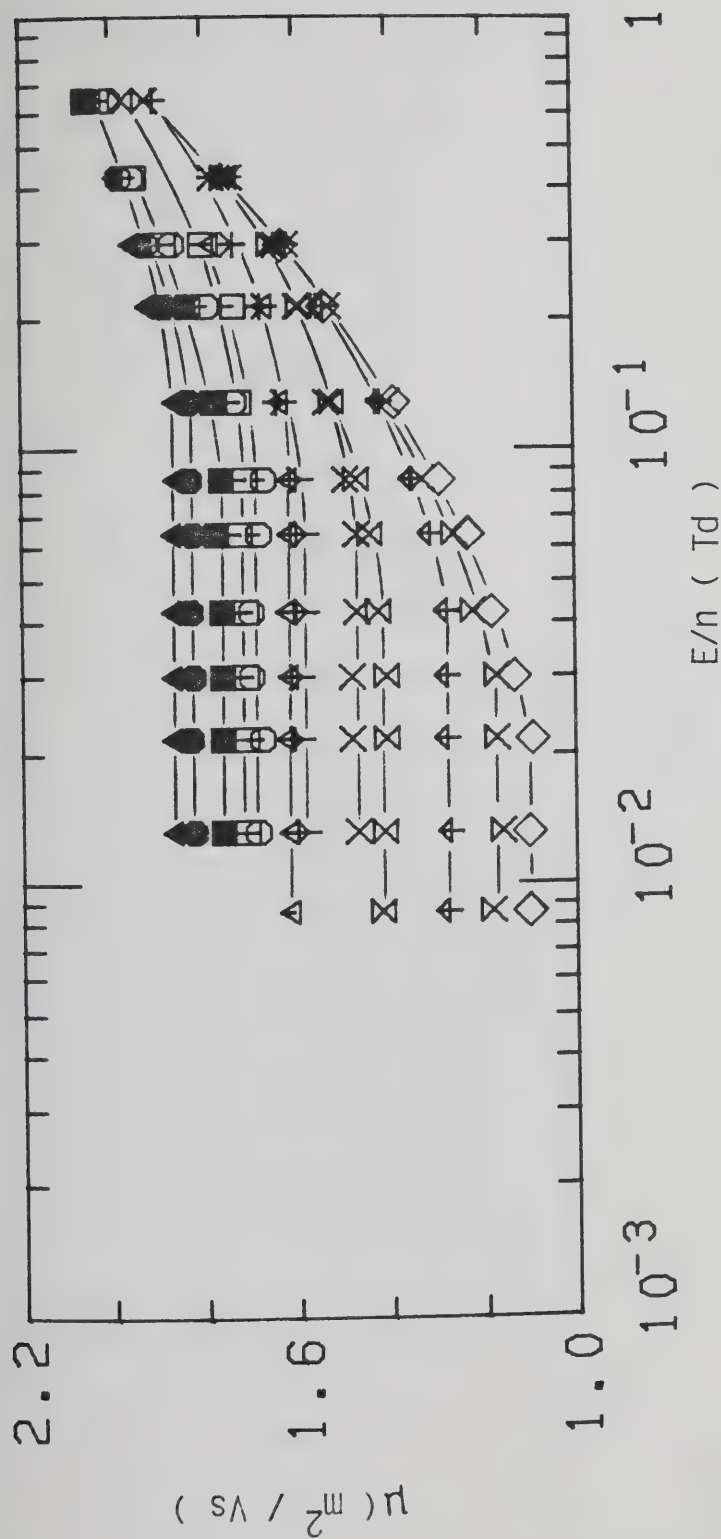


Figure III-2-1. Electron mobilities in CH_3D gas at $n = 2.35 \times 10^{25} \text{ molec/m}^3$ and different temperatures (K). \diamond , 146.3; \uparrow , 185.5; \times , 225.7; \times , 293.7; Y , 337.8; Δ , 385.8; \circ , 435.0; \square , 474.0; \blacksquare , 504.0; \bullet , 535.7; \blacktriangle , 589; \blacktriangle , 637.

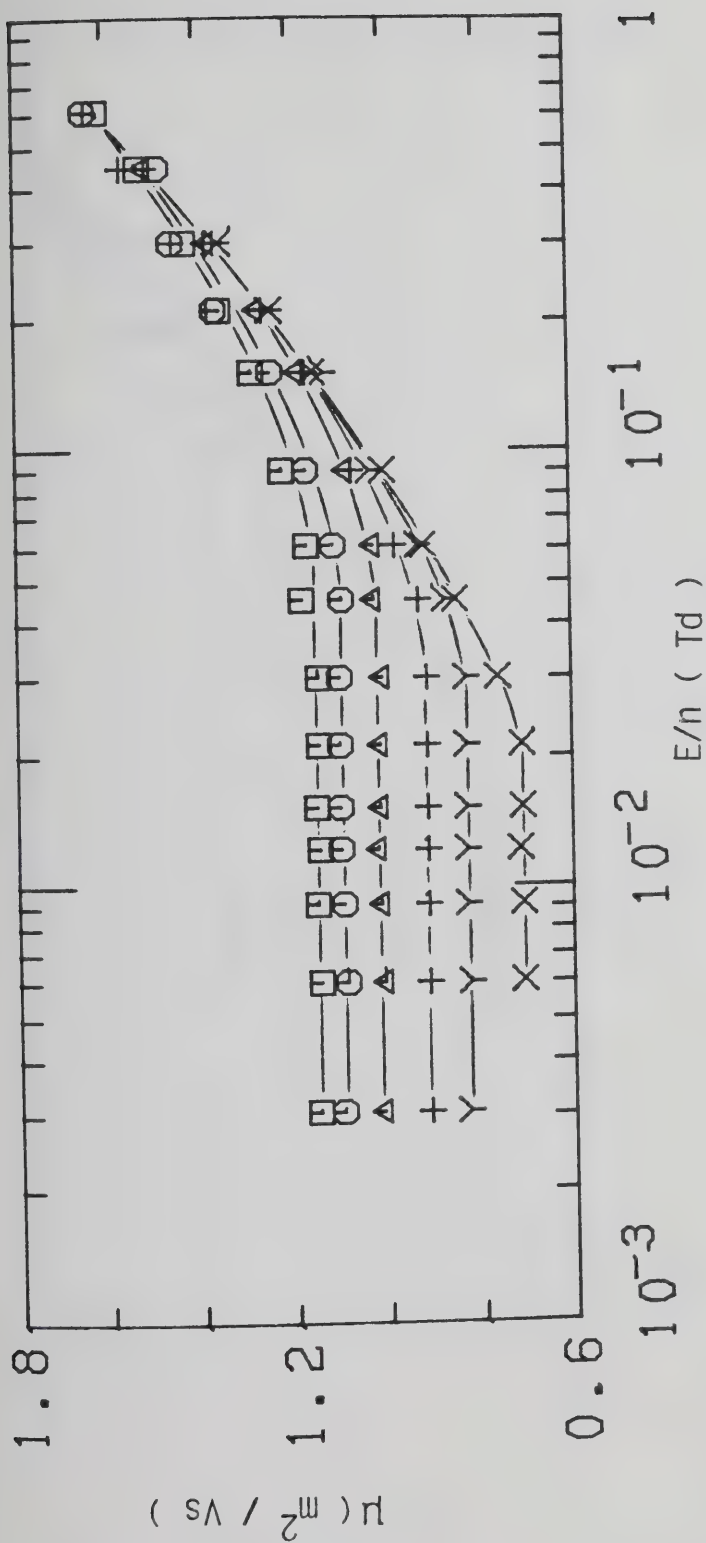


Figure III-2-2. Electron mobilities in CH_3D gas at $n = 3.30 \times 10^{25} \text{ molec/m}^3$ and different temperatures (K). X, 112.5; Y, 168.8; +, 220.7; Δ , 294.0; O, 359.0; \square , 407.

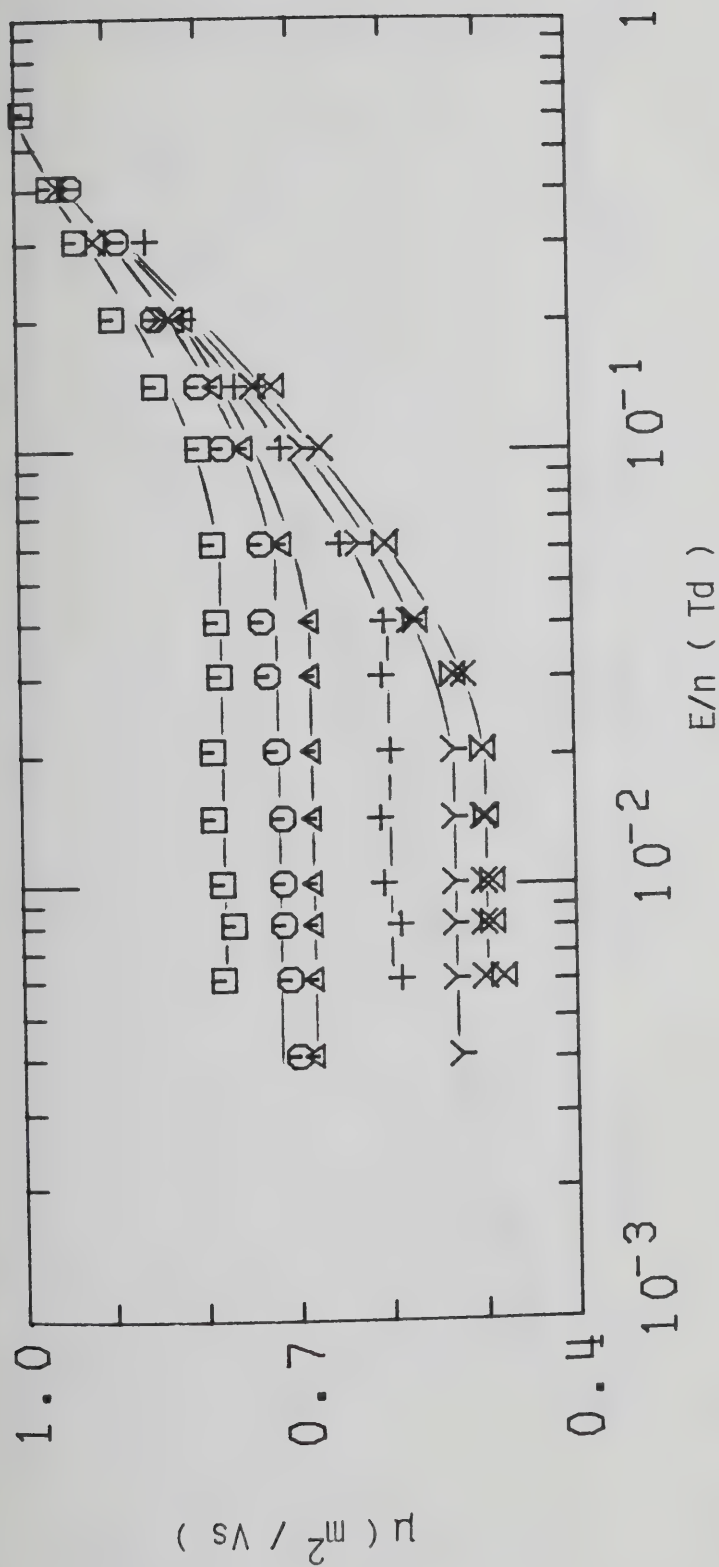


Figure III-2-3. Electron mobilities in CH_3D gas at $n = 4.9 \times 10^{25} \text{ molec/m}^3$ and different temperatures (K). Σ , 109.3; \times , 110.5; γ , 159.5; $+$, 216.2; Δ , 293.8; \circ , 360.5; \square , 423.0.

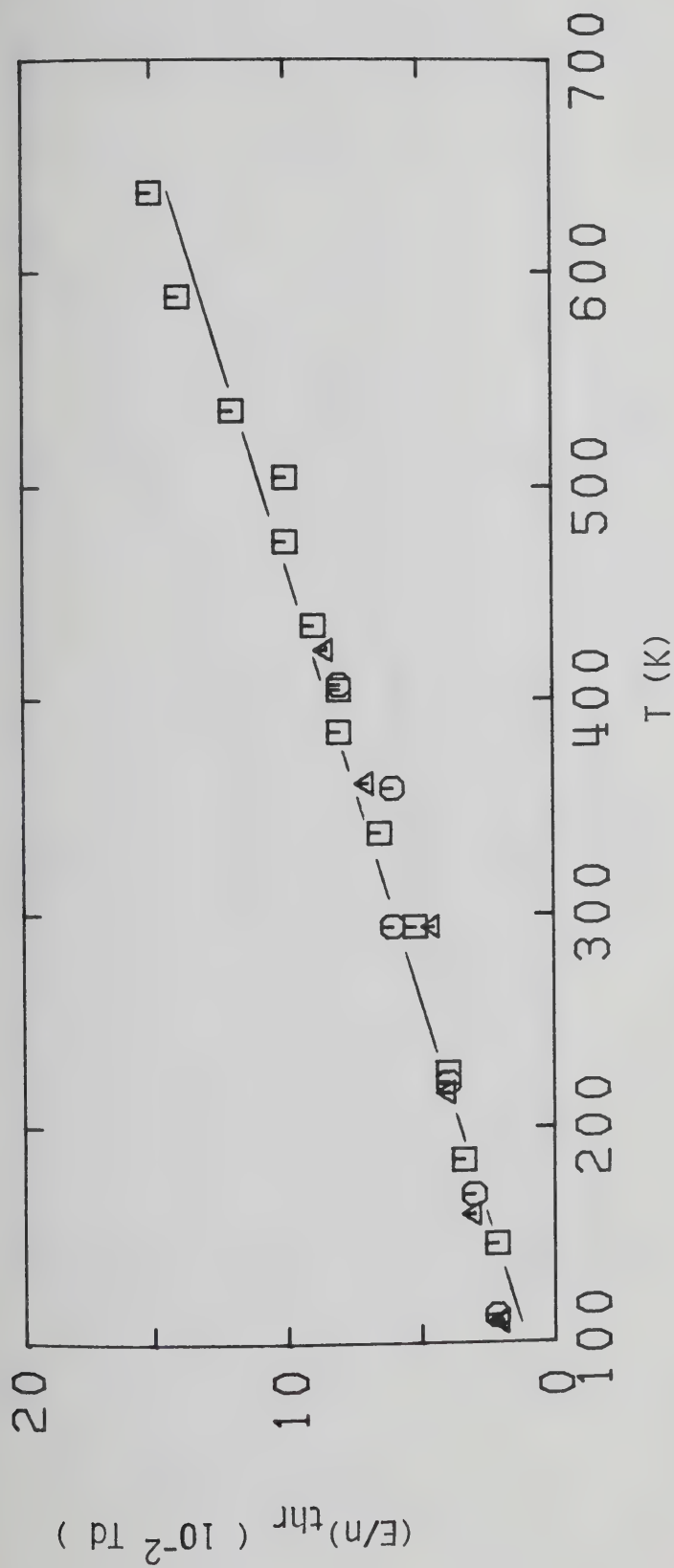


Figure III-2-4. Electric field threshold, $(E/n)_{thr}$, for electron heating in CH_3D gas at different densities (10^{25} molec/m³) as a function of temperature. \square , 2.35; \circ , 3.30; \triangle , 4.9.

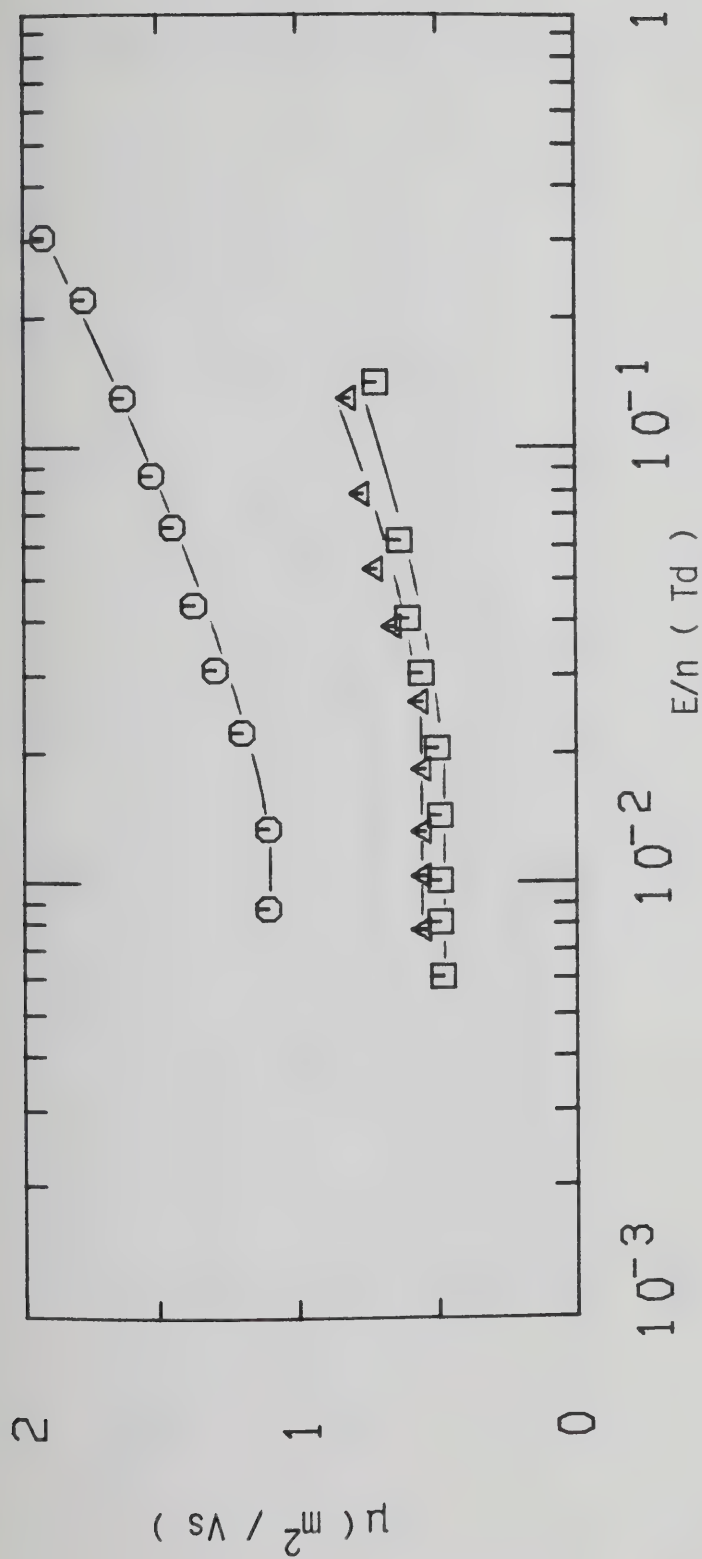


Figure III-2-5. Electron mobilities in saturated CH_3D vapor at different densities ($10^{25} \text{ molec}/\text{m}^3$) and temperatures (K). \bigcirc , 2.30, 99.0; Δ , 3.8, 104.5; \square , 4.9, 109.3.

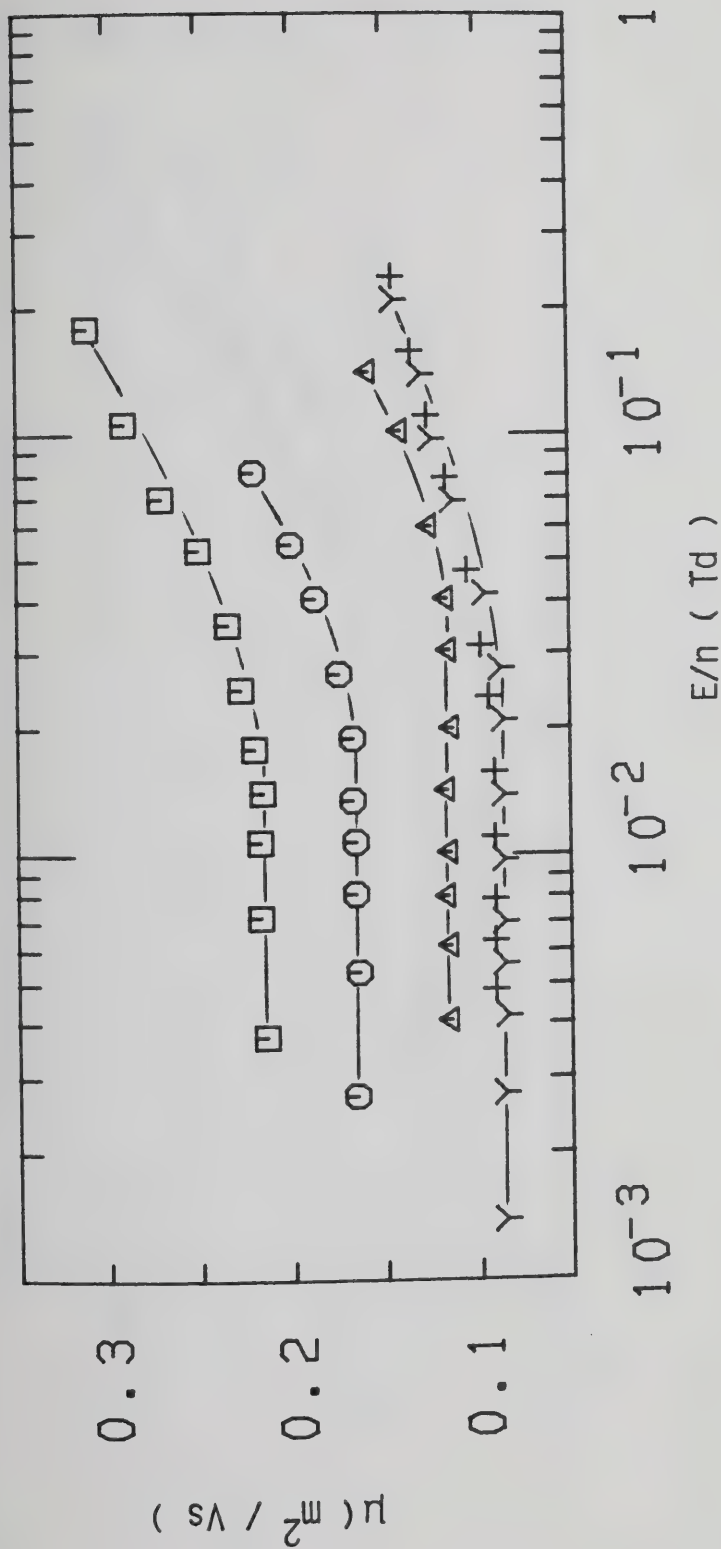


Figure III-2-6. Electron mobilities in saturated CH_3D vapor at different densities (10^{26} molec/ m^3) and temperatures (K). \square , 0.89, 115.7; \circ , 1.16, 119.5; Δ , 1.56, 124.0; $+$, 2.00, 128.5; γ , 2.26, 130.5.

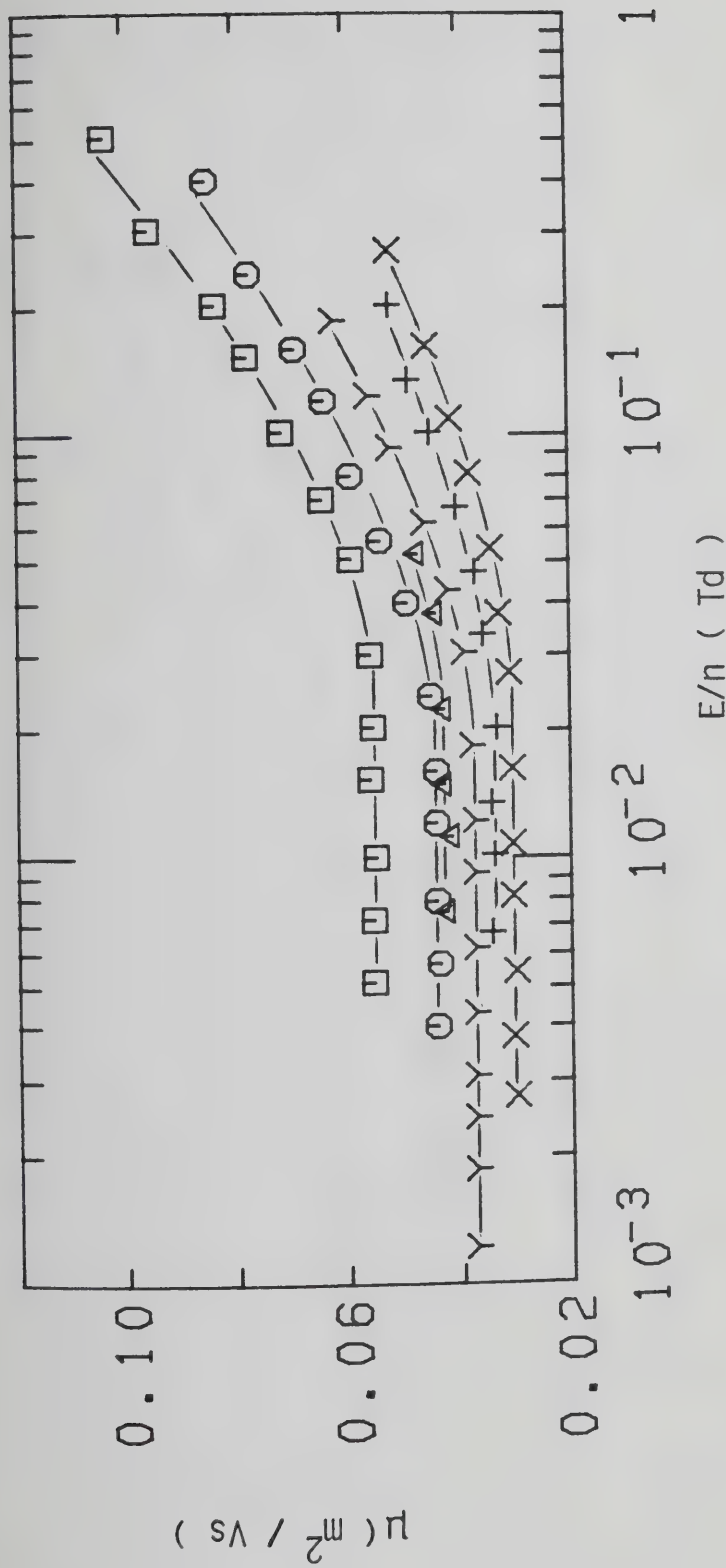


Figure III-2-7. Electron mobilities in saturated CH_3D vapor at different densities ($10^{26} \text{ molec/m}^3$) and temperatures (K). \square , 3.11, 136.5; \circ , 3.94, 141.0; Δ , 4.30, 142.7; +, 4.80, 145.5; γ , 5.1, 146.4; \times , 5.8, 149.5.

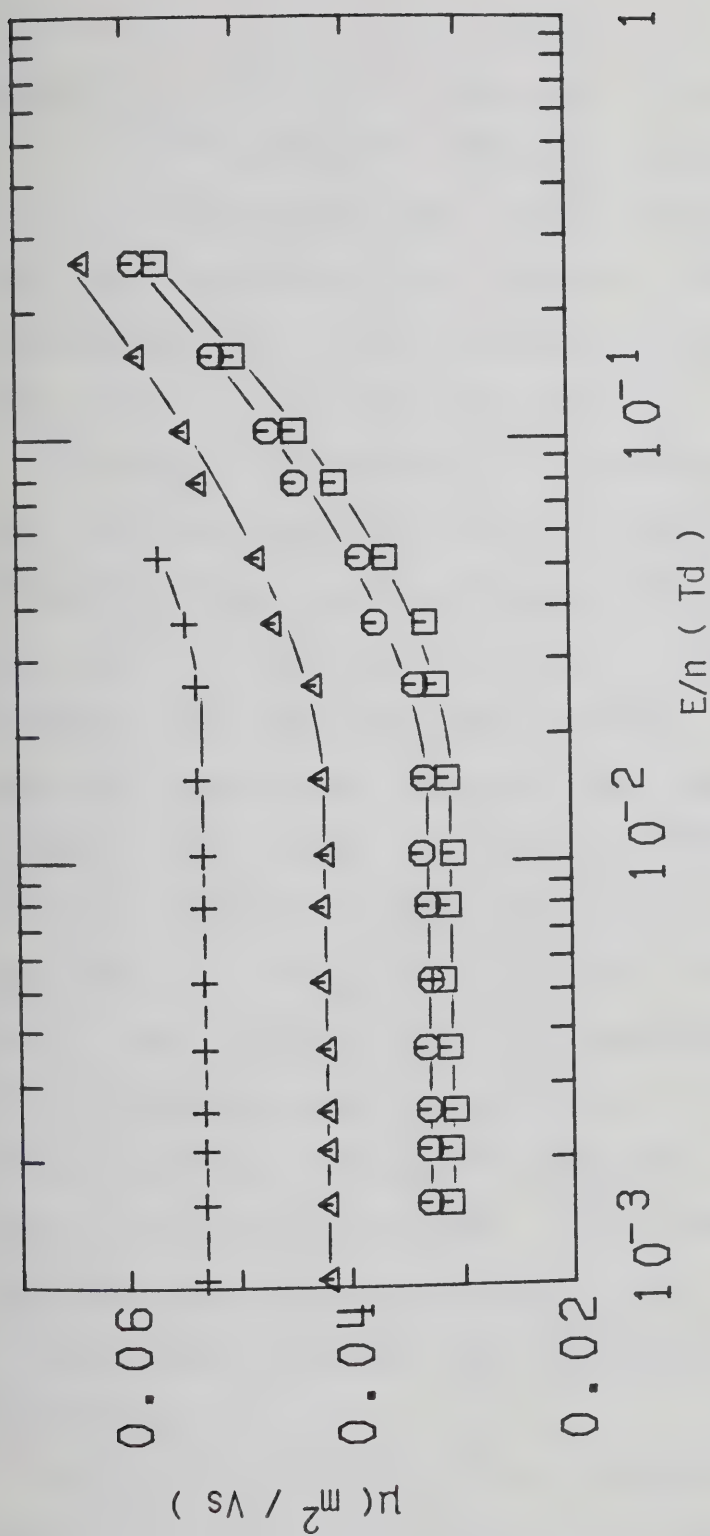


Figure III-2-8. Electron mobilities in CH_3D gas at $n = 6.0 \times 10^{26} \text{ molec/m}^3$ and different temperatures (K). □, 154.8; ○, 170.0; Δ, 215.8, +, 294.0.

produced an increase in mobility of only about 30%. At $n = 6.7 \times 10^{26}$ molec/m³ (Figure III-2-9) the low field mobility increases by 90% between 153.9K and 293.0K. At these two densities the threshold field increases with temperature from a value of about 0.026 Td at 153.9K to a value of about 0.05 Td at 294.0K.

A change in density of the coexistent vapor from 7.5×10^{26} molec/m³ to 10.7×10^{26} molec/m³ (Figure III-2-10) causes the low field mobility to decrease from 2.14×10^{-2} m²/Vs to 1.41×10^{-2} m²/Vs. No effect is noticeable on the threshold field. The corresponding change in temperature is only ~8K. Heating the gas from 171.0K to 210.0K at $n = 15 \times 10^{26}$ molec/m³ (Figure III-2-11) produces an increase in low field mobility of about 60%. In Figure III-2-12 are shown the effects of density and temperature on approaching the critical point. The coexistent vapor density increases from 23.6×10^{26} molec/m³ to 55×10^{26} molec/m³. The corresponding change in temperature is 10K. These changes lower the low field value of the mobility from 6.4×10^{-3} m²/Vs to 3.25×10^{-3} m²/Vs and increase the threshold field from 0.034 Td to 0.040 Td.

The effects of raising the temperature from 186.9K to 195.2K at $n = 27 \times 10^{26}$ molec/m³ and from 191.3K to 193.3K along the critical isochor are shown in Figures III-2-13 and III-2-14. At the lower density the low field value of

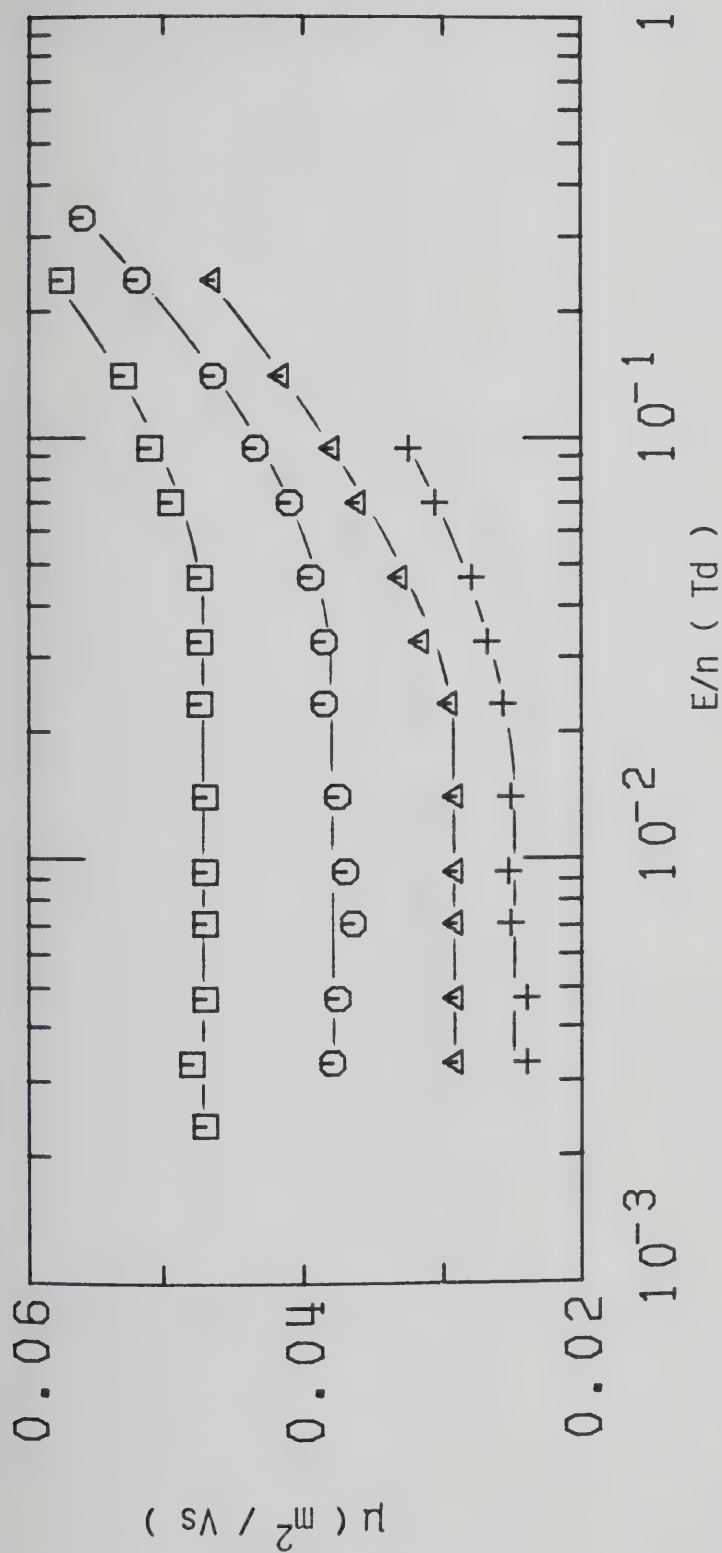


Figure III-2-9. Electron mobilities in CH_3D gas at $n = 6.7 \times 10^{26} \text{ molec/m}^3$ and different temperatures (K). + , 153.9; Δ , 172.5; \circ , 219.3; \square , 293.0.

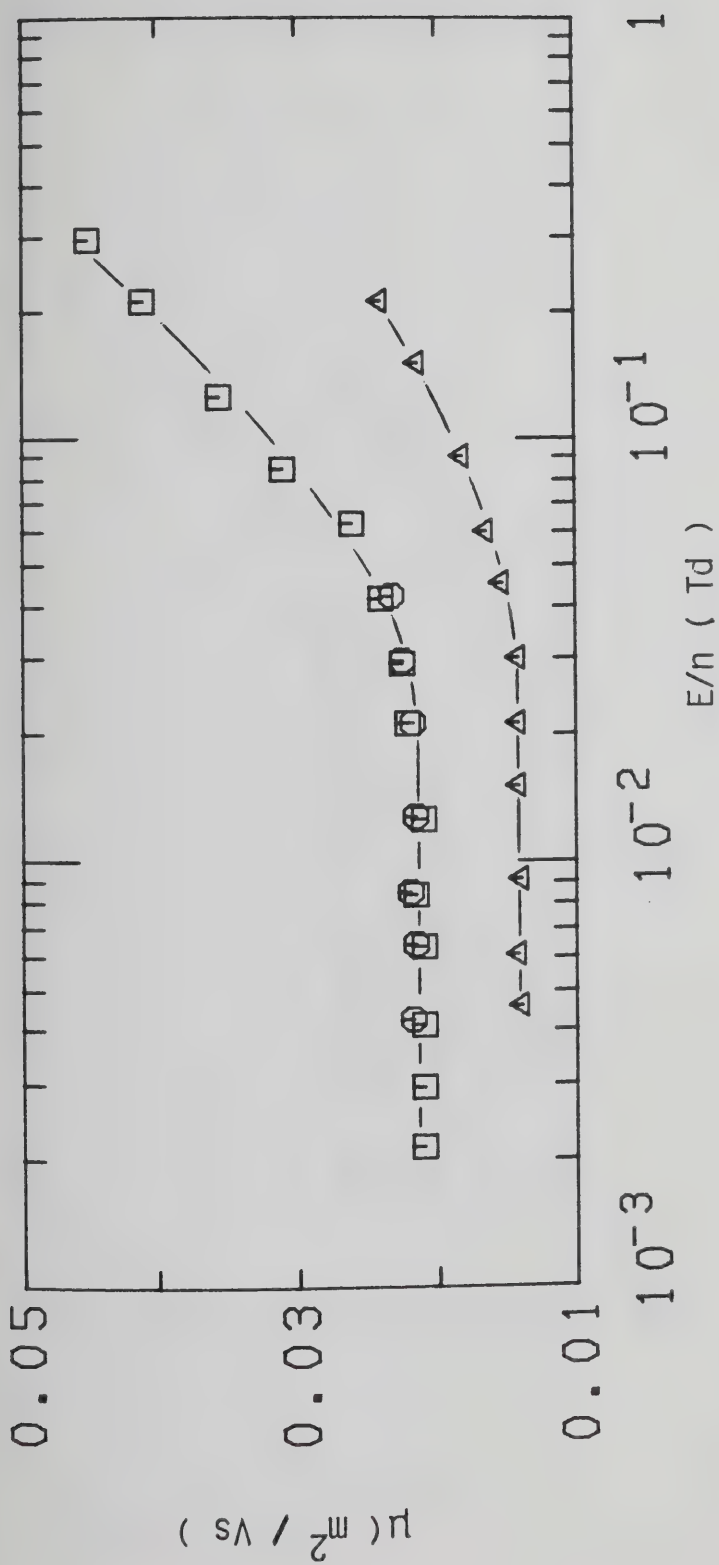


Figure III-2-10. Electron mobilities in saturated CH_3D vapor at different densities (10^{26} molec/ m^3) and temperatures (K). \square , 7.5, 154.8; \circ , 7.6, 155.0; Δ , 10.7, 163.0.

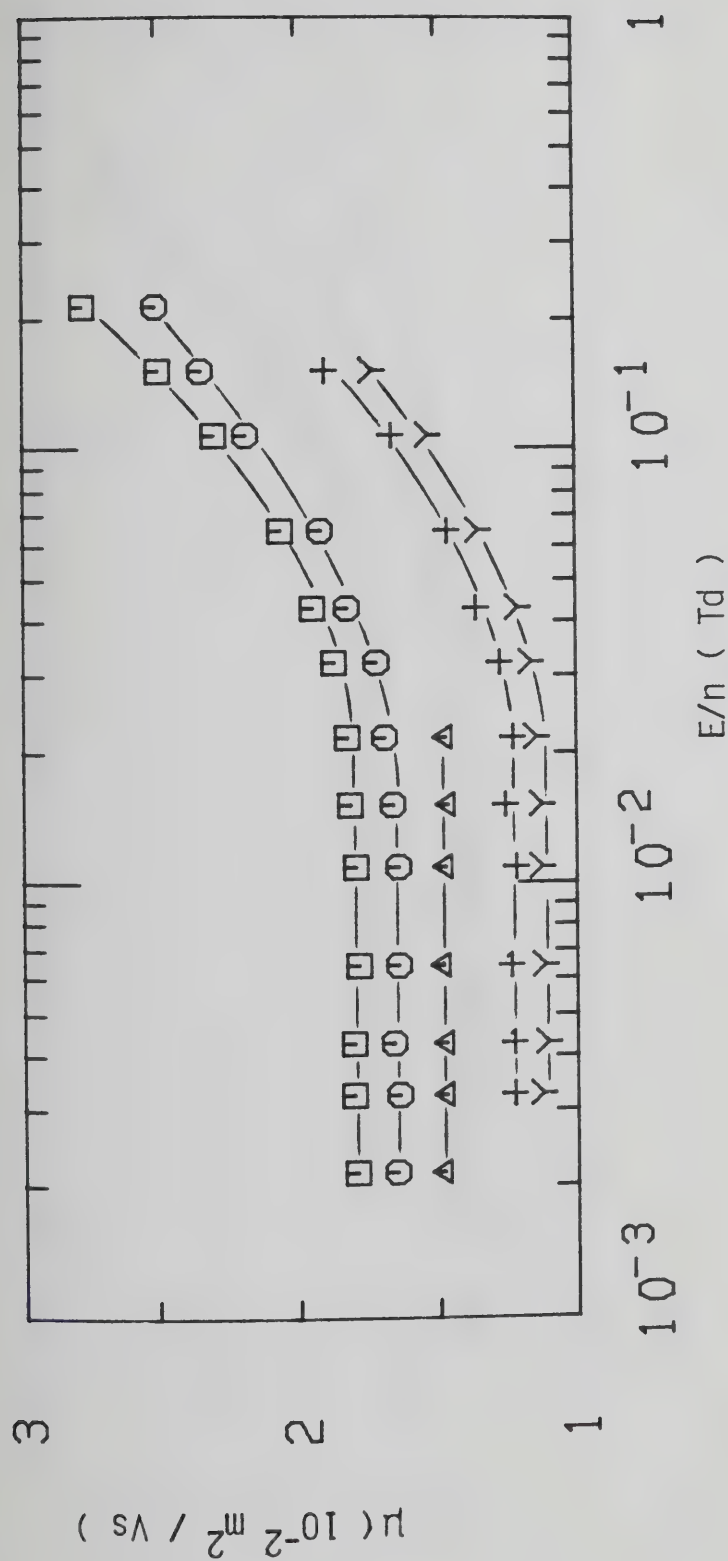


Figure III-2-11. Electron mobilities in CH_3D gas at $n = 15.0 \times 10^{26} \text{ molec/m}^3$ and different temperatures (K). \square , 210.0; \circ , 190.0; Δ , 176.0; $+$, 171.0; γ , 200.2.

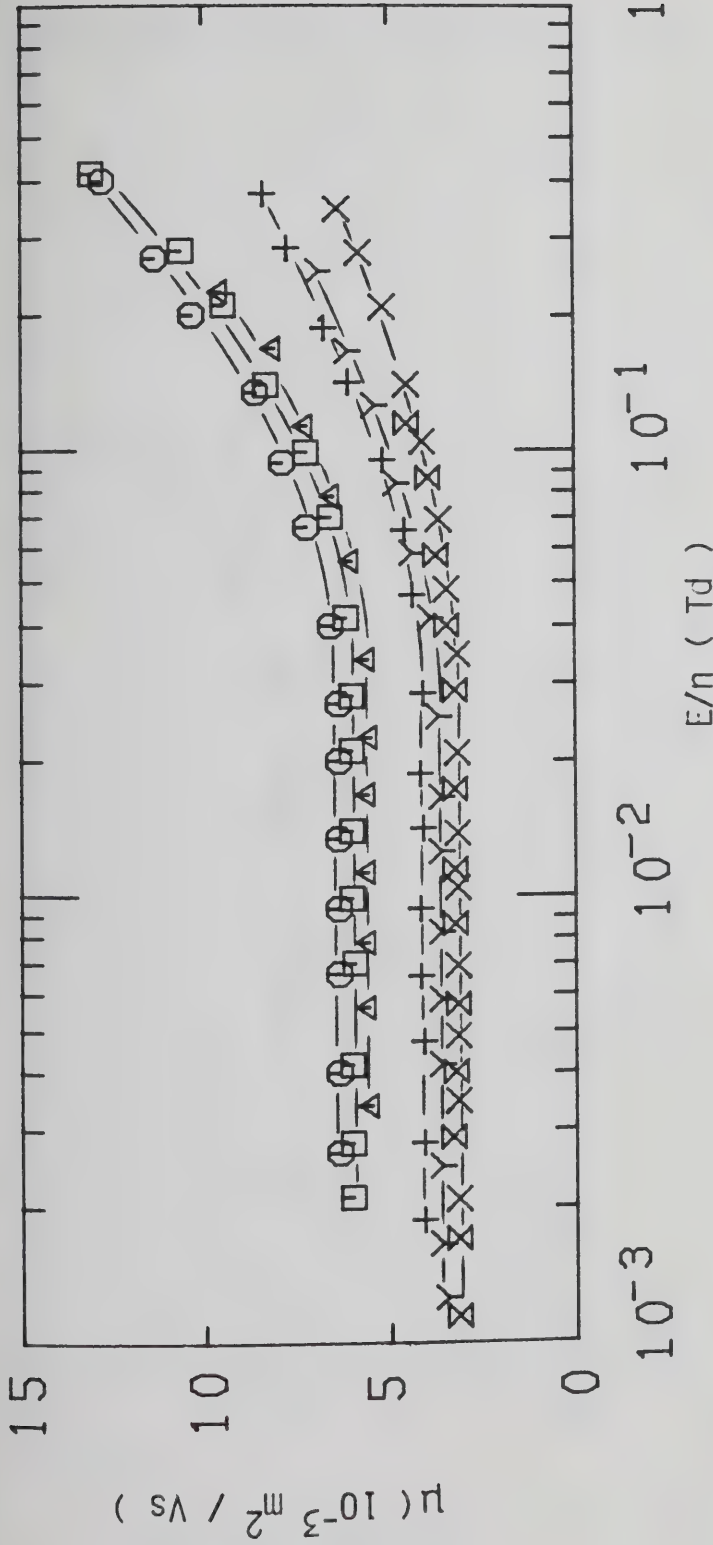


Figure III-2-12. Electron mobilities in saturated CH_3D vapor at different densities ($10^{27} \text{ molec/m}^3$) and temperatures (K). ○, 2.25, 180.0; □, 2.36, 181.0; Δ, 2.80, 184.2; +, 3.35, 187.0; Y, 3.78, 188.7; X, 4.6, 190.4; X, 5.5, 191.0.

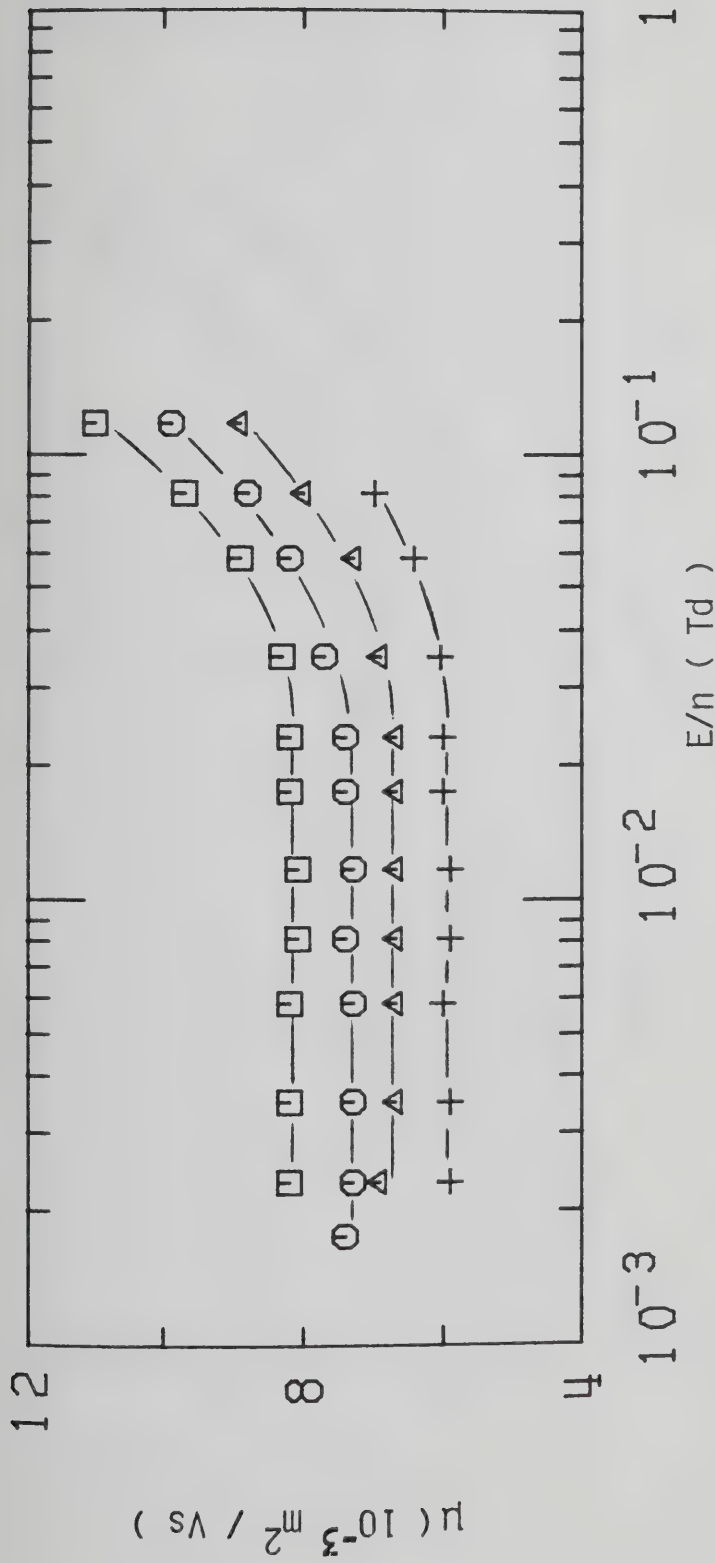


Figure III-2-13. Electron mobilities in CH_3D gas at $n = 2.70 \times 10^{27} \text{ molec/m}^3$ and different temperatures (K). + , 186.9; Δ , 190.0; \circ , 192.0; \square , 195.2.

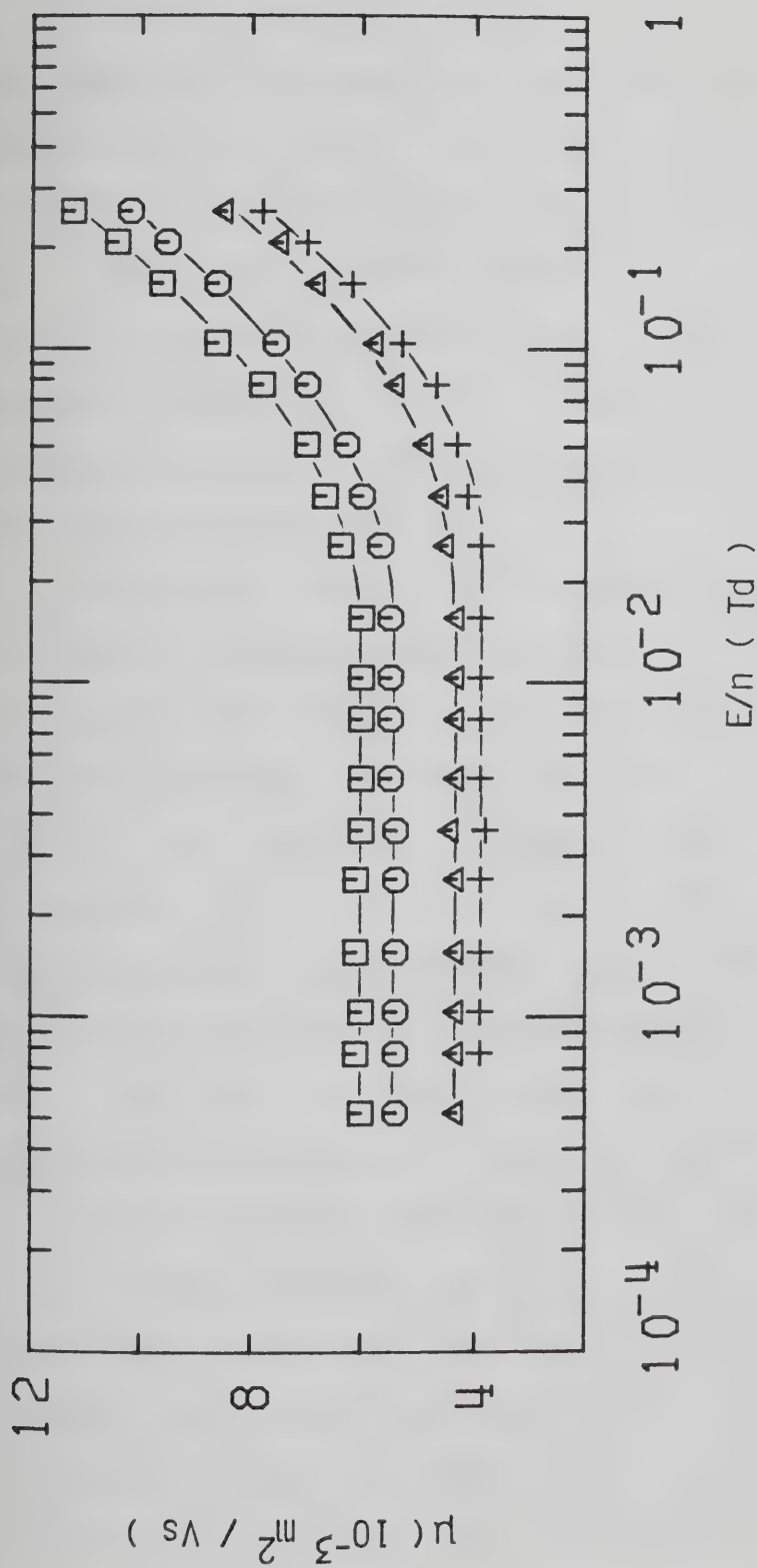


Figure III-2-14. Electron mobilities in supercritical CH_3D gas at $n_c = 6.1 \times 10^{27} \text{ molec/m}^3$ and different temperatures (K). \square , 191.1; \circ , 191.5; \triangle , 192.5; \square , 193.3. $T_c = 191.1$.

the mobility increases by about 35% for an increase in temperature of 8.3K. At the critical density ($n_c = 61 \times 10^{26}$ molec/m³) an increase in temperature of 2K causes an increase in low field mobility of about 50%. At the lower density the threshold field is approximately constant between 186.9K and 195.2K at $E/n \approx 0.035$ Td. At the critical density a slight decrease is observed by raising the temperature by 2K.

In Figure III-2-15 are reported measurements in the coexistent liquid at densities near the critical point. As previously observed in CH₄ the field effect on the electron mobility undergoes a change of sign. At $n = 7.9 \times 10^{27}$ molec/m³ the mobility increases with field above the threshold. At $n = 8.6 \times 10^{27}$ molec/m³ the mobility decreases above the threshold. The transition between the two effects can be set at value intermediate between these two. In this density region the low field mobility increases with density. A further increase in density in the liquid (Figures III-2-16 and 17) produces an increase in low field mobility up to $n = 10.6 \times 10^{27}$ molec/m³. Above this value the low field mobility decreases with density. Throughout this density range the threshold field is constant at $E/n \approx 8$ mTd. This value is lower than any value observed in the gas. The mobility curves tend to merge at $E/n \approx 0.1$ Td.

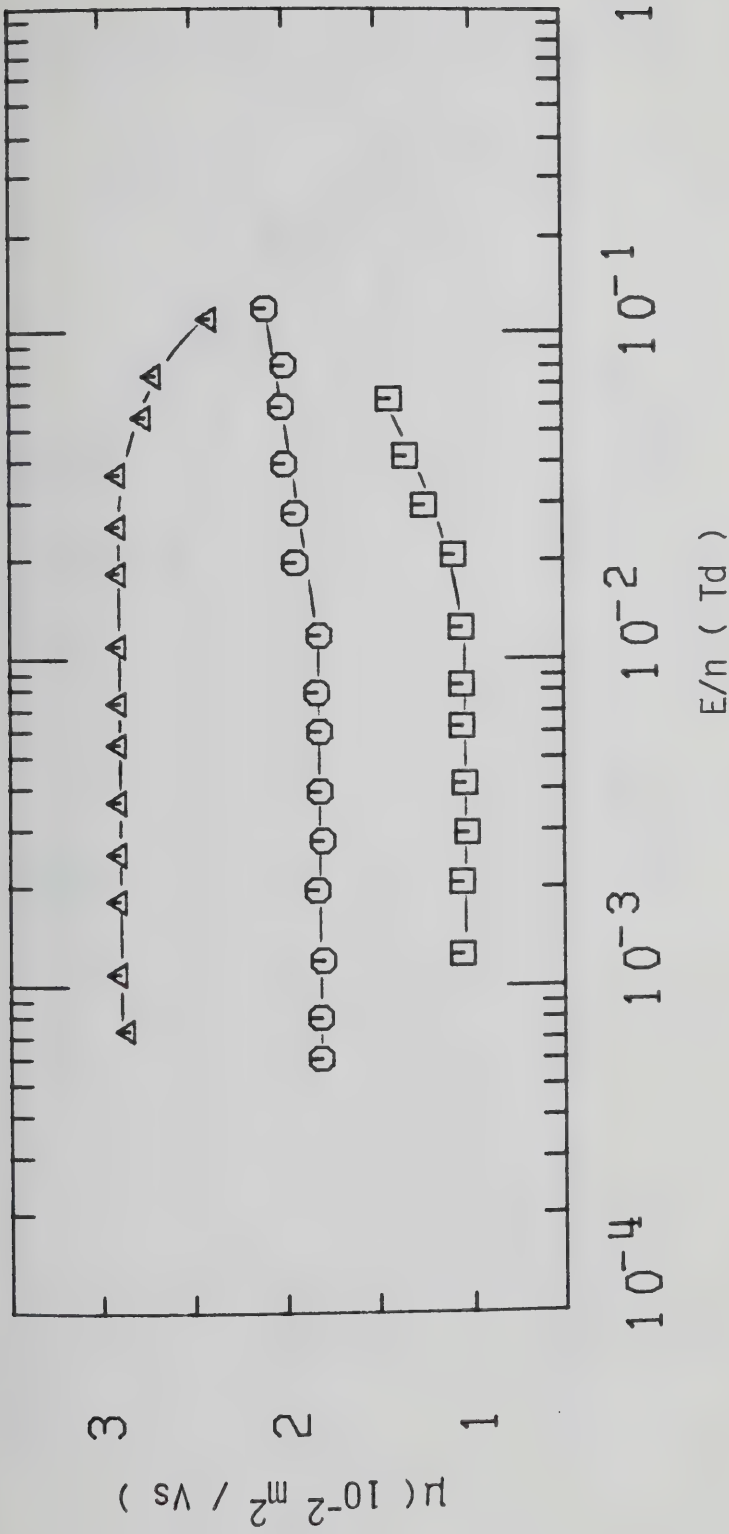


Figure III-2-15. Electron mobilities in liquid CH_3D at different densities (10^{27} molec/ m^3) and temperatures (K). \square , 7.5, 191.0; \circ , 7.9, 190.4; Δ , 8.6, 188.7.

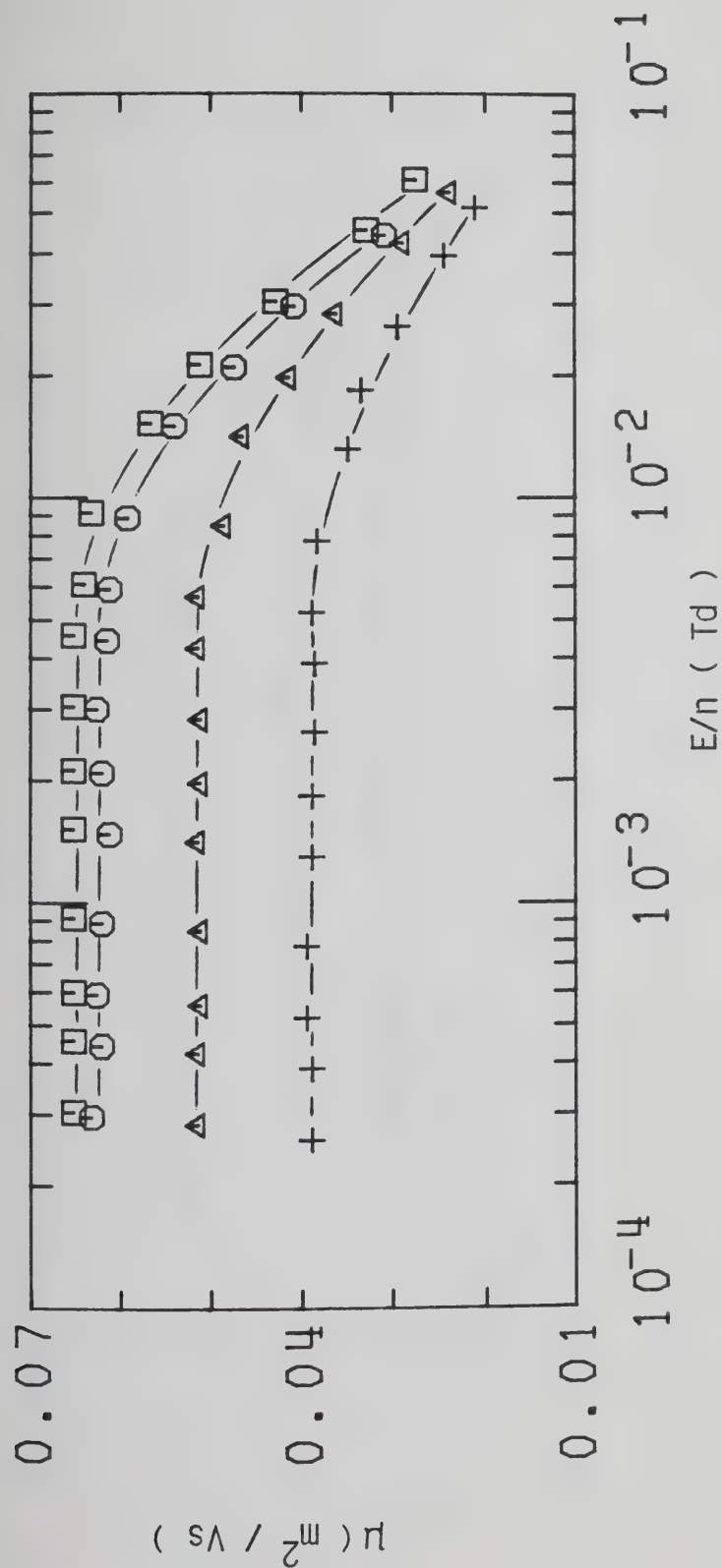


Figure III-2-16. Electron mobilities in liquid CH_3D at different densities ($10^{27} \text{ molec/m}^3$) and temperatures (K). $+$, 9.1, 187.0; Δ , 9.2, 186.9; \circ , 10.1, 181.9; \square , 10.3, 181.0.

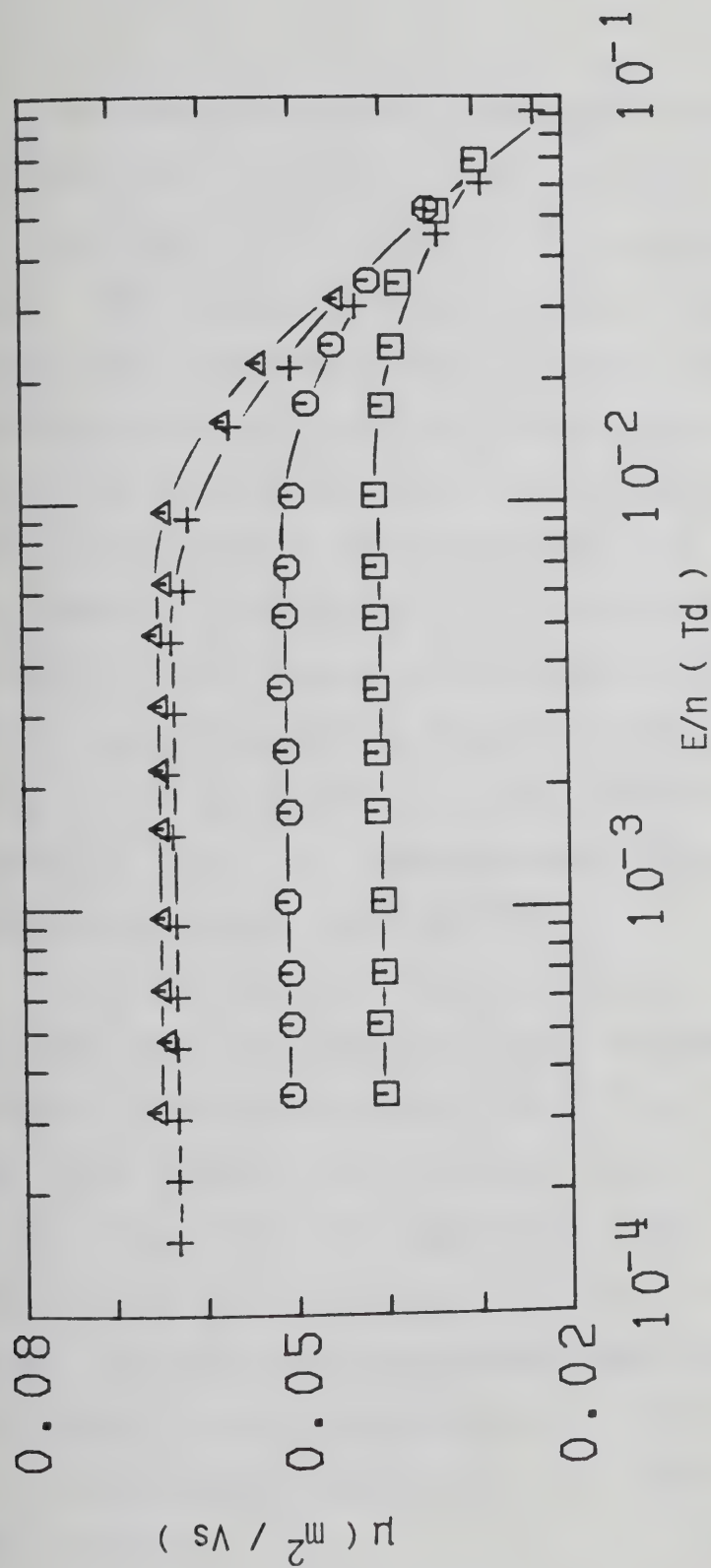


Figure III-2-17. Electron mobilities in liquid CH_3D at different densities (10^{27} molec/ m^3) and temperatures (K). Δ , 10.6, 178.7; \circ , 10.8, 177.7; \square , 11.4, 173.0; \square , 12.3, 164.5.

The electron mobility decreases with density (Figure III-2-18) up to $n = 14.8 \times 10^{27}$ molec/m³. Above this value it increases with density on approaching the triple point. The threshold field is constant at $E/n \approx 8$ mTd. In Figure III-2-19 the effect of density and temperature on the threshold field from the dilute gas to the dense liquid along the saturation curve is illustrated. The lowest density corresponds to a temperature of 99K. The highest gas density corresponds to a temperature of 191K. The threshold field increases from about 0.015 Td to about 0.04 Td. A change of sign is observed at an approximate density of 8×10^{27} molec/m³. In the liquid the value of the threshold field is approximately density (temperature) independent at $E/n \approx 8 \times 10^{-3}$ Td.

The results in Figures III-2-1 to III-2-5 were obtained with low pressure type conductance cells. The electrode separations were 1.001 ± 0.003 cm. All the other gas phase results were obtained with high pressure type cells. The electrode separations were 0.314 ± 0.004 cm. Liquid data were obtained in liquid type high pressure cells. The electrode separations were 0.315 ± 0.003 cm. A listing of the low field mobilities and threshold voltages at the different temperatures and densities is given in Table III-2.

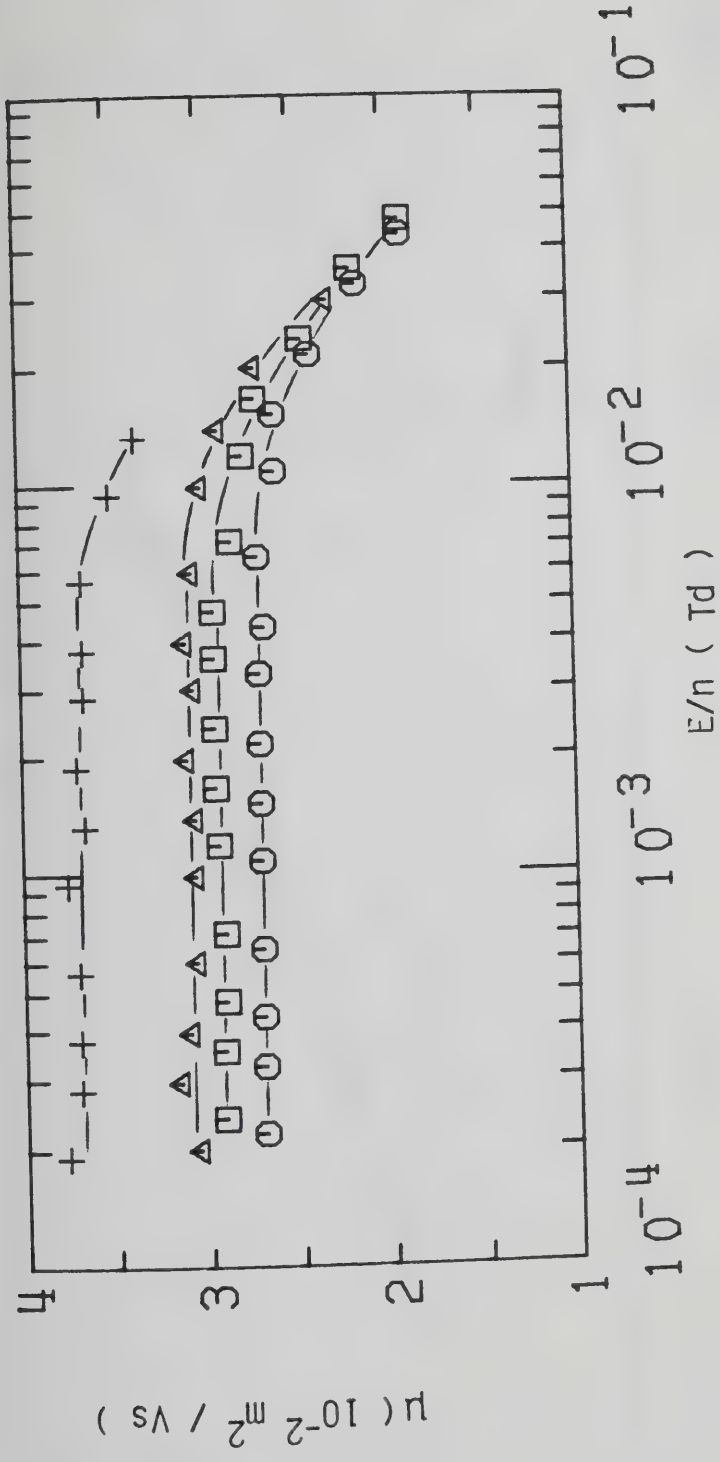


Figure III-2-18. Electron mobilities in liquid CH_3D at different densities ($10^{27} \text{ molec/m}^3$) and temperatures (K). \square , 13.5, 150.5; \circ , 14.8, 131.0; Δ , 16.2, 108.5; $+$, 17.0, 92.5.

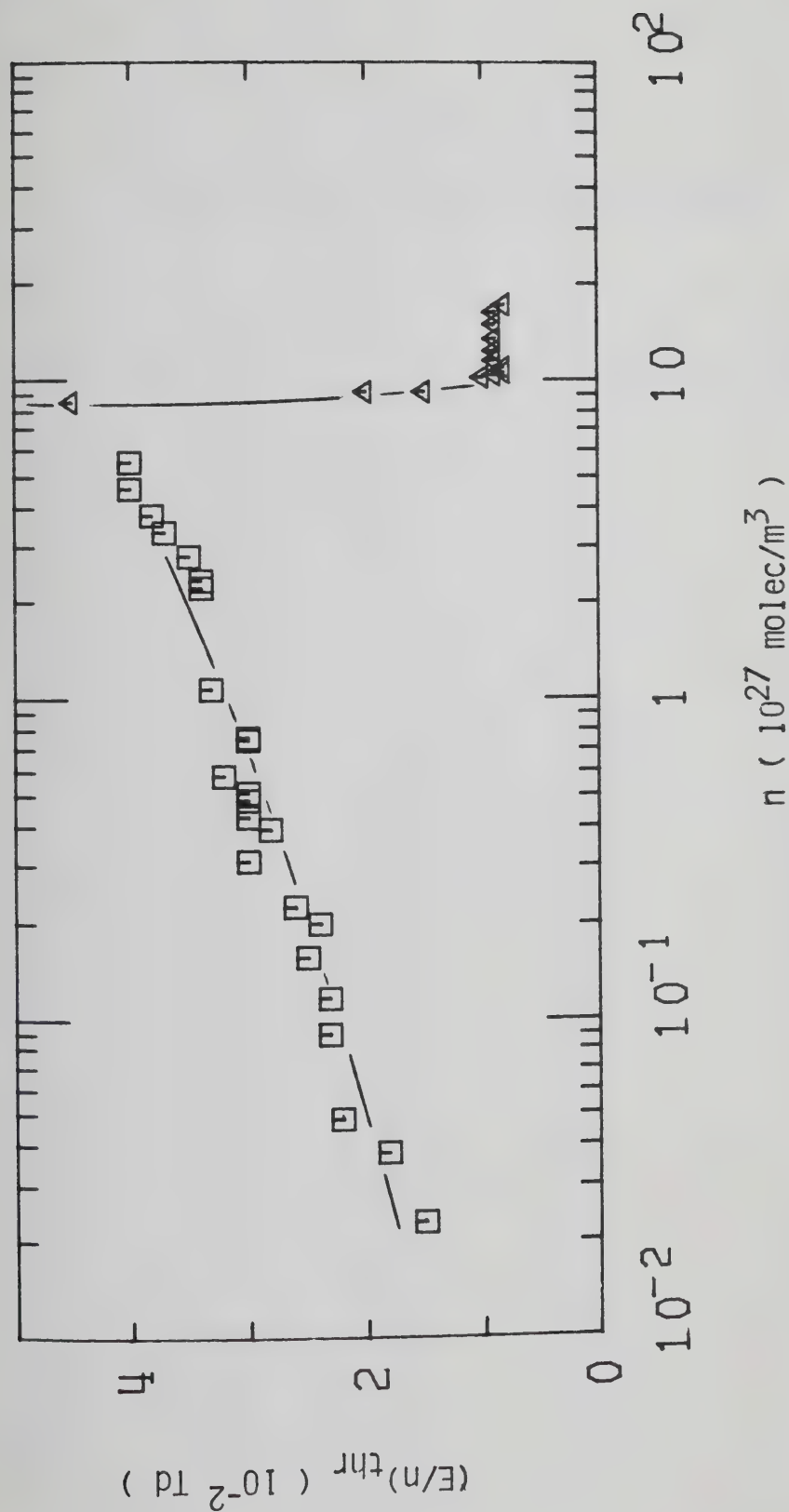


Figure III-2-19. Electric field threshold, $(E/n)_{thr}$, in coexistence vapor and liquid CH_3D as a function of density. \square , $d\mu / d(E/n) > 0$; Δ , $d\mu / d(E/n) < 0$.

TABLE III-2

Summary of Electron Results for CH_3D^a

T (K)	n (10^{26} m^{-3})	μ (m^2/Vs)	$n\mu$ [$10^{25} (\text{Vsm})^{-1}$]	(E/n) _{thr} (mTd)	$d\mu/d(E/n)$
108.2	0.235	1.00	2.35		
146.3	0.235	1.10	2.59	22	+
185.5	0.235	1.18	2.77	34	+
225.7	0.235	1.28	3.01	40	+
293.7	0.235	1.42	3.34	52	+
337.8	0.235	1.48	3.48	65	+
385.8	0.235	1.59	3.74	80	+
404.4	0.235	1.60	3.76	80	+
435.0	0.235	1.62	3.81	90	+
474.0	0.235	1.69	3.97	100	+
504.0	0.235	1.72	4.04	100	+
535.7	0.235	1.77	4.16	120	+
589	0.235	1.83	4.30	140	+
637	0.235	1.86	4.37	150	+
112.5	0.33	0.71	2.34	22	+
168.8	0.33	0.82	2.71	30	+
220.7	0.33	0.91	3.00	40	+
294.0	0.33	1.01	3.33	60	+
359	0.33	1.10	3.63	60	+
407	0.33	1.15	3.80	80	+
109.3	0.49	0.49	2.40	20	+
110.5	0.49	0.50	2.45	20	+
159.5	0.49	0.53	2.60	30	+
216.2	0.49	0.60	2.94	40	+

(continued....)

Table III-2 continued

293.8	0.49	0.68	3.33	45	+
360.5	0.49	0.72	3.53	70	+
423.0	0.49	0.79	3.87	90	+
99.0	0.230	1.10	2.53	15	+
104.5	0.38	0.55	2.09	18	+
109.3	0.49	0.49	2.40	22	+
115.7	0.89	0.218	1.94	23	+
119.5	1.16	0.168	1.95	23	+
124.0	1.56	0.115	1.79	25	+
128.5	2.00	0.091	1.82	24	+
130.5	2.26	0.085	1.92	26	+
136.5	3.11	0.056	1.74	30	+
141.0	3.94	0.044	1.73	28	+
142.7	4.30	0.0414	1.78	30	+
145.5	4.8	0.0337	1.62	30	+
146.4	5.1	0.0370	1.89	30	+
149.5	5.8	0.0247	1.43	32	+
149.8	6.0	0.0320	1.92	30	+
154.8	6.0	0.0310	1.86	28	+
170.0	6.0	0.0330	1.98	28	+
215.8	6.0	0.0422	2.53	32	+
294.0	6.0	0.053	3.18	48	+
153.9	6.7	0.0247	1.65	26	+
172.5	6.7	0.0290	1.94	28	+
219.3	6.7	0.0376	2.52	38	+
293.0	6.7	0.0473	3.17	52	+
154.8	7.5	0.0210	1.58	30	+
155.0	7.6	0.0218	1.66	30	+
163.0	10.7	0.0141	1.51	33	+
171.0	15.0	0.0112	1.68	30	+
176.0	15.0	0.0124	1.86	32	+
190.0	15.0	0.0148	2.22		

(continued....)

Table III-2 continued

200.2	15.0	0.0165	2.48	36	+
210.0	15.0	0.0179	2.69	36	+
180.0	22.5	0.0060	1.35	34	+
181.0	23.6	0.0064	1.42	34	+
186.9	27.0	0.0060	1.62	34	+
190.0	27.0	0.0068	1.84	35	+
192.0	27.0	0.0074	2.00	34	+
195.2	27.0	0.0082	2.21	38	+
184.2	28.0	0.0056	1.57	35	+
187.0	33.5	0.00410	1.37	37	+
188.7	37.8	0.00361	1.36	38	+
190.4	46	0.00320	1.47	40	+
191.0	55	0.00325	1.79	40	+
191.3	61 ^b	0.00390	2.38	30	+
191.5	61 ^b	0.00431	2.63	30	+
192.5	61 ^b	0.0055	3.36	30	+
193.3	61 ^b	0.0060	3.66	27	+
191.0	75	0.0105	7.9	20	+
190.4	79	0.0182	14.4		
188.7	86	0.0290	24.9	45	-
187.0	91	0.0405	36.9	20	-
186.9	92	0.0505	46.5	15	-
181.9	101	0.065	66	10	-
181.0	103	0.063	65	9	-
178.7	106	0.065	69	8	-
177.7	108	0.062	67	8	-
173.0	114	0.0515	59	8	-
164.5	123	0.0390	48	9	-

(continued....)

Table III-2 continued

150.5	135	0.0293	39.6	9	-
131.0	148	0.0270	40	9	-
108.5	162	0.0305	49	9	-
92.5	170	0.0370	63	8	-

a. The results appear in this table in the same order as the figures. They are given in order of increasing density.

b. $n_c = 6.1 \times 10^{27} \text{ molec/m}^3$, $T_c = 191.1\text{K}$

3. CH₂D₂

In Figure III-3-1 are reported measurements of the electron mobility in the saturated vapor as a function of field and density (temperature). The behavior is analogous to that observed previously. The mobility is field independent at low fields and it increases with field above a threshold value. This value is approximately constant in this region. The temperature variation is only $\sim 10\text{K}$. In this density region the value of the mobility at low fields is proportional to the inverse density. In Figure III-3-2 the effect of raising the temperature from 133.0K to 450K at $n = 3.7 \times 10^{25} \text{ molec/m}^3$ is illustrated. The low field mobility increases by about 50%. The value of the threshold field increases with temperature. At this density the mobility curves tend to merge at $E/n \approx 0.5 \text{ Td}$ and show a tendency to saturate above this value of field. The same features are observed at $n = 6.1 \times 10^{25} \text{ molec/m}^3$ (Figure III-3-3). The threshold field follows the same temperature dependence observed at the lower density. The low field mobility increases by about 60% for a change in temperature of 295.5K . The mobility curves merge at about 0.6 Td but no evidence of saturation is observed.

An increase in density of the coexistent vapor leads to a decrease in low field mobility (Figure III-3-4).

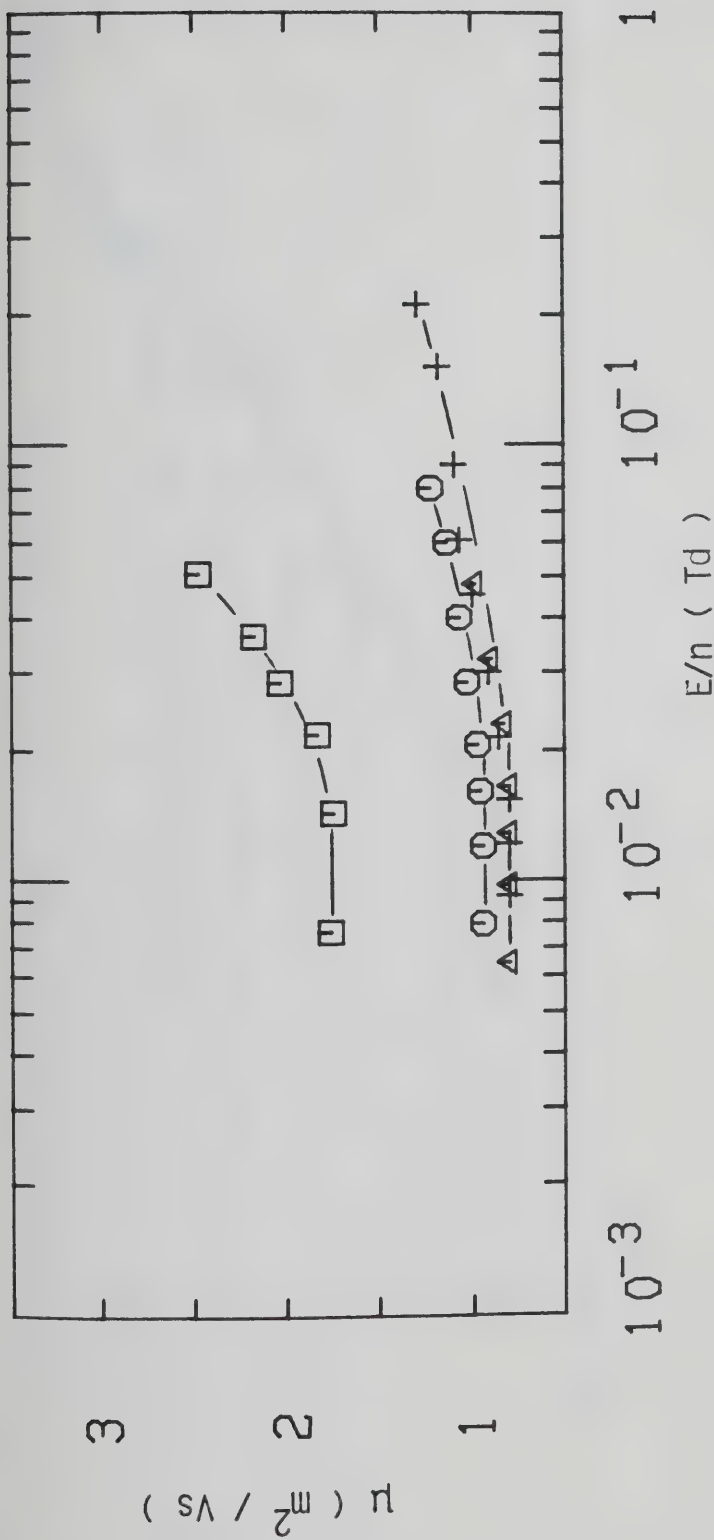


Figure III-3-1. Electron mobilities in saturated CH_2D_2 vapor at different densities (10^{25} molec/ m^3) and temperatures (K). \square , 1.43, 94.0; \circ , 2.57, 100.0; Δ , 3.12, 102.0; +, 3.30, 102.8.

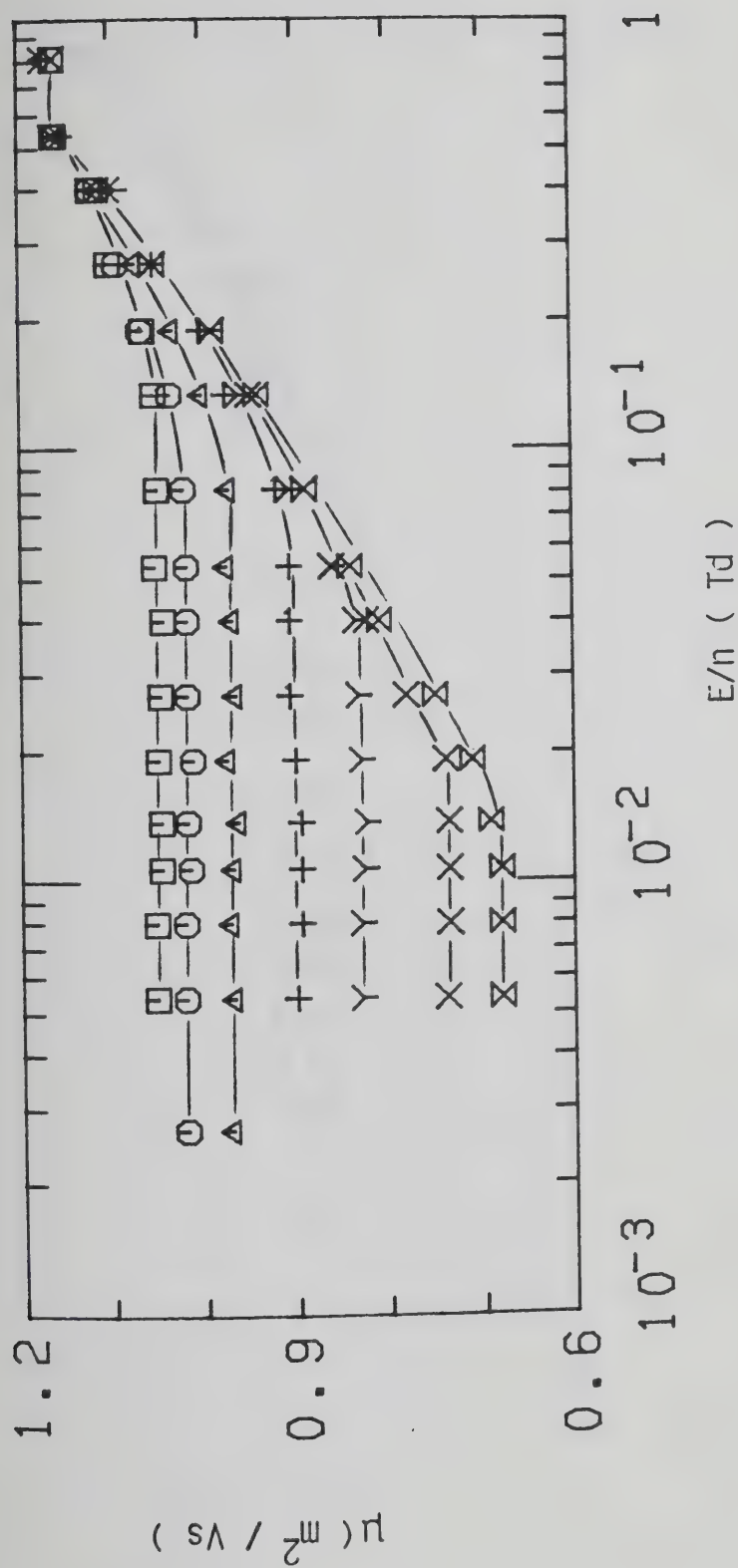


Figure III-3-2. Electron mobilities in CH_2D_2 gas at $n = 3.70 \times 10^{25} \text{ molec/m}^3$ and different temperatures (K). Δ , 133.0; \times , 170.8; γ , 230.3; $+$, 293.5; Δ , 351.7; \circ , 409.6; \square , 450.

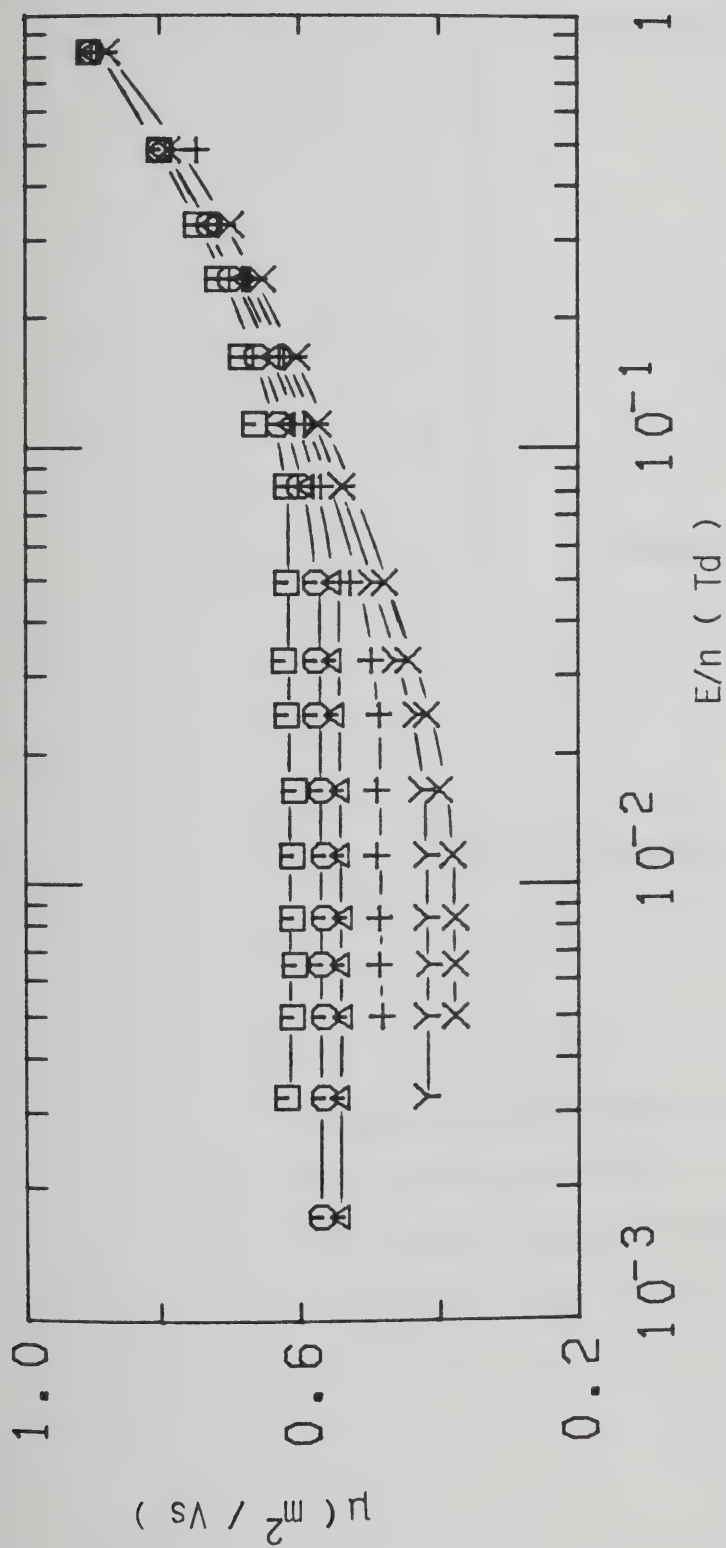


Figure III-3-3. Electron mobilities in CH_2D_2 gas at $n = 6.1 \times 10^{25} \text{ molec/m}^3$ and different temperatures (K). X, 113.0; Y, 151.0; +, 225.5; Δ , 294.0; O, 340.0; \square , 408.5.

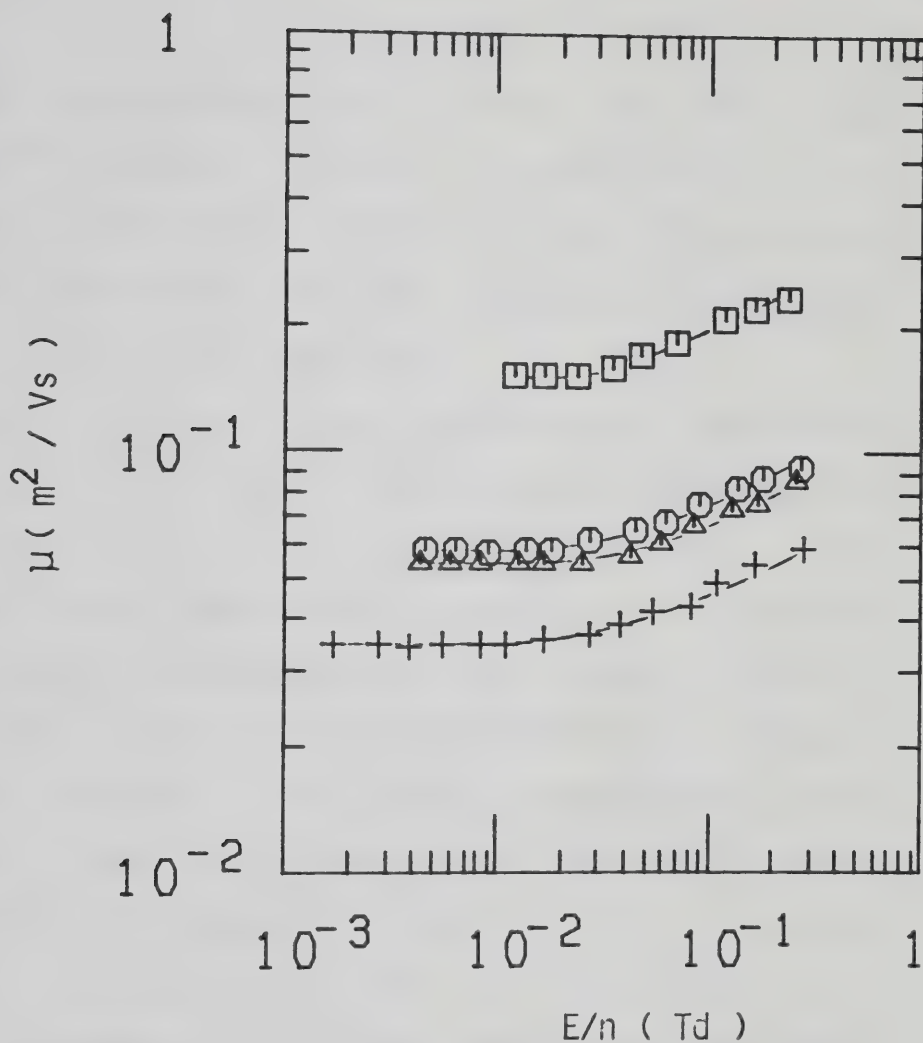


Figure III-3-4. Electron mobilities in saturated CH_2D_2 vapor at different densities (10^{26} molec/ m^3) and temperatures (K). \square , 1.37, 120.8; \circ , 3.58, 137.7; \triangle , 3.82, 139.0; $+$, 5.9, 147.8.

Raising the temperature from 155.7K to 292.0K at $n = 7.3 \times 10^{26}$ molec/m³ (Figure III-3-5) leads to an increase of the low field mobility of 78%. The rate of change of the threshold field with temperature is the same as that observed at lower densities.

In Figure III-3-6 is shown the effect of temperature on the threshold field in a density range spanning from 3.7×10^{25} molec/m³ to 73×10^{25} molec/m³. An approximately linear dependence is observed. By increasing the density of the saturated vapor by a factor of about 3 (Figure III-3-7) a drop in low field mobility by a factor of about 4 is observed. A 30K change in temperature causes the threshold field to increase from 0.038 Td to 0.045 Td. At $n = 26 \times 10^{26}$ molec/m³ (Figure III-3-8) an increase in temperature of about 10K above the coexistence curve produces an increase in low field mobility of about 50%. At the lowest density the same temperature change increased the low field mobility by less than 10%. The threshold field is approximately constant at $E/n \approx 0.04$ Td for this limited temperature variation.

In Figures III-3-9 and III-3-10 the effect of increasing the density of the vapor from 2.65×10^{27} molec/m³ to $n_c = 6.1 \times 10^{27}$ molec/m³ is shown. The low field mobility decreases with density in the vapor and it increases in the supercritical gas. This change in density corresponds to a change in temperature of about 8K. The

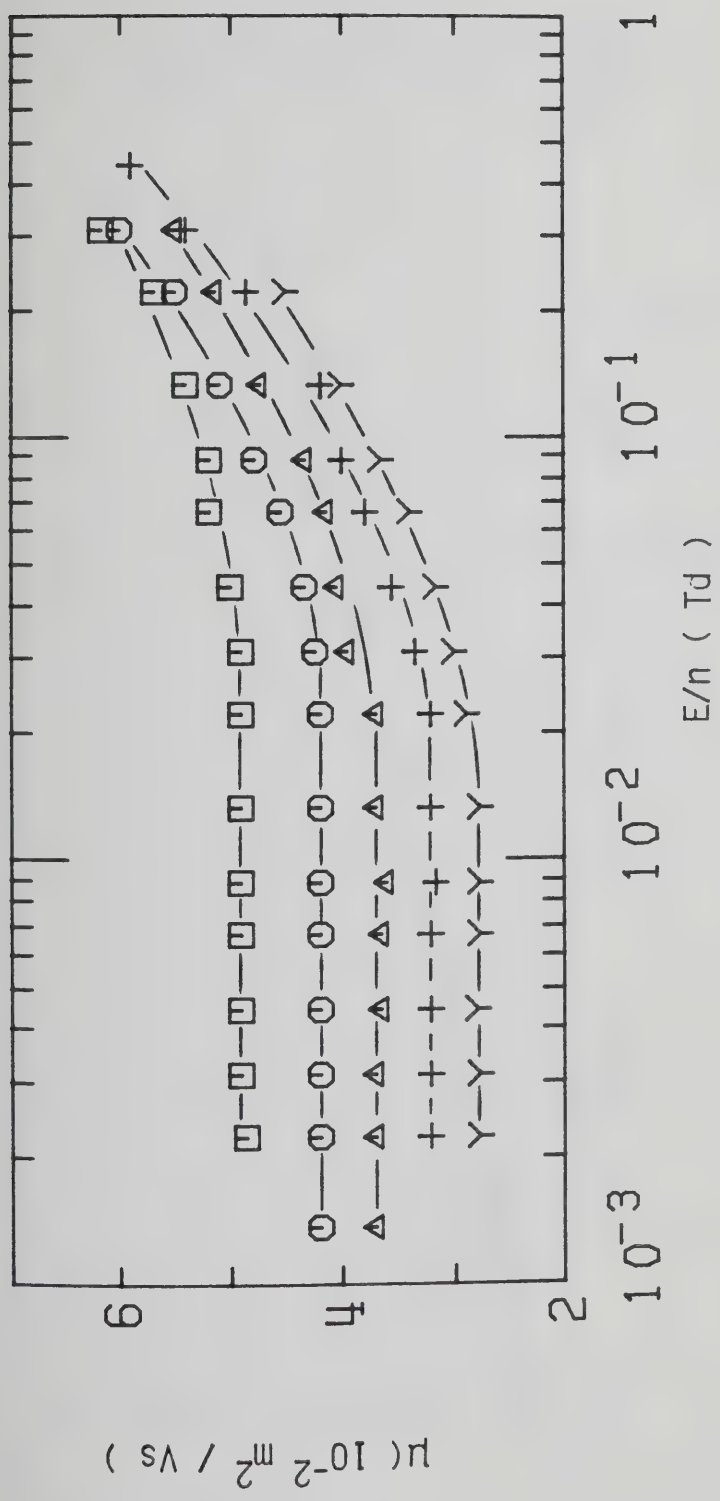


Figure III-3-5. Electron mobilities in CH_2D_2 gas at $n = 7.3 \times 10^{26} \text{ molec/m}^3$ and different temperatures (K). Y, 155.7; +, 172.5; Δ , 195.5; \circ , 231.8; \square , 292.0.

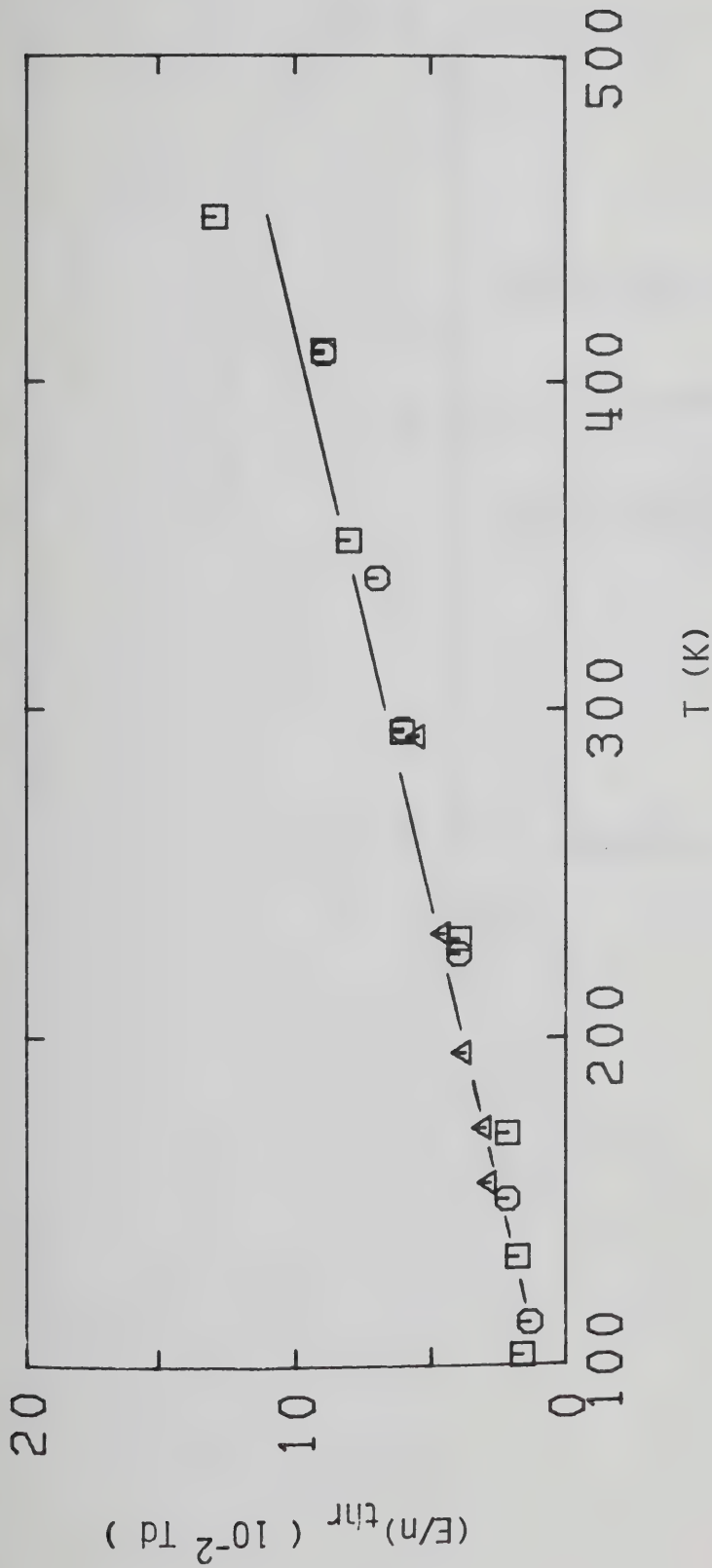


Figure III-3-6. Electric field threshold, $(E/n)_{thr}$, for electron heating in CH_2D_2 gas at different densities (10^{25} molec/ m^3) as a function of temperature \square , 3.70; \circ , 6.1; \triangle , 73.

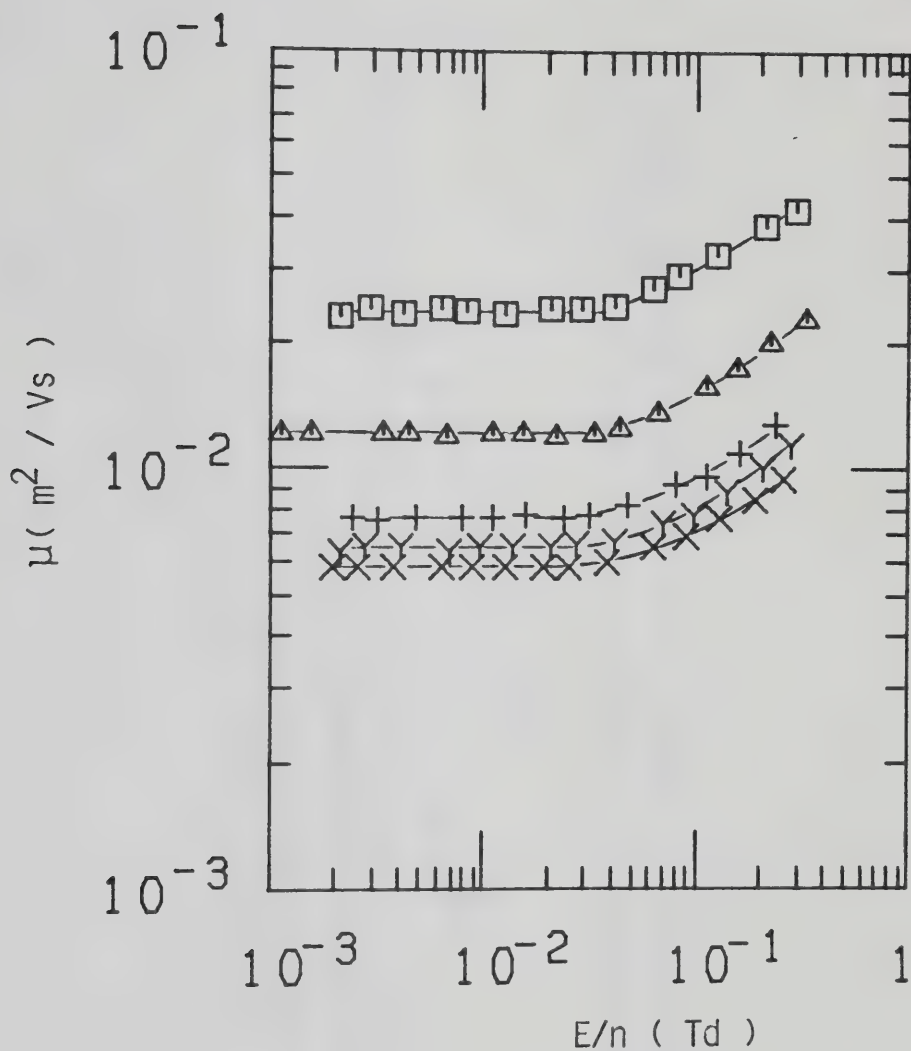


Figure III-3-7. Electron mobilities in saturated CH_2D_2 vapor at different densities ($10^{26} \text{ molec/m}^3$) and temperatures (K). \square , 7.7, 154.0; Δ , 14.6, 168.9; $+$, 19.8, 175.3; Y , 22.8, 178.5; X , 24.8, 180.1.

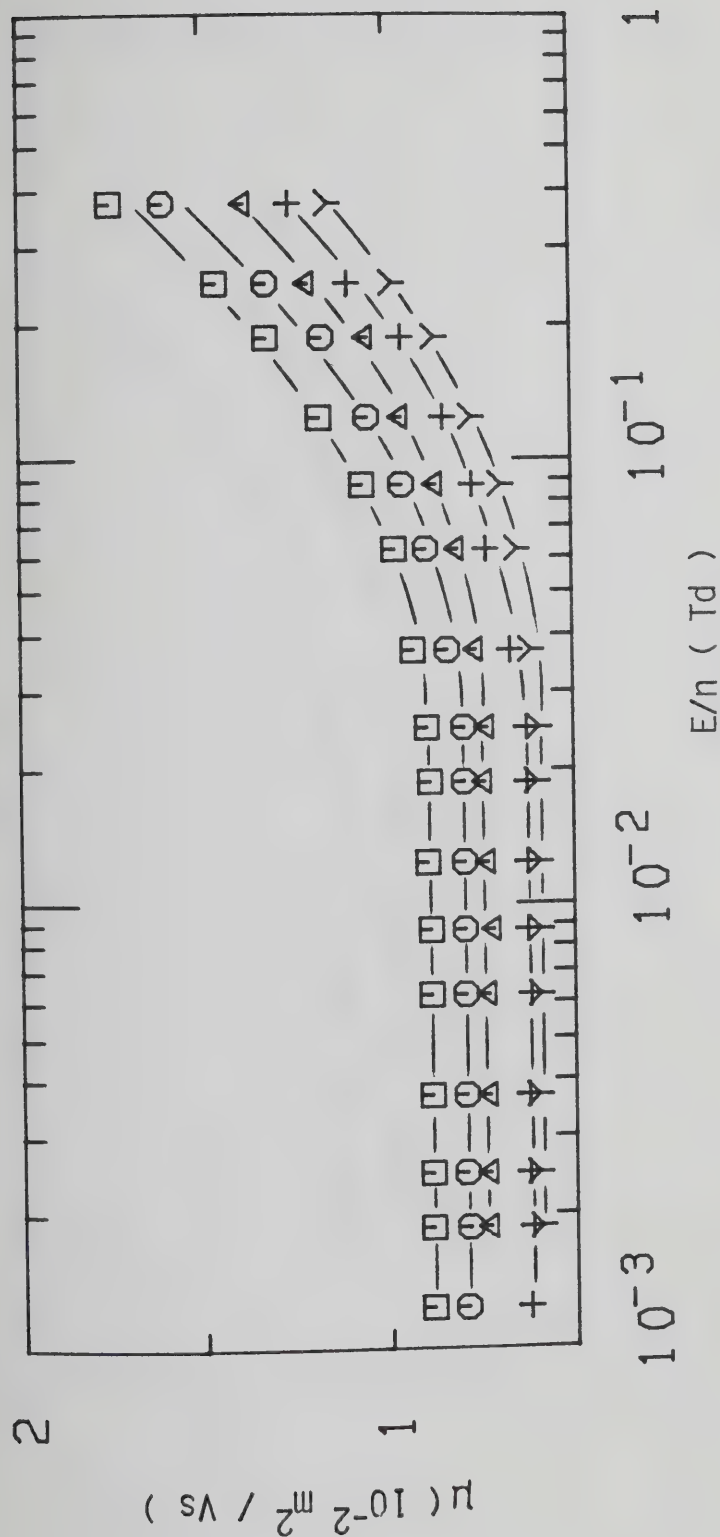


Figure III-3-8. Electron mobilities in CH_2D_2 gas at $n = 2.60 \times 10^{27} \text{ molec/m}^3$ and different temperatures (K). Y, 184.2, +, 186.0; Δ , 189.3; O, 192.0; \square , 195.5.

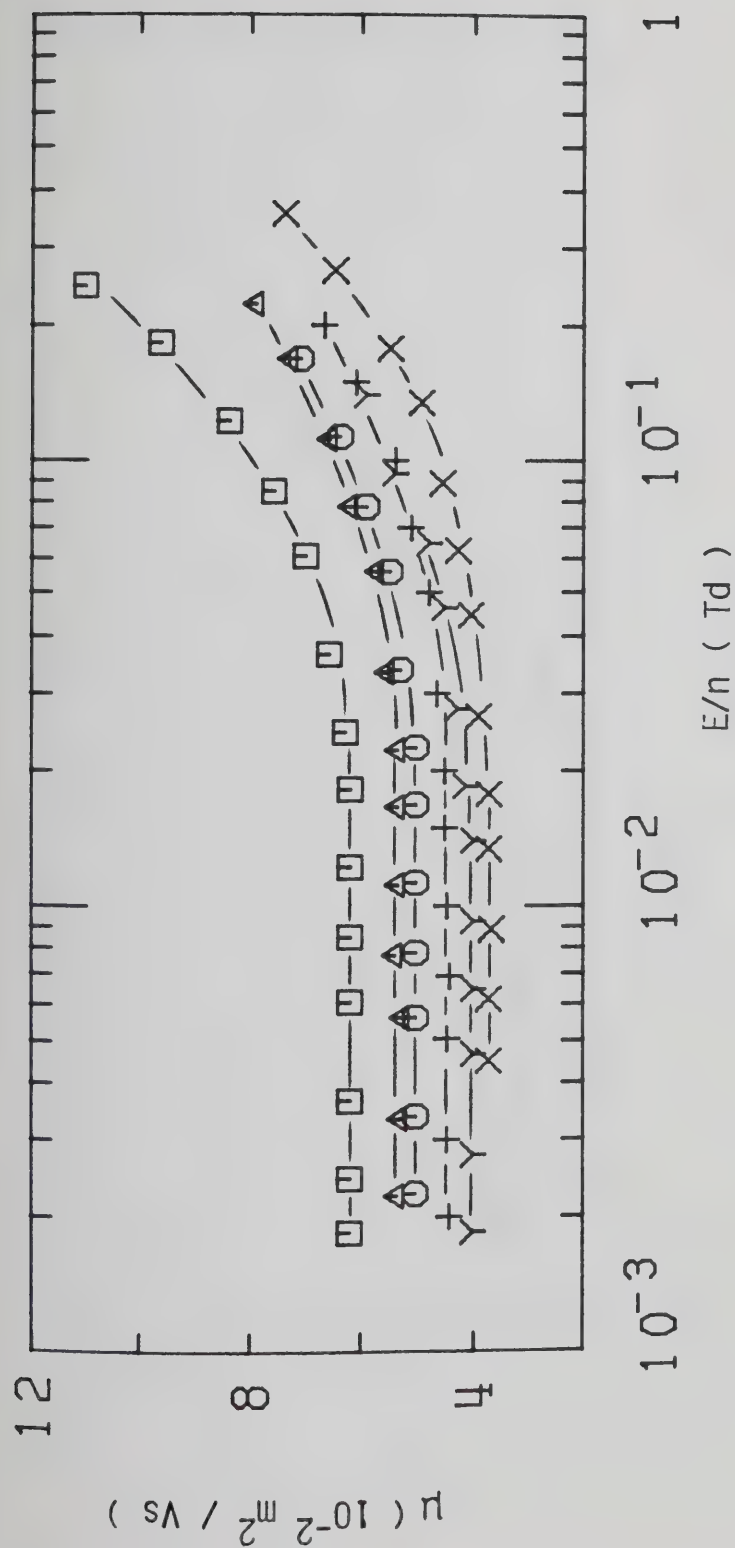


Figure III-3-9. Electron mobilities in saturated CH_2D_2 vapor at different densities (10^{27} molec/ m^3) and temperatures (K). \square , 2.65, 181.4; \circ , 2.80, 182.3; Δ 2.83, 182.6; +, 3.15, 184.2; x, 3.40, 185.5; x, 3.55, 186.0.

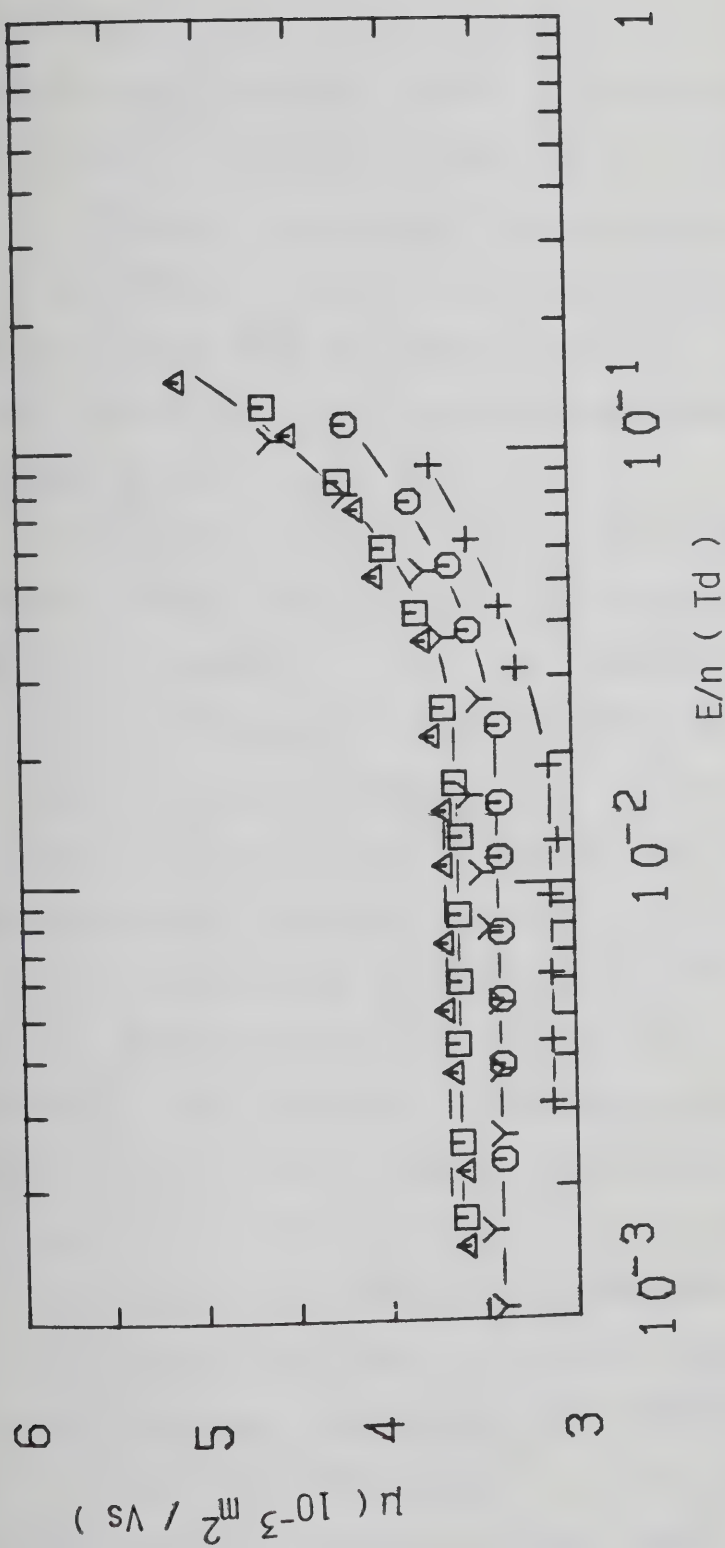


Figure III-3-10. Electron mobilities in saturated CH_2D_2 vapor at different densities ($10^{27} \text{ molec/m}^3$) and temperatures (K). \square , 3.70, 186.6; \circ , 4.20, 187.8; Δ , 4.3, 188.0; $+$, 5.2, 189.0; γ , $n_c = 6.1$, $T_c = 189.2$.

value of the threshold field is approximately constant at $E/n \approx 0.04$ Td. A slight decrease to ~ 0.03 Td is observed at $T_c = 189.2\text{K}$. An increase in temperature at the critical density (Figure III-3-10 and III-3-11) from 189.2K to 193.9K causes the low field mobility to increase by a factor of about 2.5. The threshold field is approximately constant at $E/n \approx 0.03$ Td.

In the liquid (Figure III-3-12) at densities near the critical point the effect of the electric field on the mobility changes. It is positive near zero at $n = 7.5 \times 10^{27}$ molec/m³ and negative at $n = 8.8 \times 10^{27}$ molec/m³. The transition can be set at 8×10^{27} molec/m³. In this density region the low field mobility increases with increasing density. In Figure III-3-13 the effect of increasing the density of the liquid is shown. The low field mobility increases up to $n = 10.4 \times 10^{27}$ molec/m³. The threshold field decreases to a value of about 1.0×10^{-2} Td. Again, as observed in CH₄ and CH₃D the value of the threshold field in the liquid far from the critical density is lower than any value observed in the gas. A further increase in density (Figures III-3-14 and III-3-15) in the liquid causes the mobility to decrease up to $n = 14.2 \times 10^{27}$ molec/m³ and to increase at higher densities on approaching the triple point. Throughout this density (temperature) range the threshold field is approximately constant at $E/n \approx 1.0 \times 10^{-2}$ Td. The mobility curves tend to merge at $E/n \approx 0.1$ Td.

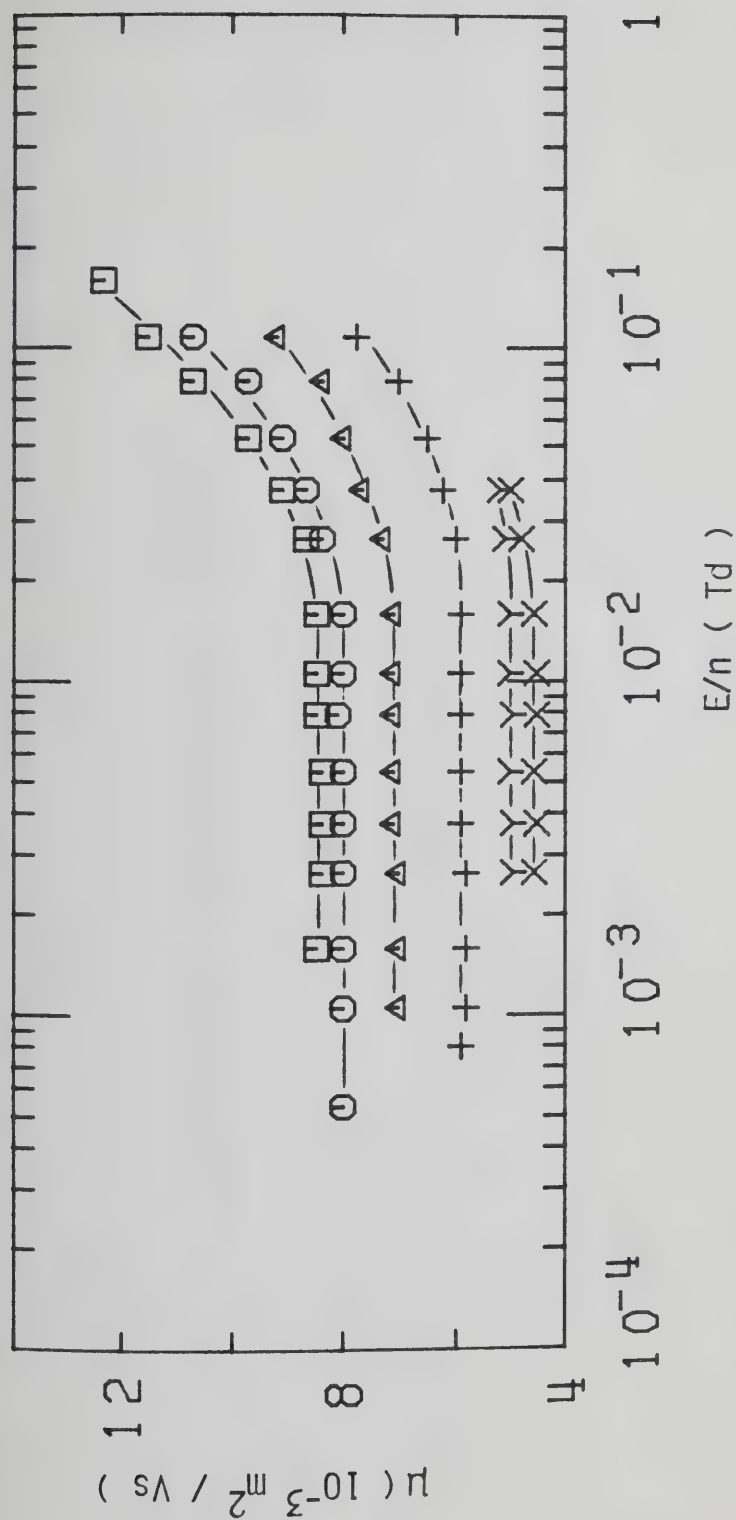


Figure III-3-11. Electron mobilities in supercritical CH_2D_2 gas at $n_c = 6.1 \times 10^{27} \text{ molec/m}^3$ and different temperatures (K). X, 189.6; Y, 189.8; +, 190.5; Δ , 191.7; O, 192.9; \square , 193.9. $T_c = 189.2$.

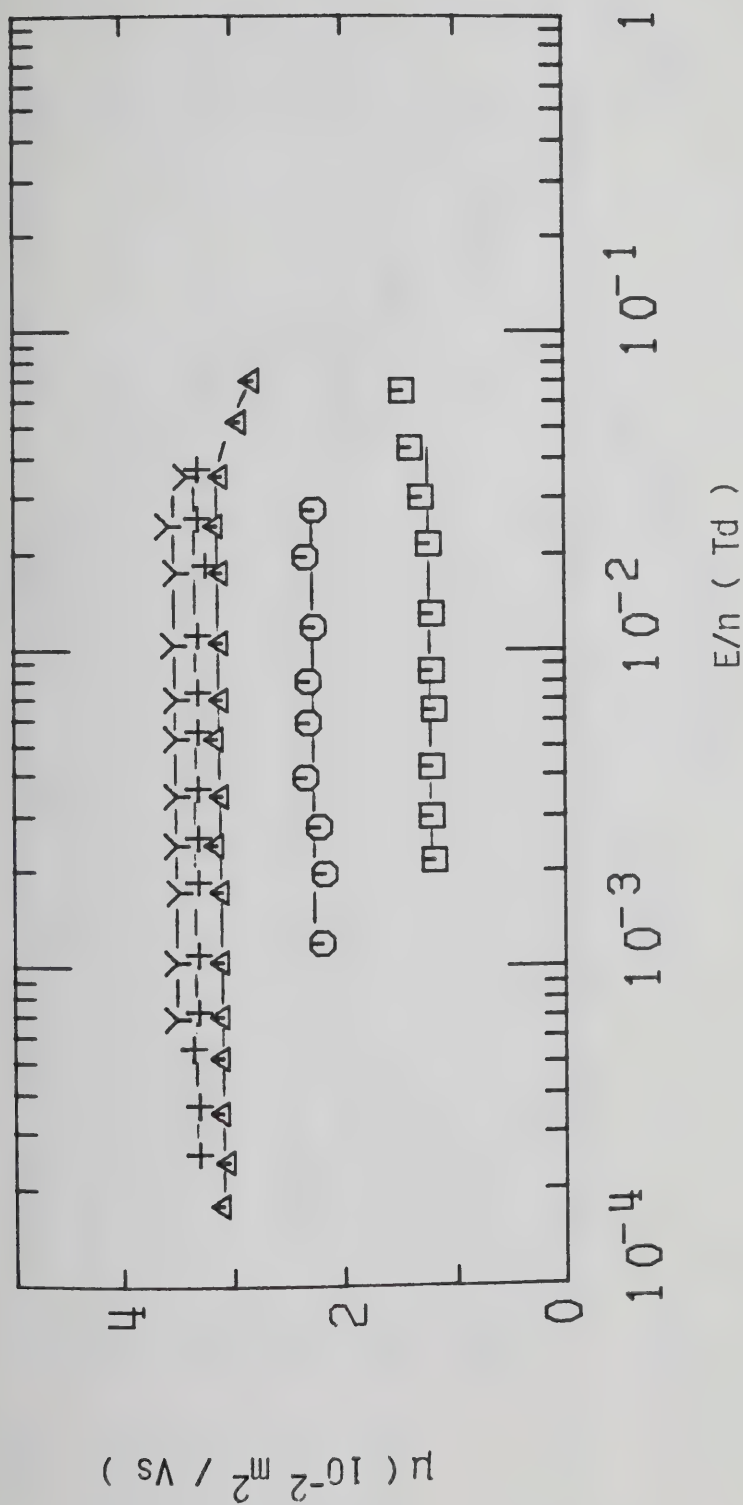


Figure III-3-12. Electron mobilities in liquid CH_2D_2 at different densities ($10^{27} \text{ molec/m}^3$) and temperatures (K). \square , 7.5, 189.0; \circ , 8.2, 187.8; Δ , 8.8, 186.2; +, 8.8, 186.1; Y, 9.1, 185.5.

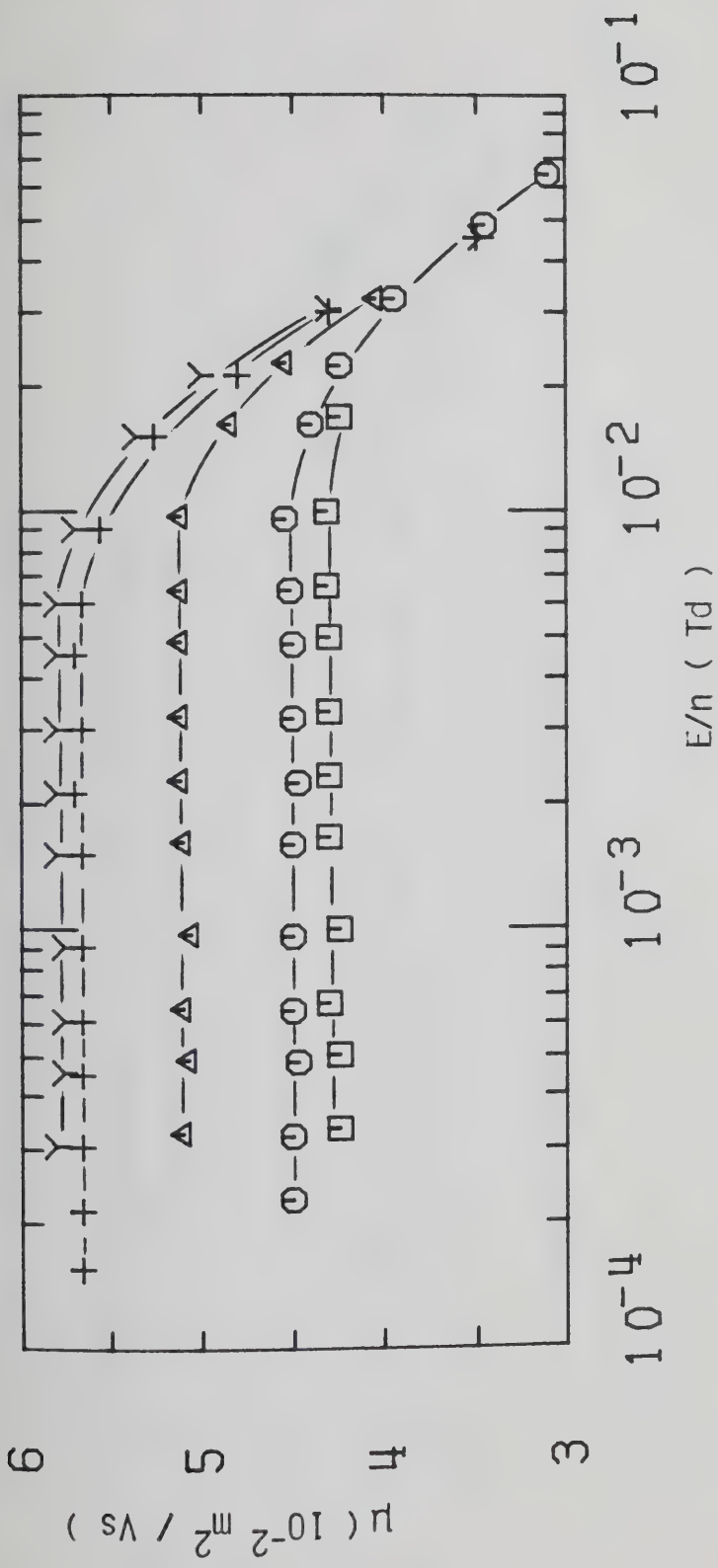


Figure III-3-13. Electron mobilities in liquid CH_2D_2 at different densities ($10^{27} \text{ molec/m}^3$) and temperatures (K). \square , 9.4, 184.2; \circ , 9.5, 183.8; Δ , 9.7, 182.3; $+$, 10.1, 180.1; \times , 10.4, 178.5.

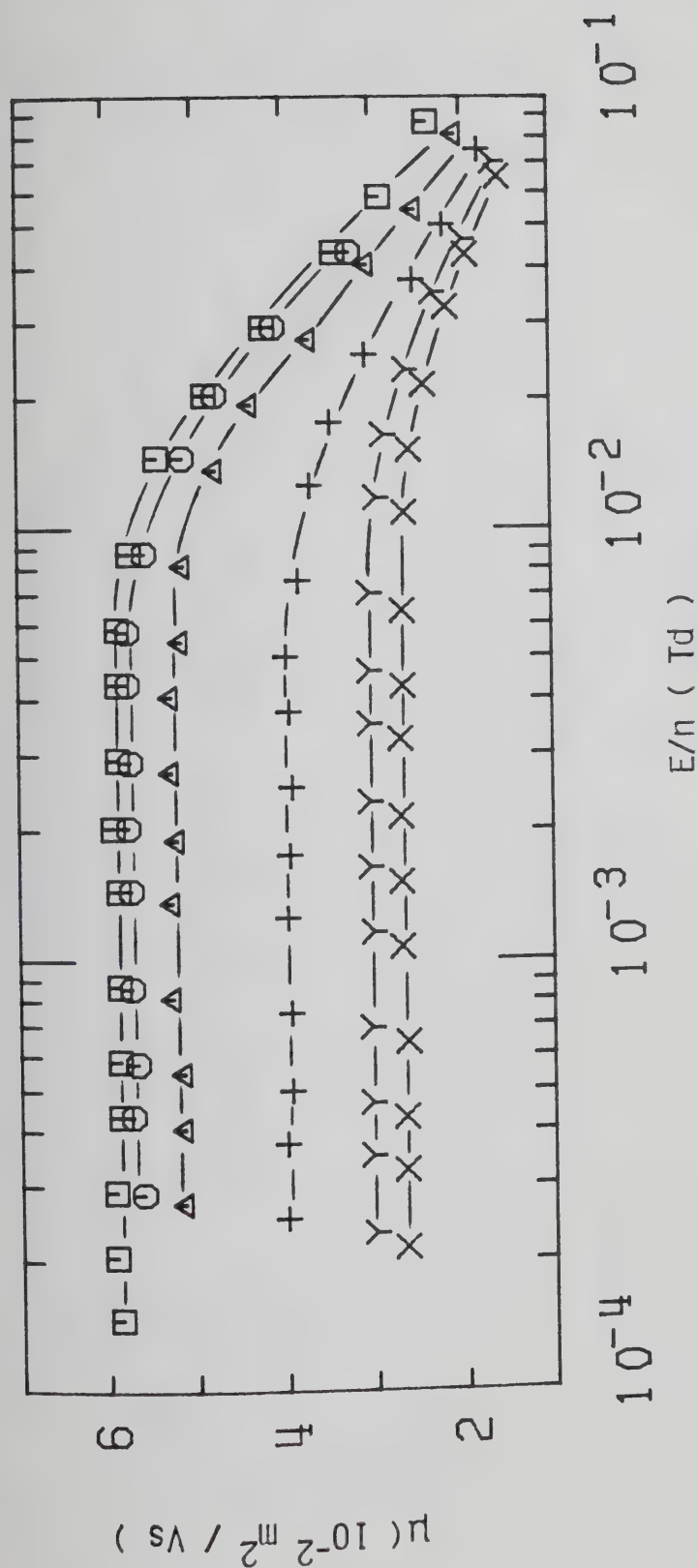


Figure III-3-14. Electron mobilities in liquid CH_2D_2 at different densities ($10^{27} \text{ molec/m}^3$) and temperatures (K). \square , 10.5, 178.0; \circ , 10.9, 175.3; Δ , 11.2, 172.7; $+$, 12.2, 163.8; \times , 13.1, 153.5; \times , 14.2, 139.0.

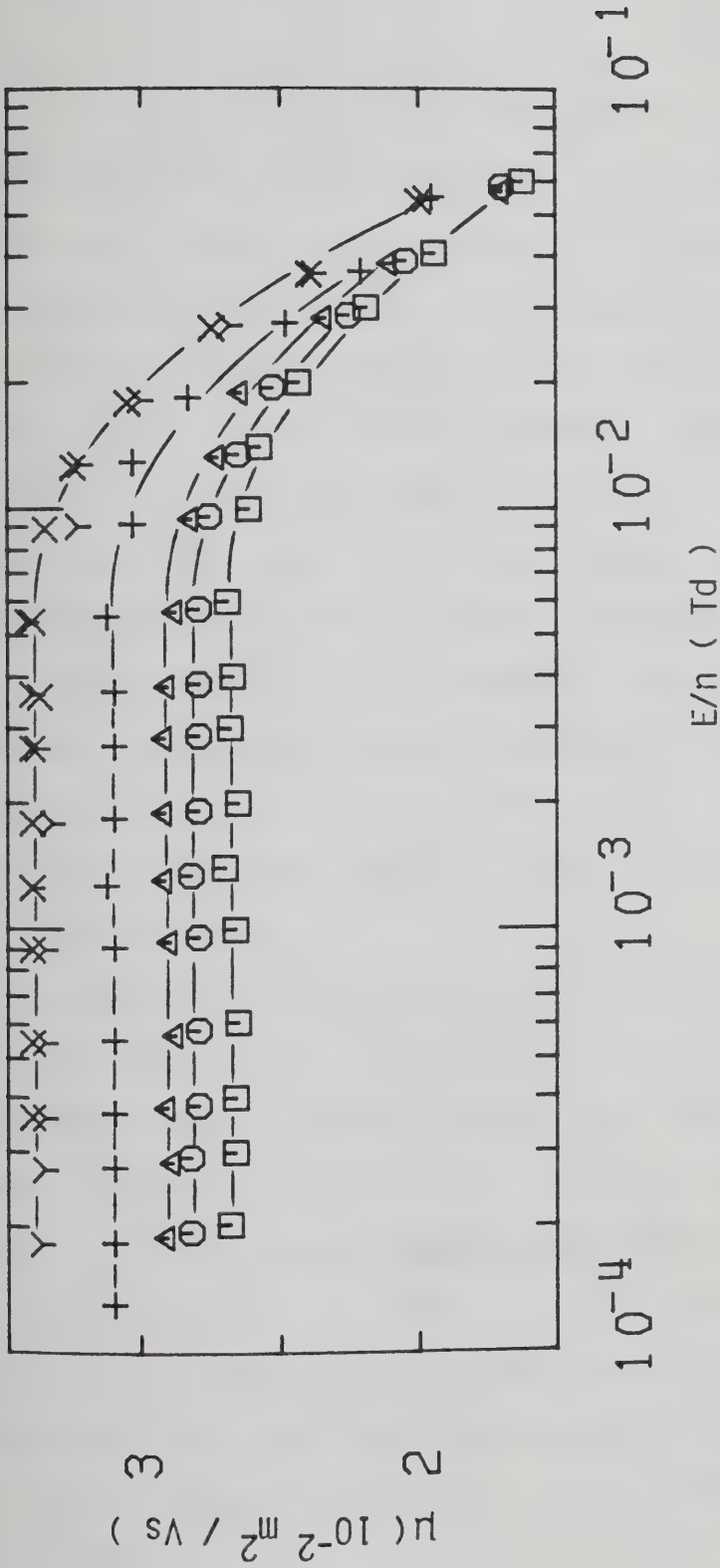


Figure III-3-15. Electron mobilities in liquid CH_2D_2 at different densities ($10^{27} \text{ molec/m}^3$) and temperatures (K). \square , 15.2, 124.0; \circ , 15.8, 114.0; Δ , 16.1, 109.0; $+$, 16.6, 100.0; Y , 16.9, 93.0; X , 17.0, 92.0.

In Figure III-3-16 is reported the variation of the threshold field in the saturated vapor and liquid from the dilute gas to the dense liquid. In the gas the mobility increases at fields above the threshold. The value of the threshold increases monotonically with density from about 0.015 Td at the lowest density corresponding to a temperature of 94K to about 0.05 Td at densities slightly lower than that at the critical temperature $T_c = 189.2\text{K}$. In the liquid the field effect undergoes a change of sign at a density of $8 \times 10^{27} \text{ molec/m}^3$. At higher densities the mobility decreases with increasing field above the threshold. At $n \gtrsim 10 \times 10^{27} \text{ molec/m}^3$ the value of the threshold field is density (temperature) independent at $E/n \approx 8 \times 10^{-3} \text{ Td}$.

Results in Figures III-3-1 to III-3-3 were obtained in low pressure type conductance cells. The electrode separations were $1.004 \pm 0.001 \text{ cm}$. All the other gas phase results were obtained in high pressure gas type cells. The electrode separations were $0.314 \pm 0.004 \text{ cm}$. Liquid data were obtained in high pressure liquid type cells. The electrode separations were $0.323 \pm 0.005 \text{ cm}$. A listing of the low field mobilities and threshold voltages at the different temperature and densities is given in Table III-3.

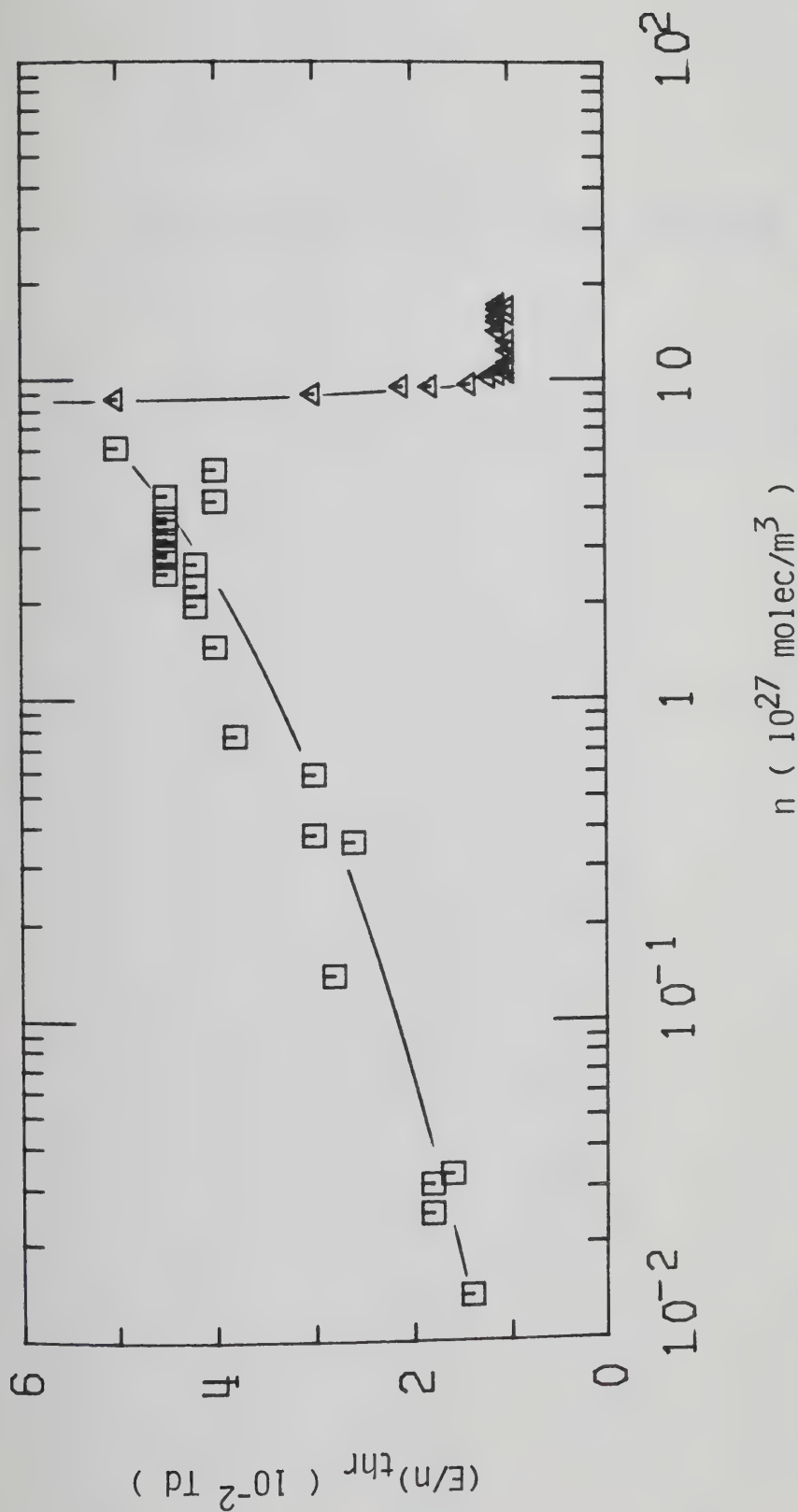


Figure III-3-16. Electric field threshold, $(E/n)_{thr}$, for electron heating in coexistence vapor and liquid CH_2D_2 as a function of density.

\square , $d\mu / d(E/n) > 0$; Δ , $d\mu / d(E/n) < 0$

TABLE III-3

Summary of Electron Results for CH₂D₂^a

T (K)	n (10 ²⁶ m ⁻³)	μ (m ² /Vs)	n _μ [10 ²⁵ (Vsm) ⁻¹]	(E/n) _{thr} (mTd)	d _μ /d(E/n)
94.0	0.143	1.76	2.52	14	+
94.3	0.145	1.80	2.61		
96.0	0.172	1.52	2.61		
100.0	0.257	0.94	2.42	18	+
102.0	0.312	0.80	2.50	18	+
102.8	0.330	0.80	2.64	16	+
133.0	0.370	0.68	2.52	18	+
170.8	0.370	0.74	2.74	22	+
230.3	0.370	0.83	3.07	40	+
293.5	0.370	0.90	3.33	60	+
351.7	0.370	0.97	3.59	80	+
409.6	0.370	1.02	3.77	90	+
450	0.370	1.05	3.89	130	+
113.0	0.61	0.379	2.31	13	+
151.0	0.61	0.42	2.56	22	+
225.5	0.61	0.49	2.99	40	+
294.0	0.61	0.54	3.29	60	+
340.0	0.61	0.57	3.48	70	+
408.5	0.61	0.61	3.72	90	+
120.8	1.37	0.153	2.10	28	+
137.7	3.58	0.058	2.08	26	+
139.0	3.82	0.054	2.06	30	+
147.8	5.9	0.0350	2.05	30	+
155.7	7.3	0.0275	2.01	28	+

(continued....)

Table III-3 continued

172.5	7.3	0.0320	2.34	30	+
195.5	7.3	0.0368	2.69	38	+
231.8	7.3	0.0422	3.08	45	+
292.0	7.3	0.049	3.58	55	+
154.0	7.7	0.0240	1.85	38	+
168.9	14.6	0.0121	1.77	40	+
175.3	19.8	0.0077	1.52	42	+
178.5	22.8	0.0064	1.46	42	+
180.1	24.8	0.0058	1.44	45	+
184.2	26.0	0.0059	1.53	40	+
186.0	26.0	0.0063	1.64	40	+
189.3	26.0	0.0073	1.90	40	+
192.0	26.0	0.0080	2.08	40	+
195.5	26.0	0.0089	2.31	40	+
181.4	26.5	0.0062	1.64	42	+
182.3	28.0	0.0050	1.40	45	+
182.6	28.3	0.0054	1.53	45	+
184.2	31.5	0.0045	1.42	45	+
185.5	34.0	0.0040	1.36	45	+
186.0	35.5	0.00370	1.31	45	+
186.6	37.0	0.00362	1.34	45	+
187.8	42	0.00341	1.43	40	+
188.0	43	0.00365	1.57	45	+
189.0	52	0.00313	1.63	40	+
189.2	61 ^b	0.00345	2.10	33	+
189.6	61 ^b	0.00452	2.76	30	+
189.8	61 ^b	0.00497	3.03	30	+
190.5	61 ^b	0.0059	3.60	30	+

(continued....)

Table III-3 continued

191.7	61 ^b	0.0071	4.33	30	+
192.9	61 ^b	0.0080	4.88	28	+
193.9	61 ^b	0.0085	5.19	27	+
189.0	75	0.0121	9.1	30	+
187.8	82	0.0225	18.5		
186.6	87	0.0250	21.8		
186.2	88	0.0310	27.3	50	-
186.1	88	0.0330	29.0		
185.5	91	0.0350	31.9	30	-
184.2	94	0.0430	40.4	21	-
183.8	95	0.0450	42.8	18	-
182.3	97	0.051	49.5	14	-
180.1	101	0.057	58	12	-
178.5	104	0.058	60	11	-
178.0	105	0.059	62	10	-
175.3	109	0.057	62	10	-
172.7	112	0.052	58	10	-
163.8	122	0.0395	48	10	-
153.5	131	0.0303	39.7	10	-
139.0	142	0.0268	38.1	11	-
124.0	152	0.0267	40.6	11	-
114.0	158	0.0280	44.2	11	-
109.0	161	0.0291	47	10	-
100.0	166	0.0310	51	11	-
93.0	169	0.0335	57	10	-
92.0	170	0.0340	58	11	-

a. The results appear in this table in the same order as the figures. They are given in order of increasing density.

b. $n_c = 6.1 \times 10^{27} \text{ molec/m}^3$, $T_c = 189.2\text{K}$.

4. CHD₃

In Figure III-4-1 is reported the variation of the mobility with field and temperature in the gas at $n = 2.30 \times 10^{25}$ molec/m³. The mobility is field independent at low fields and increases above a threshold value. The value of the threshold field increases with temperature. By raising the temperature from 102.0K to 622K the low field value of the mobility increases from 1.02 m²/Vs to 1.89 m²/Vs. The effect of an increase in density by a factor of almost two is shown in Figure III-4-2. The rate of change of the threshold field with temperature is the same as that observed at the lower density. The low field mobility increases by about 70% on raising the temperature from 106.6K to 434K.

In the saturated vapor (Figure III-4-3) the low field mobility is inversely proportional to the density. In Figure III-4-4 the effect of raising the temperature from 121.5K to 293.7K at $n = 12.2 \times 10^{25}$ molec/m³ is illustrated. The low field mobility increases by about 40% while the threshold field increases with temperature. It is 0.018 Td (1 Td = 10^{-21} m²V/molec) at $T = 121.5$ K and 0.06 Td at $T = 293.7$ K. This is consistent with the variation observed at lower densities. In this temperature region a change of about 20K causes a change in density of the saturated vapor of about a factor of 3 (Figure

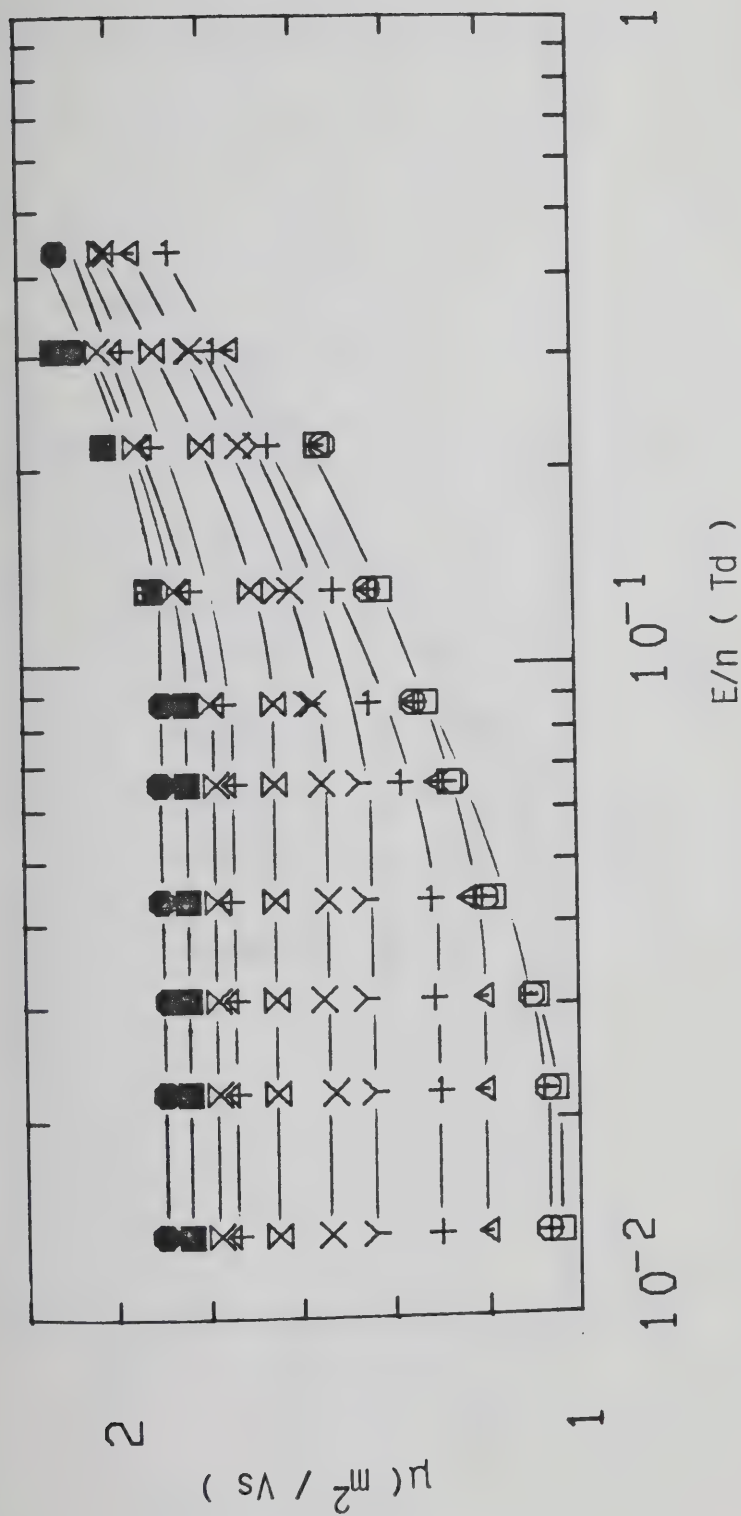


Figure III-4-1. Electron mobilities in CHD_3 gas at $n = 2.30 \times 10^{25} \text{ molec/m}^3$ and different temperatures (K). \square , 102.0; \circ , 135.0; \triangle , 175.2, $+$, 225.2; \Uparrow , 294.6; \times , 348.6; \boxtimes , 405.7; \uparrow , 465.6; \blacksquare , 516.7; \bullet , 568.7; \bullet , 622.

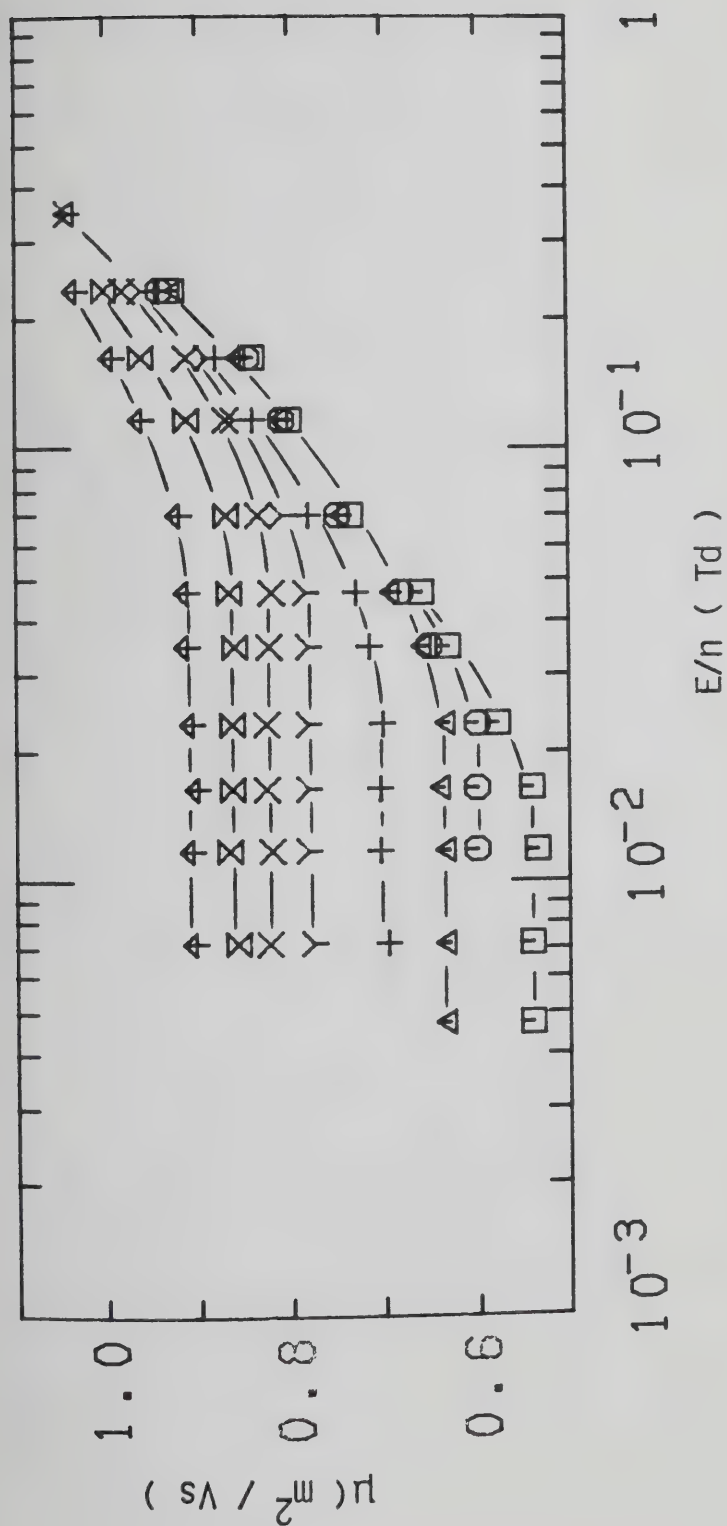


Figure III-4-2. Electron mobilities in CHD_3 gas at $n = 4.3 \times 10^{25} \text{ molec/m}^3$ and different temperatures (K). \square , 106.6; \circ , 135.5; Δ , 175.1; $+$, 235.6; Y , 294.6; X , 337.2; \otimes , 384.8; \uparrow , 434.

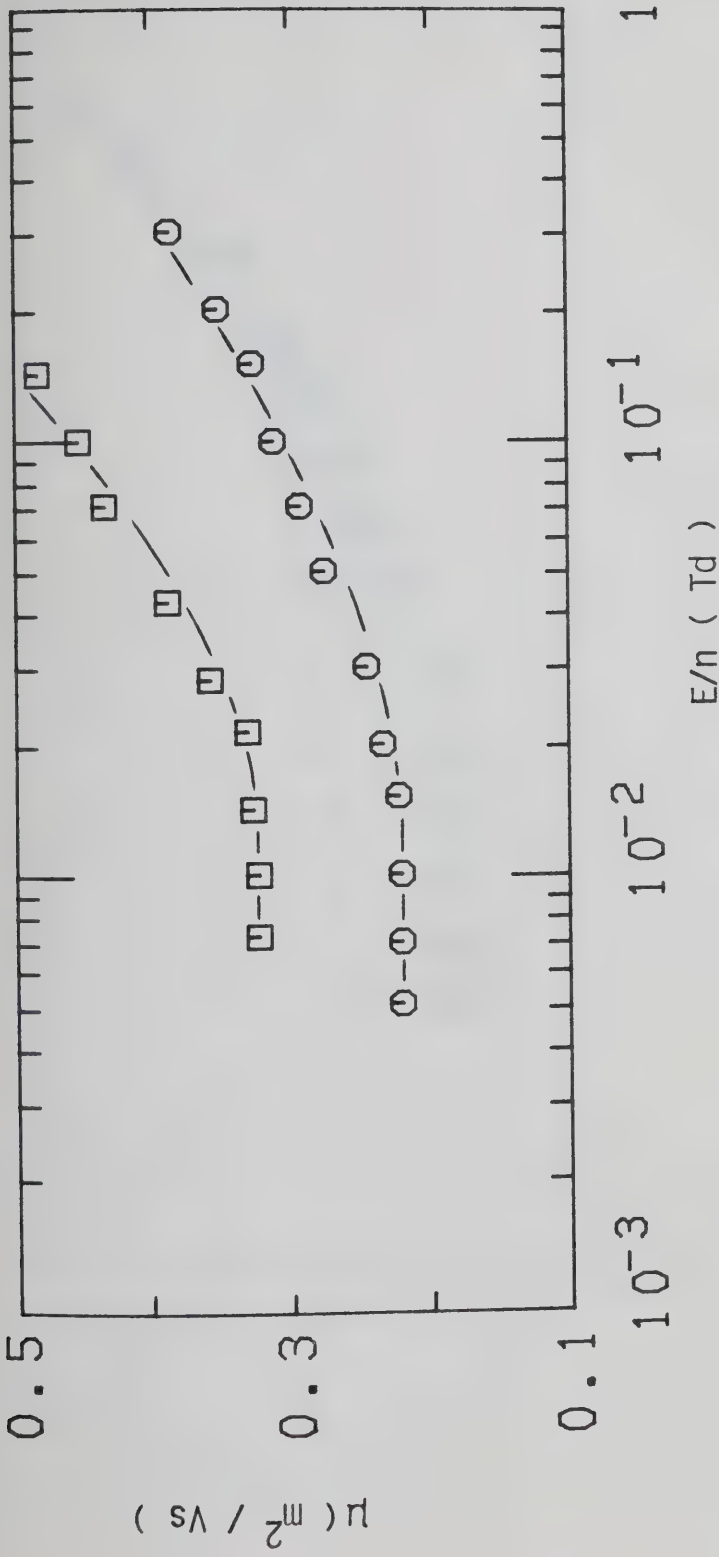


Figure III-4-3. Electron mobilities in saturated CHD_3 vapor at different densities (10^{25} molec/ m^3) and temperatures (K). \square , 7.0, 9.9, 115.8. \circ , 7.0, 111.1, 115.8.

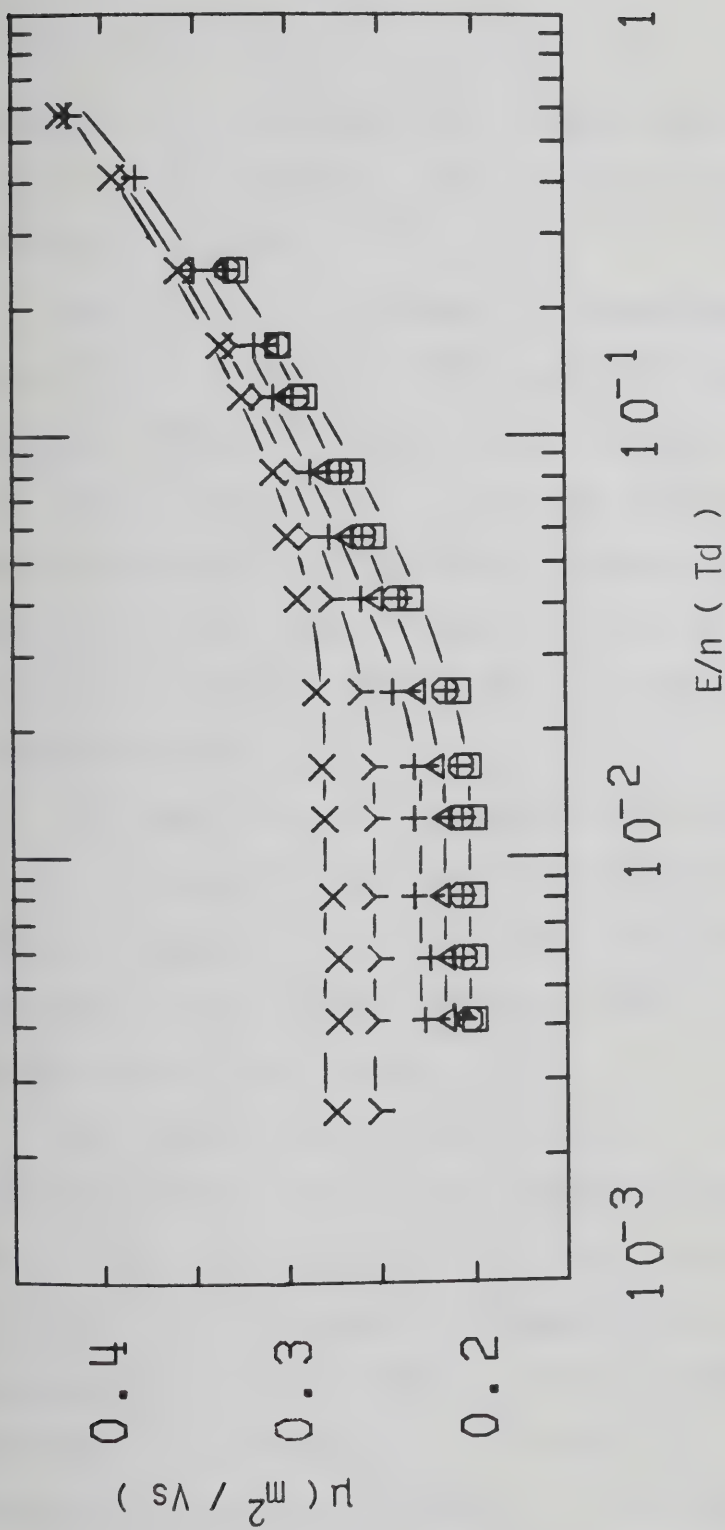


Figure III-4-4. Electron mobilities in CHD_3 gas at $n = 1.22 \times 10^{26} \text{ molec/m}^3$ and different temperatures (K). \square , 121.5; \circ , 136.0; \triangle , 156.0; +, 186.0; Y, 236.3; X, 293.7.

III-4-5). The increase in density lowers the mobility by about the same factor. The threshold field increases from 0.02 Td to 0.03 Td.

The effect of a change in temperature from 155.0K to 369.5K at $n = 6.8 \times 10^{26}$ molec/m³ is shown in Figure III-4-6. This causes the low field mobility to increase by more than a factor of 2. The same change in temperature at the lowest density produced an increase in mobility of only about 40%. The rate of change of the threshold field with temperature at this density is the same as that observed at lower densities.

In Figure III-4-7 is shown the effect of temperature on the threshold field at four densities different by a factor of about 2. An approximately linear dependence is observed in the range from about 100K to 600K, independent of density in this range.

In Figure III-4-8 are reported measurements in the saturated vapor. The small temperature and density changes show the consistency of the measurements. At $n = 9.3 \times 10^{26}$ molec/m³ (Figure III-4-9) raising the temperature from 161.0K to 293.8K causes the low field mobility to increase by a factor of about 2 and the threshold field from 0.035 Td to 0.06 Td. The effect of change in density of the saturated vapor by a factor of 2.8 is shown in Figures III-4-10 and III-4-11. The corresponding change in temperature is 22.8K. These changes

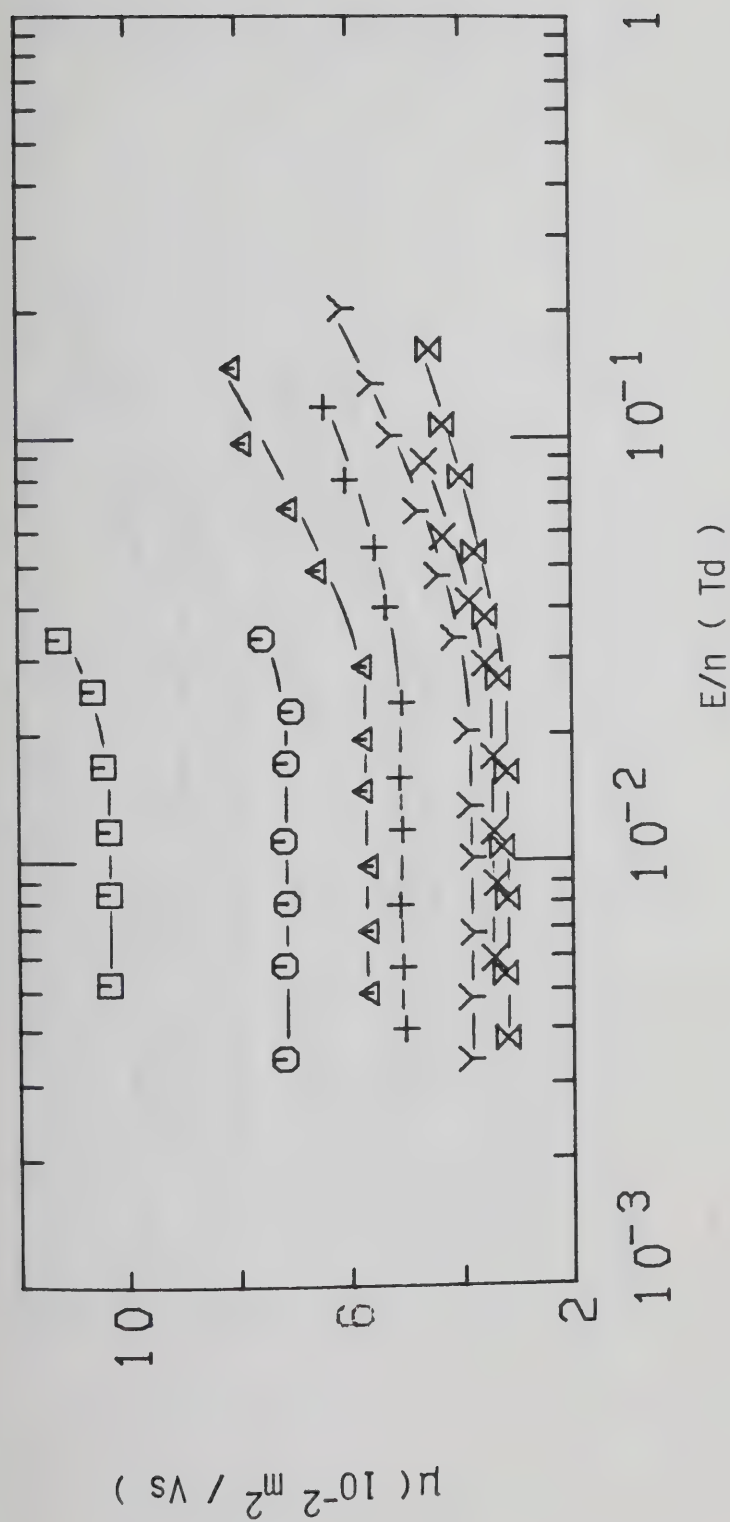


Figure III-4-5. Electron mobilities in saturated CHD_3 vapor at different densities ($10^{26} \text{ molec/m}^3$) and temperatures (K). \square , 1.85, 125.5; \circ , 2.76, 132.6; Δ , 3.22, 135.5; $+$, 3.94, 139.4; \times , 4.64, 142.8; \boxtimes , 5.5, 146.3; \boxtimes , 5.8, 147.5.

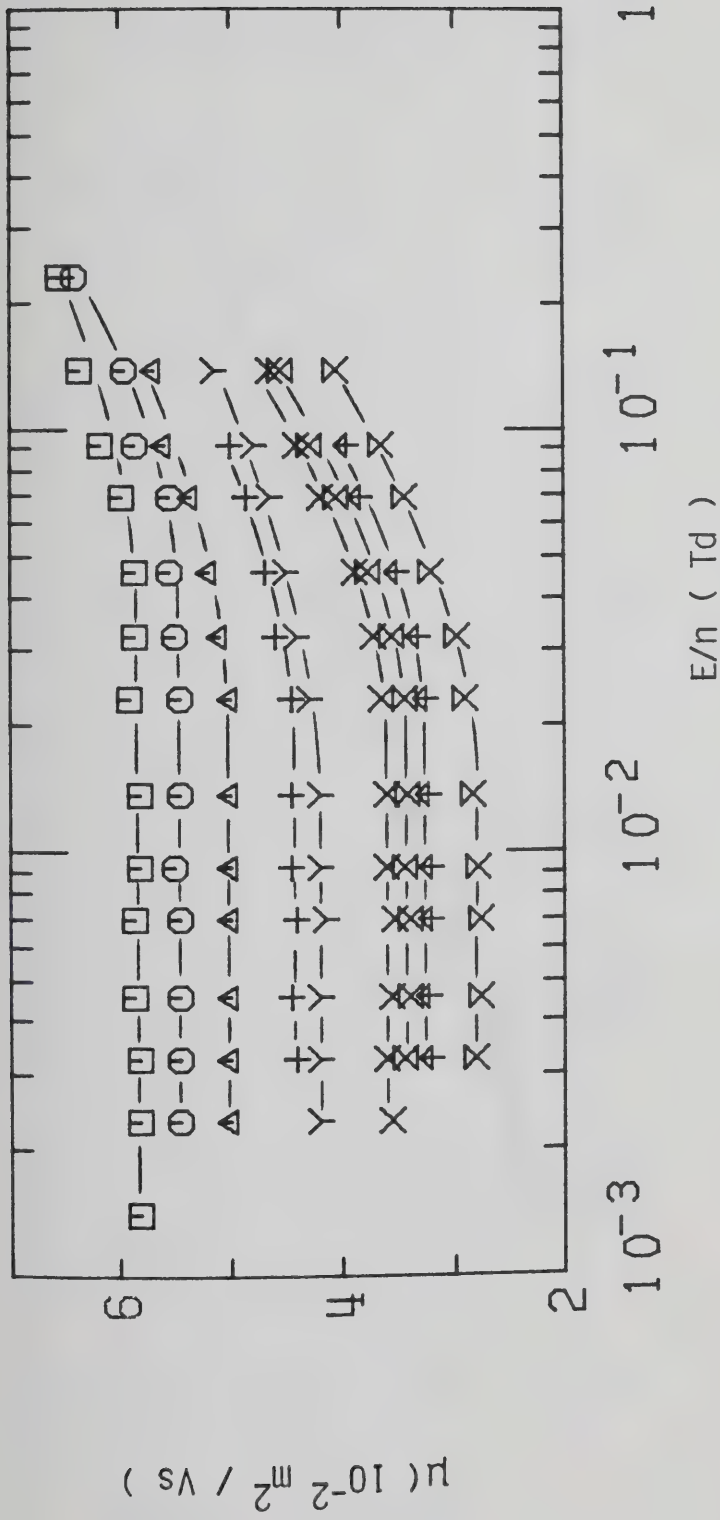


Figure III-4-6. Electron mobilities in CHD_3 gas at $n = 6.8 \times 10^{26} \text{ molec/m}^3$ and different temperatures (K). \square , 155.0; Δ , 168.5; \circ , 184.2; $+$, 194.7; \times , 235.0; \times , 250.5; Δ , 295.0; \circ , 331.0; \square , 369.5.

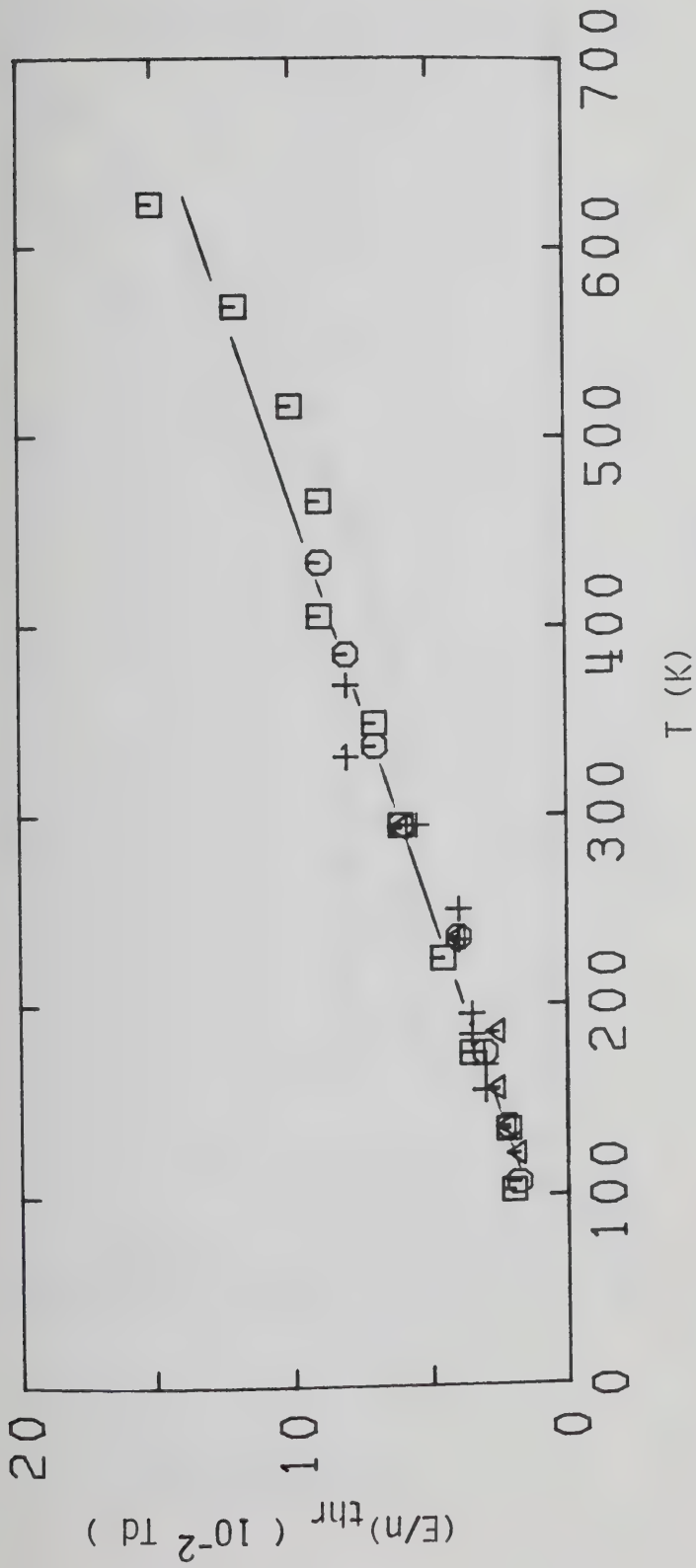


Figure III-4-7. Electric field threshold, $(E/n)_{thr}$, for electron heating in CHD_3 gas at different densities (10^{25} molec/m³) as a function of temperature. \square , 2.30; \circ , 4.3; Δ , 12.2; +, 68.

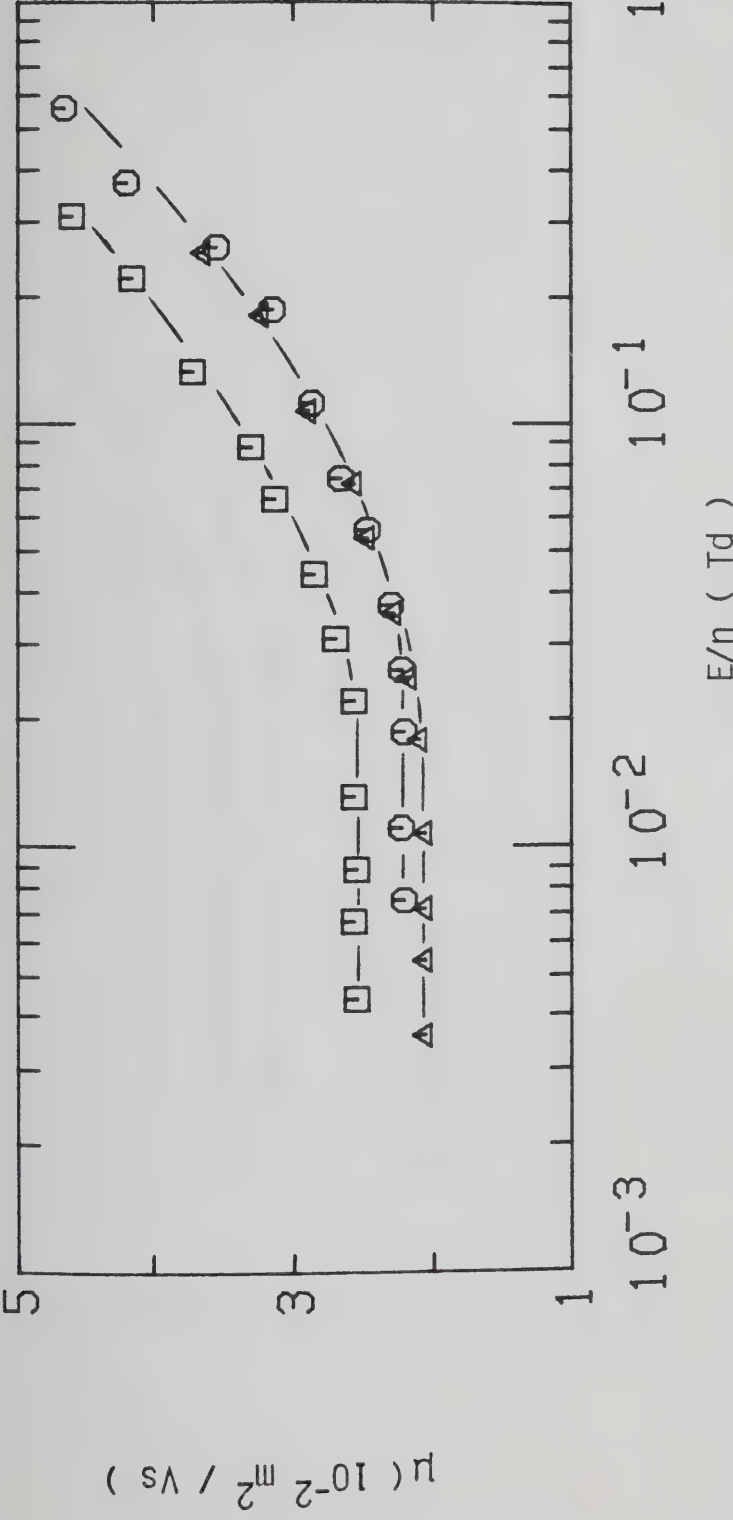


Figure III-4-8. Electron mobilities in saturated CHD_3 gas at different densities (10^{26} molec / m^3) and temperatures (K). \square , 7.1, 152.0; \circ , 8.4, 155.5; \triangle , 8.7, 156.0.

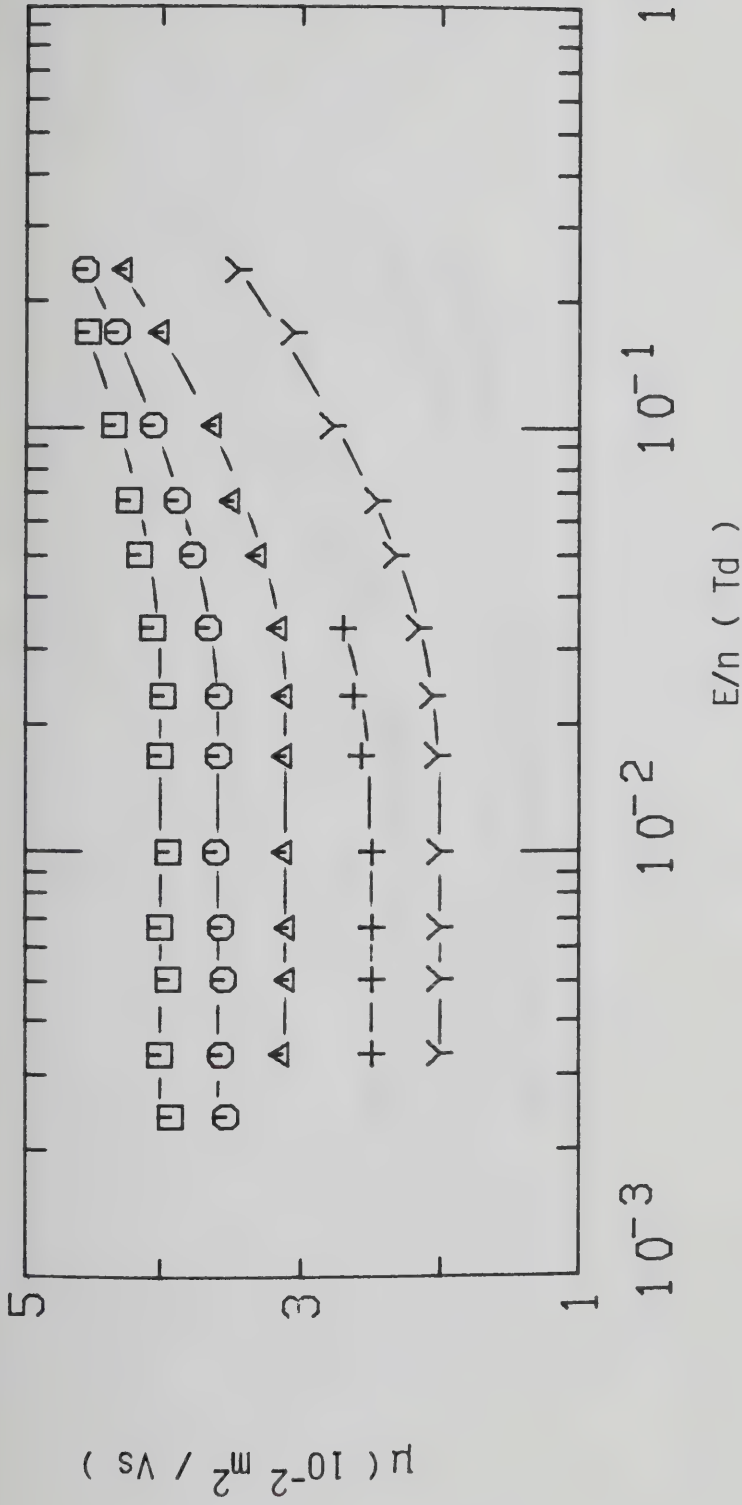
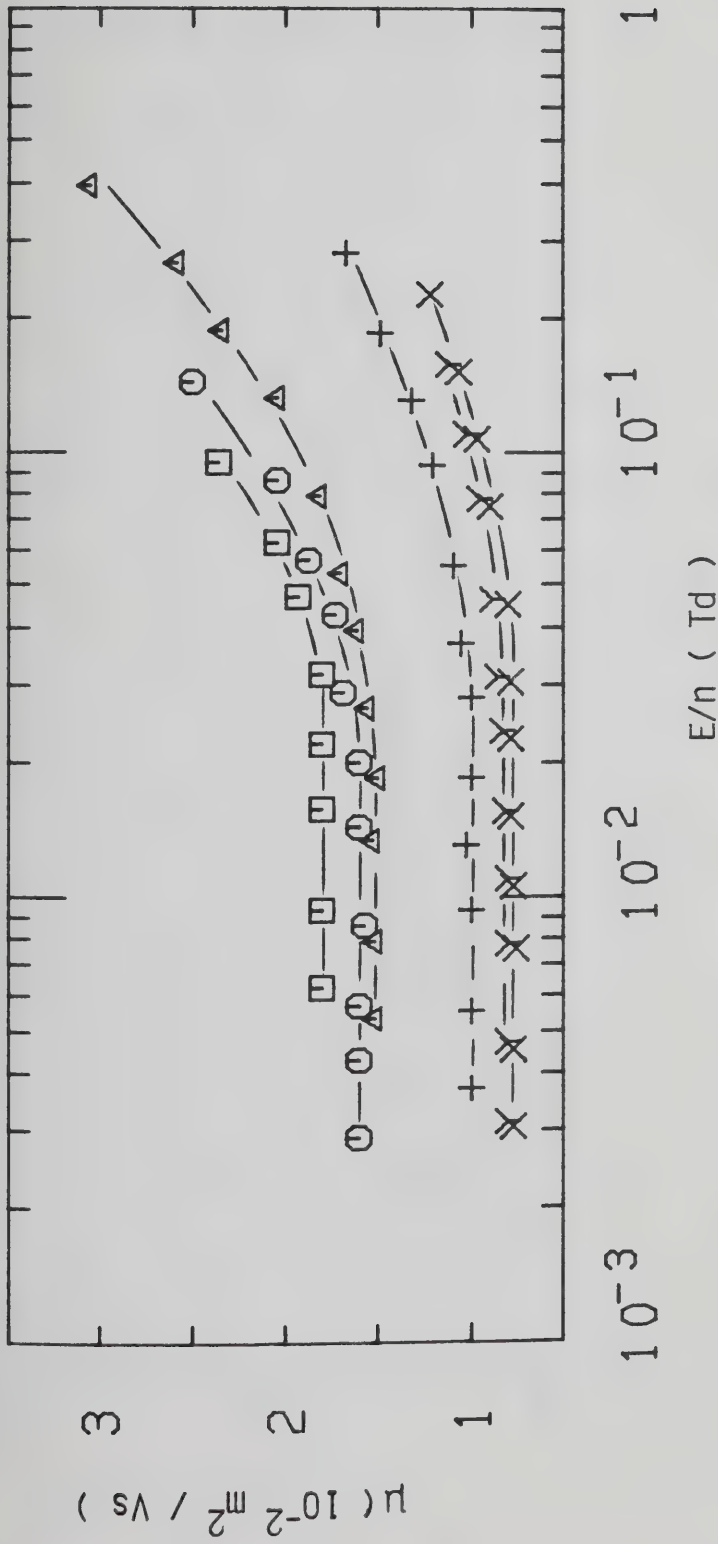


Figure III-4-9. Electron mobilities in CHD_3 gas at $n = 9.3 \times 10^{26} \text{ molec/m}^3$ and different temperatures (K). \square , 293.8; Δ , 216.0; $+$, 186.0; \circ , 256.5.



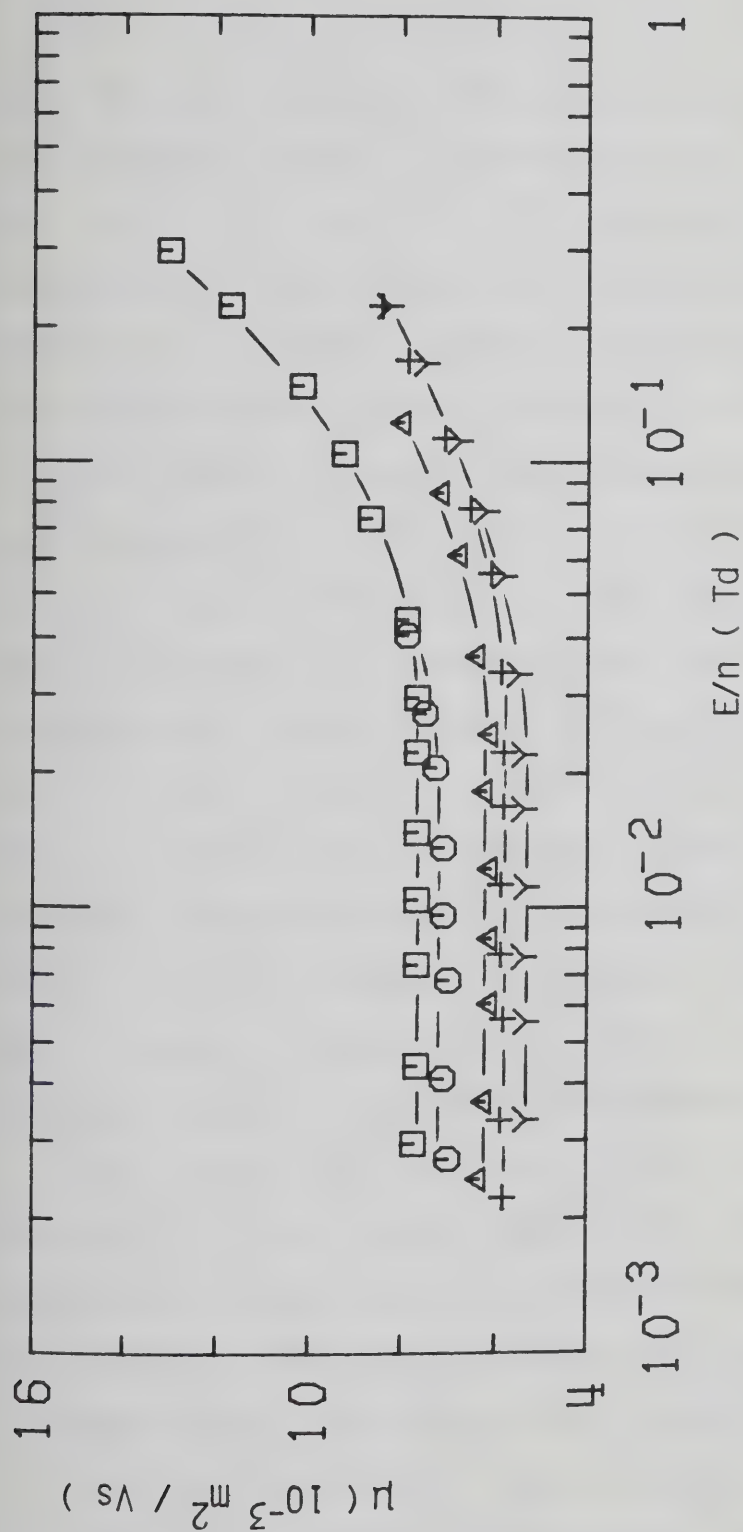


Figure III-4-11. Electron mobilities in saturated CHD_3 vapor at different densities (10^{27} molec/ m^3) and temperatures (K). \square , 2.12, 176.8; \circ , 2.37, 179.0; Δ , 2.65, 181.0; +, 2.70, 181.5; \times , 2.83, 182.3.

cause the low field mobility to drop by a factor of 3.4 and the threshold field to increase from 0.035 Td to 0.045 Td. At $n = 29.1 \times 10^{26}$ molec/m³ (Figure III-4-12) increasing the temperature from 184.0K to 192.8K causes the mobility to increase by 46%. In this limited temperature range the threshold field is constant at $E/n = 0.045$ Td.

The effect of approaching the critical density on the vapor saturation curve is shown in Figure III-4-13. The value of the threshold field does not appreciably change for an increase in temperature of only 4.9K. However the corresponding change in density is an increase by a factor of 1.6. This causes the low field mobility to drop by a factor of 1.5. At the critical density, $n_c = 6.1 \times 10^{27}$ molec/m³, (Figure III-4-14) an increase in temperature from 189.0K to 193.0K causes the low field mobility to increase by a factor of 2.3. $T_c = 189.0$ K. The value of the threshold field is approximately constant at $E/n \approx 0.03$ Td.

In Figure III-4-15 the effect of increasing the density of the liquid above the critical point is illustrated. As previously observed the field effect on the mobility undergoes a change of sign. The mobility increases with field above the threshold in the gas at $n = 6.1 \times 10^{27}$ molec/m³. The threshold value is at about 0.03 Td. At $n = 8.3 \times 10^{27}$ molec/m³ the field effect is zero up to $E/n \approx 0.06$ Td. At $n = 8.8 \times 10^{27}$ molec/m³ the mobility decreases with field above $E/n \approx 0.030$ Td. The

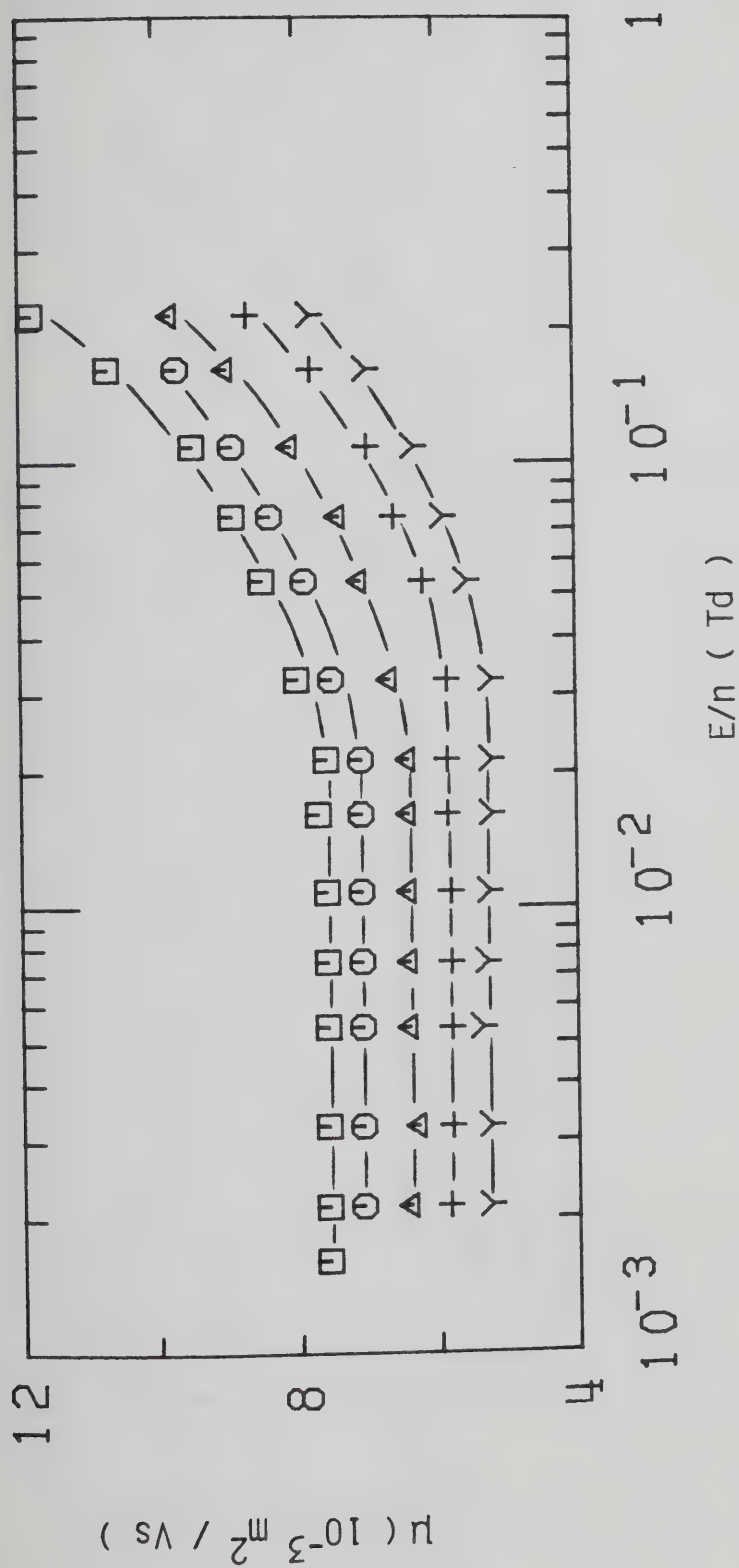


Figure III-4-12. Electron mobilities in CHD_3 gas at $n = 2.91 \times 10^{27} \text{ molec/m}^3$ and different temperatures (K). Y, 184.0; +, 187.0; Δ , 189.0; O, 192.0; \square , 193.8.

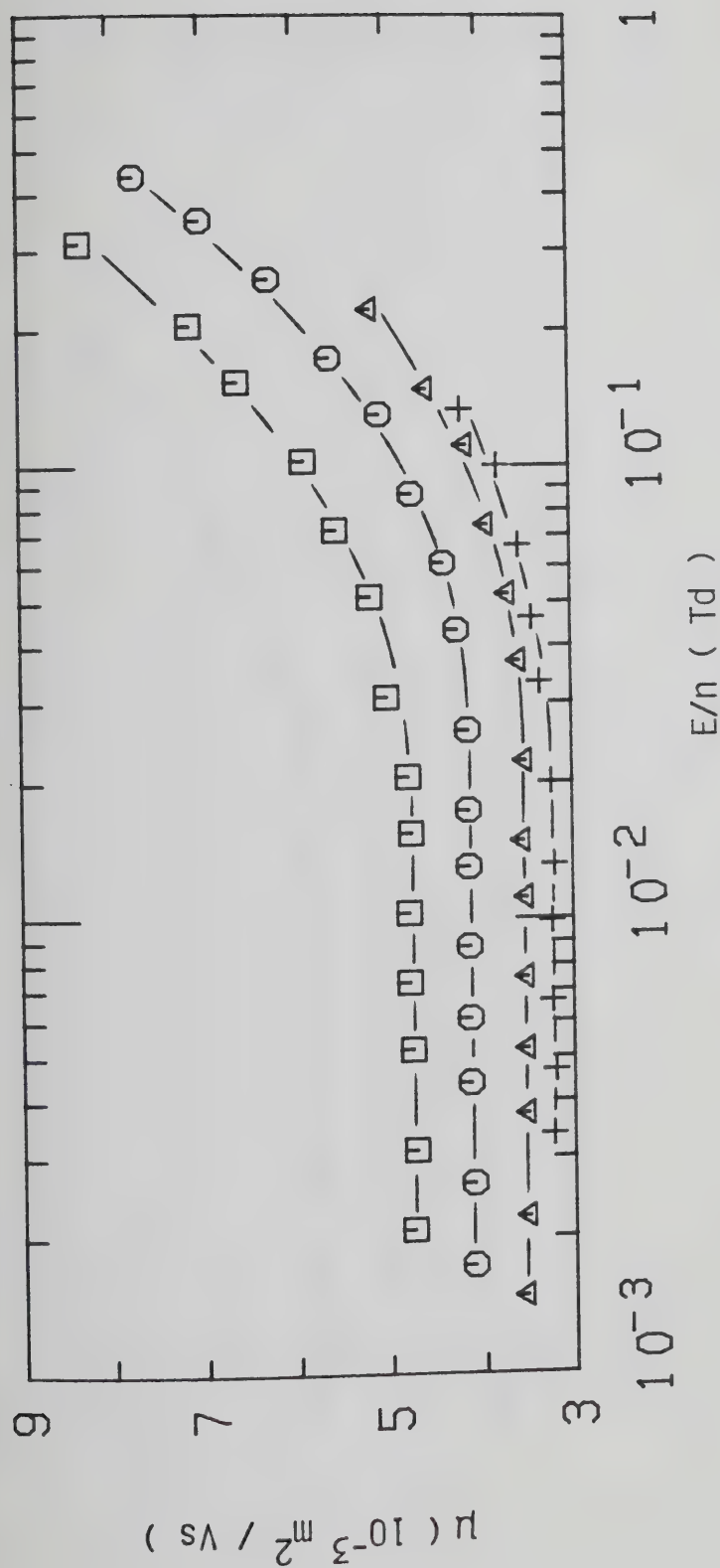


Figure III-4-13. Electron mobilities in saturated CHD_3 vapor at different densities ($10^{27} \text{ molec/m}^3$) and temperatures (K). \square , 3.03, 183.6; \circ , 3.60, 186.0; Δ , 4.22, 187.7; $+$, 4.7, 188.5.

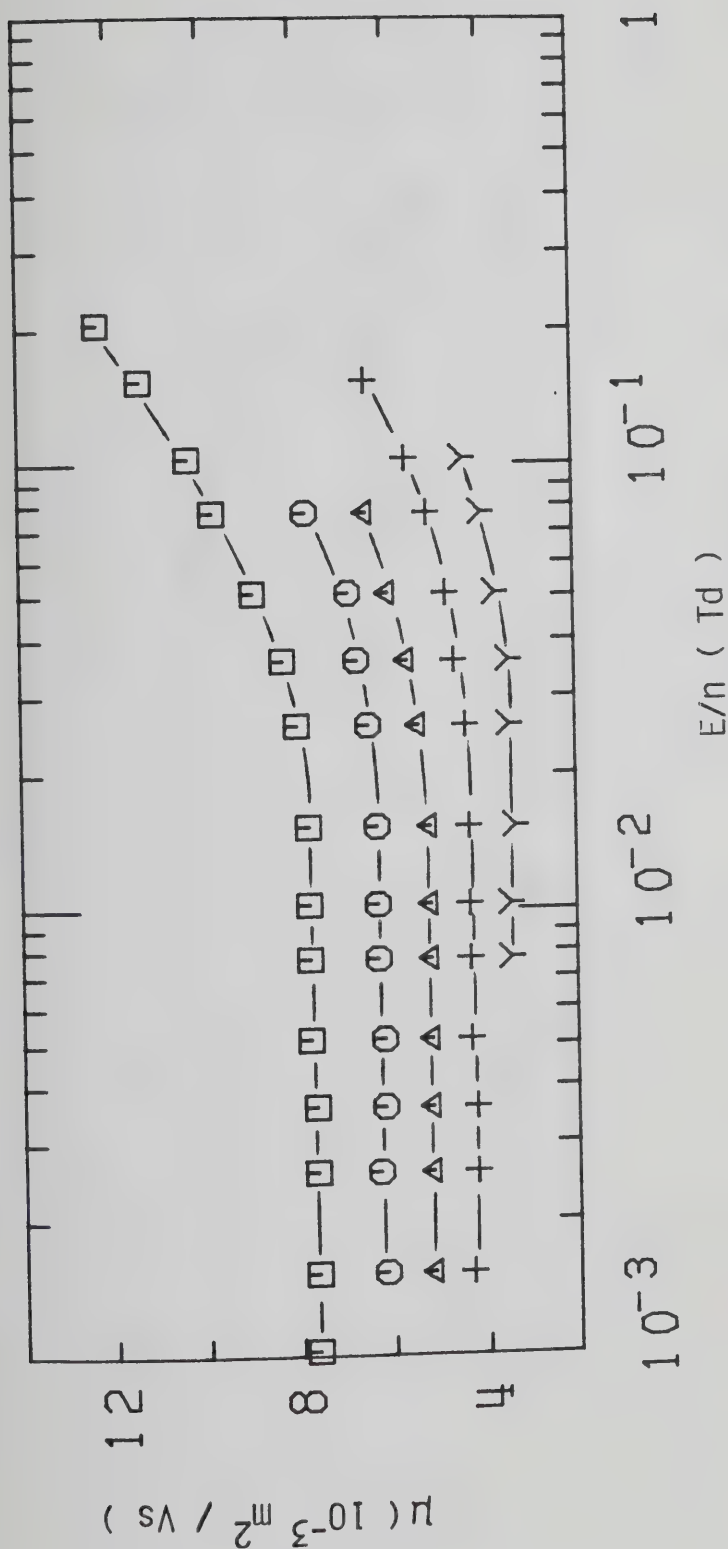


Figure III-4-14. Electron mobilities in supercritical CHD_3 gas at $n_c = 6.1 \times 10^{27} \text{ molec/m}^3$ and different temperatures (K). \circ , 191.2; \square , 193.0. $T_c = 189.0$. \triangle , 190.2; $+$, 189.5.

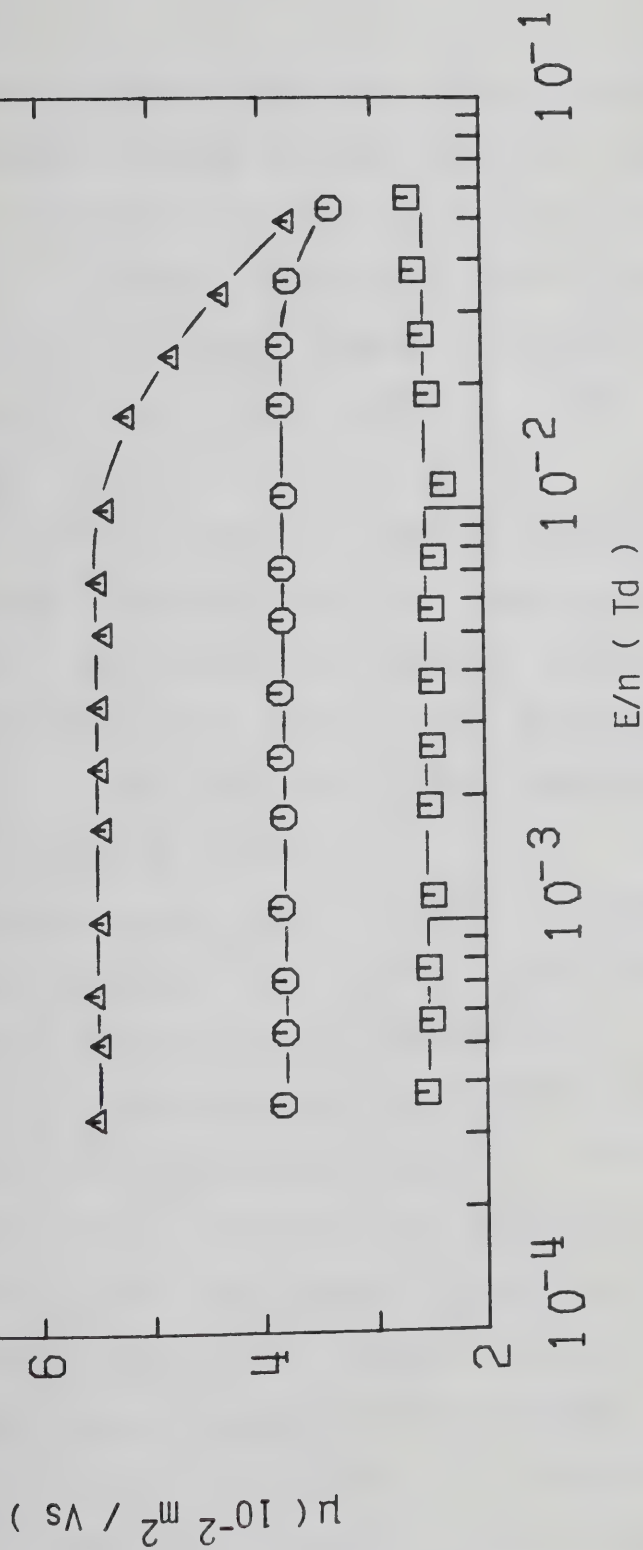


Figure III-4-15. Electron mobilities in liquid CHD_3 at different densities ($10^{27} \text{ molec/m}^3$) and temperatures (K). \square , 8.3, 187.7; \circ , 8.8, 186.0; Δ , 9.4, 183.6.

transition between the two effects occurs at a density intermediate between 8.3 and 8.8 (10^{27} molec/m³). In this density region the low field mobility increases with density. A further increase in density to $n = 10.3 \times 10^{27}$ molec/m³ in the liquid (Figure III-4-16) produces a further increase in low field mobility. The threshold field decreases from 1×10^{-2} Td to 8×10^{-3} Td. At $n > 10.6 \times 10^{26}$ molec/m³ (Figure III-4-17) a decrease in low field mobility as the density is increased is observed. The threshold field is constant at $E/n \approx 9$ mTd between 178.6K, $n = 10.6 \times 10^{27}$ molec/m³ and $T = 155.3$ K, $n = 13.0 \times 10^{27}$ molec/m³. The mobility curves tend to merge at about 0.1 Td.

In Figure III-4-18 is shown the effect of increasing the density of the liquid to $n = 16.9 \times 10^{27}$ molec/m³. The low field mobility is approximately constant between 14.0×10^{27} molec/m³ and 14.8×10^{27} molec/m³ and then it increases with increasing density. The threshold field is constant at $E/n \approx 9 \times 10^{-3}$ Td. The mobility curves tend to merge at 0.1 Td. In Figure III-4-19 the effect of density and temperature on the threshold field in the saturated vapor and liquid phases is illustrated. In the vapor the threshold field increases in a temperature range from 111.1K at the lowest density to 188.5K at the highest from a value of 0.018 Td to a value of 0.05 Td. The field effect undergoes a change of sign in the liquid at a

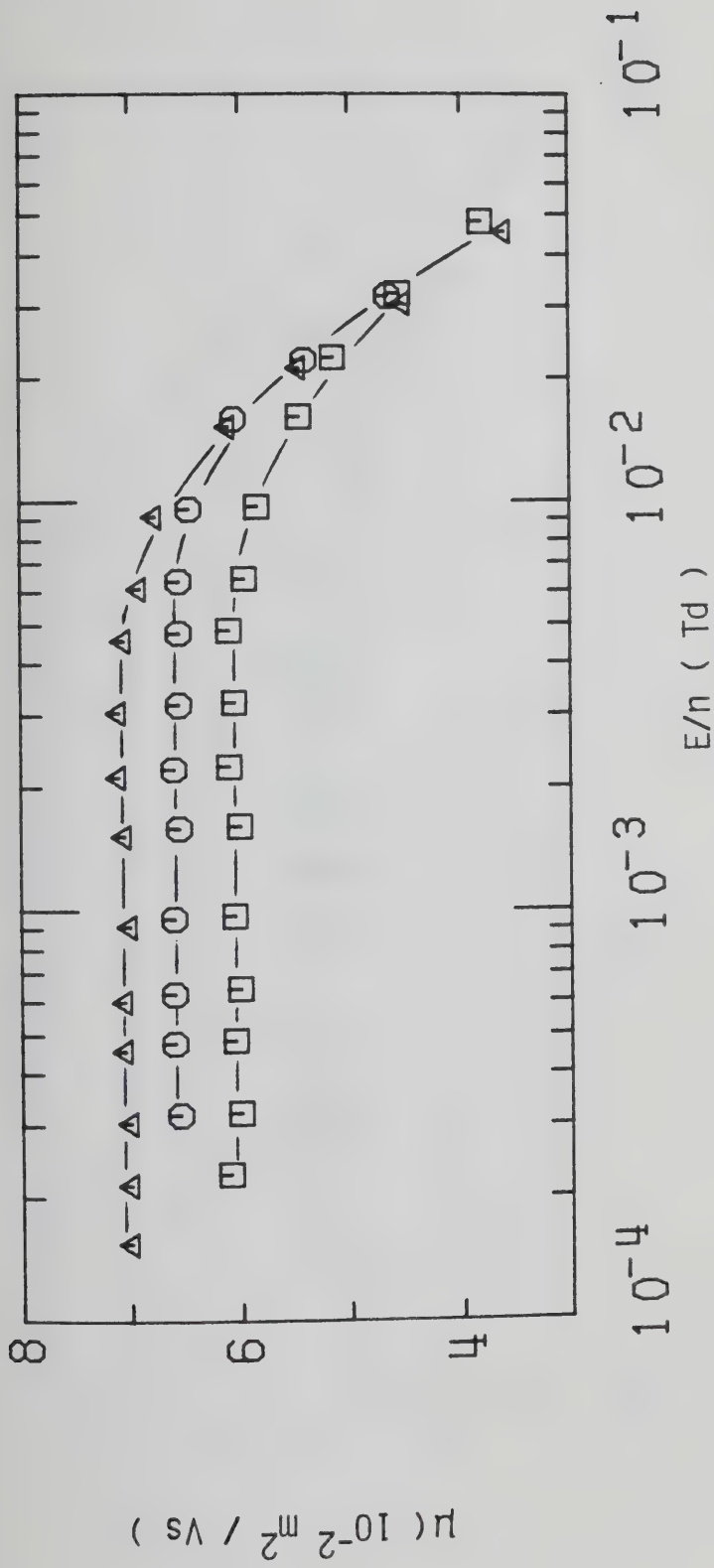


Figure III-4-16. Electron mobilities in liquid CHD_3 at different densities ($10^{27} \text{ molec/m}^3$) and temperatures (K). \square , 9.7, 182.4; O , 9.9, 181.5; Δ , 10.3, 178.9.

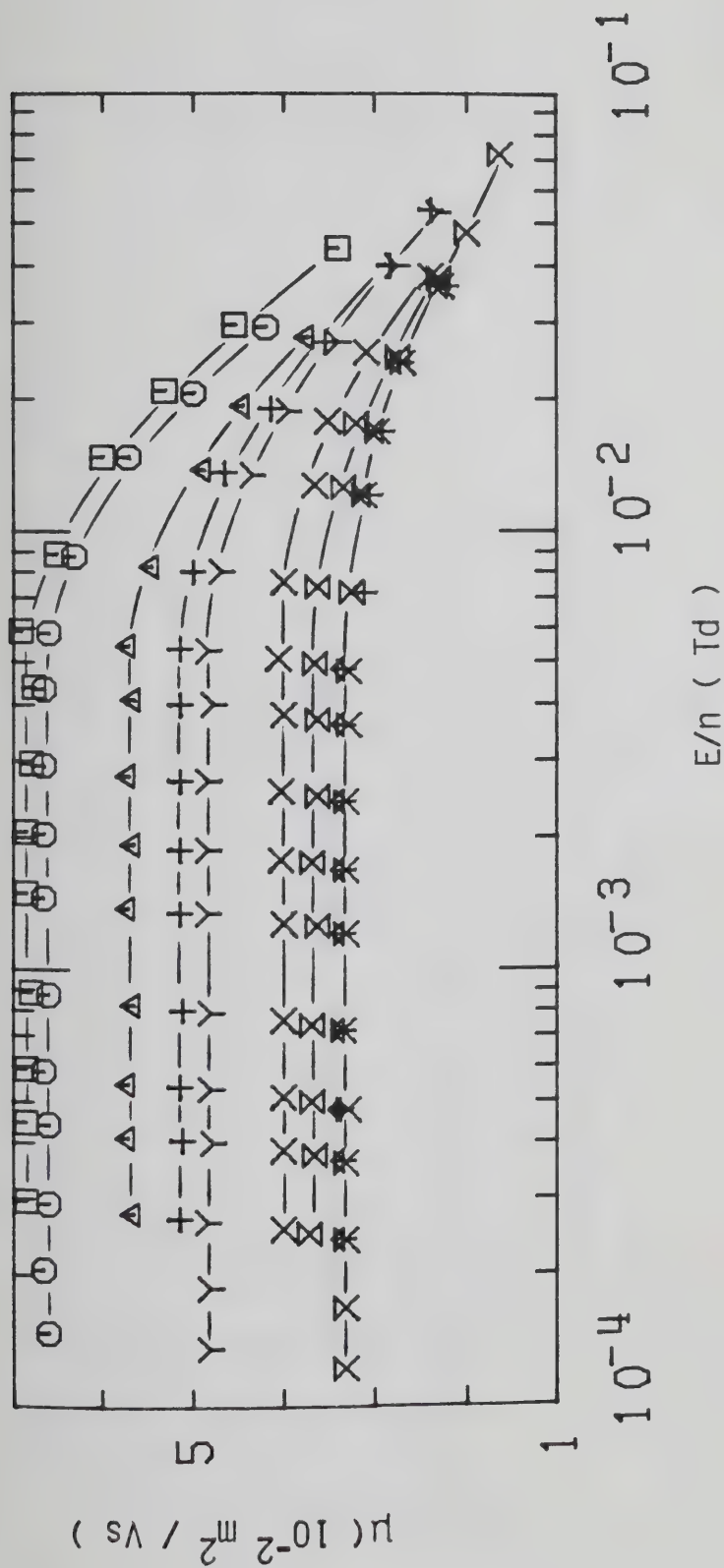


Figure III-4-17. Electron mobilities in liquid CHD_3 at different densities ($10^{27} \text{ molec/m}^3$) and temperatures (K). \square , 10.6, 178.6; \circ , 10.7, 175.4; Δ , 11.4, 171.7; $+$, 11.6, 169.5; Y , 11.7, 168.0; X , 12.3, 163.1; Σ , 12.6, 159.5; \uparrow , 13.0, 155.5; \times , 13.0, 155.3.

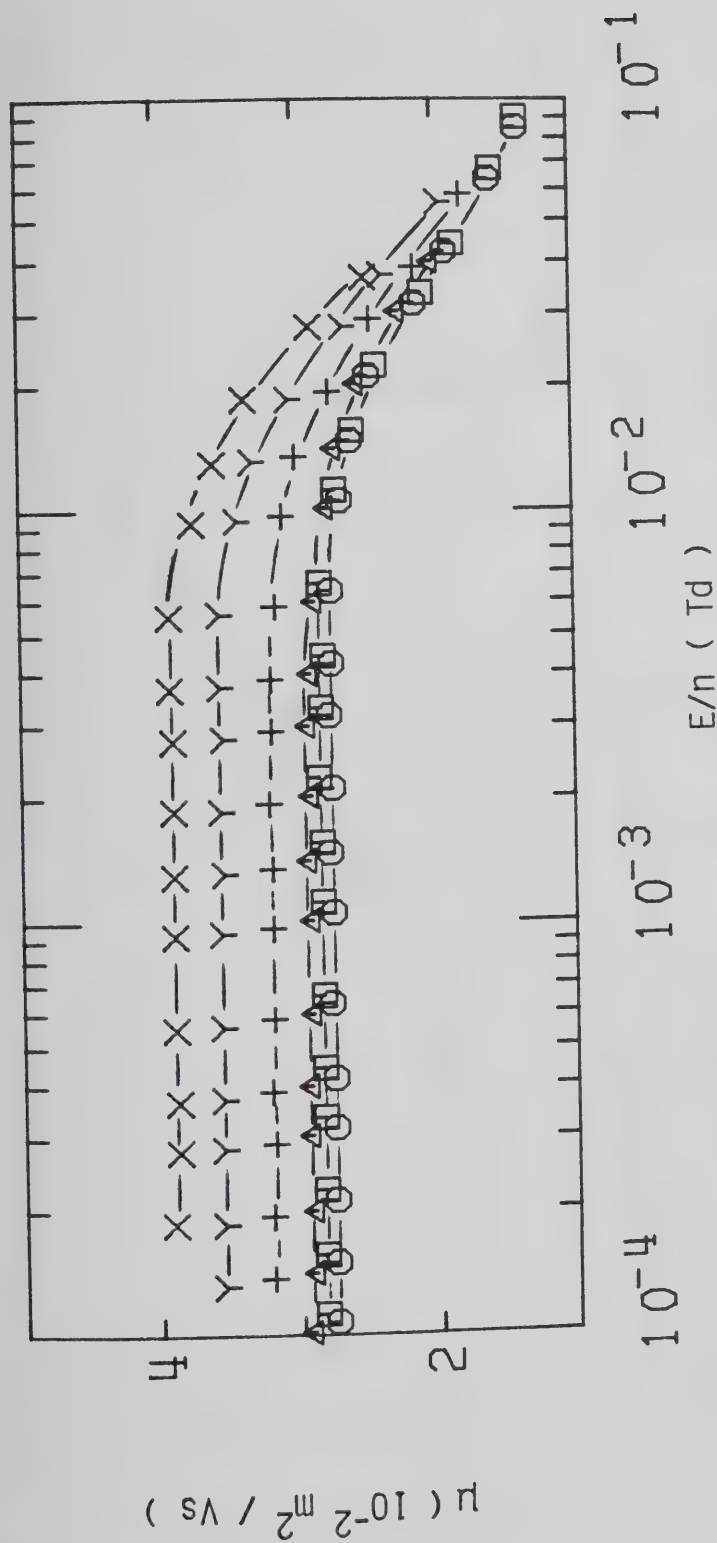


Figure-III-4-18. Electron mobilities in liquid CHD_3 at different densities ($10^{27} \text{ molec/m}^3$) and temperatures (K). \square , 14.0, 141.7; \circ , 14.8, 130.3; Δ , 15.5, 119.2; $+$, 16.1, 108.9; \times , 16.9, 92.1.

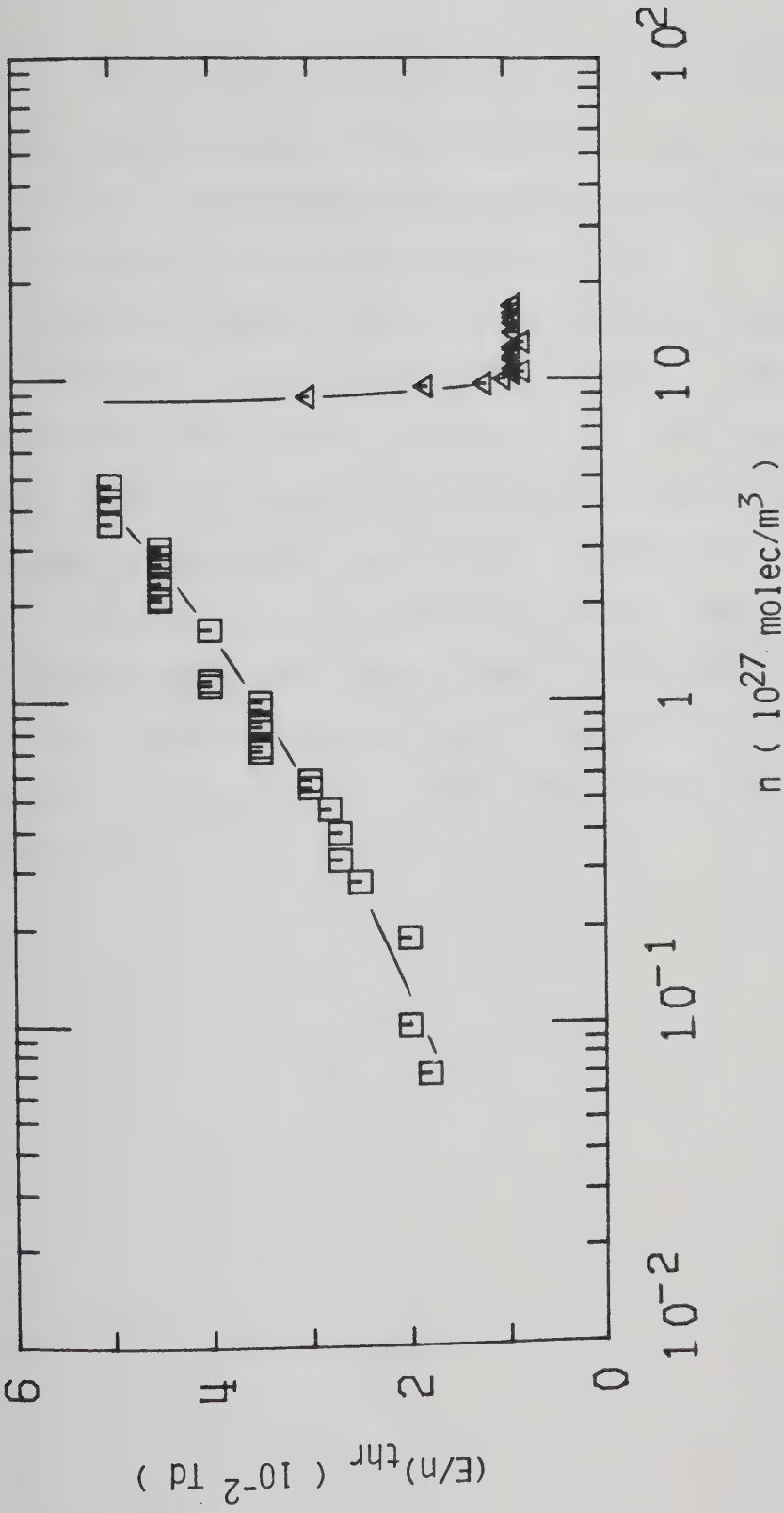


Figure III-4-19. Electric field threshold, $(E/n)_{thr}$, for electron heating in coexistence vapor and liquid CHD_3 as a function of density. \square , $d\mu / d(E/n) > 0$; \triangle , $d\mu / d(E/n) < 0$.

density intermediate between 8.3 and 8.8 (10^{27} molec/m³). In the normal liquid the threshold field is $(E/n)_{\text{thr}} \approx 9 \times 10^{-3}$ Td, independent of temperature and density and is lower than any value observed in the gas.

Data in Figures III-4-1 to III-4-4 were obtained with low pressure type conductance cells. The electrode separations were 0.999 ± 0.001 cm. All the other gas phase results were obtained in high pressure gas type cells. The electrode separations were 0.315 ± 0.005 cm. Liquid data were obtained in high pressure liquid type cells. The electrode separations were 0.320 ± 0.001 cm. A listing of the low field mobilities and threshold voltages at the different temperatures and densities is given in Table III-4.

TABLE III-4

Summary of Electron Results for CHD_3^a

T (K)	n (10^{26} m^{-3})	μ (m^2/Vs)	$n\mu$ [$10^{25} (\text{Vsm})^{-1}$]	(E/n) _{thr} (mTd)	$d\mu/d(E/n)$
102.0	0.230	1.02	2.35	20	+
135.0	0.230	1.08	2.48	22	+
175.2	0.230	1.21	2.78	35	+
225.2	0.230	1.31	3.01	45	+
294.6	0.230	1.45	3.34	60	+
348.6	0.230	1.54	3.54	70	+
405.7	0.230	1.65	3.80	90	+
465.6	0.230	1.75	4.03	90	+
516.7	0.230	1.78	4.09	100	+
568.7	0.230	1.84	4.23	120	+
622	0.230	1.89	4.35	150	+
106.6	0.43	0.54	2.32	18	+
135.5	0.43	0.60	2.58	22	+
175.1	0.43	0.63	2.71	30	+
235.6	0.43	0.70	3.01	40	+
294.6	0.43	0.78	3.35	60	+
337.2	0.43	0.82	3.53	70	+
384.8	0.43	0.86	3.70	80	+
434	0.43	0.91	3.91	90	+
111.1	0.70	0.325	2.28	18	+
115.8	0.99	0.221	2.19	20	+
121.5	1.22	0.200	2.44	18	+
136.0	1.22	0.205	2.50	22	+
156.0	1.22	0.216	2.64	25	+
186.0	1.22	0.230	2.81	25	+

(continued....)

Table III-4 continued

236.3	1.22	0.252	3.07	40	+
293.7	1.22	0.276	3.37	60	+
125.5	1.85	0.103	1.91	20	+
132.6	2.76	0.072	1.99	25	+
135.5	3.22	0.057	1.84	27	+
139.4	3.94	0.051	2.01	27	+
142.8	4.64	0.0382	1.77	28	+
146.3	5.5	0.0338	1.86	30	+
147.5	5.8	0.0323	1.87	30	+
155.0	6.8	0.0277	1.88	30	+
168.5	6.8	0.0322	2.19	30	+
184.2	6.8	0.0342	2.33	35	+
194.7	6.8	0.0358	2.43	35	+
235.0	6.8	0.0420	2.86	40	+
250.5	6.8	0.0443	3.01	40	+
295.0	6.8	0.050	3.40	55	+
331.0	6.8	0.055	3.74	80	+
369.5	6.8	0.059	4.01	80	+
152.0	7.1	0.0255	1.81	35	+
155.5	8.4	0.0222	1.86	35	+
156.0	8.7	0.0206	1.79	35	+
161.0	9.3	0.0200	1.86	35	+
186.0	9.3	0.0250	2.33		
216.0	9.3	0.0312	2.90	40	+
256.5	9.3	0.0358	3.33	50	+
293.8	9.3	0.0397	3.69	60	+
158.5	9.7	0.0186	1.80	35	+
159.5	10.0	0.0181	1.81	35	+
162.0	11.3	0.0161	1.82	40	+
163.1	11.8	0.0152	1.79	40	+

(continued....)

Table III-4 continued

171.7	16.9	0.0100	1.69	40	+
176.2	20.7	0.0080	1.66	45	+
176.2	20.7	0.0077	1.59	45	+
176.8	21.2	0.0077	1.63	45	+
179.0	23.7	0.0071	1.68	45	+
181.0	26.5	0.0062	1.64	45	+
181.5	27.0	0.0058	1.57	45	+
182.3	28.3	0.0054	1.53	45	+
184.0	29.1	0.0052	1.51	45	+
187.0	29.1	0.0058	1.69	45	+
189.0	29.1	0.0064	1.86	45	+
192.0	29.1	0.0071	2.07	45	+
193.8	29.1	0.0076	2.21	45	+
183.6	30.3	0.00475	1.44	45	+
186.0	36.0	0.00413	1.49	50	+
187.7	42.2	0.00352	1.49	50	+
188.5	47	0.00322	1.51	50	+
189.0	61 ^b	0.00340	2.07	35	+
189.5	61 ^b	0.00427	2.60	30	+
190.2	61 ^b	0.0052	3.17	30	+
191.2	61 ^b	0.0063	3.84	30	+
192.0	61 ^b	0.0068	4.15		
193.0	61 ^b	0.0078	4.76	28	+
187.7	83	0.0248	20.6	>60	
186.0	88	0.0383	33.7	30	-
183.6	94	0.054	51	19	-
182.4	97	0.061	59	12	-
181.5	99	0.066	65	10	-
178.9	103	0.071	73	9	-
176.8	106	0.069	73	8	-
175.4	107	0.067	72	9	-
171.7	114	0.057	65	9	-

(continued....)

Table III-4 continued

169.5	116	0.052	60	9	-
168.0	117	0.048	56	9	-
163.1	123	0.040	49	9	-
159.5	126	0.0367	46.2	9	-
155.5	130	0.0335	43.6	8	-
155.3	130	0.0333	43.3	8	-
141.7	140	0.0284	39.8	9	-
130.3	148	0.0276	40.8	9	-
119.2	155	0.0291	45.1	9	-
108.9	161	0.0320	52	9	-
99.8	167	0.0355	59	9	-
92.1	169	0.0390	66	9	-

a. The results appear in this table in the same order of appearance as the figures. They are given in order of increasing density.

b. $n_c = 6.1 \times 10^{27}$ molec/m³, $T_c = 189.0\text{K}$.

5. CD₄

In Figure III-5-1 are reported measurements of the mobility in the saturated vapor as a function of field and density. The mobility is independent of field strength for fields lower than a threshold value. Above this value the mobility increases with increasing field. The value of the low field mobility is inversely proportional to the density. The effect of raising the temperature at two different densities is shown in Figures III-5-2 and 3. At $n = 3.20 \times 10^{25}$ molec/m³ raising the temperature from 106.0K to 598K causes the low field mobility to increase from 0.70 m²/Vs to 1.34 m²/Vs and the threshold field from 0.015 Td to 0.15 Td ($T_d = 10^{-21}$ m²V/molec). At $n = 5.0 \times 10^{25}$ molec/m³ an increase in temperature from 111.8K to 521K produces an increase in low field mobility from the value of 0.47 m²/Vs to that of 0.83 m²/Vs. The threshold field is 0.02 Td at the lowest temperature and 0.12 Td at the highest. The mobility curves tend to merge at $E/n \approx 0.6$ Td.

In Figure III-5-4 are reported measurements in the saturated vapor as the density is increased from 1.23×10^{26} molec/m³ to 4.46×10^{26} molec/m³. The corresponding change in temperature is from 119.3K to 142.0K. In this region the low field mobility decreases by a factor of 3.6. A change in temperature of about 25K

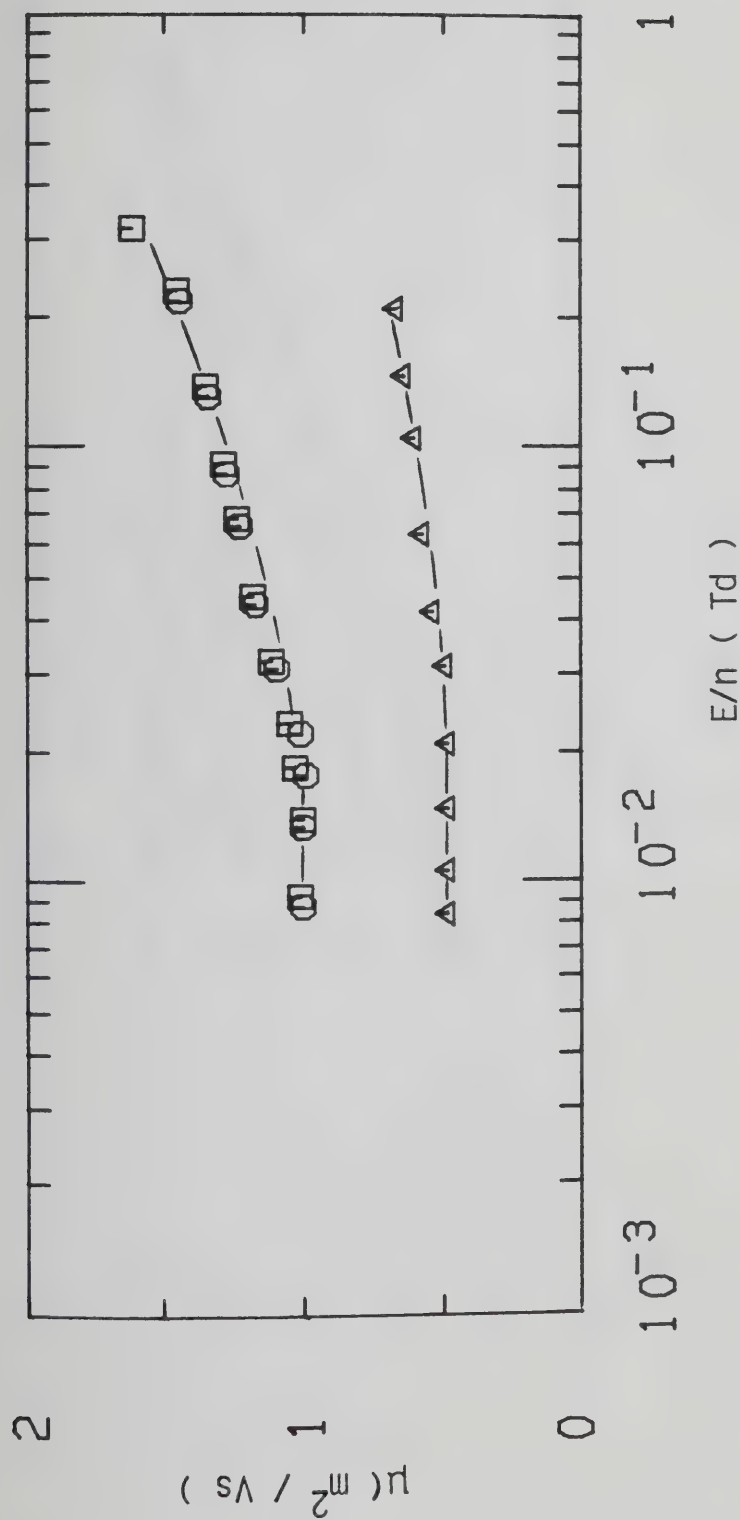


Figure III-5-1. Electron mobilities in saturated CD_4 vapor at different densities ($10^{25} \text{ molec}/\text{m}^3$) and temperatures (K). \square , 2.32, 98.3; \circ , 2.56, 99.3; Δ , 5.0, 107.8.

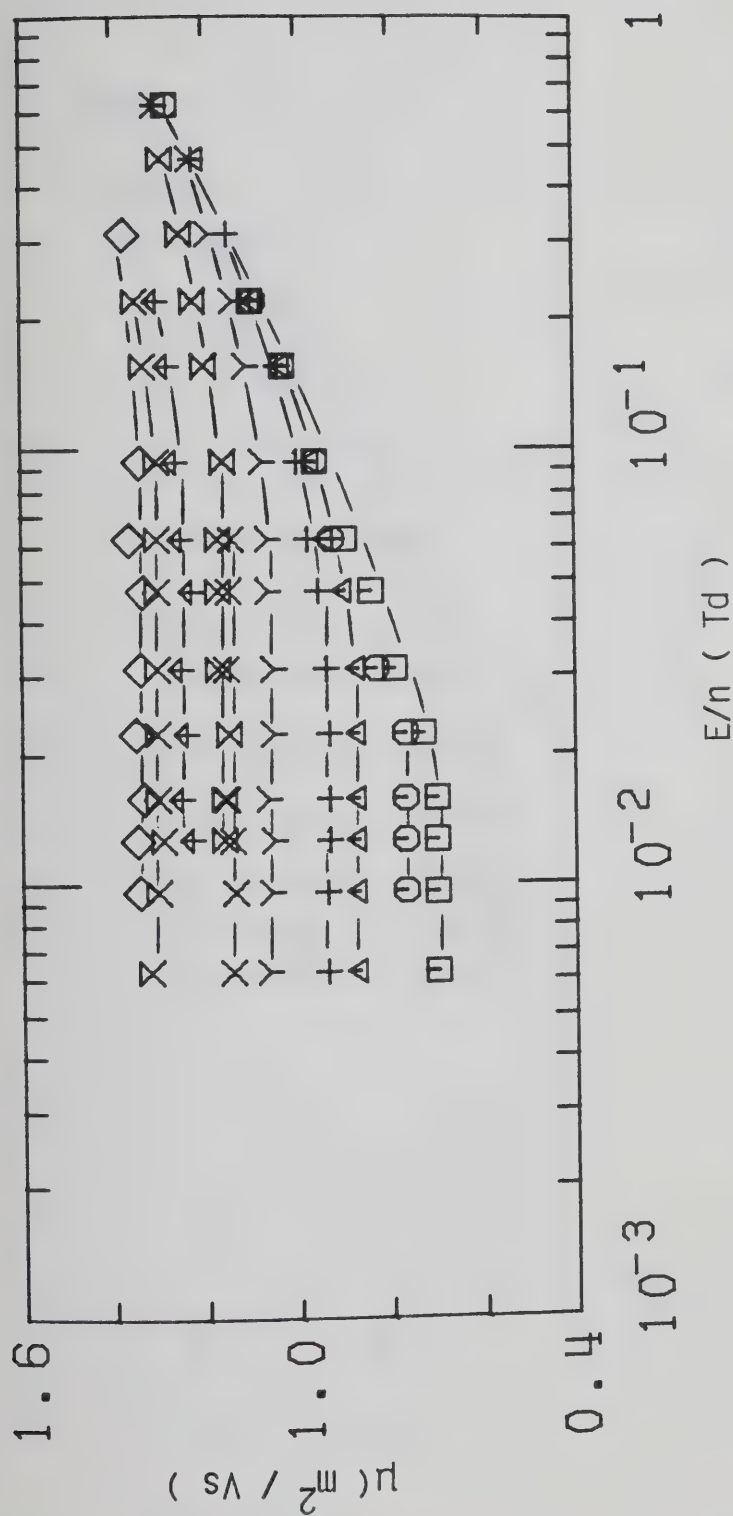


Figure III-5-2. Electron mobilities in CD_4 gas at $n = 3.20 \times 10^{25} \text{ molec/m}^3$ and different temperatures (K). \square , 106.0; \circ , 130.0; Δ , 159.2; $+$, 214.4; Y, 293.2; X, 356; Z, 414; \uparrow , 474; \times , 536; \diamond , 598.

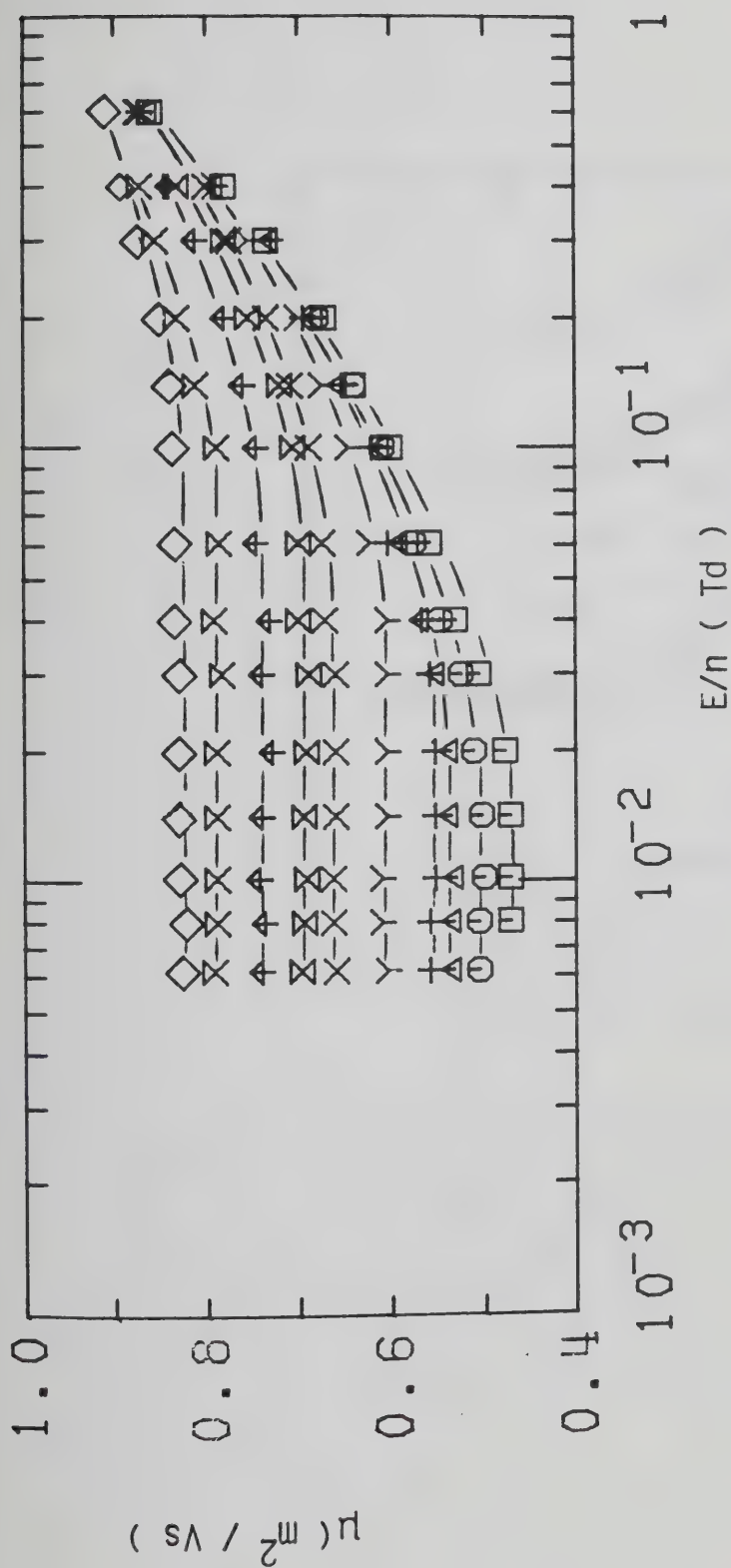


Figure III-5-3. Electron mobilities in CD_4 gas at $n = 5.0 \times 10^{25} \text{ molec/m}^3$ and different temperatures (K). \square , 111.8; \circ , 131.0; \triangle , 150.6; $+$, 179.9; γ , 230.5; \times , 294.5; \boxtimes , 337.4; \uparrow , 395; \boxtimes , 454.3; \diamond , 521.

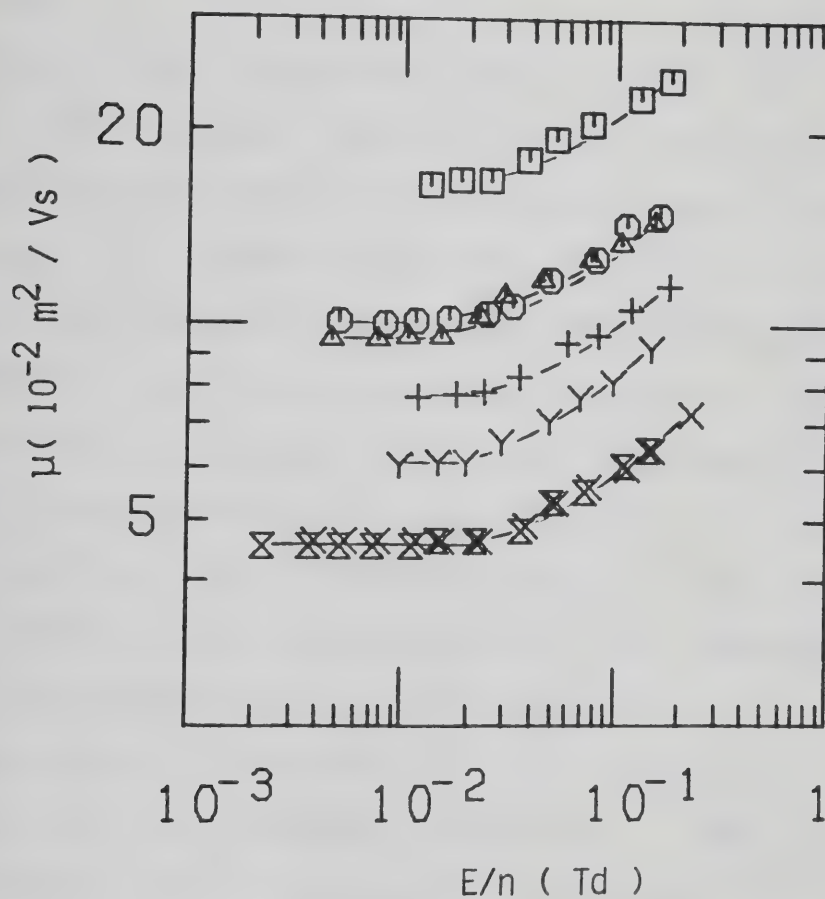


Figure III-5-4. Electron mobilities in saturated CD_4 vapor at different densities ($10^{26} \text{ molec/m}^3$) and temperatures (K). \square , 1.23, 119.3; \circ , 2.00, 127.0; Δ , 2.16, 128.2; $+$, 2.66, 132.0; Y , 3.23, 135.7; X , 4.21, 141.0; \otimes , 4.46, 142.0.

causes the threshold field to increase from about 0.02 Td to 0.03 Td.

Raising the temperature from 138.4K to 433K at $n = 3.7 \times 10^{26}$ molec/m³ (Figure III-5-5) has the effect of increasing the low field mobility by a factor of about 2. An increase in temperature from 146.5K to 397.0K at $n = 5.5 \times 10^{26}$ molec/m³ (Figure III-5-6) increases the low field mobility by the same factor. However the change in mobility which is observed by raising the temperature 15K above the coexistence curve is about 10% at the lower density and about 15% at the higher one. In both cases the rate of change of the threshold field with temperature is the same as that observed at lower densities.

Figure III-5-7 shows the effect of temperature on the threshold field at different densities. The threshold field increases with temperature independent of density between 3.20 and 55×10^{26} molec/m³.

An increase in density of the saturated vapor from 1.24 to 2.83 (10^{26} molec/m³) (Figure III-5-8) lowers the low field mobility by a factor of 2.7. The threshold field is constant at $E/n \approx 0.04$ Td. The corresponding temperature change is only about 18K. In Figure III-5-9 the effect of raising the temperature from 182.7K to 195.5K at $n = 2.90 \times 10^{27}$ molec/m³ is illustrated. The low field mobility increases by about 80%. The corresponding increase at the lowest density was less than 10%. In this

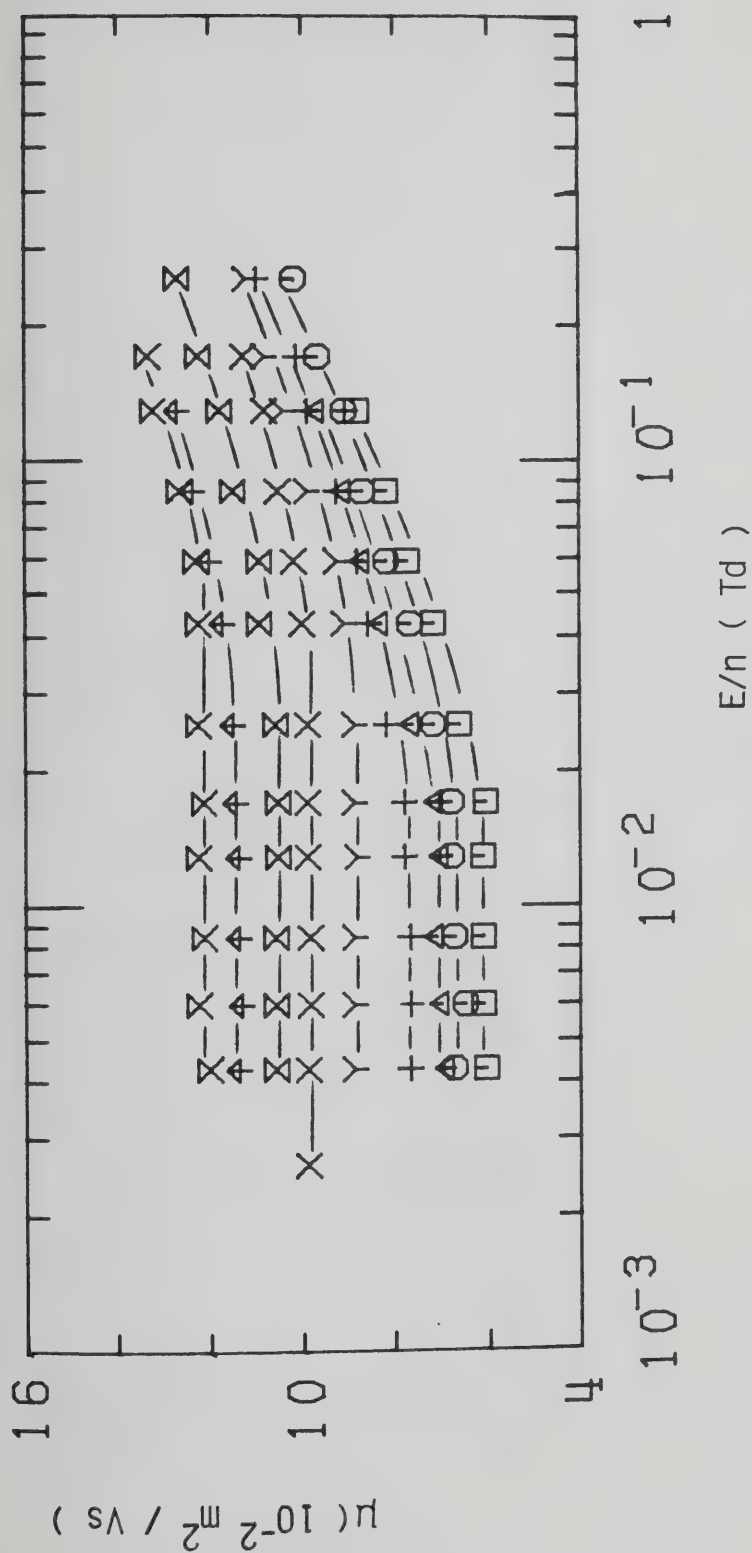


Figure III-5-5. Electron mobilities in CD_4 gas at $n = 3.7 \times 10^{26} \text{ molec/m}^3$ and different temperatures (K). \square , 138.4; \circ , 155.7; Δ , 175.5; $+$, 195.2; γ , 235.7; \times , 294.0; \boxtimes , 337; \uparrow , 385; \boxtimes , 433.

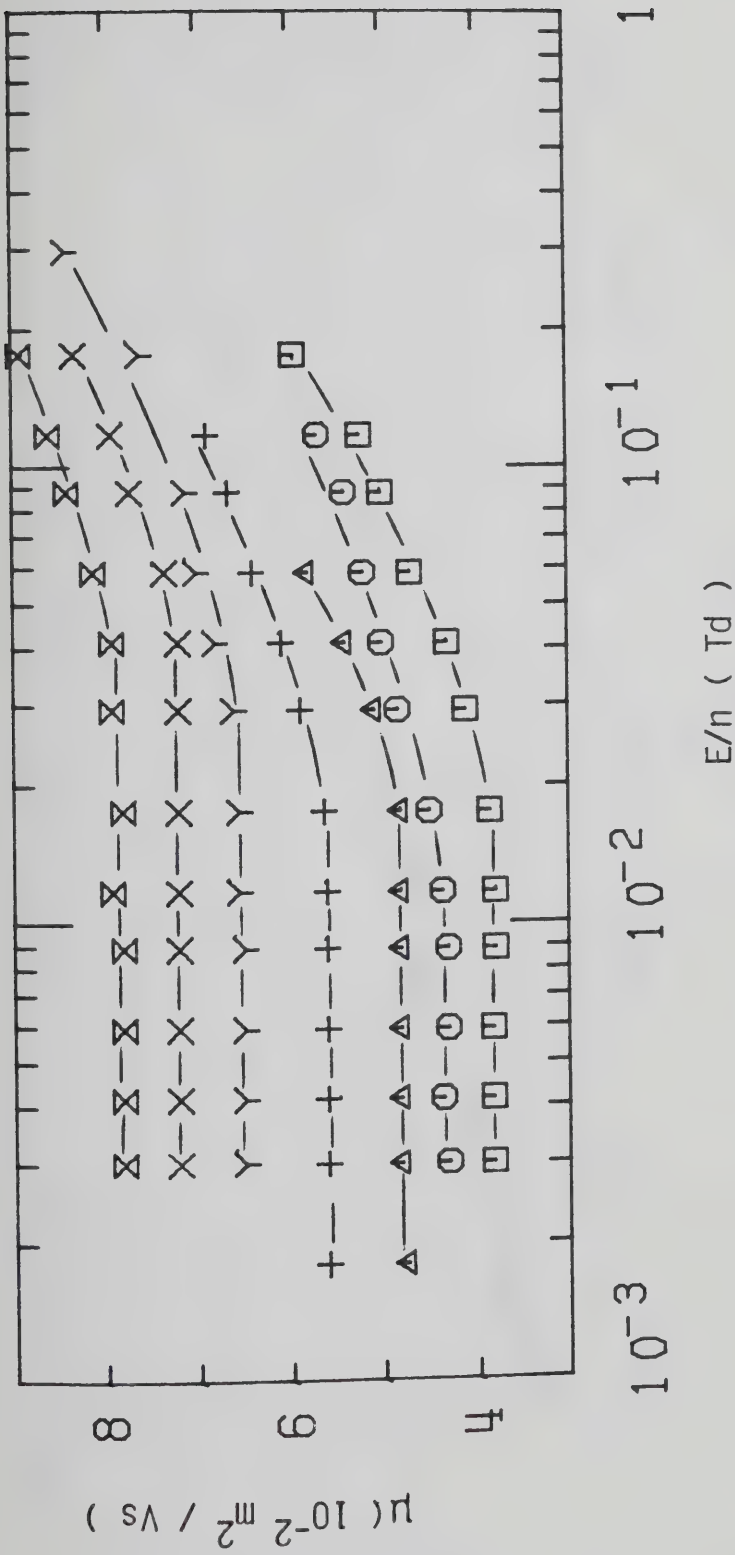


Figure III-5-6. Electron mobilities in CD_4 gas at $n = 5.5 \times 10^{26} \text{ molec/m}^3$ and different temperatures (K). \square , 146.5; \circ , 160.0; Δ , 181.5; $+$, 236.5; γ , 293.0; \times , 341; \otimes , 397.

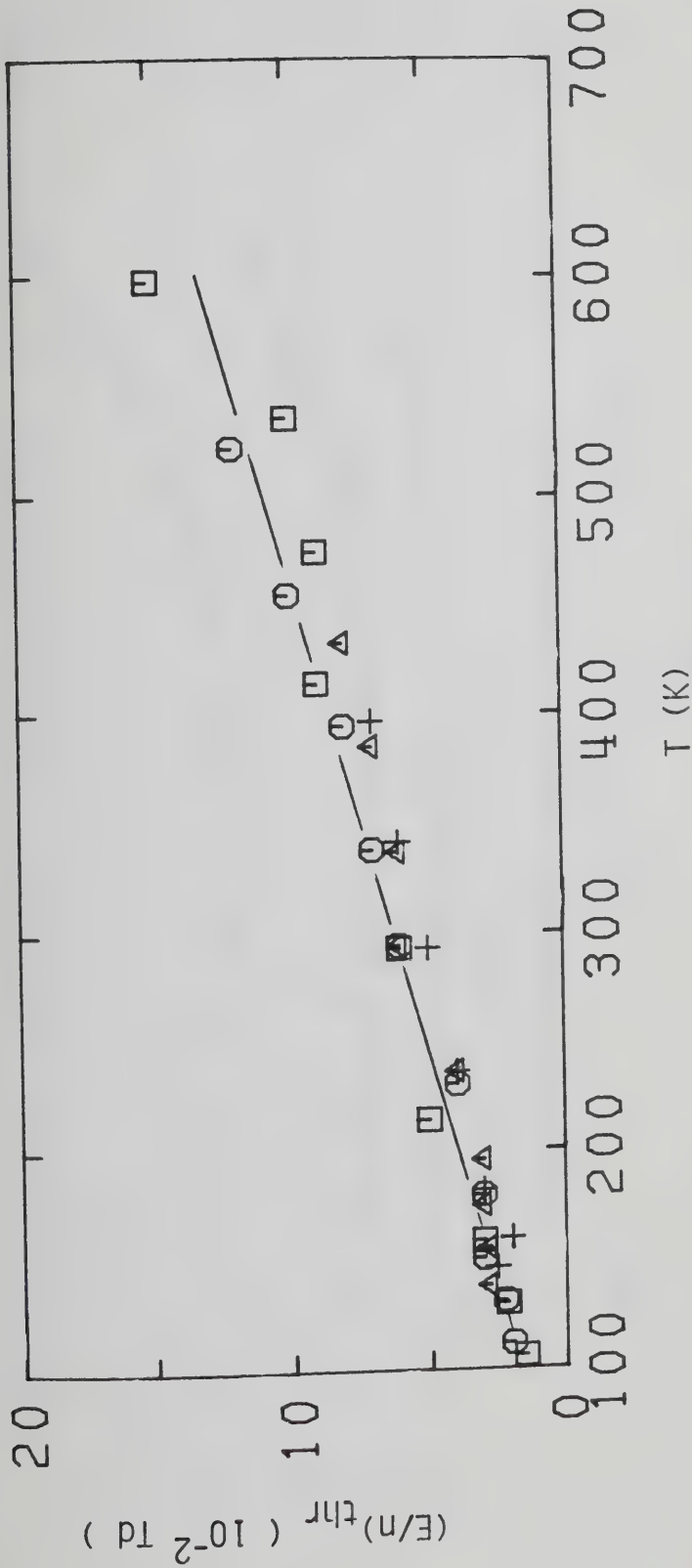
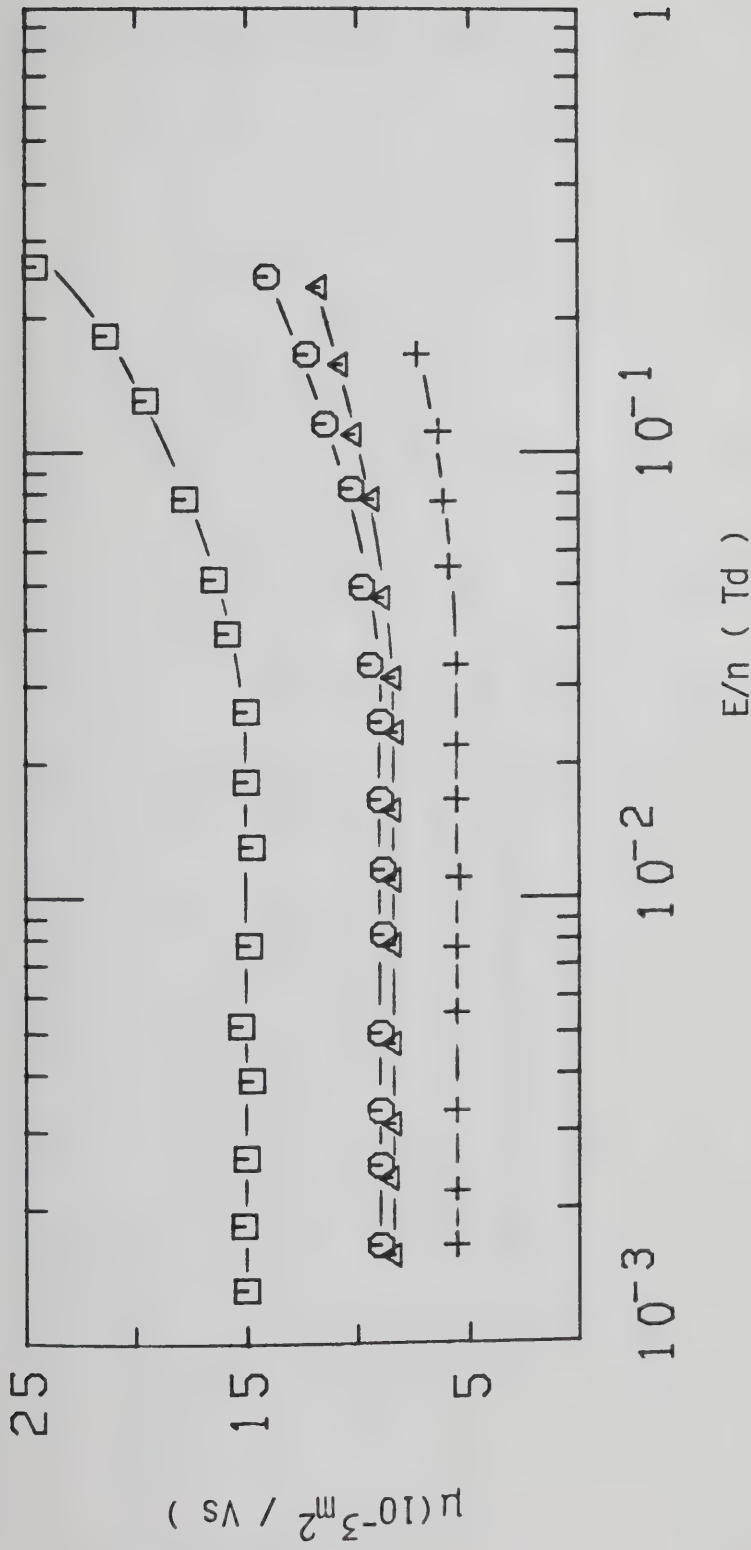


Figure III-5-7. Electric field threshold, $(E/n)_{thr}$, for electron heating in CD_4 gas at different densities (10^{25} molec/m³) as a function of temperature. \square , 3.20; \circ , 5.0; Δ , 37; $+$, 55.



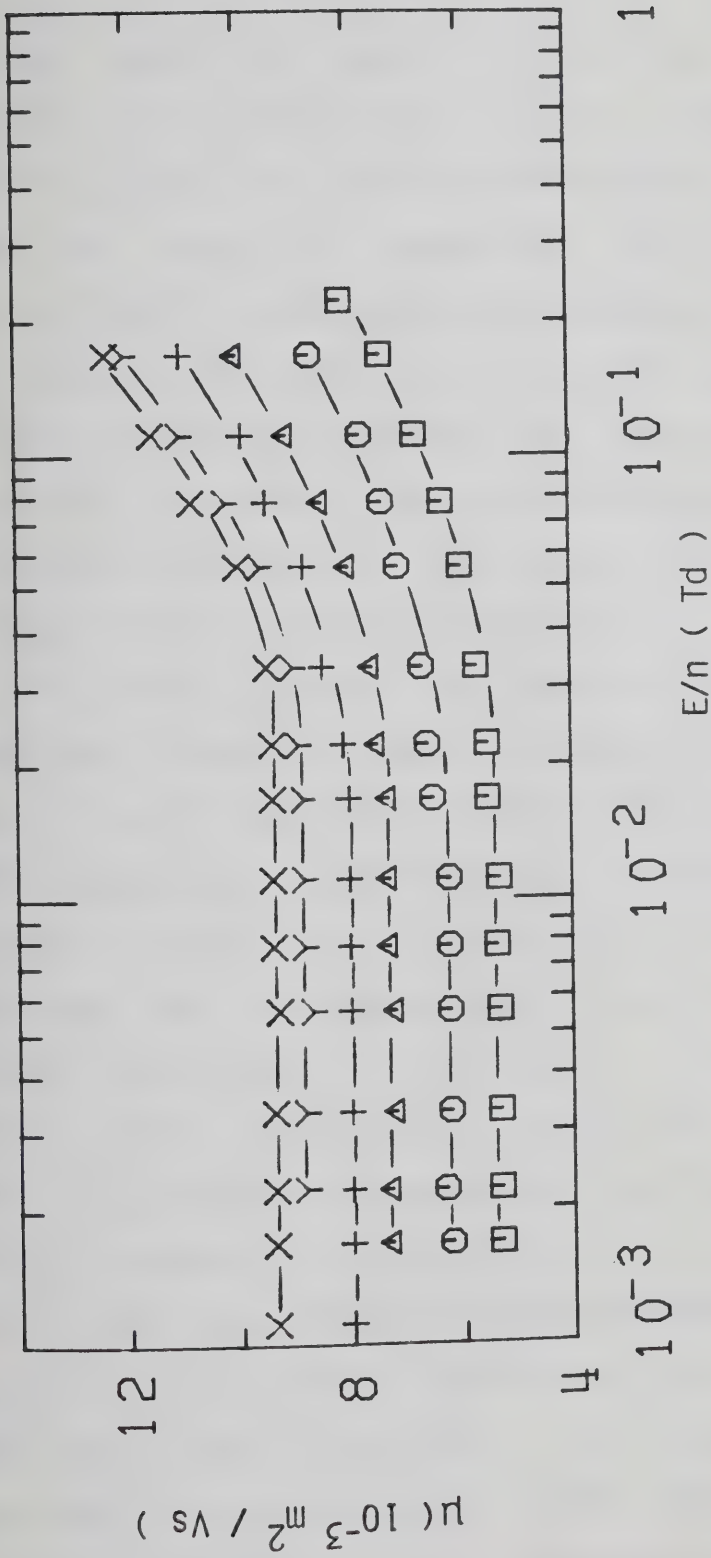


Figure III-5-9. Electron mobilities in CD_4 gas at $n = 2.90 \times 10^{27} \text{ molec/m}^3$ and different temperatures (K). \square , 182.7; \circ , 185.5; \triangle , 188.7; $+$, 191.2; \times , 193.9; \times , 195.5.

limited temperature range no effect is observed on the threshold field which stays constant at $E/n \approx 0.04$ Td. In Figure III-5-10 are reported measurements in the saturated vapor at densities approaching that of the critical point. The low field mobility decreases with density.

Raising the temperature in the supercritical gas (Figure III-5-11) increases the value of the low field mobility. On going from 189.3K to 193.2K the mobility increases by about 70%. The value of the threshold field is approximately constant at 0.03 Td.

In Figure III-5-12 are reported measurements in the coexistent liquid at densities near the critical point. The low field mobility increases with density. The field effect undergoes a change of sign at a density intermediate between 8.6 and 8.9 (10^{27} molec/m³). The threshold field increases with increasing density up to $n = 8.6 \times 10^{27}$ molec/m³ and then it decreases. A further increase in density of the liquid to $n = 10.5 \times 10^{27}$ molec/m³ (Figure III-5-13) produces an increase in low field mobility and a slight decrease in threshold field. In Figures III-5-14 and III-5-15 the effect of further increasing the density of the liquid is shown. The low field mobility decreases with density up to $n = 15.1 \times 10^{27}$ molec/m³ and then it increases on approaching the triple point. In this range no effect is observed on the threshold field, which stays constant at $E/n \approx 9 \times 10^{-3}$ Td.

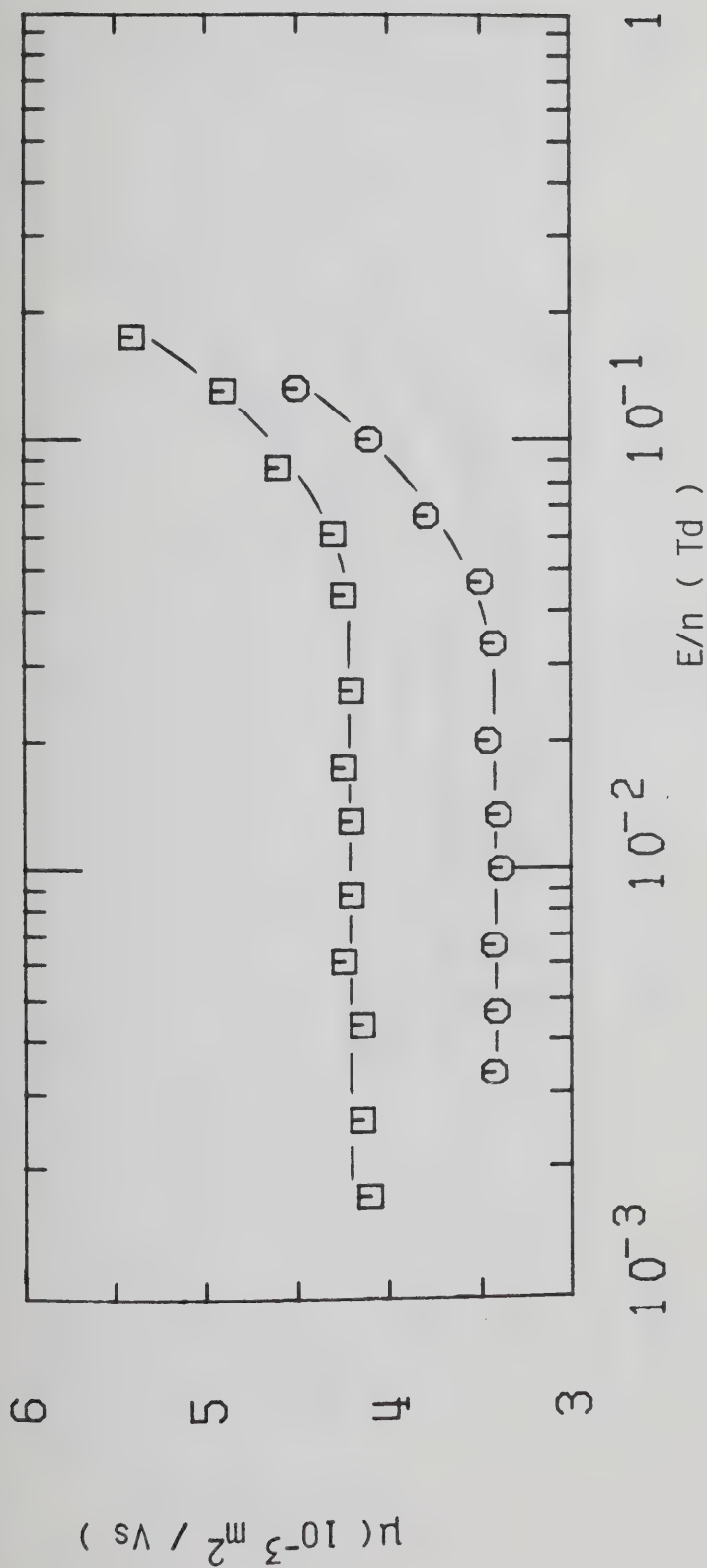


Figure III-5-10. Electron mobilities in saturated CD_4 vapor at different densities (10^{27} molec/m³) and temperatures (K). □, 3.60, 186.1; ○, 4.7, 188.7.

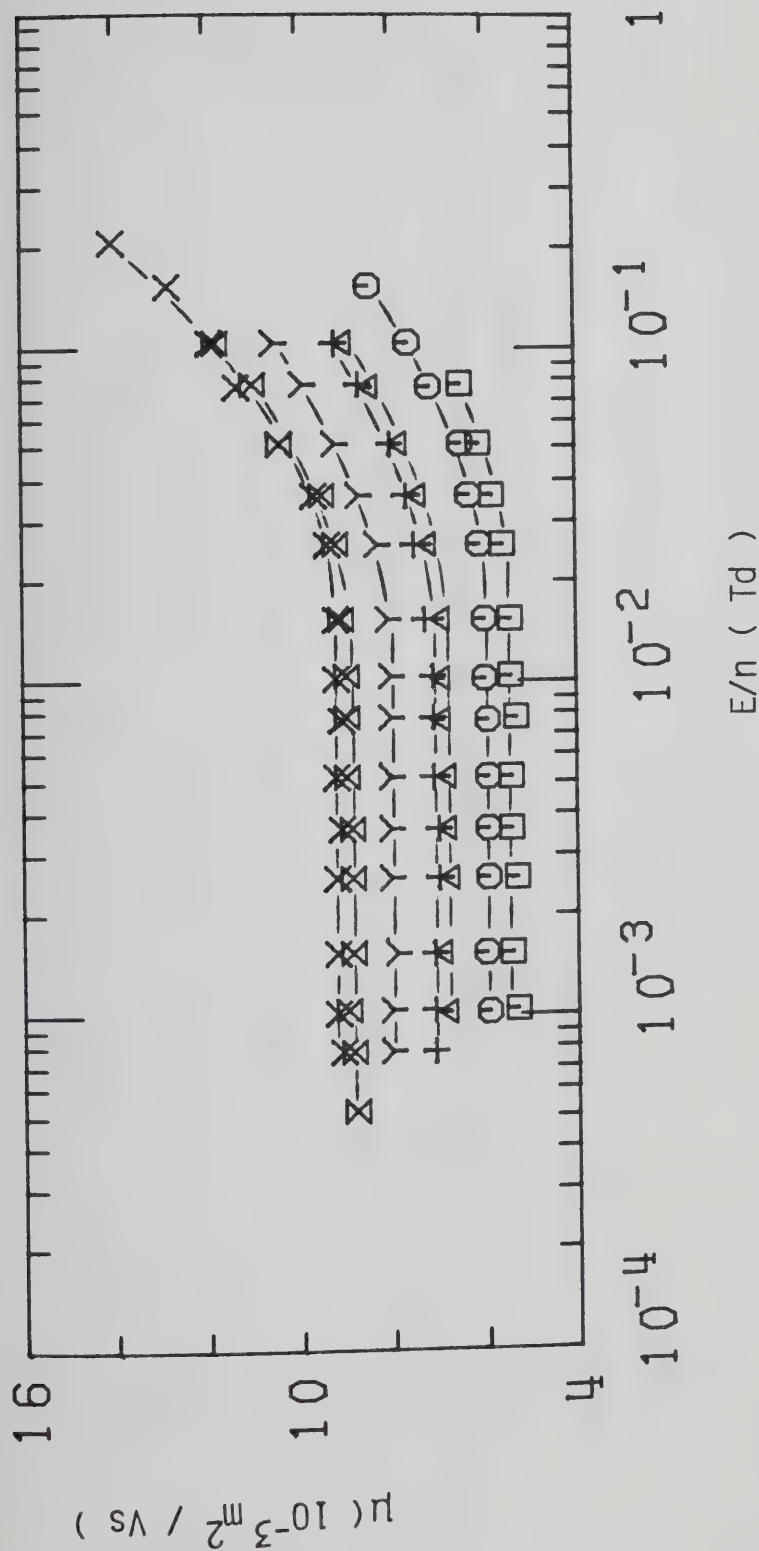


Figure III-5-11. Electron mobilities in supercritical CD_4 gas at $n_c = 6.1 \times 10^{27}$ molec/ m^3 and different temperatures (K). \square , 189.3; \circ , 189.5; \triangle , 190.5; $+$, 190.8; γ , 192.1; \times , 193.0; Σ , 193.2. $T_c = 189.2$.

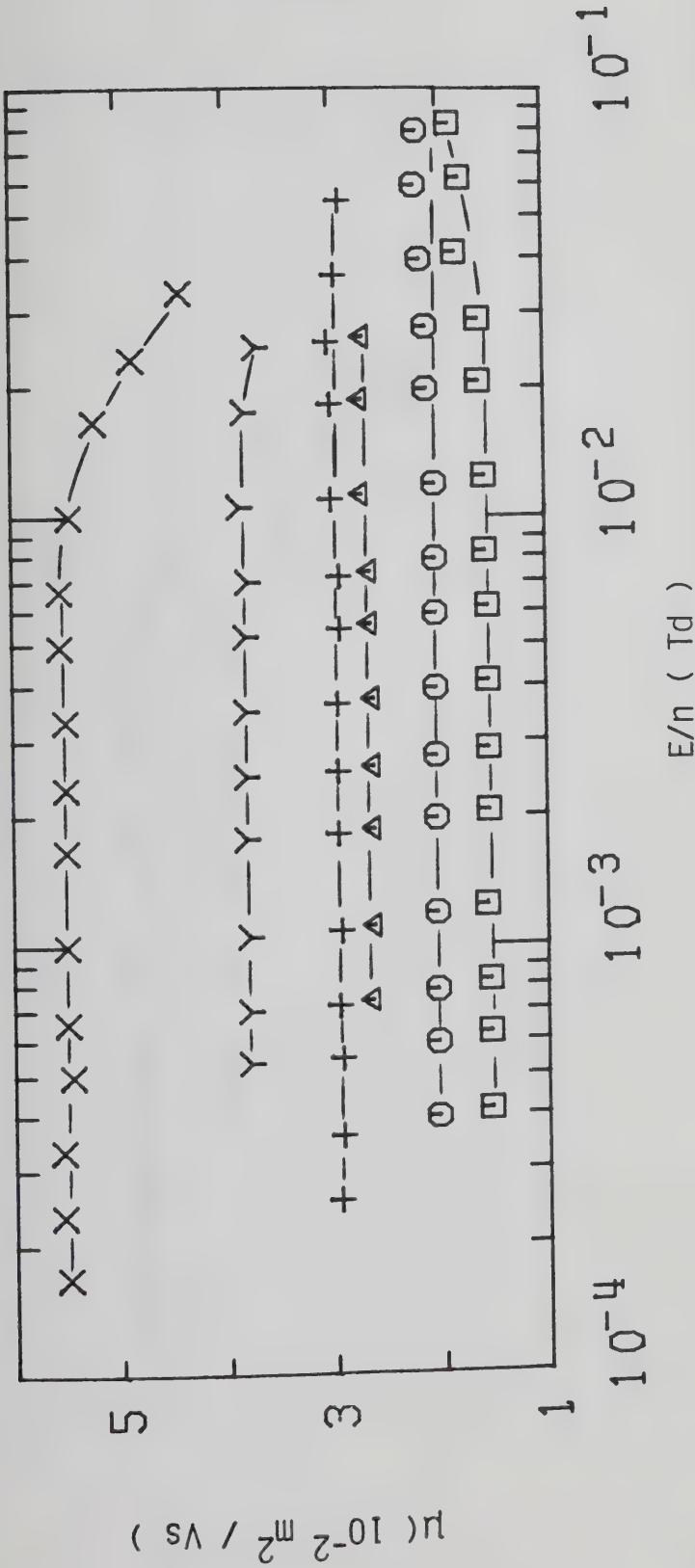


Figure III-5-12. Electron mobilities in liquid CD_4 at different densities ($10^{27} \text{ molec/m}^3$) and temperatures (K). \square , 7.6, 188.7; \circ , 7.9, 188.0; Δ , 8.4, 187.5; +, 8.6, 187.0; Y, 8.9, 186.1; X, 9.4, 184.0.

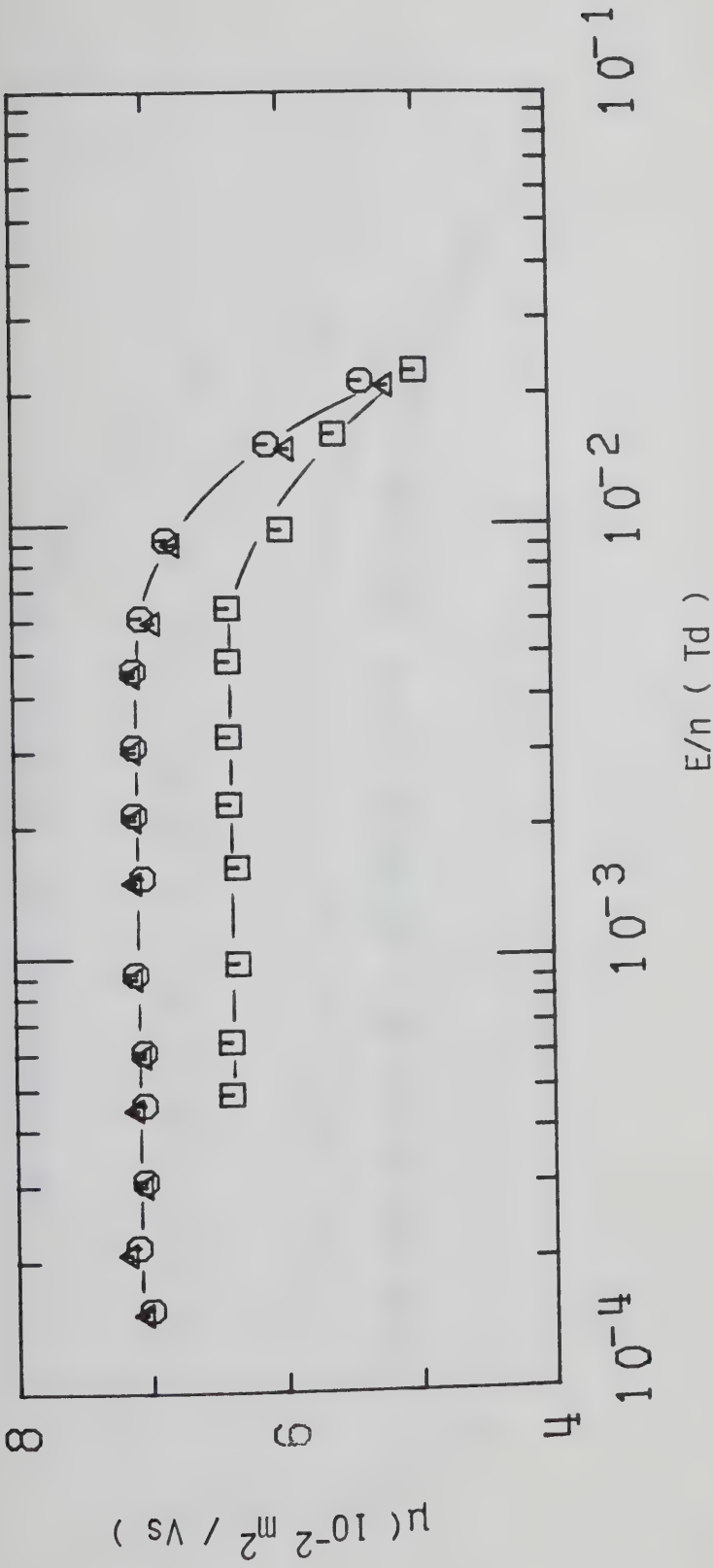


Figure III-5-13. Electron mobilities in liquid CD_4 at different densities ($10^{27} \text{ molec/m}^3$) and temperatures (K). \square , 9.7, 182.5; \circ , 10.2, 180.0; Δ , 10.5, 178.0.

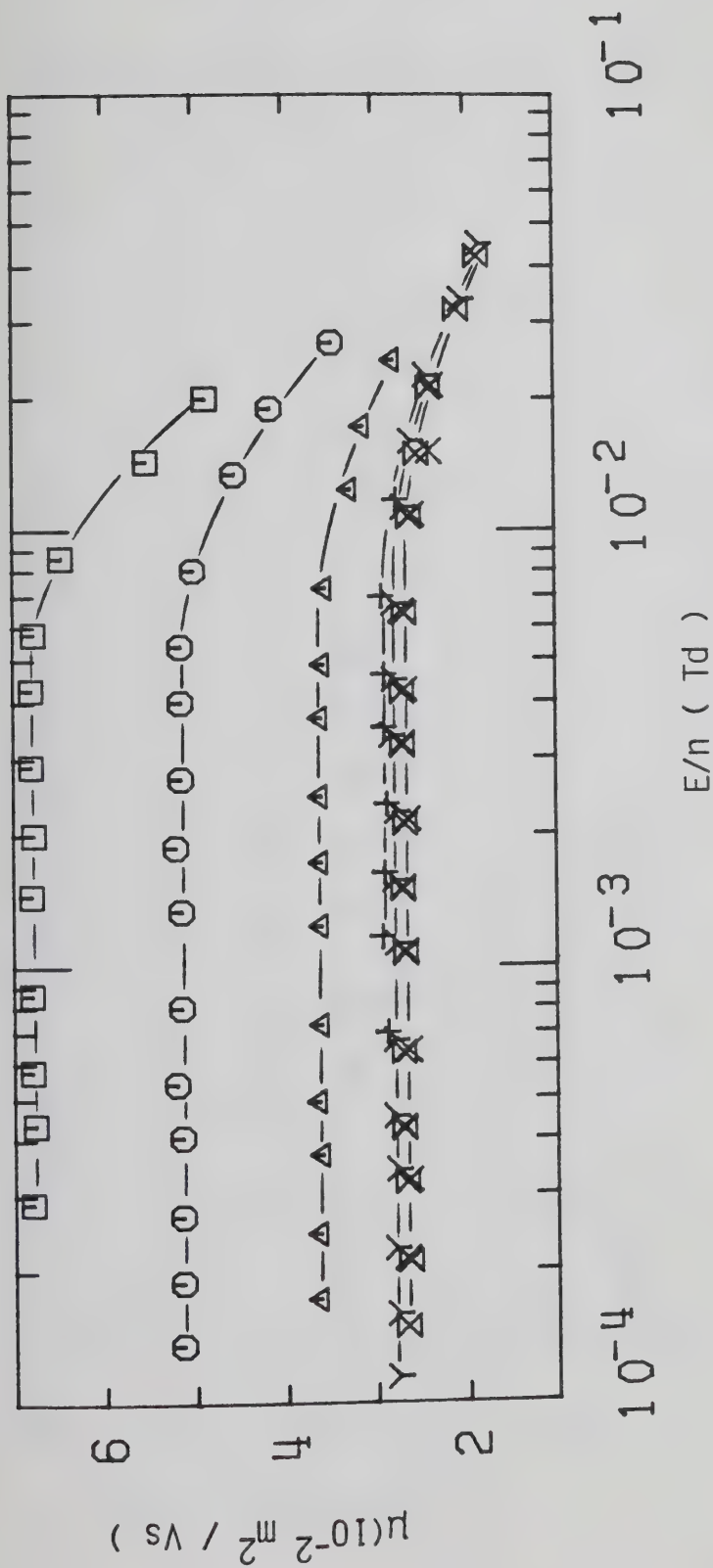


Figure III-5-14. Electron mobilities in liquid CD_4 at different densities (10^{27} molec/ m^3) and temperatures (K). \square , 10.9, 175.5; \circ , 11.6, 170.0; Δ , 12.7, 160.2; $+$, 13.4, 151.0; γ , 13.8, 145.5; \times , 14.5, 136.5; \boxtimes , 14.7, 134.0.

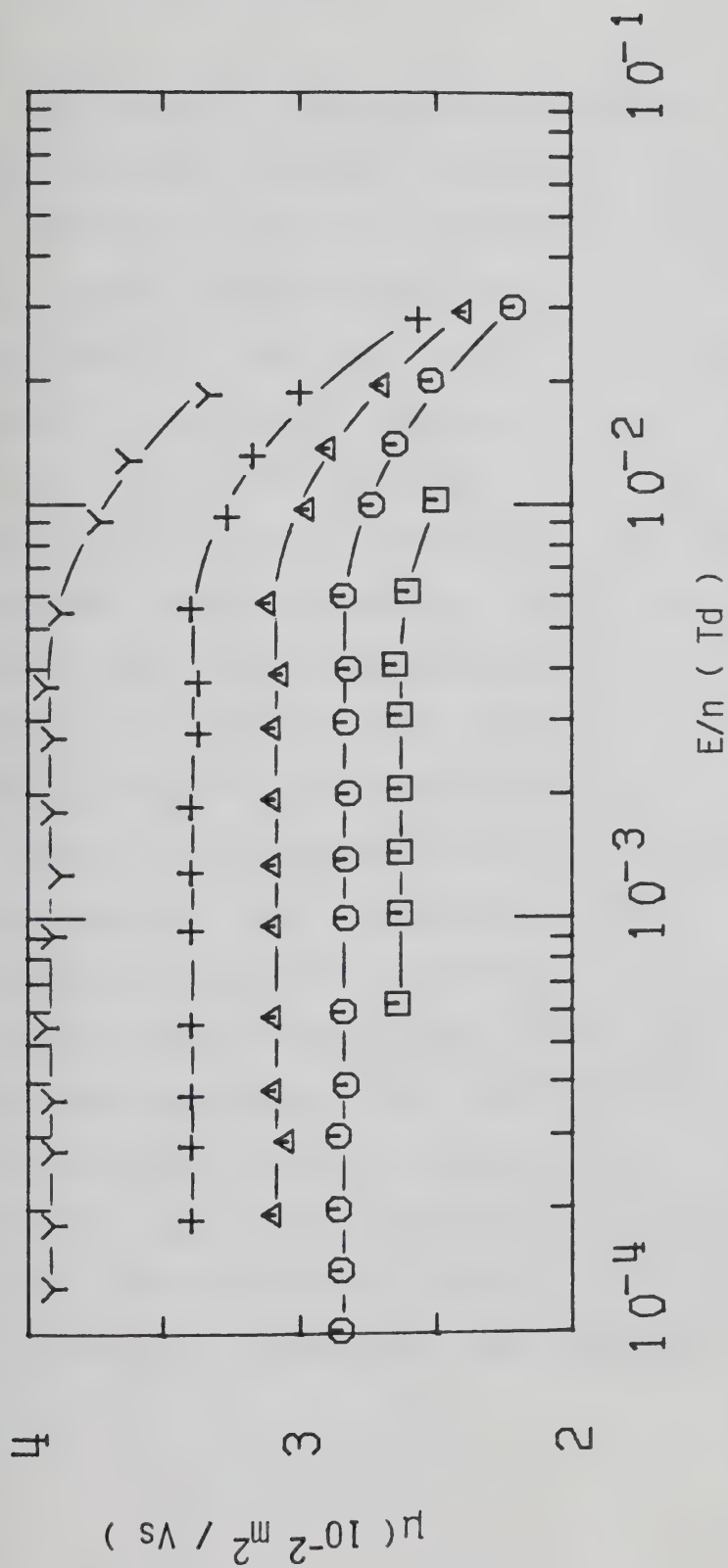


Figure III-5-15. Electron mobilities in liquid CD_4 at different densities (10^{27} molec/ m^3) and temperatures (K). \square , 15.1, 127.0; \circ , 15.6, 119.5; Δ , 16.1, 109.7; $+$, 16.7, 100.3; Y , 17.1, 92.4.

The effect of density and temperature on the threshold field is shown in Figure III-5-16. In the saturated vapor the threshold value of the field increases monotonically with density (temperature) from a value of ~ 0.02 Td at about 100K to that of ~ 0.05 Td at about 180K. In the liquid it increases sharply and at a density between 8.6 and 8.9 (10^{27} molec/m³) the field effect on the mobility is zero. At higher densities the mobility decreases with increasing field above the threshold value. This value increases with density. At densities higher than about 10×10^{27} molec/m³ the threshold field is density (temperature) independent.

Results in Figures III-5-1 to III-5-3 were obtained in low pressure type conductance cells. The electrode separations were 0.999 ± 0.002 cm. All the other gas phase results were obtained in high pressure gas type cells. The electrode separations were 0.315 ± 0.005 cm. Liquid data were obtained in high pressure liquid type cells. The electrode separations were 0.320 ± 0.001 cm. A listing of the low field values of mobility and threshold voltages at the different temperatures and densities is given in Table III-5.

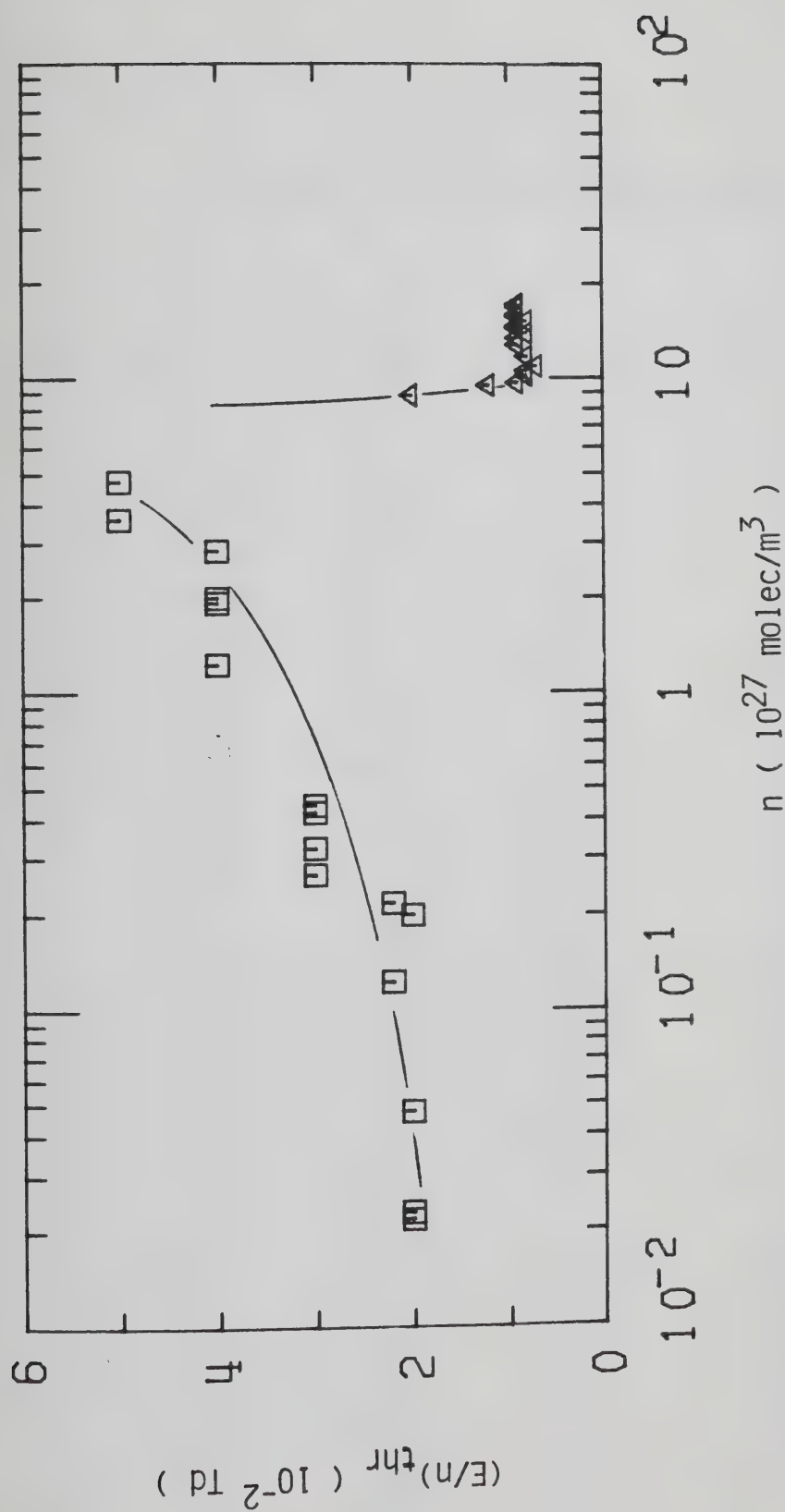


Figure III-5-16. Electric field threshold, $(E/n)_{thr}$, for electron heating in coexistence vapor and liquid CD_4 as a function of density.

\square , $d\mu / d(E/n) > 0$; Δ , $d\mu / d(E/n) < 0$.

TABLE III-5

Summary of Electron Results for CD_4^a

T (K)	n 10^{26} m^{-3}	μ (m^2/Vs)	ν $[10^{25} (\text{Vsm})^{-1}]$	$(E/n)_{\text{thr}}$ (mTd)	$d\mu/d(E/n)$
98.3	0.232	1.01	2.34	20	+
99.3	0.256	1.00	2.56	20	+
107.8	0.50	0.48	2.40	20	+
106.0	0.32	0.70	2.24	15	+
130.0	0.32	0.77	2.46	22	+
159.2	0.32	0.87	2.78	30	+
214.4	0.32	0.94	3.01	50	+
293.2	0.32	1.06	3.39	60	+
356.0	0.32	1.15	3.68		
414	0.32	1.17	3.74	90	+
474	0.32	1.25	4.00	90	+
536	0.32	1.30	4.16	100	+
598	0.32	1.34	4.29	150	+
111.8	0.50	0.47	2.35	20	+
131.0	0.50	0.51	2.55	23	+
150.6	0.50	0.54	2.70	30	+
179.9	0.50	0.56	2.80	30	+
230.5	0.50	0.61	3.05	40	+
294.5	0.50	0.67	3.35	60	+
337.4	0.50	0.70	3.50	70	+
395	0.50	0.74	3.70	80	+
454.3	0.50	0.79	3.95	100	+
521	0.50	0.83	4.15	120	+
119.3	1.23	0.166	2.04	22	+
127.0	2.00	0.100	2.00	20	+

(continued....)

Table III-5 continued

128.2	2.16	0.096	2.07	22	+
132.0	2.66	0.078	2.07	30	+
135.7	3.23	0.061	1.97	30	+
141.0	4.21	0.046	1.94	30	+
142.0	4.46	0.046	2.05	30	+
138.4	3.70	0.061	2.26	28	+
155.7	3.70	0.067	2.48	28	+
175.5	3.70	0.070	2.59	30	+
195.2	3.70	0.078	2.89	30	+
235.7	3.70	0.089	3.29	40	+
294.0	3.70	0.099	3.66	60	+
337	3.70	0.106	3.92	60	+
385	3.70	0.114	4.22	70	+
433	3.70	0.120	4.44	80	+
146.5	5.5	0.0382	2.10	25	+
160.0	5.5	0.0433	2.38	20	+
181.5	5.5	0.048	2.64	30	+
236.5	5.5	0.056	3.08	30	+
293.0	5.5	0.065	3.58	50	+
341	5.5	0.072	3.96	60	+
397	5.5	0.078	4.29	70	+
151.0	6.8	0.0280	1.90	40	+
164.8	12.4	0.0150	1.86	40	+
174.5	19.5	0.0090	1.76	40	+
175.5	20.0	0.0084	1.68	40	+
182.5	28.3	0.0055	1.56	40	+
182.7	29.0	0.0053	1.54	40	+
185.5	29.0	0.0062	1.80	40	+
188.7	29.0	0.0073	2.12	40	+
191.2	29.0	0.0080	2.32	40	+

(continued....)

Table III-5 continued

193.9	29.0	0.0088	2.55	40	+
195.5	29.0	0.0094	2.73	40	+
186.1	36.0	0.0042	1.51	50	+
188.7	47	0.0034	1.60	45	+
189.3	61 ^b	0.0054	3.29	27	+
189.5	61 ^b	0.0059	3.60	27	+
190.5	61 ^b	0.0069	4.21	25	+
190.8	61 ^b	0.0071	4.33	30	+
192.1	61 ^b	0.0080	4.88	30	+
193.0	61 ^b	0.0092	5.6	30	+
193.2	61 ^b	0.0090	5.5	28	+
188.7	76	0.0154	11.7	29	+
188.0	79	0.0203	16.0	37	+
187.5	84	0.0263	22.1		
187.0	86	0.0295	25.4	>50	
186.1	89	0.0380	33.8	25	-
184.0	94	0.055	52	14	-
182.5	97	0.064	62	9.6	-
180.0	102	0.071	72	8	-
178.0	105	0.071	75	8	-
175.5	109	0.068	74	7	-
170.0	116	0.0515	60	8	-
160.2	127	0.0363	46	9	-
151.0	134	0.0290	38.9	9	-
145.5	138	0.0277	38.2	8	-
136.5	145	0.0268	38.9	9	-
134.0	147	0.0268	39.4	9	-
127.0	151	0.0263	39.7	8	-

(continued.....)

Table III-5 continued

119.5	156	0.0284	44	9	-
109.7	161	0.0310	50	9	-
100.3	167	0.0340	57	9	-
92.4	171	0.0390	67	9	-

a. The results in this table appear in the same order as the figures. They are given in order of increasing density.

b. $n_c = 6.1 \times 10^{27} \text{ molec/m}^3$, $T_c = 189.2\text{K}$.

B. Cation Mobilities

In this section the cation results are presented as plots of the mobility μ_+ against the density normalized field strength in Townsends ($Td = 10^{-21} \text{ m}^2\text{V/molec}$).

Ion mobilities are typically four to five orders of magnitude smaller than the electron mobilities. The ions are the slowest charge carriers in the system. The electrons are swept out of the system before the cations have drifted appreciably.

The exact identity of the ions is not known. Chemical reactions involving electron irradiated methane have been studied by mass spectrometry usually at low gas densities compared to those used in this work.²⁰⁰⁻²⁰³ The ionization process in methane leads mainly to CH_4^+ and CH_3^+ . These ions react with CH_4 according to the fast bimolecular processes



The rate constants of these reactions are of the order of $10^{-15} \text{ molec/m}^3$ at about 7 torr and 295K.²⁰⁴ The lifetimes of CH_4^+ and CH_3^+ at the lowest density of CH_4 in the present work would then be approximately 10^{-10} s . In this

work the typical drift times were μs to ms . Therefore these ions could not be observed. The CH_5^+ and C_2H_5^+ ions produced by reactions III-1 and III-2 can cluster with methane. The position of the clustering equilibria depends on the temperature and density. The ions in the present study are thought to be polymeric.

Measurements were made of the ion mobilities in all compounds as a function of density in the saturated vapor and liquid phases and as a function of temperature in the gas along selected isochores, except for CH_3D where no measurements in the liquid phase were made. The ion mobilities were measured as a function of the applied electric field strength. In no case was any field effect found. It has been found²⁰³ that the mobilities of both CH_5^+ and C_2H_5^+ are field independent up to $E/n \approx 70 \text{ Td}$, and they increase above this threshold value. In the present work the highest field used for CH_4 was about 1 Td.

The results are presented in order of increasing density. Data in CH_4 are given first followed by CH_3D , CH_2D_2 , CHD_3 and CD_4 . A table summarizing the results is given at the end of each subsection.

1. CH₄

In Figure III-1-20 is shown the effect of raising the temperature from 116.5K to 494K at $n = 2.95 \times 10^{25}$ molec/m³. The mobility increases from 1.38×10^{-4} m²/Vs to 2.32×10^{-4} m²/Vs. It was impossible to measure a value of the ion mobility at higher temperatures because the voltage vs. time traces became nonlinear. The electron traces at the same temperatures were linear.

The ion mobility decreases upon increasing the density of the saturated vapor. Figure III-1-21 shows the effect of an increase in density by a factor of 2.8. The mobility decreases by approximately the same factor. On raising the temperature from 152.0 to 292.3K at $n = 5.5 \times 10^{26}$ molec/m³ the mobility increases from 6.4×10^{-6} m²/Vs to 9.5×10^{-6} m²/Vs (Figure III-1-22). A further increase in density of the saturated vapor by a factor of 3.9 (Figure III-1-23) produces a decrease in mobility by about the same factor.

Heating the gas at $n = 29.0 \times 10^{26}$ molec/m³ and $n_c = 61 \times 10^{26}$ molec/m³ (Figures III-1-24 and 25) causes the mobility to increase. At the lower density the mobility increases by 12% for a 6.5K (3.4%) change in temperature. At the higher density, $n_c = 61 \times 10^{26}$ molec/m³, the mobility increases by 9% for a 1K (0.5%) change in temperature. In the liquid (Figure III-1-26) the mobility decreases monotonically with increasing density.

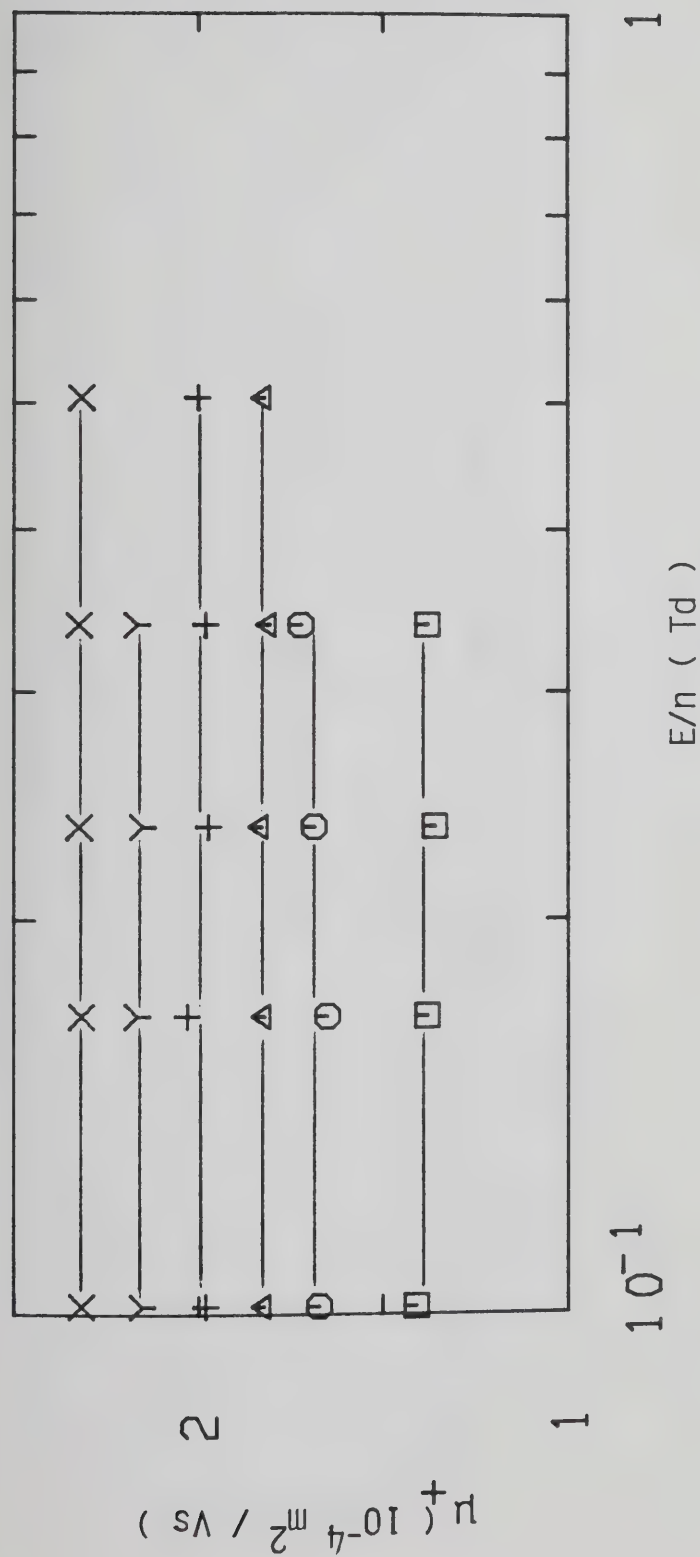


Figure III-1-20. Ion mobilities in CH_4 gas at $n = 2.95 \times 10^{25} \text{ molec/m}^3$ and different temperatures (K). \square , 116.5; \circ , 163.7; Δ , 292.5; $+$, 372.6; \times , 441.2; \times , 494.

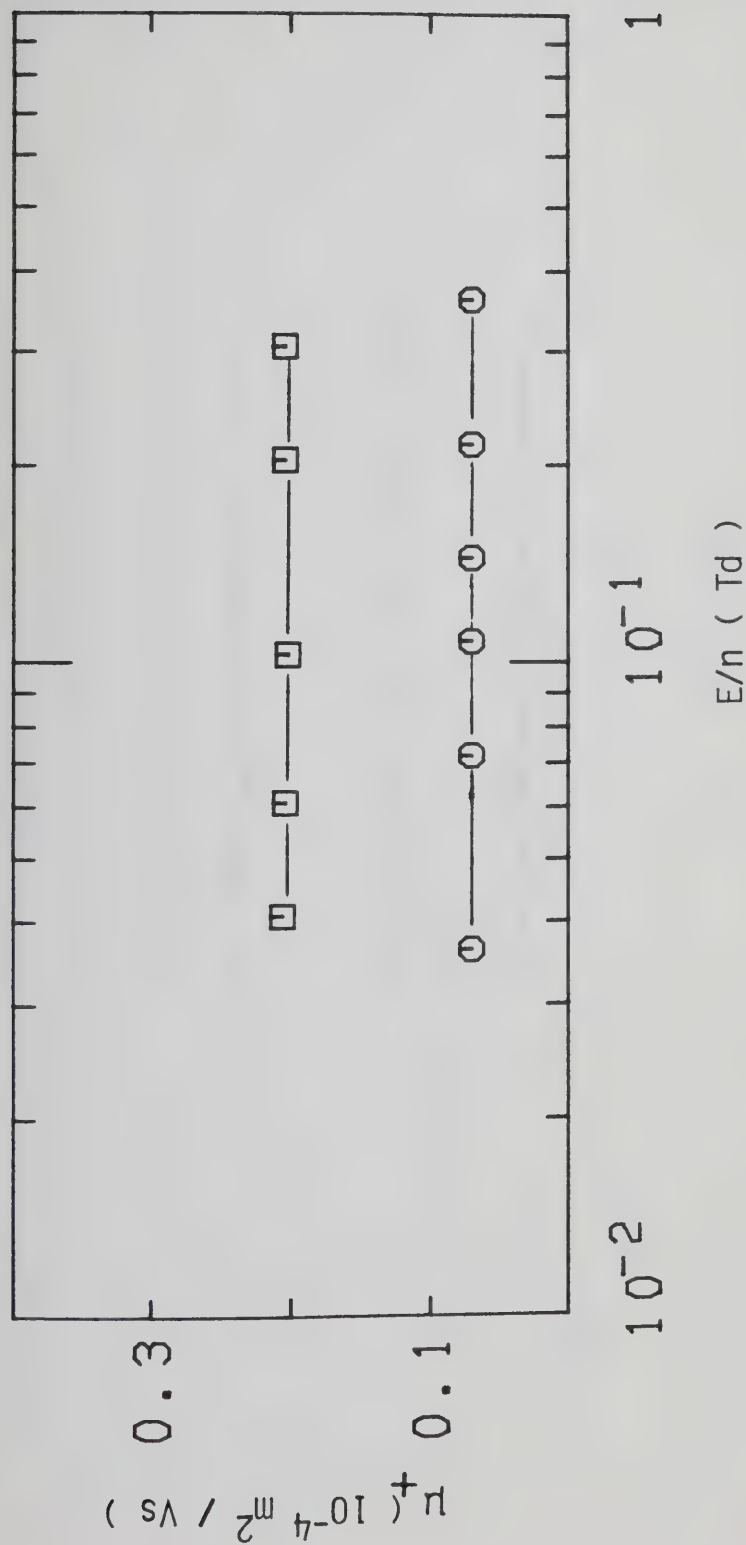


Figure III-1-21. Ion mobilities in saturated CH_4 vapor at different densities ($10^{26} \text{ molec/m}^3$) and temperatures (K). \square , 1.54, 123.5; \circ , 4.36, 142.5.

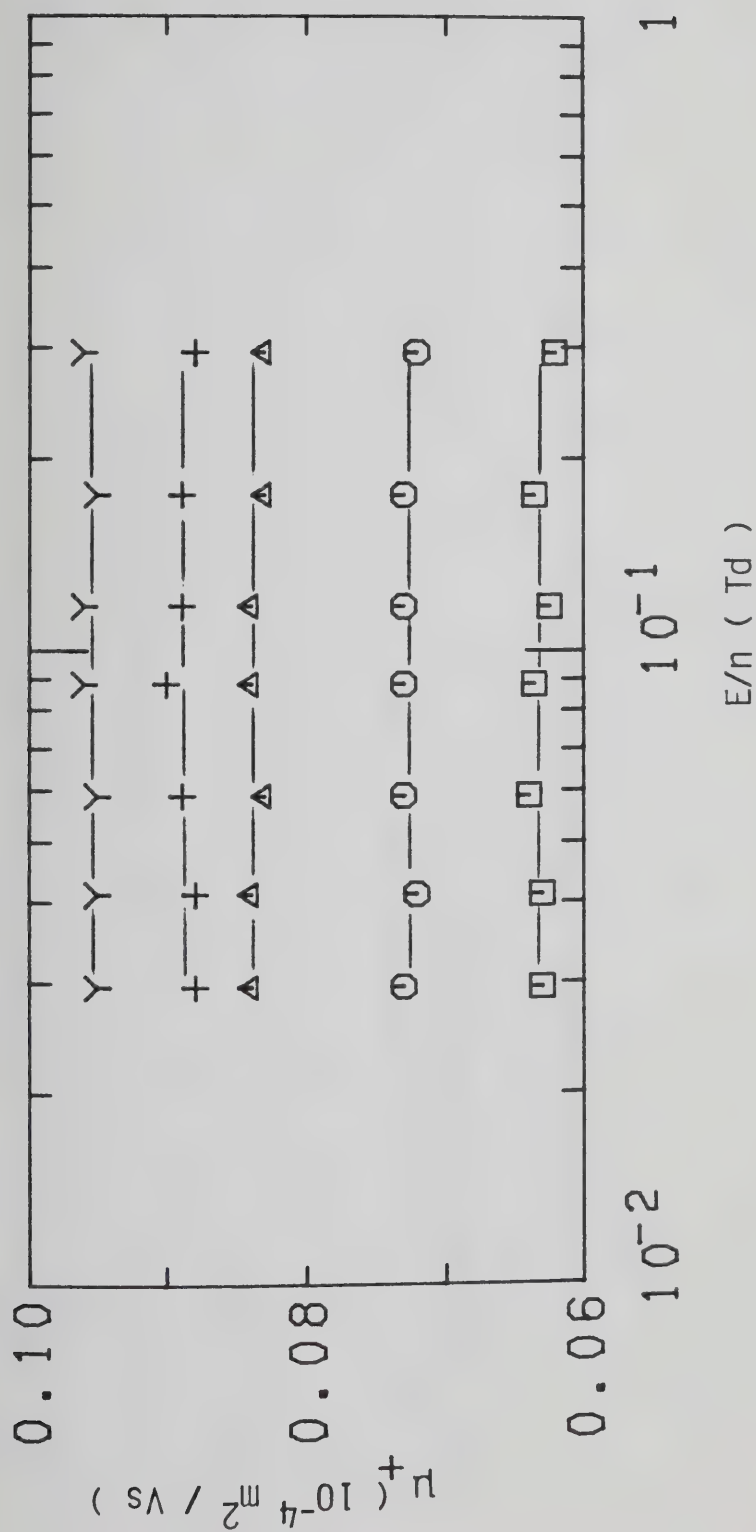


Figure III-1-22. Ion mobilities in CH_4 gas at $n = 5.5 \times 10^{26} \text{ molec/m}^3$ and different temperatures (K). \square , 152.0 ; \bigcirc , 172.5 ; Δ , 201.5 ; $+$, 228.0 ; γ , 292.3 .

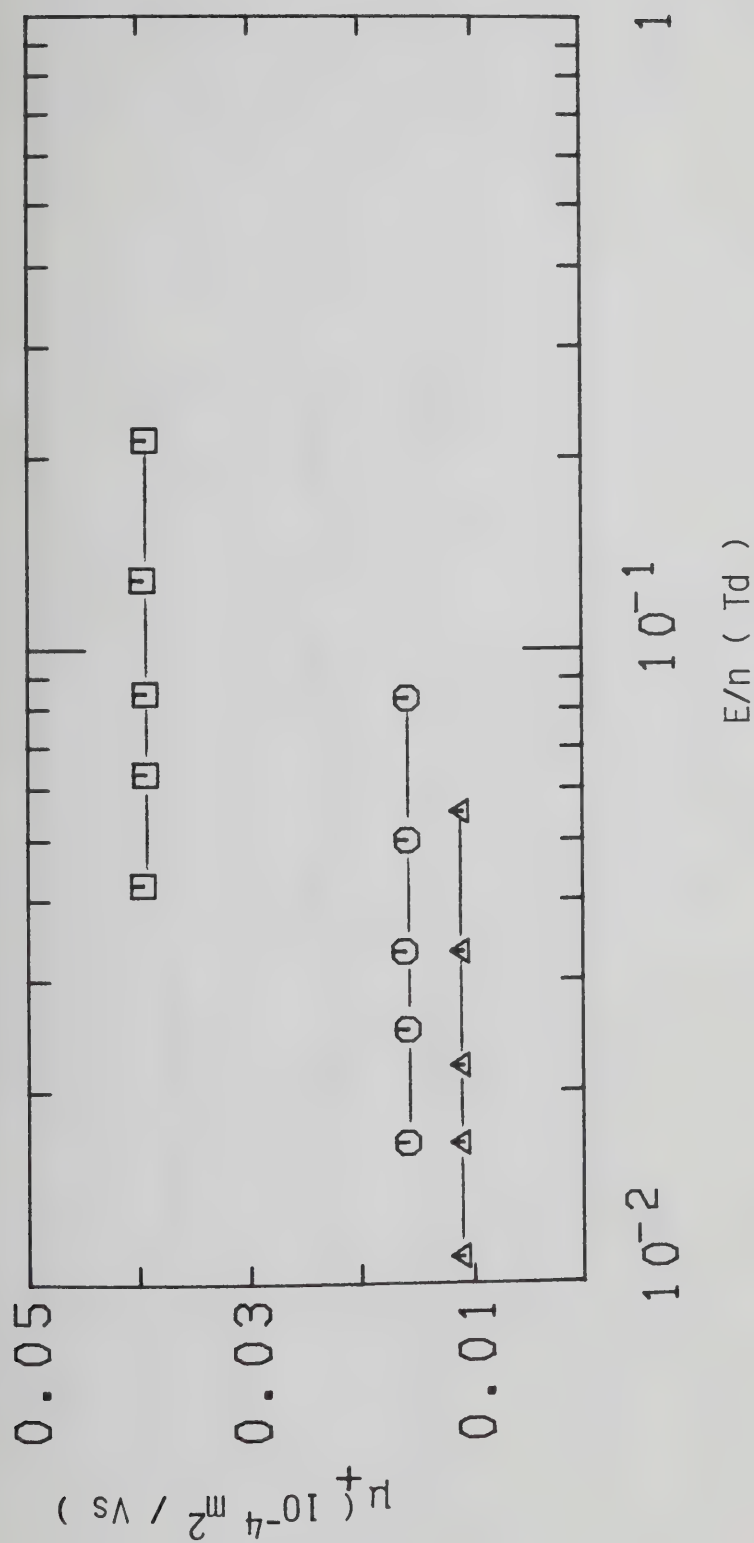


Figure III-1-23. Ion mobilities in saturated CH_4 vapor at different densities ($10^{27} \text{ molec}/\text{m}^3$) and temperatures (K). \square , 0.74, 154.0; \circ , 1.89, 175.7; Δ , 2.85, 184.0.

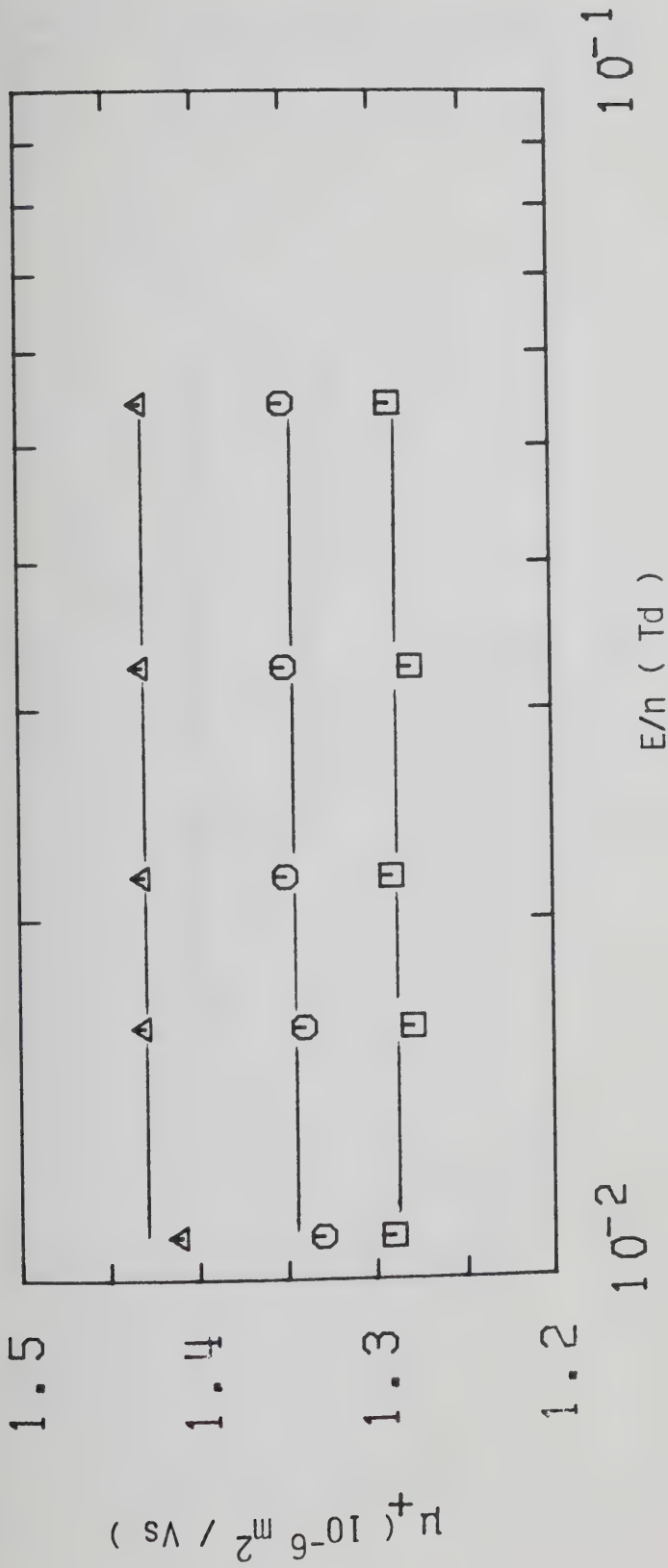


Figure III-1-24. Ion mobilities in CH_4 gas at $n = 2.9 \times 10^{27} \text{ molec/m}^3$ and different temperatures (K). \square , 188.7; \circ , 192.0; Δ , 195.2.

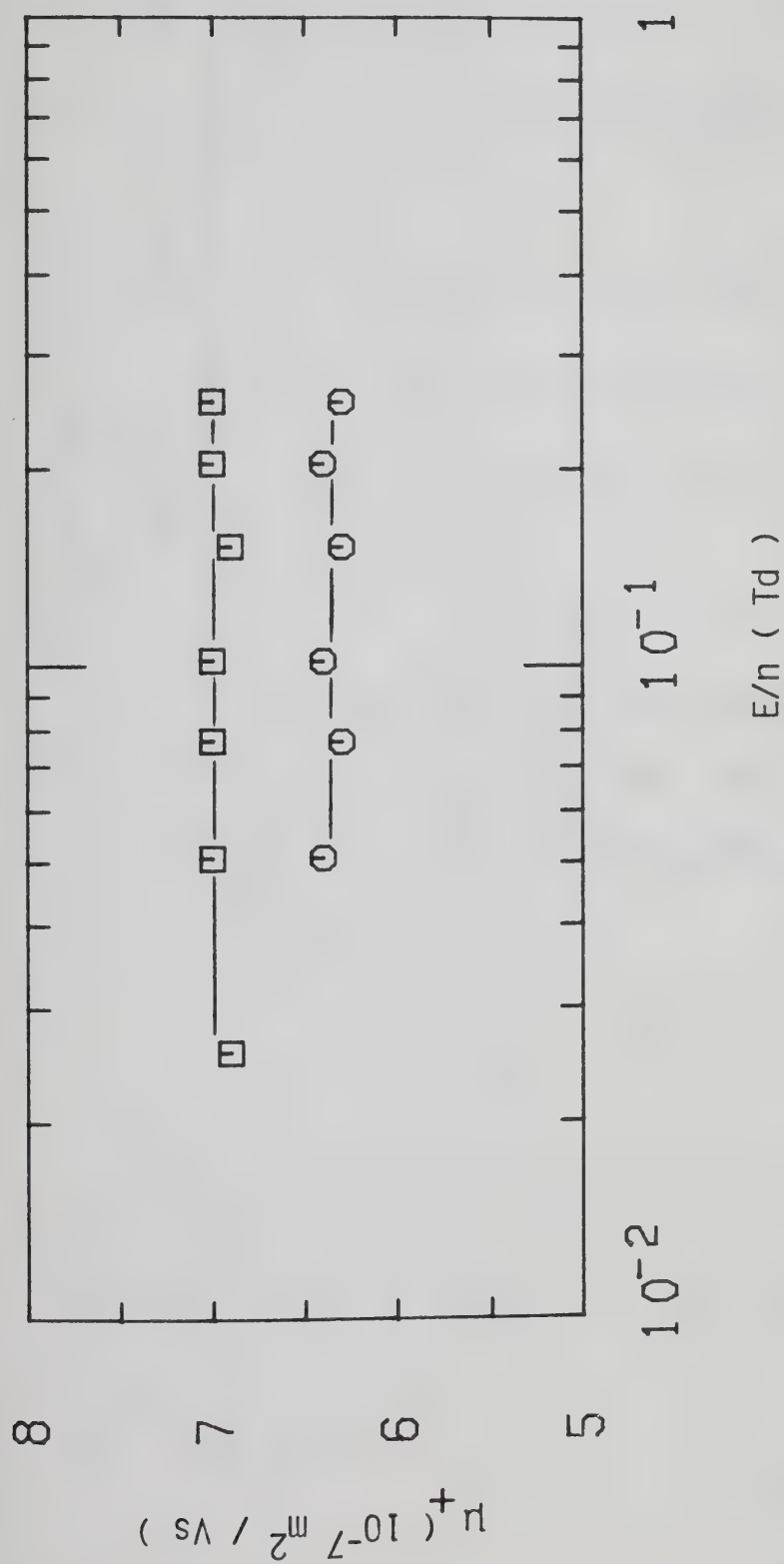


Figure III-1-25. Ion mobilities in supercritical CH_4 gas at $n_c = 6.1 \times 10^{27} \text{ molec/m}^3$ and different temperatures (K). O, 191.2; □, 192.2. $T_c = 190.6$.

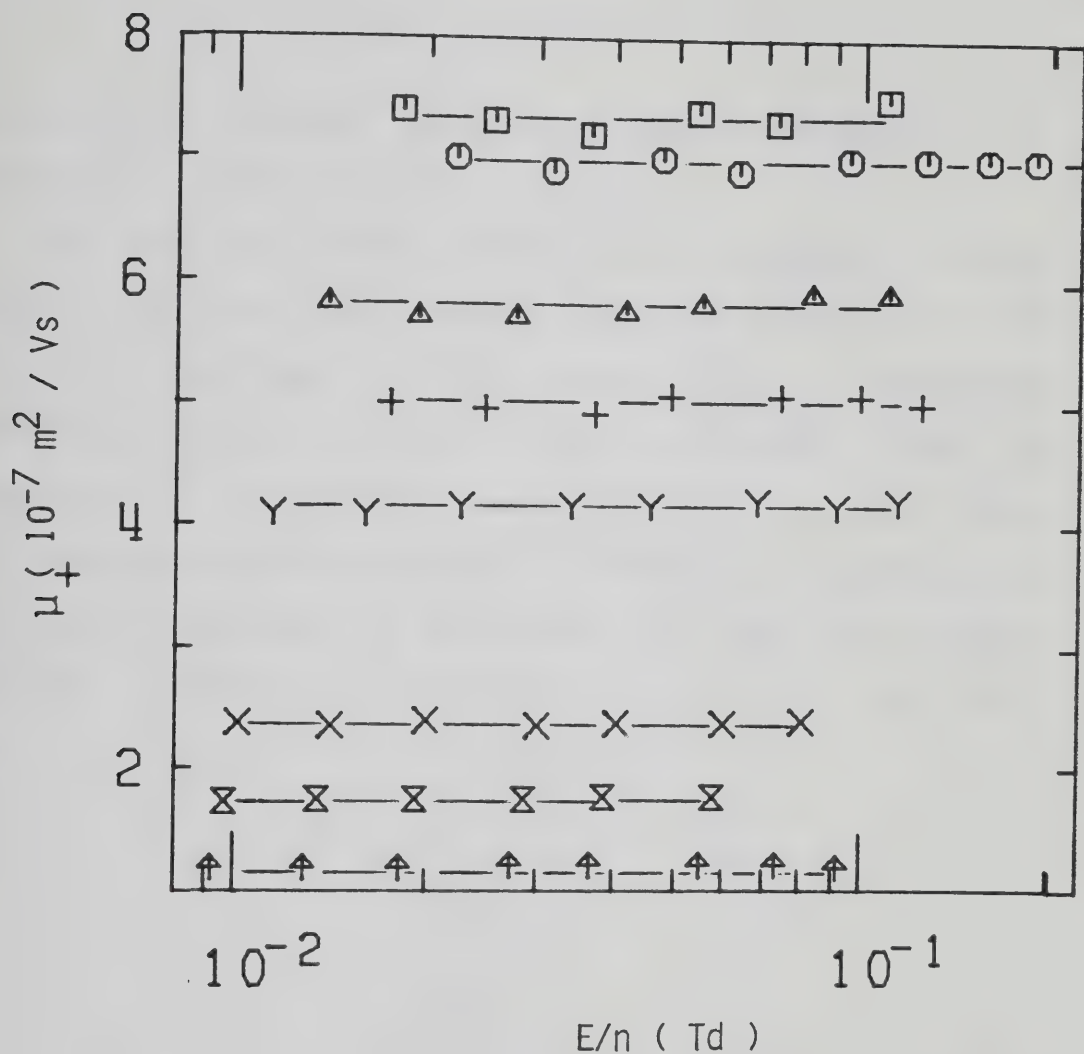


Figure III-1-26. Ion mobilities in liquid CH_4 at different densities (10^{27} molec/m³) and temperatures (K)
 □, 8.6, 188.2; ○, 9.9, 183.0; △, 11.3, 173.0; +, 12.6, 160.0; Y, 13.7, 146.5; X, 15.5, 118.5; ⊗, 16.2, 104.5; ↑, 17.0, 92.0.

A factor of 2 increase in density causes the mobility to decrease by a factor of 6.2.

All the gas phase results were obtained in high pressure gas type cells except those in Figure III-1-20 which were obtained in low pressure cells. Electrode separations were 0.315 ± 0.005 cm and 1.004 cm respectively. Liquid data were obtained in liquid type high pressure conductance cells. The electrode separations were 0.320 ± 0.001 cm. A listing of the mobilities at the different temperatures and densities is given in Table III-6.

TABLE III-6
Summary of Ion Results for CH₄^a

T (K)	n (10 ²⁶ m ⁻³)	μ_+ (10 ⁻⁴ m ² /Vs)	$n\mu_+$ [10 ²¹ (Vsm) ⁻¹]
116.5	0.295	1.38	4.07
163.7	0.295	1.68	4.96
292.5	0.295	1.82	5.4
372.6	0.295	1.99	5.9
441.2	0.295	2.16	6.4
494	0.295	2.32	6.8
123.5	1.54	0.204	3.14
142.5	4.36	0.070	3.05
152.0	5.5	0.064	3.52
172.5	5.5	0.073	4.02
201.5	5.5	0.083	4.57
228.0	5.5	0.089	4.90
292.3	5.5	0.095	5.2
154.0	7.4	0.0393	2.91
175.7	18.9	0.0159	3.01
184.0	28.5	0.0108	3.08
188.7	29.0	0.0128	3.71
192.0	29.0	0.0134	3.89
195.2	29.0	0.0143	4.15
191.2	61 ^b	0.0064	3.90
192.2	61 ^b	0.0070	4.27
188.2	86	0.0074	6.4
183.0	99	0.0069	6.8
173.0	113	0.0057	6.4

(continued....)

Table III-6 continued

160.0	126	0.0050	6.3
146.5	137	0.00415	5.7
118.5	155	0.00237	3.67
104.5	162	0.00176	2.85
92.0	170	0.00120	2.04

a. The results in this table appear in the same order of appearance as the figures. They are given in order of increasing density.

b. $n_c = 6.1 \times 10^{27} \text{ molec/m}^3$, $T_c = 190.6\text{K}$.

2. CH₃D

In Figure III-2-20 are shown measurements in the saturated vapor. The ion mobility decreases with density. An increase in density by 70% causes the mobility to drop by approximately the same factor. An increase in temperature at constant density causes the ion mobility to increase. Figure III-2-21 shows the effect of raising the temperature from 108.2K to 535K at $n = 2.35 \times 10^{25}$ molec/m³. The mobility increases from 1.63×10^{-4} m²/Vs to 3.00×10^{-4} m²/Vs. As previously observed in CH₄ the ion signals became nonlinear at higher temperatures and it was not possible to determine a mobility. At the same temperatures the electron traces were linear. An increase in density of the saturated vapor by a factor of 6.5 (Figure III-2-22) has the effect of decreasing the mobility by about the same factor.

Raising the temperature from 153.9K to 293.0K at $n = 6.7 \times 10^{26}$ molec/m³ (Figure III-2-23) increases the mobility by about 70%. The same temperature change increased the mobility by only about 20% at the lowest density. A further increase in density of the saturated vapor (Figure III-2-24) causes the mobility to decrease as approximately the inverse density. In Figures III-2-25 and III-2-26 the effect of raising the temperature from 171.0K to 210.0K at $n = 1.50 \times 10^{27}$ molec/m³ and from 190.0K to

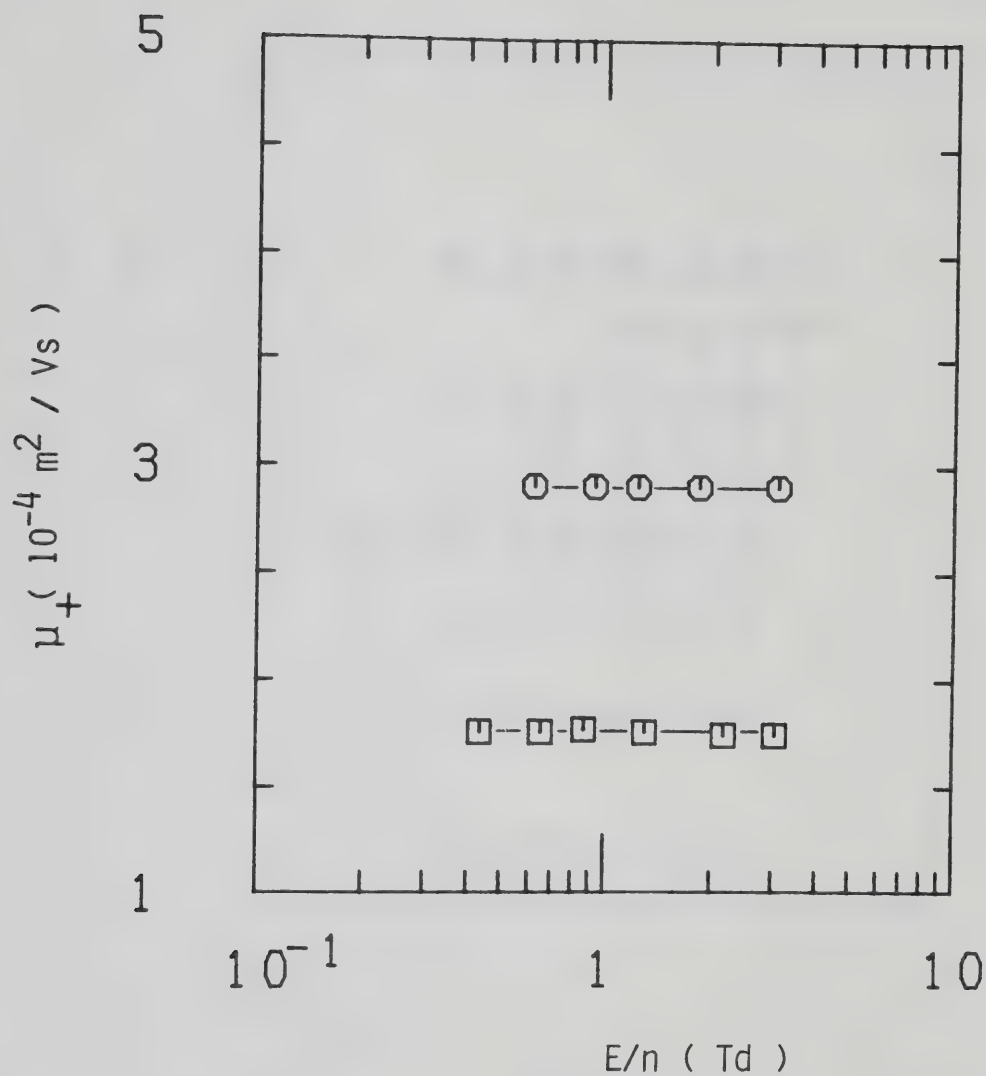


Figure III-2-20. Ion mobilities in saturated CH_3D vapor at different densities ($10^{25} \text{ molec/m}^3$) and temperatures (K). \bigcirc , 1.06, 91.9; \square , 1.78, 96.7.

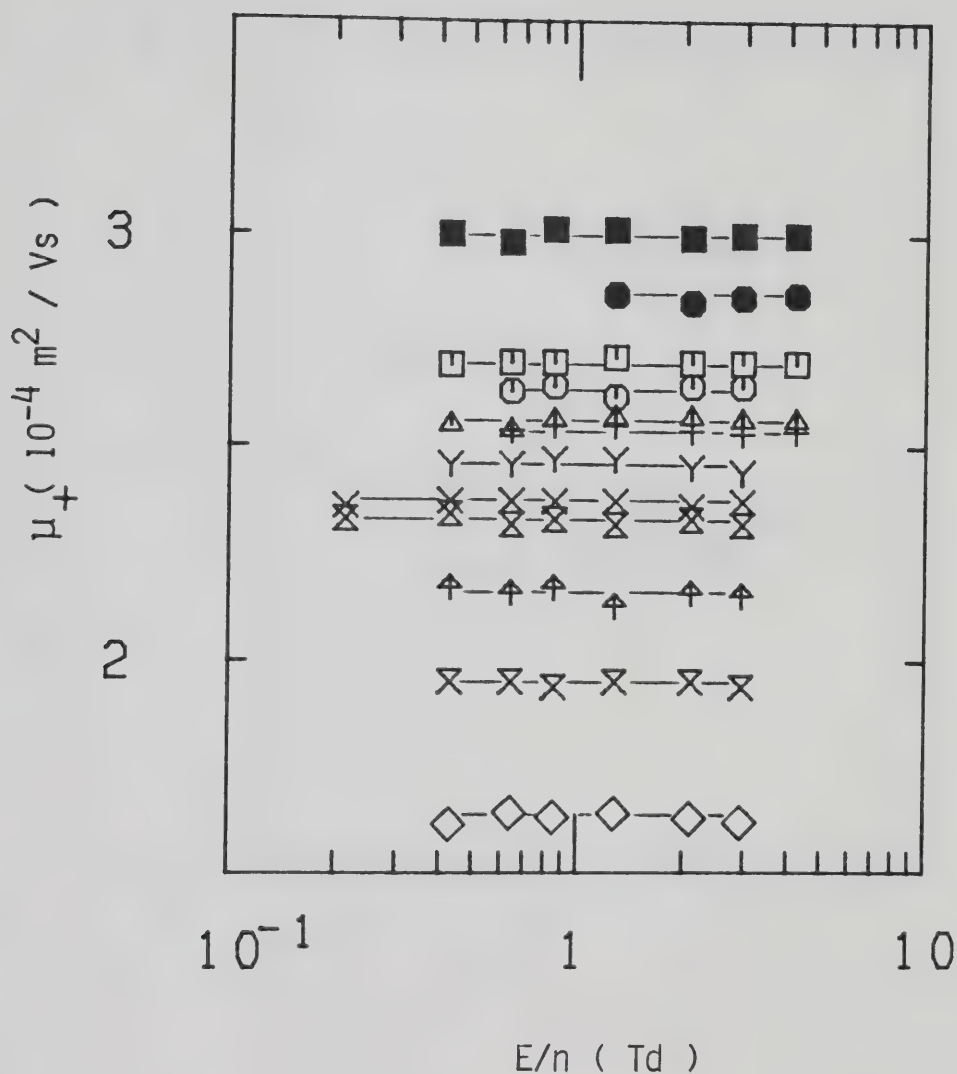


Figure III-2-21. Ion mobilities in CH_3D gas at $n = 2.35 \times 10^{25} \text{ molec/m}^3$ and different temperatures (K). \diamond , 108.2; \boxtimes , 146.3; \uparrow , 185.5; \boxtimes , 225.7; \times , 293.7; γ , 337.8; $+$, 385.8; \triangle , 404.4; \circ , 435; \square , 474; \bullet , 504; \blacksquare , 535.

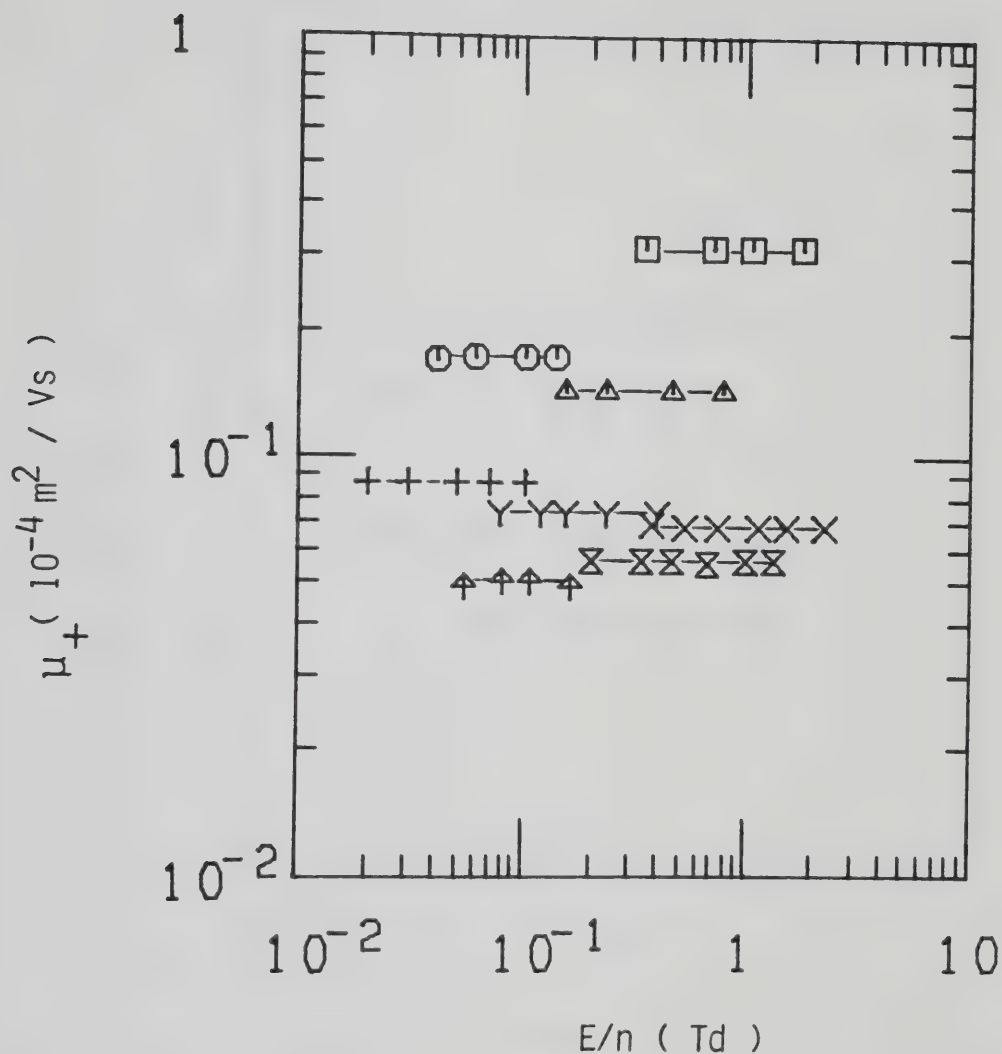


Figure III-2-22. Ion mobilities in saturated CH_3D vapor at different densities (10^{26} molec/m³) and temperatures (K). □, 0.89, 115.7; ○, 1.56, 124.0; Δ, 2.00, 128.5; +, 3.11, 136.5; Y, 3.94, 141.0; X, 4.30, 142.7; ⊗, 4.8, 145.5; ↑, 5.8, 149.5.

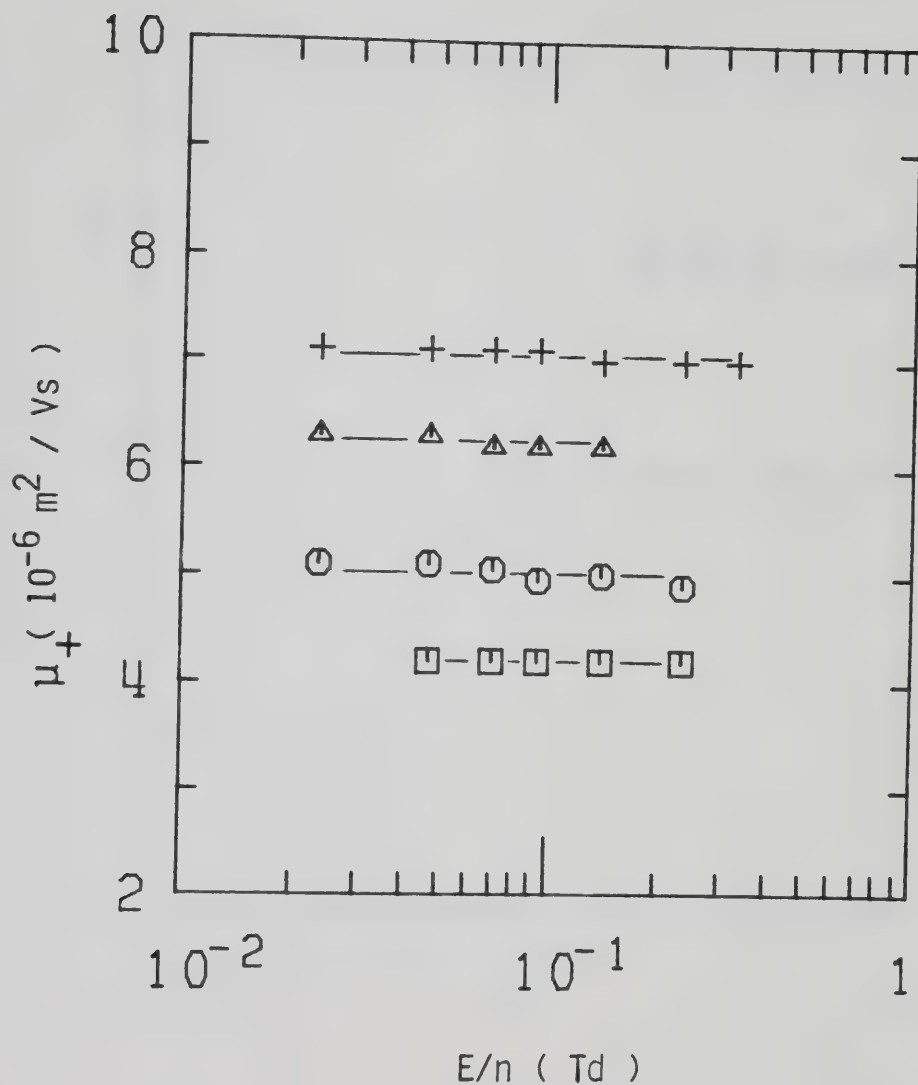


Figure III-2-23. Ion mobilities in CH_3D gas at $n = 6.7 \times 10^{26} \text{ molec/m}^3$ and different temperatures (K). \square , 153.9; \circ , 172.5; Δ , 219.3; $+$, 293.0.

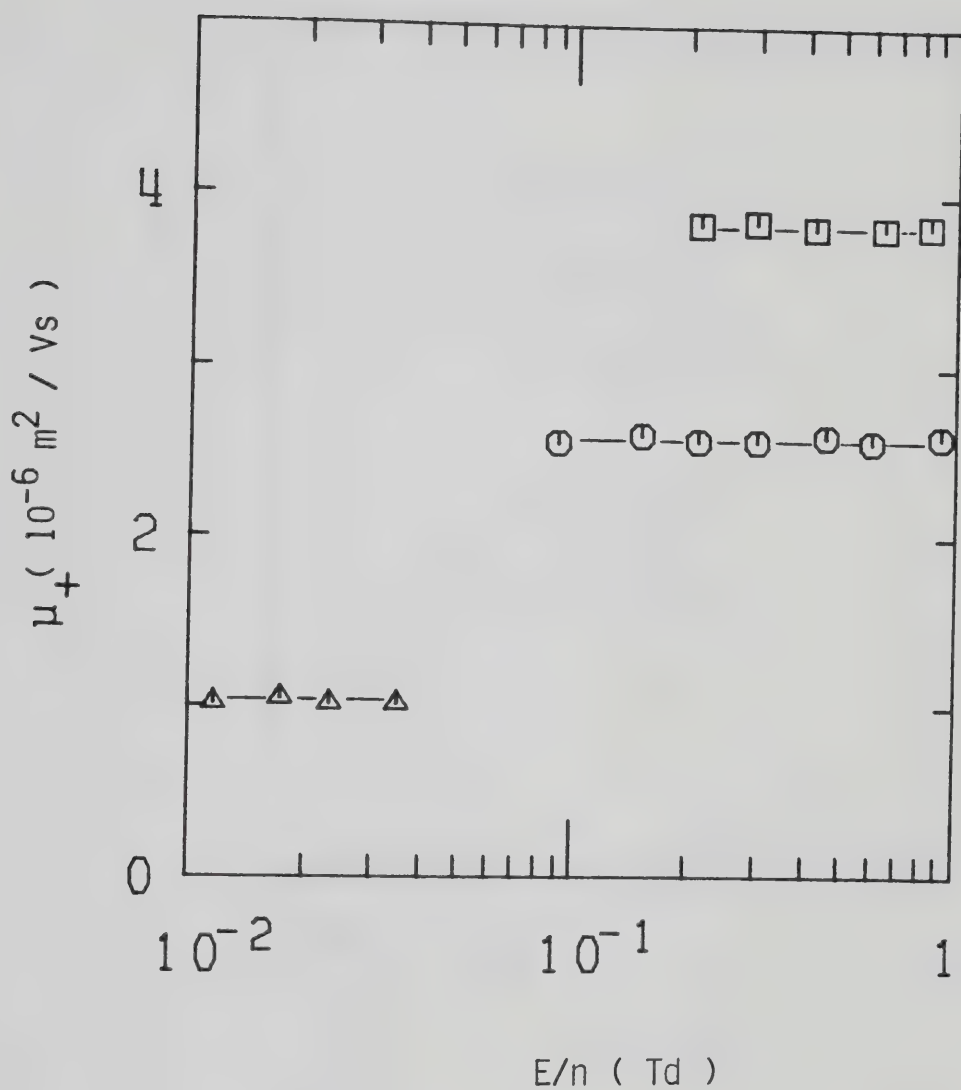


Figure III-2-24. Ion mobilities in saturated CH_3D vapor at different densities (10^{26} molec/ m^3) and temperatures (K). \square , 7.6, 155.0; \circ , 10.7, 163.0; Δ , 27.0, 184.2.

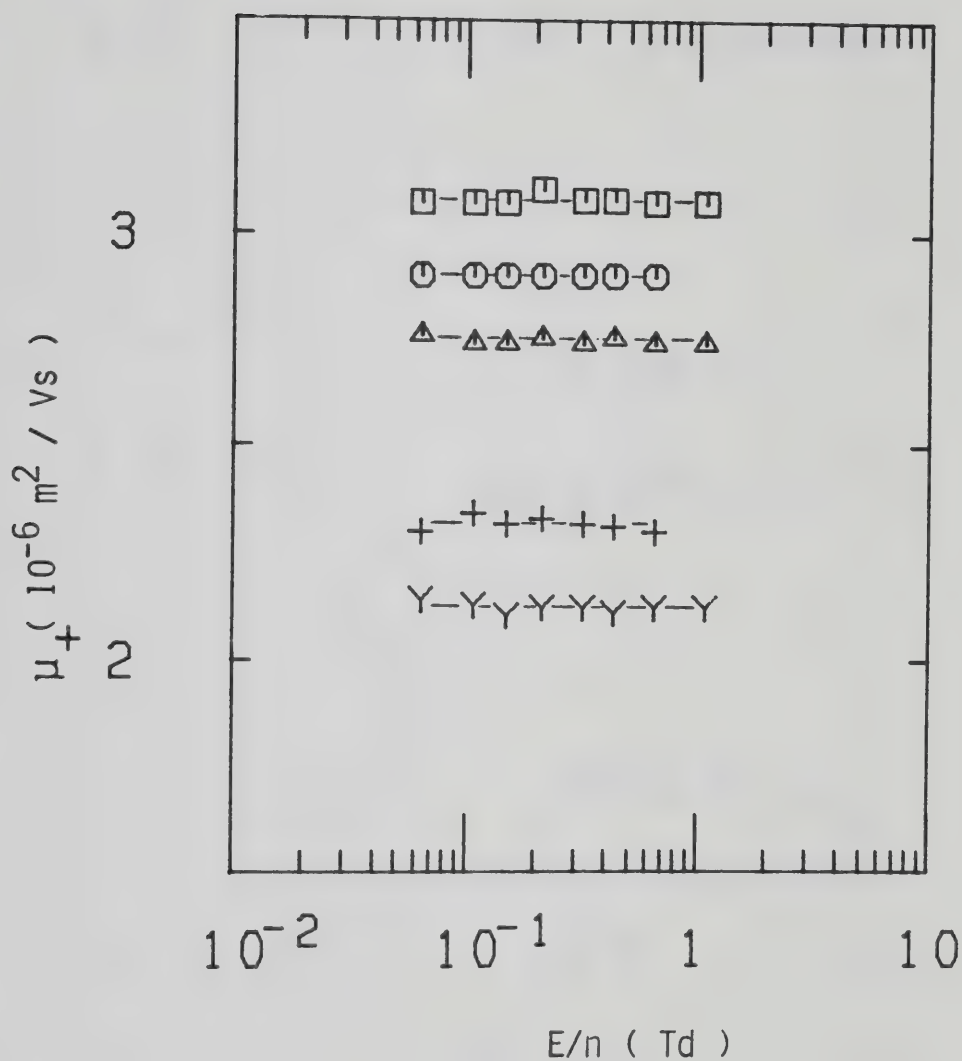


Figure III-2-25. Ion mobilities in CH_3D gas at $n = 1.50 \times 10^{27} \text{ molec/m}^3$ and different temperatures (K). Y , 171.0; + , 176.0; Δ , 190.0; \bigcirc , 200.2; \square , 210.0.

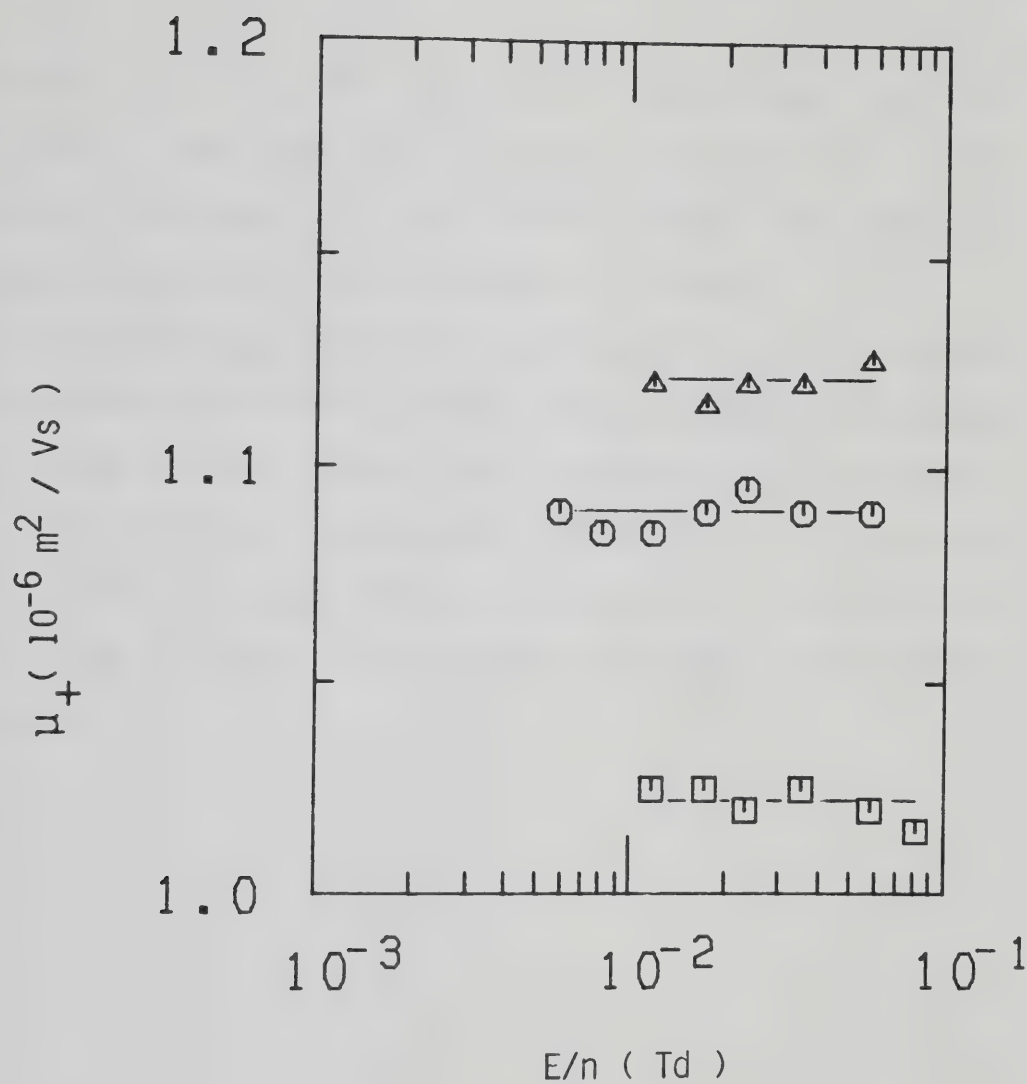


Figure III-2-26. Ion mobilities in CH_3D gas at $n = 2.70 \times 10^{27} \text{ molec/m}^3$ and different temperatures (K). \square , 190.0; \circ , 192.0; \triangle , 195.2.

195.2K at $n = 2.70 \times 10^{27}$ molec/m³ is illustrated. At the lower density the mobility increases by 45% for a 39K temperature increase. At the higher density the mobility increases by 10% for a 5K temperature increase.

All these measurements were performed in gas type high pressure conductance cells except those reported in Figures III-2-20 and III-2-21 which were obtained in low pressure cells. The electrode separations were 0.314 ± 0.004 cm and 0.999 ± 0.001 cm respectively. A listing of the mobility values at the different temperatures and densities is given in Table III-7.

TABLE III-7
Summary of Ion Results for CH₃D^a

<u>T</u> <u>(K)</u>	<u>n</u> <u>(10²⁶ m⁻³)</u>	<u>μ₊</u> <u>(10⁻⁴ m²/Vs)</u>	<u>nμ₊</u> <u>[10²¹ (Vsm)⁻¹]</u>
91.9	0.106	2.90	3.07
96.7	0.178	1.75	3.11
108.2	0.235	1.63	3.83
146.3	0.235	1.95	4.58
185.5	0.235	2.16	5.1
225.7	0.235	2.35	5.5
293.7	0.235	2.37	5.6
337.8	0.235	2.46	5.8
385.8	0.235	2.54	6.0
404.4	0.235	2.56	6.0
435	0.235	2.63	6.2
474	0.235	2.70	6.3
504	0.235	2.85	6.7
535	0.235	3.00	7.1
115.7	0.89	0.314	2.79
124.0	1.56	0.172	2.68
128.5	2.00	0.144	2.88
136.5	3.11	0.087	2.71
141.0	3.94	0.073	2.88
142.7	4.30	0.068	2.92
145.5	4.8	0.056	2.69
149.5	5.8	0.050	2.90
153.9	6.7	0.042	2.81

(continued....)

Table III-7 continued

172.5	6.7	0.050	3.35
219.3	6.7	0.063	4.22
293.0	6.7	0.071	4.76
155.0	7.6	0.0383	2.91
163.0	10.7	0.0258	2.76
184.2	27.0	0.0102	2.75
171.0	15.0	0.0212	3.18
176.0	15.0	0.0232	3.48
190.0	15.0	0.0274	4.11
200.2	15.0	0.0290	4.35
210.0	15.0	0.0308	4.62
190.0	27.0	0.0102	2.75
192.0	27.0	0.0109	2.94
195.2	27.0	0.0112	3.02

- a. The results appear in this table in the same order of appearance as the figures. They are given in order of increasing density.

3. CH₂D₂

In Figure III-3-17 the effect of raising the temperature from 133.0K to 450K at $n = 3.7 \times 10^{25}$ molec/m³ is reported. The ion mobility increases from 1.30×10^{-4} m²/Vs to 1.78×10^{-4} m²/Vs. The rate of increase of the mobility with temperature is greater at low temperatures than at high temperatures.

The same effect can be noticed by raising the temperature from 113.0K to 408.5K at $n = 6.1 \times 10^{25}$ molec/m³ (Figure III-3-18). The mobility increases by 48% on going from 113.0K to 225.5K and at higher temperature it tends to level off.

In the saturated vapor (Figure III-3-19) the mobility decreases with increasing density. An increase in density by a factor of about 20 causes a decrease in mobility by about the same factor. In Figures III-3-20 to III-3-22 the effect of temperature at three different densities is illustrated. At $n = 7.3 \times 10^{26}$ molec/m³ the mobility increases by 65% on raising the temperature from 155.7K to 292.0K. At $n = 26 \times 10^{26}$ molec/m³ an increase in temperature from 184.2K to 195.5K causes the mobility to increase by 27%. Heating the supercritical gas, $n_c = 61 \times 10^{26}$ molec/m³, from 190.5K to 193.9K increases the mobility by 21%. The rate of change of the mobility with temperature increases with increasing density.

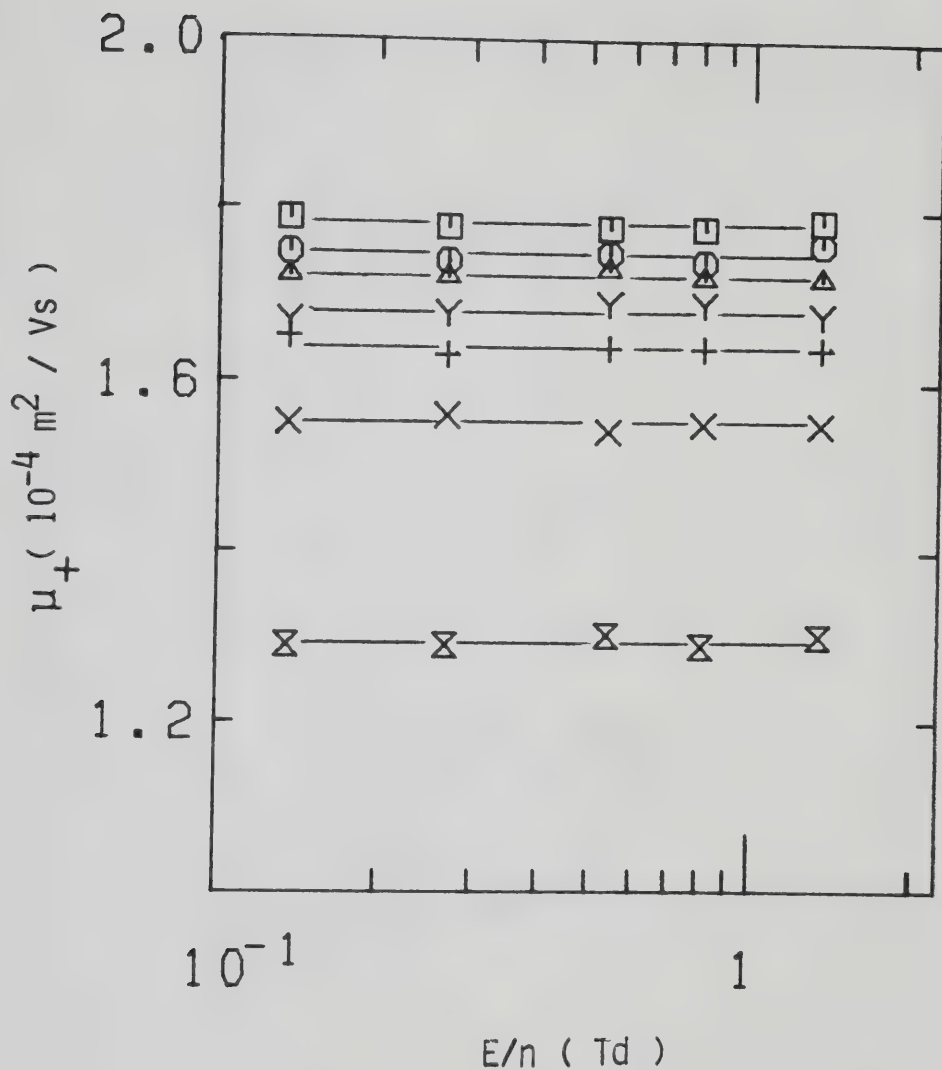


Figure III-3-17. Ion mobilities in CH_2D_2 gas at $n = 3.7 \times 10^{25} \text{ molec/m}^3$ and different temperatures (K). \otimes , 133.0; X, 170.8; +, 230.3; Y, 293.5; Δ , 351.7; \circ , 409.6; \square , 450.

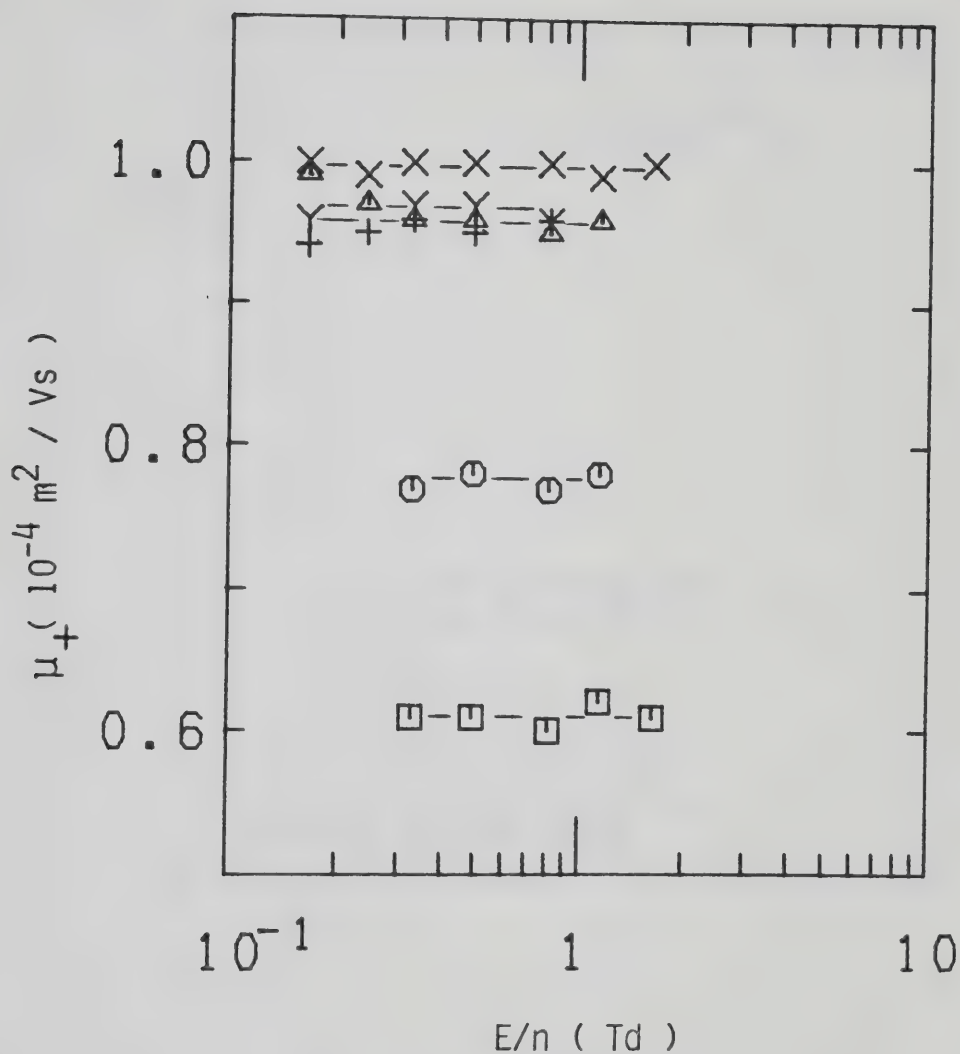


Figure III-3-18. Ion mobilities in CH_2D_2 gas at $n = 6.1 \times 10^{25} \text{ molec/m}^3$ and different temperatures (K). \square , 113.0; \circ , 151.0; Δ , 225.5; $+$, 294.0; Y , 340.0; X , 408.5.

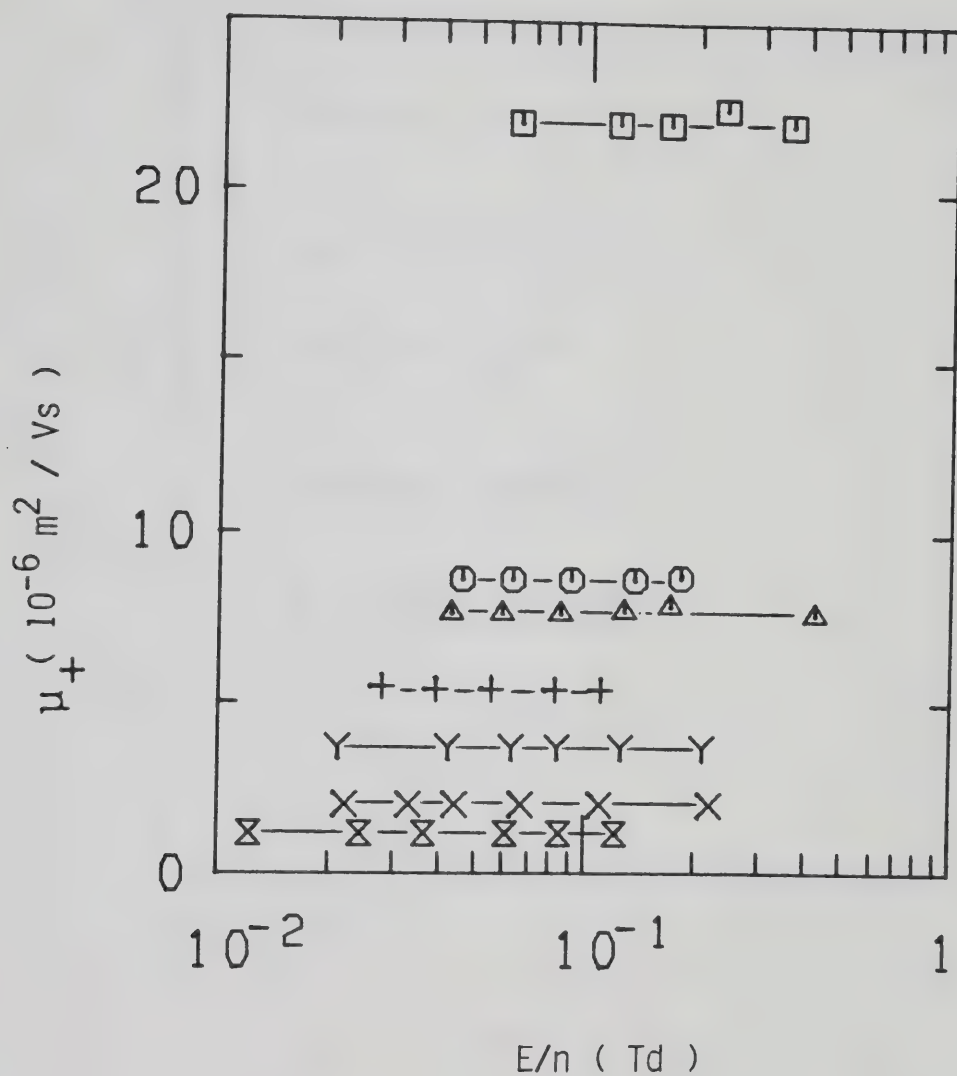


Figure III-3-19. Ion mobilities in saturated CH_2D_2 vapor at different densities ($10^{26} \text{ molec/m}^3$) and temperatures (K). □, 1.37, 120.8; ○, 3.58, 137.7; △, 3.82, 139.0; +, 5.9, 147.8; Y, 7.7, 154.0; X, 14.6, 168.9; ⊗, 26.5, 181.4.

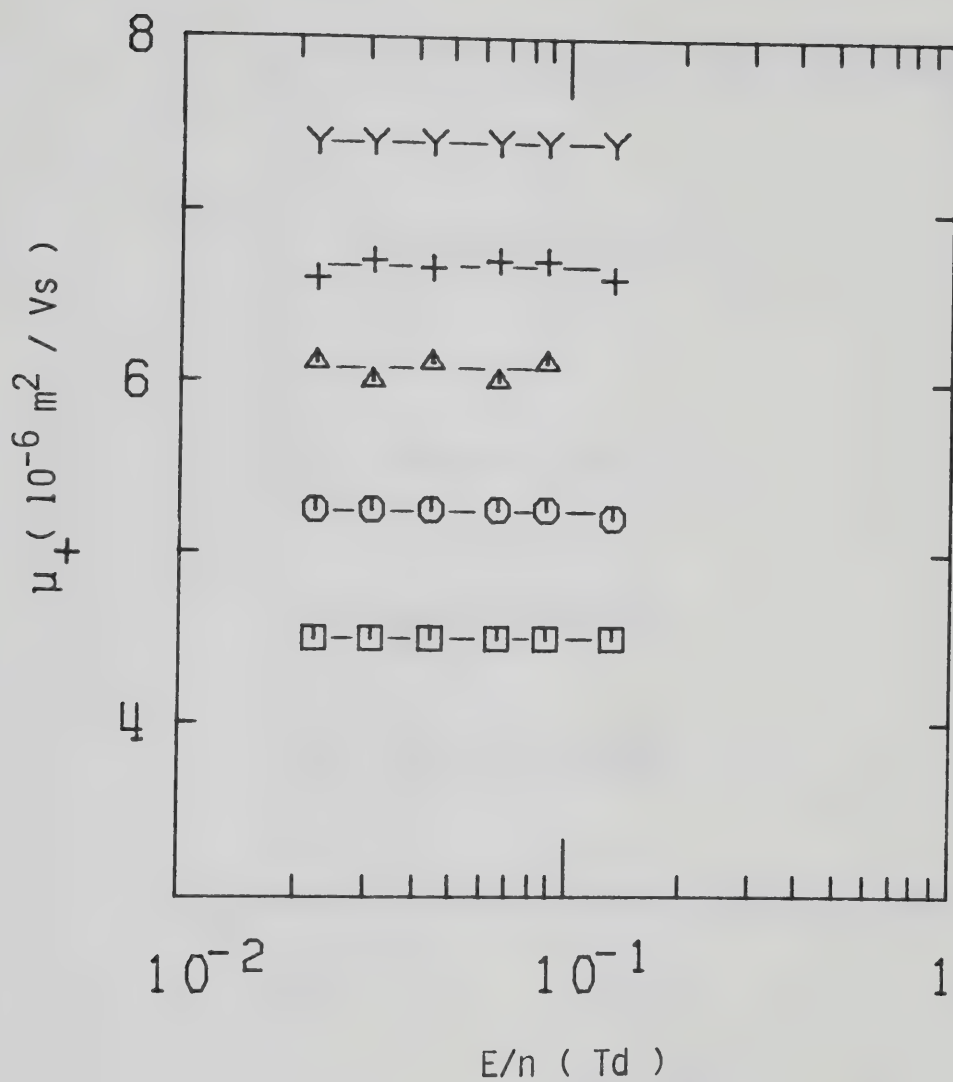


Figure III-3-20. Ion mobilities in CH_2D_2 gas at $n = 7.3 \times 10^{26} \text{ molec/m}^3$ and different temperatures (K). \square , 155.7; \circ , 172.5; \triangle , 195.5; + , 231.8; Y , 292.0.

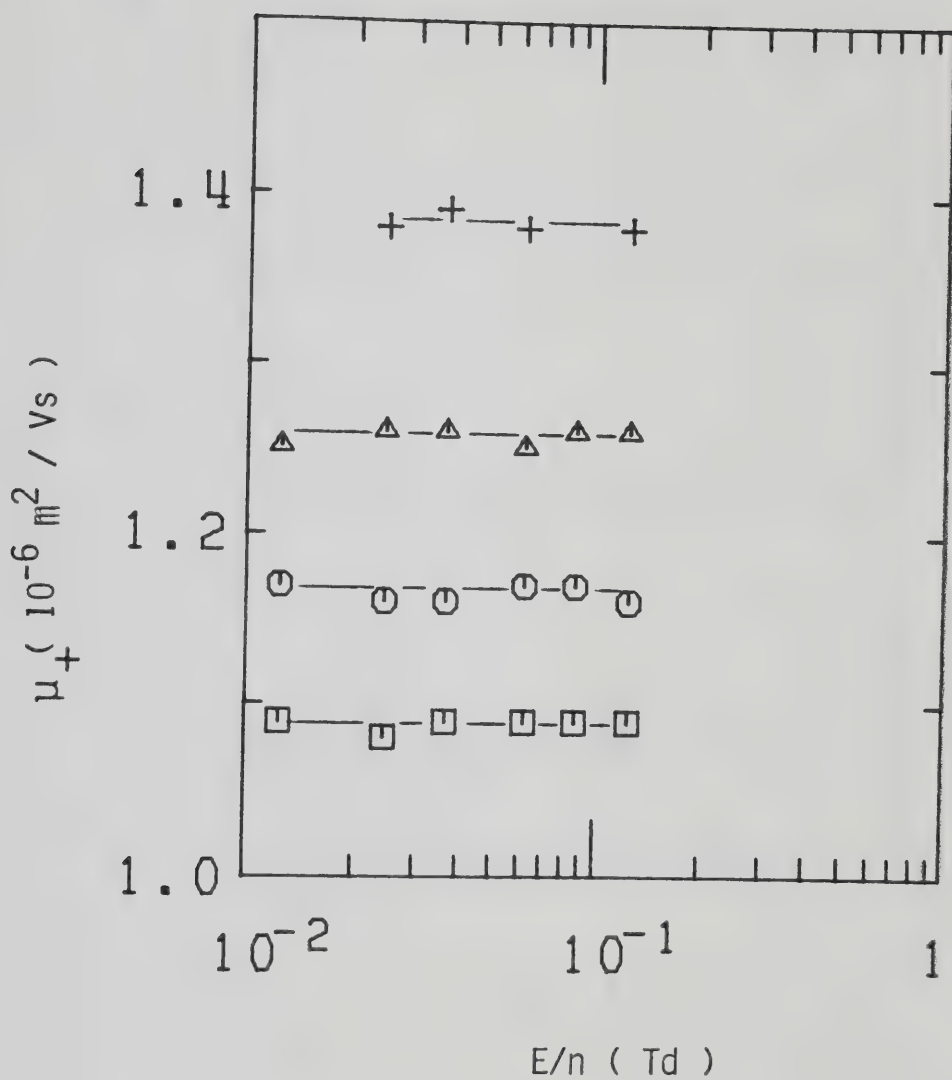


Figure III-3-21. Ion mobilities in CH_2D_2 gas at $n = 2.60 \times 10^{27}$ molec/m³ and different temperatures (K). □, 184.2; ○, 186.0; △, 189.3; +, 195.5.

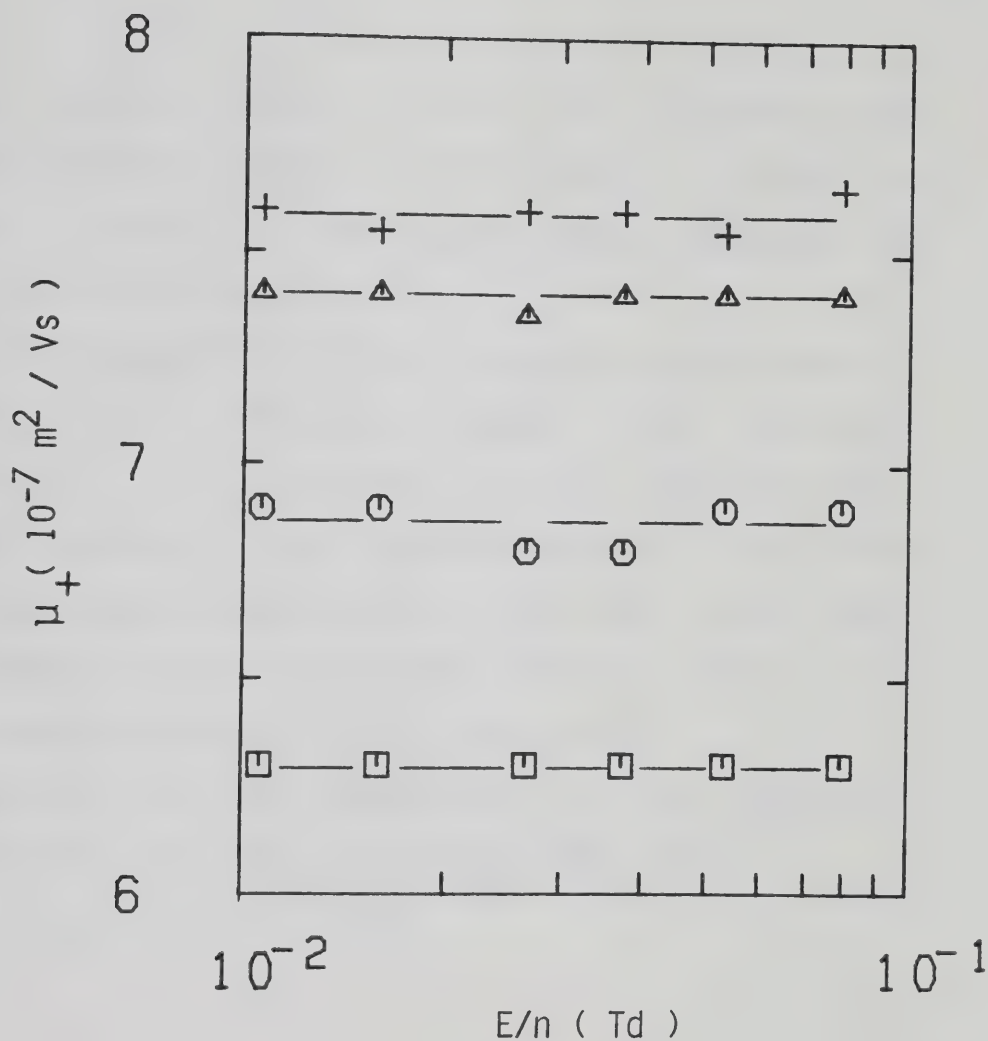


Figure III-3-22. Ion mobilities in supercritical CH_2D_2 gas at $n_c = 6.1 \times 10^{27} \text{ molec/m}^3$ and different temperatures (K). \square , 190.5; \circ , 191.7; Δ , 192.9; $+$, 193.9. $T_c = 189.2$.

In the liquid (Figures III-3-23 and III-3-24) the mobility decreases monotonically with density. A change in density by a factor of about 2 produces a decrease in mobility by a factor of 5.3.

Data in Figures III-3-17 and III-3-18 were obtained in low pressure type conductance cells. The electrode separations were 1.004 ± 0.001 cm. All the other gas phase results were obtained in high pressure gas type cells. The electrode separations were 0.310 ± 0.002 cm. Liquid data were obtained in liquid type high pressure cells. The electrode separations were 0.328 ± 0.001 cm.

A listing of the mobilities at the different temperatures and densities is given in Table III-8.

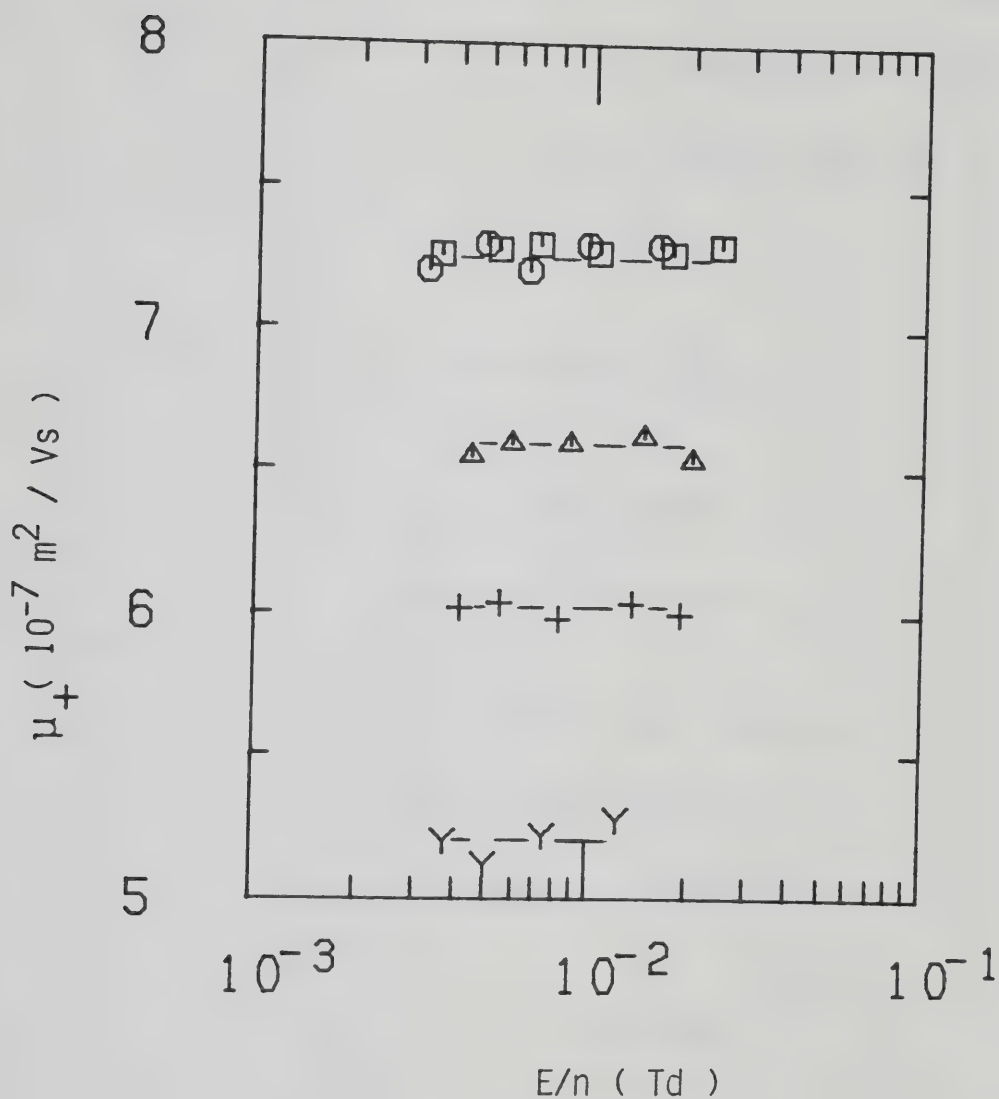


Figure III-3-23. Ion mobilities in liquid CH_2D_2 at different densities (10^{27} molec/ m^3) and temperatures (K). \square , 8.8, 186.1; \circ , 9.5, 183.8; Δ , 10.5, 178.0; +, 11.2, 172.7; Y, 12.2, 163.8.

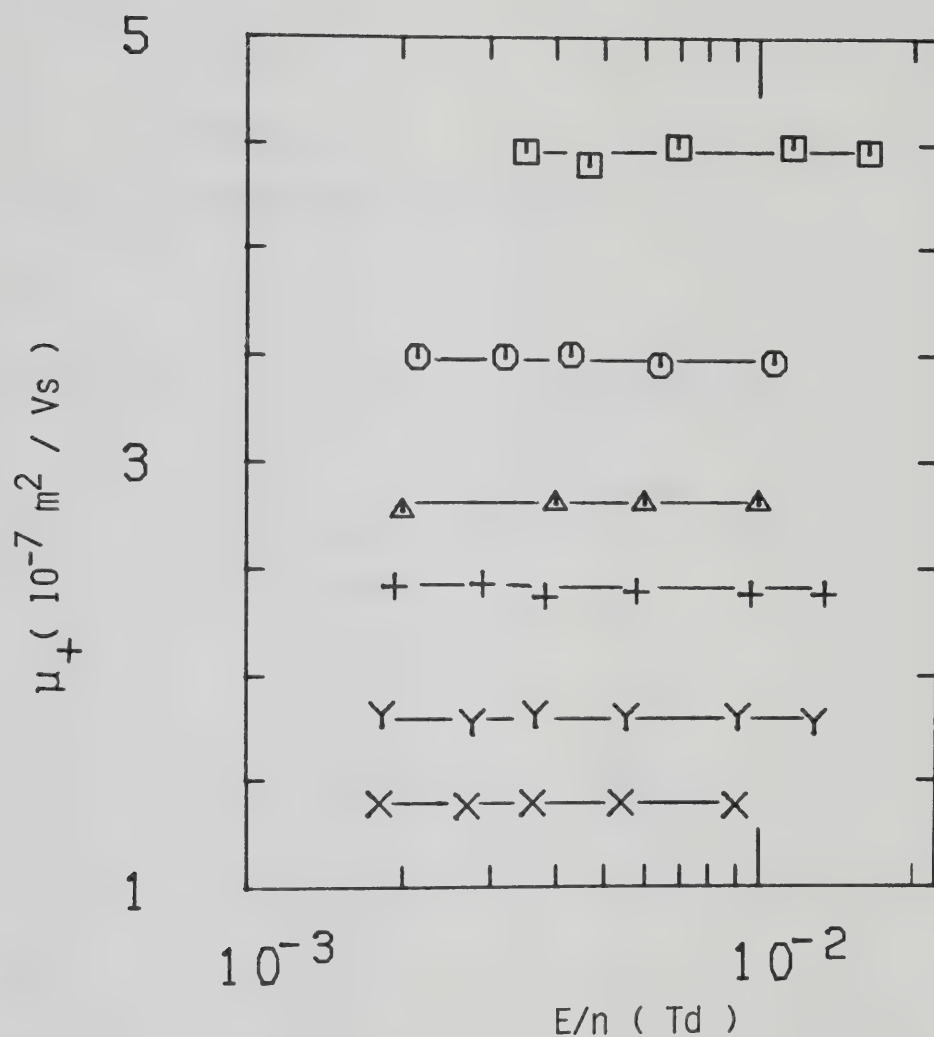


Figure III-3-24. Ion mobilities in liquid CH_2D_2 at different densities ($10^{27} \text{ molec/m}^3$) and temperatures (K). \square , 13.1, 153.5; \bigcirc , 14.2, 139.0; \triangle , 15.2, 124.0; $+$, 15.8, 114.0; Y , 16.6, 100.0; X , 16.9, 93.0.

TABLE III-8

Summary of Ion Result for CH_2D_2^a

T (K)	n (10^{26}m^{-3})	μ_+ ($10^{-4}\text{m}^2/\text{Vs}$)	$n\mu_+$ [$10^{21}(\text{Vsm})^{-1}$]
133.0	0.37	1.30	4.81
170.8	0.37	1.55	5.7
230.3	0.37	1.68	6.2
293.5	0.37	1.64	6.1
351.7	0.37	1.72	6.4
409.6	0.37	1.75	6.5
450	0.37	1.78	6.6
113.0	0.61	0.61	3.72
151.0	0.61	0.77	4.70
225.5	0.61	0.96	5.9
294.0	0.61	0.95	5.8
340.0	0.61	0.97	5.9
408.5	0.61	1.00	6.1
120.8	1.37	0.220	3.01
137.7	3.58	0.086	3.08
139.0	3.82	0.077	2.94
147.8	5.9	0.054	3.16
155.7	7.3	0.045	3.29
172.5	7.3	0.053	3.87
195.5	7.3	0.061	4.45
231.8	7.3	0.067	4.89
292.0	7.3	0.074	5.4
154.0	7.7	0.037	2.85
168.9	14.6	0.0200	2.92

(continued....)

Table III-8 continued

181.4	26.5	0.0116	3.07
184.2	26.0	0.0109	2.83
186.0	26.0	0.0117	3.04
189.3	26.0	0.0126	3.28
195.5	26.0	0.0138	3.59
190.5	61 ^b	0.0063	3.84
191.7	61 ^b	0.0069	4.21
192.9	61 ^b	0.0074	4.51
193.9	61 ^b	0.0076	4.64
186.1	88	0.0073	6.4
183.8	95	0.0073	6.9
178.0	105	0.0066	6.9
172.7	112	0.0060	6.7
163.8	122	0.0052	6.3
153.5	131	0.00446	5.8
139.0	142	0.00348	4.94
124.0	152	0.00280	4.26
114.0	158	0.00238	3.76
100.0	166	0.00180	2.99
93.0	169	0.00139	2.35

a. The results appear in this table in the same order as the figures. They are given in order of increasing density.

b. $n_c = 6.1 \times 10^{27} \text{ molec/m}^3$, $T_c = 189.2\text{K}$.

4. CHD₃

In Figure III-4-20 is reported the effect of increasing the density of the saturated vapor from 1.30×10^{25} molec/m³ to 1.56×10^{25} molec/m³. The mobility decreases by a factor of about 27%. By raising the temperature from 102.0K to 568.7K at $n = 2.30 \times 10^{25}$ molec/m³ (Figure III-4-21) the mobility increases from 1.46×10^{-4} m²/Vs to 3.19×10^{-4} m²/Vs. The rate of change of the mobility with temperature is greatest at temperatures near the coexistence curve. The same effects are noticeable at a density higher by approximately a factor of 2 (Figure III-4-22). The mobility increases from 7.9×10^{-5} m²/Vs to 1.50×10^{-4} m²/Vs on raising the temperature from 106.6K to 434K. Again, the temperature change has more effect on the ion mobility at low temperatures than at high ones.

In the saturated vapor (Figure III-4-23) the mobility decreases as the inverse density. In Figure III-4-24 the effect of heating the gas from 136.0K to 293.7K at $n = 1.22 \times 10^{26}$ molec/m³ is illustrated. The mobility increases with temperature by 24% between 136.0K and 186.0K and by only 4% between 236.3K and 293.7K. In Figure III-4-25 is shown the effect of increasing the density of the saturated vapor by a factor of about 3. The mobility decreases by about the same factor.

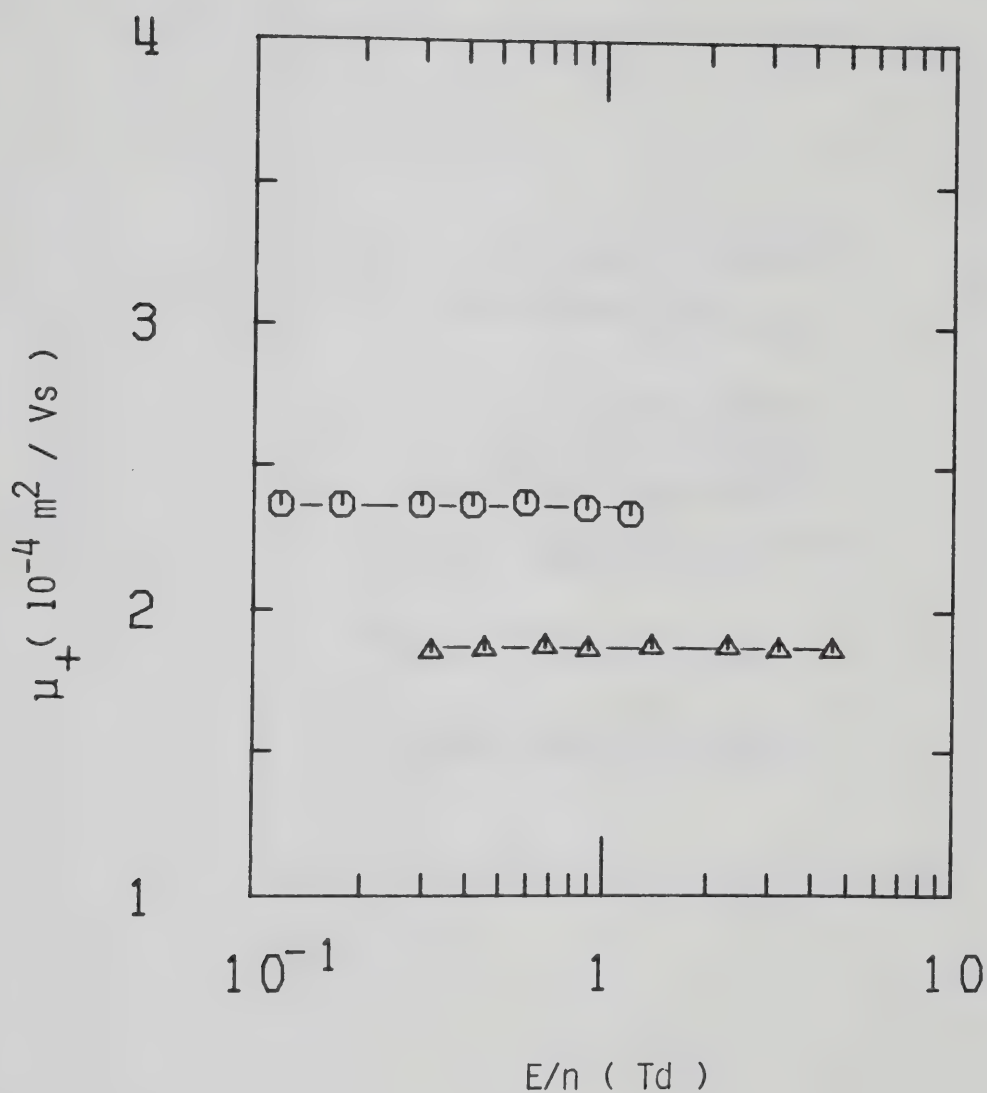


Figure III-4-20. Ion mobilities in saturated CHD_3 gas at different densities ($10^{25} \text{ molec/m}^3$) and temperatures (K). \bigcirc , 1.30, 92.6; Δ , 1.56, 94.8.

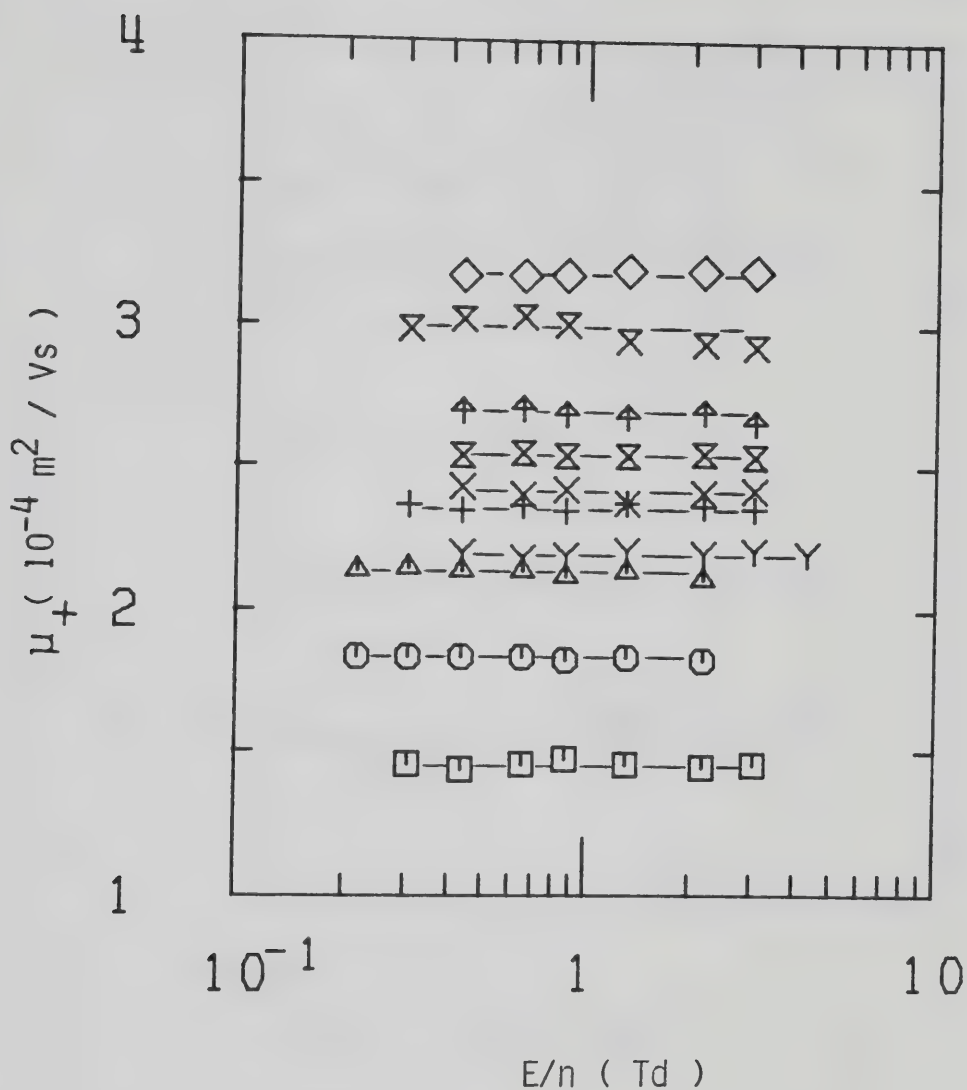


Figure III-4-21. Ion mobilities in CHD_3 gas at $n = 2.30 \times 10^{25} \text{ molec/m}^3$ and different temperatures (K). □, 102.0; ○, 135.0; △, 175.2; +, 225.2; Y, 294.6; X, 348.6; ⊠, 405.7; ↑, 465.6; ⋈, 516.7; ◇, 568.7.

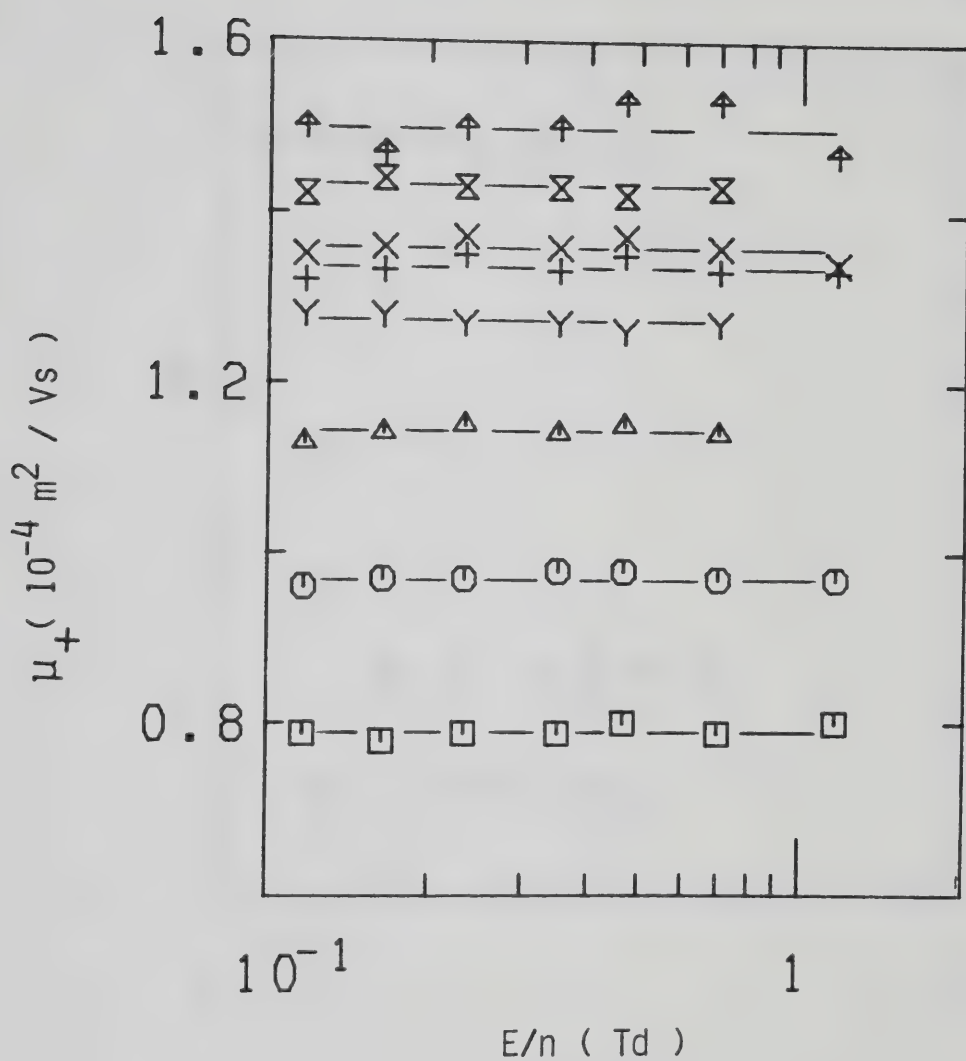


Figure III-4-22. Ion mobilities in CHD_3 gas at $n = 4.3 \times 10^{25} \text{ molec/m}^3$ and different temperatures (K). \square , 106.6; \circ , 135.5; \triangle , 175.1; $+$, 235.6; Y , 294.6; X , 337.2; \otimes , 384.8; \uparrow , 434.

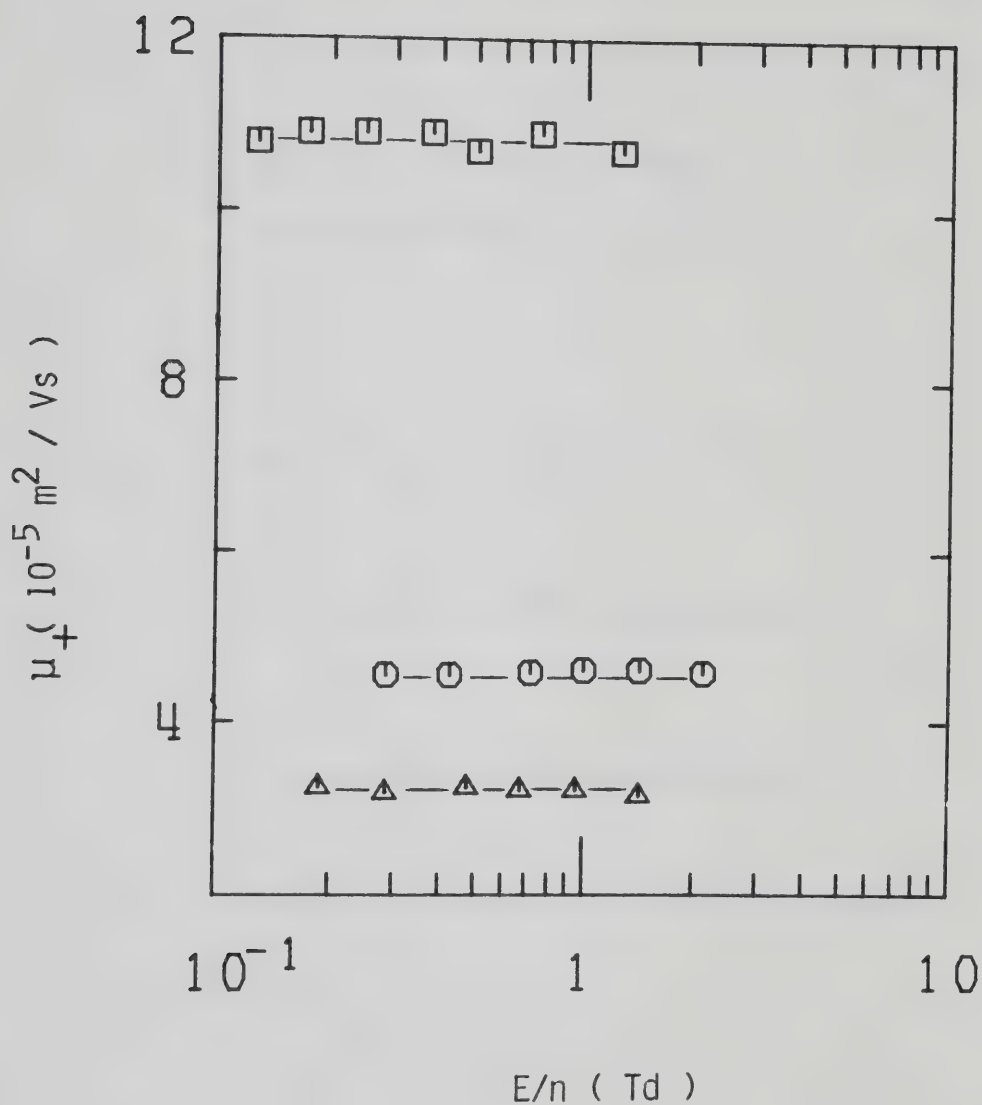


Figure III-4-23. Ion mobilities in saturated CHD_3 gas at different densities ($10^{25} \text{ molec/m}^3$) and temperatures (K). \square , 2.95, 101.0; \circ , 7.0, 111.1; Δ , 9.9, 115.8.

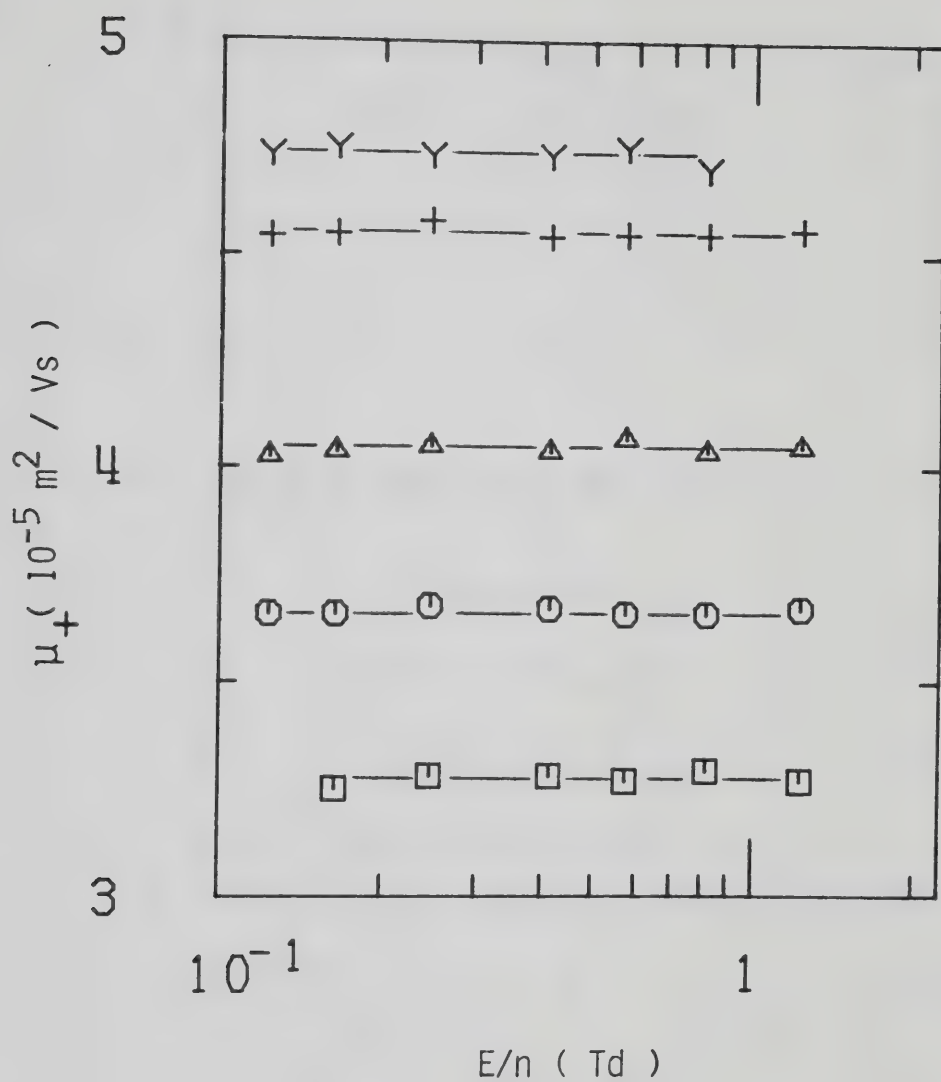


Figure III-4-24. Ion mobilities in CHD_3 gas at $n = 1.22 \times 10^{26} \text{ molec/m}^3$ and different temperatures (K). \square , 136.0; \circ , 156.0; Δ , 186.0; +, 236.3; Y, 293.7.

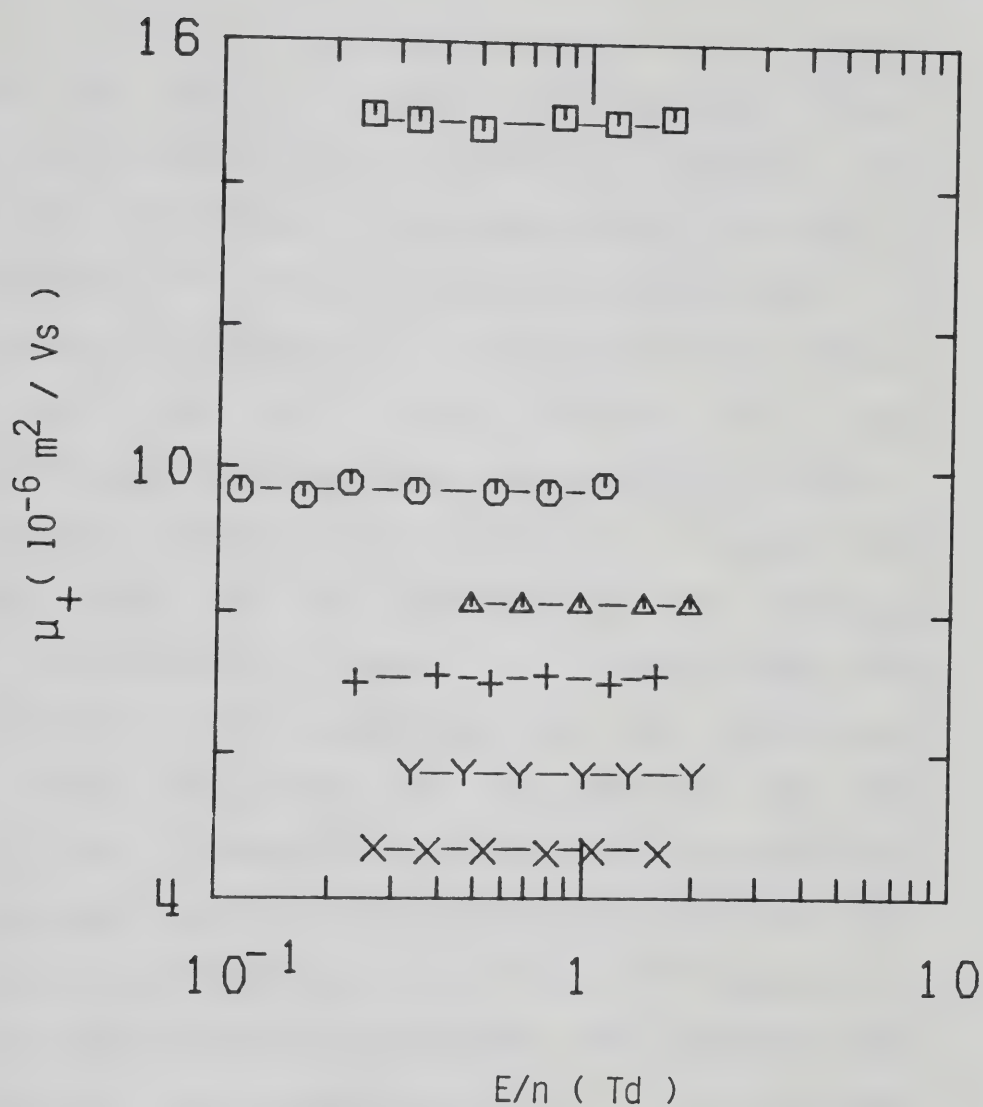


Figure III-4-25. Ion mobilities in saturated CHD_3 vapor at different densities (10^{26} molec/m³) and temperatures (K). □, 1.85, 125.5; ○, 2.76, 132.6; △, 3.22, 135.5; +, 3.94, 139.4; Y, 4.64, 142.8; X, 5.8, 147.5.

Heating the gas at $n = 6.8 \times 10^{26}$ molec/m³ (Figure III-4-26) has the effect of increasing the mobility. The effect is more noticeable at low temperatures, whereas at high temperatures the mobility tends to level off. A further increase in density of the saturated vapor (Figure III-4-27) has the same effect observed at lower densities. The mobility decreases as the inverse density.

In Figures III-4-28 and III-4-29 are reported the temperature effects on the mobility at two densities different by a factor of about 3. In both cases the mobility increases with temperature and the temperature effect is more noticeable at temperatures near the coexistence curve. However at $n = 9.3 \times 10^{26}$ molec/m³ the mobility increases by 27% for a 25K temperature change near the saturation curve whereas at $n = 29.1 \times 10^{26}$ molec/m³ an increase in temperature of only about 10K increases the mobility by 31%. An increase in density of the saturated vapor to about half the critical density (Figure III-4-30) causes the mobility to decrease in inverse ratio. At the critical density (Figure III-4-31) an increase in temperature of 3.5K produces an increase in mobility of about 40%. Increasing the density of the liquid (Figures IV-4-32 and 33) causes the mobility to decrease monotonically with density. It drops by a factor of 5.9 on raising the density by a factor of 1.9.

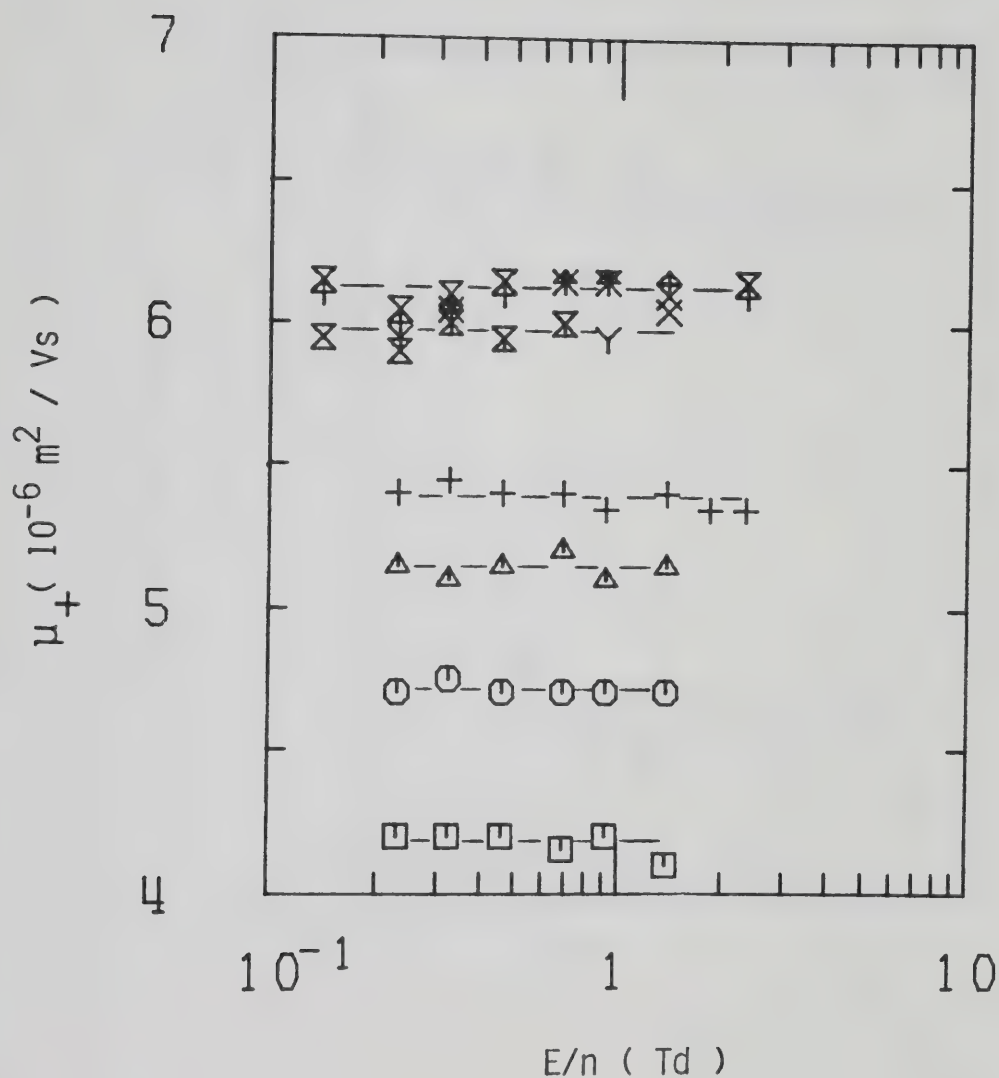


Figure III-4-26. Ion mobilities in CHD_3 gas at $n = 6.8 \times 10^{26} \text{ molec/m}^3$ and different temperatures (K). \square , 155.0; \circ , 168.5; \triangle , 184.2; $+$, 194.7; γ , 235.0; \times , 250.5; \boxtimes , 295.0; \uparrow , 331; \boxtimes , 369.5.

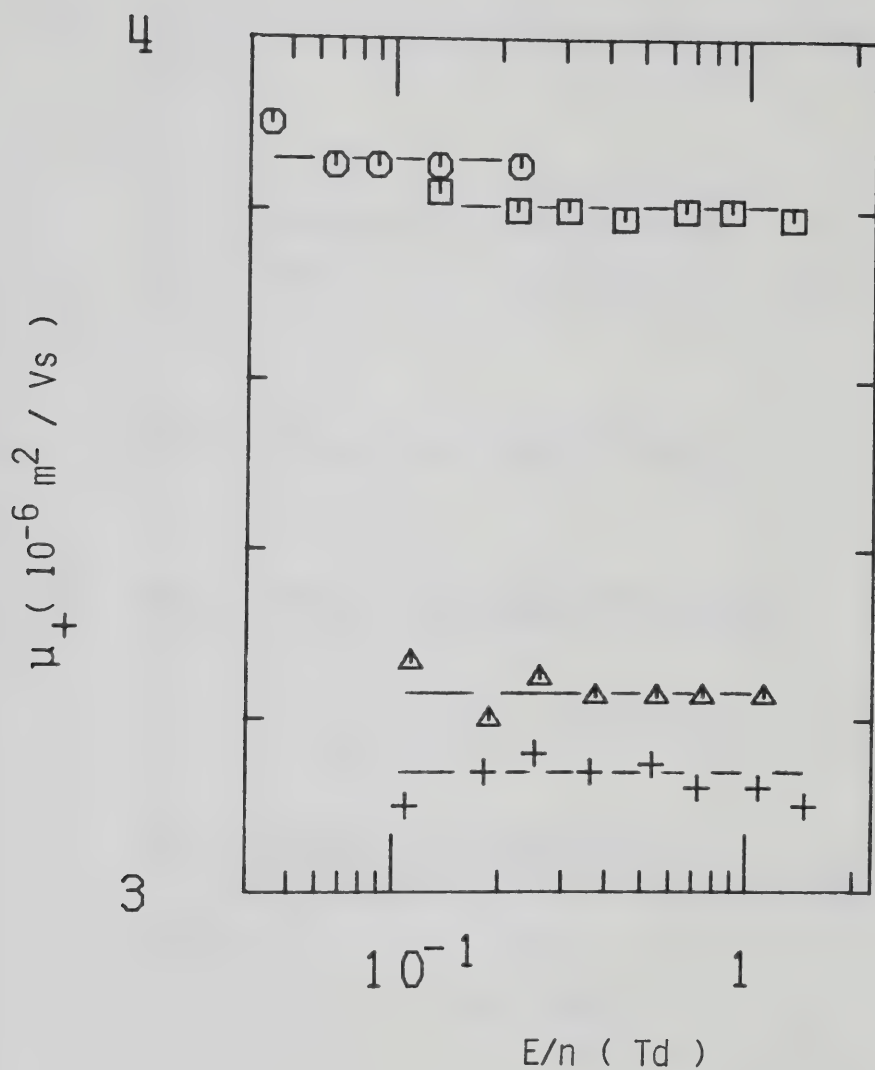


Figure III-4-27. Ion mobilities in saturated CHD_3 at different densities ($10^{26} \text{ molec/m}^3$) and temperatures (K). \square , 7.1, 152.0; \circ , 7.3, 152.3; Δ , 8.4, 155.5; +, 8.7, 156.0.

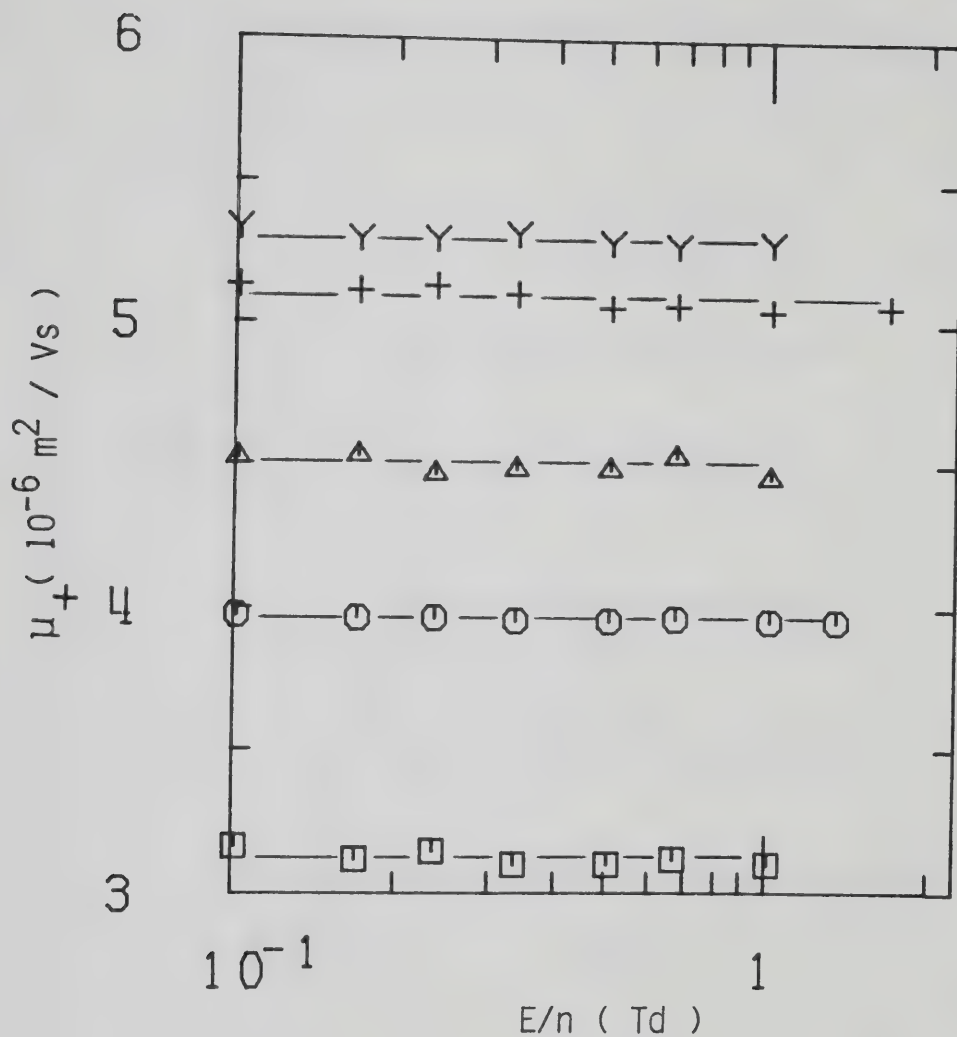


Figure III-4-28. Ion mobilities in CHD_3 gas at $n = 9.3 \times 10^{26} \text{ molec/m}^3$ and different temperatures (K). \square , 161.0; \circ , 186.0; Δ , 216.0; $+$, 256.5; Y , 293.8.

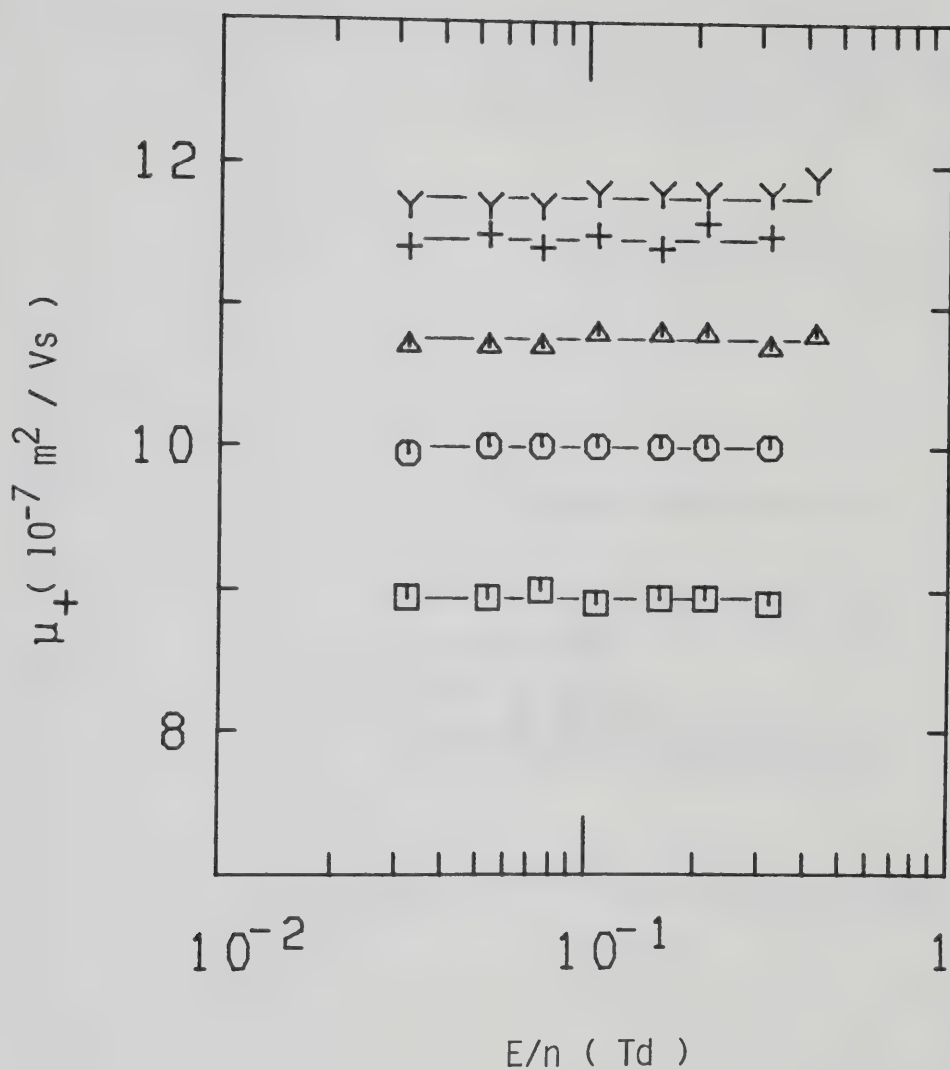


Figure III-4-29. Ion mobilities in CHD_3 gas at $n = 2.91 \times 10^{27} \text{ molec/m}^3$ and different temperatures (K). \square , 184.0; \circ , 187.0; \triangle , 189.0; $+$, 192.0; Y , 193.8.

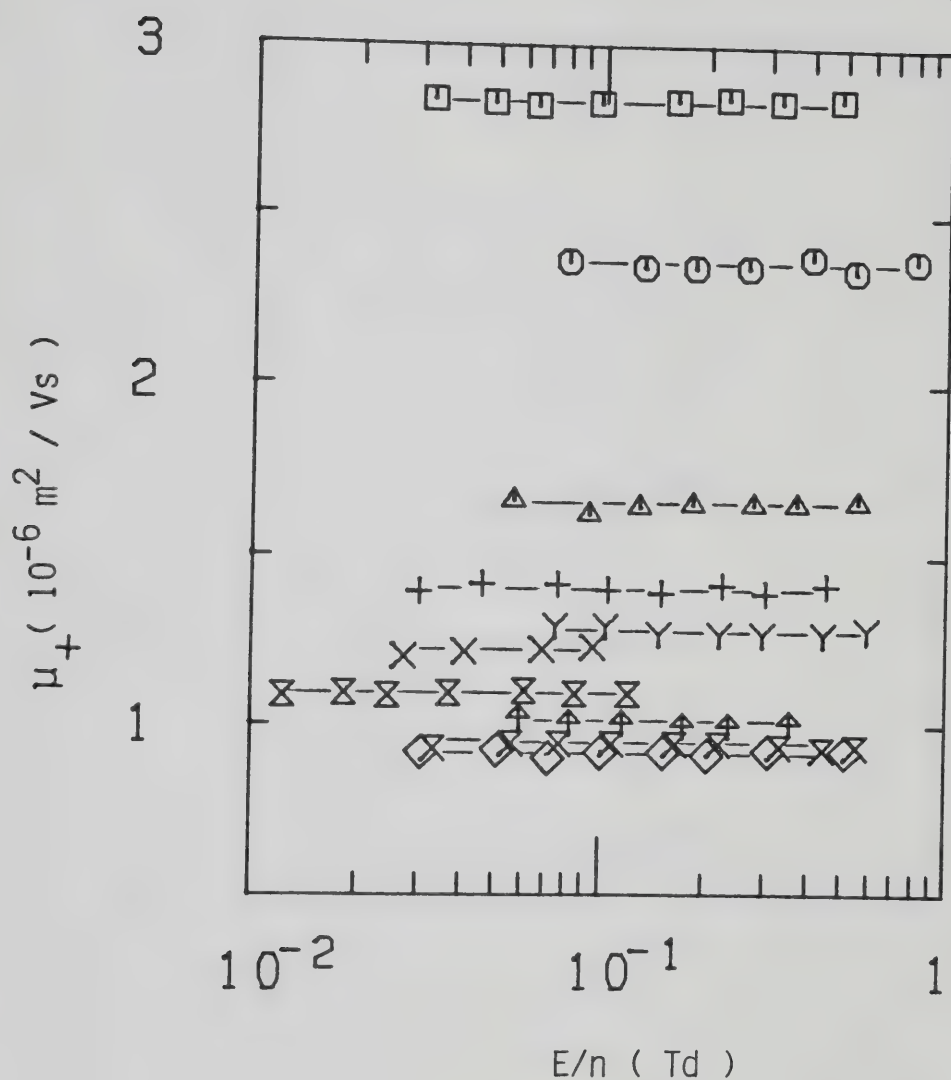


Figure III-4-30. Ion mobilities in saturated CHD_3 vapor at different densities ($10^{27} \text{ molec/m}^3$) and temperatures (K). \square , 0.97, 158.5; \circ , 1.18, 163.1; \triangle , 1.69, 171.7; $+$, 2.07, 176.2; γ , 2.12, 176.8; \times , 2.37, 179.0; \boxtimes , 2.65, 181.0; \uparrow , 2.70, 181.5; \boxtimes , 2.83, 182.3; \diamond , 3.03, 183.6.

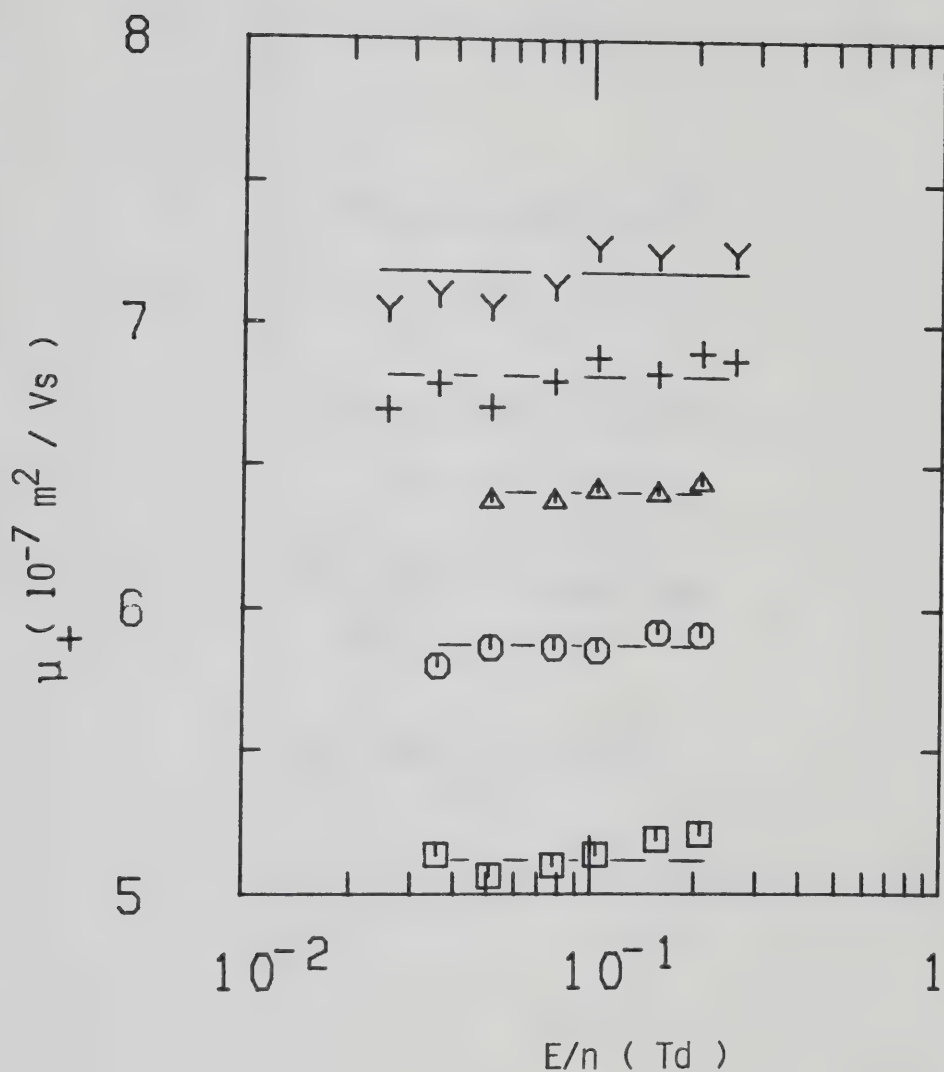


Figure III-4-31. Ion mobilities in supercritical CHD_3 at $n_c = 6.1 \times 10^{27} \text{ molec/m}^3$ and different temperatures (K). \square , 189.5; \circ , 190.2; \triangle , 191.2; $+$, 192.0; Y , 193.0. $T_c = 189.0$.

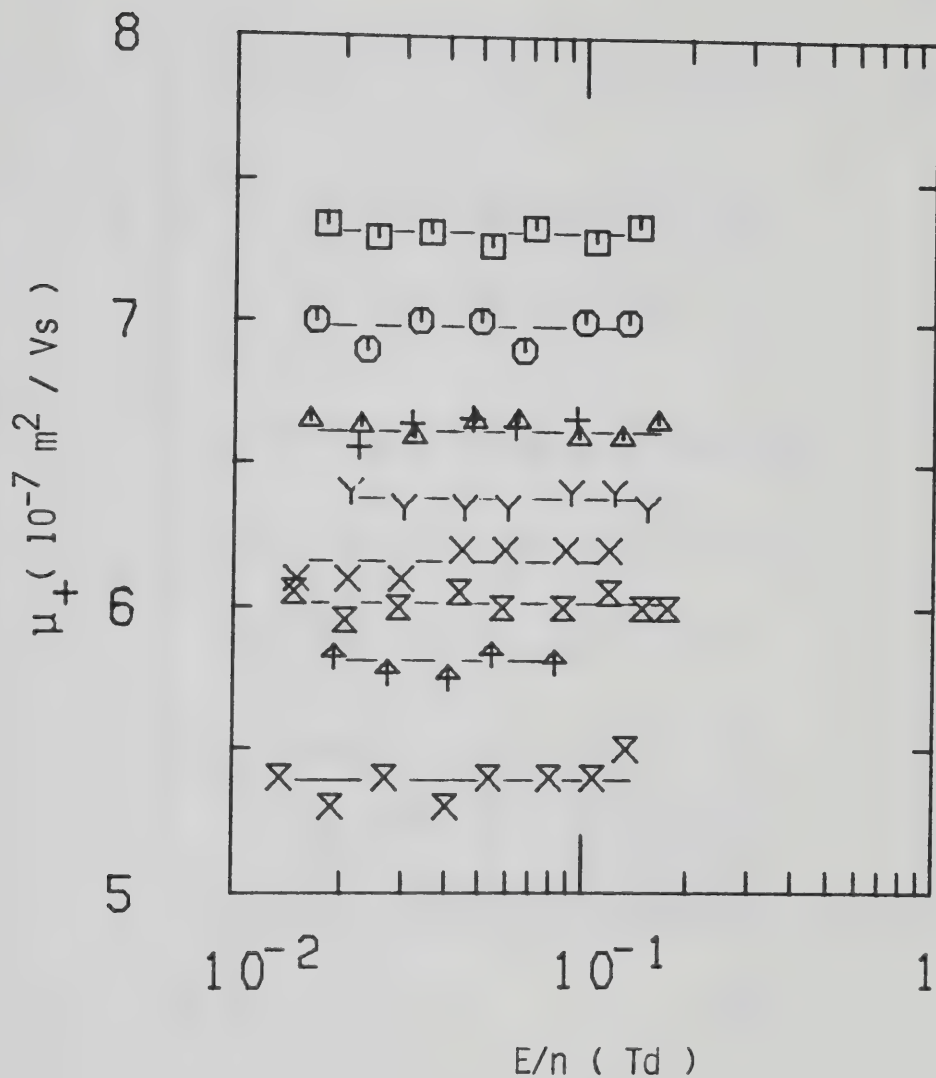


Figure III-4-32. Ion mobilities in liquid CHD_3 at different densities ($10^{27} \text{ molec/m}^3$) and temperatures (K). \square , 8.8, 186.0; \circ , 9.4, 183.6; \triangle , 9.7, 182.4; $+$, 9.9, 181.5; γ , 10.3, 178.9; \times , 10.6, 176.8; \boxtimes , 10.7, 175.4; \uparrow , 11.4, 171.7; \boxtimes , 11.7, 168.0.

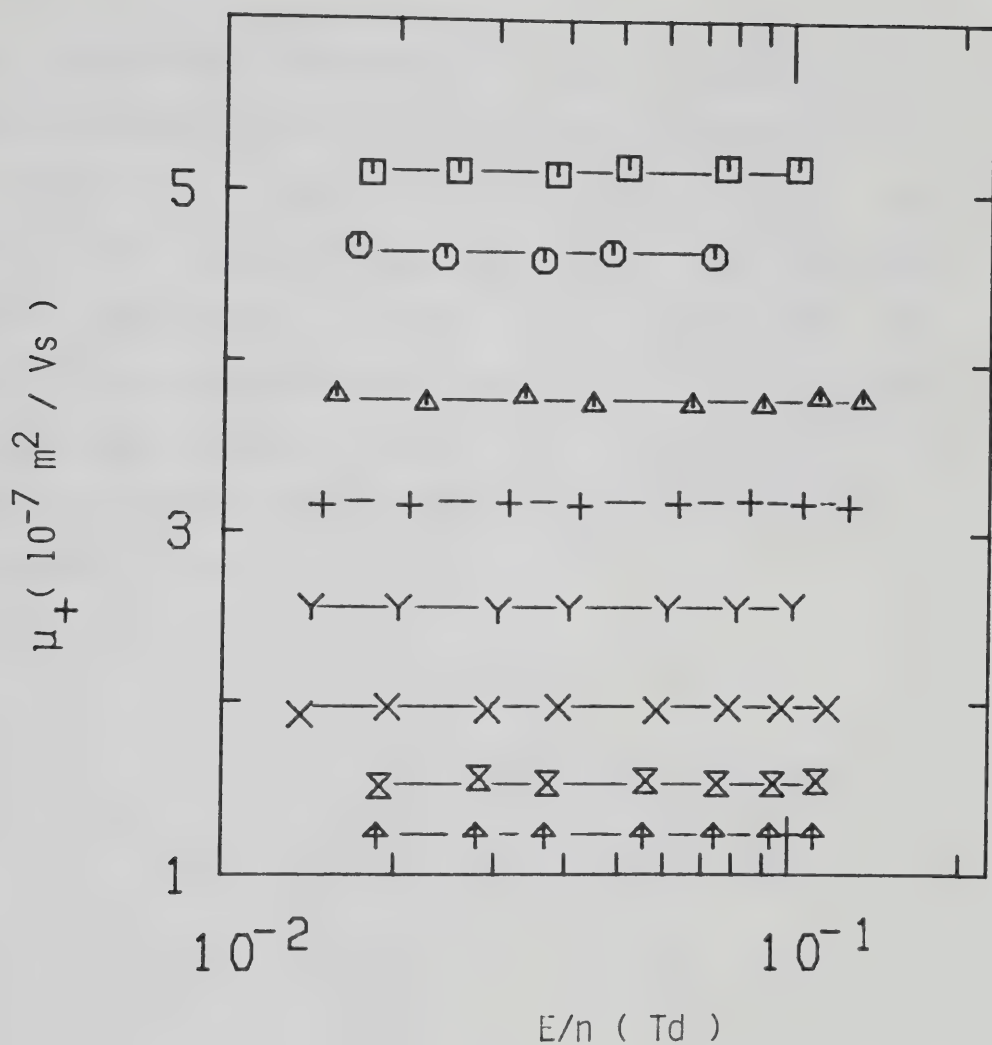


Figure III-4-33. Ion mobilities in liquid CHD_3 at different densities ($10^{27} \text{ molec/m}^3$) and temperatures (K). \square , 12.3, 163.1; \bigcirc , 13.0, 155.5; \triangle , 14.0, 141.7; $+$, 14.8, 130.3; Y , 15.5, 119.2; \times , 16.1, 108.9; \boxtimes , 16.7, 99.8; \uparrow , 16.9, 92.1.

Data in Figures III-4-20 to 24 were obtained in low pressure conductance cells. The electrode separations were 0.998 ± 0.001 cm. All other gas phase results were obtained in high pressure gas type cells. The electrode separations were 0.315 ± 0.005 cm. Liquid data were obtained in high pressure liquid type cells. The electrode separations were 0.320 ± 0.001 cm. A listing of the mobilities at the different temperatures and densities is given in Table III-9.

TABLE III-9
Summary of Ion Results for CHD₃^a

T (K)	n (10 ²⁶ m ⁻³)	μ_+ (10 ⁻⁴ m ² /Vs)	$n\mu_+$ [10 ²¹ (Vsm) ⁻¹]
92.6	0.130	2.37	3.08
94.8	0.156	1.86	2.90
102.0	0.230	1.46	3.36
135.0	0.230	1.83	4.21
175.2	0.230	2.14	4.92
225.2	0.230	2.37	5.5
294.6	0.230	2.20	5.1
348.6	0.230	2.41	5.5
405.7	0.230	2.55	5.9
465.6	0.230	2.69	6.2
516.7	0.230	2.98	6.9
568.7	0.230	3.19	7.3
101.0	0.295	1.08	3.19
111.1	0.70	0.46	3.22
115.8	0.99	0.32	3.17
106.6	0.43	0.79	3.40
135.5	0.43	0.97	4.17
175.1	0.43	1.14	4.90
235.6	0.43	1.33	5.7
294.6	0.43	1.27	5.5
337.2	0.43	1.36	5.8
384.8	0.43	1.43	6.1
434	0.43	1.50	6.5

(continued....)

Table III-9 continued

136.0	1.22	0.327	3.99
156.0	1.22	0.366	4.47
186.0	1.22	0.404	4.93
236.3	1.22	0.455	5.6
293.7	1.22	0.473	5.8
125.5	1.85	0.150	2.78
132.6	2.76	0.097	2.68
135.5	3.22	0.081	2.61
139.4	3.94	0.071	2.80
142.8	4.64	0.057	2.64
147.5	5.8	0.0465	2.70
155.0	6.8	0.0418	2.84
168.5	6.8	0.0473	3.22
184.2	6.8	0.051	3.47
194.7	6.8	0.054	3.67
235.0	6.8	0.061	4.15
250.5	6.8	0.061	4.15
295.0	6.8	0.060	4.08
331.0	6.8	0.061	4.15
369.5	6.8	0.061	4.15
152.0	7.1	0.0380	2.70
152.3	7.3	0.0385	2.81
155.5	8.4	0.0323	2.71
156.0	8.7	0.0313	2.72
161.0	9.3	0.0312	2.90
186.0	9.3	0.0395	3.67
216.0	9.3	0.0450	4.19
256.5	9.3	0.051	4.74
293.8	9.3	0.053	4.93

(continued....)

Table III-9 continued

158.5	9.7	0.0282	2.74
163.1	11.8	0.0236	2.78
171.7	16.9	0.0165	2.79
176.2	20.7	0.0140	2.90
176.8	21.2	0.0128	2.71
179.0	23.7	0.0122	2.89
181.0	26.5	0.0109	2.89
181.5	27.0	0.0101	2.73
182.3	28.3	0.0094	2.66
184.0	29.1	0.0090	2.62
187.0	29.1	0.0100	2.91
189.0	29.1	0.0108	3.14
192.0	29.1	0.0115	3.35
193.8	29.1	0.0118	3.43
183.6	30.3	0.0092	2.79
186.0	36.0	0.0073	2.63
187.7	42.2	0.0064	2.70
189.5	61 ^b	0.0051	3.11
190.2	61 ^b	0.0059	3.60
191.2	61 ^b	0.0064	3.90
192.0	61 ^b	0.0068	4.15
193.0	61 ^b	0.0072	4.39
187.7	83	0.0064	5.3
186.0	88	0.0073	6.4
183.6	94	0.0070	6.6
182.4	97	0.0067	6.5
181.5	99	0.0066	6.5

(continued....)

Table III-9 continued

178.9	103	0.0064	6.6
176.8	106	0.0062	6.6
175.4	107	0.0060	6.4
171.7	114	0.0058	6.6
168.0	117	0.0055	6.4
163.1	123	0.0052	6.4
155.5	130	0.0046	6.0
141.7	140	0.00378	5.3
130.3	148	0.00317	4.7
119.2	155	0.00256	3.97
108.9	161	0.00197	3.17
99.8	167	0.00153	2.56
92.1	169	0.00123	2.08

a. The results in this table appear in the same order of appearance as the figures. They are given in order of increasing density.

b. $n_C = 6.1 \times 10^{27} \text{ molec/m}^3$, $T_C = 189.0\text{K}$.

5. CD₄

In Figure III-5-17 is shown the effect of raising the temperature from 95.0K to 535.5K at $n = 2.50 \times 10^{24}$ molec/m³. The mobility increases by a greater factor at low temperatures than at high temperatures. The ion traces showed a pronounced curvature at $T \gtrsim 550$ K.

In the coexistent vapor an increase in density (Figure III-5-18) leads to a decrease of the mobility. On going from 1.50×10^{25} molec/m³ to 5.0×10^{25} molec/m³ the mobility decreases from 2.00×10^{-4} m²/Vs to 6.1×10^{-5} m²/Vs. At $n = 3.2 \times 10^{25}$ molec/m³ and 5.0×10^{25} molec/m³ (Figures III-5-19 to 21) an increase in temperature leads to an increase in mobility. Again a marked curvature in the voltage vs time traces was observed at high temperatures. The corresponding electron current decays were linear. In Figure III-5-22 the effect of increasing the density of the saturated vapor from 1.25×10^{26} molec/m³ to 3.22×10^{26} molec/m³ is illustrated. The ion mobility decreases by a factor of 2.5. At $n = 3.70 \times 10^{26}$ molec/m³ (Figure III-5-23) raising the temperature from 138.4K to 175.5K produces an increase in mobility of about 30%. Heating the gas from 385K to 433K increases the mobility by only 3%.

In Figure III-5-24 are reported measurements in the saturated vapor between 4.21 and 6.8 (10^{26} molec/m³). The mobility decreases by 65%. Heating the gas at

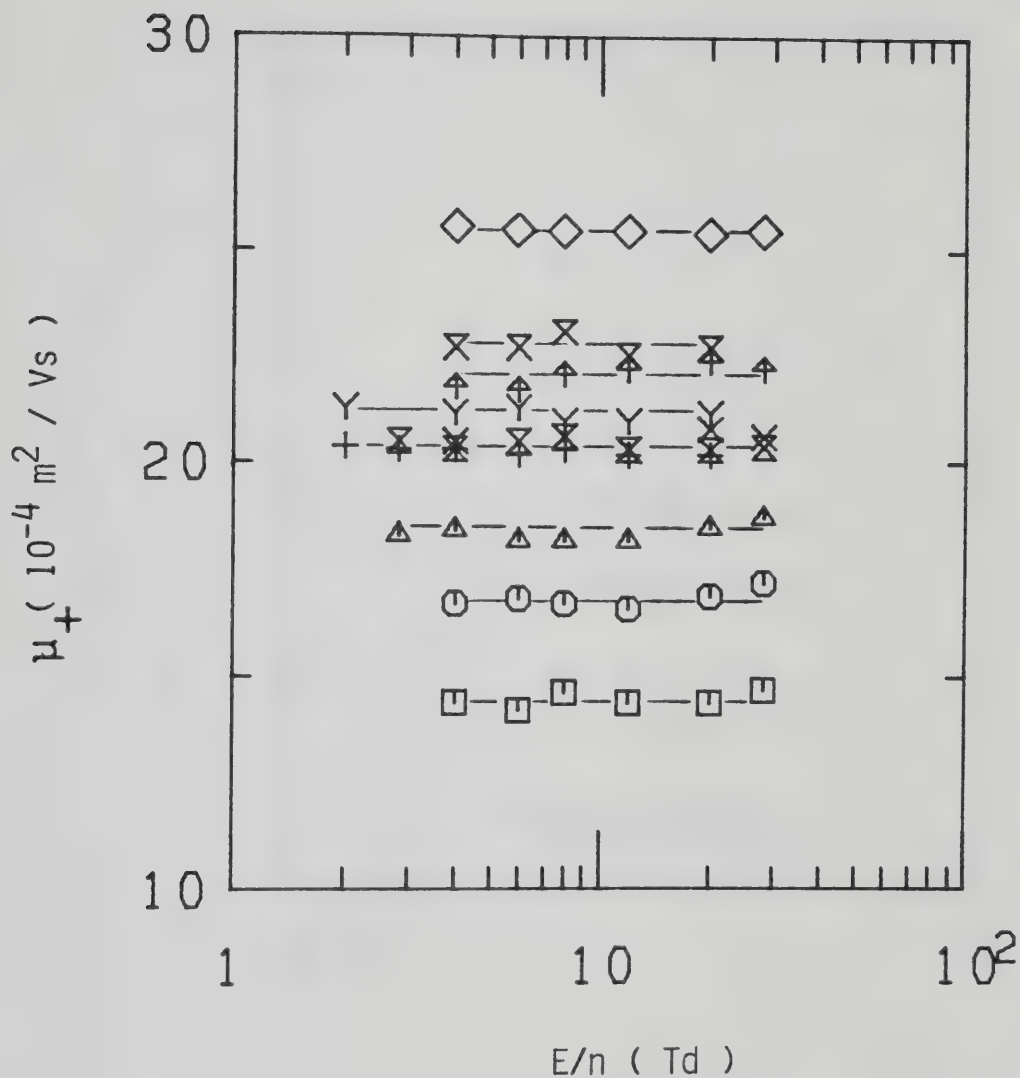


Figure III-5-17. Ion mobilities in CD_4 gas at $n = 2.50 \times 10^{24} \text{ molec/m}^3$ and different temperatures (K). \square , 95.0; \circ , 120.5; \triangle , 150.0; $+$, 185.0; γ , 235.5; \times , 294.0; \boxtimes , 337; \uparrow , 404; \bowtie , 463.5; \diamond , 535.5.

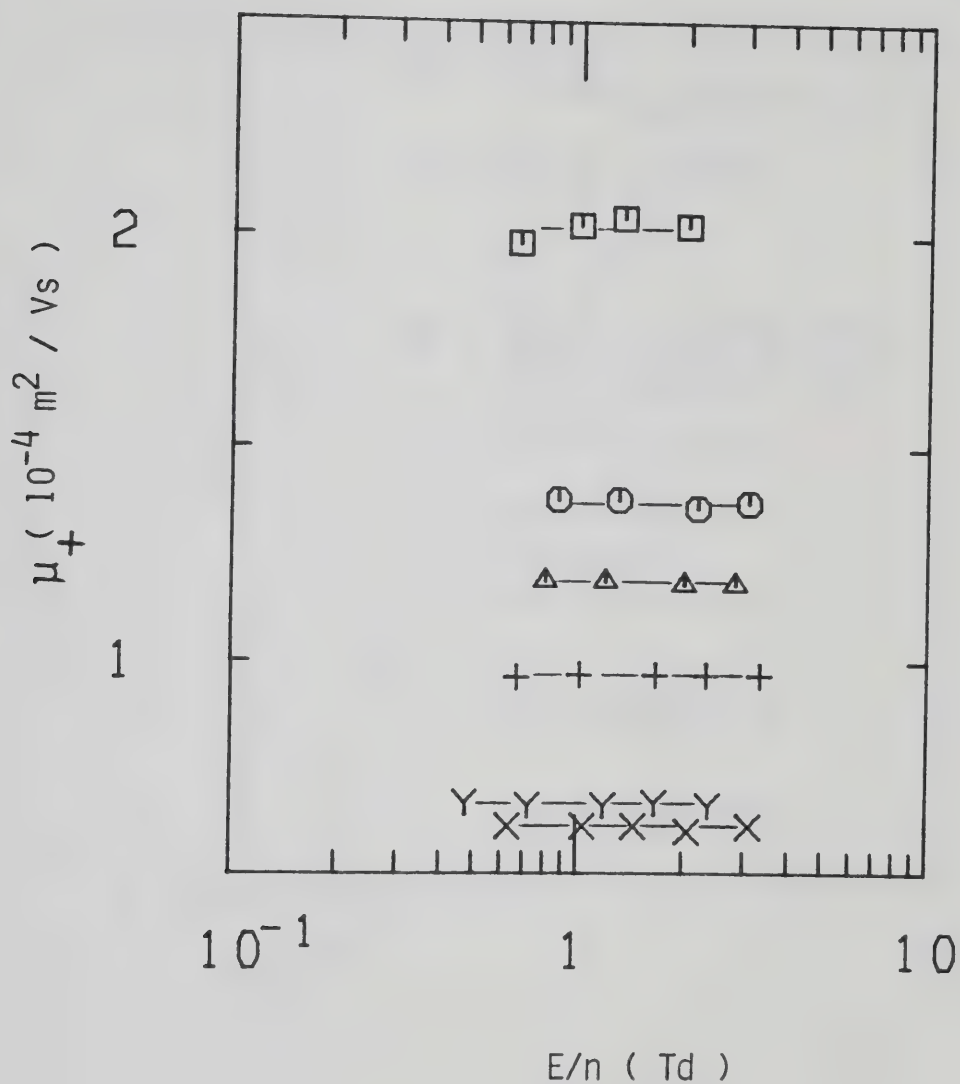


Figure III-5-18. Ion mobilities in saturated CD_4 vapor at different densities ($10^{25} \text{ molec/m}^3$) and temperatures (K). □, 1.50, 94.0; ○, 2.32, 98.3; △, 2.56, 99.3; +, 3.18, 101.6; Y, 4.8, 106.3; X, 5.0, 107.8.

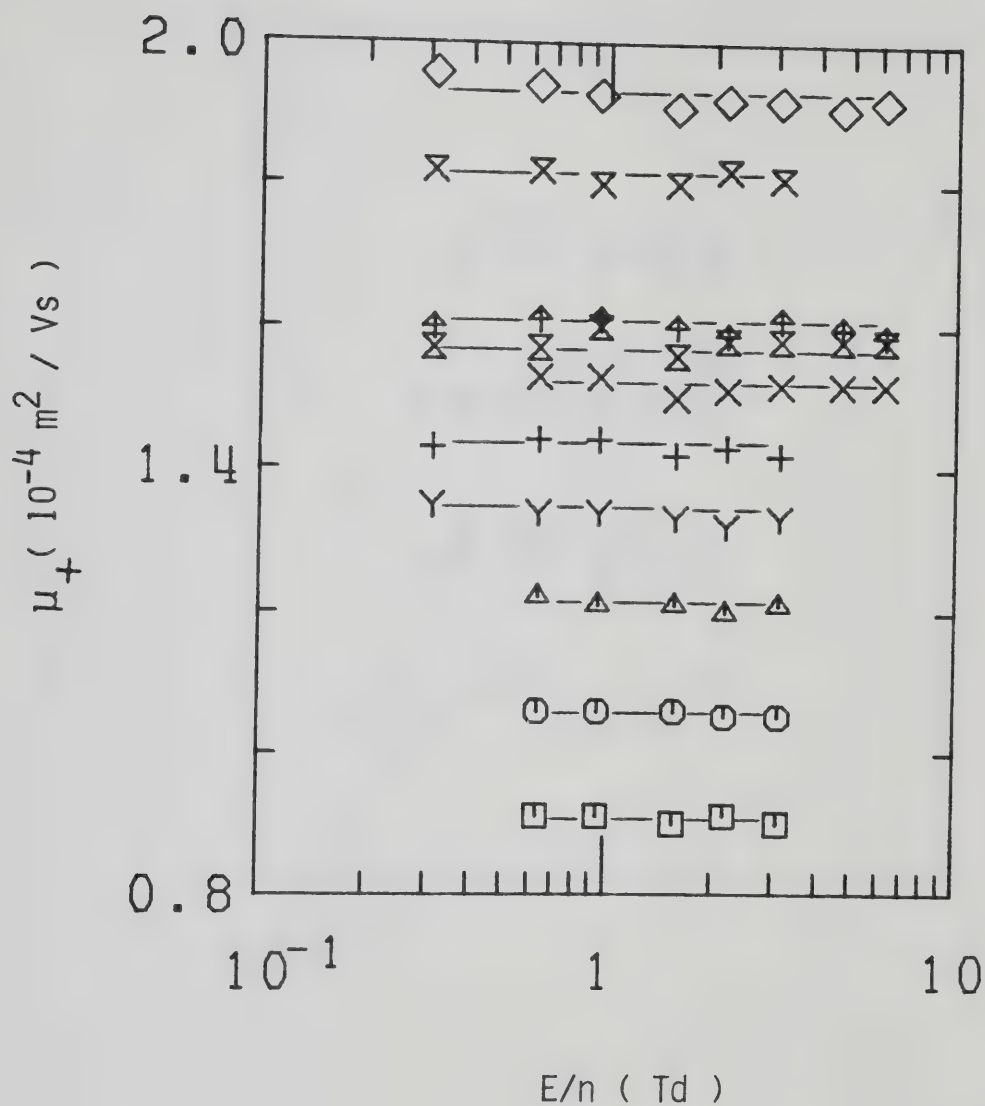


Figure III-5-19. Ion mobilities in CD_4 gas at $n = 3.20 \times 10^{25} \text{ molec/m}^3$ and different temperatures (K). \square , 106.0; \circ , 130.0; \triangle , 159.2; +, 214.4; Y, 293.2; X, 356; \boxtimes , 414; \uparrow , 474; \times , 536; \diamond , 598.

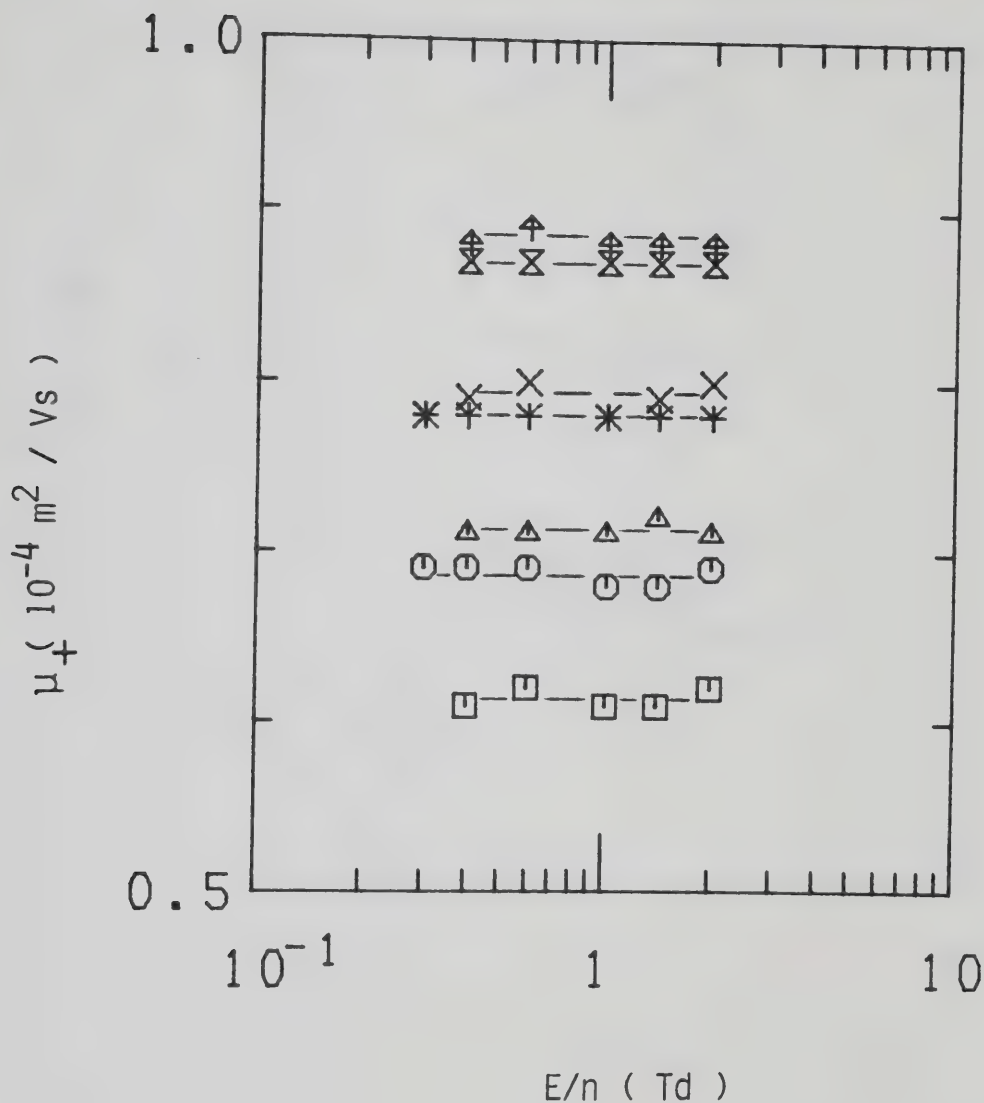


Figure III-5-20. Ion mobilities in CD_4 gas at $n = 5.0 \times 10^{25} \text{ molec/m}^3$ and different temperatures (K). \square , 111.8; \circ , 125.2; \triangle , 131.0; $*$, 150.6; \times , 155.4, \otimes , 179.9; \uparrow , 184.7.

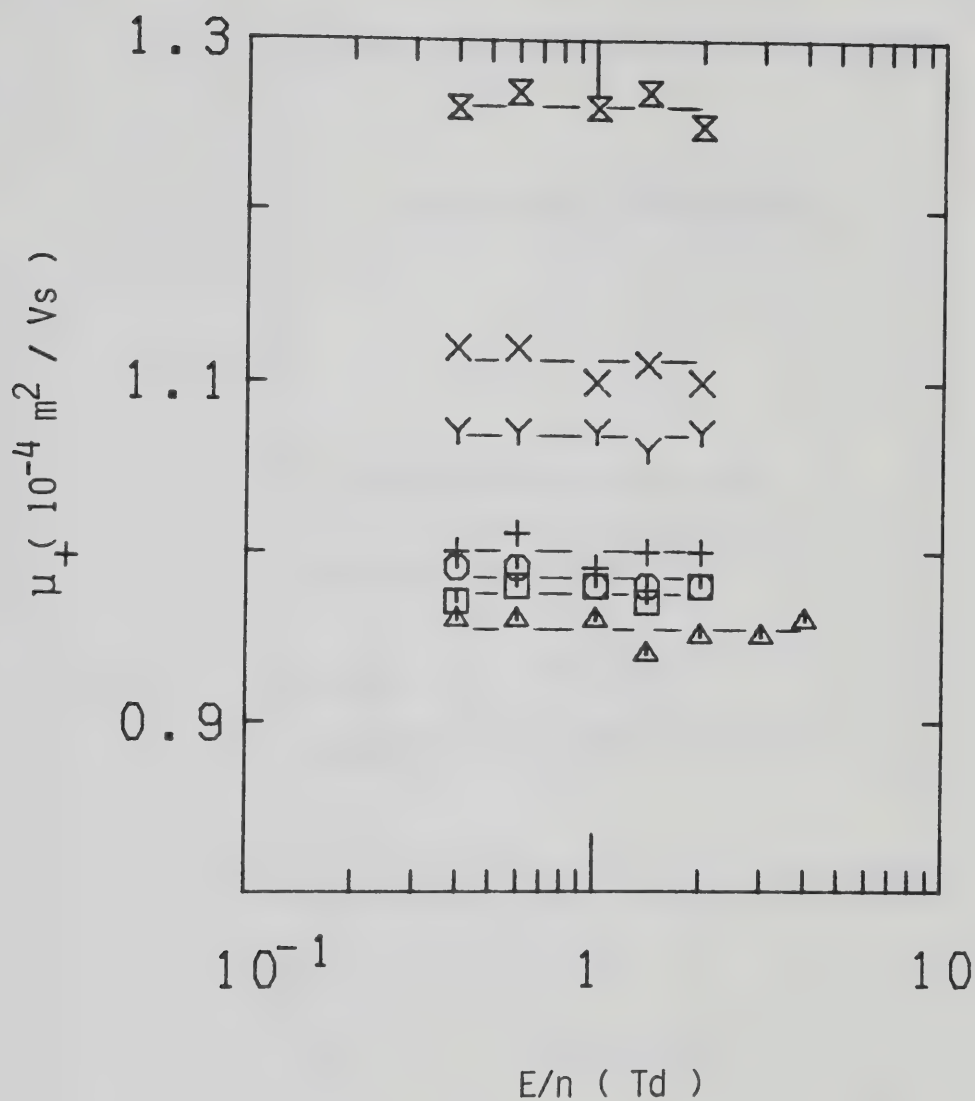


Figure III-5-21. Ion mobilities in CD_4 gas at $n = 5.0 \times 10^{25} \text{ molec/m}^3$ and different temperatures (K). \square , 225.0; \circ , 230.5; Δ , 293.8; $+$, 337.4; Y , 395.0; X , 454.3; \boxtimes , 521.

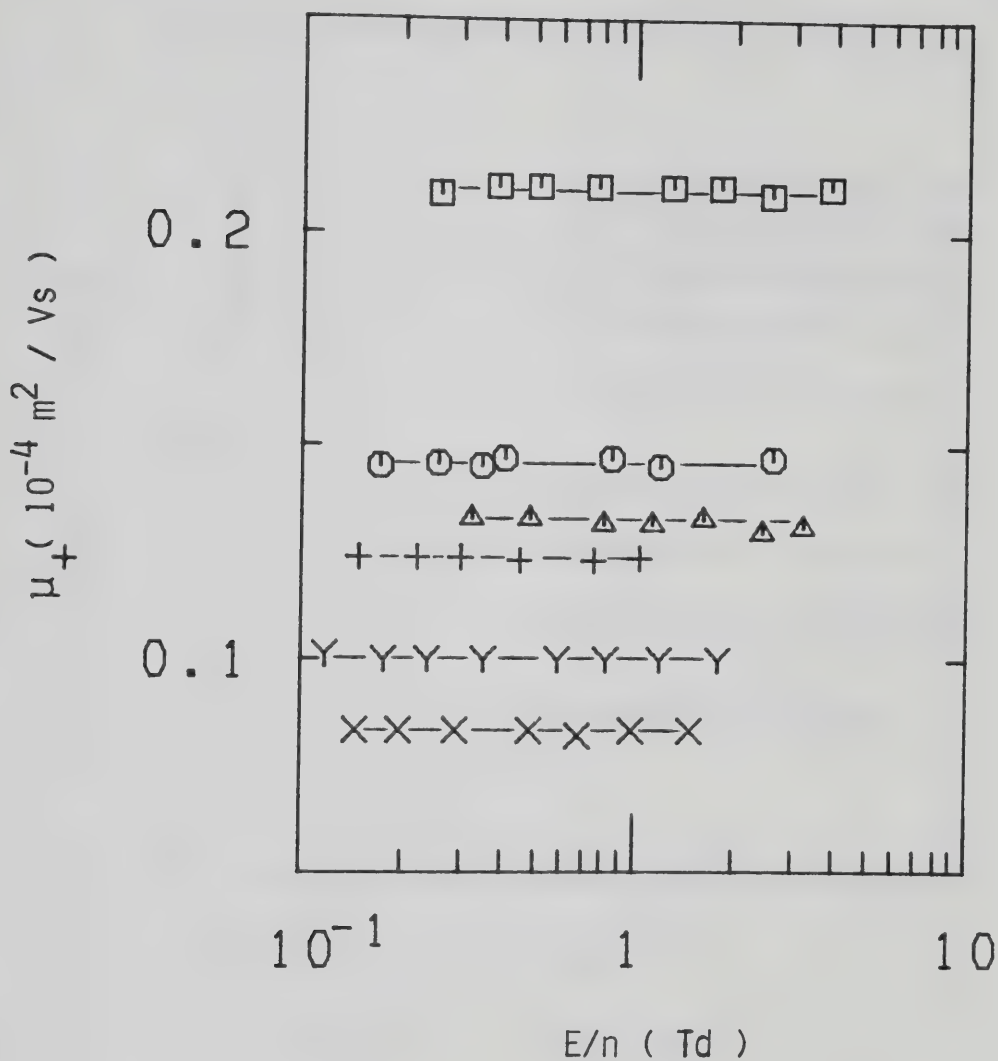


Figure III-5-22. Ion mobilities in saturated CD_4 vapor at different densities (10^{26} molec/ m^3) and temperatures (K). \square , 1.23, 119.3; \circ , 1.83, 125.5; Δ , 2.00; 127.0; +, 2.16, 128.2; Y, 2.66, 132.0; x, 3.23, 135.7.

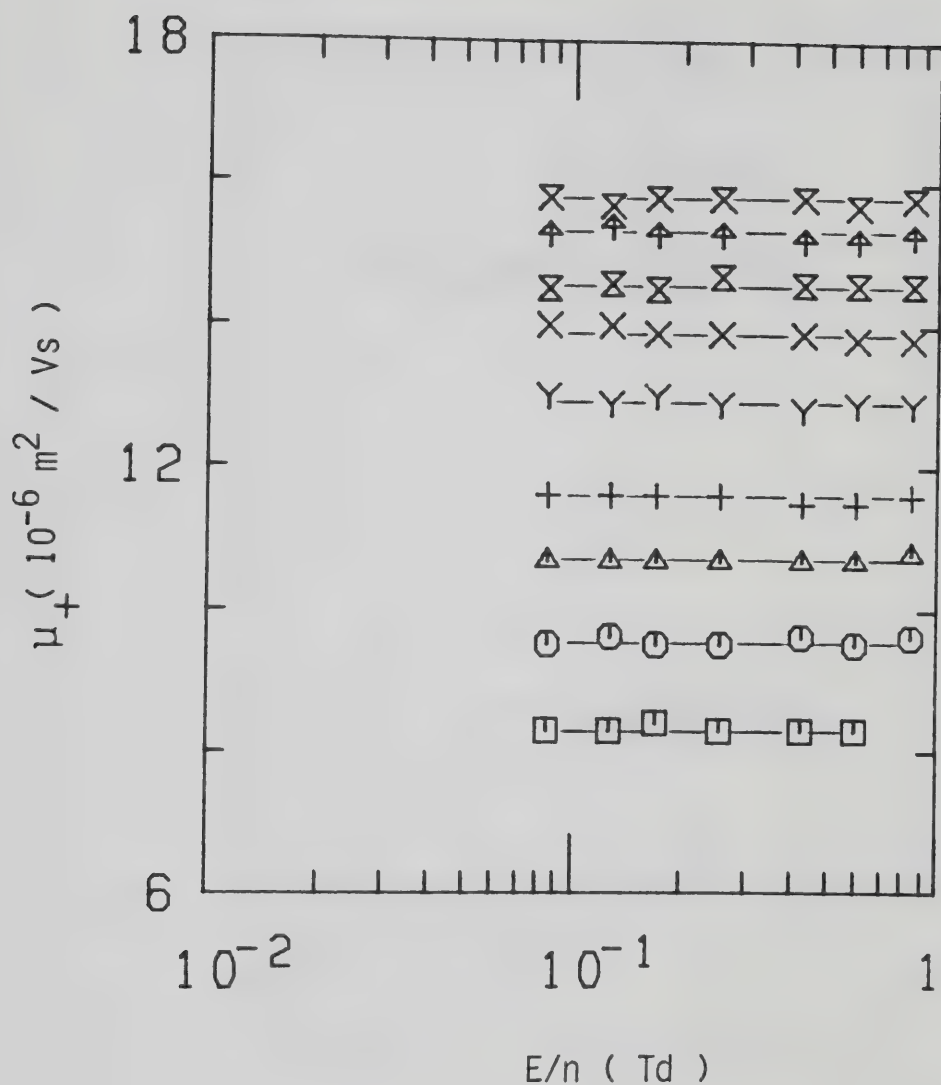


Figure III-5-23. Ion mobilities in CD_4 gas at $n = 3.7 \times 10^{26} \text{ molec/m}^3$ and different temperatures (K). \square , 138.4; \circ , 155.7; \triangle , 175.5; $+$, 195.2; Y , 235.7; X , 294.0; \boxtimes , 337; \uparrow , 385; \times , 433.

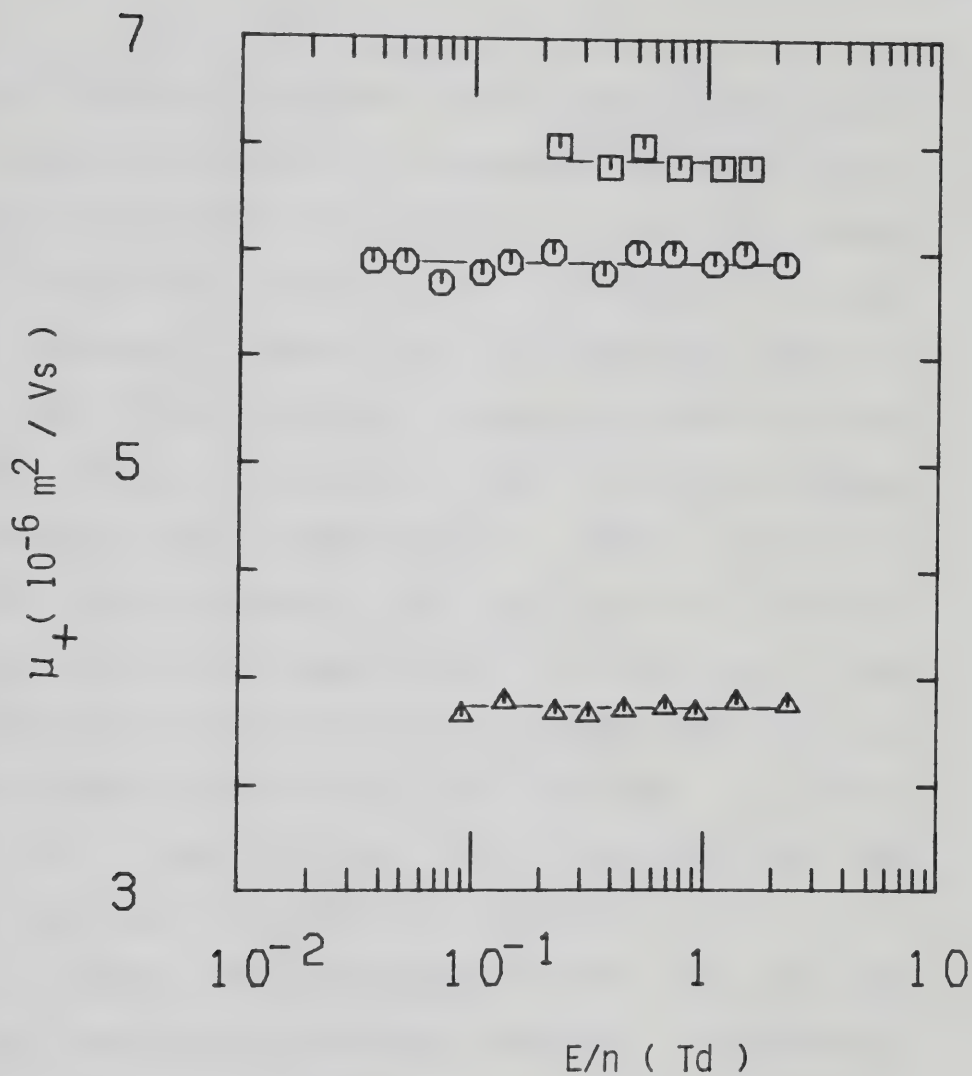


Figure III-5-24. Ion mobilities in saturated CD_4 vapor at different densities (10^{26} molec/ m^3) and temperatures (K). \square , 4.21, 141.0; \circ , 4.46, 142.0; \triangle , 6.8; 151.0.

$n = 5.5 \times 10^{26}$ molec/m³ between 146.5K and 397.0K (Figure III-5-25) has the effect of increasing the mobility by 85%. However the rate of increase is about 27% between 146.5K and 181.5K and approximately 1% between 341K and 397K. An increase in density of the saturated vapor to about half the critical density (Figure III-5-26) has the same effect previously observed. The mobility decreases with the inverse ratio of the density. Heating the gas at $n = 29 \times 10^{26}$ molec/m³ and $n_c = 61 \times 10^{26}$ molec/m³ (Figures III-5-27 and 28) has the same effect in both cases. The mobility increases with temperature. However the increase at the lower density is 22% on going from 182.7 to 188.7K whereas at the higher density it is about 50% as the temperature is raised from 189.3K to 193.0K.

In the liquid phase (Figures III-5-29 and 30) the mobility decreases with increasing density. A change in density by a factor of about 2 produces a drop in mobility by a factor of 5.7.

Data contained in Figures III-5-17 to III-5-21 were obtained in low pressure type conductance cells. The electrode separations were 1.000 ± 0.002 cm. All the other gas phase results were obtained in high pressure gas type cells. The electrode separations were 0.315 ± 0.005 cm. Liquid data were obtained in high pressure liquid type cells. The electrode separations were 0.319 ± 0.002 cm. A listing of the mobility values at the different temperatures and densities is reported in Table III-10.

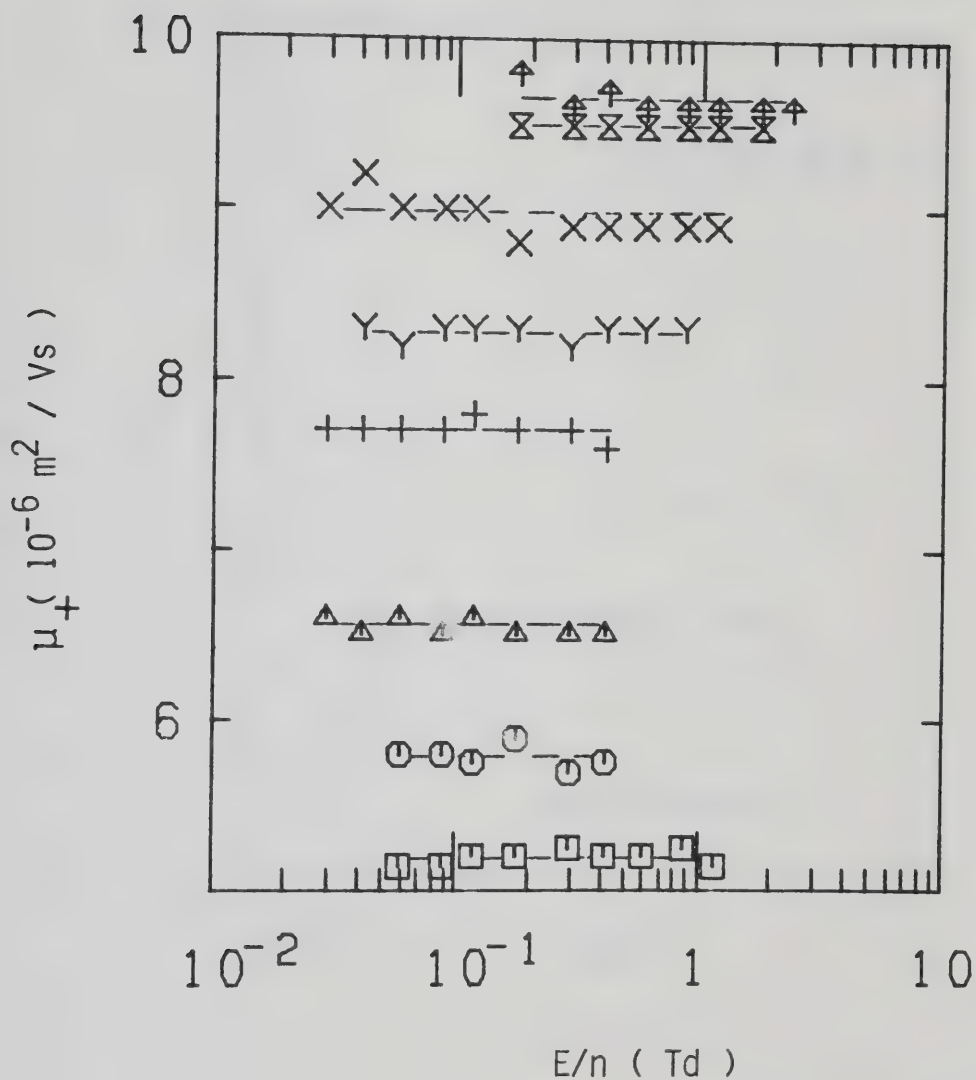


Figure III-5-25. Ion mobilities in CD_4 gas at $n = 5.5 \times 10^{26} \text{ molec/m}^3$ and different temperatures (K). \square , 146.5; \circ , 160.0; \triangle , 181.5; $+$, 219.7; γ , 236.5; \times , 293.0; \boxtimes , 341; \uparrow , 397.

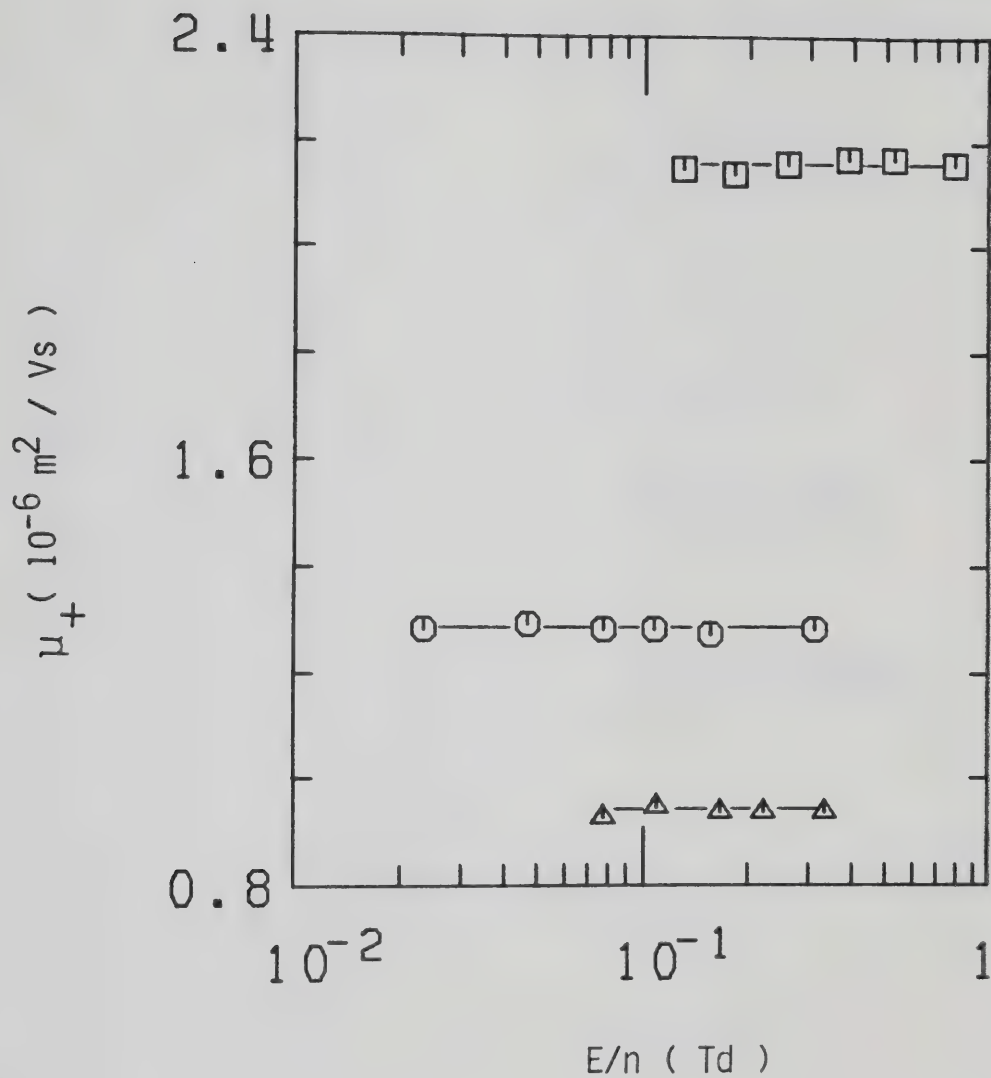


Figure III-5-26. Ion mobilities in saturated CD_4 vapor at different densities (10^{27} molec/ m^3) and temperatures (K). \square , 1.24, 164.8; \circ , 2.00, 175.5; \triangle , 2.83, 182.5.

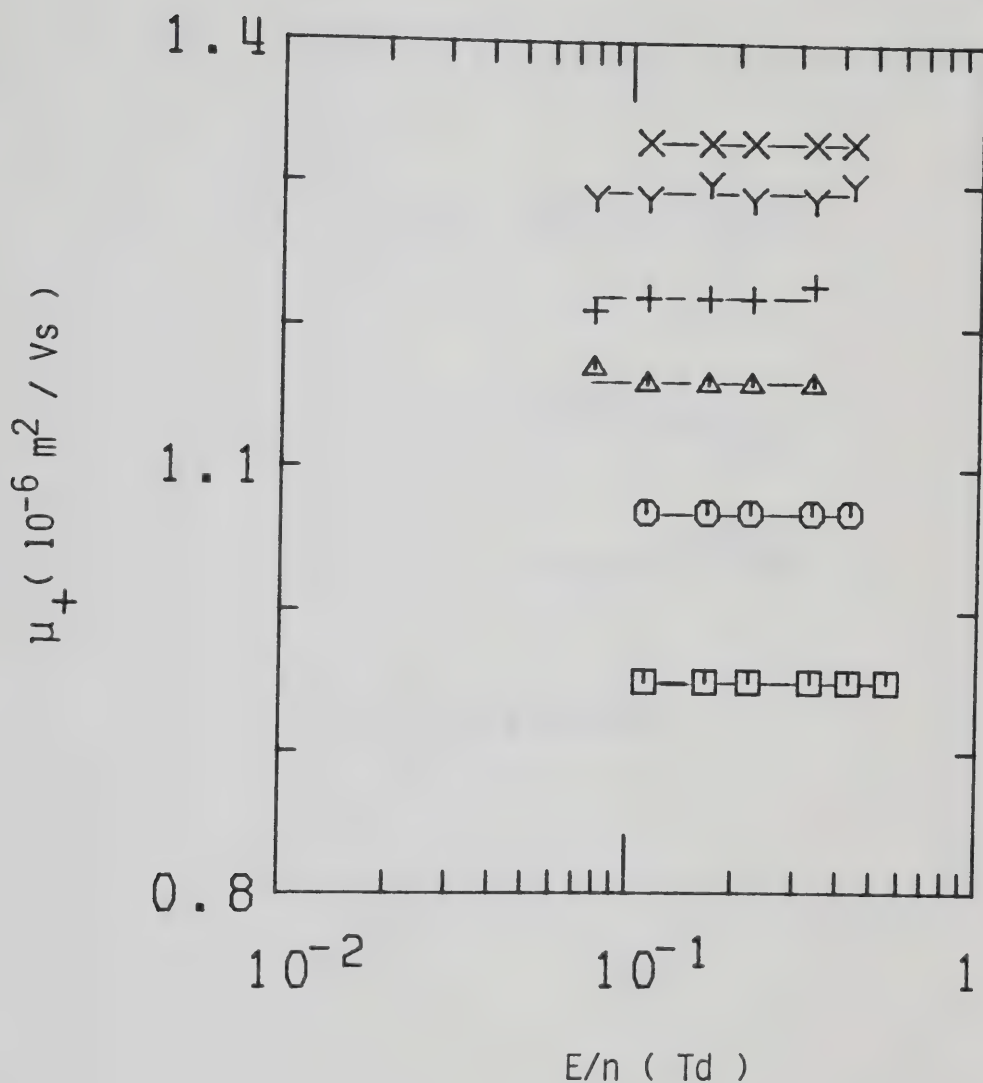


Figure III-5-27. Ion mobilities in CD_4 gas at $n = 2.9 \times 10^{27} \text{ molec/m}^3$ and different temperatures (K). \square 182.7; \circ , 185.5; Δ , 188.7; +, 191.2; Y, 193.9; X, 195.5.

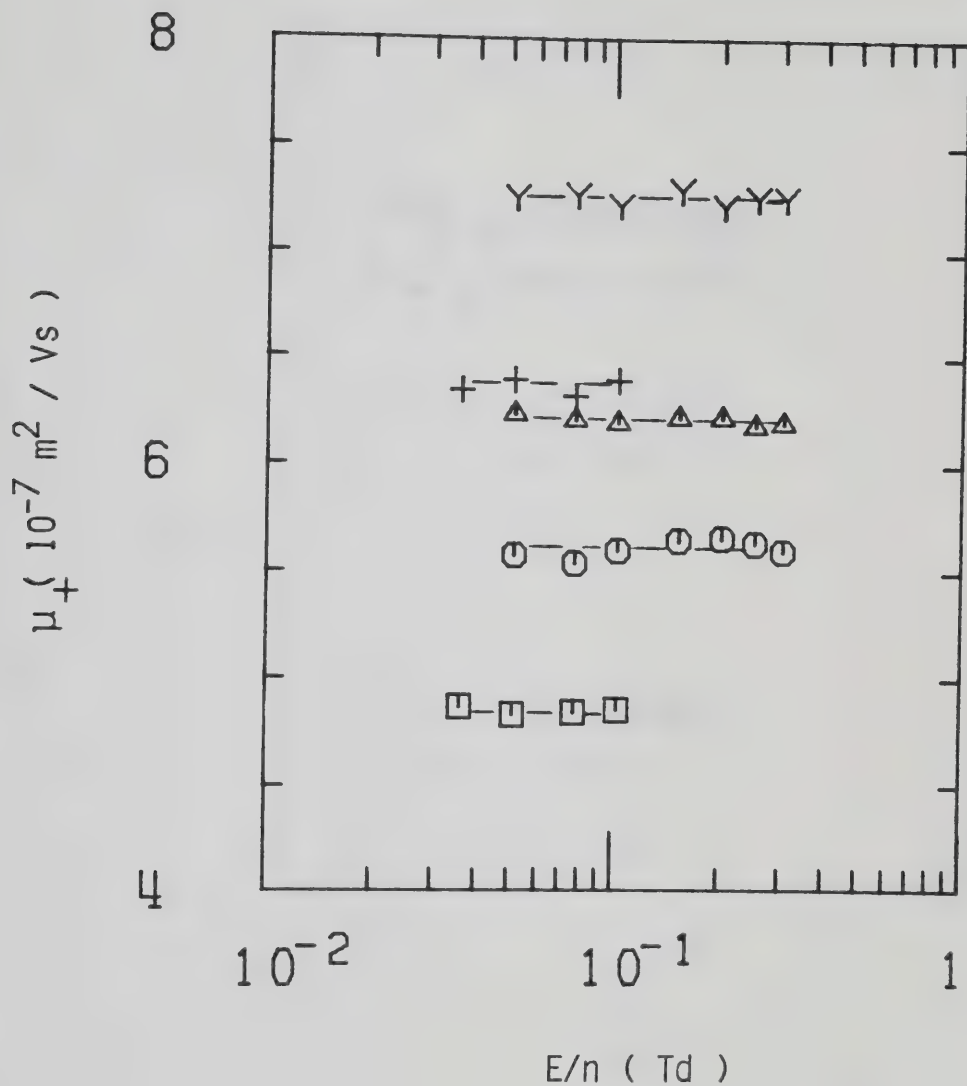


Figure III-5-28. Ion mobilities in supercritical CD_4 gas at $n_c = 6.1 \times 10^{27} \text{ molec/m}^3$ and different temperatures (K). \square , 189.3; \circ , 189.5; \triangle , 190.5; $+$, 192.1; Y , 193.0. $T_c = 189.2$.

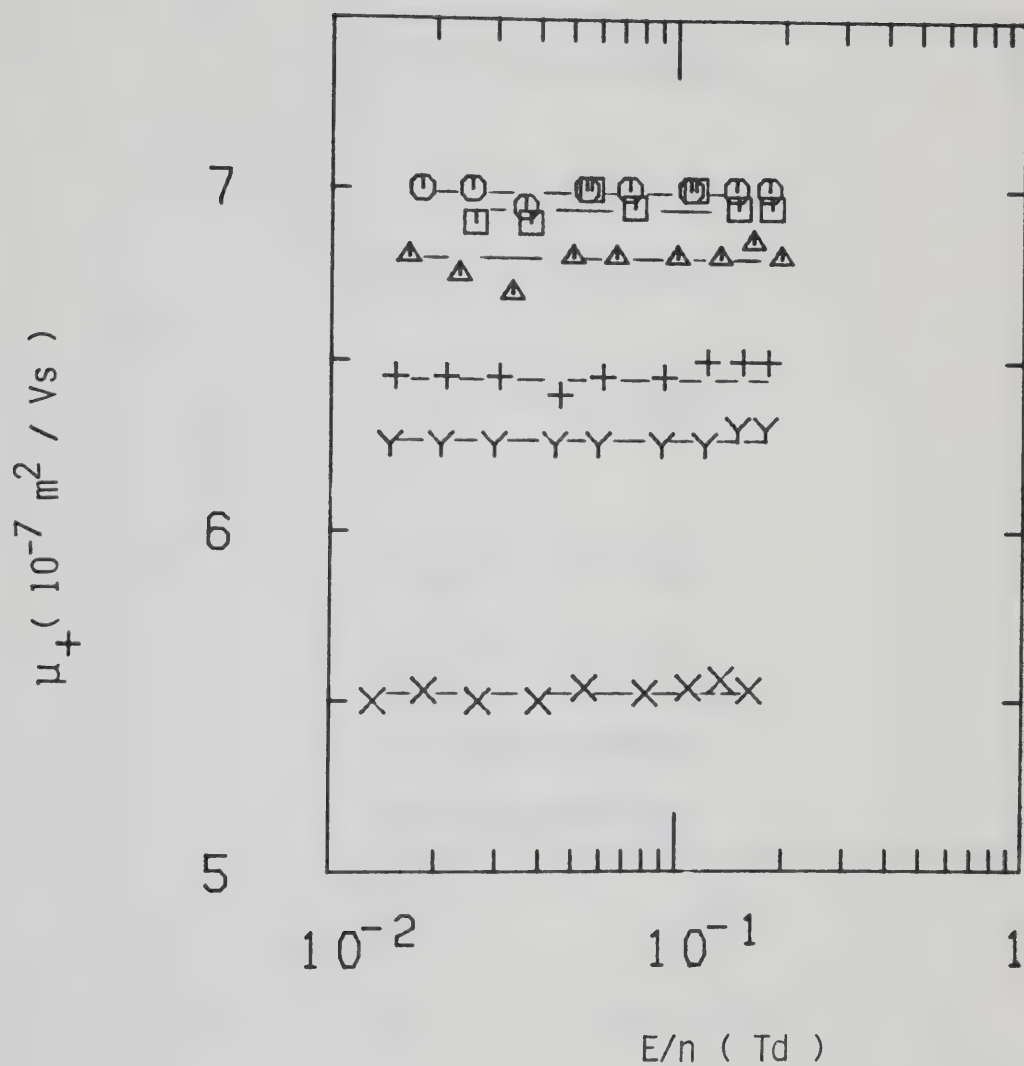


Figure III-5-29. Ion mobilities in liquid CD_4 at different densities ($10^{27} \text{ molec/m}^3$) and temperatures (K). \square , 8.4, 187.5; \circ , 8.6, 187.0; Δ , 9.4, 184.0; +, 10.2, 180.0; Y, 10.5, 178.0; X, 11.6, 170.0.

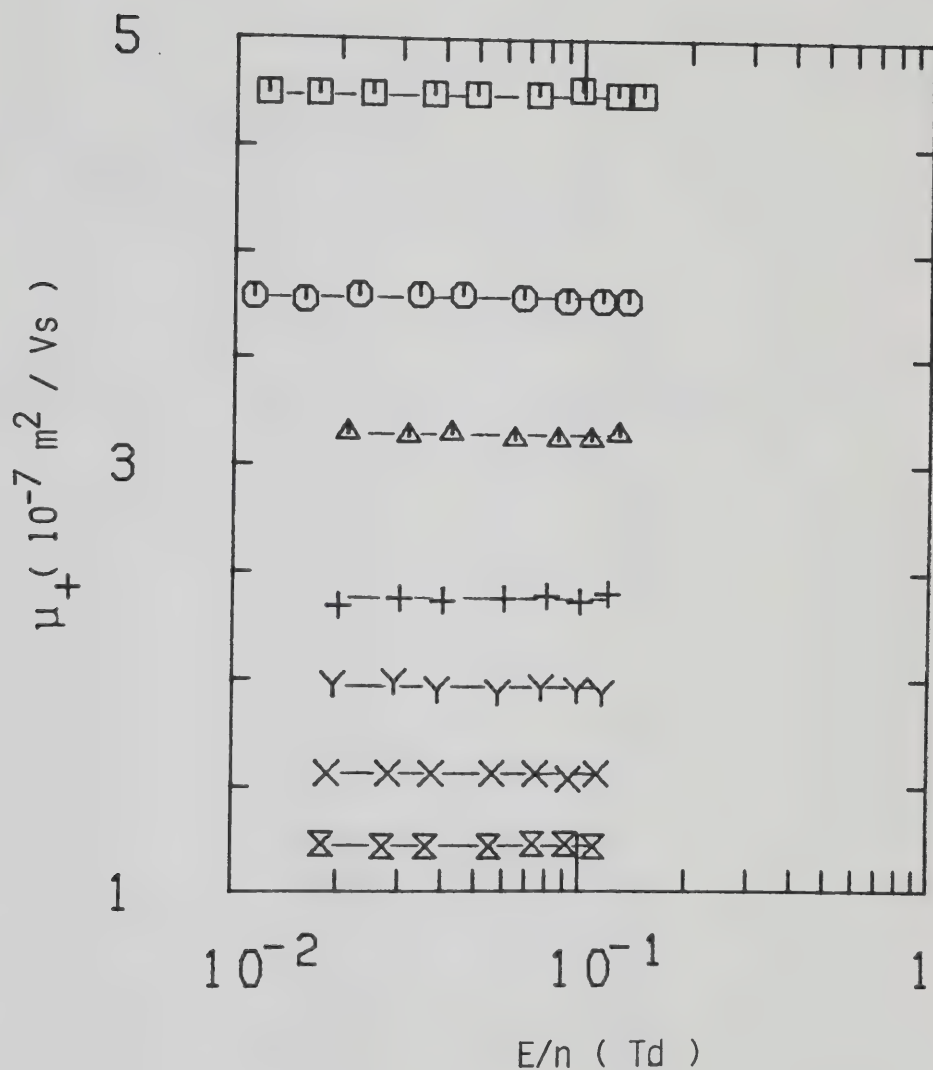


Figure III-5-30. Ion mobilities in liquid CD_4 at different densities ($10^{27} \text{ molec/m}^3$) and temperatures (K). \square , 12.7, 160.2; \circ , 13.8, 145.5; \triangle , 14.7, 134.0; $+$, 15.6, 119.5; Y , 16.1, 109.7; X , 16.7, 100.3; \boxtimes , 17.1, 92.4.

TABLE III-10
Summary of Ion Results for CD₄^a

T (K)	n (10 ²⁶ m ⁻³)	μ_+ (10 ⁻⁴ m ² /Vs)	$n\mu_+$ [10 ²¹ (V _{sm}) ⁻¹]
95.0	0.025	14.4	3.60
120.5	0.025	16.8	4.20
150.0	0.025	18.4	4.60
185.0	0.025	20.3	5.1
235.5	0.025	21.2	5.3
294.0	0.025	20.6	5.2
337	0.025	20.5	5.1
404	0.025	22.1	5.5
463.5	0.025	22.8	5.7
535.5	0.025	25.5	6.4
94.0	0.150	2.00	3.00
98.3	0.232	1.38	3.20
99.3	0.256	1.19	3.05
101.6	0.318	0.97	3.08
106.3	0.48	0.67	3.22
107.8	0.50	0.61	3.05
106.0	0.32	0.91	2.91
130.0	0.32	1.06	3.39
159.2	0.32	1.21	3.87
214.4	0.32	1.43	4.58
293.2	0.32	1.34	4.29
356	0.32	1.52	4.86
414	0.32	1.58	5.1
474	0.32	1.60	5.1

(continued....)

Table III-10 continued

536	0.32	1.81	5.8
598	0.32	1.93	6.2
111.8	0.50	0.61	3.05
125.2	0.50	0.69	3.45
131.0	0.50	0.71	3.55
150.6	0.50	0.78	3.90
155.4	0.50	0.79	3.95
179.9	0.50	0.87	4.35
184.7	0.50	0.88	4.40
225.0	0.50	0.98	4.90
230.5	0.50	0.98	4.90
293.8	0.50	0.96	4.80
337.4	0.50	1.00	5.0
395	0.50	1.07	5.4
454.3	0.50	1.11	5.6
521	0.50	1.27	6.4
119.3	1.23	0.214	2.64
125.5	1.83	0.146	2.67
127.0	2.00	0.132	2.64
128.2	2.16	0.124	2.68
132.0	2.66	0.100	2.66
135.7	3.23	0.083	2.68
138.4	3.70	0.083	3.07
155.7	3.70	0.096	3.55
175.5	3.70	0.107	3.96
195.2	3.70	0.116	4.29
235.7	3.70	0.129	4.77
294.0	3.70	0.139	5.1
337	3.70	0.146	5.4
385	3.70	0.153	5.7
433	3.70	0.158	5.8

(continued....)

Table III-10 continued

141.0	4.21	0.064	2.69
142.0	4.46	0.060	2.68
151.0	6.8	0.0387	2.63
146.5	5.5	0.052	2.86
160.0	5.5	0.058	3.19
181.5	5.5	0.066	3.63
219.7	5.5	0.077	4.24
236.5	5.5	0.083	4.57
293.0	5.5	0.089	4.90
341	5.5	0.095	5.2
397	5.5	0.096	5.3
164.8	12.4	0.0216	2.68
175.5	20.0	0.0130	2.60
182.5	28.3	0.0094	2.66
182.7	29.0	0.0095	2.76
185.5	29.0	0.0107	3.10
188.7	29.0	0.0116	3.36
191.2	29.0	0.0122	3.54
193.9	29.0	0.0129	3.74
195.5	29.0	0.0133	3.86
189.3	61 ^b	0.0049	2.99
189.5	61 ^b	0.0056	3.42
190.5	61 ^b	0.0062	3.78
192.1	61 ^b	0.0064	3.90
193.0	61 ^b	0.0073	4.45
187.5	84	0.0070	5.9
187.0	86	0.0070	6.0

(continued....)

Table III-10 continued

184.0	94	0.0068	6.4
180.0	102	0.0065	6.6
178.0	105	0.0063	6.6
170.0	116	0.0055	6.4
160.2	127	0.0048	6.1
145.5	138	0.00379	5.2
134.0	147	0.00314	4.62
119.5	156	0.00237	3.70
109.7	161	0.00196	3.16
100.3	167	0.00155	2.59
92.4	171	0.00122	2.09

a. The results appear in this table in the same order as the figures. They are given in order of increasing density.

b. $n_c = 6.1 \times 10^{27} \text{ molec/m}^3$, $T_c = 189.2\text{K}$.

DISCUSSION

A. Electrons

The effects of electric field strength and temperature on the electron mobility were investigated as functions of density in the region between the dilute gas and the dense liquid.

Simple gas theory suggests that the mobility of a charged particle in a medium at density n and in the presence of an electric field E should be inversely proportional to n . The mobility is a measure of the maximum velocity attained by the particle under the acceleration by the electric field between collisions with the molecules. The maximum velocity depends on the length of time that the particle is accelerated by the field, that is the time between collisions. This time is inversely proportional to the density. It follows that the mobility is inversely proportional to n and the density normalized mobility (low field limit) $n\mu$ should be density independent.

In Figure IV-1 is reported the density variation of the density normalized mobility (low field) $n\mu$ in CH_4 in

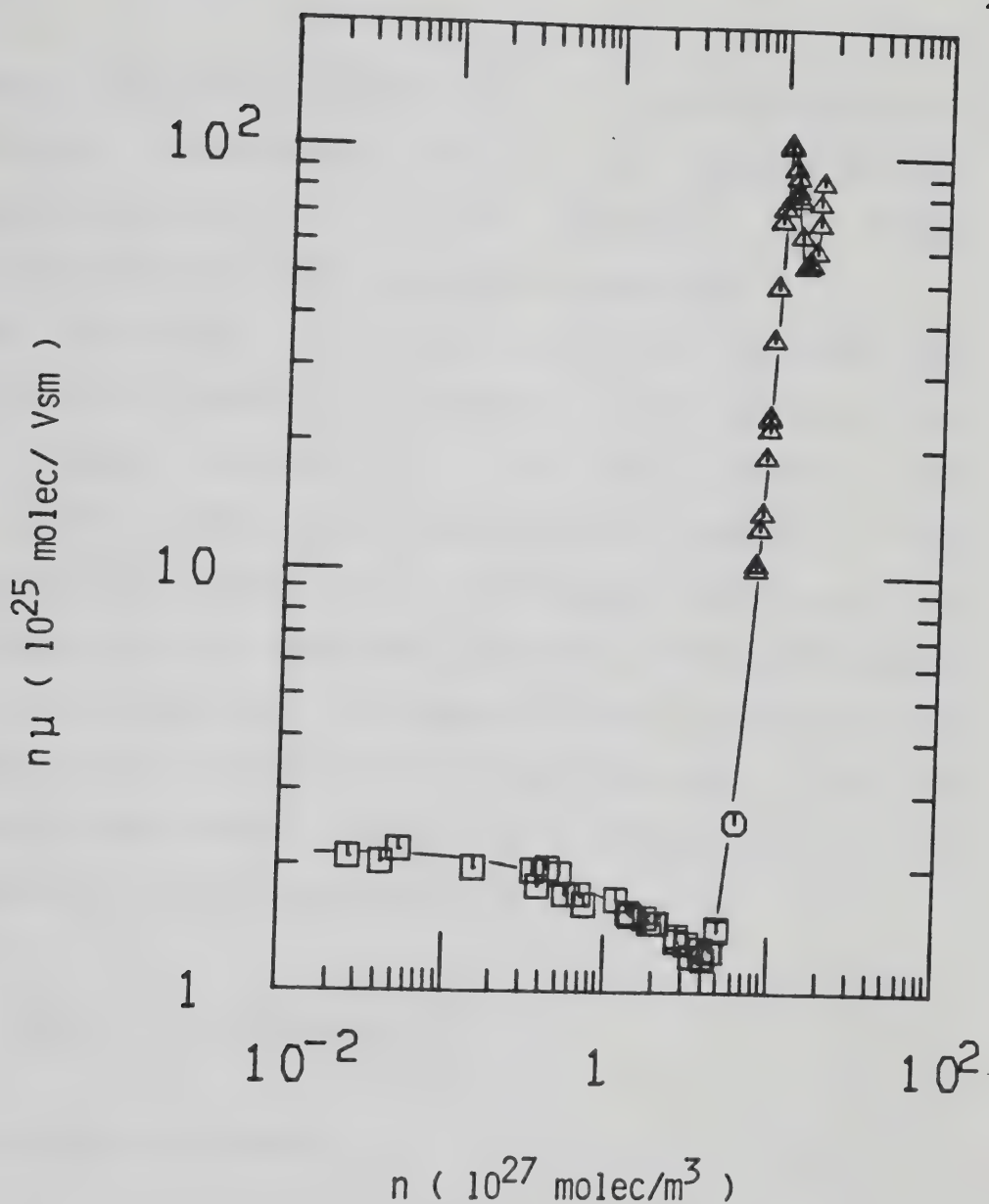


Figure IV-1. Density dependence of the density normalized electron mobility (low field) in the coexistent vapor (\square) and liquid (Δ) phases of CH_4 . \circ represents the slightly supercritical fluid at n_c and $T_c + 0.1\text{K}$.

the vapor and liquid phases along the coexistence curve. The density normalized mobility is indeed density independent up to $n \approx 3 \times 10^{26}$ molec/m³. At higher densities deviations from ideality are observed.

The discussion of the results will be divided into three sections according to density. The first section will contain results in the low density gas ($n/n_c \lesssim 0.05$). The second will contain results in the dense gas ($0.05 \lesssim n/n_c \leq 1$). Finally the behavior in the liquid phase will be examined. In each section the effect of electric field will be examined first in CH₄ and then compared to that in the deuterated compounds. Then the temperature and density effects will be discussed in CH₄ and compared to the other compounds.

1. Low Density Gas ($n/n_c \lesssim 0.05$)

a. Electric Field Effect

i) CH₄

The electron mobility in CH₄ gas at densities between 2.95-5.8 (10^{25} molec/m³) and temperatures near the saturation curve is field independent up to $E/n \approx 0.02$ Td (Table III-1). Above this threshold value the mobility increases with increasing field. The value of the

threshold field increases with temperature (Figure III-1-18). The drift velocity at $(E/n)_{thr}$ is usually compared to the speed of low frequency sound c_0 .^{48,54,55,205-209} In Figure IV-2 are reported data in CH_4 gas at $n = 5.3 \times 10^{25}$ molec/ m^3 and $T = 293.5K$ as a plot of the drift velocity v_d against E/n . In this case measurements were taken at field strengths up to $E/n \sim 8$ Td. The drift velocity reaches a saturation value of approximately 1×10^5 m/s at $E/n \approx 4$ Td. If elastic collisions were the dominating process in moderating the electron energy the ratio $(v_d^{thr})/c_0$ would be about unity.^{125,126} Increased inelastic contributions would increase this ratio.⁵⁴ Drift velocities at the threshold fields were estimated from v_d vs E/n plots. Speeds of sound were taken from Reference 196. The ratios $(v_d^{thr})/c_0$ at the different temperatures in CH_4 at two different densities are shown in Figure IV-3. The ratio is close to unity at low temperatures but it increases with temperature indicating that inelastic losses are unimportant near the saturation curve but appreciably contribute in moderating the electron energy at higher temperatures.

In Figure IV-4 are shown the Maxwellian energy distribution functions

$$F(\epsilon) = (2\pi\epsilon^{1/2})/(\pi kT)^{3/2} \exp(-\epsilon/kT) \quad IV-1$$

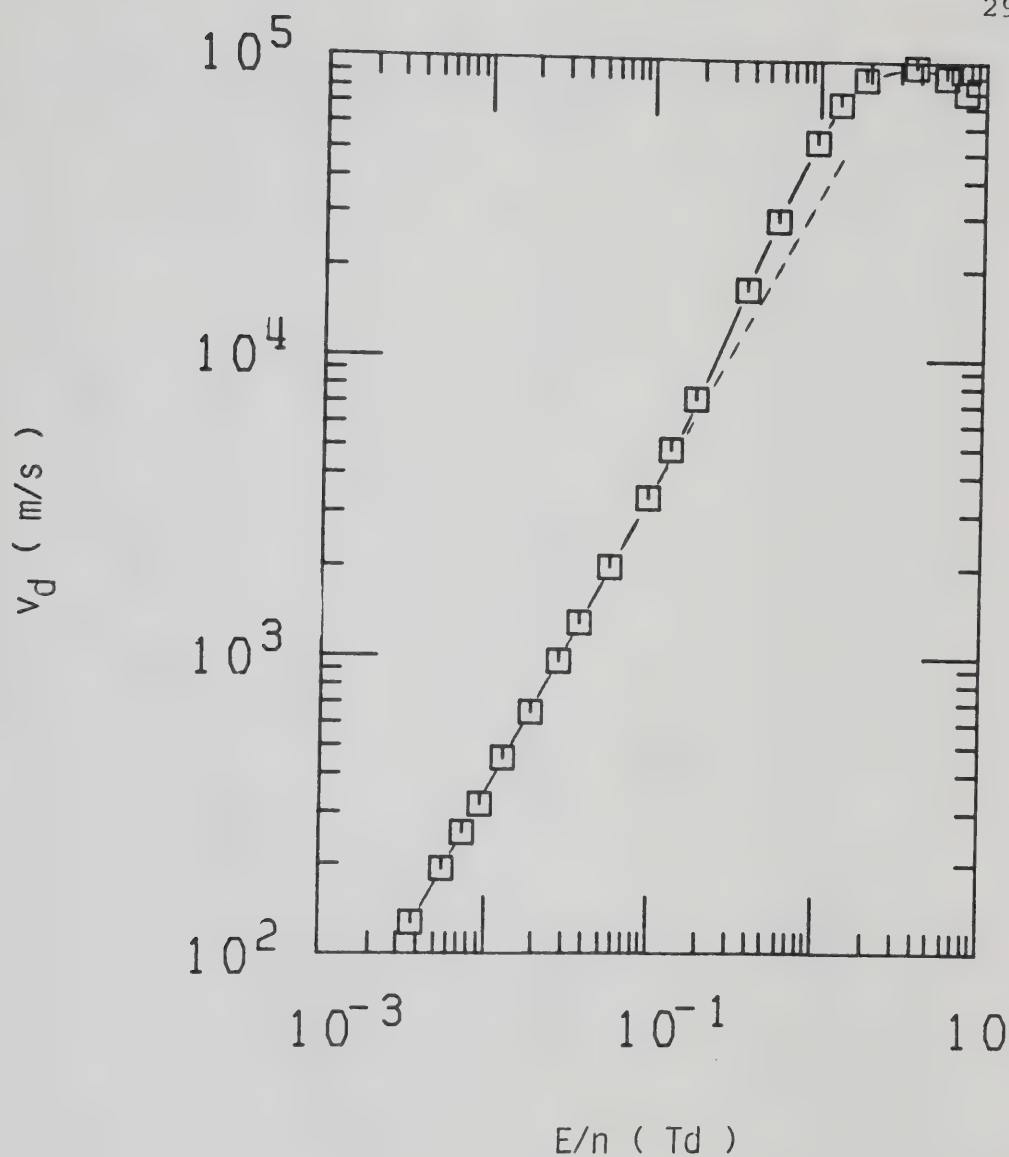


Figure IV-2. Electron drift velocities v_d in CH_4 gas at $n = 5.3 \times 10^{25} \text{ molec/m}^3$ and $T = 293.5\text{K}$ as functions of E/n . The dashed line has a slope of unity for reference.

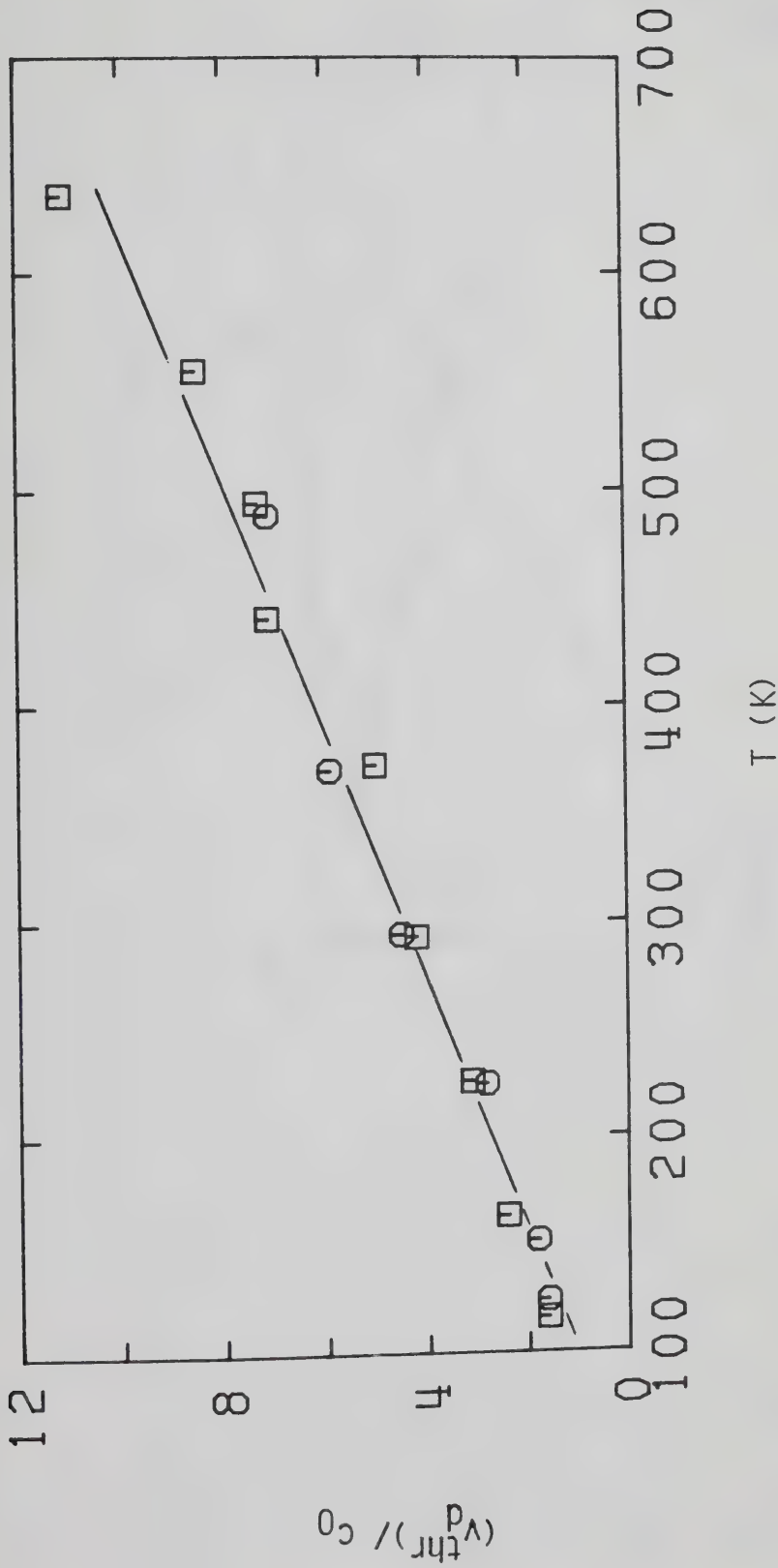


Figure IV-3. Ratios of the electron drift velocity at the threshold fields to the speed of sound c_0 in CH_4 gas at different densities ($10^{25} \text{ molec/m}^3$) as functions of temperature. \square , 2.95; \circ , 5.8.

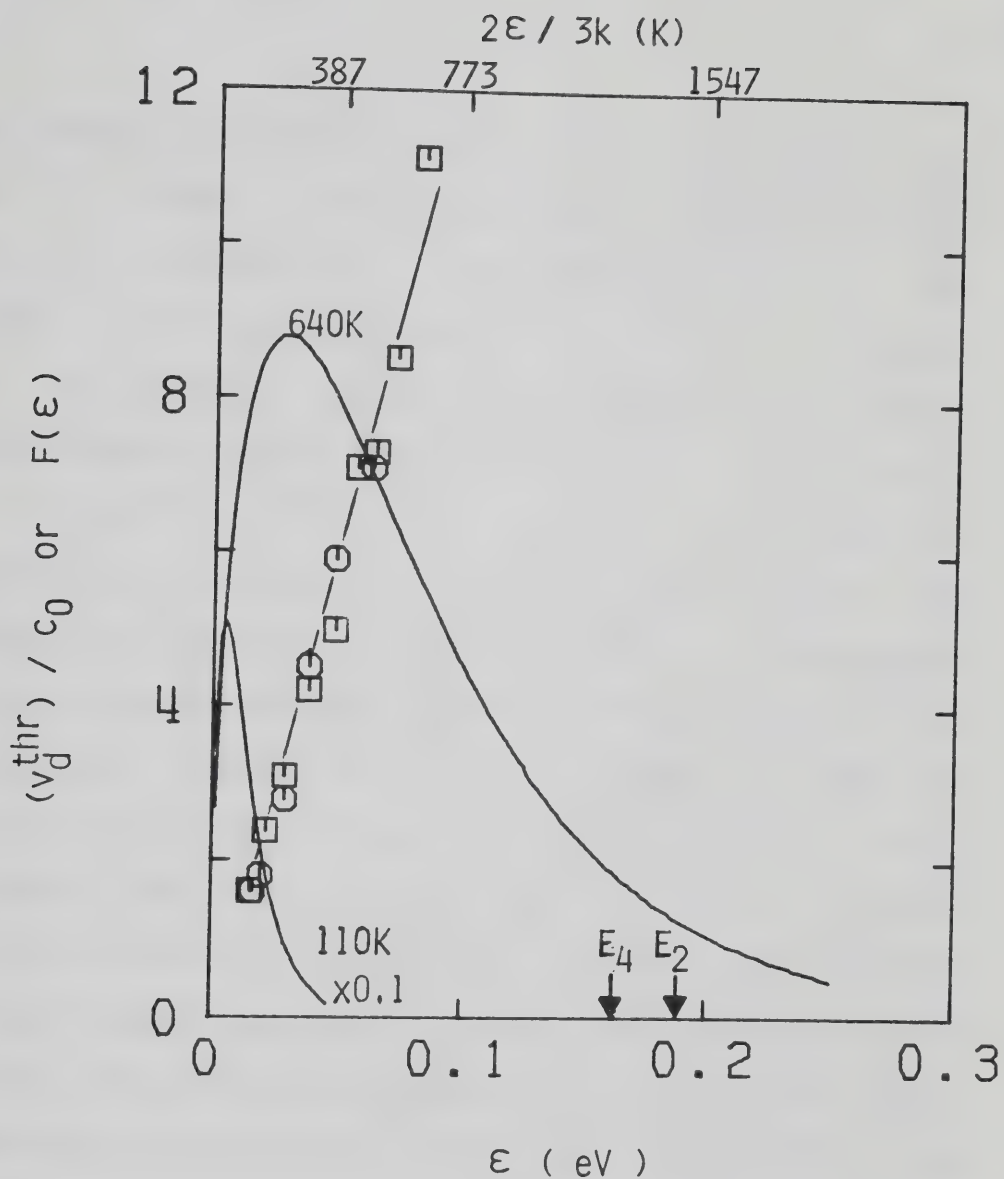


Figure IV-4. Maxwellian electron energy distributions $F(\epsilon)$ at 110K and 640K. The curve at 110K has been divided by 10. Values of $(v_d^{thr}) / c_0$ in CH_4 gas at the different average electron energies $\epsilon = 1.5kT$ from Figure IV-3 are reported for comparison. The arrows indicate the two lowest vibrational energies in CH_4 .

at the lowest temperature used, $T \approx 110\text{K}$ and at the highest, $T \approx 640\text{K}$. The same points of Figure IV-3 are reported for comparison. The temperatures have been converted to average energies $\epsilon = 1.5 kT$. Possible channels for inelastic losses are excitations of rotational and vibrational motions. The dipole moment of methane is only $5.4 \times 10^{-6} \text{ D}^{183}$ and, since the molecular polarizability in gas phase is essentially isotropic, the excitation of rotations by the electron is improbable. Methane has four fundamental vibrational frequencies¹⁹⁹ at $\nu_4 = 1306 \text{ cm}^{-1}$ (0.162 eV), $\nu_2 = 1526 \text{ cm}^{-1}$ (0.189 eV), $\nu_1 = 2914 \text{ cm}^{-1}$ (0.361 eV) and $\nu_3 = 3020 \text{ cm}^{-1}$ (0.374 eV). From Figure IV-4 it can be seen that at the highest temperature there is an appreciable fraction of electrons with energy sufficient to excite at least the first two vibrations. At the lowest temperature, on the other hand, the distribution has already appreciably dropped before the first vibrational threshold energy has been reached. The fraction of electrons, q , with a given energy, ϵ , at temperature T can be estimated from

$$q = \frac{\exp(-\epsilon/kT)}{1 - \exp(-\epsilon/kT)} \quad \text{IV-2}$$

Using $\epsilon = 0.162 \text{ eV}$, the lowest methane vibrational energy, the value of this fraction is 3.8×10^{-8} at $T = 110\text{K}$ and 5.6×10^{-2} at $T = 640\text{K}$.

A similar temperature dependence of $(v_d^{\text{thr}})/c_o$ has been found in gaseous ethane⁵² where at $n = 6.8 \times 10^{25}$ molec/m³ the ratio increased from 2.5 at $T = 197\text{K}$ to 7.9 at $T = 326\text{K}$.

ii) Deuterated Methanes

In Figures III-2-4 , III-3-6, III-4-7 and III-5-7 are shown the values of $(E/n)_{\text{thr}}$ as functions of temperature in the gases CH_3D , CH_2D_2 , CHD_3 and CD_4 . These plots are very similar to that for CH_4 (Figure III-1-18). Within experimental scatter the values of the drift velocities at the threshold fields are the same in all compounds. It was shown in the previous subsection that in CH_4 the excitation of vibrational modes is responsible for the increase in the value of $(v_d^{\text{thr}})/c_o$ with temperature. The difference in vibrational energy levels between CH_4 and CD_4 is equal to the square root of the reduced masses, ~35%. Vibrational levels in CD_4 are 35% lower than those in CH_4 .¹⁹⁹ The speed of sound is proportional to the square root of the molecular mass M

$$c_o = \left(\frac{\gamma kT}{M} \right)^{1/2} \quad \text{IV-3}$$

where γ is the heat capacity ratio. The speed of sound in CD_4 is ~12% lower than that in CH_4 . The estimated values

of the drift velocity at the threshold fields are not reliable to less than about 15%, therefore it is concluded that the contribution of inelastic losses is about the same in all compounds.

b. Temperature Effect

i) CH₄

A plot of the density normalized low field mobility $n\mu$ against the temperature at low gas densities is given in Figure IV-5. In this region the value of the low field mobility is inversely proportional to the number density and increases with increasing temperature. The temperature variation of the low field mobility, normalized by the density, can be used to extract the energy dependence of the electron-molecule momentum transfer cross section σ_m .³²

By assuming a Maxwellian distribution of electron velocities

$$f_0 = (m/2\pi kT)^{3/2} \exp(-mv^2/2kT) \quad \text{IV-4}$$

Equation I-9 can be written as

$$n\mu = (8\pi^2 e/3m)(m/2\pi kT)^{5/2} \int_0^\infty \frac{v^3}{\sigma_m} \exp(-mv^2/2kT) dv \quad \text{IV-5}$$

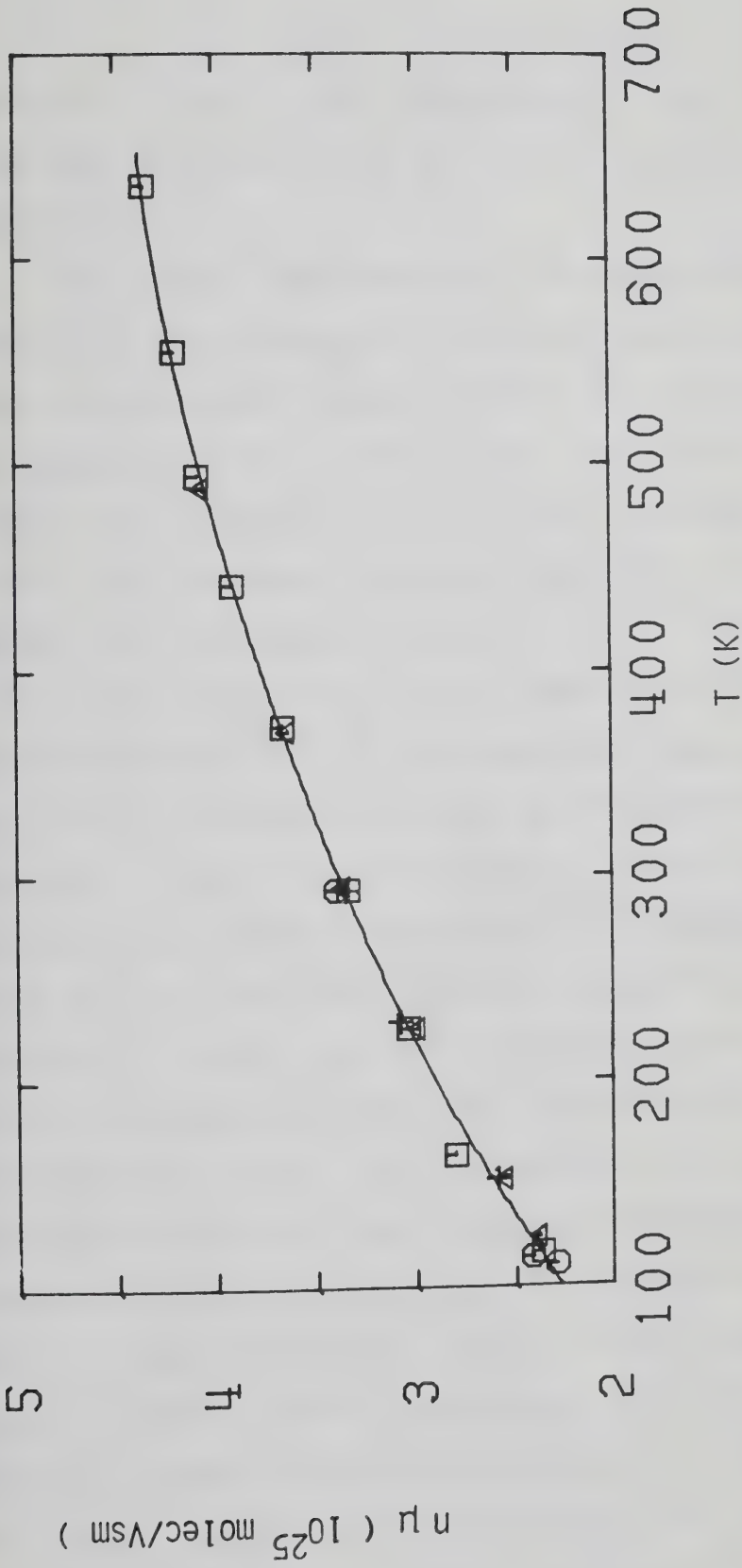


Figure IV-5. Density normalized electron mobilities (low field) in CH_4 gas at different densities ($10^{25} \text{ molec/m}^3$) as functions of temperature. \square , 2.95; \circ , 5.3; Δ , 7.5.

where e , m , and v are, respectively, the electron charge, mass and velocity, k is Boltzmann's constant and T is the temperature.

The energy dependence of the momentum transfer cross section σ_m was obtained by matching the experimental $(n\mu, T)$ sets to calculated values obtained by numerical integration of Equation IV-5. A trial cross section as a function of energy ϵ or velocity v ($\epsilon = mv^2/2$) was chosen and adjusted until the agreement between calculated and experimental values was considered satisfactory. In Figure IV-6A the solid line represents the result of this procedure. Earlier results^{42,45,48} are shown for comparison. The line in Figure IV-5 was calculated by using the extracted cross section. The average deviation between calculated and experimental values was 1.1% for all densities ranging from 0.3% at $n = 7.5 \times 10^{25}$ molec/m³ to 1.9% at $n = 5.3 \times 10^{25}$ molec/m³. The region of greatest sensitivity in the fitting procedure is that near the maximum of the integrand in Equation IV-5. The functions $f(\epsilon)$ in Figure IV-6B show the percent of the integral in the equation that has been contributed by electrons in the swarm with energies up to ϵ . These functions refer to the lowest temperature used, $T = 110\text{K}$, and to the highest, $T = 636\text{K}$. Electrons at energies between those corresponding to $f(\epsilon) \sim 10$ and 90 make the major contribution to transport of the swarm. At $T = 110\text{K}$ this energy range is $\sim 0.009 - 0.05$ eV. At $T = 636\text{K}$ it is $\sim 0.05 - 0.25$ eV.

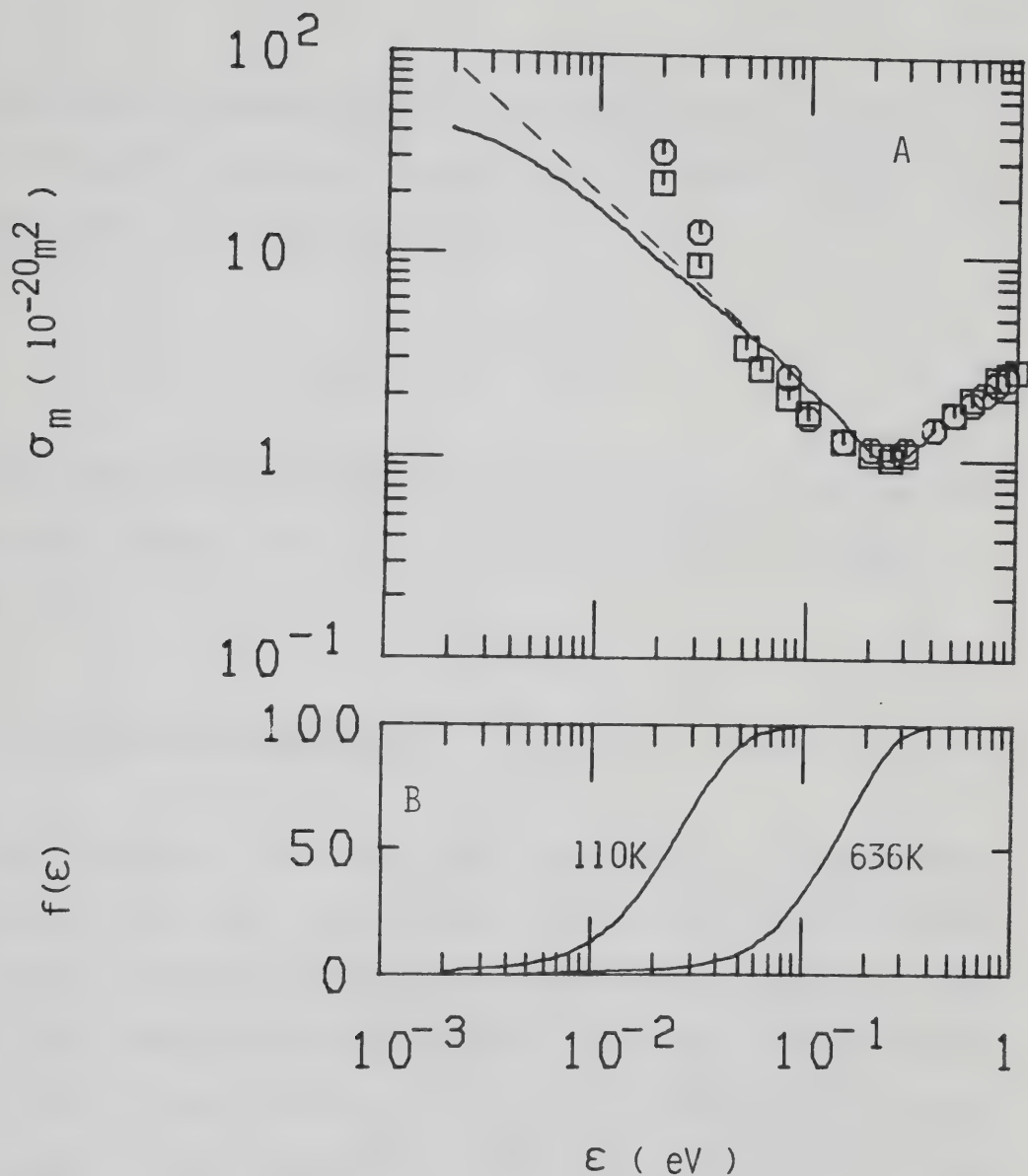


Figure IV-6. A: Momentum transfer cross section σ_m of low density CH_4 gas as a function of energy ϵ . The solid line represents results of the present work producing the solid line in Figure IV-5. - - -, Reference 48; \bigcirc , Reference 42; \square , Reference 45. B: Plots of $f(\epsilon)$ vs ϵ at 110K and 636K. $f(\epsilon)$ is the percent of the integral in Equation IV-5 that has been contributed by electrons with energy up to ϵ .

Taking an average cross section (assuming a Maxwellian distribution of electron velocities) equivalent to one that is independent of velocity leads to

$$\sigma_{ave} = \langle v \rangle / \langle v / \sigma_m \rangle \quad \text{IV-6}$$

The temperature variation of the average cross section calculated using the curve of Figure IV-6A is shown in Figure IV-7.

ii) Deuterated Methanes

In Figures IV-8 and IV-9 are shown the density normalized low field mobilities in the low density gases CH_3D , CH_2D_2 , CHD_3 and CD_4 as functions of temperature. The lines have been calculated using the cross section vs. energy curve shown in Figure IV-6A. The agreement between experimental and calculated values is similar to that obtained for CH_4 . The average deviations over all densities were 1.2%, 1.2%, 0.9% and 1.2% for CH_3D , CH_2D_2 , CHD_3 and CD_4 , respectively. In this density and energy region there is no isotope effect. This is in agreement with what was found in a previous study of the system $\text{CH}_4\text{-CD}_4$.^{39,42} In these density and energy regions the scattering process is thought to be mainly elastic. The small differences in sizes between methane and the

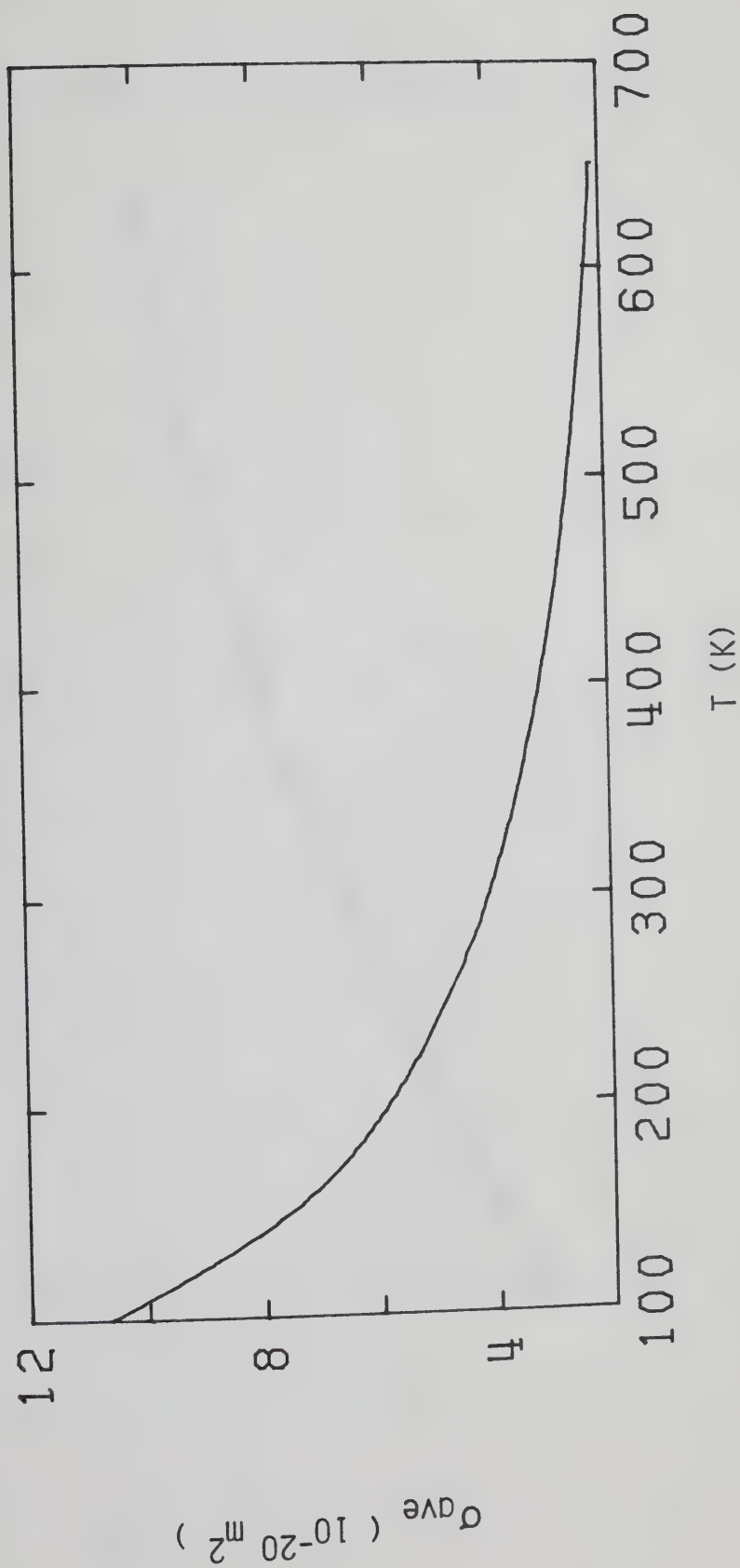


Figure IV-7. Temperature dependence of the average cross section of low density CH_4 gas, from Equation IV-6 and the solid line in Figure IV-5A.

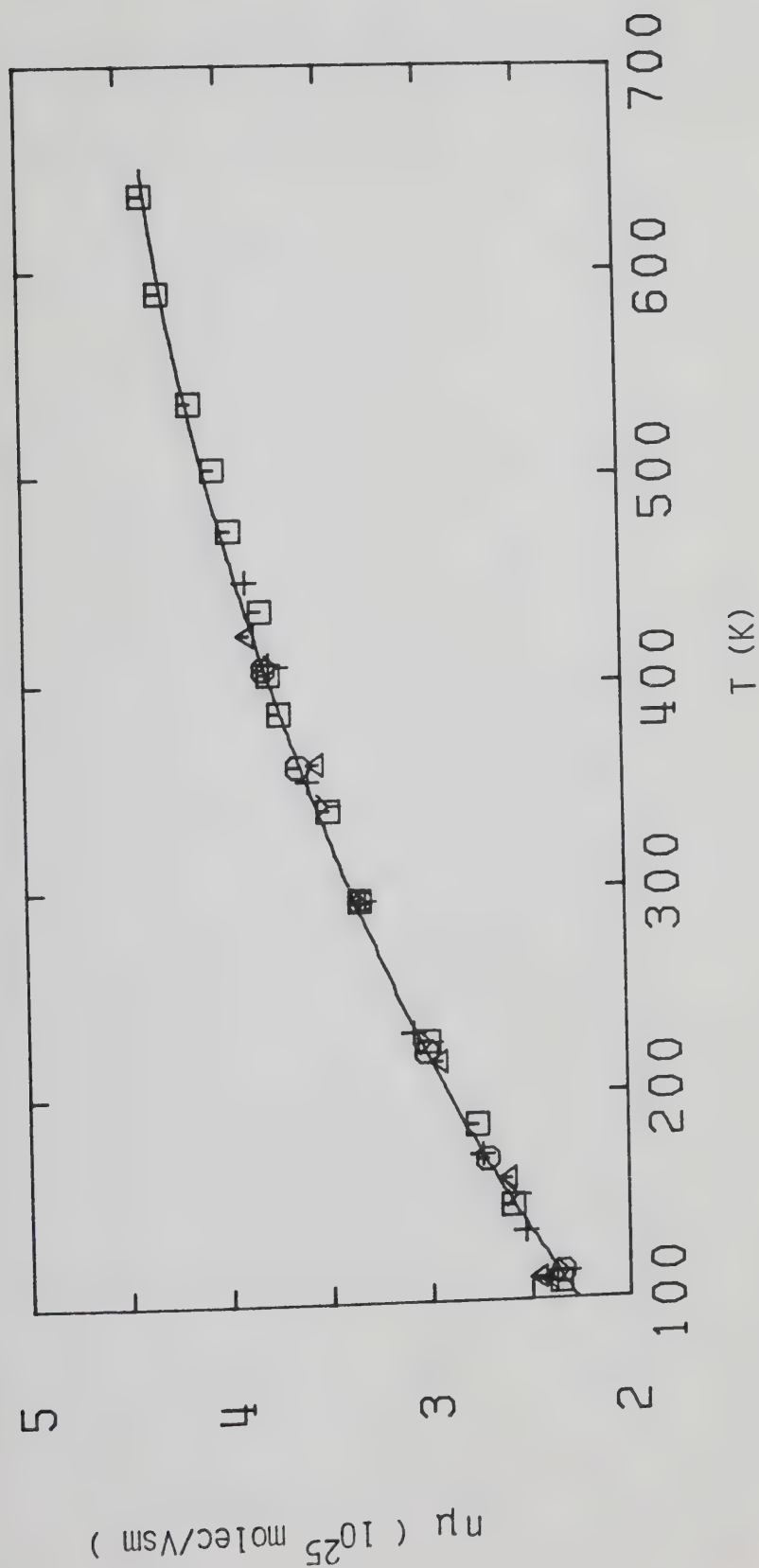


Figure IV-8. Density normalized electron mobilities (low field) in CH_3D and CH_2D_2 gases at different densities ($10^{25} \text{ molec/m}^3$) as functions of temperature.
 CH_3D : \square , 2.35; \circ , 3.3; \triangle , 4.9. CH_2D_2 : +, 3.7; γ , 6.1. The line is from Figure IV-5.

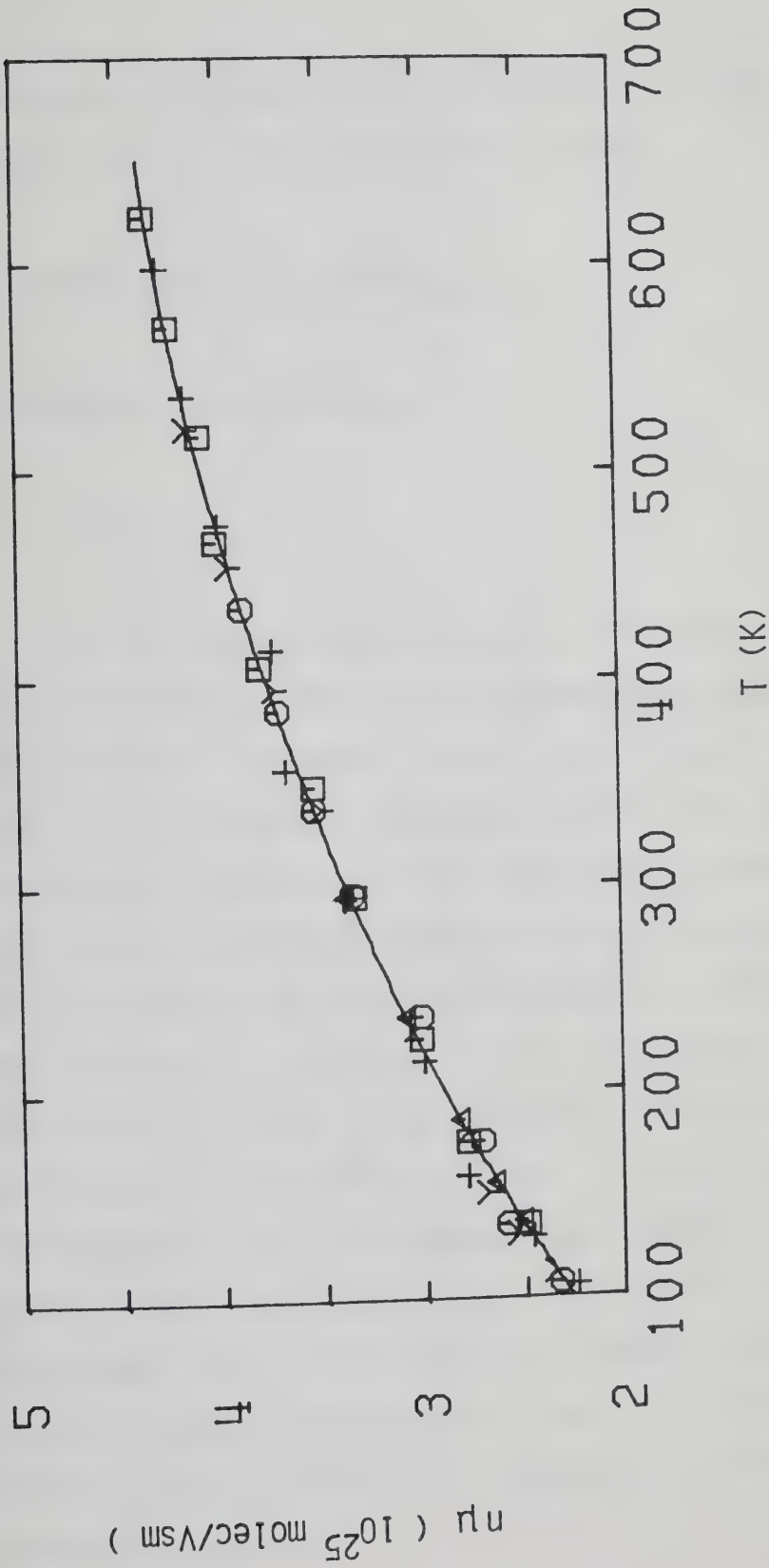


Figure IV-9. Density normalized electron mobilities (low field) in CHD_3 and CD_4 gases at different densities ($10^{25} \text{ molec/m}^3$) as functions of temperature.
 CHD_3 : \square , 2.30; \circ , 4.3; \triangle , 12.2. CD_4 : +, 3.20; γ , 5.0. The line is from

Figure IV-5.

deuterated compounds are too small to produce a detectable difference in scattering cross section.

2. Dense Gas ($0.05 \lesssim n/n_c \lesssim 1$)

a. Electric Field Effect

i) CH₄

On the saturation curve, in the region ($n \gtrsim 3 \times 10^{26}$ molec/m³) where the density normalized mobility decreases with density (Figure IV-1), the value of the ratio $(v_d^{thr})/c_0$ increases (Figure IV-10). At lower densities this ratio is constant at 1 implying predominantly elastic contributions. The decrease in $n\mu$ at $n \gtrsim 3 \times 10^{26}$ molec/m³ is attributed to quasilocalization of the electron by van der Waals clusters of molecules (see next subsection). This is an inelastic process which leads to an increase in $(v_d^{thr})/c_0$. At $T = 190K$, the temperature corresponding to the highest gas density used in Figure IV-10, the fraction q of electrons with an energy sufficient to excite isolated methane molecules to the lowest excited vibrational level is 5.1×10^{-5} . The increase in $(v_d^{thr})/c_0$ is therefore a density and not a temperature effect.

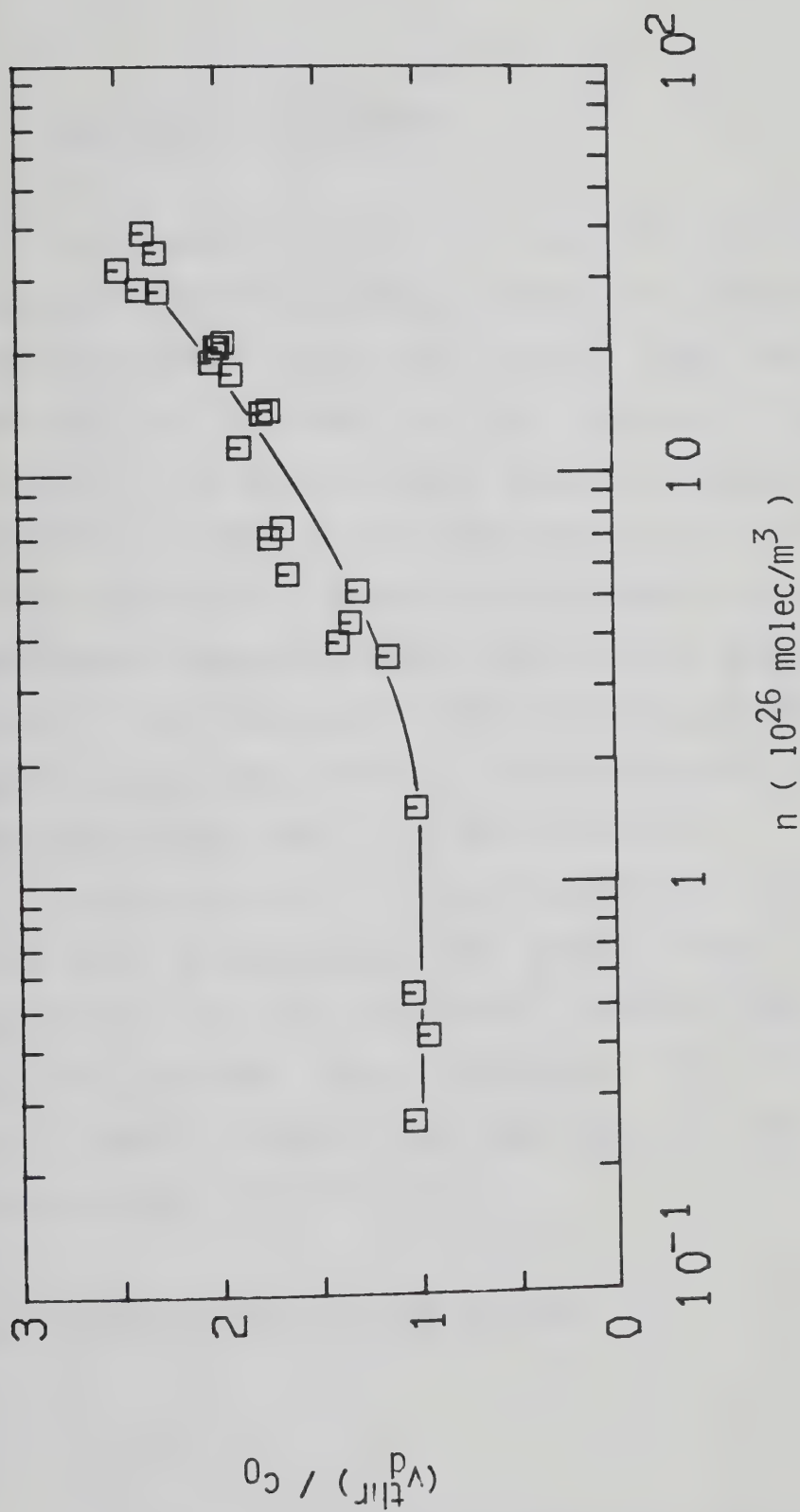


Figure IV-10. Plot of the ratio of the electron threshold drift velocity v_d^{thr} to the speed of sound c_0 in saturated CH_4 vapor as a function of density n .

ii) Deuterated Methanes

In Figures III-2-19, III-3-16, III-4-19, and III-5-16 are shown plots of $(E/n)_{\text{thr}}$ against the number density in the saturated vapors CH_3D , CH_2D_2 , CHD_3 and CD_4 . The behavior is the same as that observed in CH_4 (Figure III-1-19). In saturated CH_4 vapor the speed of sound goes through a maximum at $T \approx 145\text{K}$ and $n \approx 5 \times 10^{26} \text{ molec/m}^3$. It is reasonable to expect that the same will happen in the deuterated compounds whose experimental values were not found in the literature. The ratios $(v_{\text{dthr}})/c_0$ would then also increase with density in the isotopic molecules at densities higher than $\sim 3 \times 10^{26} \text{ molec/m}^3$.

Plots of n_μ vs. n (see Figures IV-13 to IV-16) also show that n_μ decreases with density above $n \approx 3 \times 10^{26} \text{ molec/m}^3$. It is therefore concluded that the same inelastic process (quasilocalization) operating in CH_4 in this density region is important in the deuterated analogues as well.

b. Temperature and Density Effects

i) CH_4

The effect of density on n_μ in the saturated vapor and liquid can be seen from Figure IV-1. At low densities,

$n \lesssim 3 \times 10^{26}$ molec/m³, the low field mobility decreases as the inverse density. In this region the density normalized mobility is density independent because multi-body effects are not important. The value of $n\mu$ decreases as the density is further increased and reaches a minimum in the vicinity of the critical point. The sharp increase in $n\mu$ at $n > 6.1 \times 10^{27}$ molec/m³ is due to conduction band formation. Results in this region will be discussed separately.

In Figures IV-11 and IV-12 are reported Arrhenius plots of the thermal electron mobility (low field strength limit) in CH₄ gas at different densities. At low densities the temperature coefficient of the mobility is related to the energy variation of the momentum transfer cross section. At higher densities the temperature coefficient of mobility increases superlinearly with density.

The effect of increasing the density above $n \approx 3 \times 10^{26}$ molec/m³ in the saturated vapor is to decrease the value of $n\mu$ (Figure IV-1). In the same density region where $n\mu$ decreases with density and the temperature coefficient increases, the value of the quasifree electron mobility, μ_0 , increases.⁴⁶ At $n \gtrsim 3 \times 10^{26}$ molec/m³ quasilocalization of the electron in van der Waals clusters of molecules is thought to occur.^{48,207}

Gee and Freeman⁴⁸ have shown that, by taking the low field values of mobility from Reference 46 as a measure of

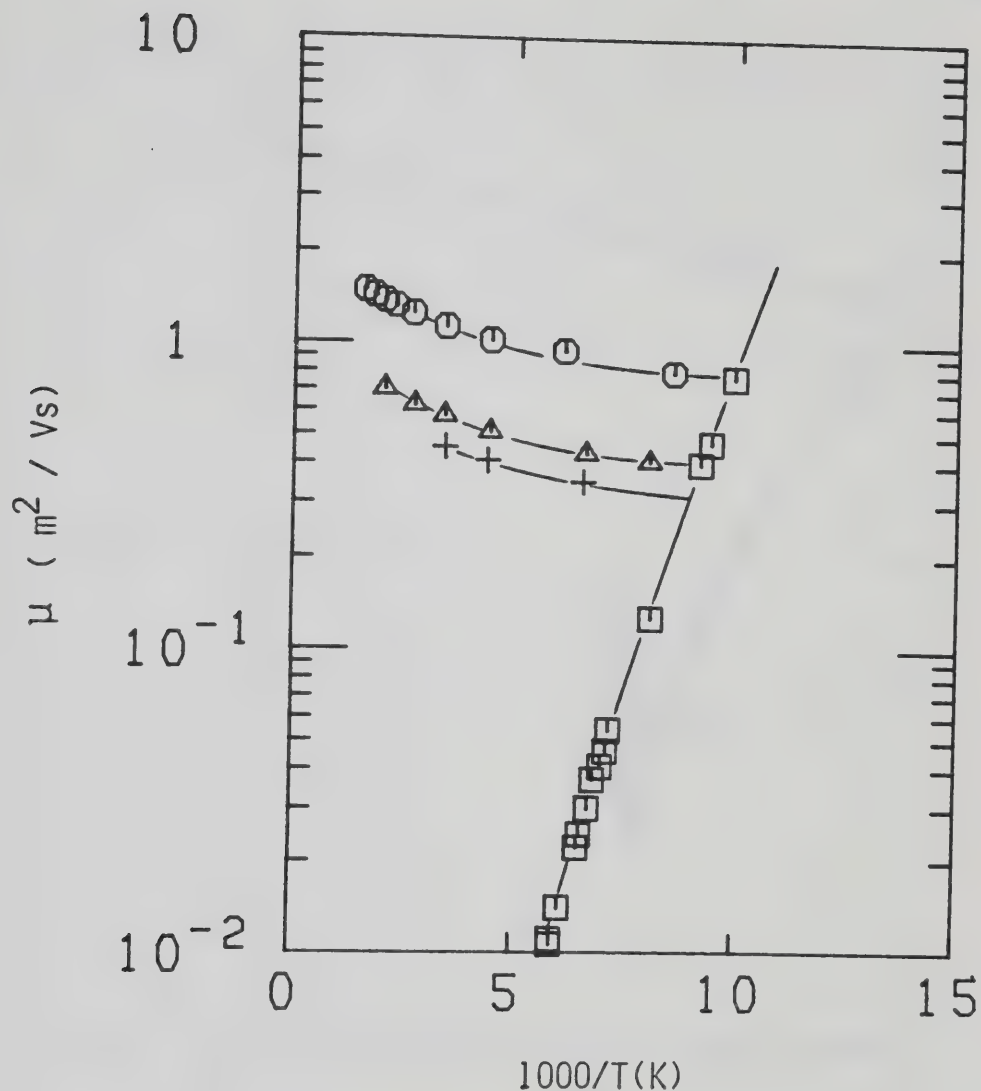


Figure IV-11. Arrhenius plot of thermal electron mobilities (low field) in CH_4 gas at different densities ($10^{25} \text{ molec/m}^3$). Mobilities in the gas along the vapor-liquid coexistence curve are represented by \square . \circ , 2.95; Δ , 5.3; +, 7.5.

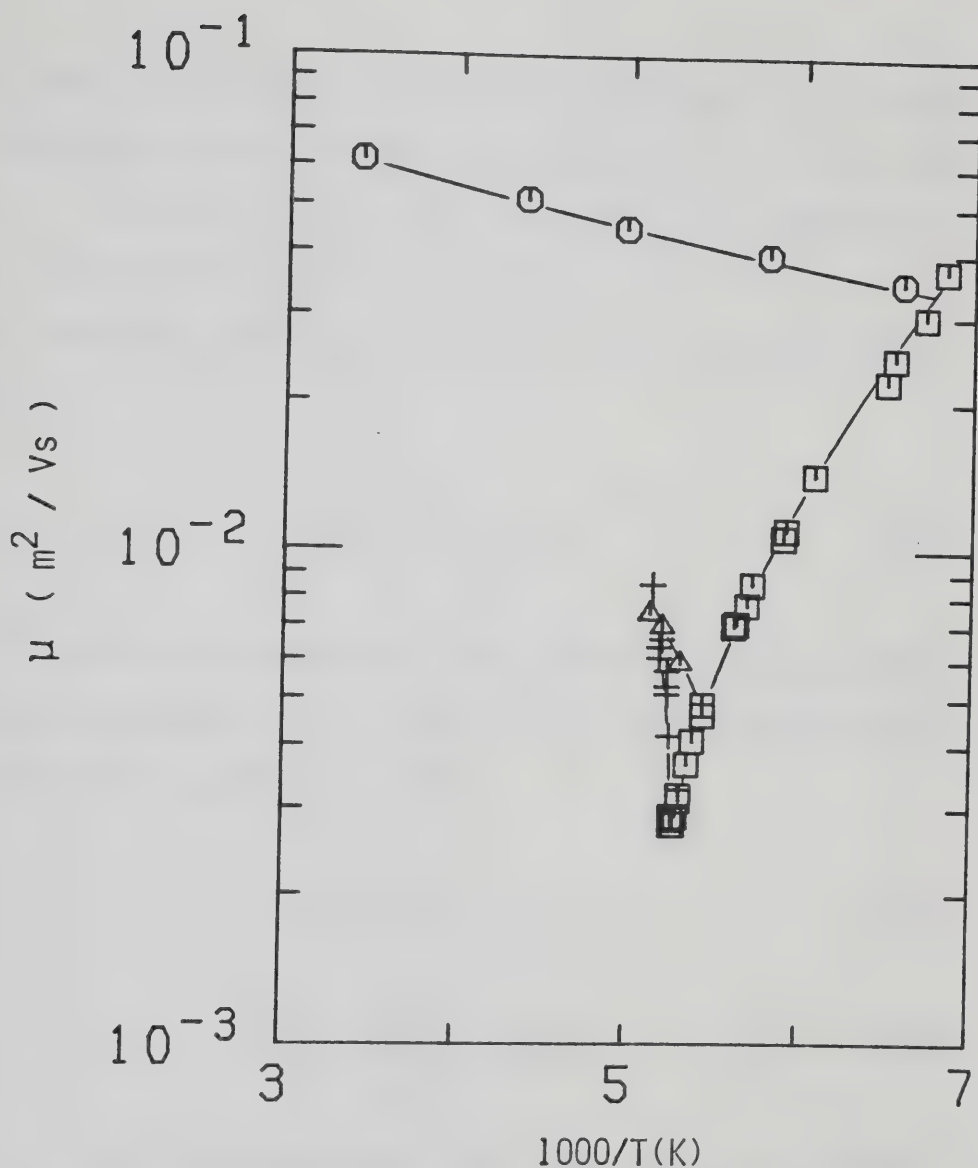


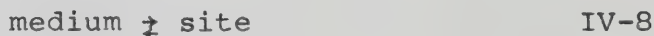
Figure IV-12. Arrhenius plot of thermal electron mobilities (low field) in CH_4 gas at different densities (10^{26} molec/ m^3). Mobilities in the gas along the vapor-liquid coexistence curve are represented by □. ○, 5.5; Δ, 29.0; +, $n_c=61$.

μ_0 , the ratio of $(n\mu_0)_n$ at density n to the low density limit $(n\mu_0)_{ld}$ is $(n\mu_0)_n/(n\mu_0)_{ld} = 1.05$ at $n = 3 \times 10^{26}$ molec/m³, 1.25 at $n = 11 \times 10^{26}$ molec/m³ and extrapolates to 3 ± 1 at $n_c = 6.1 \times 10^{27}$ molec/m³.

The density normalized mobility for any values of T and n is

$$n\mu = (n\mu_0)_n f \quad \text{IV-7}$$

where f is the fraction of electrons in the quasifree state. In the dense gas the quasilocalization sites may be regarded as density fluctuations



where e^-_{qf} is the quasifree electron, e^-_{ql} the quasi-localized electron and "site" represents a density fluctuation of sufficient magnitude and breadth.

The concentration of sites depends on the free energy change of process IV-8.

$$k_8 = [\text{site}] = \exp[-\Delta G^0_8/RT] = \exp[\Delta S^0_8/R - \Delta H^0_8/RT] \quad \text{IV-10}$$

where k_8 is the equilibrium constant and R is gas constant.

The concentration of e^-_{qf} can be written in terms of the equilibrium constant of process IV-9, k_9 , as

$$[e^-_{qf}] = \frac{[e^-_{q1}]}{k_9[\text{site}]} = \frac{[e^-_{q1}]}{k_8 k_9} = \frac{[e^-_{q1}]}{k'} \quad \text{IV-11}$$

$$k_9 = \exp\left[-\frac{\Delta G^0_9}{RT}\right] = \exp\left[\frac{\Delta S^0_9}{R} - \frac{\Delta H^0_9}{RT}\right] \quad \text{IV-12}$$

It follows then that the fraction of quasifree electrons, f , is

$$f = \frac{[e^-_{qf}]}{[e^-_{qf}] + [e^-_{q1}]} = \left\{1 + \frac{[e^-_{q1}]}{[e^-_{qf}]}\right\}^{-1} = \{1 + [\text{site}]k'\}^{-1} \quad \text{IV-13}$$

and

$$\frac{(n_{\mu O})_n}{n_{\mu}} - 1 = k' = \exp\left(\frac{\Delta S^{0'}}{R} - \frac{\Delta H^{0'}}{RT}\right) \quad \text{IV-14}$$

where

$$\Delta S^{0'} = \Delta S^0_8 + \Delta S^0_9 \quad \text{IV-15}$$

$$\Delta H^{0'} = \Delta H^0_8 + \Delta H^0_9 \quad \text{IV-16}$$

Values of the temperature coefficient E_μ at the different densities were calculated from Figure IV-12. They were $E_\mu = 1.5, 15$ and 135 kJ/mol at $n = 5.5, 29$ and 61 (10^{26} molec/m³) respectively. The present value at the critical density is considerably higher than that reported in Reference 48. The difference is attributed to the better temperature control that was achieved in the present study. For comparison the values obtained in the supercritical gases Ar²⁰⁸ and Xe²⁰⁷ were 18 and 130 kJ/mol respectively.

ii) Deuterated Methanes

In Figures IV-13 to IV-16 are reported plots of the density normalized low field mobility, n_μ , against the density, n , in the saturated vapors and liquids CH₃D, CH₂D₂, CHD₃ and CD₄. The dashed line drawn in each plot in the vapor region represents values in CH₄.

In Figures IV-17 to IV-20 are shown Arrhenius plots at different vapor densities in the same compounds. The lower densities have been omitted because the Arrhenius model is not applicable.

As for CH₄, values of the temperature coefficient of mobility were calculated. They are given, together with those found in CH₄, in Table IV-1 and Figure IV-21.

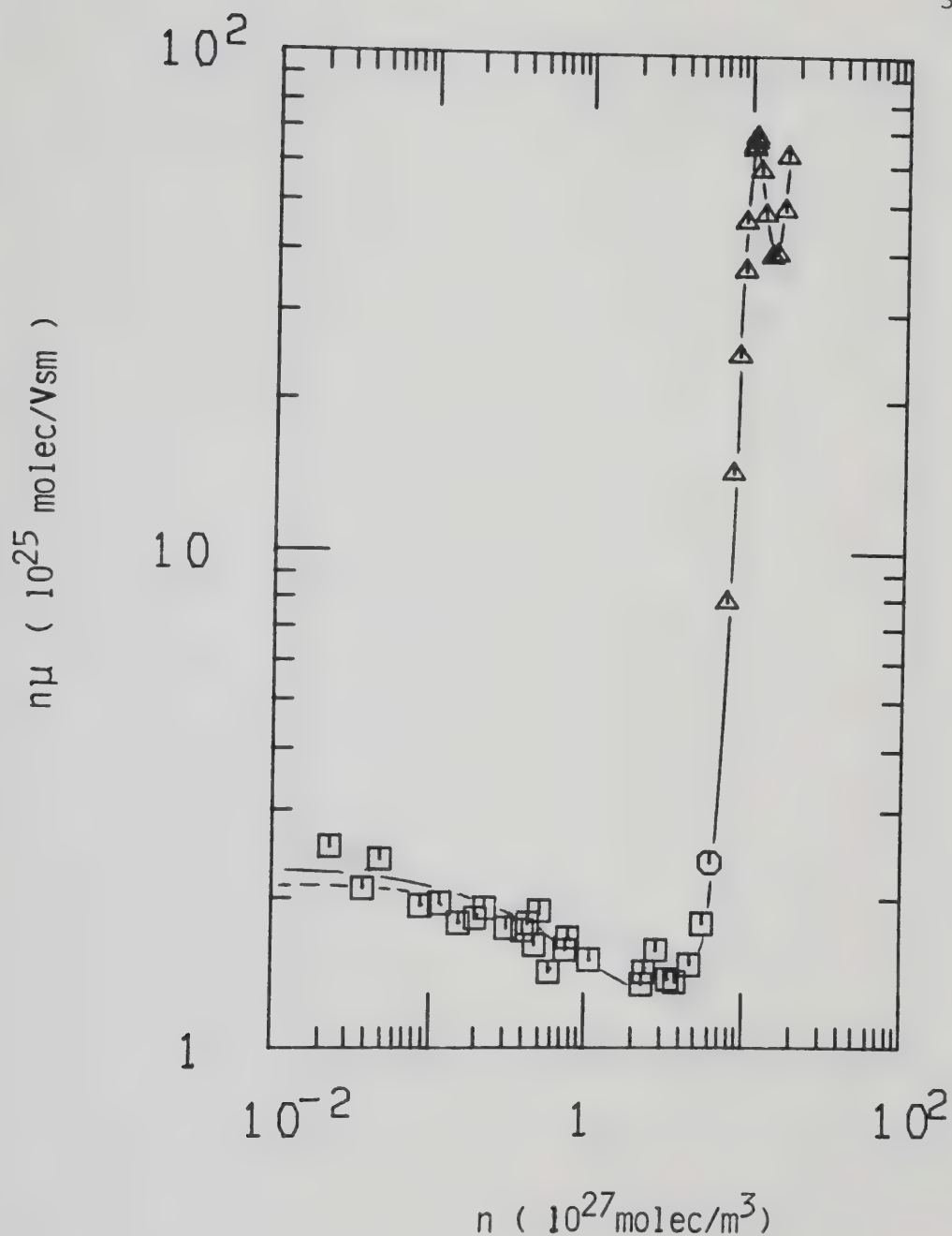


Figure IV-13. Density normalized electron mobility (low field) against n for thermal electrons in coexistence vapor (\square) and liquid (Δ) CH_3D . \bigcirc , represents the supercritical fluid at n_c and $T_c + 0.2\text{K}$. The dashed line is for CH_4 from Fig. IV-1.

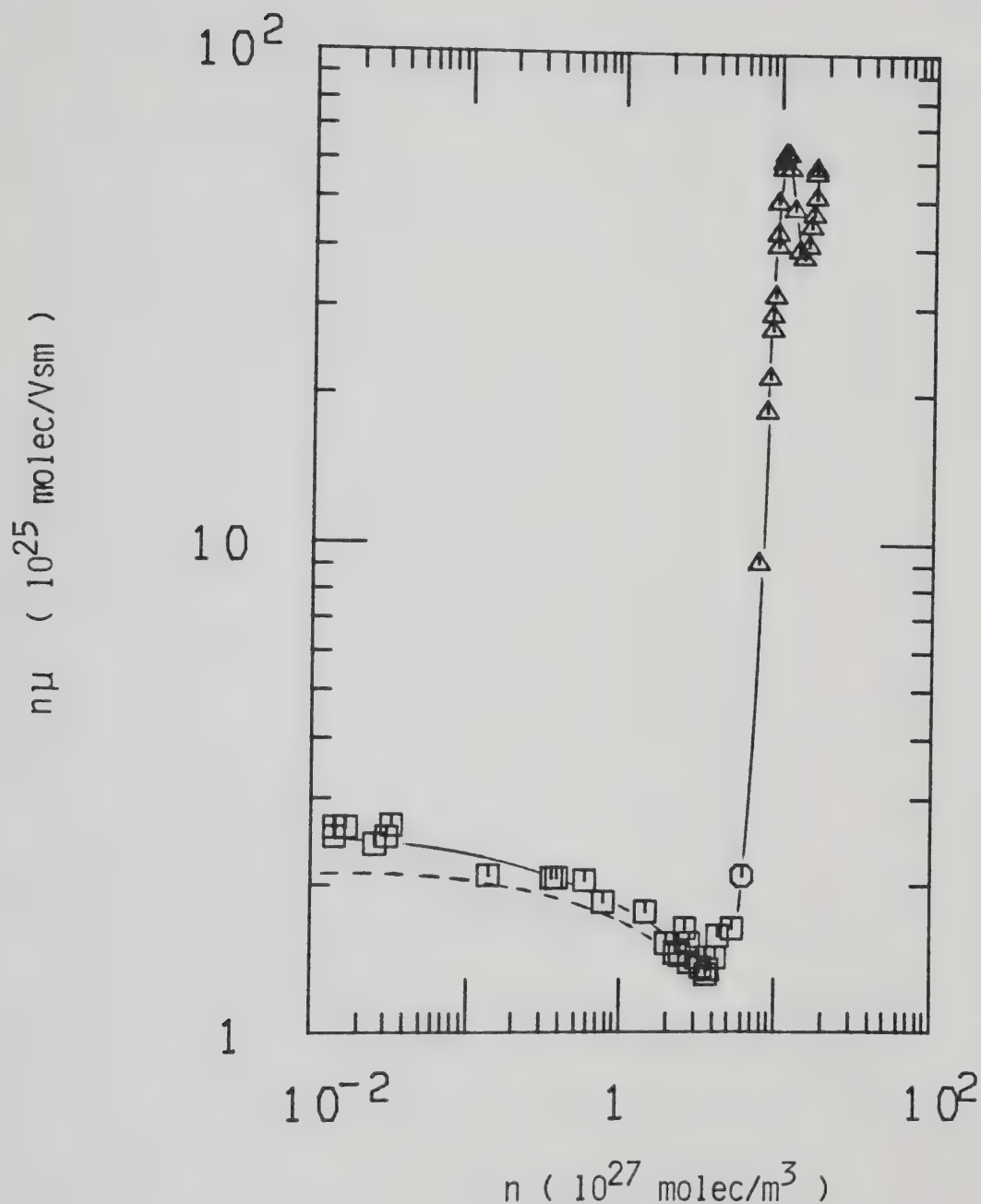


Figure IV-14. Density normalized electron mobility (low field) for thermal electrons in coexistence vapor (\square) and liquid (Δ) CH_2D_2 . \circ represents the supercritical fluid at n_c and T_c . The dashed line is for CH_4 from Figure IV-1.

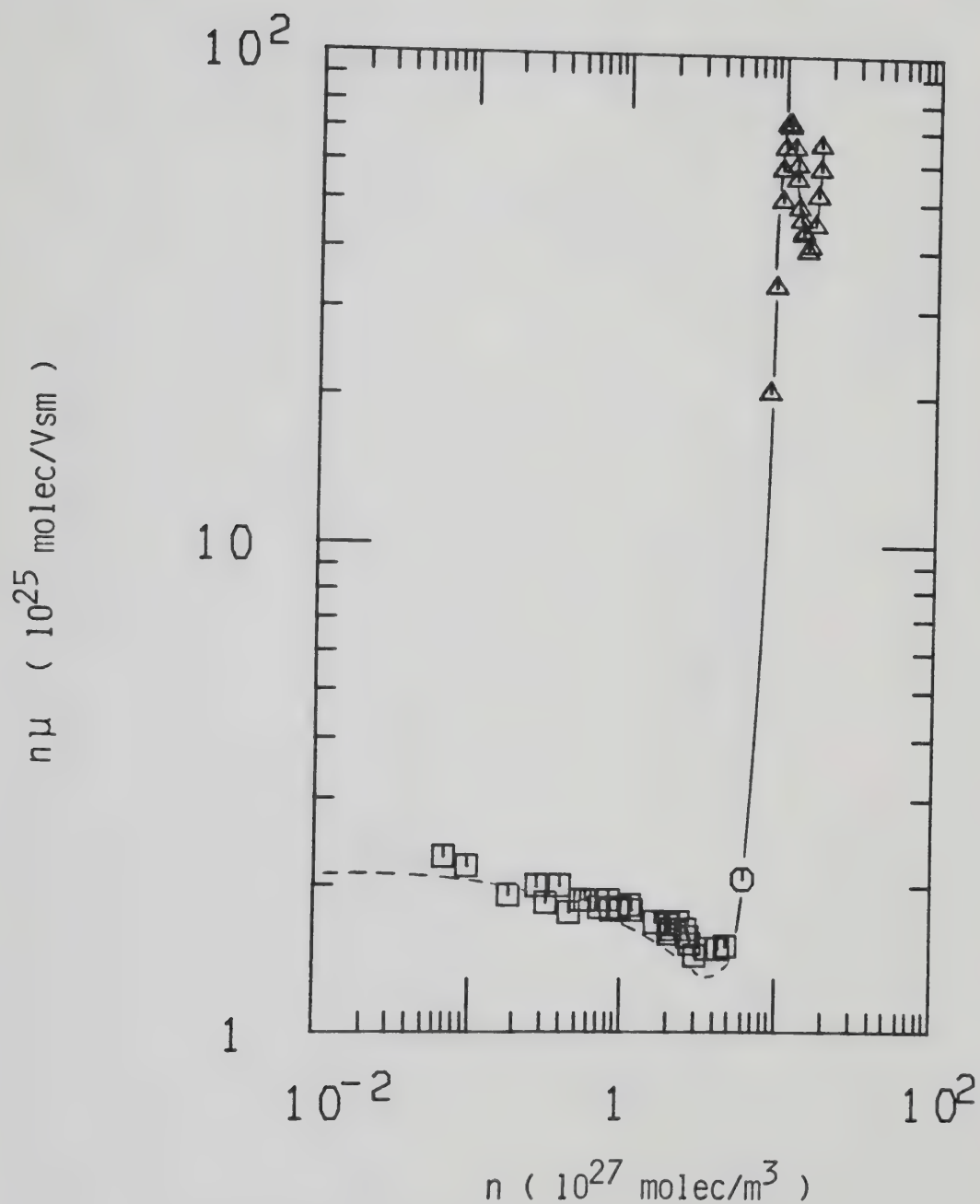


Figure IV-15. Density normalized mobilities against n (low field) for thermal electrons in coexistence vapor (\square) and liquid (Δ) CHD_3 . \circ represents the supercritical fluid at n_c and T_c . The dashed line is for CH_4 from Figure IV-1.

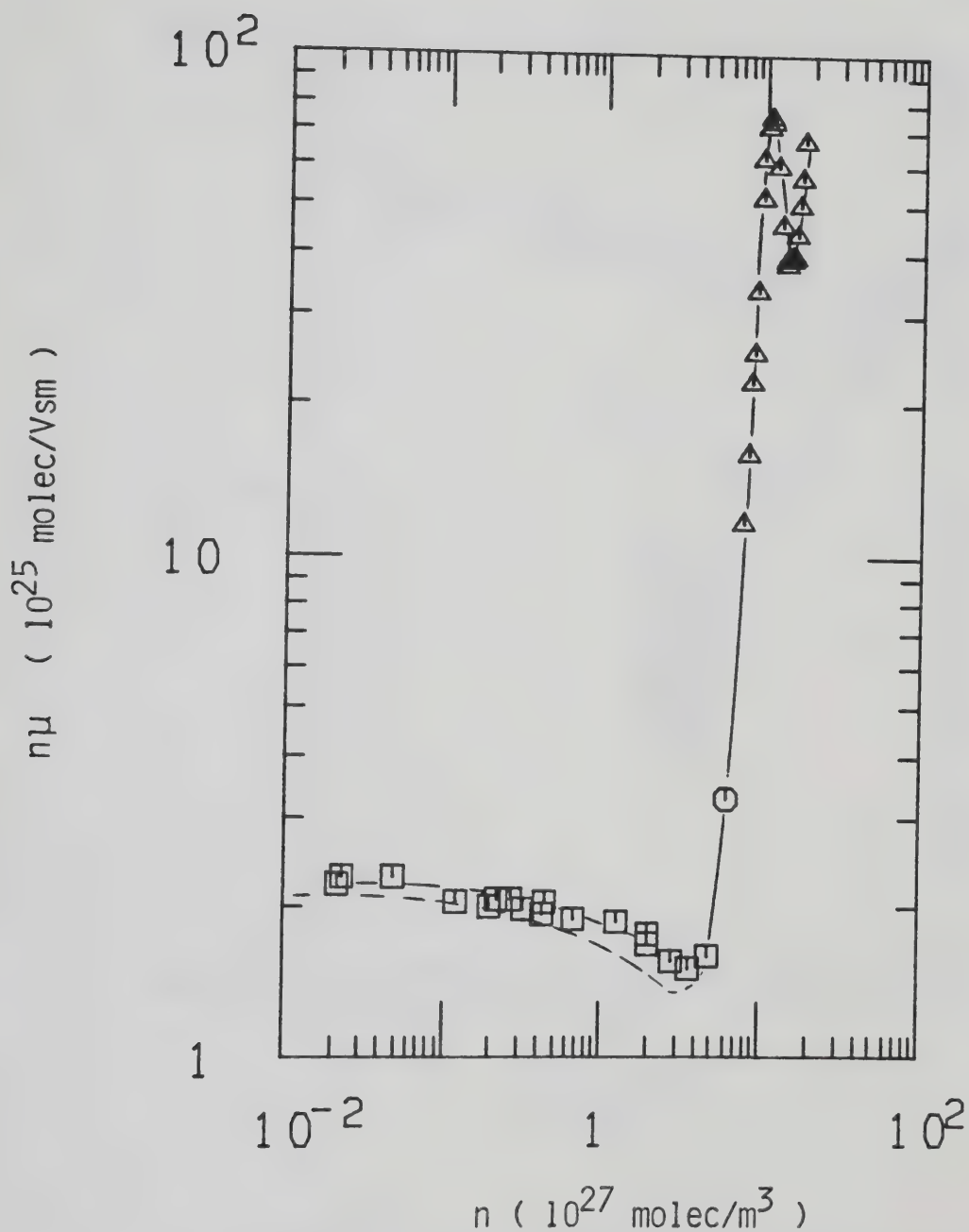


Figure IV-16. Density normalized mobilities (low field) against n for thermal electrons in coexistence vapor (\square) and liquid (Δ) CD_4 . \circ represents the supercritical fluid at n_c and $T_c + 0.1\text{K}$. The dashed line is for CH_4 from Figure IV-1.

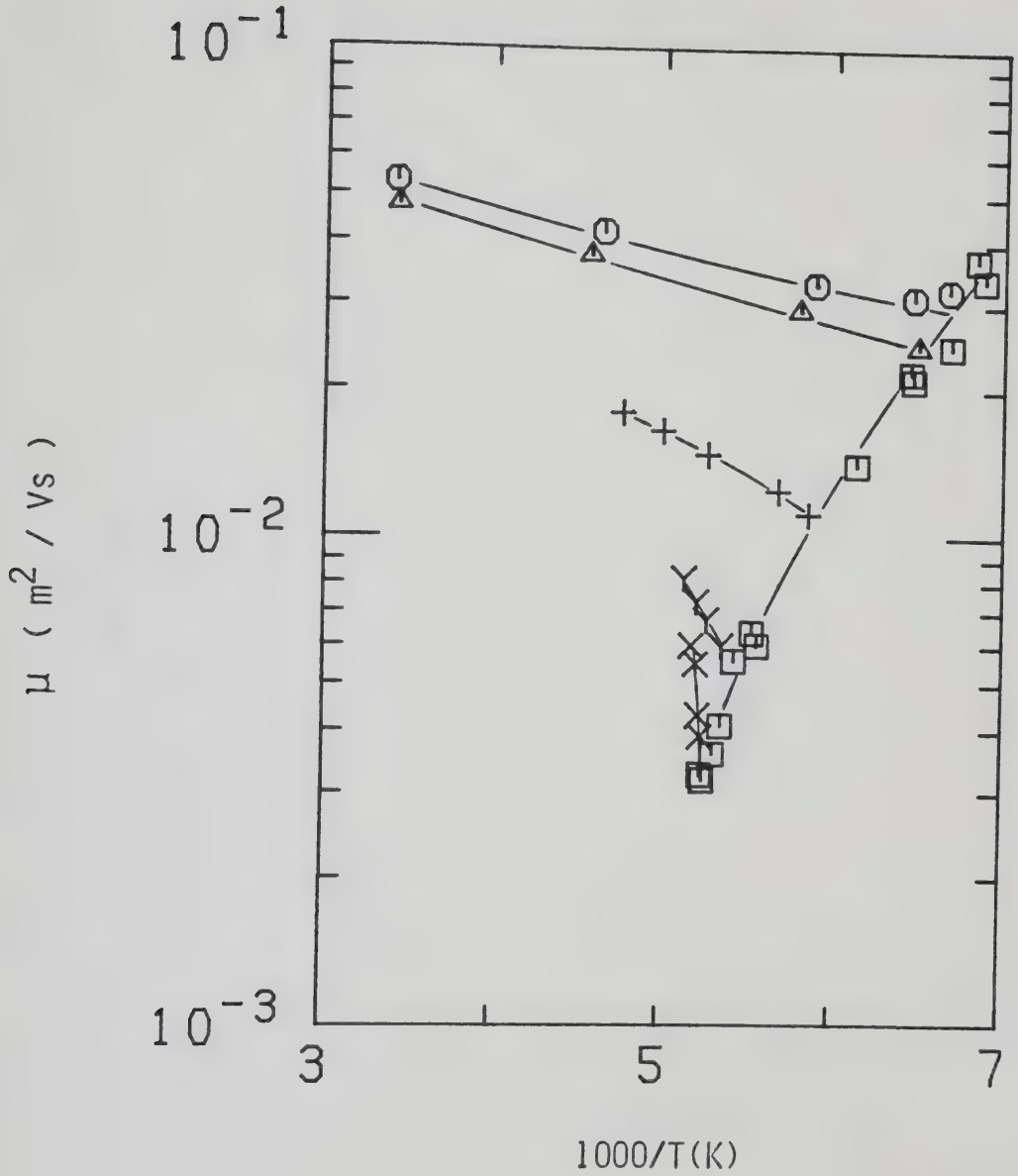


Figure IV-17. Arrhenius plot of thermal electron mobility (low field) in CH_3D gas at different densities ($10^{26} \text{ molec/m}^3$). Mobilities in the gas along the vapor-liquid coexistence curve are represented by \square . \bigcirc , 6.6; \triangle , 6.7; +, 15.0; Y, 27.0; X, $n_c=61$.

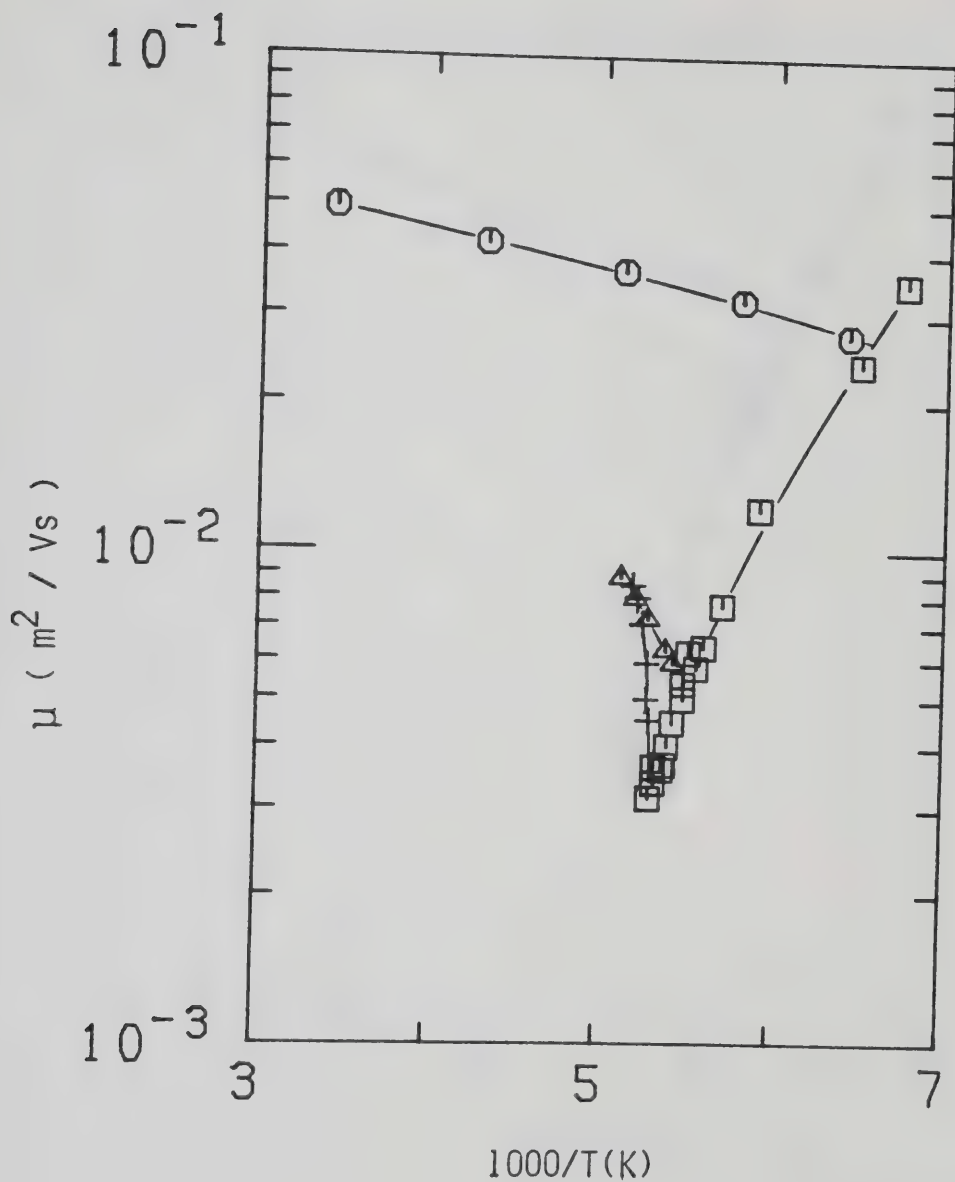


Figure IV-18. Arrhenius plot of thermal electron mobilities (low field) in CH_2D_2 gas at different densities (10^{26} molec/ m^3). Mobilities in the gas along the vapor-liquid coexistence curve are represented by \square . \circ , 7.3; \triangle , 26.0; +, $n_c=61$.

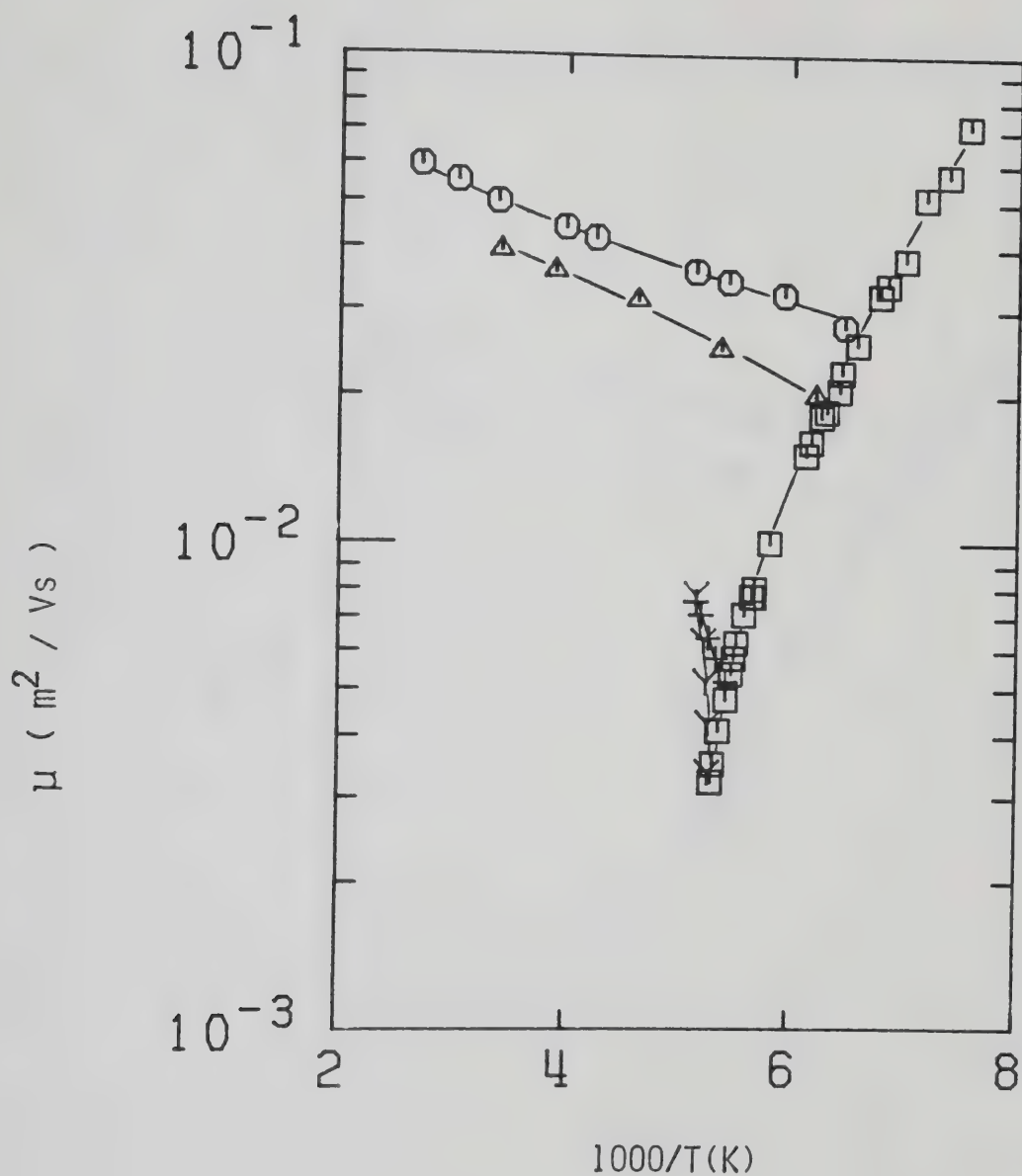


Figure IV-19. Arrhenius plot of thermal electron mobilities (low field) in CHD_3 gas at different densities ($10^{26} \text{ molec/m}^3$). Mobilities in the gas along the vapor-liquid coexistence curve are represented by \square . \circ , 6.8; \triangle , 9.3; +, 29.1; γ , $n_c=61$.

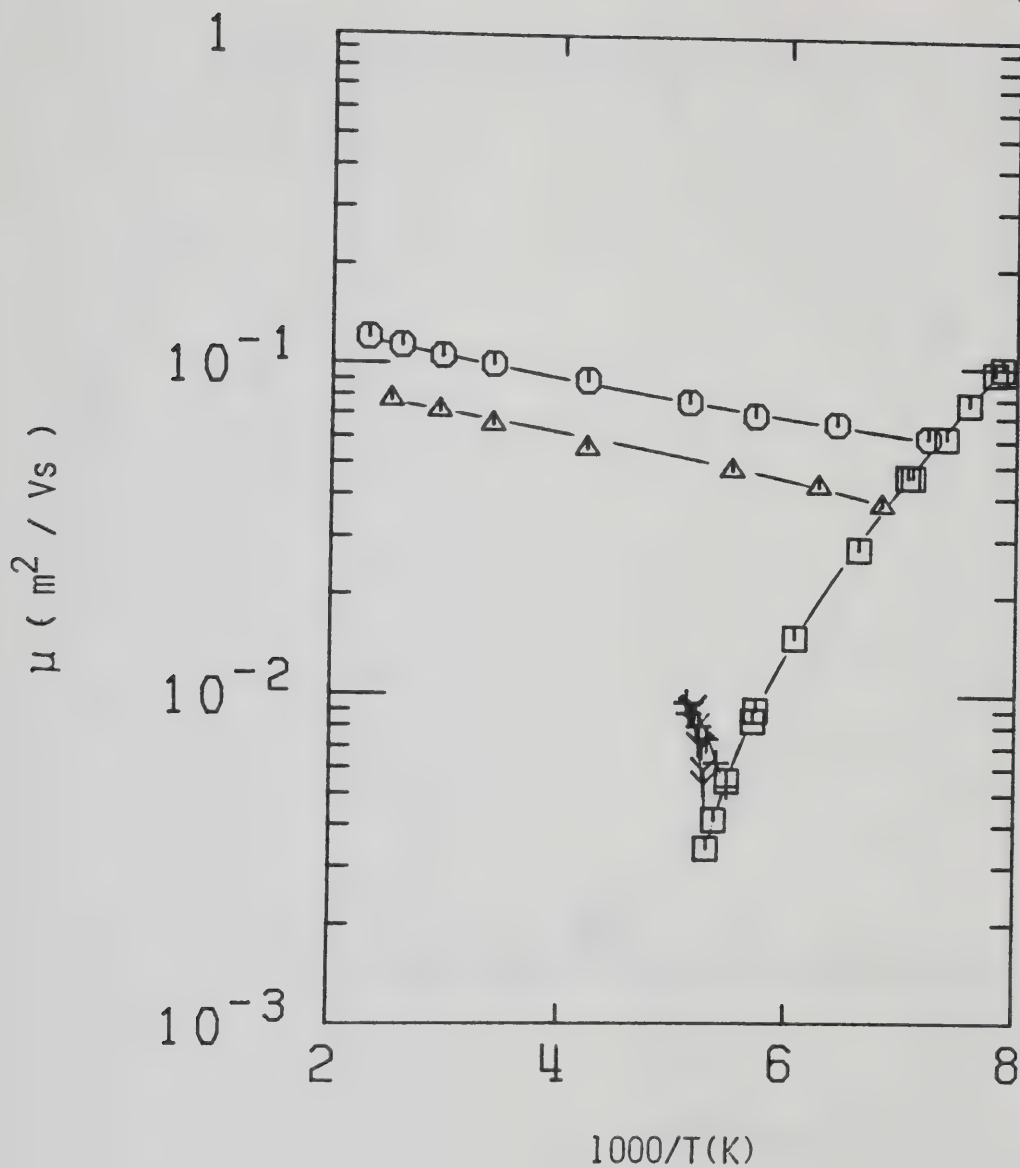


Figure IV-20. Arrhenius plot of thermal electron mobilities (low field) in CD_4 gas at different densities ($10^{26} \text{ molec/m}^3$). Mobilities in the gas along the vapor-liquid coexistence curve are represented by \square . \circ , 3.7; \triangle , 5.5; +, 29.0; γ , $n_c=61$.

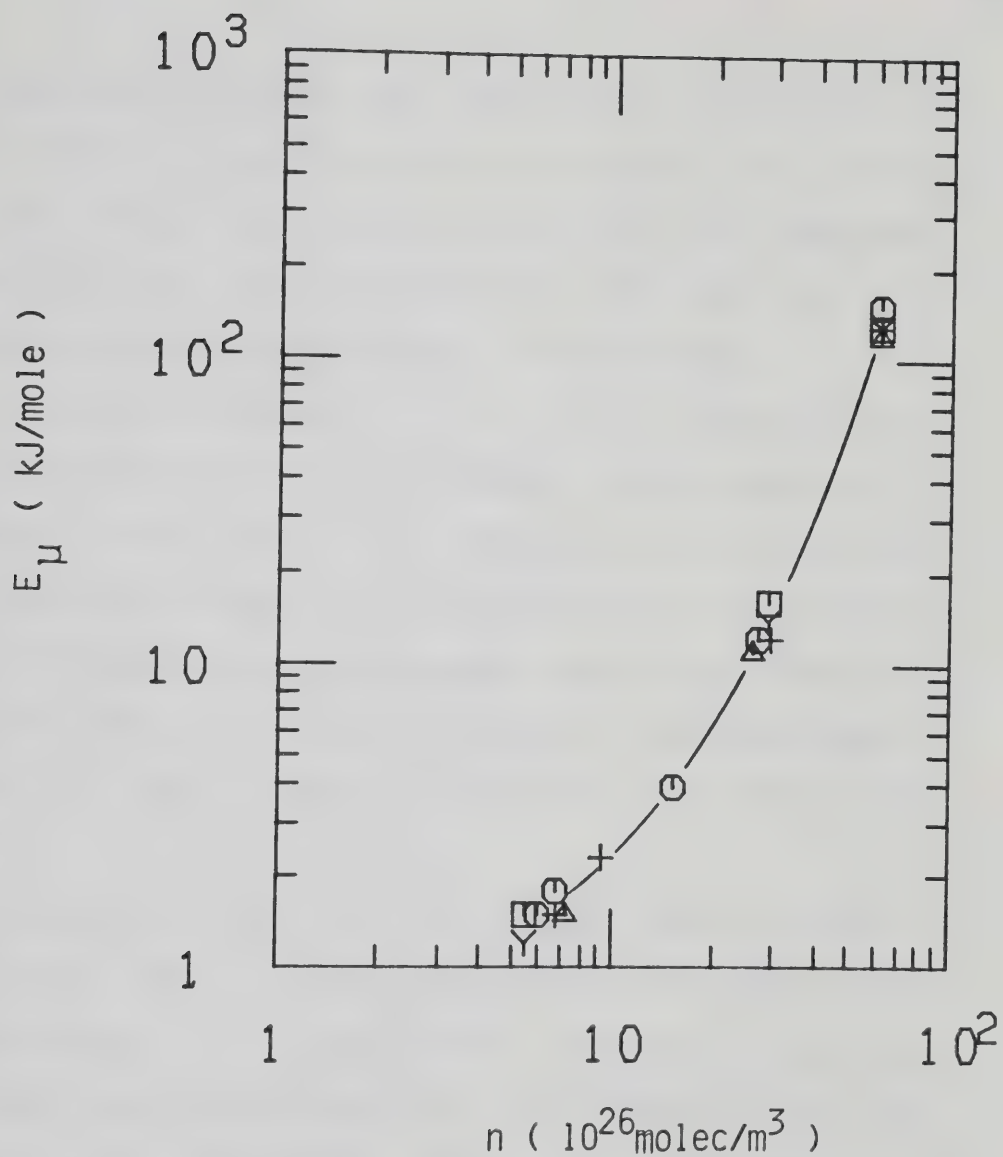


Figure IV-21. Density dependence of the temperature coefficient of mobility E_μ in CH₄ (□), CH₃D (○), CH₂D₂ (Δ), CHD₃ (Y) and CD₄ (+) gases.

As mentioned earlier the temperature coefficient of mobility increases superlinearly with density. At a given density the values of E_μ are the same for all compounds. The energy of the quasilocalization sites has not been appreciably altered by the isotopic substitution.

At the critical density, $n_c = 6.1 \times 10^{27}$ molec/m³, the temperature coefficient is ~ 140 kJ/mol. Considering that a localization energy of kT is sufficient to produce the observed decrease in mobility on going from the low density to the high density gas, the average localization energy is taken to be $-\Delta H^0_9 = \Delta H^0_{-9} \approx kT \approx 2$ kJ/mol. The remaining is attributed to $-\Delta H^0_8$. Thus, in the critical gas, $\Delta H^{0'} \approx \Delta H^0_8$.

From equation IV-14 it can be seen that a plot of $\lg\{[(n\mu_0)_n/n\mu] - 1\}$ vs. $1/T$ yields a line of slope $\Delta H^{0'}/R$ and intercept at $T^{-1} = 0$ of $\Delta S^{0'}/R$. Values of $n\mu_0$ at a given density were estimated for all compounds using the low density $n\mu$ vs. T curve from Figure IV-5 and multiplying by $(n\mu_0)_n/(n\mu_0)_{ld}$ from Reference 46. The slopes and intercepts were calculated by a least square method. The results are tabulated in Table IV-1 and displayed in Figures IV-22 and IV-23. As observed earlier,⁴⁸ the values of $\Delta S^{0'}$ are approximately proportional to the structure factor of the fluid, $S(0)$, which is related to the magnitude of the density fluctuations. The density fluctuations are largest in the saturated vapor. The

TABLE IV-1

Electron Mobility Activation Parameters

Compound	n (10^{26}m^{-3})	n/n_c	T_{range} (K)	E_u^a (kJ/mol)	$-\Delta H^b$ (kJ/mol)	$-\Delta S^b$ (J/mol K)	Corr ^c	$S(0)^d$	$-\Delta S/S(0)$
CH ₄	5.5	0.09	152- 292	1.5	3.1	26	0.97	1.3	20
	29.0	0.48	189- 195	16	15.9	78	0.98	5.4	14
	61	1.00	190.7- 192.4	130	110	620	0.96	29	21
	6.0	0.10	150- 294	1.5	2.8	23	0.96	1.3	18
CH ₃ D	6.7	0.11	154- 293	1.8	3.5	24	0.999	1.4	17
	15.0	0.25	171- 210	3.9	6.3	35	0.999	1.8	19
	27.0	0.44	187- 195	12	16.9	84	0.999	4.8	18
	61	1.00	191.3- 193.3	150	100	520	0.98	29	18

(continued....)

CH ₂ D ₂	7.3	0.12	156- 292	1.5	3.9	30	0.996	1.5	20
	26.0	0.43	184- 196	11	16.5	83	0.999	4.5	18
	61	1.00	189.2- 193.9	120	92	480	0.97	29	17
	6.8	0.11	155- 251	1.5	3.2	25	0.99	1.4	18
CHD ₃	9.3	0.15	161- 294	2.3	5.0	33	0.998	1.7	19
	29.1	0.48	184- 194	12	17.4	86	0.999	5.4	16
	61	1.00	189.0- 193.0	130	99	510	0.986	29	18
	5.5	0.09	147- 293	1.2	3.3	29	0.97	1.3	22
CD ₄	29.0	0.48	183- 196	14	20	103	0.999	5.4	19
	61	1.00	189.3- 193.0	130	86	480	0.996	29	17

a. from Arrhenius plots

b. from Equation IV-14.

c. Correlation factor of the least square fit (see text)

d. calculated from $S(0) = nkt\chi_T$ at the average temperature in the range.

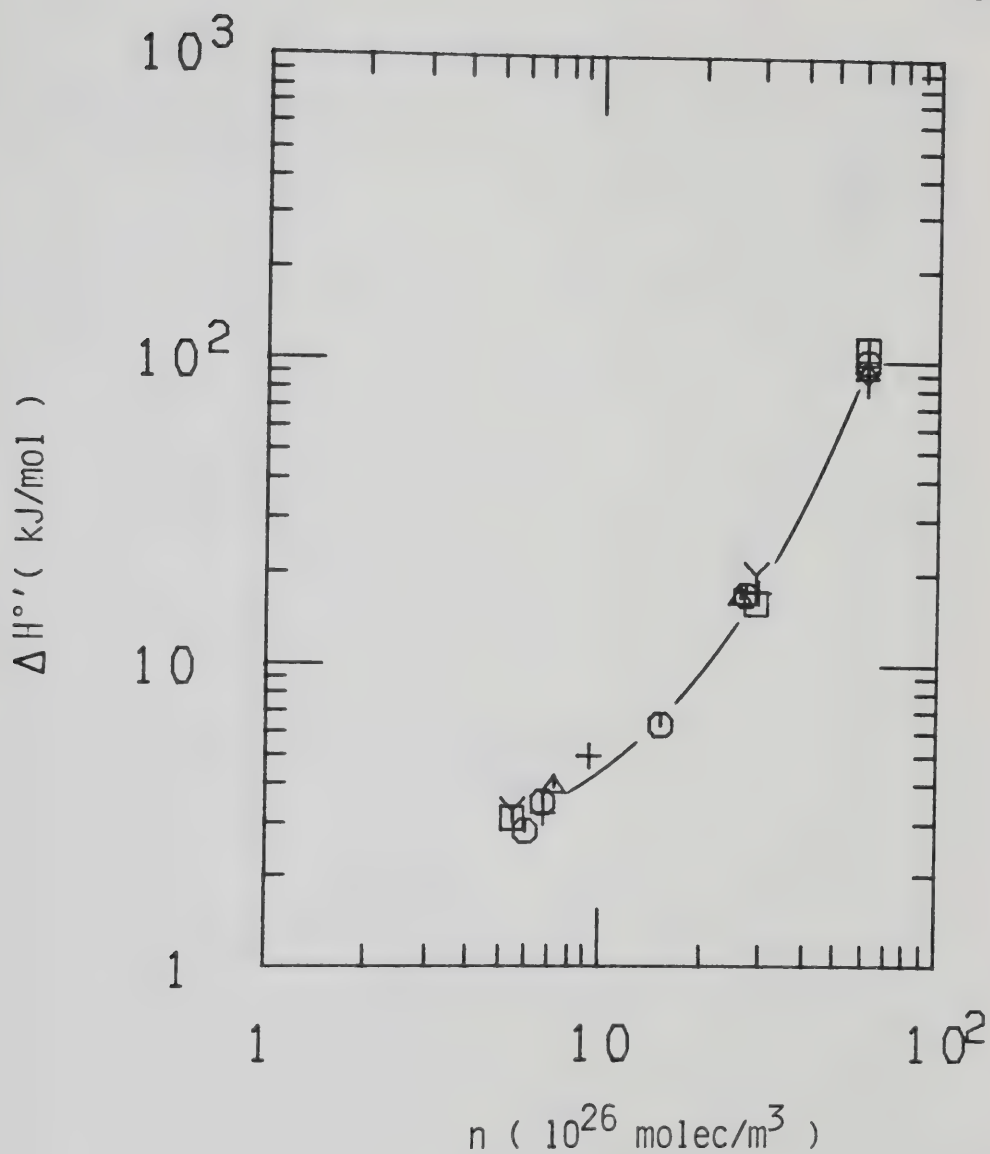


Figure IV-22. Density dependence of the enthalpy of equilibrium IV-14, $\Delta H^{\circ'}$, in the gases CH_4 (□), CH_3D (○), CH_2D_2 (△), CHD_3 (Y) and CD_4 (+).

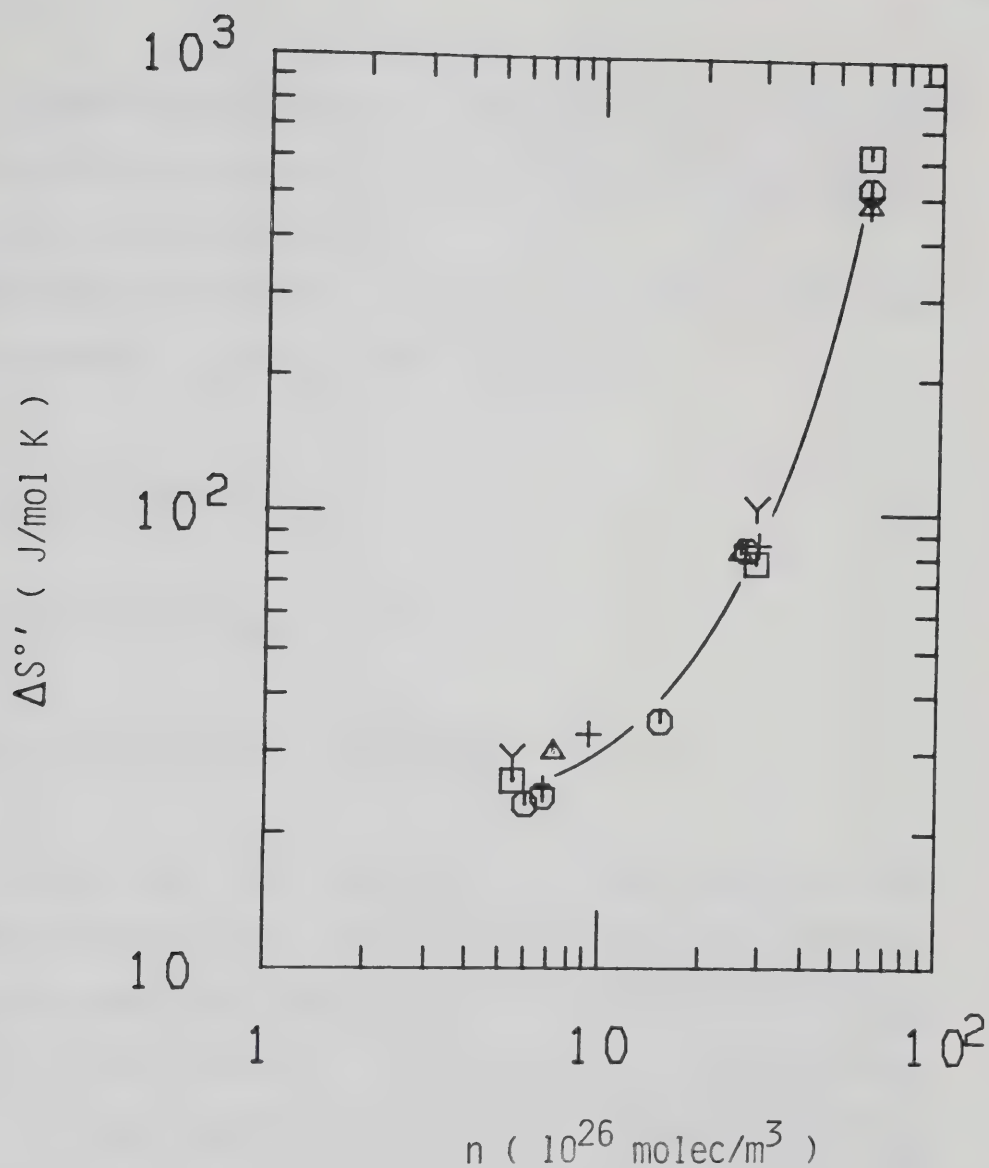


Figure IV-23. Density dependence of the entropy of equilibrium IV-14, ΔS° , in the gases CH_4 (\square), CH_3D (\circ), CH_2D_2 (\triangle), CHD_3 (Y) and CD_4 (+).

extent of quasilocalization of the electron is therefore largest near the coexistence curve and decreases as the gas is heated at constant density.

Differences between compounds in Table IV-1 are attributed mainly to experimental scatter.

3. Liquid ($1 < n/n_c \lesssim 2.8$)

a. Electric Field Effect

i) CH₄ and Deuterated Analogues

In Figure IV-24 is reported the density variation of the threshold field for electron heating in the liquid and supercritical methanes. The density dependence of $(E/n)_{thr}$ is similar in all compounds. Beginning at the high density end near the triple point, $n = 17 \times 10^{27}$ molec/m³, $(E/n)_{thr}$ remains constant at 9 mTd as n is decreased to 14×10^{27} molec/m³. The threshold then decreases to a shallow minimum of 8 mTd at 11×10^{27} molec/m³, then increases progressively rapidly as the density is decreased towards 8.5×10^{27} molec/m³, where the field effect changes sign. The threshold fields in CH₄ appear to be ~15% lower, and those in CH₂D₂ ~15% higher than those quoted (Figure IV-24). At densities $< 8.5 \times 10^{27}$ molec/m³, $(E/n)_{thr}$ remains relatively constant at ~30 mTd, even in the fluid at n_c and temperatures up to $T_c + 4K$ (Figure IV-24).

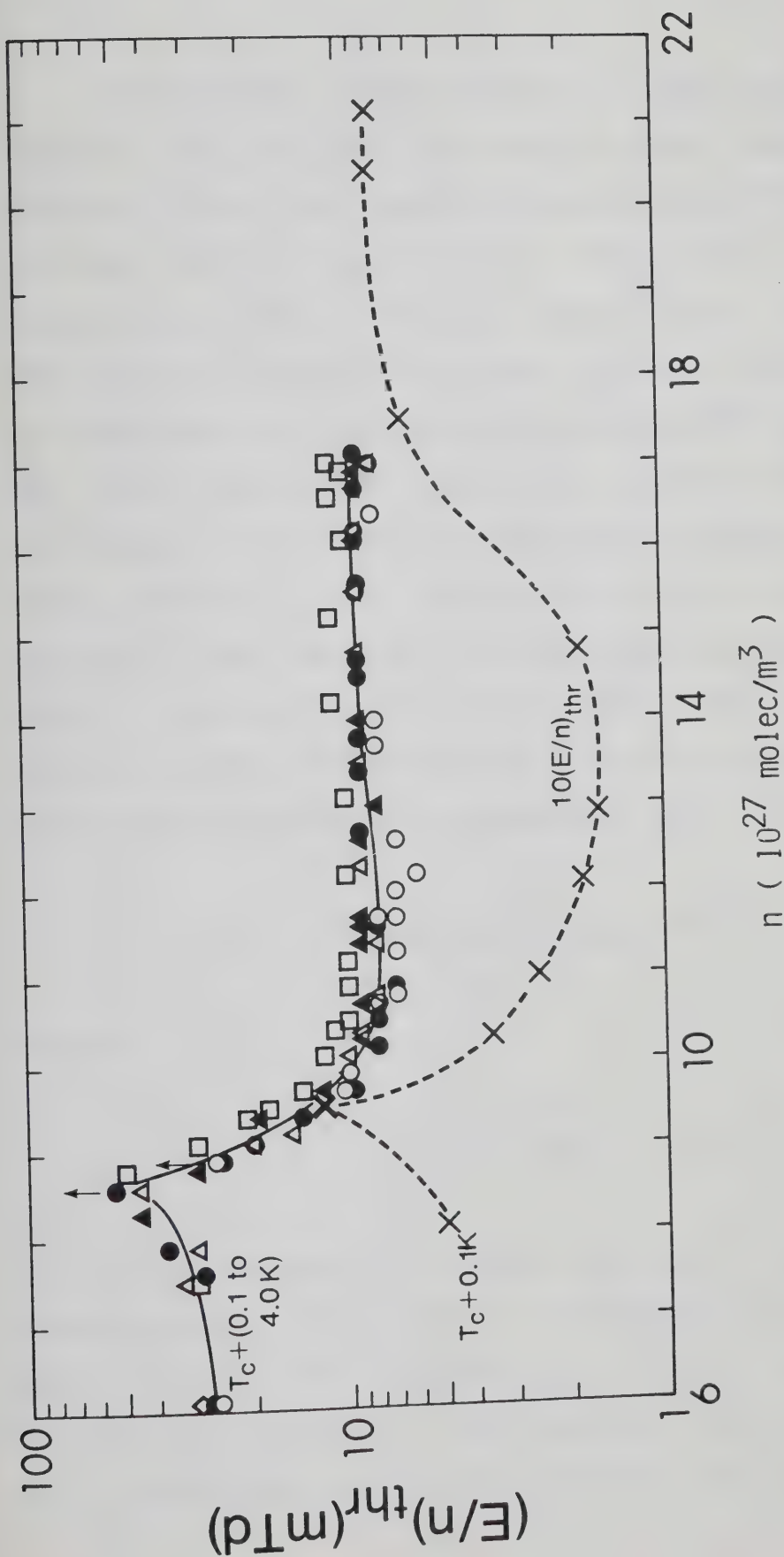


Figure IV-24. Electric field threshold, $(E/n)_{thr}$, for electron heating in the coexistence liquid methanes and argon, as functions of density n . \circ , CH_4 ; \triangle , CH_3D ; \square , CH_2D_2 ; \blacktriangle , CHD_3 ; \bullet , CD_4 ; \times , Ar, Ref. 208; the larger \times at the cusp represents an interpolation of data in Figures 6 then 4 in Ref. 208. The points with temperature labels refer to the supercritical gases at n_c , 0.1–4.0 K above T_c ; $\diamond = \triangle$, \square , \blacktriangle . The sign of $d\mu/dE$ is positive at densities below that of the cusp and negative above. \uparrow indicates a lower limit.

In liquid CH_4 at 101.5K ($T/T_c = 0.533$) and 16.4×10^{27} molec/m³ ($n/n_c = 2.70$) the electron drift velocity at the threshold field for electron heating is $v_d^{\text{thr}} = 6200$ m/s (Figures III-1-17 and IV-24). This value is 24 times greater than that in the low density gas at $n/n_c = 0.0049$ and the same temperature (Figure III-1-1). The difference is consistent with the model of Schnyders^{127a} and Lekner¹²⁶ and their co-workers, which is suitable for quasifree electrons in the heavier monoatomic liquids near their triple points.⁹¹ In this model the scattering cross section of the molecules is reduced by the long wavelength limit of the structure factor $S(0)$. The ratio of the threshold drift velocities at the low and high density limits might therefore be expected to be⁴⁸

$$(v_d^{\text{thr}})_{\text{hd}} / (v_d^{\text{thr}})_{\text{ld}} \approx S(0)^{-1} \quad \text{IV-17}$$

where²¹⁰

$$S(0) = nkT\chi_T \quad \text{IV-18}$$

where k is Boltzmann's constant and χ_T is the isothermal compressibility of the fluid. In liquid CH_4 at $T = 101.5\text{K}$, with $n = 16.4 \times 10^{27}$ molec/m³ and $\chi_T = 1.68 \times 10^{-9}$ Pa⁻¹,¹⁹⁵ one has $S(0) = 0.039$. The predicted ratio of threshold drift velocities is 26 which agrees with the observed 24.

The quantity $[(v_d^{\text{thr}})_{\text{hd}}/(v_d^{\text{thr}})_{\text{ld}}]S(0)$ is plotted against T/T_c and n/n_c in Figure IV-25. The value is approximately unity, in agreement with Equation IV-17, for the dense liquid at $n/n_c > 2.2$ and $T/T_c < 0.80$. This range is similar to the "normal liquid" regime $n/n_c > 2.0$ postulated on the basis of electron mobility as a function of density.^{60,208} At lower densities, in the "low density liquid" regime, the above quantity increases due to the rapid increase of χ_T . The density fluctuations increase with χ_T . In Section I it was mentioned that in the critical fluid, where $\chi_T \rightarrow \infty$, it had been predicted that electron localization would occur.⁵⁸ However, localization does not occur,⁵⁹ because the effective electron-molecule interaction distance is much smaller than the correlation length of the density fluctuations in the critical fluid.²¹¹ The above quantity therefore increases rapidly as the critical region is approached (Figure IV-25).

The theory can reproduce experimental results in supercritical ethane²¹² and propane²¹³ if χ_T is replaced by the isentropic compressibility χ_S ,²¹⁴ so $S(0)$ in Equation IV-17 was replaced by $S(K)$ for the low density liquid regime.^{132,139}

$$S(K) = kT/Mc_0^2 = nkT\chi_S \quad \text{IV-19}$$

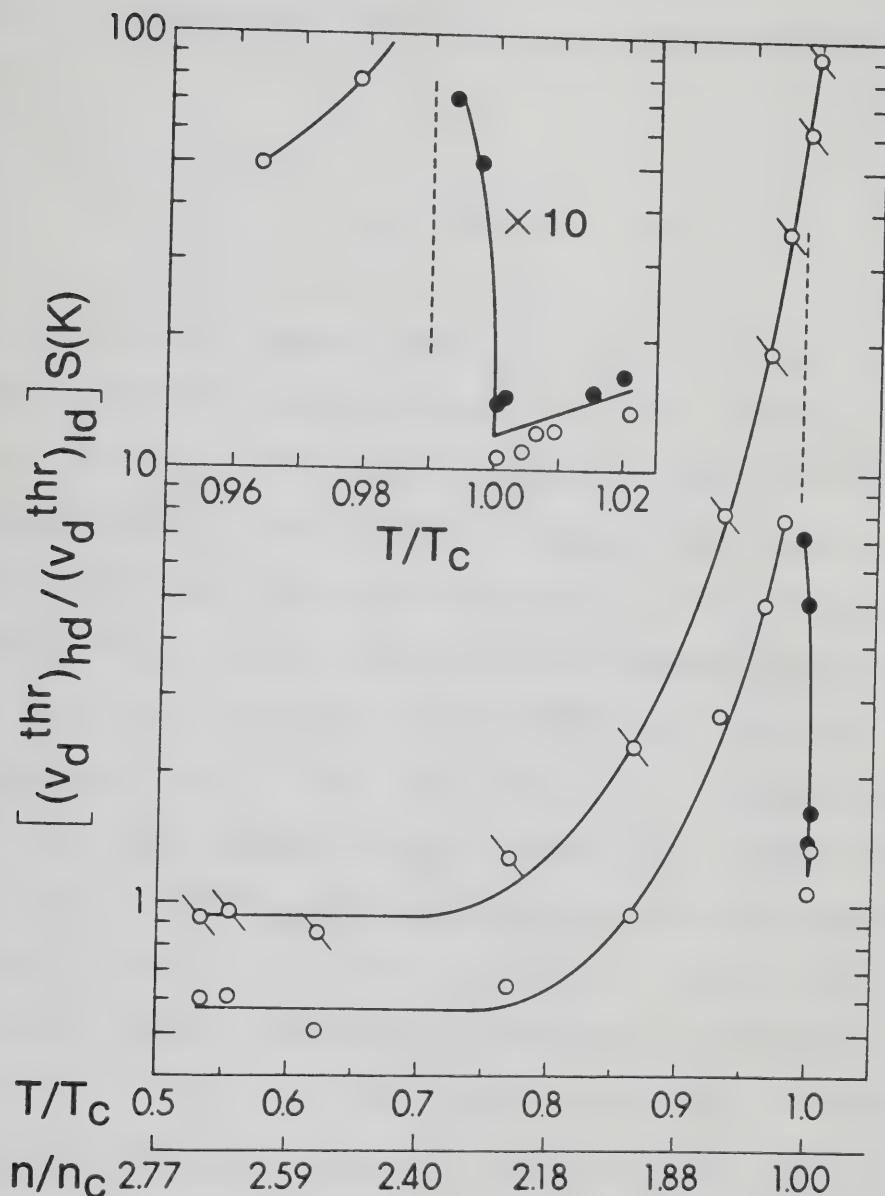


Figure IV-25. Density and temperature dependences of the ratio of the threshold drift velocities in the dense fluids and low density gas normalized by $S(K)$; hd refers to the coexistence liquid and the supercritical gas at n_c ; ld refers to $n=2.95 \times 10^{25}$ molec/m³ and the same temperature as hd. Open points, CH₄; filled points, CD₄; slashed points, $K=0$. The insert is an expansion of the critical region.

where M = molecular mass and c_0 = speed of sound in the fluid.

$$\chi_S = 1/\rho c_0^2 = \chi_T/\gamma \quad \text{IV-20}$$

where ρ = fluid density and γ = heat capacity ratio. The value of $S(K)$ remains finite in the critical fluid.²¹⁴ Values of χ_S for liquid methane were obtained from Reference 214. Those for the supercritical gas at n_c were calculated from the speed of sound in the critical fluid, obtained by a small interpolation between values for the near critical gas and liquid,¹⁹⁶ and adjusted to the appropriate T/T_c by comparison with measurements in critical and supercritical xenon.²¹⁵ The value of $[(v_d^{\text{thr}})_{\text{hd}}/(v_d^{\text{thr}})_{\text{ld}}]S(K)$ is about 0.6 in the normal liquid at $n/n_c > 2.2$. In the low density liquid the quantity increases with increasing density, reaching ~ 9 at $n/n_c = 1.4$ ($T/T_c = 0.99$), passes through a maximum and decreases towards unity in the critical fluid. The quantity increases again with increasing T in the supercritical fluid at n_c . The maximum coincides with the change of sign of $d\mu/dE$ (Figure IV-24).

In Figure IV-26 is reported the variation of the ratio $(v_d^{\text{thr}})/c_0$ with density in all liquids. Threshold drift velocities were estimated from plots of v_d against E/n . Speeds of sound in the liquid deuterio compounds were

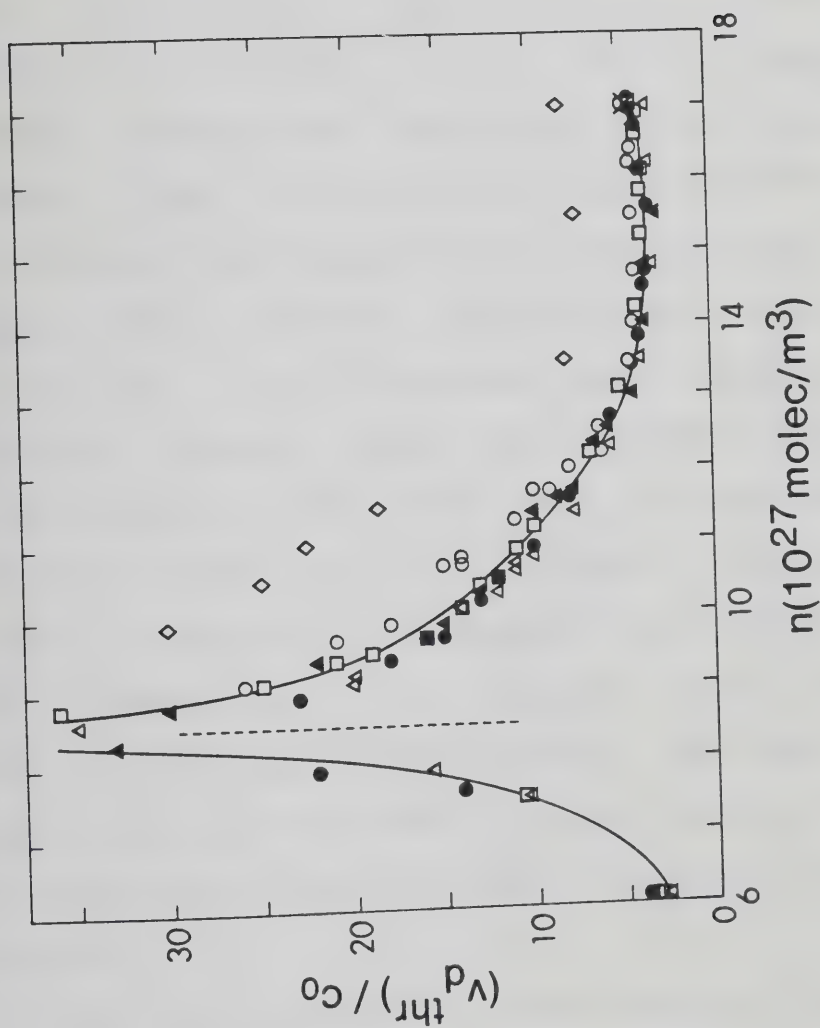


Figure IV-26. Ratio of the threshold drift velocity v_d^{thr} for electron heating to the speed of sound c_0 , as a function of liquid density. Symbols as in Fig. IV-24. Data from Ref. 48, \diamond , reduce to the present curve when the high field drift times are corrected for the radiation pulse width. The X at $n=17 \times 10^{27}$ is an example. The sign of $d\mu/dE$ reverses at 8.5×10^{27} molec/m³ (dashed line).

calculated by reducing the CH_4 values¹⁹⁶ by the square root of the mass ratios. The experimental speeds of sound in liquid CD_4 at 90-115K are 11% lower than those in CH_4 ,¹⁸² compared to the above calculated 12%.

In all methane isomers the ratio $(v_d^{\text{thr}})/c_0 \approx 4$ in the dense liquid (Figure IV-26). In the monoatomic liquids argon, krypton and xenon near their triple points the ratios were approximately unity.²⁰⁶⁻²⁰⁸ Inelastic processes were negligible in the monatomic liquids, but appreciable in methane. The relevant electron energies are $\lesssim 0.1$ eV. No differences were observed between the isotopic isomers, within the experimental uncertainty of $\pm 10\%$ (Figure IV-26). The ratio increases with decreasing density below 14×10^{27} molec/m³, passes through a cusp ≥ 35 at 8.5×10^{27} molec/m³ where the field dependence of μ changes sign, then decreases again. It equals 3 in the slightly supercritical fluids. Near the cusp, electron heating occurs at fields $< (E/n)_{\text{thr}}$ because μ is relatively insensitive to small increases of electron energy in this region.

In Reference 48 the values reported for v_d^{thr} in CH_4 were too high (Figure IV-26) because the X-ray pulse width was not negligible compared to the drift times at high fields, and no correction (see Experimental section) was applied. The value of v_d^{thr} obtained at $n = 17 \times 10^{27}$ molec/m³ from Reference 48 agrees with that in the present

work when the correction is applied (see the X at $n = 17$ in Figure IV-26).

The difference in behavior between methane and the noble liquids is attributed to the contribution of inelastic processes. The behavioral difference between electrons in methane and argon is also noticeable in $(E/n)_{thr}$ (Figure IV-24). The threshold field has a pronounced minimum in argon, but only a shallow minimum in methane. The minima are related to the increase in μ with decreasing n in this region. The differences are again attributed to the larger contribution of inelastic processes to electron-molecule energy exchange in methane.

In methane the ratio $(v_d^{thr})/c_0$ approaches unity in the low density gas (Figure IV-10) and equals approximately 4 at $n \geq 14 \times 10^{27}$ molec/m³. At intermediate densities the ratio rises to a cusp at 8.5×10^{27} molec/m³. Although the increase of the ratio at intermediate densities probably contains a contribution from inelastic processes, the cusp is due simply to the change of sign of $d\mu/dE$. Near the cusp, electron heating becomes appreciable at a field strength lower than that indicated by v_d^{thr} . The heating is not detected because increasing the electron energy ϵ has little effect on μ in this region: $d\mu/d\epsilon \approx 0$.

b. Density Effect

In Figure IV-1 is reported the density normalized mobility as a function of density in the coexistent vapor and liquid phases of CH_4 . The density region up to $n_c = 6.1 \times 10^{27} \text{ molec/m}^3$ has been discussed in the previous sections. In this section the region corresponding to the liquid under its vapor pressure will be examined. The density of the liquid was increased by decreasing the temperature.

The increase in $n\mu$ at densities greater than the critical (Figure IV-1) has been attributed to the formation of a conduction band by overlapping of unoccupied molecular orbitals. This process is not exclusively connected to liquid phase behavior; it begins to be important in the dense gas. It was mentioned in the previous section that in the region where $n\mu$ decreases with n in the saturated CH_4 vapor, the value of the quasifree electron mobility μ_0 increases.⁴⁶ This means that electron motion is less hindered as the vapor density is increased. In the saturated vapor, however, the effect of quasilocalization in density fluctuations tends to overcome the effect of conduction band formation. In Figure IV-27 are reported values of the low field mobility as functions of the saturated vapor density. Around the critical density the mobility goes through a minimum. In this figure the last

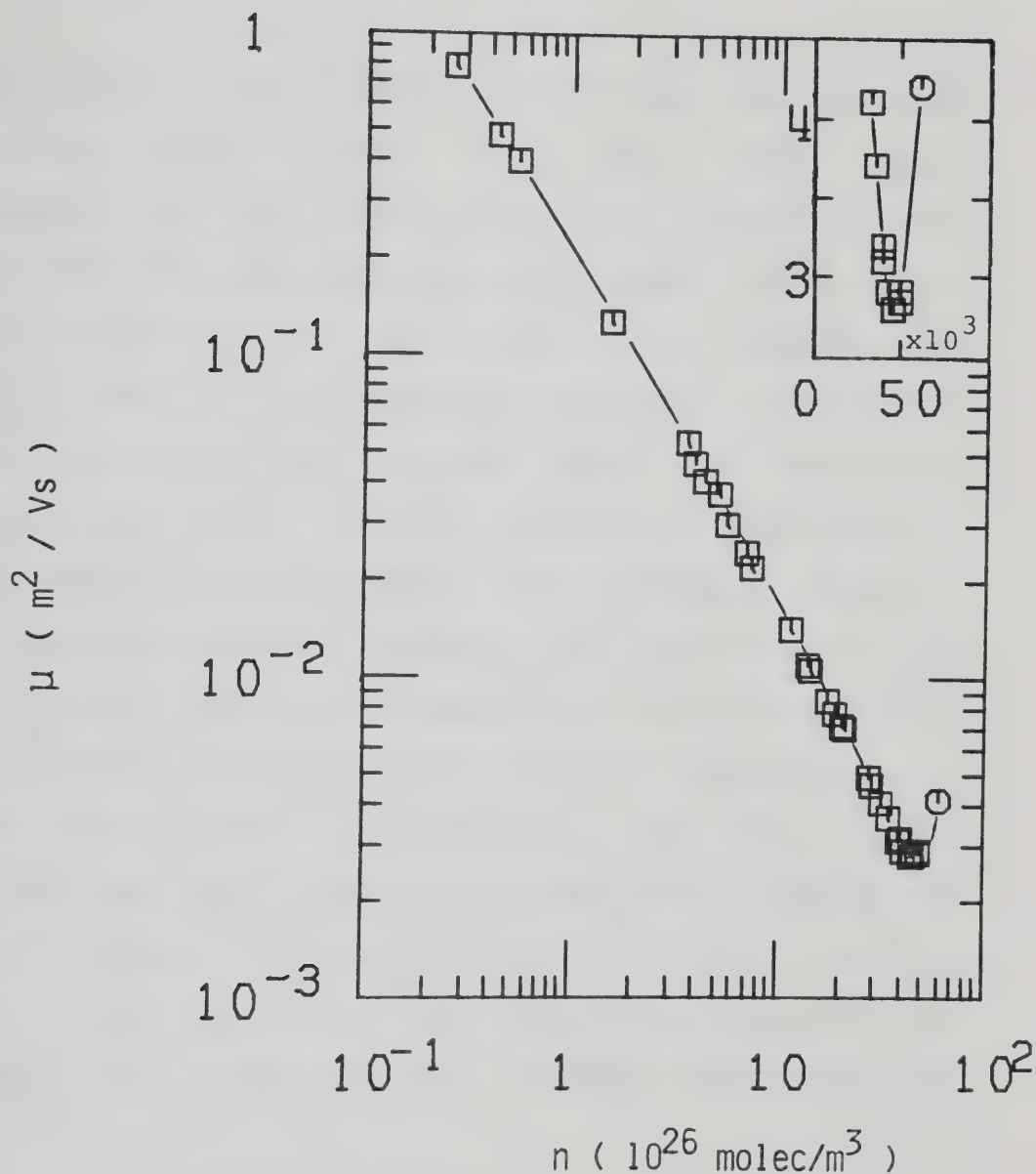


Figure IV-27. Plot of the electron mobility (low field) against the density in saturated CH_4 vapor. \circ represents the supercritical fluid at n_c and $T_c + 0.1\text{K}$. The insert is an expansion of the critical region. These points have been multiplied by 1000.

point on the coexistence curve and the first point in the supercritical fluid differ by 0.5K. The point corresponding to the critical fluid is thought to be between these two points but somewhat closer to the value in the supercritical gas since the latter is $T_c + 0.1K = 190.7K$. Conduction band formation counteracts quasilocalization in the coexistent vapor. This phenomenon takes place in a very limited temperature range which, however, corresponds to a fairly large change in density. It was also monitored by observing the appearance of two ramps on cooling from the supercritical fluid in the cell (see Experimental section) which allowed measurements in vapor and liquid phases simultaneously. The measurements in the critical region were always performed on cooling to minimize the effect of gravity which would induce density gradients. For this reason the top part of the cell was also kept two or three tenths of a degree cooler than the bottom.

The most important molecular property affecting electron transport in the liquid phase of simple hydrocarbons is the degree of sphericity.^{72,75} The density dependence of n_μ in spherelike methane is similar to that in spherical argon and xenon (Figure IV-28). On going from the near critical fluid to the mobility maximum, n_μ increases 5300 fold in xenon, 40 fold in methane and 10 fold in argon. Although it would have been more direct to

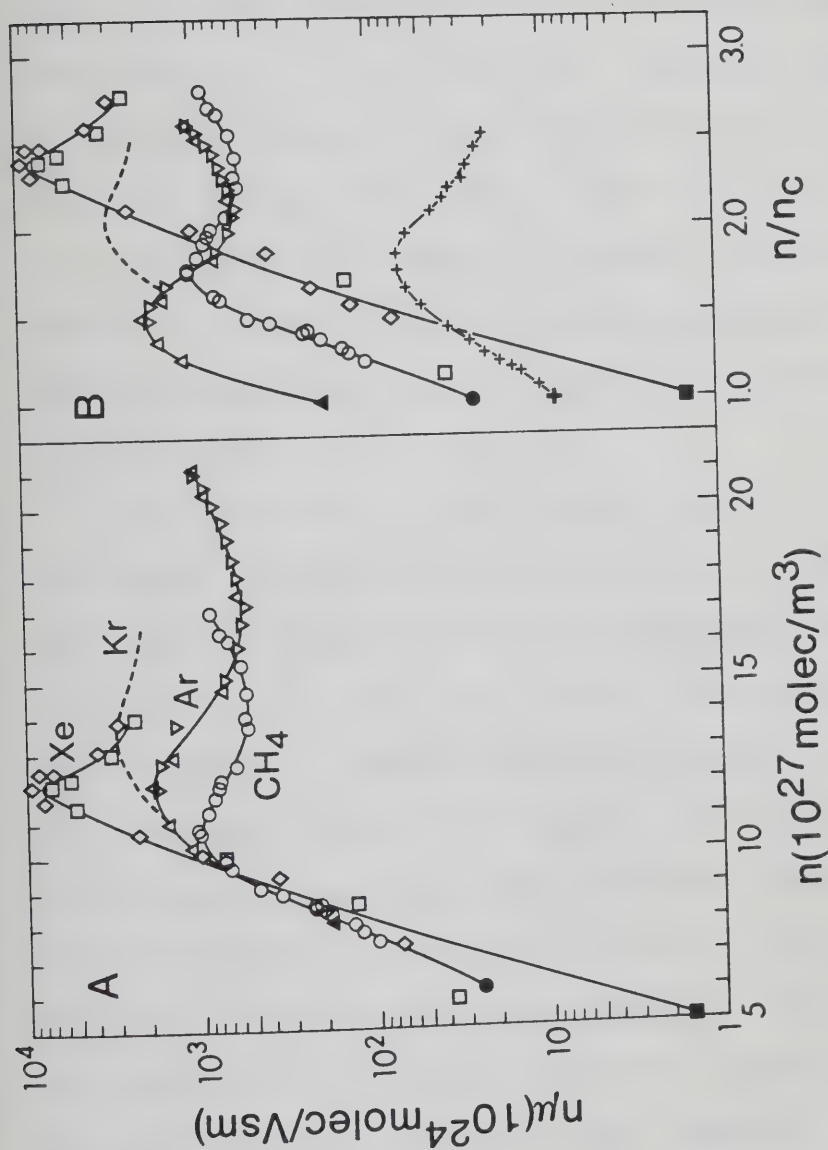


Figure IV-28. Density normalized electron mobilities plotted against the density (A) and reduced density (B) in the noble liquids and CH_4 . The critical densities ($10^{27} \text{ molec/m}^3$), symbol, Reference, pressure and field strength were as follows. CH_4 , 6.1, \circ , this work, vp (vapor pressure), 1fl (low field limit). Ar, 8.1, ∇ , Ref. 91, 55 atm, extrapolated to zero field; Δ , Ref. 208, vp, 1fl. Kr, 6.6, ---, Ref. 127a, 15-69 atm, -10 KV/m. Xe, 5.1, \diamond , Ref. 58, vp, 1fl; \square , Ref. 207, vp, 1fl. The results of Ref. 58 were low by a factor of 2 and have been corrected. Neopentane, 1.92, +, Ref. 57 and 98, vp, 1fl. The dark points represent near critical vapors at $n_c, T_c + 0.1 \text{ K}$.

plot μ against n for the liquid phase, $n\mu$ was chosen to facilitate comparison with gas phase results (see Figure IV-1). The data are presented both as functions of n and of n/n_c . The densities at the mobility maxima increase in the order $\text{CH}_4 < \text{Ar} \approx \text{Xe} < \text{Kr}$. However, the value of n/n_c at $n\mu_{\text{max}}$ increases on increasing the molecular size in the order $\text{Ar} < \text{CH}_4 < \text{Xe} < \text{Kr}$. The value of $n_c\mu$ in the near critical gas is lowest in xenon because xenon has the largest polarizability (largest scattering cross section in the gas phase) and the lowest n_c . The reverse is true for $n_c\mu$ in argon.

The increase in $n\mu$ (Figure IV-28) in methane and in the noble liquids at densities above the critical is due to the establishment of the conduction band and to the decrease in magnitude of density fluctuations connected to the decrease in compressibility of the liquids. In Ar and CH_4 the mean free path between scattering events of the thermal electrons is ~ 100 molecular diameters. A large angle scattering event will randomize the momentum of the electron. In Ar and CH_4 the electron will travel for about 100 molecular diameters suffering small angle collisions during its path before the momentum is randomized. Electrons in the band are scattered by potential fluctuations produced by spacial and orientational disorder. Argon and methane are spherelike species, of roughly the same size and isotropically polarizable. In

these liquids the conduction band is relatively smooth. Potential fluctuations are small compared to thermal energy, therefore isolated scattering events will only contribute a fraction to the randomization of the electron momentum. On the other hand, in liquid ethane, a rodlike molecule, a potential fluctuation can be deep and wide enough that an electron can become localized in it.

A maximum in mobility is observed in methane and in the noble liquids (Figure IV-28). The density normalized mobility maximum $n\mu_{\max}$ occurs at 10.8, 12.0, 12.1 and 13.7 (10^{27} molec/ m^3) in methane, argon, xenon and krypton, respectively. The maximum is interpreted in terms of the zero scattering length model of Lekner.^{132,139} The scattering length changes from positive at high densities to negative at low densities. Although it passes through zero at a certain density, the mobility remains finite due to density fluctuations. The change of sign of the scattering length is confirmed by the change of sign of the field dependence of μ : $d\mu/dE$ changes from negative at high densities to positive at a density ~20% below that of the mobility maximum in methane, argon²⁰⁸ and xenon.²⁰⁷

The Lekner equation for μ_{\max} is¹³²

$$\mu_{\max} = \left[\frac{63eM\delta^7}{24} \left(\frac{2}{\pi m} \right)^{1/2} \left(\frac{a_o}{R_s \alpha f_L} \right)^2 \right] \frac{c_o^2}{(kT)^{3/2}}, \text{ m}^2/\text{Vs} \quad \text{IV-21}$$

where $e(C)$ and $m(kg)$ are the electron charge and mass, respectively, δ is the molecular hard core diameter which is taken as $n_s^{-1/3}$ for the solid at the triple point, a_0 is the Bohr radius, $R_s = (3/4\pi n)^{1/3}$ is the Wigner-Seitz radius for the liquid at the density of μ_{max} , α is the molecular polarizability, and $f_L = [1 + (8/3) \pi n \alpha]^{-1}$ is the Lorentz local-field function.

Equation IV-21 gave μ_{max} about 20% larger than the experimental values in argon, krypton and xenon.²⁰⁸ For methane the calculated values of μ_{max} are too high by a factor of 2.1 in CH_4 and 2.6 in CD_4 (Table IV-2). Equation IV-21 applies less well to molecules that are less perfect spheres and that have internal degrees of freedom, which provide greater undulations in the conduction band lower potential surface and sources of inelastic scattering. It was suspected then that the trend would continue to neopentane, $C(CH_3)_4$, which is a still more distorted sphere and has more internal degrees of freedom than methane. The ratio calc/expt is 4.7 (Table IV-2). Mobilities in neopentane^{57,98} are included in Figure IV-28B. Physical data required in Table IV-2 and not otherwise listed were obtained from References 216-220.

The maximum in the mobility curve has been correlated with a minimum in the conduction band energy V_0 as a function of density, which minimizes the potential fluctuations.¹³⁶⁻¹³⁹ In the absence of accurate electron-

Table IV-2 Calculation of μ_{\max} from equation IV-21.

	Ar	Kr	Xe	CH ₄	CD ₄	C(CH ₃) ₄
M(10 ⁻²⁸ kg)	663	1391	2180	266	333	1198
α (10 ⁻³⁰ m ³)	1.63 ^a	2.47 ^a	4.01 ^a	2.60 ^f	2.54 ^f	10.2 ⁱ
T _C (K)	150.9 ^a	209.4 ^a	289.7 ^a	190.6	189.2	433.8 ^m
n _C (10 ²⁶ molec/m ³)	80.8 ^a	66 ^a	51 ^a	60.8	61.4	19.4 ^m
T _{μ_{\max}} (K)	147 ^b	180 ^d	223 ^e	177	179	405 ^j
n _{μ_{\max}} (10 ²⁶ molec/m ³)	121 ^b	133 ^d	120 ^e	107	104	35 ^j
c _O (m/s)	257 ^c	398 ^c	470 ^c	540 ^g	475 ^g	435 ^k
δ (10 ⁻¹⁰ m)	3.44 ^a	3.67 ^a	3.95 ^a	3.80 ^h	3.78 ^h	5.59 ^l
R _S (10 ⁻¹⁰ m)	2.70	2.62	2.71	2.81	2.84	4.09
f _L	0.86	0.78	0.71	0.81	0.82	0.77

Table IV-2 (continued)

calc (m^2/Vs) μ_{max}	0.19	0.61	0.69	0.21	0.19	0.089
expt (m^2/Vs) μ_{max}	$\geq 0.16^b$	$\sim 0.50^d$	$\geq 0.60^e$	0.10	0.072	0.019 ^j
calc/expt	1.2	1.2	1.2	2.1	2.6	4.7

a. Ref. 216. δ obtained from density of solid at triple point.

b. Ref. 208. μ measured at 2.4 kV/m, which is in the field-dependent region at this density.

c. Ref. 217.

d. Ref. 127a. μ estimated from field-dependent values at 1.5, 1.0 and 0.5 kV/m.

e. Ref. 207. μ measured at 3.0 kV/m, in the field dependent region at this density.

f. Ref. 182.

g. Ref. 196. In CD_4 , $c_0 = \sqrt{16/20}$ x value in CH_4 at same T/T_c .

h. Ref. 198.

i. Ref. 218.

j. Refs. 57 and 98.

k. Calculated from c_0 in iso-pentane at same T/T_c from ref. 219.

l. Ref. 77.

m. Ref. 220.

molecule interaction potentials, it is not yet possible to calculate from theory the values of n where $V_{O,min}$ and μ_{max} occur. All the models require an adjustable parameter such as the hard core diameter,²²¹ or input of the observed value of $n_{\mu_{max}}$.¹³²

The factors in Equation IV-21 that favor a large μ_{max} are: a) large molecules with not much space to move around, $\delta^7/R_s^2 = (n_{\mu_{max}})^{2/3}/(n_s)^{7/3}$; b) large c_o , which reflects a small compressibility; c) large molecular mass and low temperature, $M/T^{3/2}$, which gives a small molecular displacement velocity; d) small polarization interaction, but it must be large enough to give a negative scattering length at low densities so that a conduction band can form at high densities. Factors a), b) and c) lead to low positional disorder, hence low potential fluctuations; d) refers to the nature of the electron-molecule interactions and is why the model does not apply to helium and neon, which have positive scattering lengths in the gas phase.²²²

If the molecules are not spherical, orientational disorder also contributes to the potential fluctuations that scatter electrons in the conduction band. There is no factor in Equation IV-21 that accounts for orientational disorder, so for progressively less spherelike molecules μ_{max} falls farther below that calculated from the equation. When the potential fluctuations are sufficiently large, quasilocalized^{48,207,208,223} and localized⁵² states

of the electron can form, which further decrease the measured μ . A possible interpretation of the relative insensitivity of $(E/n)_{thr}$ to deuteration of methane (Figure IV-24) is that shallow trapped states²²⁴ are involved. The same would then be true in neopentane, although shallow trapped states are negligible in argon and xenon at $n \gtrsim n_{\mu max}$.^{208,225}

Returning now to the discussion of the variation of $n\mu$ with n (Figure IV-28), the shallow minimum at $n \approx 14 \times 10^{27}$ molec/m³ arises from the transition between a region where decreasing the density loosens the structure and decreases the magnitude of the positive scattering length, and a region where increasing the density creates more order and decreases the structure factor. The liquids are under their vapor pressure, so increasing density is associated with decreasing temperature.

c. Isotope Effect

In Figure IV-29 the density normalized mobility in CH₄ is compared to that in the deuterated analogues. The same comparison is reported in Figure IV-30 as plots of the mobility against the reduced temperature T/T_c . The reduced temperature was used to normalize for small differences in critical temperatures (Table II-1). In Figure IV-31 is reported an expansion of the critical region. All of the

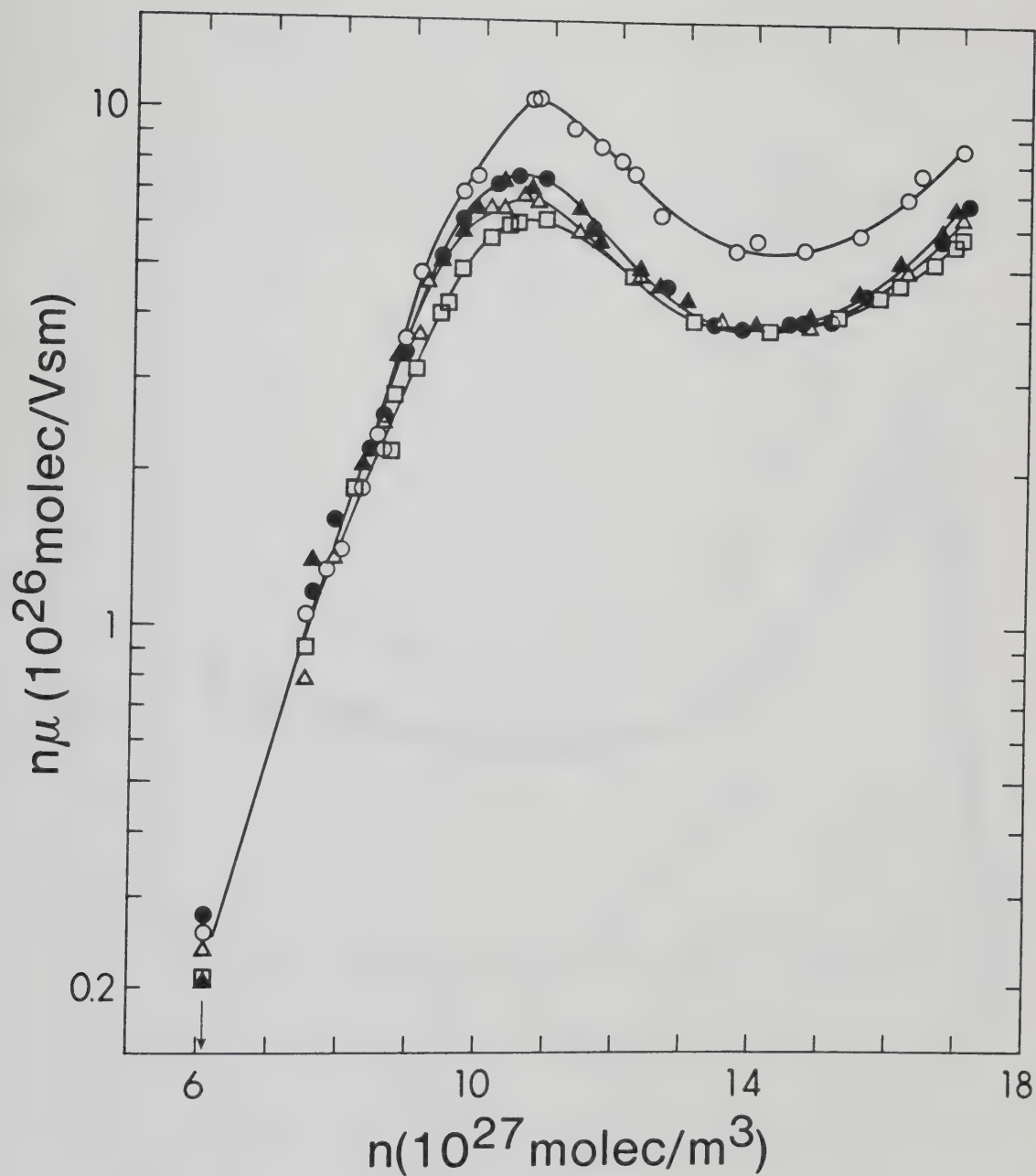


Figure IV-29. Density dependence of low field $n\mu$ in the liquid methanes. Symbols as in Figure IV-24. The arrow indicates the critical density.

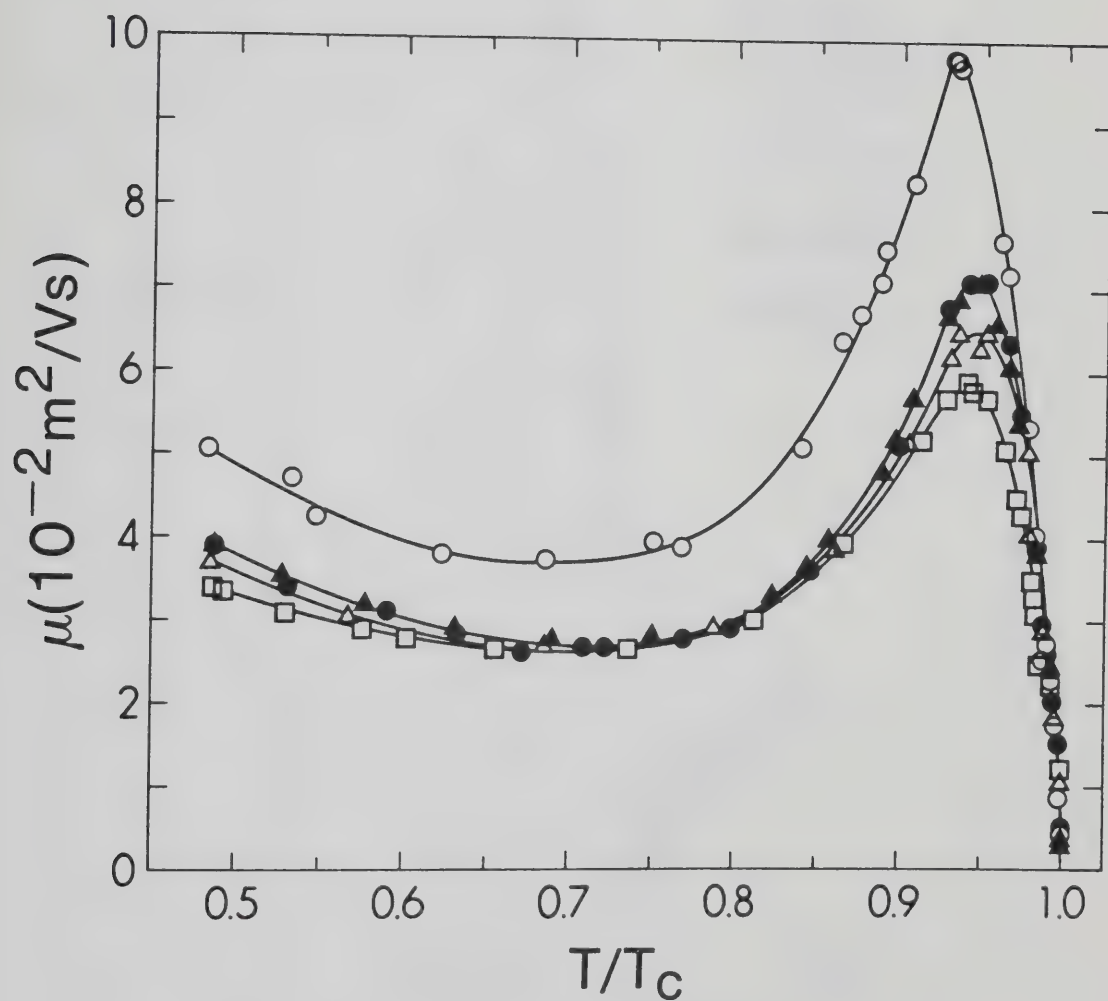


Figure IV-30. Thermal electron mobilities (low field) in coexistence liquid methanes as functions of the reduced temperature T/T_C . Symbols as in Figure IV-24.

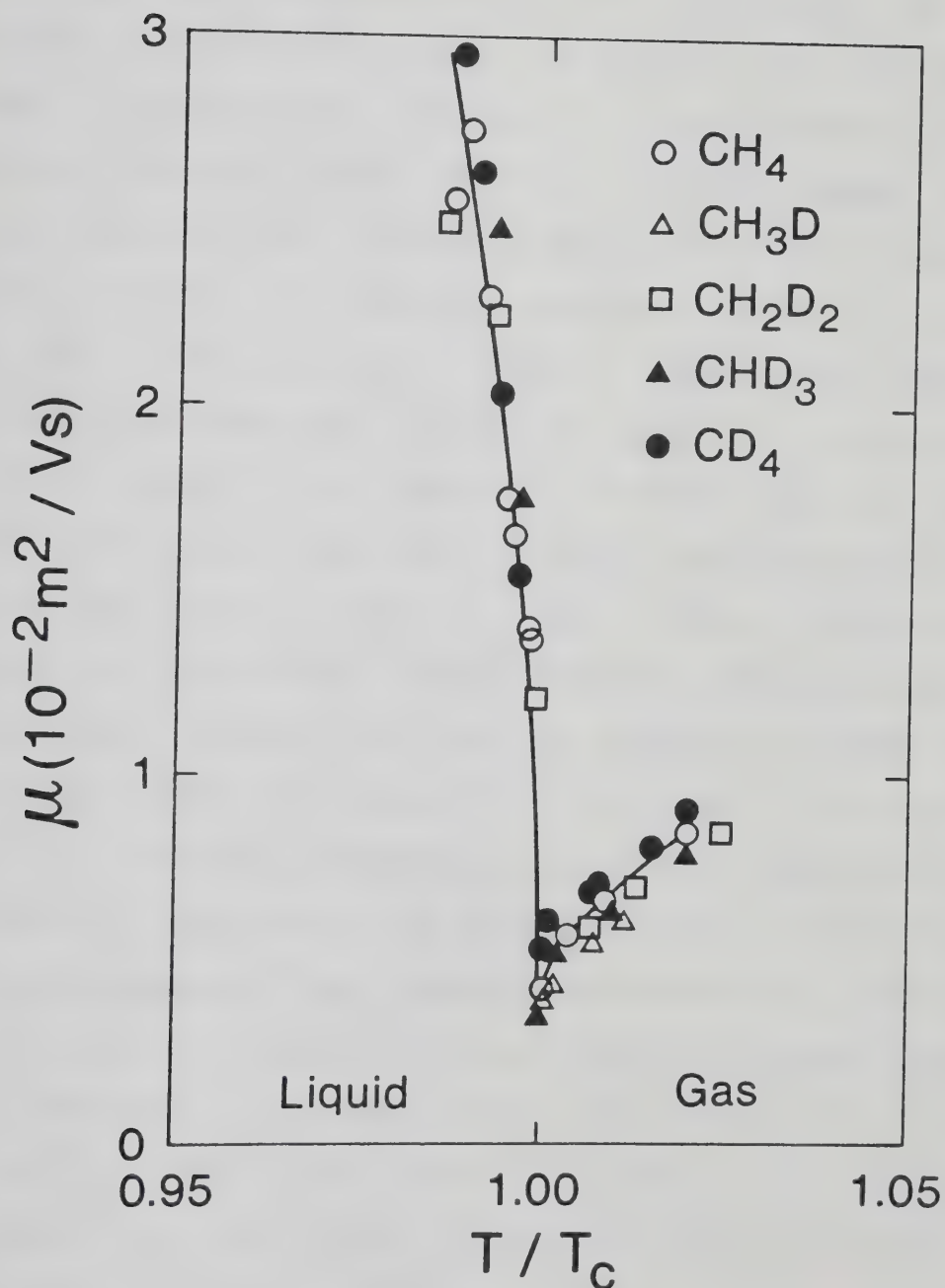


Figure IV-31. Thermal electron mobilities (low field) in coexistence liquid and supercritical methanes as functions of the reduced temperature T/T_c in the vicinity of T_c . Symbols as in Figure IV-24.

features observed in CH_4 are also present in the deuterated derivatives. The variation of μ with temperature in the coexistence liquid is similar in each of the isotopic methanes (Figure IV-30). However, μ is ~30% lower in the deuterated methanes than in CH_4 . In each liquid the mobility has a shallow minimum at $T/T_c \approx 0.7$ and a maximum at $T/T_c \approx 0.94$. The mobility maximum decreases in the order $\text{CH}_4 > \text{CD}_4 \approx \text{CHD}_3 > \text{CH}_3\text{D} > \text{CH}_2\text{D}_2$ with ratios 1.00:0.73:0.72:0.66:0.59. A similar pattern occurs near the triple point. By contrast the mobilities at the minimum are nearly the same in each of the deuterio-methanes and 0.72 of that in CH_4 . These differences disappear at the critical point (Figures IV-30 and 31). The molecular symmetry of CH_4 is slightly altered by deuteration. The CH_4 molecule in the ground vibrational state is a regular tetrahedron, which is isotropically polarizable. Replacement of hydrogen atoms by deuterium introduces asymmetry and changes the moment of inertia (Table II-1). On going from CH_4 to CH_3D the average dipole moment increases a thousand times from 5.4×10^{-6} D to 5.6×10^{-3} D. Two of the moments of inertia increase by 35%, and so on. The values of μ_{max} are quite different, being largest in CH_4 and smallest in CH_2D_2 (Figure IV-32), which has the largest dipole moment and largest unbalance in moments of inertia (Table II-1). In the critical region the mobilities are the same in all the isotopic methanes,

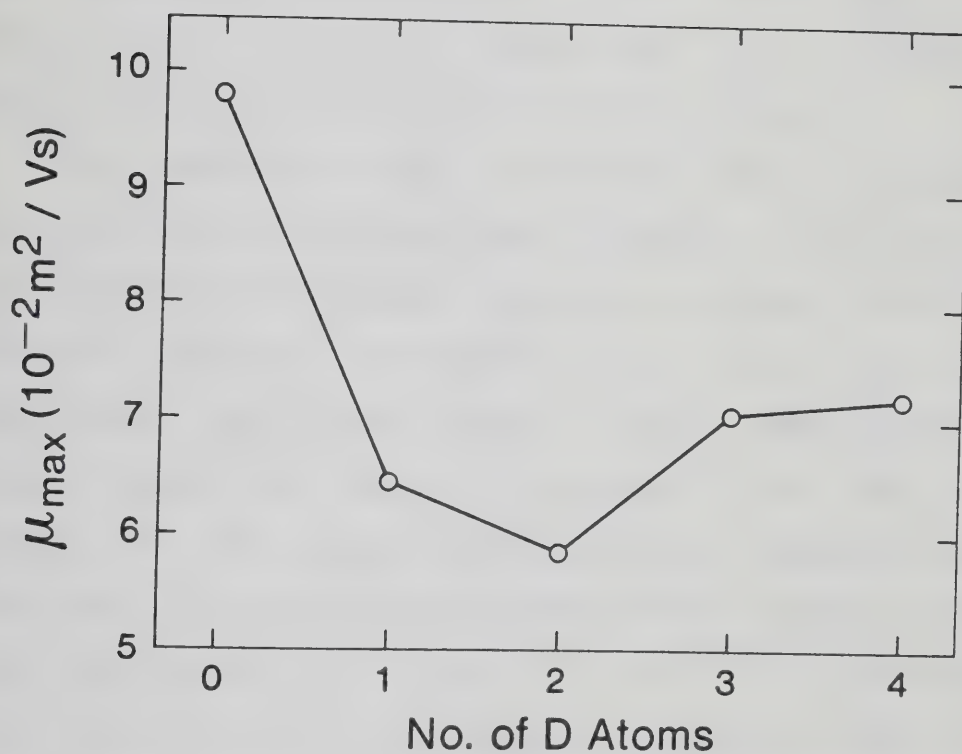


Figure IV-32. Electron mobilities at the temperature of the maximum μ_{max} as functions of the number of deuterium atoms substituted for hydrogen in CH_4 .

within the experimental uncertainty (Figure IV-31). The density fluctuations in this region dominate the electron scattering, and small differences in molecular properties are relatively unimportant at a given $n/n_C < 1.4$, $T/T_C > 0.990$. By comparison μ_{\max} occurs at $n/n_C \approx 1.72 \pm 0.05$, with $T/T_C = 0.94 \pm 0.01$.

The relative changes in mobility caused by deuteration are displayed by plotting the ratios of μ in CH_4 to that in the deuterated compounds against n (Figure IV-33). On average, electron mobilities in the liquids are in the order $\text{CH}_4 > \text{CD}_4 \approx \text{CHD}_3 > \text{CH}_3\text{D} > \text{CH}_2\text{D}_2$. The curves have a shape similar to that of μ against n , but the relative changes in the ratios are an order of magnitude smaller than that in the mobilities themselves (Figures IV-33 and 29). The factors that govern the mobility are sensitive to the unbalancing of the molecule by isotopic substitution. The ratio $\mu_{\text{CH}_4}/\mu_{\text{D}}$ is largest for the most unbalanced molecule, CH_2D_2 , and the next largest for CH_3D . However, it is not clear why the ratio is nearly the same for CD_4 and for CHD_3 .

Inelastic collisions make an important contribution to electron-molecule energy exchange in liquid methane even at energies < 0.1 eV. The low energy indicates that phonons²²⁶ and molecular rotations are involved. Both motions are affected by isotopic substitution. The lattice vibrational energies are related to the van der Waals forces and are

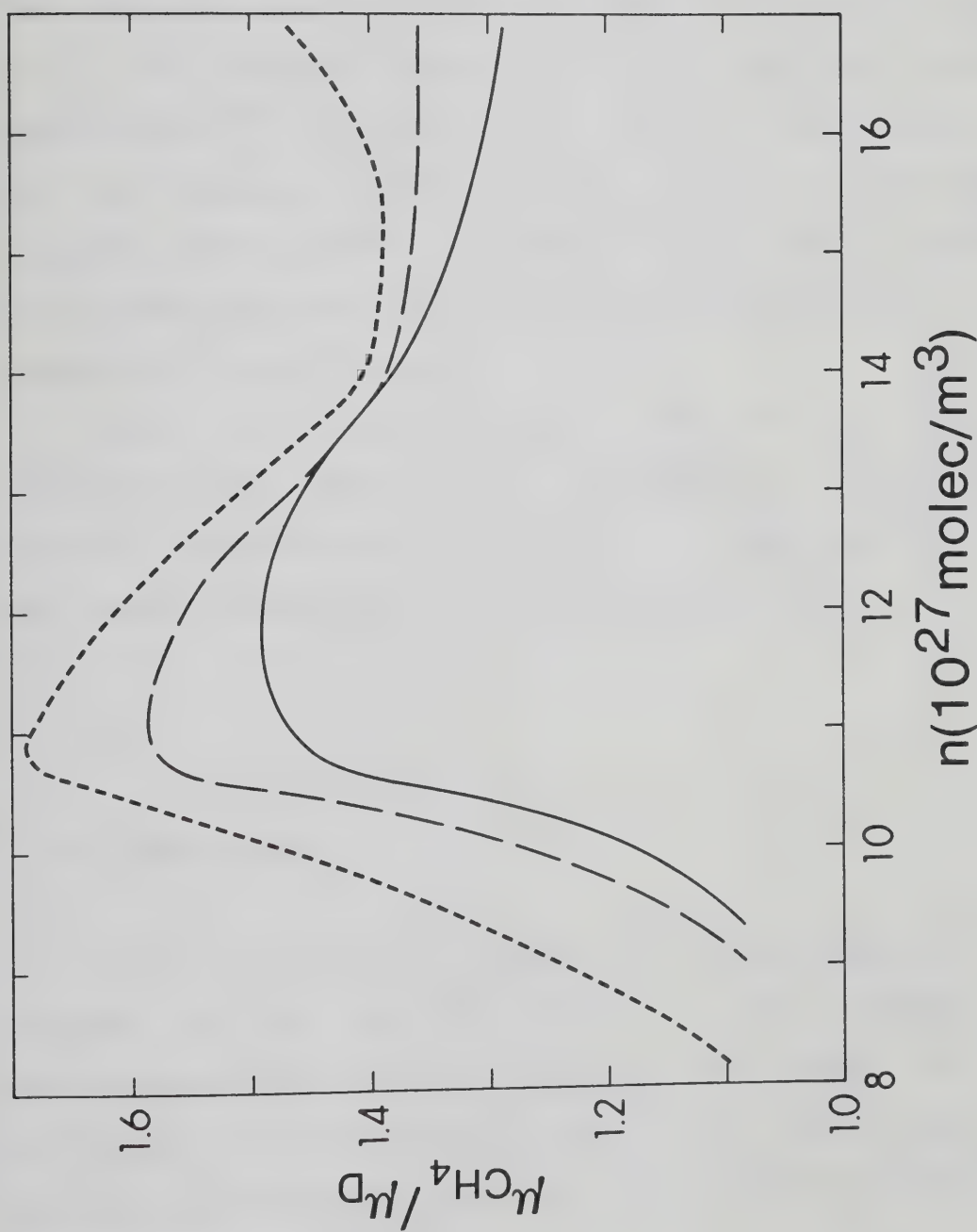


Figure IV-33. Ratios of the mobility in liquid CH_4 to that in the deuterated compounds $\mu_{\text{CH}_4}/\mu_{\text{D}}$, as functions of density n . —, CH_4 and CD_4 ; ---, CH_3D ; ····, CH_2D_2 .

inversely proportional to the square root of the mass. The intermolecular forces are nearly the same in CH_4 and CD_4 . The moment of inertia of CD_4 is double that of CH_4 (Table II-1); the rotational constants $2B_0$ are 0.64 and 1.30 meV, respectively.¹⁹⁹ Quasispherical molecules such as CH_4 and CD_4 are commonly treated as free rotors, but the vapor pressure isotope effect (see Section I-E) offers evidence of hindered rotation in the liquid and solid phases in the temperature range 70-120K.

It is not clear why the curves of the deuterio compounds come together in the vicinity of 14×10^{27} molec/ m^3 (Figures IV-29, 30 and 33). There might be two overlapping mechanisms that are shape sensitive.

B. Ions

1. Low Density Gas

As in the case of electrons, an ion of mass m in the presence of an electric field E will undergo an acceleration eE/m , gaining energy. The energy lost by collisions with molecules of mass M is proportional to m/M . The average drift velocity in the direction of the field is given by^{104,227}

$$v_d = \frac{3}{4} \frac{e}{M_r \langle v \rangle \sigma} \left(\frac{E}{n} \right) \quad \text{IV-22}$$

where M_r is the reduced mass of the ion-molecule system

$$M_r = \frac{mM}{m+M} \quad \text{IV-23}$$

$\langle v \rangle$ is the average relative velocity which for a Maxwellian distribution is given by

$$\langle v \rangle = (8kT/\pi M_r)^{1/2} \quad \text{IV-24}$$

e is the electronic charge, k Boltzmann's constant, T the absolute temperature, n the number density of the molecules and σ the scattering cross section.

Equation IV-22 can be rewritten as

$$\frac{nv_d}{E} = n\mu_+ = 0.47 \frac{e}{(M_r)^{1/2} (kT)^{1/2} \sigma} \quad \text{IV-25}$$

where μ_+ is the mobility of the ion.

According to Equation IV-25, if σ were independent of temperature, that is velocity, the density normalized mobility should vary as $T^{-1/2}$

In Figures IV-34 and 35 are reported the temperature dependencies of the density normalized ion mobility in gaseous CH_4 at $n = 2.95 \times 10^{25}$ molec/ m^3 and in gaseous CD_4 , where measurements were taken in a wider density range, at $n = 0.25, 3.2$ and 5.0 (10^{25} molec/ m^3). From these data it

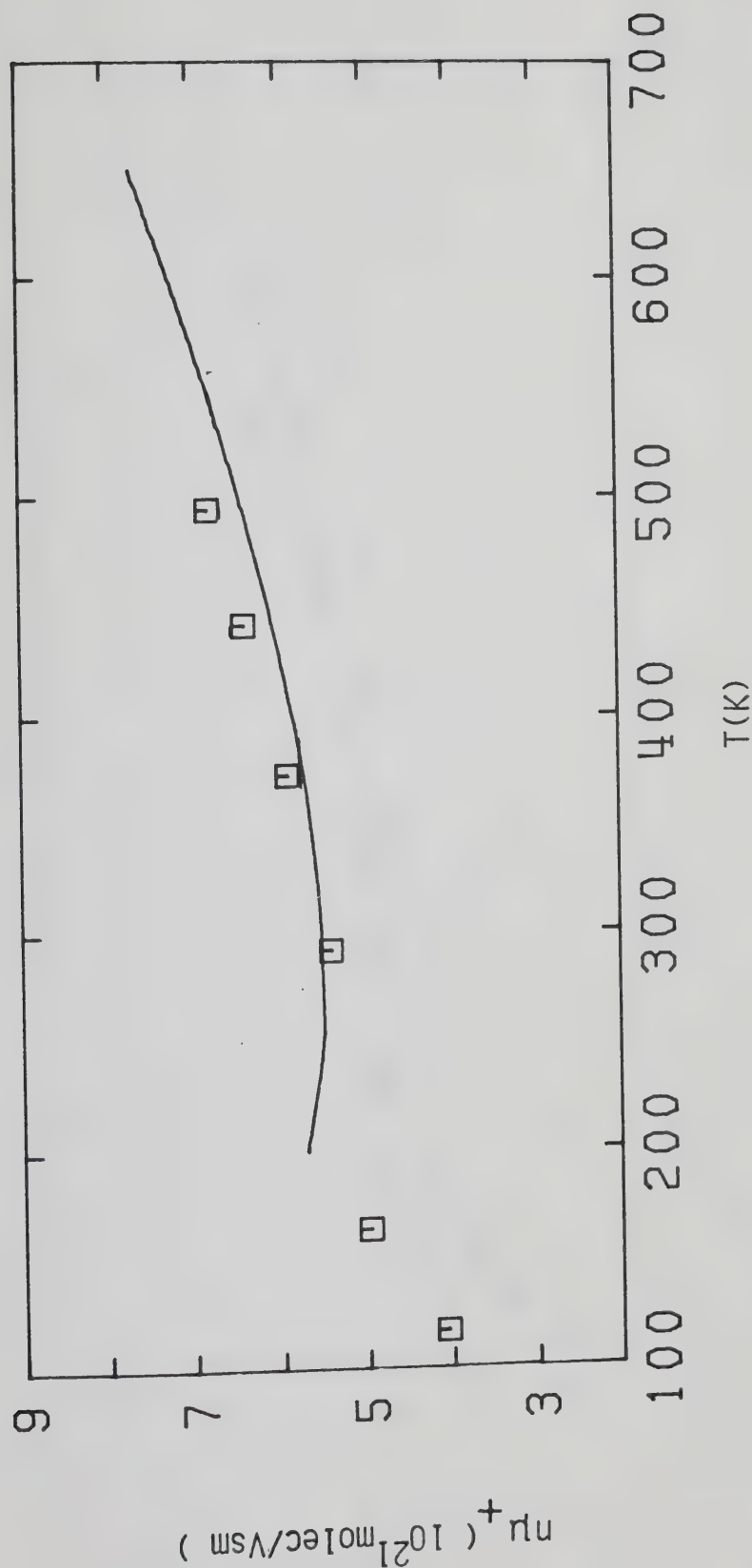


Figure IV-34. Density normalized cation mobilities in CH₄ gas at $n = 2.95 \times 10^{25} \text{ molec/m}^3$ as functions of temperature. The solid line was obtained from curve A in Fig. IV-36.

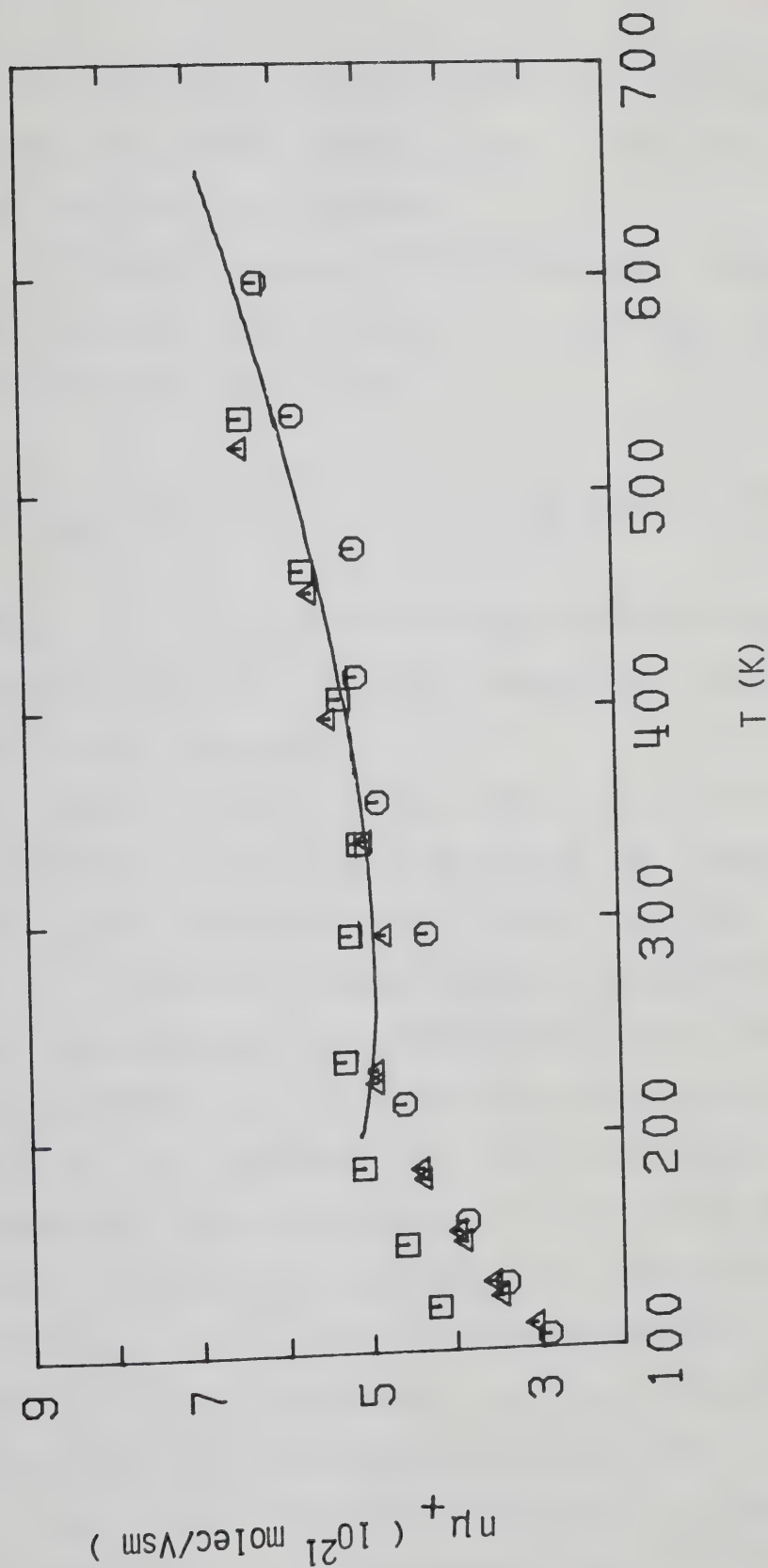


Figure IV-35. Density normalized cation mobilities in low density CD_4 gas at different density ($10^{25} \text{ molec/m}^3$) as function of temperature. \square , 0.25; \circ , 3.20; Δ , 5.0. The solid line was obtained from curve A in Figure IV-36.

can be seen that $n\mu_+$ does not follow a $T^{-1/2}$ dependence and in CD_4 the lowest density gives a higher set of values in the low temperature region.

Viehland and Mason^{116,117} developed a model similar to that proposed for electrons to calculate ion mobilities. The resulting equation is

$$n\mu_+ = \frac{3e}{8M_r} \sqrt{\pi} \left(\frac{2kT}{M_r}\right)^{5/2} / \int_0^{\infty} v^5 \sigma_m^+ \exp(-M_r v^2/2kT) dv \quad \text{IV-26}$$

where v is the relative velocity of the ion with respect to molecule and σ_m^+ is the ion-molecule scattering cross section for velocity v .

Equation IV-26 was used to calculate density normalized mobilities as functions of temperature in CH_4 and CD_4 in a manner similar to that used for electrons. A σ_m^+ vs. ϵ curve was chosen and adjusted until the calculated $n\mu_+$ values matched the experimental ones. The calculation was performed in the temperature region 200-600K. Below 200K it was thought that the variation of $n\mu_+$ with temperature was dominated by clustering effects which should become more important on approaching the vapor saturation curve. This argument is supported by the higher values of $n\mu_+$ obtained in CD_4 at a density lower by a factor of 20 than the other two densities.

The result of this calculation is shown in Figure IV-36 by line A. It was assumed that the ions were mainly

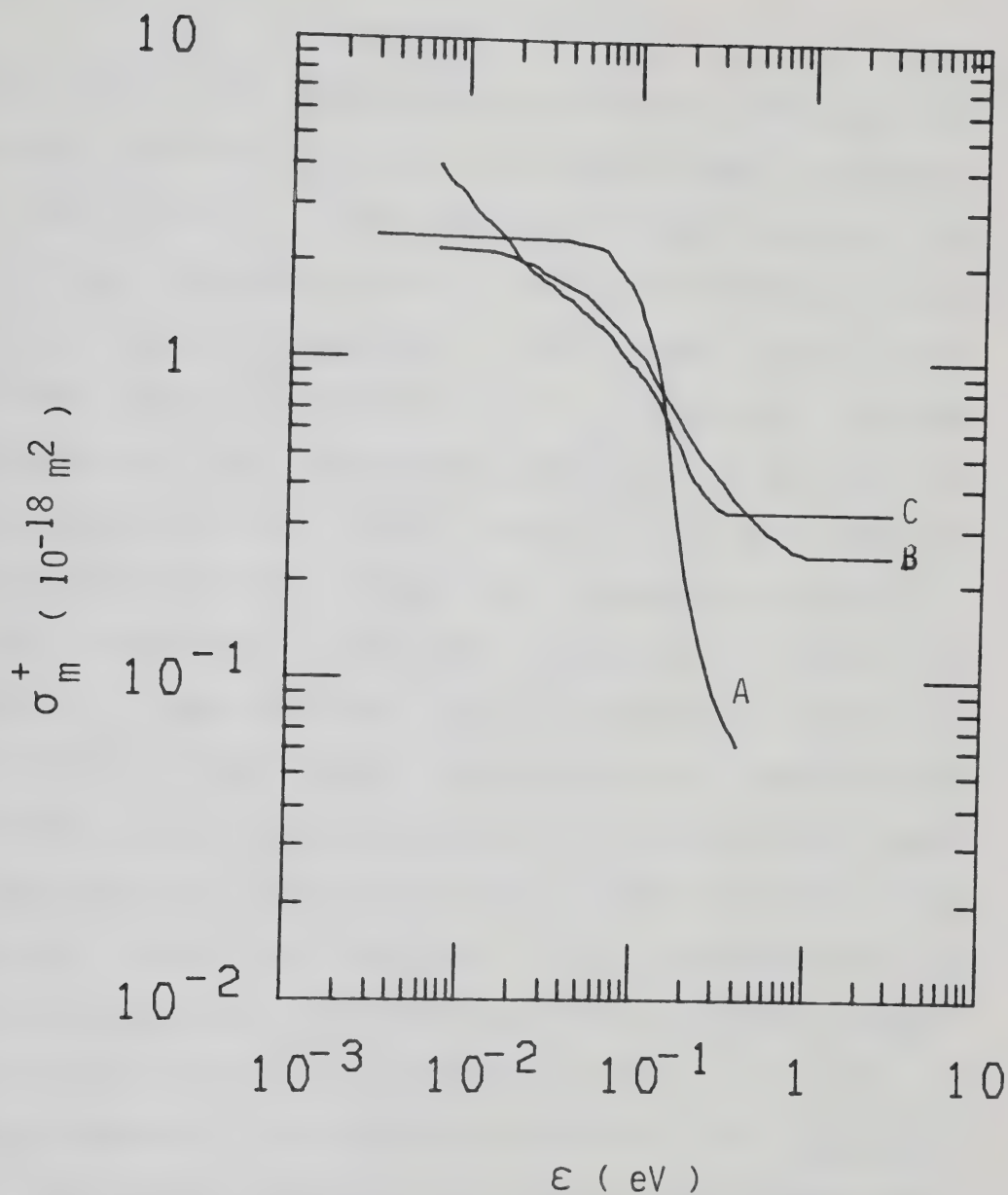


Figure IV-36. Ion-molecule momentum transfer cross sections σ_m^+ of CH_4 molecules as functions of energy .
 A : present data, CH_5^+ ions. B: obtained from data of Reference 203, CH_5^+ ions. C: obtained from data of Reference 203, C_3H_7^+ ions.

CH_5^+ (or CD_5^+). The calculated values of $n\mu_+$ obtained with this cross section are shown as solid lines in Figures IV-34 and IV-35. The extracted cross section is approximately constant up to $\epsilon \approx 0.05$ eV and then it drops sharply at higher energies. This rapid drop is an indication that clustering is an important process contributing to the temperature variation of $n\mu_+$ even at those temperatures ($T > 200\text{K}$) where $n\mu_+$ is the same for densities different by a factor of 20 (see Figure IV-35).

Gee and Freeman⁵² found that the effect of clusters is to produce a steep minimum in the calculated scattering cross section. They forced the behavior in dense ethane gas into the single-scatterer model for electrons and found that increasing the density to $n/n_c = 0.25$ had the effect of greatly raising the apparent cross sections at low energies and lowering the cross sections at high energies thereby giving raise to a deep minimum.

Saporoshenko²⁰³ measured mobilities of ions identified by mass spectrometry as functions of the applied electric field strength normalized by density, E/n (Td), in electron irradiated CH_4 gas as $300 \pm 5\text{K}$ in the pressure range 0.7 - 1.3 torr. He measured mobilities for CH_5^+ , C_2H_5^+ , C_3H_5^+ and C_3H_7^+ . The results for CH_5^+ and C_3H_7^+ are shown in Figure IV-37. They are given as density normalized mobilities, $n\mu_+$, against the density normalized electric field strength, E/n . The density normalized mobility in

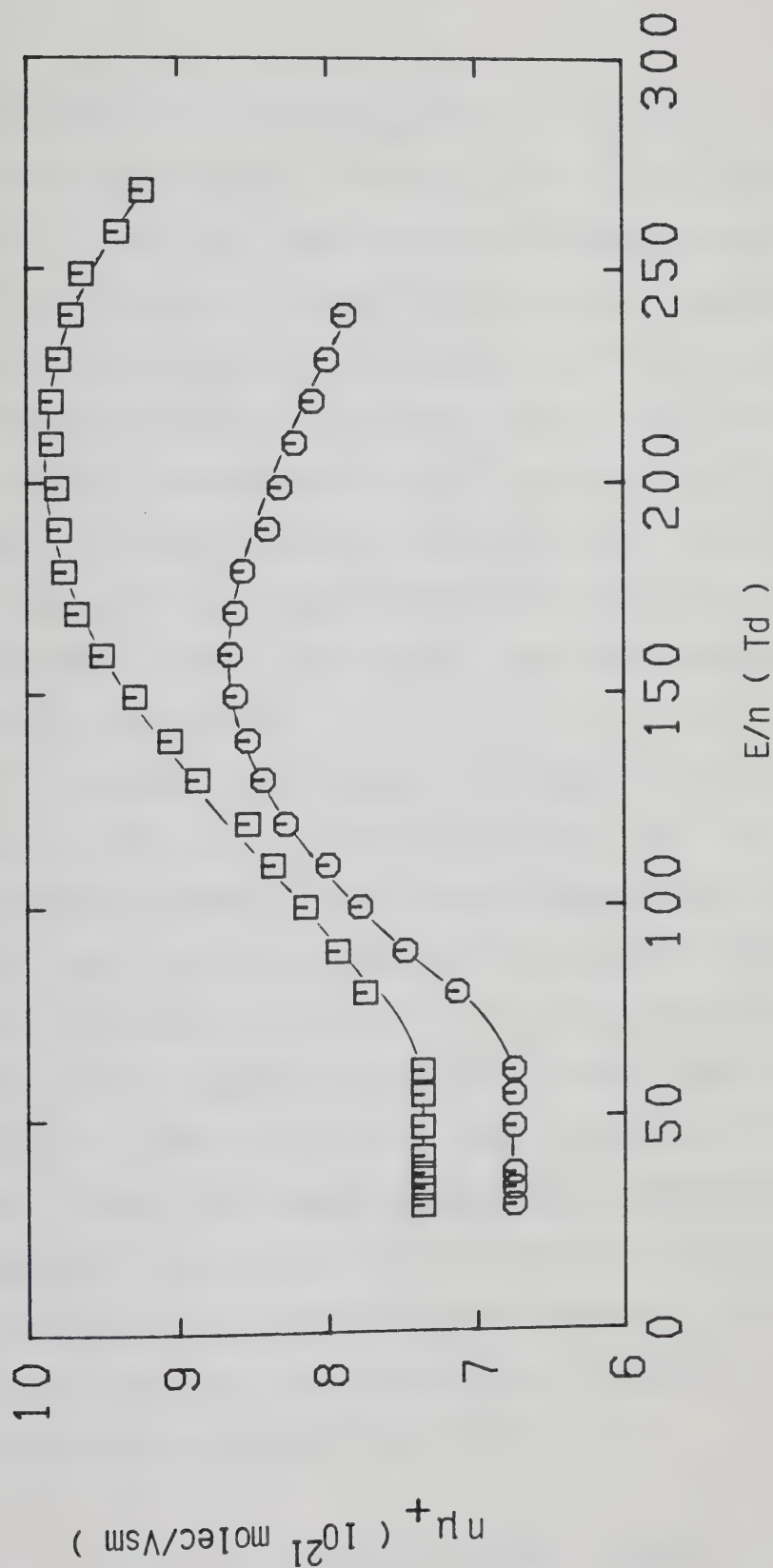


Figure IV-37. Density normalized cation mobilities as functions of E/n from Reference 203. \square , CH_5^+ ; \circ , C_3H_7^+ . $P_{\text{CH}_4} = 0.7\text{--}1.3$ torr. $T = 300 \pm 5\text{K}$.

both cases is field independent up to $E/n \approx 60$ Td. In CH_5^+ it increases with increasing field to a maximum at $E/n \approx 220$ Td. In C_3H_7^+ the maximum is located at a lower field, at $E/n \approx 160$ Td. Above the maxima the mobilities decrease with increasing field strength. The low field density normalized mobility obtained from these data at 293K is 7.9×10^{21} molec/Vsm for CH_5^+ and 7.2×10^{21} molec/Vsm for C_3H_7^+ , the most massive ion observed. The value obtained in this work in CH_4 at the same temperature is 5.4×10^{21} molec/Vsm, again indicating that the observed ions were heavily clustered.

In order to examine the shape of the cross section curve that can be obtained from data not affected by multibody effects, the field dependences of mobility of CH_5^+ and C_3H_7^+ reported by Saporoshenko were transformed into "effective temperature" dependences by use of the two-temperature approximation.²²⁸ This model is a kinetic theory in which the trace ions present in a drift chamber are allowed to have a different temperature than the neutrals, as a result of the field E acting on them. In this model the average kinetic energy of the ions is taken to be the sum of the average thermal energy plus a contribution given by the field.

$$\frac{3}{2} kT_{\text{eff}} = \frac{3}{2} kT + \frac{1}{2} Mv_d^2 \quad \text{IV-27}$$

where T_{eff} is an "effective temperature" of the ions, T is the temperature of the neutrals, k is Boltzmann's constant, M is the neutral mass and v_d is the ion drift velocity. The results of this transformation are shown in Figure IV-38 as plots of the density normalized mobility, $n\mu_+$, against the effective temperature, T_{eff} . These data were used to extract cross sections in the same manner previously described. Curve B in Figure IV-36 represents the result of this calculation for CH_5^+ and curve C the scattering cross section extracted from data relative to C_3H_7^+ . Calculated values of $n\mu_+$ using these cross sections are shown as solid lines in Figure IV-38. The scattering cross sections calculated from data not affected by clustering decrease much more gently in the energy region ($\epsilon \gtrsim 0.1$ eV) where curve A drops sharply. Curves B and C decrease with increasing energy in the region where curve A is constant. From these considerations it is concluded that the ions observed in the present study are polymeric and that the variation of mobility between 200K and 600K is not only accounted for by the change of the momentum transfer cross section with energy.

Hiraoka and Kebarle²⁰² measured the temperature dependence of the equilibria



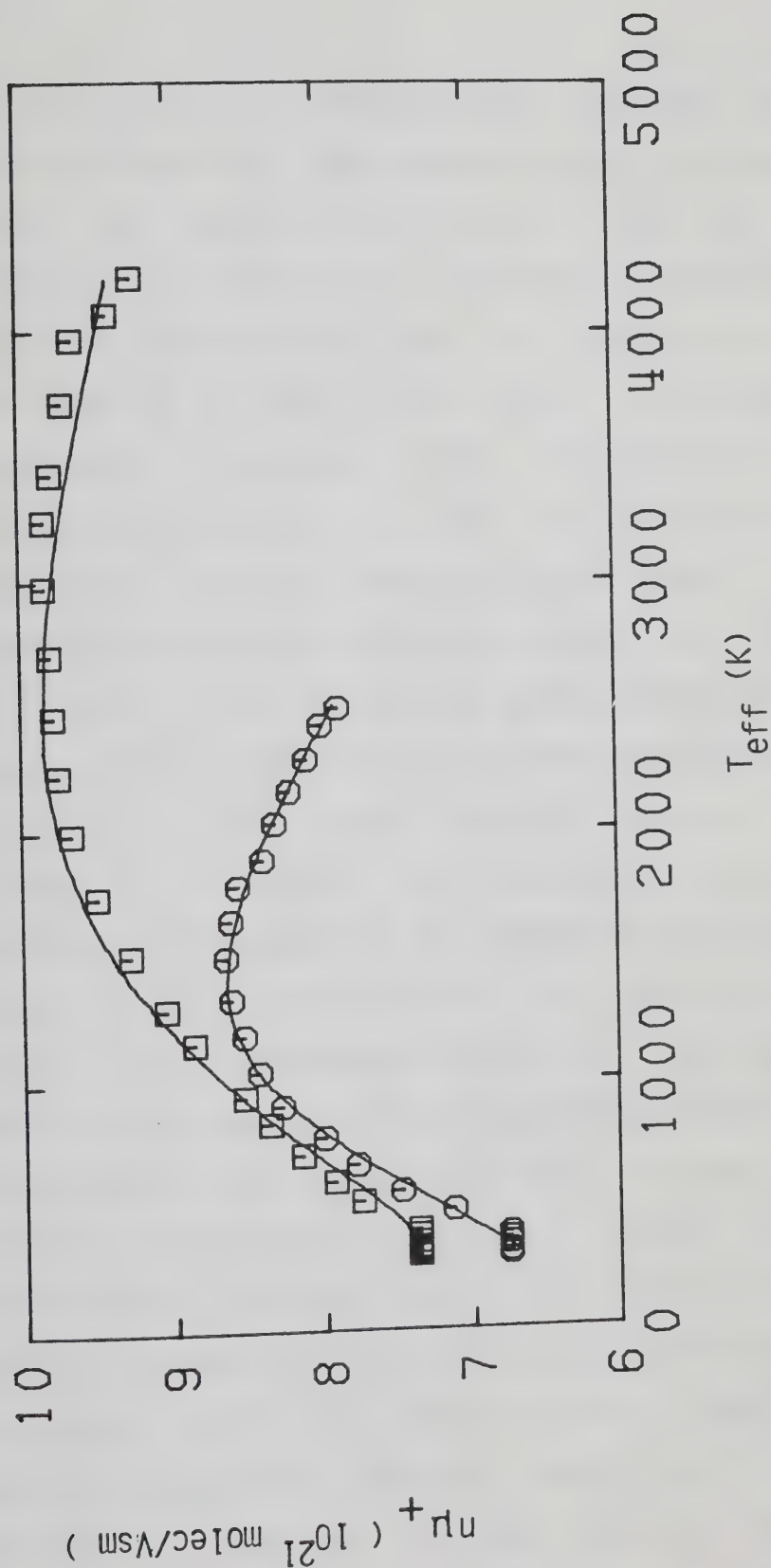


Figure IV-38. Density normalized cation mobilities for CH_5^+ (□) and C_3H_7^+ (○) from Reference 203 as functions of the effective temperature T_{eff} . The lines were obtained from curves B and C in Figure IV-36 for CH_5^+ and C_3H_7^+ respectively.

for $m = 1$ to 5. Measurements were made with a pulsed electron beam mass spectrometer in CH_4 at pressures up to 4 torr and temperatures between 110K and 290K. The constants of each of the equilibria IV-28 were measured at different temperatures from the observed ion intensities and reported as Van't Hoff plots. The values of these equilibrium constants were extrapolated at higher temperatures, up to $T = 667\text{K}$ and at lower temperatures, down to $T = 100\text{K}$ as shown in Figure IV-39. The relative concentrations of the various species, from the monomer to the hexamer were calculated using these constants at a density of CH_4 corresponding to the experimental conditions in use, $n = 2.95 \times 10^{25} \text{ molec/m}^3$ giving a pressure of 1.2 atm at $T = 300\text{K}$. The distribution of species as a function of temperature is shown in Figure IV-40. In Figure IV-41 is reported how the average cluster size changes with temperature (curve A). In the temperature region of interest in this work, between 200K and 600K, the most abundant ions change from mainly trimers, $(\text{CH}_5^+)(\text{CH}_4)_2$ at 200K, to monomers, CH_5^+ , at $T \gtrsim 500\text{K}$. Below 200K the concentration of large clusters increases quickly and this explains the marked curvature of the experimental $n_{\mu+}$ curve represented by line B in Figure IV-41. These observations support the previous findings, namely the low value of the observed $n_{\mu+}$ compared to that obtained from data not affected by clustering and the shape of the scattering

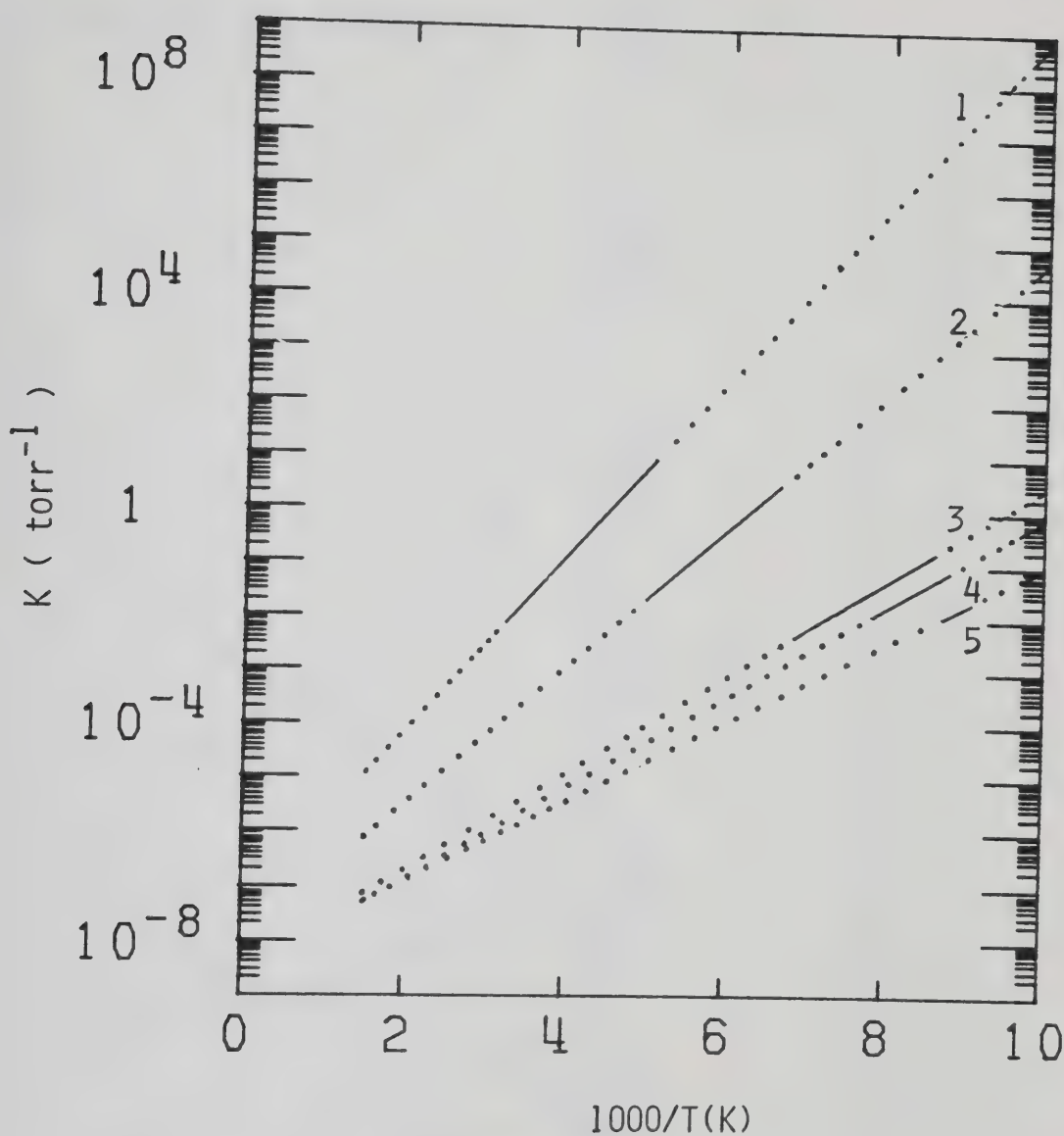


Figure IV-39. Van't Hoff plots for reactions $\text{CH}_5^+(\text{CH}_4)_{m-1}^+ + \text{CH}_4 = \text{CH}_5^+(\text{CH}_4)_m^+$. The numbers labeling the lines are values of m . The solid lines represent experimental values from Reference 202. The dotted lines represent the extrapolations used in this work.

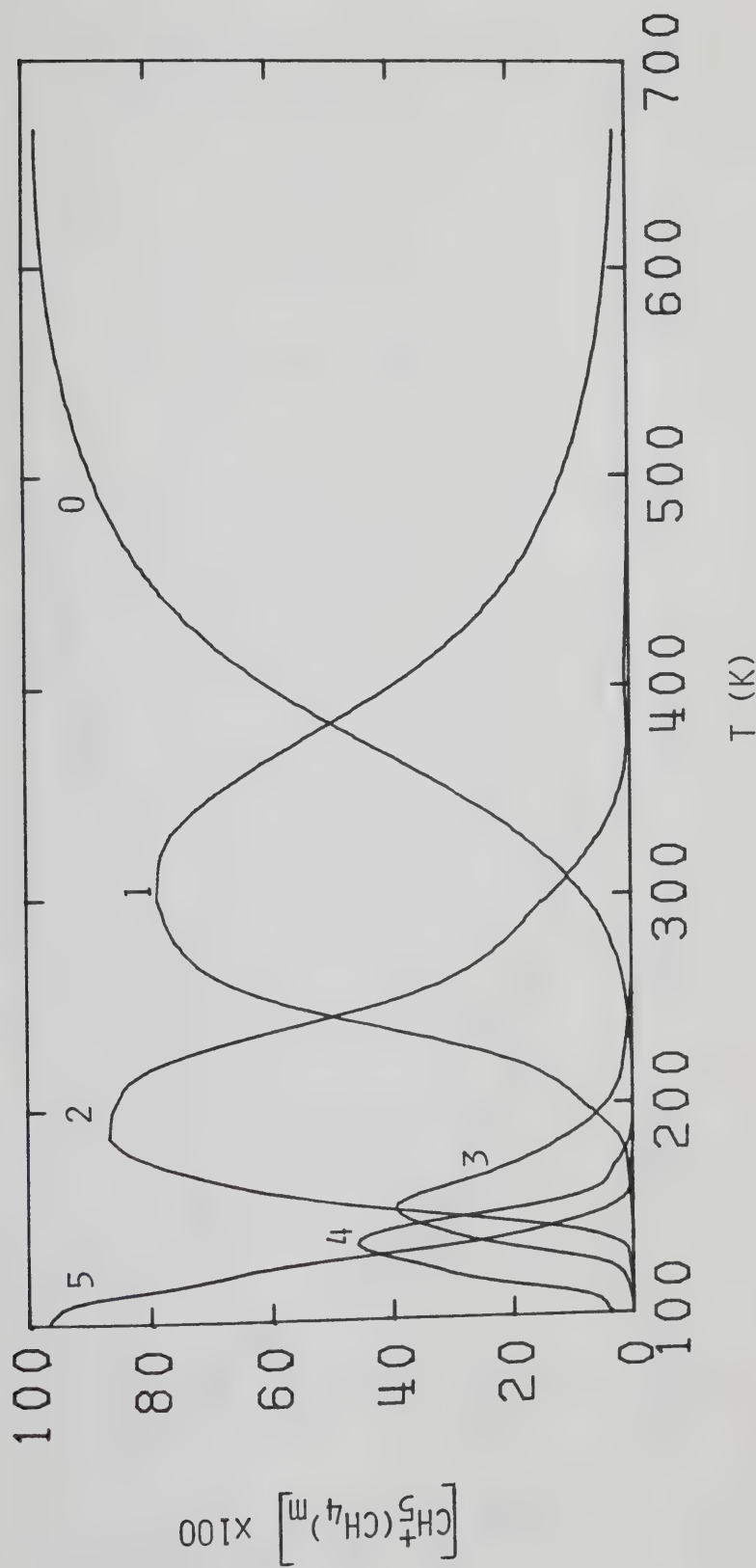


Figure IV-40. Relative percent concentrations of specie $\text{CH}_5^+(\text{CH}_4)_m$ as functions of temperature. The numbers labeling the curves are values of m . $n_{\text{CH}_4} = 2.95 \times 10^{25}$ molec/ m^3 .

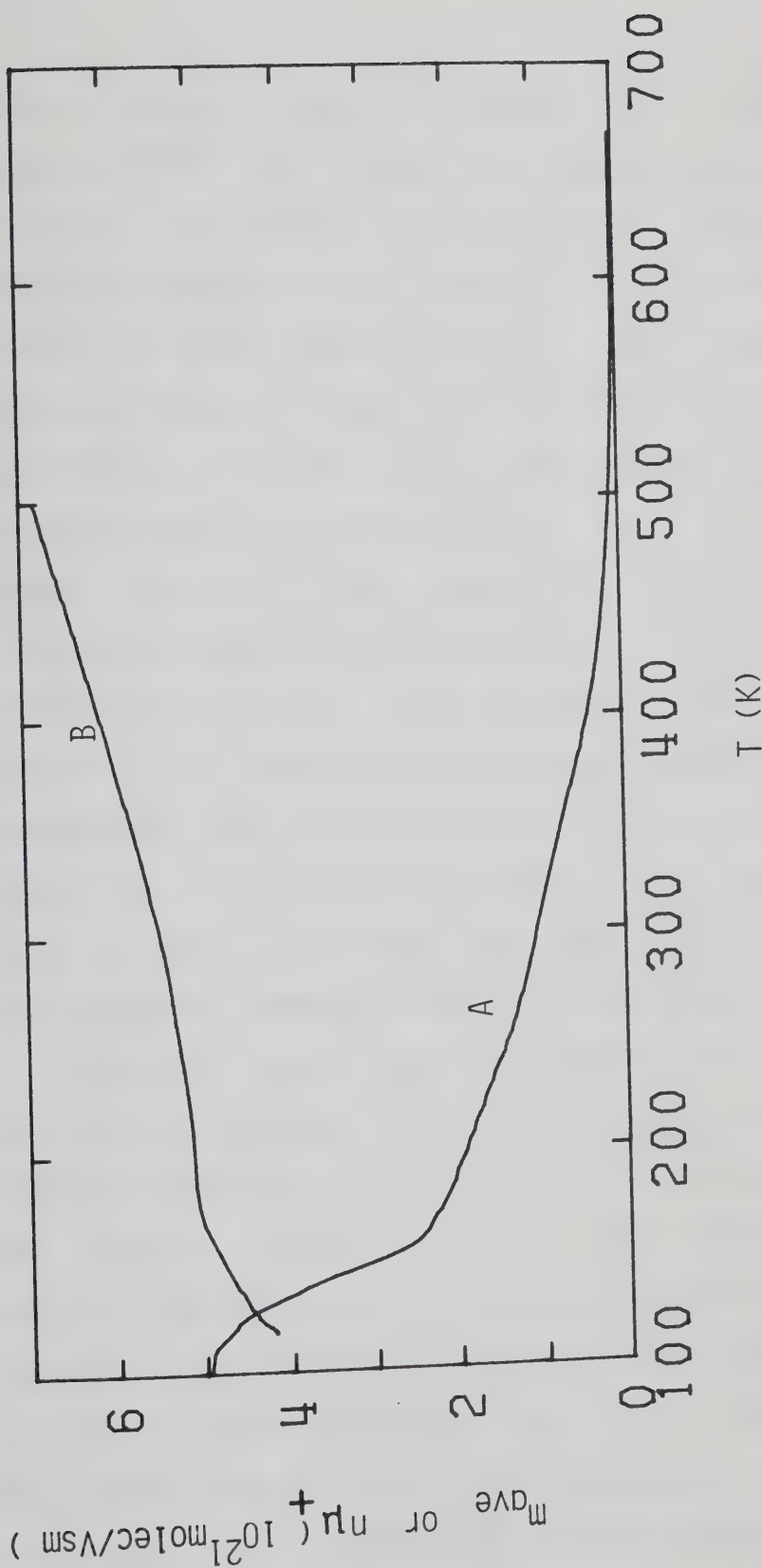


Figure IV-41. A: Average value of m in $\text{CH}_5^+(\text{CH}_4)_m$ as a function of temperature.
 B: Experimental density normalized cation mobilities $n\mu_+$ in CH_4 gas at $n=2.95 \times 10^{25}$ molec/ m^3 as functions of temperature from Figure IV-34.

cross section curve. Within the framework of the theory,^{116,117} the change of mobility with temperature is entirely attributed to the energy dependence of the momentum transfer cross section. Clustering is taken into account by using the appropriate reduced mass for the ion-molecule system. The cross section varies as $(M_r)^{-1/2}$. Considering the ions to be unclustered yields $M_r = M/2$ whereas heavy clustering yields $M_r = M$. Inclusion of cluster effects in the calculation of curve A in Figure IV-36 would have simply decreased the cross section without altering its shape. What has been found in the present study is that the temperature dependence of the density normalized mobility at low temperatures is dominated by changes in mass. At intermediate temperatures the apparent cross section is probably the combination of declustering and the energy dependence of the true cross section.

From the experimental mobilities it is possible to calculate an average cross section, σ_{ave}^+ , by inserting in formula IV-25 the values of reduced mass corresponding to the average cluster size at each temperature. The variation of σ_{ave}^+ obtained in this way with temperature is shown in Figure IV-42. The average cross section decreases with increasing temperature much more steeply in the low temperature region because heating the gas has the effect of reducing the concentration of large clusters.

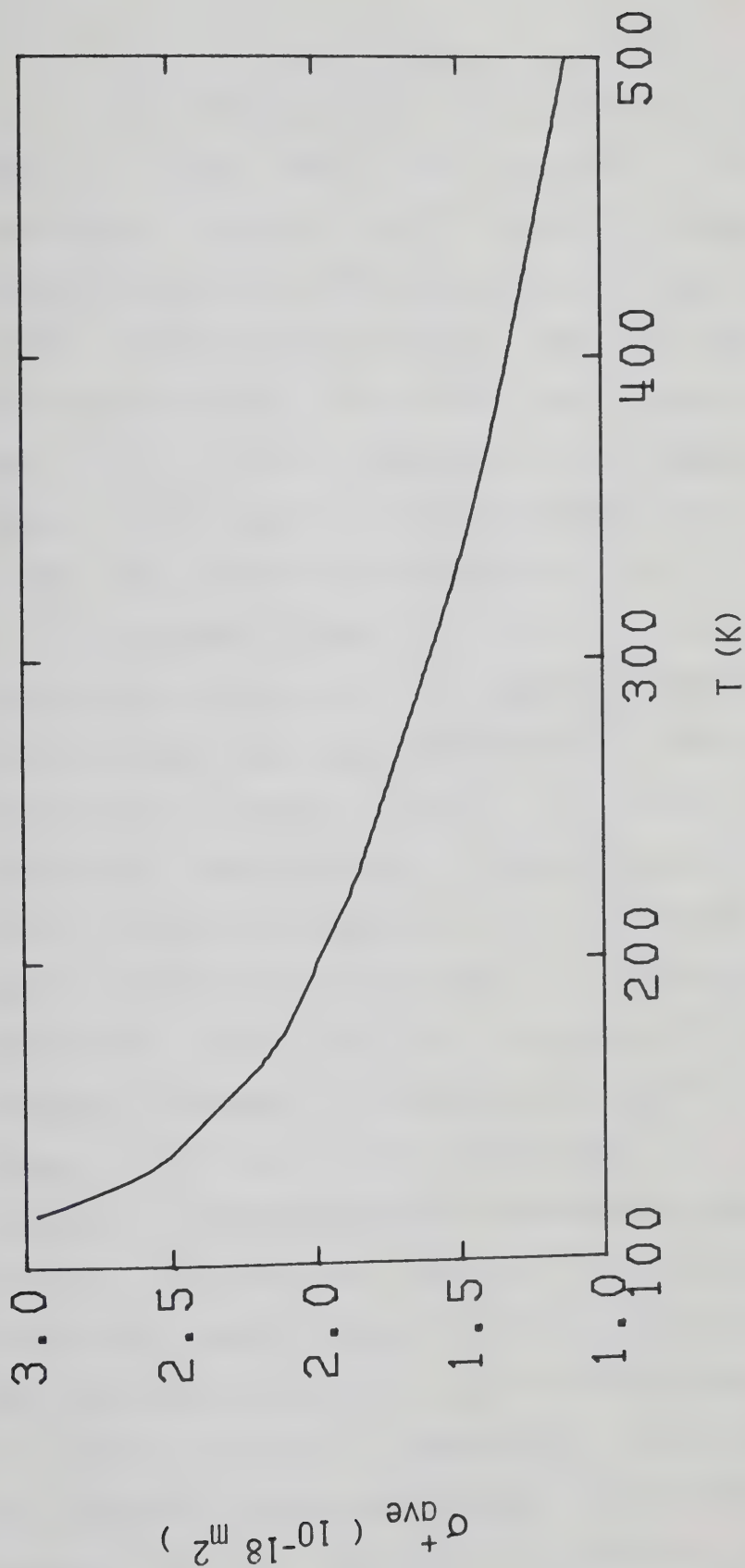


Figure IV-42. Temperature variation of the average ion-molecule scattering cross section σ_{ave}^+ calculated from the experimental mobility data in CH_4 at $n = 2.95 \times 10^{25} \text{ molec/m}^3$ reported in Figure IV-34.

It is concluded that the observed ion mobilities are those of ions which are clustered. The extent of clustering decreases with increasing temperature. At temperatures below 200K clustering has the dominant effect on the mobility while between 200K and 600K the density normalized mobility increases both because of decreasing mass of the ions and because of the decreasing momentum transfer cross section with increasing energy as indicated by data not affected by multibody effects.

In Figures IV-43, 44 and 45 are reported the temperature variations of the density normalized mobilities in CH_3D , CH_2D_2 and CHD_3 respectively. The solid lines were calculated by using curve A in Figure IV-36 and the appropriate reduced masses. The cross section used for CH_4 and CD_4 does not reproduce the experimental data in the partially deuterated compounds. The calculated values are constantly lower than the experimental ones and the deviation between calculated and experimental values is largest for CH_2D_2 . If clustering, as indicated, is important in determining the temperature dependence of the mobility, differences between compounds at a given temperature can be attributed to the same effect. A larger mobility corresponds to a lower reduced mass and therefore to a smaller extent of clustering. A possible reason for the observed differences between the partially deuterated compounds and the isotropic compounds CH_4 and CD_4 is a

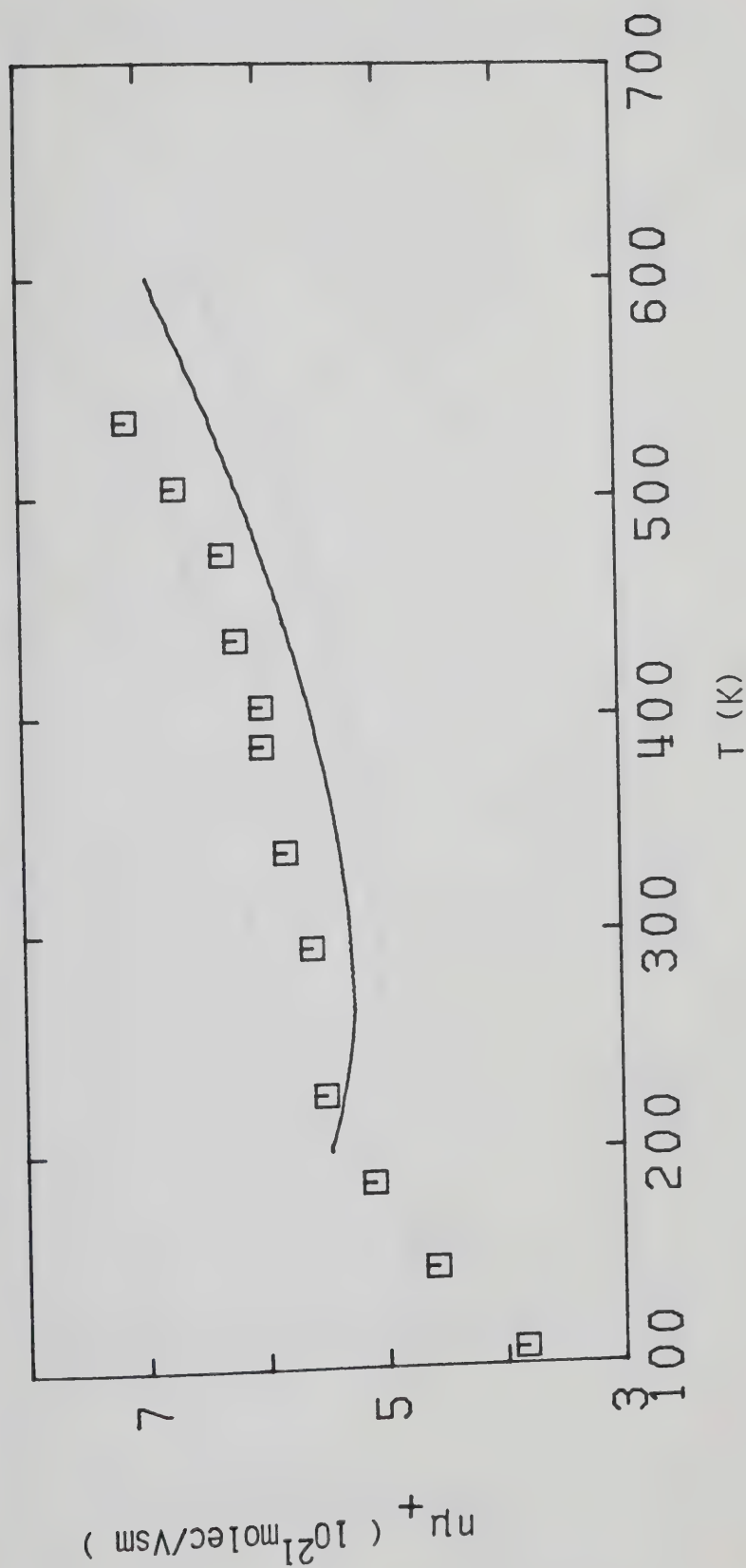


Figure IV-43. Density normalized cation mobilities in CH_3D gas at $n=2.35 \times 10^{25}$ molec/ m^3 as functions of temperature. The line was obtained from curve A in

Figure IV-36.

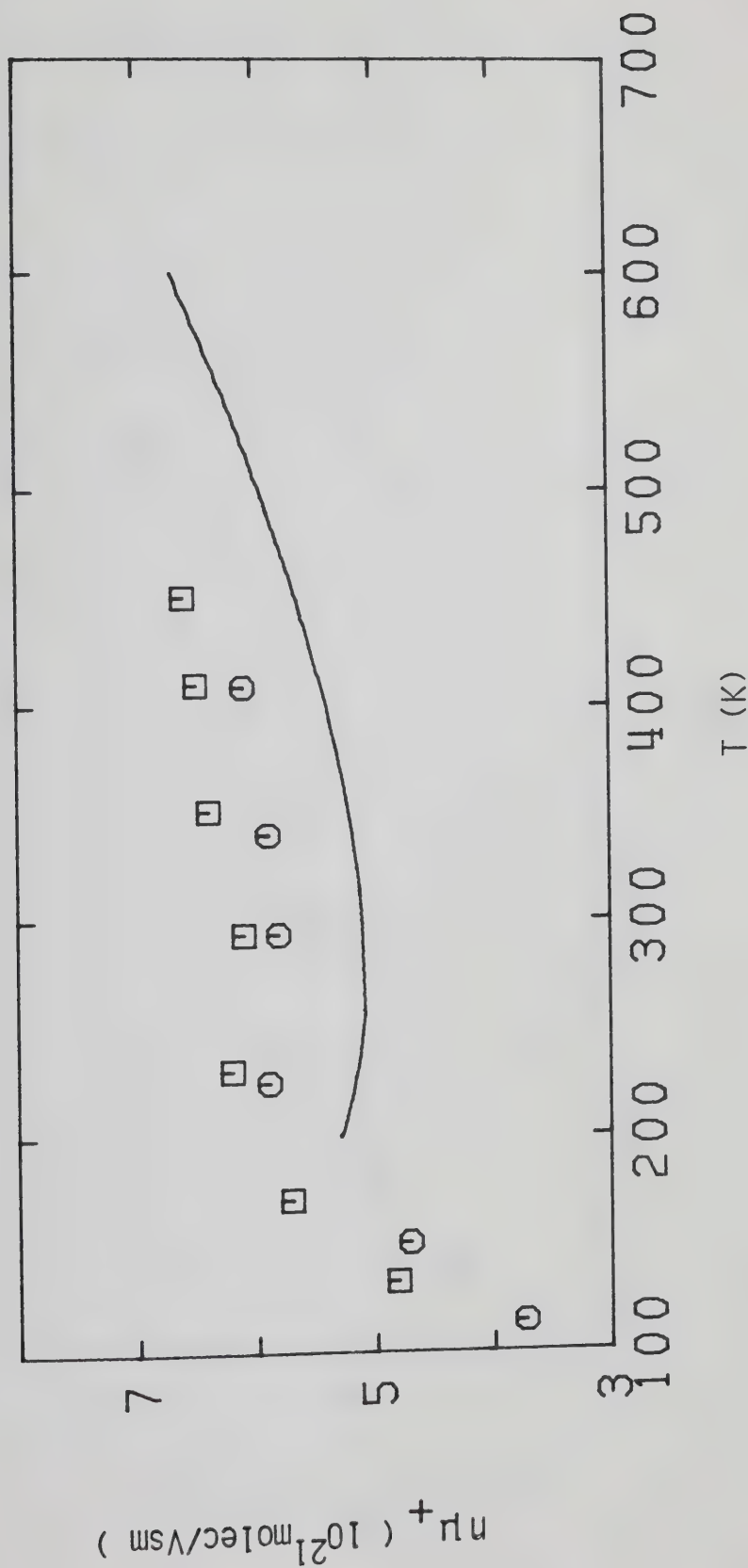


Figure IV-44. Density normalized cation mobilities in CH_2D_2 gas at different densities ($10^{25} \text{ molec/m}^3$) as functions of temperature. \square , 3.70; \circ , 6.1. The line was obtained from curve A in Figure IV-36.

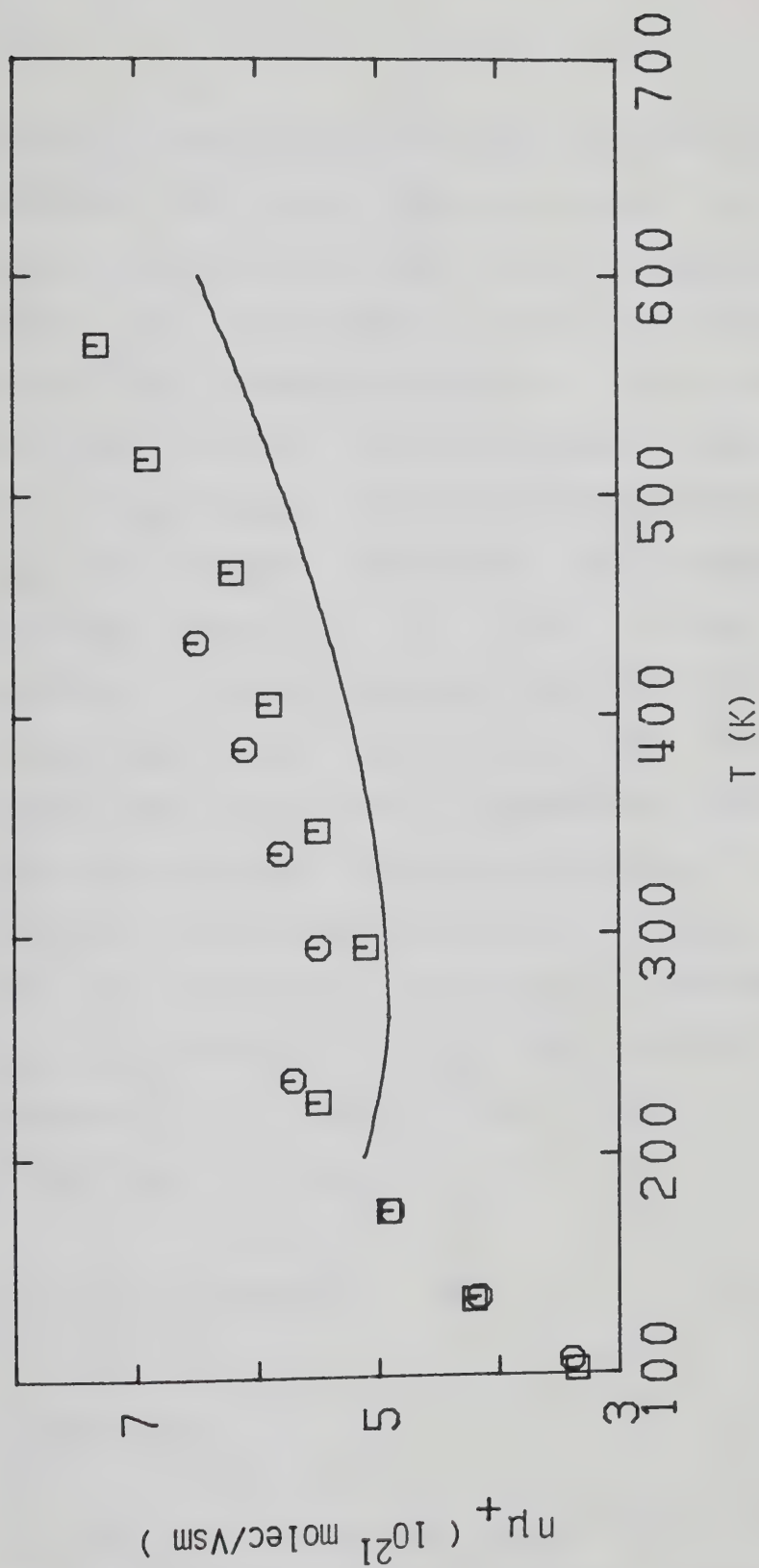


Figure IV-45. Density normalized cation mobilities in CHD_3 gas at different densities ($10^{25} \text{ molec/m}^3$) as functions of temperature. \square , 2.30; \circ , 4.3. The line was obtained from curve A in Figure IV-36.

different extent of clustering. A cluster of molecules is stabilized if excess thermal energy can be distributed among several vibrational levels. However, for this to happen, the vibrational levels of different molecules forming the cluster should match. The vibrational energies of CH and CD bonds are proportional to the square root of the reduced masses. C-D vibrational levels are 35% lower than C-H levels. Therefore, in a cluster composed of molecules containing both CH and CD bonds there is less matching of levels between different molecules and the cluster will break apart at a lower temperature. This should show up in the temperature coefficient of the mobility calculated near the coexistence curve where the effect of clustering is greatest. However, the scatter of the points does not allow a precise determination of E_μ . The values obtained in CD_4 , CH_2D_2 and CHD_3 between ~100K and 200K are all about 1 ± 0.2 kJ/mol. For comparison RT at 150K is 1.2 kJ/mol.

2. Effect of Density

a. Dense Gas

Along the saturation curve in the gas the cation mobility decreases with increasing density (see Results section). The same behavior was observed for electrons. This is attributed to a crowding effect.

In Figure IV-46 are reported the electron and ion mobilities as functions of temperature in saturated vapor and liquid CH_4 . The ion mobilities are between six and three orders of magnitude smaller than the electron mobilities on decreasing the density of the liquid from that at the triple point to that at the critical point. The curve in Figure IV-46 shows the variation of the density of the equilibrium liquid and vapor between 90K and $T_c = 190.6\text{K}$.

The density normalized electron mobility (Figure IV-1) is density independent at low gas densities. It decreases to a minimum in the dense gas and increases to a maximum in the liquid at $n \approx 10.7 \times 10^{27} \text{ molec/m}^3$. In Figure IV-47 is reported the density normalized ion mobility, $n\mu_+$, against the number density of the saturated vapor and liquid phases in all compounds. Within the experimental scatter no isotope effect is observed. The density normalized mobility is density independent between approximately $1 \times 10^{25} \text{ molec/m}^3$ and $n_c = 6.1 \times 10^{27} \text{ molec/m}^3$ at $(2.9 \pm 0.2) \times 10^{21} \text{ molec/Vsm}$ for 70 experimental points. The mobilities of electrons are four orders of magnitude greater than those of the ions in the low density vapor (Figure IV-46). This is more than the difference that would be caused by the 10^5 fold difference in masses.

It has been already mentioned that the ions are thought to be clustered even at low gas densities and at

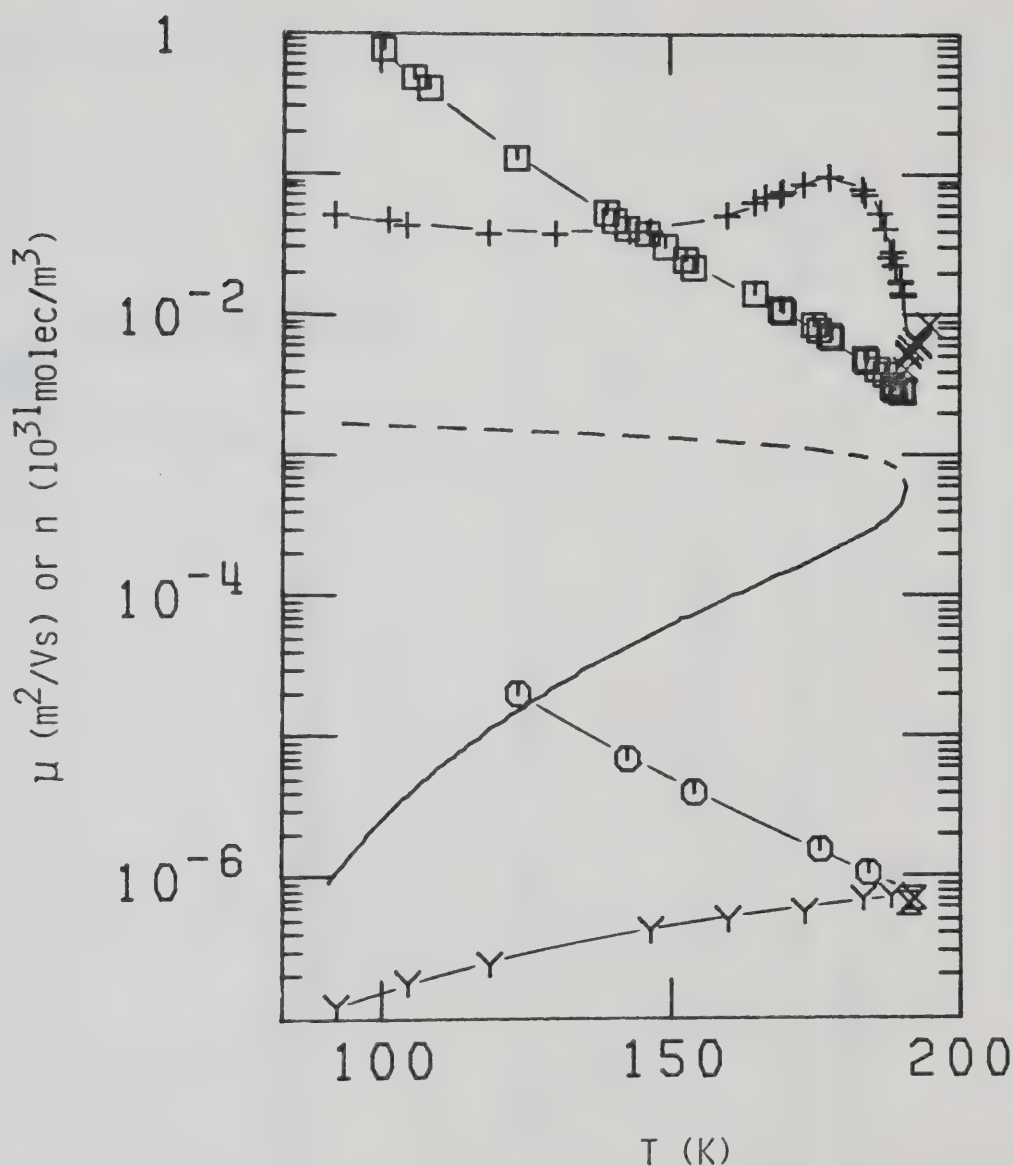


Figure IV-46. Electron and ion mobilities in coexistence vapor and liquid CH_4 as functions of temperature. Electrons: \square , vapor; $+$, liquid; \times , supercritical gas at n_c . Ions: \circ , vapor; Y , liquid; \boxtimes , supercritical gas at n_c . The temperature variations of the vapor (—) and liquid (----) densities n are reported for comparison.

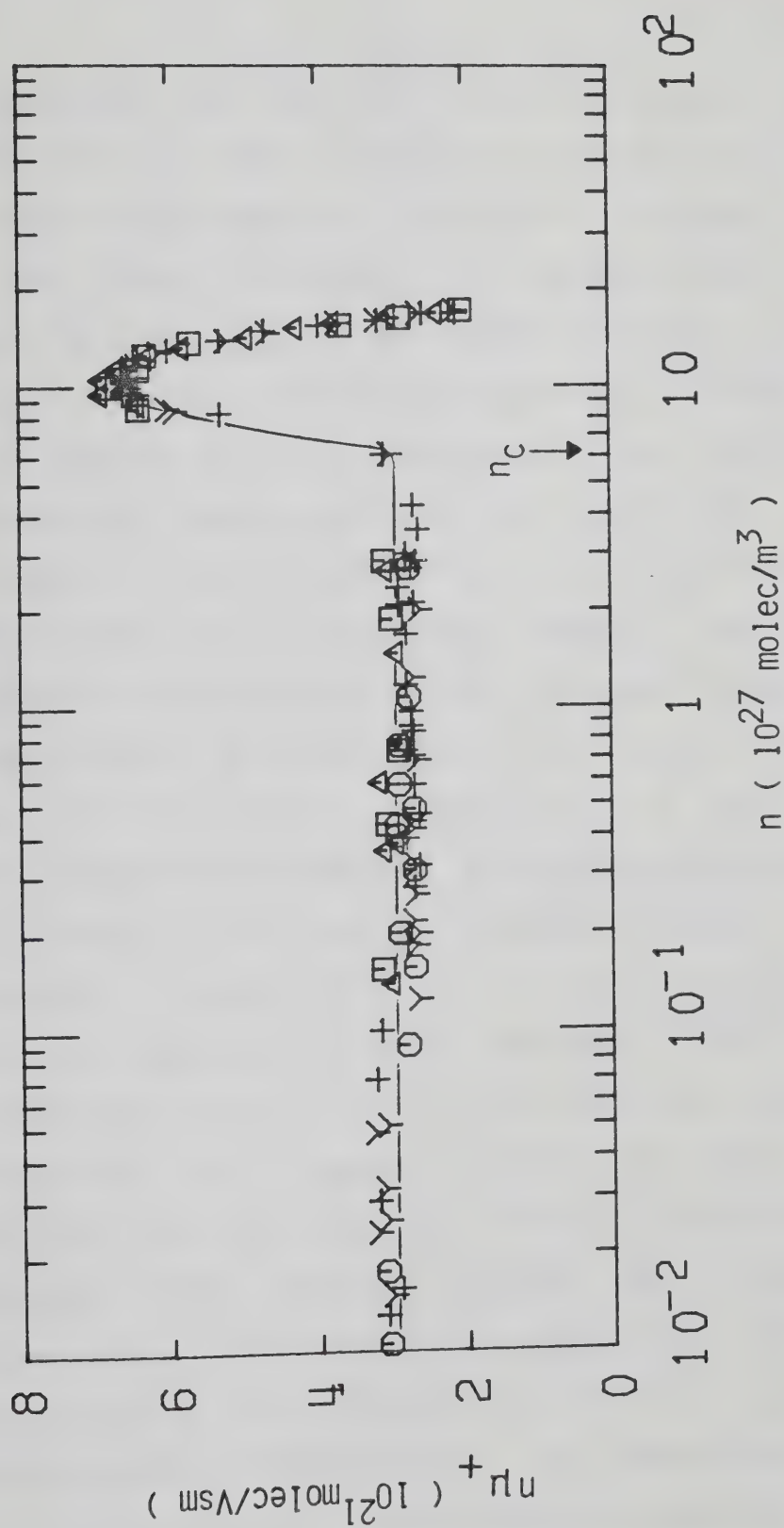


Figure IV-47. Density dependence of the density normalized cation mobility in coexistence vapor and liquid methanes. \square , CH_4 ; \circ , CH_3D ; \triangle , CH_2D_2 ; $+$, CHD_3 ; Y , CD_4 .

temperatures far from the saturation curve. This effect should be even more important in the saturated vapor. By increasing the density, the extent of density fluctuations in the solvent increases. It has been shown that in the dense gas, at $n \gtrsim 3 \times 10^{26}$ molec/m³, electrons can become quasilocalized in transient molecular clusters. The fact that the ion mobility normalized by the density does not change with density even in the region where the solvent molecules are clustered can be attributed to the achievement of a relatively stable configuration of neutrals around the ion and to the small change in reduced mass produced by clustering of the solvent molecules. If the ions are heavily clustered $M_r \approx M$ and a relatively small change is produced by further cluster growth.

Heating the gas at constant density raises the mobility. Figures IV-48 to 53 report Arrhenius plots of the ion mobility in all compounds. The temperature coefficients of mobility, at the densities indicated, were calculated in a manner similar to that used for electrons. At the critical density the measurements in all compounds were plotted against the reduced inverse temperature, T_c/T as shown in Figure IV-53. The scatter in the points is attributed mainly to errors in density and uncertainties in temperature. The temperature coefficient at n_c was calculated using the low temperature points of CD₄ and CHD₃. The value obtained, 180 kJ/mol, is assumed

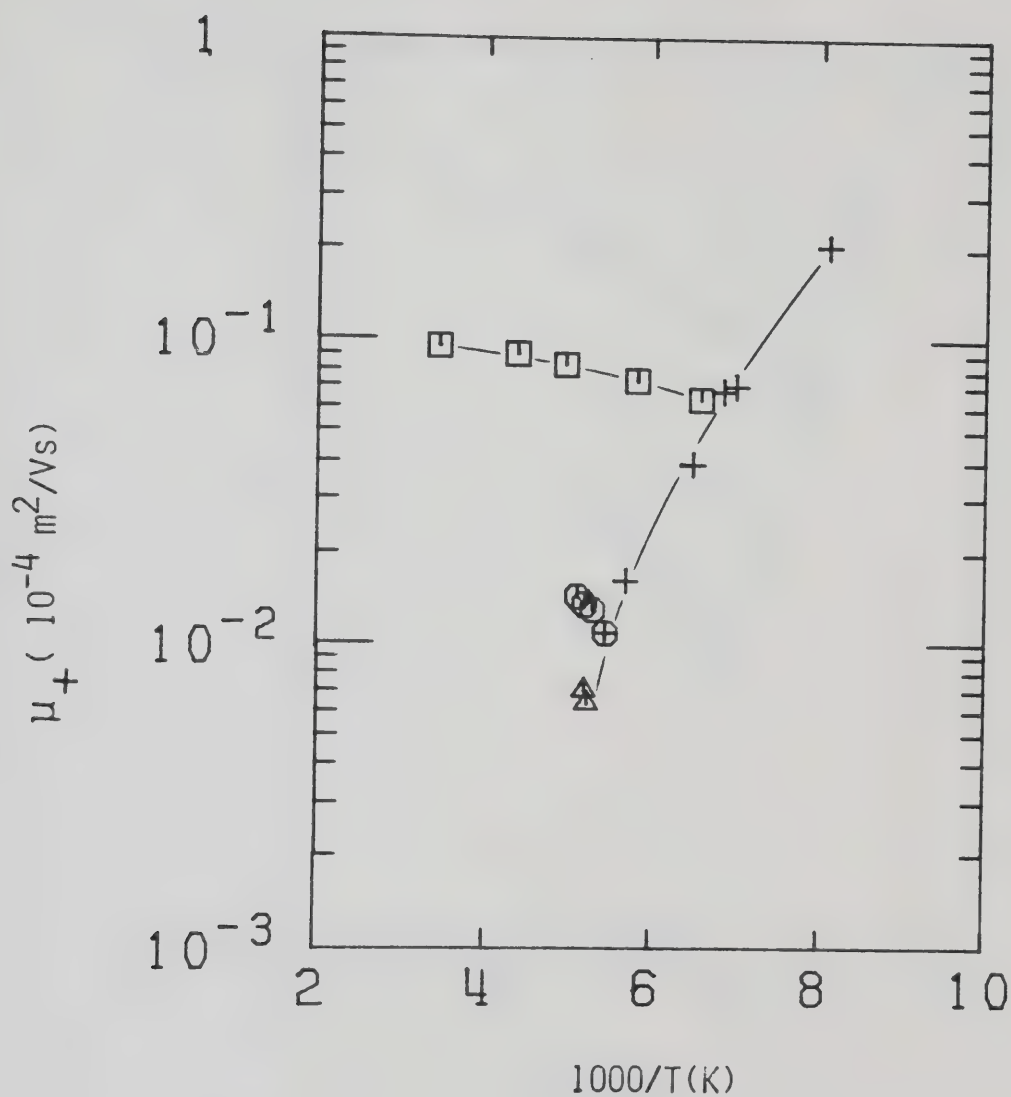


Figure IV-48. Arrhenius plot of cation mobilities in CH_4 gas at different densities ($10^{26} \text{ molec/m}^3$). Mobilities in the gas along the vapor-liquid coexistence curve are represented by +. \square , 5.5; \circ , 29.0; \triangle , $n_c = 61$.

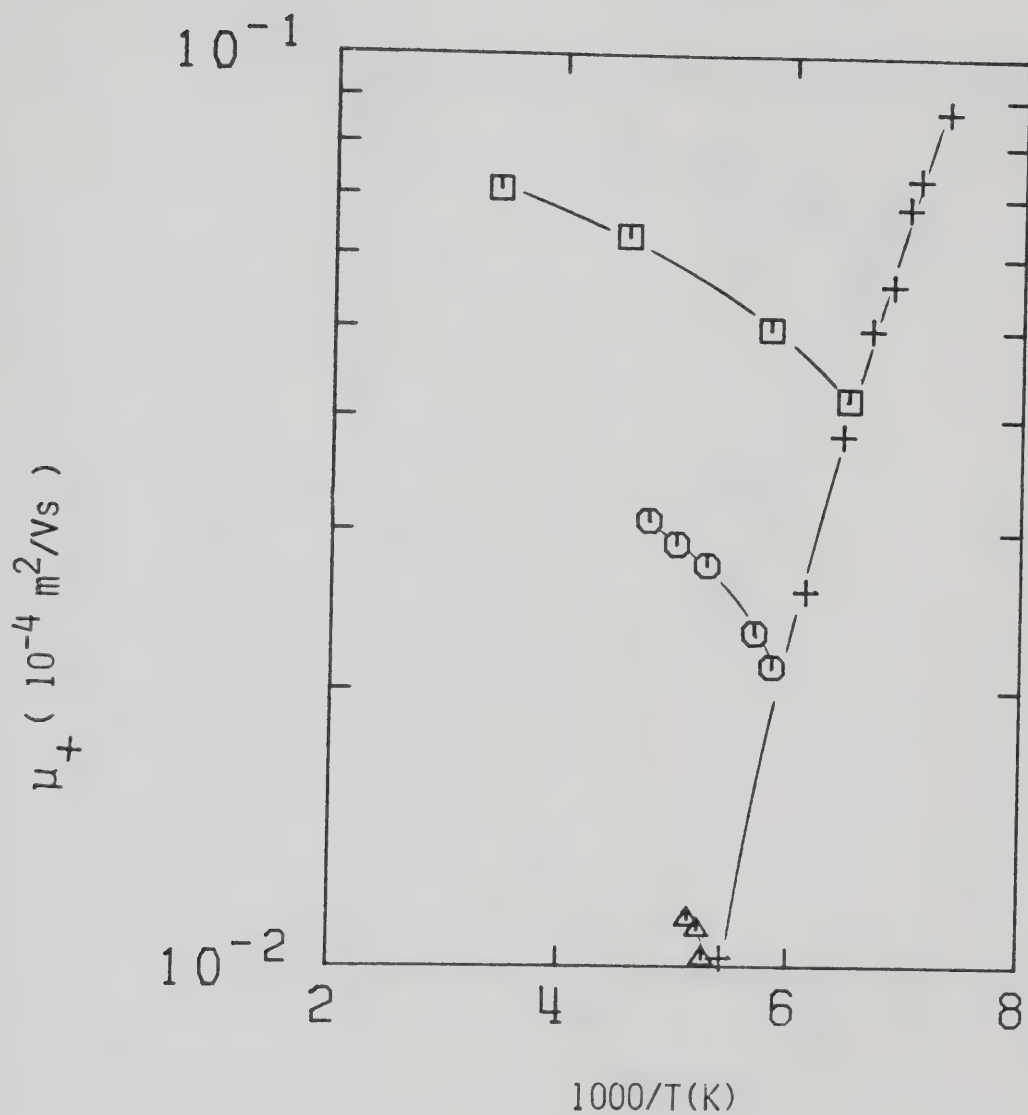


Figure IV-49. Arrhenius plot of cation mobilities in CH_3D gas at different densities ($10^{26} \text{ molec/m}^3$). Mobilities in the gas along the vapor-liquid coexistence curve are represented by +. \square , 6.7; \circ , 15.0; \triangle , 27.0.

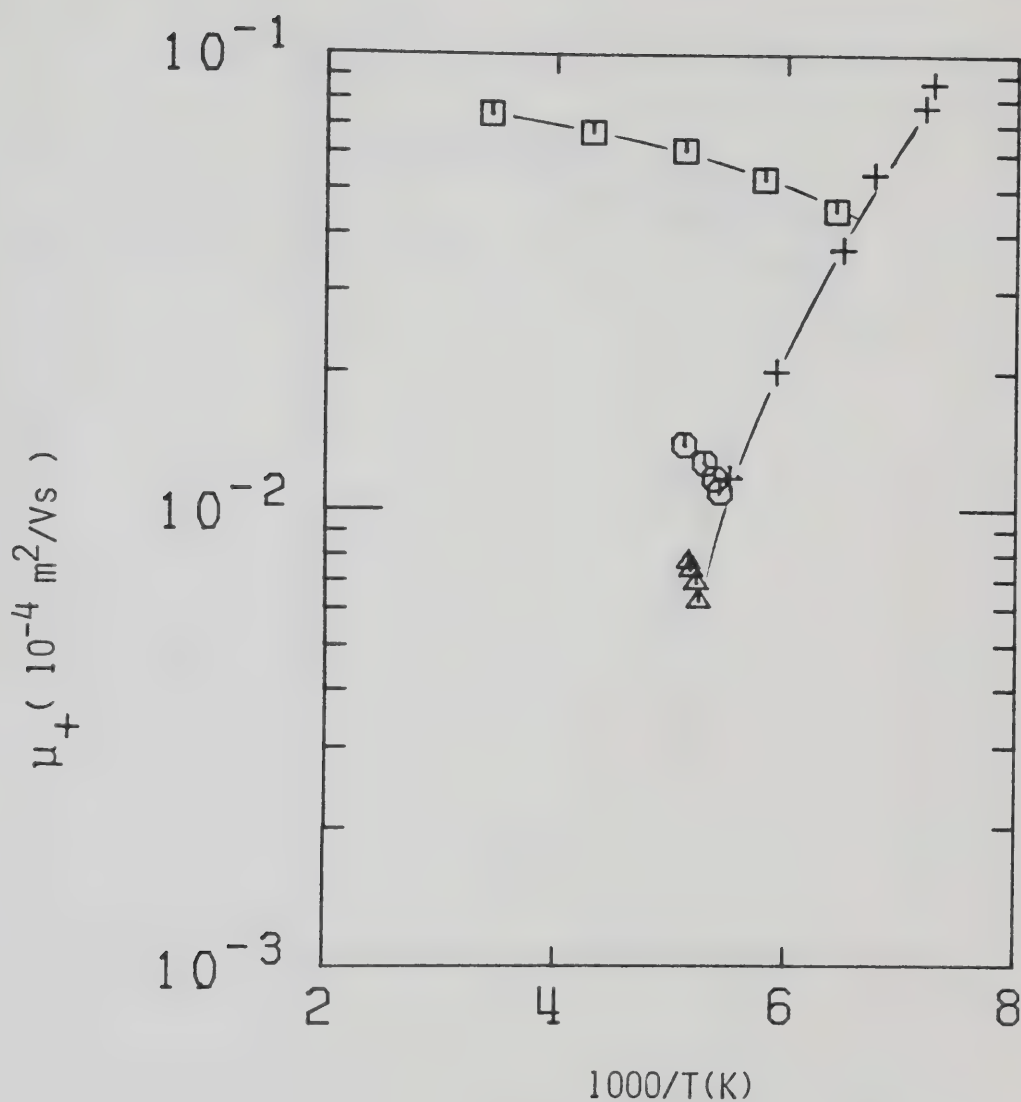


Figure IV-50. Arrhenius plot of cation mobilities in CH_2D_2 gas at different densities ($10^{26} \text{ molec/m}^3$). Mobilities in the gas along the vapor-liquid coexistence curve are represented by +. \square , 7.3; \circ , 26.0; Δ , $n_c=61$.

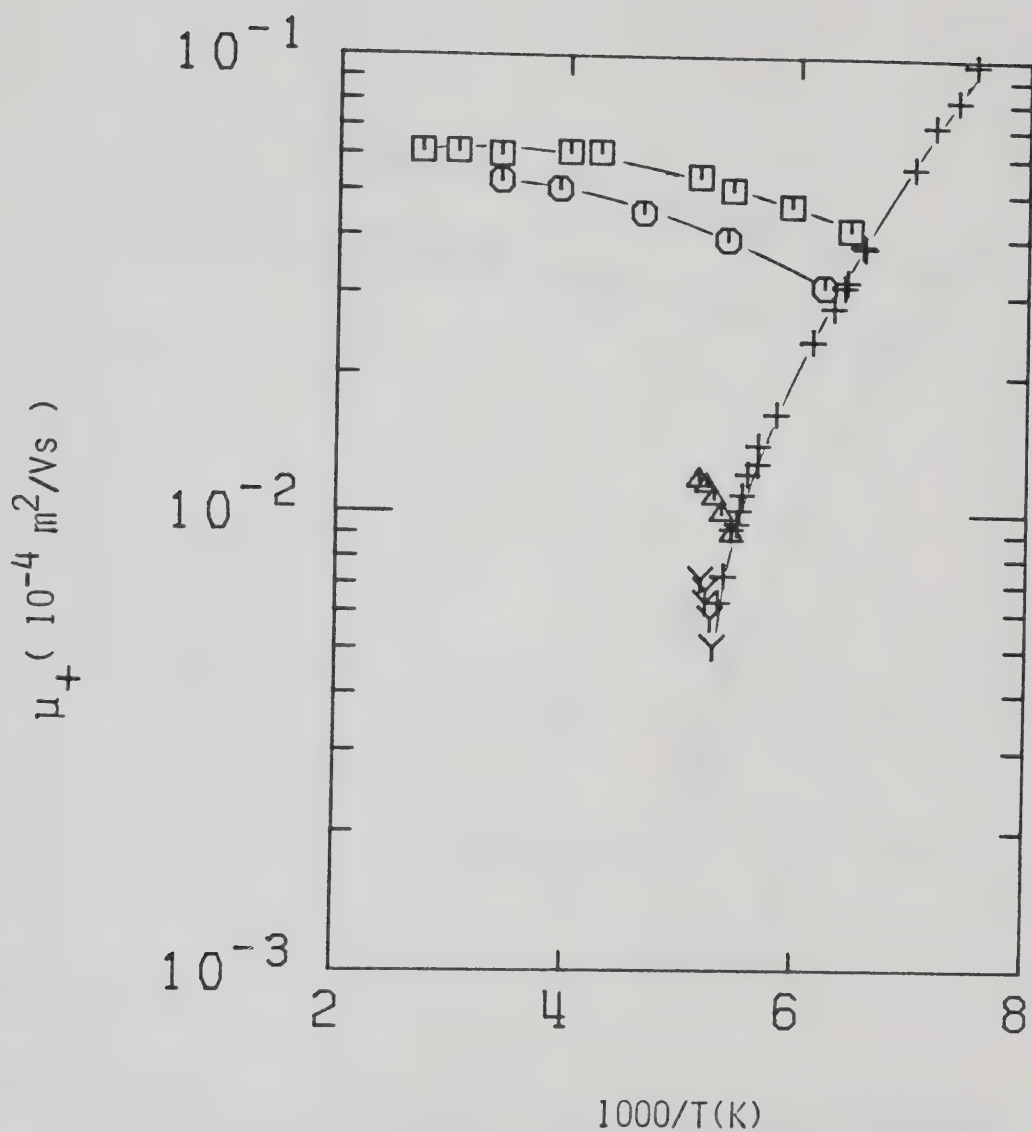


Figure IV-51. Arrhenius plot of cation mobilities in CHD_3 gas at different densities ($10^{26} \text{ molec/m}^3$). Mobilities in the gas along the vapor-liquid coexistence curve are represented by $+$. \square , 6.8; \circ , 9.3; Δ , 29.1; γ , $n_c = 61$.

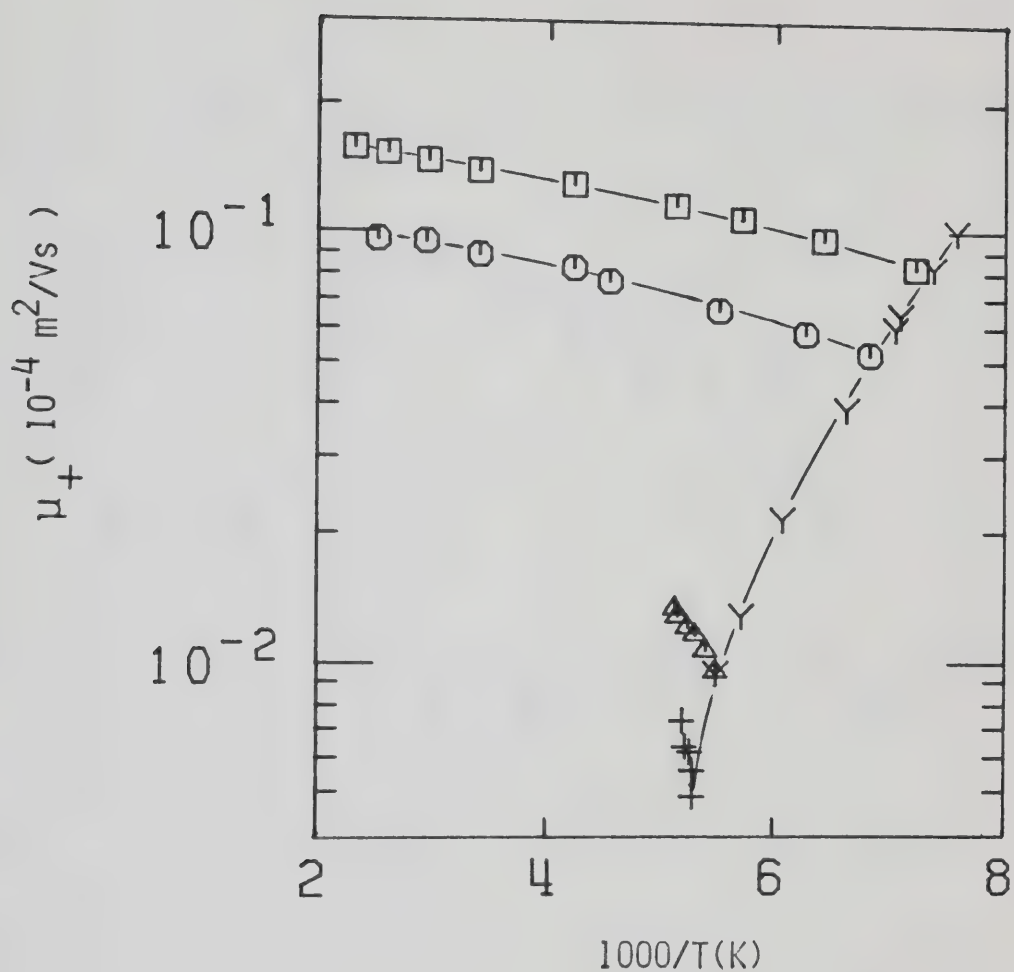


Figure IV-52. Arrhenius plot of cation mobilities in CD_4 gas at different densities ($10^{26} \text{ molec/m}^3$). Mobilities in the gas along the vapor-liquid coexistence curve are represented by Y. \square , 3.7; \circ , 5.5; \triangle , 29.0; $+$, $n_c=61$.

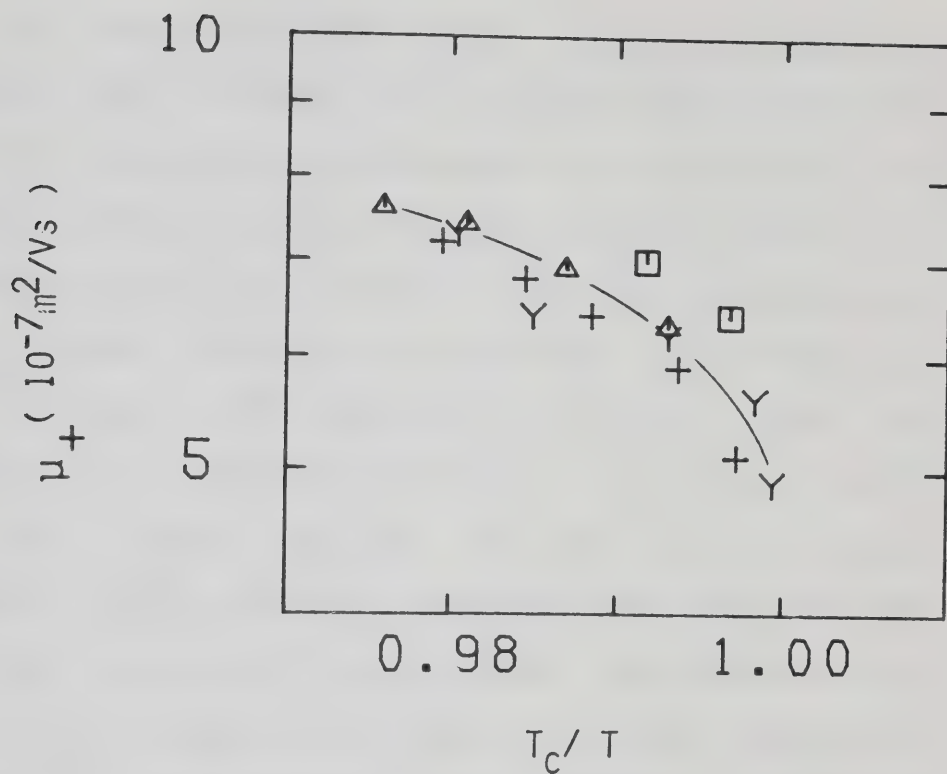


Figure IV-53. Cation mobilities in supercritical methane gases at $n_c = 6.1 \times 10^{27} \text{ molec/m}^3$ plotted against the reduced reciprocal temperature T_c/T .

\square , CH_4 ; Δ , CH_2D_2 ; +, CHD_3 ; Y, CD_4 .

to be the same for the other compounds where no measurements near enough the critical temperature were taken. The temperature coefficients of ion mobility are compared to those obtained for electrons in Table IV-3. The energies of mobility activation for ions are remarkably similar to those obtained for electrons. For example in CH_4 at $n = 5.5 \times 10^{26} \text{ molec/m}^3$, E_μ is 1.5 kJ/mol for electrons and 1.3 kJ/mol for ions. At $n = 29 \times 10^{27} \text{ molec/m}^3$ the values obtained are 16 and 11 kJ/mol respectively. This similarity indicates that the processes involved are the same in the two cases. The increase in μ for electrons on heating the gas at constant density is attributed to the decrease in the extent of density fluctuations and therefore in the concentration of "sites" for electron quasilocalization (see Equation IV-8 and following).

b. Liquid Phase

At densities greater than n_c , in the coexistence liquid, the density normalized cation mobility increases to a maximum located at $n \approx 10.5 \times 10^{27} \text{ molec/m}^3$ (Figure IV-47). At approximately the same density a maximum was also found in the density normalized electron mobility (Figures IV-1 and 28). However the value of $n\mu_+$ at the maximum is only a factor of approximately 2 higher than

TABLE IV-3

Electron and Ion Mobility Temperature Coefficients

Compound	n (10^{26} m^{-3})	n/n_c	E_{μ}^a (kJ/mol)	E_{μ}^b (kJ/mol)
CH ₄	5.5	0.09	1.5	1.3
	29.0	0.48	16	11
	61	1.00	130	
CH ₃ D	6.0	0.10	1.5	
	6.7	0.11	1.8	2.0
	15.0	0.25	3.9	4.4
	27.0	0.44	12	12
	61	1.00	150	
CH ₂ D ₂	7.3	0.12	1.6	2.1
	26.0	0.43	11	12
	61	1.00	120	
CHD ₃	6.8	0.11	1.5	1.6
	9.3	0.15	2.3	2.4
	29.1	0.48	12	11
	61	1.00	130	
CD ₄	3.7	0.06	1.1	1.3
	5.5	0.09	1.2	1.5
	29.0	0.48	14	12
	61	1.00	130	180

a. Electrons. From Arrhenius plots

b. Ions. From Arrhenius plots.

that in the low density gas. For electrons an increase by a factor of approximately 50 was observed (Figure IV-1).

Diffusion of an ion in a liquid involves concerted motions of many molecules. For this reason the ion mobility is correlated to the viscosity η .^{73,78,79,99,109,110} In Figure IV-54 are shown the ion mobility and the viscosity²²⁹ in liquid and supercritical CH_4 as functions of temperature. At high densities, when the mean free path between collisions is small compared to the molecular radius, Stokes' law²³⁰ applies

$$\eta\mu_+ = \frac{e}{cr} \quad \text{IV-29}$$

where r is the ionic radius and c a constant equals 6π for ions (stick conditions). This equation states that $\eta\mu_+$ will be viscosity independent if r is constant.

In Figure IV-55 are reported the ion mobilities in the deuterated compounds as functions of the reduced temperature T/T_c . CH_4 is included for comparison. Within the experimental scatter there is no isotope effect. In Figure IV-56 the product of the ion mobility and the viscosity is plotted as a function of the viscosity. The values of η were taken to be the same in all compounds at the same T/T_c . This plot confirms the validity of Stokes' law for $\eta \gtrsim 0.5 \times 10^{-4}$ kg/sm corresponding to $T/T_c \lesssim 0.87$ and $n/n_c \gtrsim 2.0$. In this region the radius of the ion can

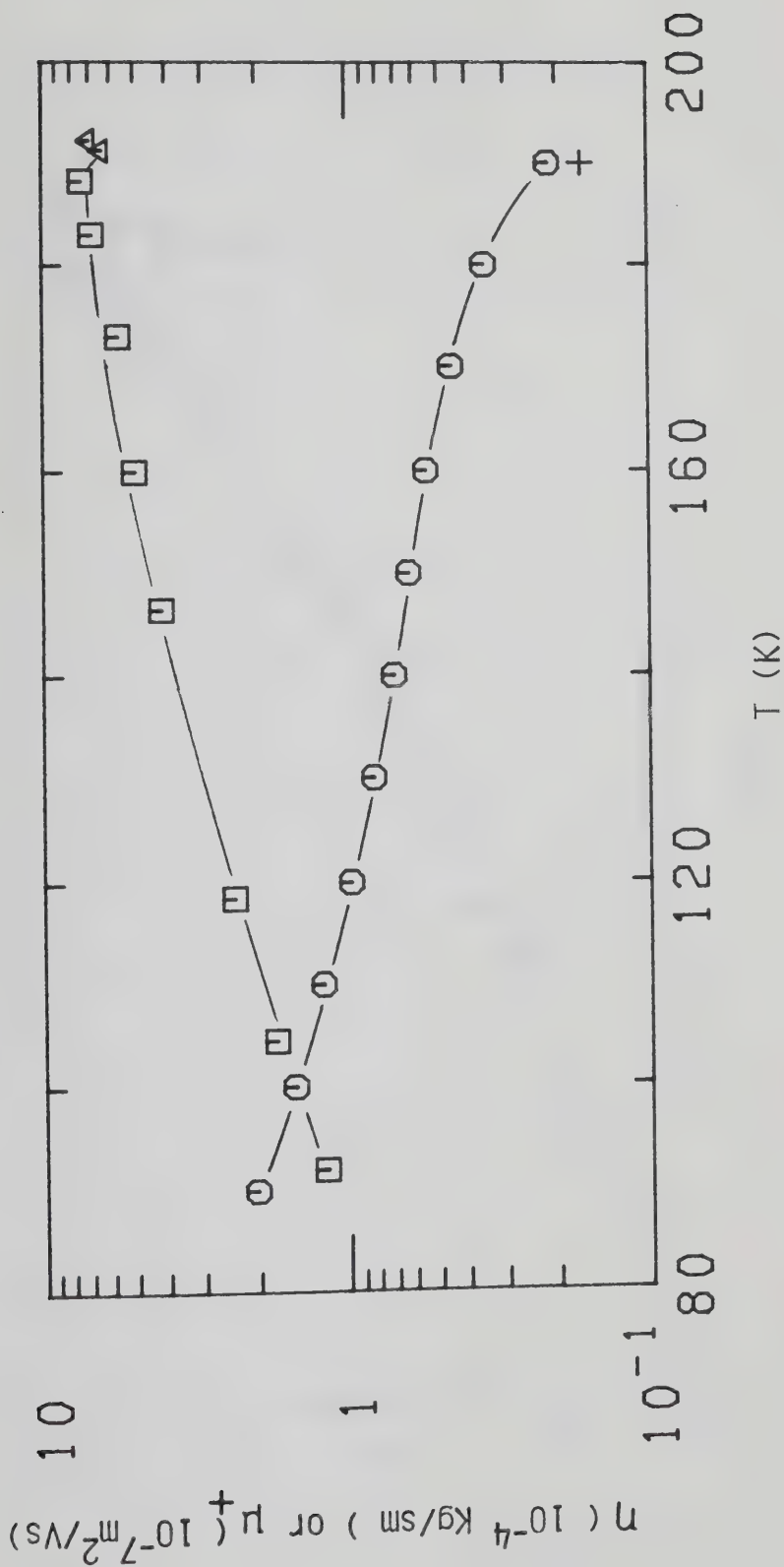


Figure IV-54. Cation mobilities (\square, Δ) and viscosities ($\circ, +$) in liquid CH_4 at the equilibrium vapor pressure. Δ and $+$ represent the supercritical fluid at n_c .

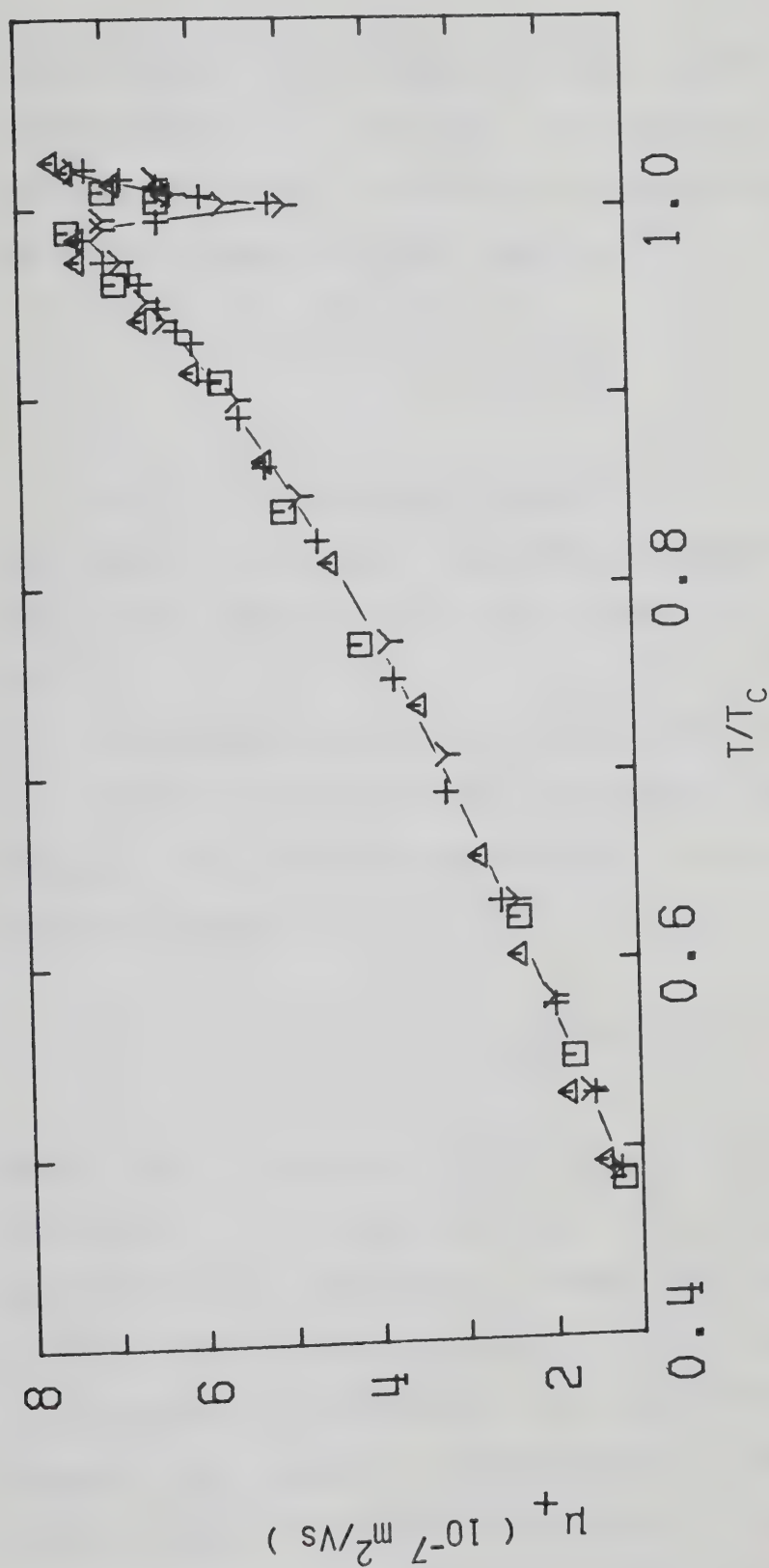


Figure IV-55. Cation mobilities in equilibrium liquid and supercritical methanes plotted as functions of the reduced temperature T/T_c . \square , CH_4 ; Δ , CH_2D_2 ; $+$, CHD_3 ; Y , CD_4 .

be estimated. The value $\eta\mu_+ = 2.4 \times 10^{-11} \text{ kgm/Vs}^2$ (Figure IV-56) gives $r = 0.35 \text{ nm}$. The molecular radius can be obtained by values of the self-diffusion coefficient D by use of the Nerst-Einstein equation.²³¹

$$\mu = \frac{De}{kT} \quad \text{IV-30}$$

In CH_4 the quantity $\eta De/kT$ is $6.3 \times 10^{-4} \text{ kgm/Vs}^2$ ²³² and gives $r = 0.20 \text{ nm}$. This value agrees with estimates of the rigid sphere radius of methane in the low density gas.²³³

An attempt to take into account the effect of changing the density of the fluid to explain the breakdown of Stokes' law at low viscosities is a modification of Equation IV-29.^{150,234}

$$\eta\mu_+ = \left(\frac{e}{6\pi r}\right)\left(1 + \frac{b\lambda}{r}\right) \quad \text{IV-31}$$

where b is a constant and λ is the mean free path between collisions. At high densities ($n/n_c \gtrsim 2.0$), $\lambda \ll r$ so Stokes' law is recovered. When $b\lambda/r$ approaches unity, Equation IV-31 indicates that $\eta\mu_+$ should increase above the value expected from Stokes' law. A maximum in $\eta\mu_+$ has been observed in several hydrocarbons¹¹² and, within the scatter, there seems to be the hint of a slight maximum in the present data (Figure IV-56). However the major feature

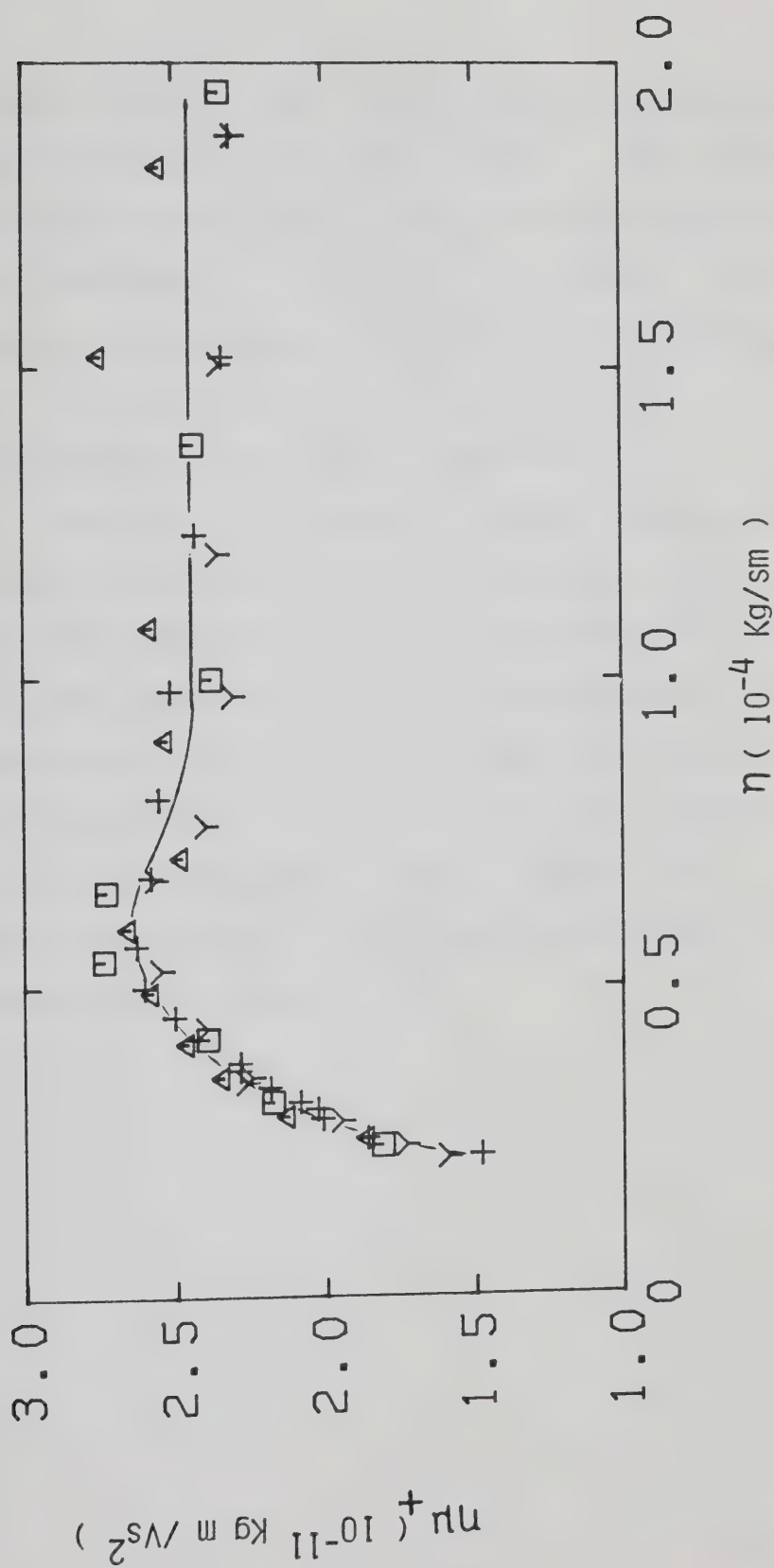


Figure IV-56. Product of the viscosity and the cation mobility in liquid methanes under the equilibrium vapor pressures. \square , CH_4 ; Δ , CH_2D_2 ; +, CHD_3 ; Y, CD_4 .

of the region at low viscosities is the **decrease** in $\eta\mu_+$ on approaching the critical point. The decrease is not predicted by the model since one would expect λ to increase as the density is further decreased. The decrease is mainly attributable to enhanced electrostriction²³⁵⁻²³⁷ due to the increased compressibility of the liquid as it approaches the critical region.^{108,112}

The dip in μ_+ observed in the critical region (Figure IV-55) can be attributed to the same effect. It has been observed before in cyclic hydrocarbons^{106,107,111} but not in other hydrocarbons.¹¹¹ A small dip in mobility on approaching the critical region has been recently found also in dimethyl ether.²³⁸ It is now believed that this is a general phenomenon which happens in a very limited temperature region ($\sim 5K$) and that can be obscured by temperature inhomogeneities.

REFERENCES

1. A.N. Gerritsen and J. Kolhaas, *Physica* **10**, 49 (1943).
2. A. Mozumder and J.L. Magee, *J. Chem. Phys.* **47**, 939 (1967).
3. G.R. Freeman, *Int. J. Radiat. Phys. Chem.* **4**, 237 (1972).
4. L. Onsager, *Phys. Rev.* **54**, 554 (1938).
5. E.W. McDaniel, Collision Phenomena in Ionized Gases, J. Wiley (1964), chapter 9.
6. G.R. Freeman, *J. Chem. Phys.* **39**, 1580 (1963).
7. A. Hummel and W.F. Schmidt, *Radiat. Res. Rev.* **5**, 199 (1974).
8. J.-P. Dodelet, *Can. J. Chem.* **55**, 2050 (1977) and references therein.
9. N. Gee and G.R. Freeman, *Phys. Rev. A* **28**, 3568 (1983).
10. J.J. Thomson, *Nature* **55**, 606 (1897).
11. J.S. Townsend, *Nature* **620**, 340 (1900).
12. J.S. Townsend, *Philos. Mag.* **1**, 198 (1901).
13. P. Curie, *Comp. Rend.* **134**, 420 (1902).
14. C. Ramsauer, *Ann. Phys.* **66**, 546 (1921).
15. C. Ramsauer and R. Kollath, *Ann. Phys.* **3**, 536 (1929).
16. C. Ramsauer and R. Kollath, *Ann. Phys.* **4**, 91 (1930).
17. E. Brück, *Ann. Phys.* **4**, 387 (1930); **5**, 281 (1930).
18. R. Kollath, *Phys. Zeitschr.* **31**, 985 (1930).
19. Reference 5, Chapter 4.

20. L.B. Loeb, Basic Processes of Gaseous Electronics, 2nd ed., University of California Press, 1961.
21. A.M. Tyndall, The Mobility of Positive Ions in Gases, Cambridge University Press, 1938.
22. J.S. Townsend and H.T. Tizard, Proc. Roy. Soc. **A88**, 336 (1913).
23. J.S. Townsend, Philos. Mag. **42**, 873 (1921).
24. J.S. Townsend and V.A. Bailey, Philos. Mag. **43**, 593 (1922).
25. J.S. Townsend and V.A. Bailey, Philos. Mag. **44**, 1033 (1923).
26. J.S. Townsend and V.A. Bailey, Philos. Mag. **46**, 657 (1923).
27. N.E. Bradbury and R.A. Nielson, Phys. Rev. **49**, 388 (1936).
28. R.A. Nielson and N.E. Bradbury, Phys. Rev. **51**, 69 (1937).
29. L.B. Loeb, Phys. Rev. **19**, 24 (1922).
30. L.B. Loeb, Phys. Rev. **20**, 397 (1922).
31. W.B. Wahlin, Phys. Rev. **21**, 517 (1923).
32. L.G.H. Huxley and R.W. Crompton, The Diffusion and Drift of Electrons in Gases, J. Wiley, (1974).
33. T.L. Cottrell and I.C. Walker, Quarterly Rev. **XX**, 153 (1966).
34. A.V. Phelps, Rev. Mod. Phys. **40**, 399 (1968).

35. A. Gilardini, Low Energy Electron Collisions in Gases, Wiley-Interscience (1972).
36. J. Dutton, J. Phys. Chem. Ref. Data, **4**, 577 (1975).
37. W.N. English and C.C. Hanna, Can. J. Phys. **31**, 768 (1953).
38. J.C. Devins and R.W. Crowe, J. Chem. Phys. **25**, 1053 (1956).
39. T.L. Cottrell and I.C. Walter, Trans. Farad. Soc. **61**, 1585 (1965).
40. C.R. Bowman and D.E. Gordon, J. Chem. Phys. **46**, 1878 (1967).
41. E.B. Wagner, F.D. Davis and G.S. Hurst, J. Chem. Phys. **47**, 3138 (1967).
42. W.J. Pollock, Trans. Farad. Soc. **64**, 2919 (1968).
43. T.L. Cottrell and I.C. Walker, Trans. Farad. Soc. **63**, 549 (1967).
44. D.R. Nelson and F.J. Davis, J. Chem. Phys. **51**, 2322 (1969).
45. C.W. Duncan and I.C. Walker, J.C.S. Faraday II, **68**, 1514 (1972).
46. H. Lehning, Phys. Rev. Lett. **29A**, 719 (1969).
47. N.E. Cipollini, R.A. Holroyd and M. Nishikawa, J. Chem. Phys. **67**, 4636 (1977).
48. N. Gee and G.R. Freeman, Phys. Rev. **A20**, 1152 (1979).
49. T.L. Cottrell, W.J. Pollock and I.C. Walker, Trans. Farad. Soc. **64**, 2260 (1968).

50. L.G. Christophorou, M.W. Grant and D. Pittman, Chem. Phys. Lett. **38**, 100 (1976).
51. D.L. McCorkle, L.G. Christophorou, M.V. Maxey and J.G. Carter, J. Phys. B**11**, 3067 (1978).
52. N. Gee and G.R. Freeman, Phys. Rev. **A22**, 301 (1980).
53. L.G. Christophorou, Atomic and Molecular Radiation Physics, Wiley-Interscience (1971).
54. I. György and G.R. Freeman, J. Chem. Phys. **70**, 4769 (1979).
55. S.S.-S. Huang and G.R. Freeman, Can. J. Chem. **56**, 2388 (1976).
56. L.G. Christophorou, R.P. Blaustein and D. Pittman, Chem. Phys. Lett. **18**, 509 (1973).
57. S.S.-S. Huang and G.R. Freeman, J. Chem. Phys. **69**, 1585 (1978).
58. J. Lekner and A.R. Bishop, Philos. Mag. **27**, 297 (1973).
59. T. Kimura and G.R. Freeman, Can. J. Phys. **52**, 2220 (1974); J. Chem. Phys. **60**, 4081 (1974).
60. N. Gee and G.R. Freeman, J. Chem. Phys. **78**, 1951 (1983).
61. I. György, N. Gee and G.R. Freeman, J. Chem. Phys. **79**, 2009 (1983).
62. M.S. Malkin and H.L. Schultz, Phys. Rev. **83**, 1051 (1951).

63. P.H. Tewari and G.R. Freeman, J. Chem. Phys. **49**, 4394 (1968).
64. P.H. Tewari and G.R. Freeman, J. Chem. Phys. **51**, 1276 (1969).
65. E.E. Conrad and J. Silverman, J. Chem. Phys. **51**, 450 (1969).
66. P.M. Minday, L.D. Schmidt and H.T. Davis, J. Chem. Phys. **50**, 1473 (1969).
67. W.F. Schmidt and A.O. Allen, J. Chem. Phys. **50**, 5037 (1969).
68. W.F. Schmidt and A.O. Allen, J. Chem. Phys. **52**, 4768 (1970).
69. R.M. Minday, L.D. Schmidt and H.T. Davis, J. Chem. Phys. **54**, 3112 (1971).
70. R.M. Minday, L.D. Schmidt and H.T. Davis, Phys. Rev. Lett. **26**, 360 (1971).
71. R.M. Minday, L.D. Schmidt and H.T. Davis, J. Phys. Chem. **76**, 442 (1972).
72. J.-P. dodelet and G.R. Freeman, Can. J. Chem. **50**, 2667 (1972).
73. G. Bakale and W.F. Schmidt, Z. Naturforsch. **28A**, 511 (1973).
74. J.-P. Dodelet, K. Shinsaka and G.R. Freeman, J. Chem. Phys. **59**, 1293 (1973).
75. M.G. Robinson and G.R. Freeman, Can. J. Chem. **52**, 440 (1974).

76. K. Shinsaka and G.R. Freeman, Can. J. Chem. **52**, 3495 (1974).
77. K. Shinsaka and G.R. Freeman, Can. J. Chem. **52**, 3556 (1974).
78. J.-P. Dodelet and G.R. Freeman, Can. J. Chem. **53**, 1263 (1975).
79. W.F. Schmidt, G. Bakale and U. Sowada, J. Chem. Phys. **61**, 5275 (1975).
80. K. Shinsaka, J.-P. Dodelet and G.R. Freeman, Can. J. Chem. **53**, 2714 (1975).
81. J.-P. Dodelet, K. Shinsaka and G.R. Freeman, Can. J. Chem. **54**, 744 (1976).
82. A.A. Balakin and B.S. Yakolev, High Energy Chem. **9**, 22 (1975).
83. A.A. Balakin and B.S. Yakolev, High Energy Chem. **9**, 69 (1975).
84. G.F. Novikov and B.S. Yakolev, Int. J. Radiat. Phys. Chem. **8**, 517 (1976).
85. A.A. Balakin, I.A. Boriev, and B.S. Yakolev, High Energy Chem. **12**, 171 (1978).
86. G. Bakale, W. Tauchert and W.F. Schmidt, J. Chem. Phys. **63**, 4470 (1975).
87. G. Bakale, U. Sowada and W.F. Schmidt, 1974 Annual Report, Conference of Electrical Insulation and Dielectric Phenomena, Nat. Acad. of Sci., p. 41.

88. I. Adamczewski and J.H. Calderwood, J. Phys. D8, 1211 (1975).
89. I. Adamczewski and J.H. Calderwood, J. Phys. D9, 2479 (1976).
90. H. Schnyders, S.A. Rice and L. Meyer, Phys. Rev. 150, 127 (1966).
91. J.A. Jahnke, L. Meyer and S.A. Rice, Phys. Rev. A3, 734 (1971).
92. J.M.L. Engels and A.J.M. Van Kimmenade, Chem. Phys. Lett. 42, 250 (1976).
93. J.M.L. Engels and A.J.M. Van Kimmenade, Phys. Lett. 59A, 43 (1976).
94. J.M.L. Engels and A.J.M. Van Kimmenade, Chem. Phys. Lett. 48, 451 (1977).
95. W. Döeldissen, G. Bakale and W.F. Schmidt, Proc. of the VIth Int. Conf. on Conductance and Breakdown in Dielectric Liquids, Edition Frontieres, Dreux, France (1978), p. 197.
96. W. Döeldissen, G. Bakale and W.F. Schmidt, Chem. Phys. Lett. 56, 347 (1978).
97. I. György and G.R. Freeman, Proc. of the VIth Int. Conf. on Conductance and Breakdown in Dielectric Liquids, Edition Frontieres, Dreux, France (1978), p. 203.
98. J.-P. Dodelet and G.R. Freeman, Can. J. Chem. 55, 2264 (1977).

99. J.-P. Dodelet and G.R. Freeman, *Can. J. Chem.* **55**, 2893 (1977).
100. T.G. Ryan and G.R. Freeman, *J. Chem. Phys.* **68**, 5144 (1978).
101. J.M. Warman, P.P. Infelta, M.P. de Haas and A. Hummel, *Can. J. Chem.* **55**, 2249 (1977).
102. J.M. Warman, *Proc. of the NATO Adv. Study Institute*, D. Reidel Pub. Co. (1982), p. 433.
103. W.F. Schmidt, *Can. J. Chem.* **55**, 2197 (1977).
104. E.W. McDaniel and E.A. Mason, The Mobility and Diffusion of Ions in Gases, J. Wiley (1973) and references therein.
105. T. Wada and G.R. Freeman, *Phys. Rev. Lett.* **42**, 715 (1979).
106. S.S.-S. Huang and G.R. Freeman, *J. Chem. Phys.* **70**, 1538 (1979).
107. N. Gee and G.R. Freeman, *Can. J. Chem.* **59**, 2988 (1981).
108. N. Gee and S.S.-S. Huang, T. Wada and G.R. Freeman, *J. Chem. Phys.* **77**, 1411 (1982).
109. I. Adamczewski, Ionization, Conductivity and Breakdown in Dielectric Liquids, Taylor and Francis Ltd., London (1969).
110. I. Adamczewski, *Ann. de Phys.* **8**, 309 (1937).
111. S.S.-S. Huang and G.R. Freeman, *J. Chem. Phys.* **72**, 1989 (1980).

- 112. N. Gee and G.R. Freeman, Can. J. chem. **58**, 1490 (1980).
- 113. Reviewed in Chapter 13 of reference 32.
- 114. Reference 32, p. 69.
- 115. J.L. Pack and A.V. Phelps, Phys. Rev. **121**, 798 (1961).
- 116. L.A. Viehland and E.A. Mason, Ann. Phys. (N.Y.) **91**, 499 (1975).
- 117. F.W. Morrison, G.R. Akridge, H.W. Ellis, R.Y. Pai, E.W. McDaniel, L.A. Viehland and E.A. Mason, J. Chem. Phys. **63**, 2238 (1975).
- 118. J.L. Pack, R.E. Voshall and A.V. Phelps, Phys. Rev. **127**, 2084 (1961).
- 119. P. Langevin, Ann. de Chim. et Phys. **5**, 245 (1905) cited in chapter 1 of reference 20, chapter 4 of reference 21 and in Appendix of reference 104.
- 120. A.C. Prior, J. Phys. Chem. Solids **12**, 175 (1959).
- 121. E.J. Ryder, Phys. Rev. **90**, 766 (1953).
- 122. J.B. Gunn, J. Electronics **2**, 87 (1956).
- 123. A.F. Gibson and J.W. Granville, J. Electronics **2**, 259 (1956).
- 124. M.B. Prince, Phys. Rev. **92**, 681 (1953).
- 125. J. Lekner, Phys. Rev. **158**, 130 (1967).
- 126. M.H. Cohen and J. Lekner, Phys. Rev. **158**, 305 (1967).
- 127. (a) H. Schnyders, S.A. Rice and L. Meyer, Phys. Rev. **150**, 127 (1966);

- (b) D.W. Swan, *Nature* **196**, 977 (1962);
- (c) D.W. Swan, *Proc. Phys. Soc. (London)* **83**, 659 (1964).
128. H.T. Davis and R.G. Brown, Low Energy Electrons in Non Polar Fluids, in *Adv. in Chem. Phys.*, edited by I. Prigogine and S.A. Rice, J. Wiley, New York (1975), p. 329.
129. J. Bardeen and W. Shockley, *Phys. Rev.* **80**, 72 (1950).
130. W. Shockley, Electrons and Holes in Semiconductors, Van Nostrand, New Jersey (1950).
131. E.M. Conwell, Solid State Physics, supplement n.9, Academic Press (1967).
132. (a) J. Lekner, *Phys. Lett.* **A27**, 341 (1968);
(b) *Philos. Mag.* **18**, 1281 (1968).
133. H.T. Davis, L.D. Schmidt and R.M. Minday, *Phys. Rev.* **A3**, 1027 (1971).
134. K. Fueki, *Can. J. Chem.* **50**, 3379 (1972).
135. K. Fueki, D.-F. Feng and L. Kevan, *Chem. Phys. Lett.* **13**, 616 (1972).
136. R.A. Holroyd and N.E. Cipollini, *J. Chem. Phys.* **69**, 502 (1978).
137. (a) R. Reininger, U. Asaf and I.T. Steinberger, *Chem. Phys. Lett.* **90**, 287 (1982); **100**, 363 (1983).
(b) K. Nagakawa, K. Ohtake and M. Nishicawa, *J. Electros.* **12**, 157 (1982).

138. Y.A. Berlin, L. Nyikos and R. Schiller, J. Chem. Phys. **69**, 2401 (1978).
139. S. Basak and M.H. Cohen, Phys. Rev. **B20**, 3404 (1979).
140. J.T. Richards and J.K. Thomas, Chem. Phys. Lett. **10**, 317 (1971).
141. L.M. Magnussen, J.T. Richards and J.K. Thomas, Int. J. Rad. Phys. Chem. **3**, 295 (1971).
142. H.A. Gillis, N.V. Klassen, G.G. Teather and K.L. Lokan, Chem. Phys. Lett. **10**, 481 (1971).
143. J.H. Baxendale, C. Ball and P. Wardman, Chem. Phys. Lett. **12**, 347 (1971).
144. L. Kevan, H.A. Gillis, K. Fueki and T. Kimura, J. Chem. Phys. **68**, 5203 (1978).
145. H. Kobayashi, T. Ueda, T. Kobayashi, M. Washio, Y. Tabata and S. Tagawa, Radiat. Phys. Chem. **21**, 13 (1983).
146. R. Schiller, J. Chem. Phys. **57**, 2222 (1972).
147. R. Schiller, Sz. Vass and J. Mandics, Int. J. Rad. Phys. Chem. **5**, 491 (1973).
148. J.-P. Dodelet, F.-Y. You and G.R. Freeman, J. Phys. Chem. **79**, 2876 (1975).
149. S. Glasstone, Textbook of Physical Chemistry, Van Nostrand, New York, 2nd ed. (1946), p. 897.
150. E. Cunningham, Proc. R. Soc. London Ser. A **83** 357 (1910).

151. O. Stern (1914), see W.H. Keesom and H. Van Dijk, Proc. Roy. Acad. Sci. Amsterdam **34**, 42 (1931).
152. F.A. Lindemann and F.W. Aston, Phil. Mag. **37**, 523 (1919).
153. F.A. Lindemann, Phil. Mag., **38**, 173 (1919).
154. E. Roth and J. Bigeleisen, J. Chem. Phys. **32**, 612 (1960).
155. J. Bigeleisen and E. Roth, J. Chem. Phys. **35**, 68 (1961).
156. M.W. Lee, S. Fucks and J. Bigeleisen, J. Chem. Phys., **53**, 4066 (1970).
157. M.W. Lee, D. Eshelman and J. Bigeleisen, J. Chem. Phys. **56**, 4585 (1972).
158. F. Mandel, J. Chem. Phys. **57**, 3929 (1972).
159. J. Bigeleisen, M.W. Lee and F.Mandel, Ann. Rev. Phys. Chem. **24**, 407 (1973).
160. K.F. Herzfeld and E. Teller, Phys. Rev. **54**, 912 (1938).
161. E. Wigner, Phys. Rev. **40**, 749 (1932).
162. G.T. Armstrong, F.G. Brickwedde and R.B. Scott, J. Res. Natl. Bur. Std., **55**, 39 (1955).
163. J. Bigeleisen, J. Chem. Phys. **34**, 1485 (1961).
164. J. Bigeleisen and M.G. Mayer, J. Chem. Phys. **15**, 261 (1947).
165. D.H. Rank, E.R. Shull and D.W.E. Axford, J. Chem. Phys. **18**, 116 (1950).

- 166. M.F. Crawford, H.L. Welsh and J.H. Harrold, *Can. J. Phys.* **30**, 81 (1952).
- 167. L.H. Jones and R.S. McDonald, *J. Mol. Spectr.* **3**, 632 (1959).
- 168. M. Wolfsberg, *J. Chim. Phys. Physiochim. Biol.*, **60**, 15 (1963).
- 169. M.J. Stern, W.A. van Hook and M. Wolfsberg, *J. Chem. Phys.* **39**, 3179 (1963).
- 170. J. Bigeleisen, C.B. Cragg and M. Jeevanandam, *J. Chem. Phys.* **47**, 4335 (1967).
- 171. G.E. Ewing, *J. Chem. Phys.* **40**, 179 (1964).
- 172. A.F. Grigor and W.A. Steele, *J. Chem. Phys.* **48**, 1032, 1038 (1968).
- 173. Y.D. Harker and R.M. Brugger, *J. Chem. Phys.* **42**, 275 (1965).
- 174. K. Otnes, *Bull. Am. Phys. Soc.* **10**, 42 (1965).
- 175. G. Kosaly and G. Solt, *Physica*, **32**, 1571 (1966); Y.D. Harker and R.M. Brugger, *J. Chem. Phys.* **46**, 2201 (1967); V.F. Sears, *Can. J. Phys.* **45**, 237 (1967).
- 176. K.J. Lushington, K. Maki, J.A. Morrison, A. Heidemann and W. Press, *J. Chem. Phys.* **75**, 4010 (1981).
- 177. Z.C. Kornblum and T. Ishida, *J. Chem. Phys.* **69**, 1814 (1978).
- 178. J.S. Pollin and T. Ishida, *J. Chem. Phys.* **66**, 4442 (1977).

179. (a) R.C. Weast, ed., Handbook of Chemistry and Physics, 55th Ed. (CRC Press, Cleveland, 1974).
(b) Landolt - Börnstein Kalorische Zustandsgrossen (Springer, Berlin, 1961) p. 262.
180. O.E. Von Frivold, O. Hassel and E. Hetland, Phys. Z. **40**, 29 (1938).
181. J.O. Hirshfelder, C.F. Curtis and R.B. Bird, Molecular Theory of Gases and Liquids, 2nd Ed. Wiley, New York (1964), p. 950.
182. A. Yoshihara, A. Anderson, R.A. Aziz and C.C. Lim, Chem. Phys., **48**, 183 (1980).
183. I. Ozier, Phys. Rev. Lett., **27**, 1329 (1971).
184. J.K.G. Watson, M. Takami, T. Oka, J. Chem. Phys. **70**, 5376 (1979).
185. M. Bloom and J.A. Morrison, in Surface and Defects Properties of Solids, the Chemical Society, Burlington House, London, Vol. 2, p. 6 (1973).
186. R. Savoie and R.P. Fournier, Chem. Phys. Lett. **7**, 1 (1970).
187. R.G. Gordon, J. Chem. Phys., **43**, 1307 (1965).
188. D.G. Bounds, M.L. Klein, G.N. Patey, J. Chem. Phys. **72**, 5348 (1980).
189. M.J. Stern, W.A. van Hook and M. Wolfsberg, J. Chem. Phys. **39**, 3179 (1963).
190. T. Ishida and J. Bigeleisen, J. Chem. Phys. **49**, 5498 (1968).

191. J. Bigeleisen and S.V. Ribnikar, J. Chem. Phys. **35**, 1927 (1961).
192. T. Wada and G.R. Freeman, Can. J. Chem. **57**, 2716 (1979).
193. G.M. Barrow, Physical Chemistry (McGraw-Hill Book Co., 4th ed. 1979).
194. G.R. Freeman, private communication.
195. R.D. Goodwin, The Thermophysical Properties of Methane from 90 to 500K at Pressures to 700 Bar, Natl. Bur. Stand. Tech. Note 653 U.S.G.P.O., Washington, D.C. (1974).
196. S. Angus, B. Armstrong and K.M. de Reuck, International Thermodynamic Tables of the Fluid State- 5: Methane, International Union of Pure and Applied Chemistry Chemical Data Series no. 16, Pergamon, Oxford (1978).
197. A.F. Grigor, The Measurements and Correlation of Some Physical Properties of Methane and Perdeuromethane, Ph.D. Thesis, Pennsylvania State University (1966).
198. S.C. Rand and B.P. Stoicheff, Can. J. Chem. **60**, 287 (1982).
199. G. Herzberg, Molecular Spectra and Molecular Structure. II. Infrared and Raman Spectra of Polyatomic Molecules. D. van Nostrand Co. Inc., Princeton (1945).

200. V.L. Talroze and A.L. Lyubimova, Dokl. Akad. Nauk. SSSR **86**, 509 (1952).
201. M.S.B. Munson and F.H. Field, J. Am. Chem. Soc. **87**, 3294 (1965).
202. K. Hiraoka and P. Kebarle, J. Am. Chem. Soc. **97**, 4179 (1975).
203. M. Saporoshenko, Int. J. Mass Spectr. and Ion Phys. **42**, 285 (1982).
204. K. Hiraoka and P. Kebarle, J. Chem. Phys. **63**, 394 (1975).
205. W. Shockley, Bell Syst. Tech. J. **30**, 990 (1951), see pp. 1018-24.
206. L.S. Miller, S. Howe and W.E. Spear, Phys. Rev. **166**, 871 (1968).
207. S.S.-S. Huang and G.R. Freeman, J. Chem. Phys. **68**, 1355 (1978).
208. S.S.-S. Huang and G.R. Freeman, Phys. Rev. **A24**, 714 (1981).
209. B.V. Paranjape, Phys. Rev. **A21**, 405 (1980).
210. D.L. Goodstein, States of Matter, Prentice Hall, Englewood Cliffs (1975) Chapter 4.
211. G.R. Freeman, J. Phys. Soc. Japan, **48**, 683 (1980).
212. M. Nishikawa, R.A. Holroyd and U. Sowada, J. Chem. Phys. **72**, 3081 (1980).
213. M. Nishikawa and R.A. Holroyd, J. Chem. Phys. **77**, 4678 (1982).

214. G.C. Straty, *Cryogenics* **14**, 367 (1974).
215. J. Thoen and C.W. Garland, *Phys. Rev.* **A10**, 1311 (1974).
216. (a) Argon, Helium and the Rare Gases, edited by G.A. Cook, Interscience, New York (1961), Vol. 1, pp. 151, 277, 354-9.
- (b) E. Mathias, C.A. Crommelin and J.J. Meihuizen, *Physica* **4**, 1200 (1937).
217. R.A. Aziz, D.H. Bowman and C.C. Lim, *Can. J. Chem.* **45**, 2079 (1967).
218. J. Applequist, J.R. Carl and K.-K. Fung, *J. Am. Chem. Soc.* **94**, 2952 (1972).
219. V.F. Nozdrev, Application of Ultrasonics in Molecular Physics, Gordon and Breach, New York (1963), p. 455.
220. T.R. Das, C.O. Reed and P.T. Eubank, *J. Chem. Eng. Data* **22**, 16 (1977).
221. B.E. Springett, J. Jortner and M.H. Cohen, *J. Chem. Phys.* **48**, 2720 (1968).
222. T.F. O'Malley, *Phys. Rev.* **130**, 1020 (1963).
223. R.C. Muñoz and G. Ascarelli, *Phys. Rev. Lett.* **51**, 215 (1983).
224. G. Ascarelli, *J. Chem. Phys.* **71**, 5030 (1979).
225. G.R. Freeman, *J. Chem. Phys.* **74**, 3079 (1981).
226. J. Kestin and J.R. Dorfman, A Course in Statistical Mechanics, Academic Press, New York (1971).

227. N. Gee and G.R. Freeman, Can. J. Chem. **61**, 1664 (1983).
228. L.A. Viehland and E.A. Mason, Ann. Phys. (N.Y.) **110**, 287 (1978).
229. Y.S. Touloukian, S.C. Saxena and P. Hestermans, Viscosity, Thermophysical Properties of Matter, IFI/Plenum, New York (1975), Vol 11.
230. G.G. Stokes, Trans. Cambridge Philos. Soc. **9**, 8 (1850) in Mathematical and Physical Papers, edited by G.G. Stokes, Cambridge University, Cambridge (1901), Vol III, p. 1.
231. A. Einstein, Zeit. fur Electrochemie **14**, 235 (1908) in Investigations on the Theory of the Brownian Motion by A. Einstein, edited by R. Furth, translated by A.D. Cowper, Dover, New York (1956) pp. 73,75.
232. P.H. Oosting and N.J. Trappeniers, Physica (Utrecht) **51**, 418 (1971).
233. Ref. 181, p. 545.
234. J.J. Thomson and C.P. Thomason, Conduction of Electricity Through Gases, Cambridge University Press (1928), Vol. 1, 3rd ed.
235. K.R. Atkins, Phys. Rev. **116**, 1339 (1959).
236. R.M. Fuoss, Proc. Natl. Acad. USA **45**, 807 (1959).
237. S.A. Rice and P. Gray, The Statistical Mechanics of Simple Liquids, Interscience Publ., New York (1965).

238. N. Gee and G.R. Freeman, Can. J. Chem. **60**, 1034 (1982).
239. J.D. Cobine, Gaseous Conductors, Dover Publ. Inc. New York (1958), pp. 55-58.

APPENDIX

Average Deviations

The average percent error was calculated for several sets of data in Chapter III, to illustrate their magnitude. The sets chosen in a Figure were those displaying more scatter. The results are given in Tables A-1 and A-2. The average percent error was taken to be

$$\text{average \% errors} = \frac{100}{n} \sum \frac{|\text{expected} - \text{experimental}|}{\text{experimental}}$$

where n is the number of experimental points. The expected value was taken to be the average mobility.

TABLE A-1
Electron Mobility Errors*

Figure	T(K)	n (10^{26} molec/m ³)	Average % error
1-1	163.7	0.295	0.5
1-1	636	0.295	0.5
1-3	294.0	0.58	0.8
1-8	149.0	5.7	0.5
1-9	183.7	28.0	1.4
1-13	194.6	61	0.4
1-16	146.5	137	0.6
2-3	109.3	0.49	1.0
2-9	219.3	6.7	1.6
2-17	178.7	106	0.8
3-2	351.7	0.370	0.3
3-10	189.2	61	1.2
3-14	172.7	112	0.9
4-4	236.3	1.22	0.3
4-11	179.0	23.7	1.6
4-15	183.6	94	1.2
5-5	433	3.70	1.2
5-10	186.1	36.0	0.9
5-13	175.5	105	0.4

*based on the field independent region only.

TABLE A-2
Ion Mobility Errors

Figure	T(K)	n (10^{26} molec/m ³)	Average % error
1-20	372.6	0.295	1.0
1-22	228.0	5.5	0.7
1-25	191.2	61	0.8
1-26	173.0	113	1.4
2-25	171.0	15.0	0.4
2-26	192.0	27.0	1.5
3-21	189.3	26.0	0.3
3-23	183.8	95	0.6
4-20	94.8	0.156	0.3
4-22	434	0.43	1.1
4-26	235.0	6.8	1.2
4-31	193.0	61	1.3
4-32	168.0	117	1.7
5-19	598	0.320	0.7
5-21	293.8	0.50	0.8
5-24	142.0	4.46	0.9
5-28	189.5	61	0.6
5-29	184.0	94	0.4

B30423